THE DESIGN, SYNTHESIS, AND USE OF PHOSPHONIC ACIDS FOR THE SURFACE MODIFICATION OF METAL OXIDES

A Dissertation
Presented to
The Academic Faculty

By

Peter J. Hotchkiss

In Partial Fulfillment
Of the Requirements for the Degree
Doctor of Philosophy in Chemistry

Georgia Institute of Technology

December 2008

THE DESIGN, SYNTHESIS, AND USE OF PHOSPHONIC ACIDS FOR THE SURFACE MODIFICATION OF METAL OXIDES

Approved by:

Dr. Seth Marder, Advisor
School of Chemistry and Biochemistry
Georgia Institute of Technology

Dr. Jean-Luc Brédas
School of Chemistry and Biochemistry
Georgia Institute of Technology

Dr. Nils Kröger
School of Chemistry and Biochemistry
Georgia Institute of Technology

Dr. Joseph Perry
School of Chemistry and Biochemistry
Georgia Institute of Technology

Dr. Ken Sandhage
School of Materials Science and Engineering
Georgia Institute of Technology

Date Approved: October 16, 2008

ACKNOWLEDGEMENTS

I wish to thank my advisor, my coworkers, and especially my friends and family for all the support they have given me throughout the years.

TABLE OF CONTENTS

LIST OF TABLES

LIST OF FIGURES

SUMMARY

The design and synthesis of a large variety of novel phosphonic acids has been described. Phosphonic acids are known to bind strongly to the surface of a number of metal oxides. The phosphonic acids designed and synthesized herein were used to modify the surface of both planar and nanoparticle metal oxides for use in a variety of applications. Indium tin oxide (ITO) substrates were modified with different fluorinated phosphonic acids in order to tune both the work function and the surface energy of the material. These changes in surface properties resulted in increased performance when the surface-modified ITO was incorporated into organic electronic devices. Additionally, the binding of phosphonic acids to a number of metal oxide species was studied. It has been shown that phosphonic acids bind strongly (bi- and tridentate) to ITO, zinc oxide (ZnO), and barium titanate ($BaTiO_3$). Phosphonic acids bind to a variety of other metal oxides *via* at least a monodentate binding. More generally, the roles of monolayers in surface science and the properties they can tune are discussed.

Chapter 1

Introduction

The goal of my graduate research has been to be able to control the surface properties of metal oxides *via* their surface modification with phosphonic acids. While there exist a number of different molecules which can bind to the surface of metal oxides, only phosphonic acids were used herein. The scientific field on the research of monolayers involves three basic parts: the design and synthesis of organic ligands, characterization of formed monolayers on surfaces, and the study of the properties that these monolayers can impart to a surface. This thesis addresses all three of these topics for the modification of metal oxides with phosphonic acids.

1.1 General Introduction to Monolayers: Their History and Use

This general introduction serves to introduce the concept of organic monolayers as well as their role in organic and molecular electronics. This introduction is intended to provide a brief description of some of the key properties and applications of organic monolayers and is not intended to be a comprehensive review of the literature as many such reviews spanning the field of organic monolayers and their role in organic electronics have recently been published.[1-10]

1.1.1 Discovery of Monolayers of Organic Molecules and Their Growth in the Scientific Field

The popular Langmuir–Blodgett technique[a] for the formation of organic monolayers was first reported in 1920 by Langmuir.[11] However, it would be another 25 years before Bigelow *et al.* introduced the idea that silanes bind on oxidized silicon to form monolayers.[12] The science and technology of monolayers saw little growth in the next 40 years or so, until the early 80s when Maoz and Sagiv reported advances in the modification of metal oxides[13] (including one of the earliest depositions of phosphate monolayers) and Allara and Nuzzo reported the first evidence of alkylthiolate monolayers on gold.[14]

While the concept of using monolayers of organic molecules has been around for almost 90 years, it has only been in the last 25 years that the field has attracted significant interest. This is due to a combination of the need for smaller feature sizes in emerging technologies as well as new and improved ways in which these systems can be studied. The advent of ultra–high vacuum (UHV) techniques as well as scanning probe microscopy has provided new and powerful characterization tools for the study of the physical properties of monolayers, and, more generally, surfaces and interfaces.[15] UHV is incredibly important in surface science, as the presence of contaminants can significantly affect surface properties. Minimal surface contamination is critical for meaningful studies of monolayers of organic species as the contaminants will often have elemental

[a] A Langmuir-Blodgett film is a film produced by controlled deposition of monolayers onto a solid substrate from a liquid. Each deposition adds a new monolayer. Thus, multilayers can be built with well-defined and controlled thickness. Amphiphilic molecules are usually used in this technique.

compositions, which include carbon and oxygen, similar to those of the monolayers. UHV technology has paved the way for many surface characterization techniques, such as X–ray photoelectron spectroscopy (XPS), ultraviolet photoelectron spectroscopy (UPS), Auger electron spectroscopy (AES), low energy electron diffraction (LEED), Rutherford Backscattering spectroscopy (RBS), and Secondary ion mass spectrometry (SIMS), to name a few.

Additionally, other techniques whose development have facilitated the field of surface science include: infrared reflection absorption spectroscopy (IRRAS), ellipsometry, scanning electron microscopy (SEM), and the field of scanning probe microscopy (SPM), which includes the popular techniques of atomic force microscopy (AFM) and scanning tunneling microscopy (STM). These two SPM techniques in particular have helped further the study of organic monolayers as they provide the necessary depth and lateral resolution to determine with nm precision the location of molecules on surfaces,[16] and importantly, where there may be multilayers rather than monolayers.[17]

The above–mentioned techniques for studying monolayers are particularly important because they can provide surface–sensitive information about a material. This is due to either reflection off of surfaces (IRRAS, ellipsometry), topographical imaging techniques (SEM, AFM, STM), or analysis of the emission of electrons (AES, UPS, XPS) or ions (SIMS) which are energetically limited to emission from the top few nanometers of a material.

1.1.2 Use of the Term SAM (Self–Assembled Monolayer)

The term self–assembled monolayer (SAM) is widely use in the literature and not necessarily in a consistent manner. Ulman defines a SAM as a monomolecular film of a surfactant formed spontaneously on a substrate upon exposure to a surfactant solution.[18] This term, coined for the attachment of thiols to gold in solution, is often used without discretion in the literature for all types of organic monolayers. While some may argue that even monolayers on gold are not "self–assembled", as the reactivity of the gold is dependent on the cleanliness and hence pre–cleaning procedures, the use of this term for many other monolayer systems is not appropriate. This thesis focuses on the attachment of phosphonic acids to metal oxides to form monolayers and the use of the "self–assembled" term has been used in the literature to describe these systems. However, it has been shown that oftentimes physisorbed and hydrogen–bonded multilayers of phosphonic acids are first deposited on a given surface, only to become monomolecular after heating and/or washing.[17, 19, 20] It is thus hard to justify the deposition of monolayers of phosphonic acids as "self–assembled". Consequently, this term will not be used to describe this system herein.

1.1.3 Different Binding Groups and the Types of Surfaces They Modify

As discussed above, many different types of inorganic surfaces can be modified with organic molecules. Monolayers on surfaces with various geometries, from planar

substrates, to nanoparticles, to porous networks, have been investigated.[4] However, as the chemistries of the inorganic surfaces can vary greatly (from noble metals to metal oxides to alloys), different types of binding groups need to be used (Table 1.1). The most common and most studied modifier–substrate system has been that of thiols and gold.

Table 1.1 Table of some of the most common ligands used to form monolayers on inorganic substrates and for which substrates they are most often used. Adapted from Love *et al*., where a more comprehensive listing can be found.[4]

Ligand	Substrate
RSH	noble metals (esp. gold, silver)
ROH	iron oxide, silicon, glass
RCOOH	various metal oxides (esp. glass, ITO)
RNH_2	cadmium selenide, gold
$RSiX_3$ (X = H, Cl, OR')	various metal oxides (esp. glass, ITO)
$RP(O)(OH)_2$	various metal oxides (esp. ITO, TiO_2), cadmium selenide

While the interactions of each type of binding group on various substrates will not be discussed in detail, it is important to know that there often exists more than one type of ligand which can bind to a given surface. The same is true of metal oxides, and our choice for using phosphonic acids exclusively is presented later in the chapter.

1.1.4 Current Trends and Future of Monolayers in Technology

Applications such as coatings, catalysis, drug delivery, biomaterials, organic and

molecular electronics, and sensors, to name a few, can all be impacted by organic monolayers.[4] In particular, in the context of this thesis, there is potential for organic monolayers to make large contributions in molecular and organic electronics. The ability to change the way in which a material interacts with another material at their interface by attaching a monolayer is a powerful way to tune the interfacial properties of devices.

For certain studies and applications, organic-based monolayers can have advantages over other thicker organic films in that they can be more well–defined, are the thinnest coating possible (in many cases having minimal impact upon the optical properties associated with the material), and can be covalently bound to the surface. This last point is especially important when chemical robustness is necessary. Organic thin films can delaminate from the surface they are coating which can affect their long–term integrity. In comparison, many monomolecular layers can be covalently bound to surfaces, allowing for more stable, robust modification of the surface.

Progress is continually made in the field of monolayer science. Specifically, the surface modification and use of metal oxides, which can often be inexpensive and non-toxic (though not true of ITO), in a variety of applications is becoming an important area of research and development. For example, the groups of Halik[21, 22] and Marks[23-25] have used monolayers of phosphonic acids and silanes, respectively, to significantly improve the properties, such as operating voltage and flexibility, of organic–based transistors. Schwartz and coworkers, at Princeton, have shown that coating titanium implant materials with monolayers of phosphonic acids can help their adhesion to biological tissue as well as increase bone–growth on their surface.[26, 27] Monolayers have been used to significantly protect metals, such as iron, from corrosion.[28] Numerous groups have

shown an ability to tune the electrodes of organic electronic devices by use of a monolayer, which have the potential to improve their transport properties.[29-32]

1.2 Properties which ligands can impart on a substrate

There are many properties of a substrate that can be changed by modification of the surface with organic monolayers. While the ability to change surface wetting is the property most widely studied, there are other key properties of inorganic materials that can be modified with organic monolayers, such as chemical functionality, electronic, and optical properties. The work function of materials is a property that will be discussed in detail in this thesis.

Conceptually, monolayer–forming molecules can be broken down into three distinct parts (Figure 1.1): the binding group, which is responsible for the attachment of the molecules to the substrate; the spacer, or linker, which is a saturated or unsaturated chain serving primarily as a connection between the binding groups and terminal functional group, but also providing the possibility to impact thickness, stability, and a physical barrier to the substrate; and the terminal functional group, which largely determines the overall surface properties and chemistry.

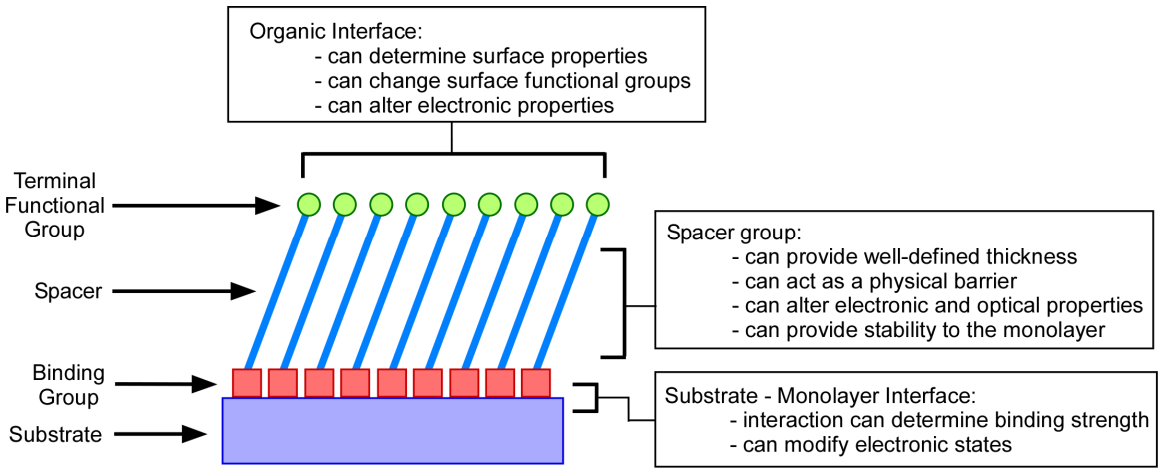

Figure 1.1 Schematic of an organic monolayer attached to a substrate, the various constituents of the monolayer, and the role that each constituent plays. Figure adapted from Love *et al.*[4]

One way to consider the discipline of monolayer science is to divide it into three distinct thrusts:

1. Design and synthesis of the ligands: While many ligands are already commercially available, the design and synthesis of new organic molecules that can bind to inorganic substrates and impart specific properties to these surfaces is an important element of the research field, specifically in the search for a better understanding of the effect of the ligands on the substrate properties, on the interaction between the binding groups and the surface, and between the surface and the environment.
2. Characterization of monolayers on surfaces: The kinetics of monolayer formation, the nature of the binding group–substrate interaction, the surface coverage, and homogeneity and robustness of the monolayer are among the properties of interest. Often the need to characterize specific properties of surfaces has spurred

the development of new measurement techniques. Conversely, the availability of commercial instrumentation for surface analysis in the last ten or twenty years, as well as continuous advances in their sensitivity and resolution, has supported the expansion of the research field.

3. Properties and applications of monolayers: The ways in which monolayers can be used to tune or enhance the properties of materials and therefore change the operation of devices made from them is an expanding area of applied research. Once the fundamental properties of monolayers are determined for specific systems, then the correct one can be identified for a given application.

1.2.1 Surface Chemistry

The addition of a monolayer to a material can change that materials' surface chemistry. By altering the chemistry on a surface, it may be possible to enable new chemistry which previously would have been impossible. Many organic reactions, such as nucleophilic substitution, oxidation/reduction, and free radical halogenation can be performed on surfaces in a manner similar to the analogous bulk media.[1] While in principle many different types of reactions can be performed on and off of surfaces, in practice most reactions are performed on monolayers with terminal carboxyl, amino, or hydroxyl groups, and are affected by the following factors:[1] solvent effects (the solvation of the functional groups on the monolayer can differ from that in the bulk), steric effects (the molecules in monolayers tend to have a particular orientation with respect to the

surface and/or conformation and this may affect sterically demanding reactions), and electronic effects (close proximity of other functional groups may affect reactivity through field effects or hydrogen bonding).

The ability to pattern surfaces either *via* microcontact printing,[33] dip–pen nanolithography,[34] ink–jet printing,[35, 36] or some other lithography technique,[37, 38] can allow for the controlled attachment of groups of ligands that have different terminal functional groups.[4] Additionally, using multiple substrates and ligands that have orthogonal interactions with one another can allow for the patterning of different functional groups (Figure 1.2).[39, 40] The ability to pattern substrates with multiple chemical functionalities in a controlled fashion potentially opens the door to custom–tailored surfaces for a variety of applications.

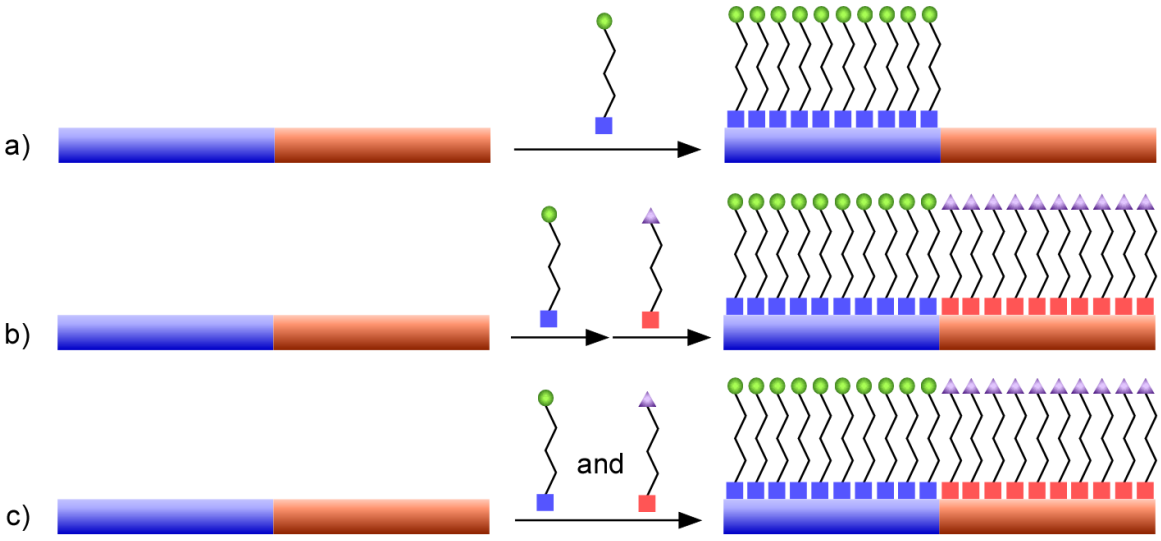

Figure 1.2 Schematic of orthogonal ligand–substrate systems where the substrate is comprised of two different materials. a) Only one of the substrate materials is modified by an organic ligand with an appropriate binding group, b) both materials are modified by ligands with different binding groups in a sequential fashion, and c) both materials are modified by ligands with different binding groups at the same time. Figure adapted from Mutin *et al.*[39]

The ability to polymerize or crosslink polymers to a surface may be possible once the correct chemical functionalities have been attached. Surfaces coated with polymers can be desirable as they can be very mechanically and chemically robust.[41] There exists a number of ways by which to coat surfaces with polymers (Figure 1.3). Various types of polymerizations, including different radical polymerizations, such as conventional radical polymerization, atom transfer radical polymerization (ATRP), reversible addition–fragmentation chain transfer (RAFT, nitroxide–mediated polymerization (NMP), and ring opening polymerization, as well as ring opening metathesis polymerization (ROMP) and anionic polymerizations have all been initiated off of both planar and/or nanoparticle surfaces.[42, 43] Polymer–coated surfaces already play a large role in biomedical applications (including biomaterials,[44] drug delivery,[45, 46] and implants[47, 48]) as well as in microfluidics[49] and smart, responsive surface applications,[50-52] and stands to increase in future designs of materials.

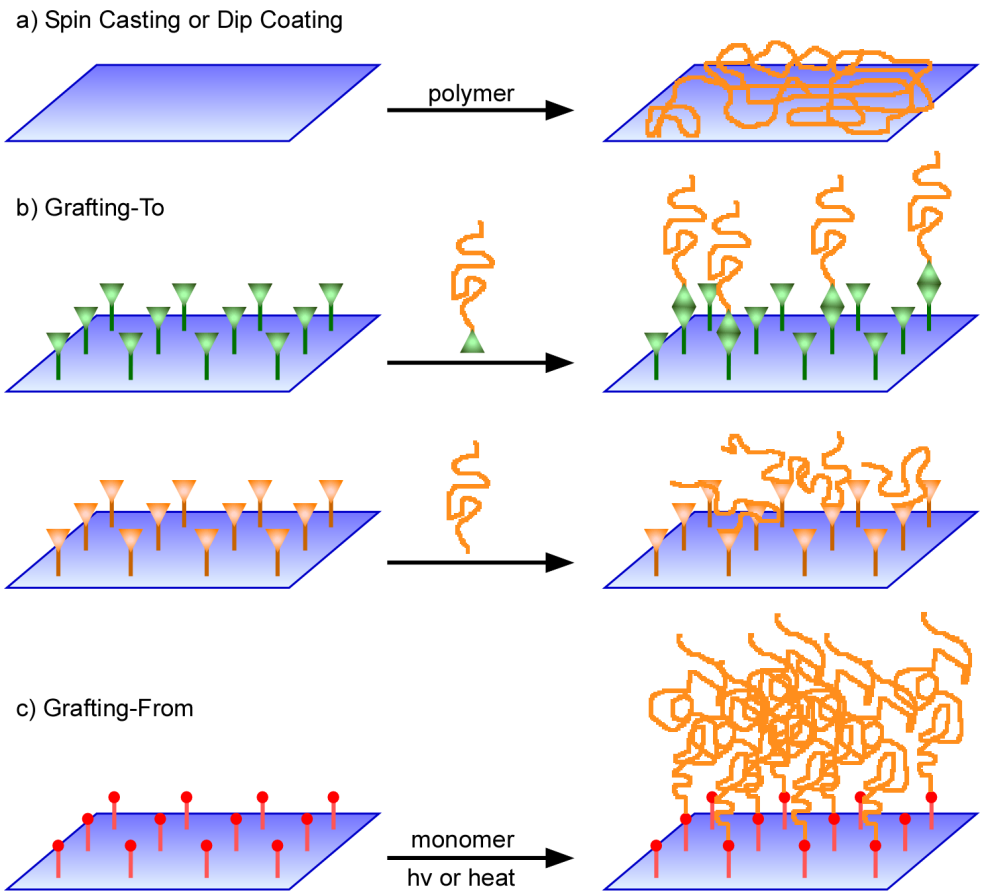

Figure 1.3 Two ways in which polymers can be attached to a surface: b) 'grafting to' approach where already formed polymers are attached to the surface *via* some sort of crosslinking group; c) 'grafting from' approach where polymers are initiated at and grown from the surface. In a) the polymer is not chemically bound to the surface. Figure adapted from Dyer.[42]

1.2.2 Changing the Wetting Properties of Inorganic Materials

The attachment of organic species to a substrate's surface can affect its interaction with other materials. This is often referred to as changing the substrate's surface energy, or more colloquially, the surface's wetting to various materials. This property of a surface

dictates how it interacts with other materials, including solvents or different organic materials with which the substrates are to be in contact. This ability to compatibilize materials is extremely important, as for nanoparticles it can help define their solubility or dispersibility in solvents or their compatibility in organic matrices for hybrid materials. For planar substrates, it can determine how the substrate interacts with subsequent deposited materials, such as, for instance, in the fabrication of organic light-emitting diodes (OLEDs), where multiple layers of components are stacked on one-another.

There are many accounts in the literature where the surface energies of substrates have been modified by attaching organic monolayers.[53-55] One common theme is the control of hydrophobicity and hydrophilicity of a surface.[56, 57] One treatment that has been often used to render surfaces hydrophobic is to attach a monolayer which is heavily fluorinated.[58, 59] Conversely, attaching a monolayer with a terminal carboxyl group can help the surface become more hydrophilic.[60] The ability to tune the surface energy, coupled with the architecture of the surface, can allow for a wide range of wetting–related surface properties (Figure 1.4).

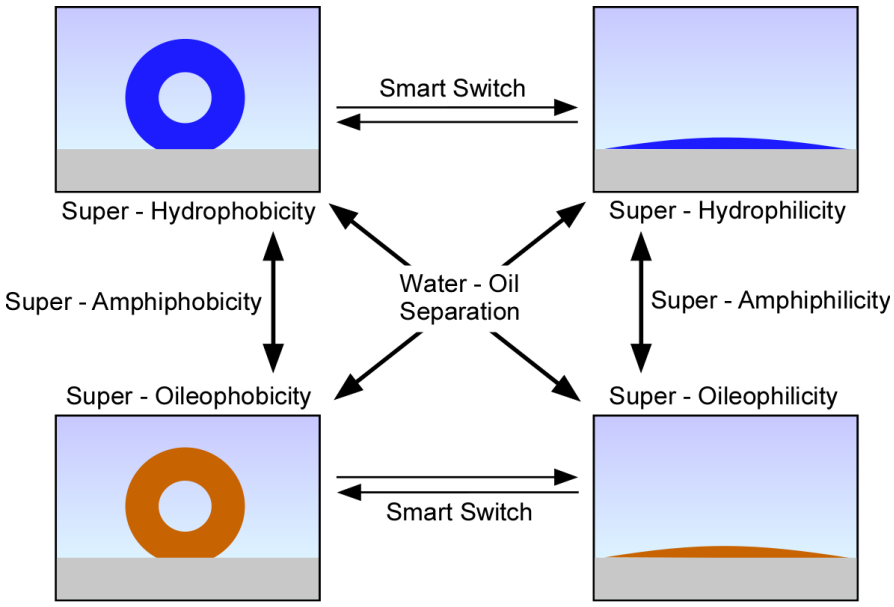

Figure 1.4 Schematic of the relationship between the 4 fundamental wetting/antiwetting properties and the special surface properties obtained when either two of the fundamental properties are combined. Double–headed arrows indicate coexistence of two properties whereas reversible arrows indicate switching between two properties. Figure adapted from Feng *et al*.[55]

The ability to tune the surface energy and, perhaps, to switch between extremes is of key importance in the area of coatings and separation technologies.

For nanoparticle modification, organic monolayers can completely change the solubility properties of a given nanoparticle.[61] This can allow for previously water–insoluble particles to become completely soluble in aqueous conditions, for instance (Figure 1.5). Or, for larger particles, the ability to suspend them for long periods of time in various media is important for depositing homogeneous, well–dispersed films of these particles or for doing further chemistry.

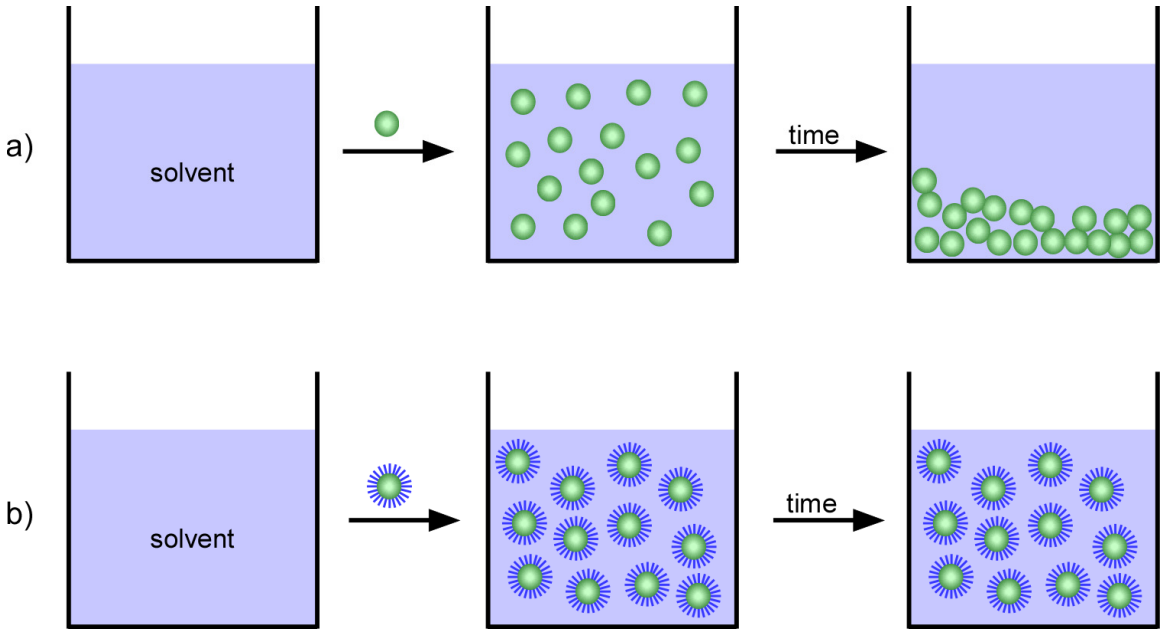

Figure 1.5 Illustration of how monolayers on nanoparticles can affect their compatibility with solvents. a) Loading of bare nanoparticles into a solvent where the nanoparticles settle after a specific period of time, and b) loading of monolayer protected nanoparticles into the same solvent where after the same amount of time the nanoparticles are still well–dispersed in solution.

1.2.3 Electronic Properties

Monolayers of organic materials can also be used to tune the electronic properties of a material. In particular, the work function of various metals and metal oxides can be shifted by attaching monolayers which change the electronic nature of the surface.[62] This concept will be discussed in detail in a later section.

1.3 Organic Monolayers in Organic and Molecular Electronics

This section provides a brief introduction to the field of organic and molecular electronics and how surface modification by organic molecules has become an integral part of the technology.

1.3.1 Introduction to Organic Electronics

Organic electronics is a branch of electronics that attempts to use organic materials either fully or in conjunction with inorganic materials to realize electronic devices. The motivation for these attempts is that organic–based devices might exhibit advantages with respect to inorganic counterparts, the most commonly cited ones being cost reduction, ease of manufacturing, improved device performance, and new device characteristics.[63] Organic materials have certainly become essential to the electronics industry, however currently only in a passive role; organics are often used either as sacrificial stencils such as photoresists or as passive insulators. It has been in only the last 30 years or so that the potential for organics to play active roles in electronics has been investigated. While the field of organic electronics started in the late 70's with the discovery of the conductivity of polyacetylene,[64, 65] research has since expanded to the point where organic materials are currently being sought after to replace almost every component of most devices, including the substrate.

The field of molecular electronics also saw its beginning in the mid 70's, as researchers realized the role that organic molecules could play in electronics.[66, 67] The future and development of smaller feature sizes was realized, and the exploration of using organic molecules, which are on the order of 1–2 nm in size, began.

While inorganic materials still hold several key advantages over organics in device performance, such as overall efficiency and lifetime, organic materials are continually improving in these key areas, and offer advantages in other areas, such as less–expensive processing and expanded structural capabilities, such as flexible devices, to name a few.[63] These inherent properties of organic materials are one of the driving forces for research in the field.

1.3.2 Use of Monolayers in Organic Electronics

Since the first reports on the electronic properties of organic monolayers by Mann and Kuhn in 1971,[67] and the first concept of single molecule electronics by Aviram and Ratner in 1974,[66] monolayers have become increasingly desirable in organic electronic applications for a number of reasons. First, they can affect the energy levels or electronic conduction of the system by either changing the work function of the substrate they modify[62] or by creating a dielectric layer in a system[10], respectively. Secondly, they are being used in order to improve the physical characteristics of interfaces between the inorganic and organic layers in devices. This includes helping to match surface energies between these interfaces and helping to induce phase segregation and subsequently better

device performance in materials.[68, 69] These topics are addressed in more detail in the following sections.

1.3.2.1 Work–Function Tuning

Before the concept of the work function will be discussed, it is important to explain why it is relevant for electronic devices. As the tuning of the work function relates to a material's function and use in organic light emitting diodes (OLEDs) and organic photovoltaics (OPVs), these concepts need to be introduced and briefly discussed.

OLEDs and OPVs are very similar in their basic constituents; they both contain an anode and a cathode, usually ITO and an alkali metal, respectively; an organic hole transport layer (HTL) and electron transport layer (ETL). While almost all devices will contain these basic components, many have designs and architectures which include more layers for various reasons which will not be discussed here.

The process of light absorption and conversion to a current in an OPV can be broken down into five steps: 1) photon absorption, 2) exciton formation and diffusion, 3) exciton dissociation and charge separation, 4) charge transport to the electrodes, 5) charge collection at the electrodes. In an OLED the process is basically reversed, so that light is generated by applying a voltage to the device: 1) a voltage is applied between the electrodes, 2) the current flows from the cathode to the anode (cathode gives electrons to the emissive layer and the anode removes electrons from the conductive layer), 3)

electrons and holes move towards and build up at the organic heterojunction, 4) electrons and holes recombine, 5) a photon is emitted. (Figure 1.6).

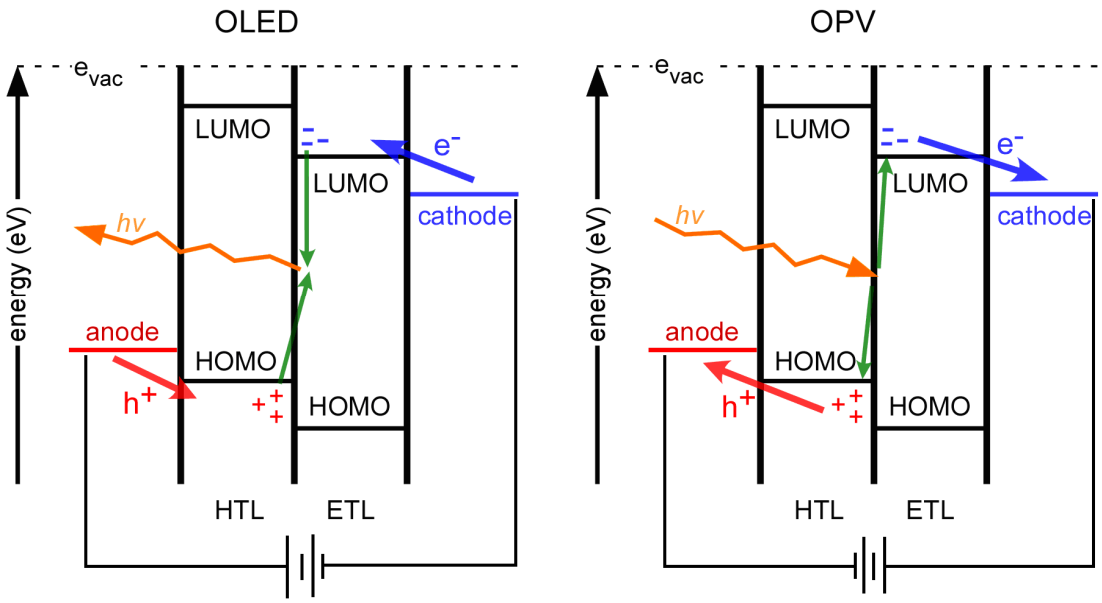

Figure 1.6 Energy diagrams and processes involved when an OLED emits light and when an OPV absorbs light. The orange arrow corresponds to a photon, a red arrow indicates the transport of holes, a blue arrow indicates the transport of electrons, and the green arrows indicate the charge recombination or separation in an OLED or OPV, respectively.

One of the major challenges in these devices is to minimize the charge injection barriers between the electrodes and the organic layers.[70, 71] In an OLED, for example, the highest occupied molecular orbital (HOMO) of the HTL is often lower in energy than the work function of the anode (usually ITO). This results in higher voltages needed to inject the charges through to the HTL. Conversely, the LUMO of the ETL is often too high in energy compared to the work function of the cathode.

The work function can be described as the energy difference between two states, where one state is the Fermi level of the solid and the second state is the absolute vacuum level.[62] As the absolute vacuum level is experimentally impossible to obtain, a more realistic second state to consider is that of a singly ionized solid with its electron at rest just outside the vacuum level of a sample ($E_{vac}(s)$).

$$\Phi_m = E_K^{min} + h\nu - E_K^{max} \qquad \text{(Equation 1.1)}$$

The work function of a metal (Φ_m) can be determined by measuring the secondary electron edge (SEE), E_K^{min} by ultraviolet photoelectron spectroscopy (UPS) using equation 1.1, where E_K^{max} is the kinetic energy of a primary electron photoexcited from the Fermi level and $h\nu$ is the energy of the light used to excite the electrons (a He(I) line at 21.2 eV is used in most UPS experiments).

As previously mentioned briefly, attaching a monolayer of an organic species that can effectively change the surface dipole of a metallic surface can change the work function of that surface. A change in the work function corresponds to a change in E_K^{min}, caused by a change in $E_{vac}(s)$ due to the surface dipole. In the case of Figure 1.7b, polar molecules are absorbed to the metal surface such that they form a dipole with its negative end pointing away from the surface. The dipole opposes the escape of electrons by effectively raising the work function of the metal.

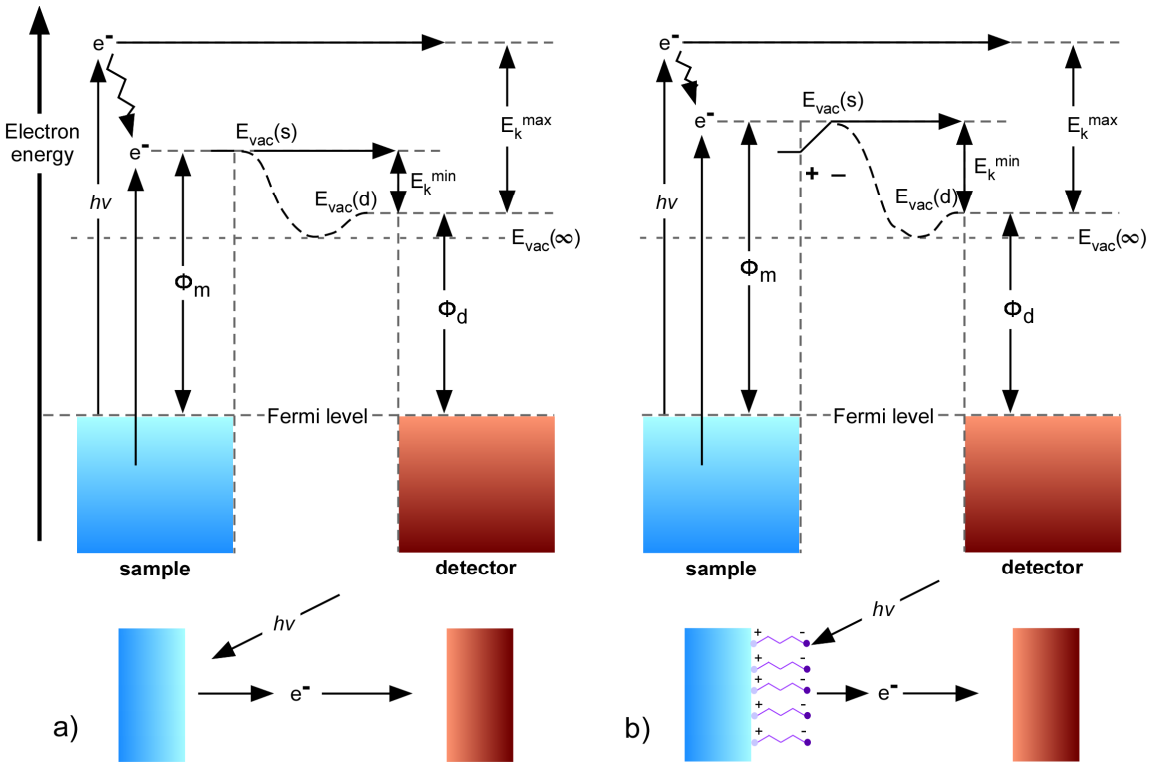

Figure 1.7 a) Energy diagram of a metal surface and detector in equilibrium, where the Fermi level is aligned across the system. $E_{vac}(s)$ is the vacuum level of the metal surface, $E_{vac}(d)$ is the vacuum level of the detector, Φ_m is the work function of the metal surface, Φ_d is the work function of the detector, E_K^{min} is the kinetic energy of a secondary electron just above $E_{vac}(s)$, and E_K^{max} is the kinetic energy of a primary electron photoexcited from the Fermi level. b) the same energy diagram as (a), but now with an additional molecule–induced dipole which raises both $E_{vac}(s)$ and E_K^{min}. Figure adapted from Cahen and Kahn.[62]

Conversely, if the negative end of the dipole is pointing towards the surface, the positive charge inside the surface would be decreased, and the work function would be decreased.

There are several factors at play when considering how a monolayer can tune the work function of a surface. A recent review by Heimel *et al*. discusses the various factors responsible for the overall surface work function.[3] First, in any metal, there is going to be

a natural spilling out of electronic density from the surface resulting in a negatively charged region just above the metal surface and a positively charged region just below the surface. This surface dipole effectively raises the work function of the metal. When any sort of molecule is close enough to interact with the surface, whether the molecule be covalently attached or not, then the electron density gets pushed back into the surface, and the work function is effectively lowered. The amount that the surface dipole is reduced is called the interface dipole. If the molecules are attached to the surface, such as in a covalently attached monolayer, then the change in dipole induced by this attachment can be considered to be composed of two main parts. The first, more important aspect of the dipole is the terminal functional group(s) on the molecule. This can affect the overall polarity and thus have the largest contribution to the surface dipole. The second component comes from the interaction between the binding group and the metal surface, which can also be polar in nature. For more detailed information on the tuning of the work function, the reader is referred to several excellent papers in the literature.[3, 32, 62, 72]

The charge injection barriers can be decreased by tuning the work functions of the electrodes[71, 72] or the position of the HOMOs and LUMOs of the charge transport materials[73, 74] and both approaches have been discussed in the literature. While in theory the work functions of both electrodes can be shifted using the appropriate dipolar monolayers, it is often only practical to focus on the anode because it is the transparent electrode in most architectures and also serves as the substrate. The cathode is usually thermally evaporated lastly on top of the other layers, making it challenging to insert a monolayer between the cathode and the ETL, though groups have recently reported an ability to do so.[29, 75, 76]

1.3.2.2 Interfacial Surface Energy Matching

Another important aspect of organic electronic devices is the physical interfacial characteristics. If two materials in a device are not in good physical contact with one another then the potential electronic interactions can be severely undermined. This is particularly important at the interface between the anode and the hole–transport material and the cathode and the electron–transport material in OLEDs and OPVs, as well as between the dielectric layer and the semiconductor in organic transistors. These are the interfaces that couple organic and inorganic materials in common device architectures. If poor physical interaction is seen in any of these interfaces then the device's performance and/or lifetime could be decreased.[6, 77, 78]

Thermodynamically, surfaces are less energetically favored than the bulk of a material. Hence it requires energy to form a surface, and if a specific amount of energy is needed to cleave a solid into two pieces, with two new surfaces, then half of that energy would be equal to the surface energy of one of the surfaces. Hence, surface energy is a quantification of the disruption of molecular bonds when a surface is created. Four types of Van der Waals forces contribute to the surface energy: permanent and induced dipoles and hydrogen bonding (polar component) and instantaneous dipoles (dispersion component).[79]

The surface of a solid therefore possesses energy (the surface energy) but this energy is not directly observable, so it has to be observed indirectly. One common way to do this is through the interaction of liquids, with known surface energies and

characteristics, with the solid surface. Young's equation relates the balance of forces present when a drop of a liquid comes into contact with a solid surface (Equation 1.2)

$$\gamma_{SL} + \gamma_{LV}(\cos\theta_c) = \gamma_{SV} \qquad \text{(Equation 1.2)}$$

where γ_{SL}, γ_{LV}, and γ_{SV} are the interfacial tensions between the solid and the liquid, the liquid and the vapor, and the solid and the vapor, respectively; and θ_c is the measured contact angle between the surface and the liquid drop (Figure 1.8).

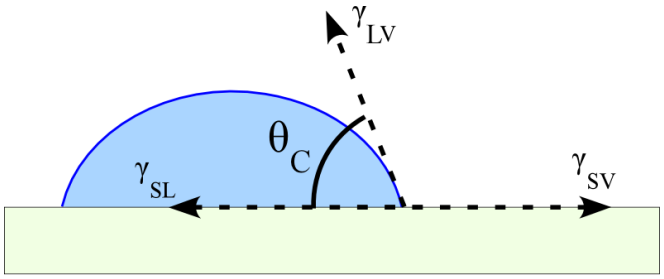

Figure 1.8 Schematic of the forces involved and contact angle measured for a drop of liquid on a solid substrate.

The total surface free energy, including its dispersion and polar components, can be calculated by two methods that have been used in similar studies: the geometric–mean method,[80, 81] and the harmonic–mean method.[79, 81, 82] Both approaches use the tension components of two probing liquids (taken from Ström *et al.*[83]) and their contact angles on the substrates, to solve simultaneously a system of coupled equations. The geometric–mean method requires the use of Equation 1.3, while the harmonic–mean method requires the use of Equation 1.4, where γ represents the individual surface tensions; *i* refers to the probe liquid; *s* represents the surface in question; *d* is the dispersion component; and *p* is

the polar component:

$$(1+\cos\theta_i)(\gamma_i^{\,d}+\gamma_i^{\,p}) = 2\left(\sqrt{\gamma_i^{\,d}\gamma_s^{\,d}}+\sqrt{\gamma_i^{\,p}\gamma_s^{\,p}}\right) \qquad \text{(Equation 1.3)}$$

$$(1+\cos\theta_i)(\gamma_i^{\,d}+\gamma_i^{\,p}) = 4\left(\frac{\gamma_i^{\,d}\gamma_s^{\,d}}{\gamma_i^{\,d}+\gamma_s^{\,d}}+\frac{\gamma_i^{\,p}\gamma_s^{\,p}}{\gamma_i^{\,p}+\gamma_s^{\,p}}\right) \qquad \text{(Equation 1.4)}$$

It has been shown, for instance, that many common hole transport materials do not wet ITO properly, due to poor surface energy matching.[78] This can be seen conceptually in Figure 1.9. If the organic material to be deposited and the substrate do not have similar surface energies, then the organic will not wet the surface well and will not coat the surface evenly. By attaching a monolayer that creates an interface with a similar energy to the organic being deposited, the wetting can be improved and the organic can be more evenly deposited (Figure 1.9).

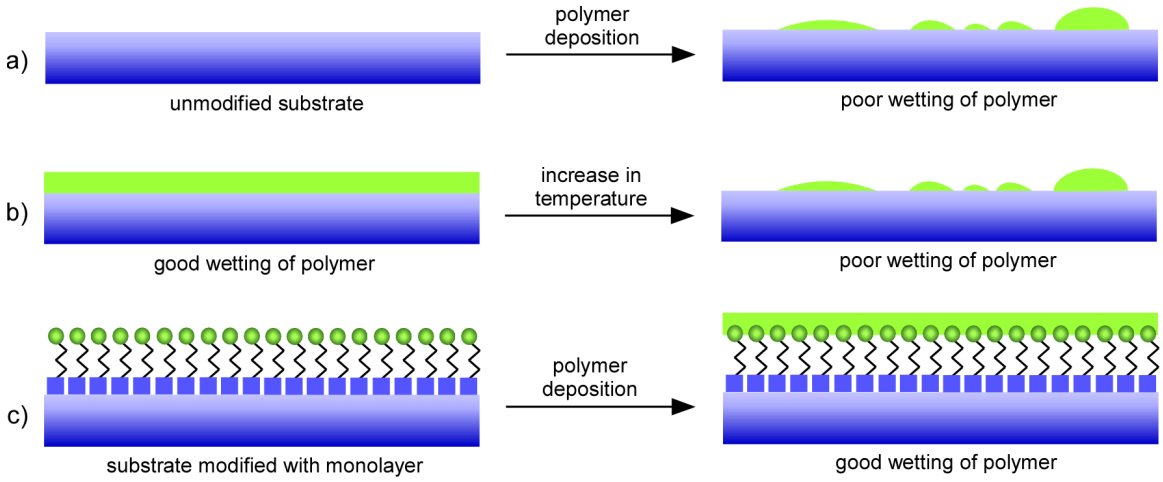

Figure 1.9 Illustration of the role a monolayer can play on the surface energy of a material. a) A hydrophilic substrate that does not interact well with the deposited polymer, thereby causing inhomogeneous coating of the polymer on the surface. b) Initial good wetting of the polymer which displays poor wetting after an increase in temperature and over time. c) A substrate modified with a monolayer that changes the surface energy of the material in such a way as to interact more favorably with the polymer, resulting in homogeneous film deposition.

The mismatch in surface energies is not always a problem during deposition of the organic, but can oftentimes arise after annealing or continued use of the device, when the rise in temperature allows the organic material to reach a more thermodynamically favorable conformation, which might create pinholes or even islands of organic material on the substrate (Figure 1.9b).

1.3.2.3 Use of Monolayers in Transistors

A transistor is a semiconductor device used to amplify or switch electronic signals. Field Effect Transistors (FETs) are a subtype of transistor that uses either

electrons (n–type) or holes (p–type) to conduct electricity. Current flows between the source and drain, controlled by the electric field produced when a voltage is applied between the gate and the source.

Organic field effect transistors (OFETs) use an organic material as the semiconductor in its channel. The organic material is typically usually either a composition of vacuum evaporated small molecules or a solution–cast film of polymers or small molecules. Many of the same materials that are used in OLEDs and OPVs can be used in OFETs, as the material needs to be able to transport charge. However, as hole–transport materials have the highest charge transport properties, these materials are often the choice for OFETs.[84]

Additionally, organic monolayers are currently being explored as the dielectric gate electrode in organic field–effect transistors (OFETs).[10, 25] For example, the presence of tightly–packed long alkyl chains creates an insulating coating on a surface, allowing for nanometer–thin dielectric layers as well as increased compatibility between the dielectric and the semiconductor. Reduced operating voltages,[21, 22] increased mobilities,[85, 86] as well as alignment of the semiconductor[87] can all be realized by using an organic monolayer in a transistor device (Figure 1.10).

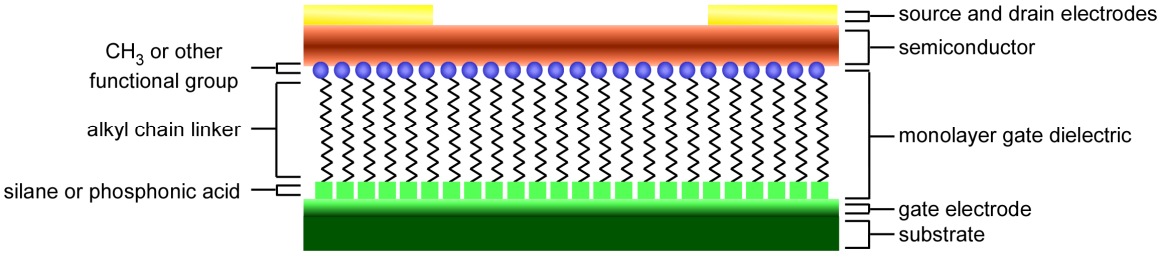

Figure 1.10 A common transistor architecture (top contact, bottom gate) comprised of a gate electrode which doubles as the substrate, a monolayer gate dielectric, an organic semiconductor, and source / drain electrodes.

The potential of organic monolayers to make an impact in the field of transistors is large, as oftentimes the addition of a monolayer does not change any of the other aspects of the device structure, and usually only gains in performance are seen after attaching a monolayer of the appropriate structure (i.e. there is little to no trade–off in properties).

1.4 Phosphonic Acids

As previously shown, there exists more than one particular functional group that will bind to a given inorganic surface. However, each binding moiety may have certain advantages and disadvantages. This section outlines the choice and reasons behind our decision to use phosphonic acids for the surface modification of metal oxides.

1.4.1 What are Phosphonic Acids

Phosphonic acids are compounds which contain the phosphonic acid moiety; namely, a tetravalent phosphorus atom in the +5 oxidation state that is bound to two hydroxyl groups and a double–bonded oxygen (known as a phosphoryl group). The fourth group can be to a variety of species, though it is most often a carbon, and is the position where changes can be made to the compound. The chemical and physical properties of phosphonic acids are discussed in the next chapter.

1.4.2 Applications of Phosphonic Acids

Phosphonic acids have been used in a variety of applications. They are often used as ligands in various organic–inorganic frameworks and hybrid materials,[88, 89] as additives in fertilizers[90] and dental adhesives,[91, 92] and are found naturally in many lipid and protein materials.[93] It has been only since the early nineties when phosphonic acids were considered for use as monolayers on metal oxide supports.[2] The amphiphilic nature of alkylphosphonic acids propagated first their use in Langmuir–Blodgett films.[2] However, as research continued on the affinity of phosphonic acids and phosphonates for metal oxides, the use of these functionalities as surface modifiers correspondingly increased. The last decade has seen an incredible increase in the use of phosphonic acids for surface modification, as their ability to form hydrolytically robust monolayers has been shown.

1.4.3 Why use Phosphonic Acids Rather Than Other Functional Groups for Metal Oxide Surface Modification

As was previously mentioned, there are several different binding groups which have been successfully used to bind to metal oxides. Alcohols, carboxylic acids, silanes, sulfonic acids, phosphinic acids and phosphonic acids have all been used to modify various metal oxides.[94] Of these, carboxylic acids, silanes, and phosphonic acids have been the most widely studied and used. Carboxylic acids have been used successfully to bind to different metal oxides, but usually through a variety of binding moieties, including as an uncoordinated anion, a monodentate ligand, a bidentate chelate or a bridging bidentate.[95] Despite the fact that high–coverage monolayers can be prepared utilizing carboxylic acids, the combination of binding modes and their relative weakness means that the monolayers are often not bound strongly to the surface and can be easily removed, sometimes by simple rinsing in solvents.[96] Additionally, the presence of additional polar sites on the carboxylic acid molecules can result in competition for surface sites, thus preventing well–organized, high coverage monolayers.[95]

Silanes have been and still are a widely used functionality that binds to metal oxides, in particular silicon dioxide. There are many types of silanes that are commercially available. They have been used to form very dense monolayers for a variety of applications and on a variety of surfaces *via* a covalent bond to the surface and among other silanes.[10] However, the formation of robust monolayers based on silanes can be difficult as it depends heavily on the hydrolysis of the silane, which is dependent on the water content, pH, and temperature. If the modification conditions are such that the

amount of hydrolysis is not sufficient (such as when not enough water is present) then an incomplete monolayer will be formed (Figure 1.11).[94, 97]

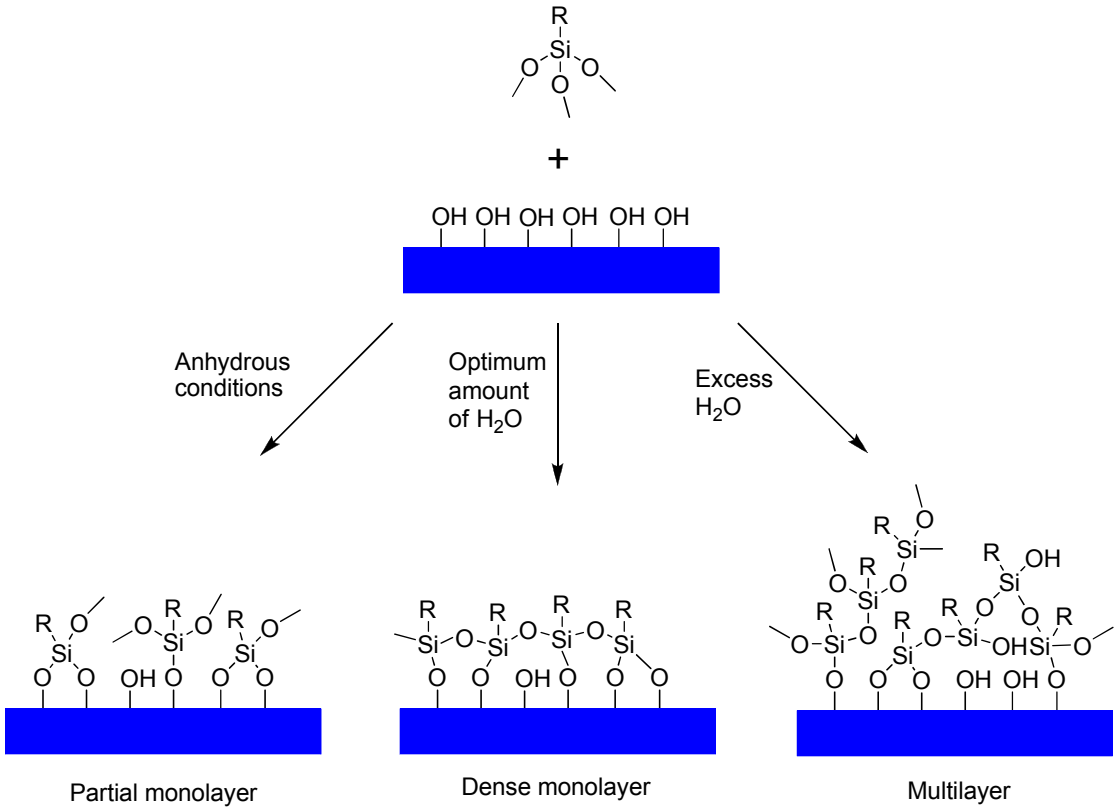

Figure 1.11 Illustration showing the effects of no, optimum, and excess water on the formation of monolayers from silanes (trimethoxy is shown, but this phenomenon holds true for other alkoxy silanes and chlorosilanes). Adapted from Mutin *et al.*[97]

When an excess of water is present then the rate and extent of hydrolysis will be too high and self–condensation will occur and multilayers can be formed on the surface. It is only when the conditions can be carefully monitored and controlled that robust, well–formed monolayers can be formed using silanes. Another drawback to silanes is that to ensure their long–term integrity they need to be stored in anhydrous conditions as they

may self–condense over time.

Phosphonic acids, while similar to silanes in that they can have up to three covalent bonds to the surface of metal oxides, are different in other respects. Phosphonic acids are thought to bind to a metal oxide surface by first coordination of the phosphoryl oxygen to Lewis acid sites on the surface, followed by condensation of the P–OH groups with surface hydroxyl groups or other surface oxygen species.[94] One important difference between phosphonic acids and silanes is that the homocondensation of P–OH and $P–O^-$ bonds does not occur at mild conditions and/or in aqueous conditions. Thus, multilayers should not form *via* this mechanism on the surface.[94] The fact that the quality of modification is independent of the amount of water present means that less stringent conditions need to be followed when using phosphonic acids with respect to silanes. One other advantage of phosphonic acids is their stability. Assuming any additional organic groups on the compound are inert, they are almost always white crystalline solids which are stable in ambient conditions over long periods of time.

Despite the advantages of phosphonic acids they have as yet not become as popular as silanes. This is partially due to their limited commercial availability. Most surface chemistry groups do not possess the means to synthesize their own compounds and as such tend to buy the materials they need. A recent search in Sci–Finder showed ~50 commercially available phosphonic acids, most available only in small amounts and at high costs. Silanes (including trichloro, triethoxy, and trimethoxy), on the other hand, have ~400 commercially available analogues and tend to be less expensive. However, the synthesis of phosphonic acids is often not difficult and will be discussed in the next chapter.

Additionally, there is question as to the surface coverage that can be obtained with phosphonic acids. Because they do not self–condense easily, the formation of robust, complete monolayers is more dependent on the functional group present on the surface of the oxide such as hydroxyl groups. This has some limitations on the use of phosphonic acids, as incomplete monolayers can be formed if the materials are not heavily hydroxylated.[94]

Based upon the evidence at hand, we decided to focus our efforts on the design, synthesis, and use of phosphonic acids for the surface modification of metal oxides.

1.5 Organization of the Thesis

While the material presented in this thesis could have been organized in a variety of ways, I believe that a logical structure is: A general introduction, followed by synthesis of the phosphonic acids, followed by how they bind and what sorts of coverages can be expected, followed by the modification of planar substrates, the modification of nanoparticles, and then a conclusion and appendix. Sections dealing with planar substrates and nanoparticles are separated accordingly as the methods of characterization and end applications are generally different.

In terms of background discussion, a general overview of the use and ability of monolayers in general has been discussed. More narrow literature discussions pertaining to phosphonic acids and metal oxides in regards to specific projects are presented when

necessary. Characterization methods are briefly described unless a method has had considerable utility in which case it may be discussed in more detail.

Minor contributions to publications that are not pertinent to the main theme of the dissertation have been omitted from general discussion. However, copies of these and all other publications can be found in the appendices.

1.6 References

1. Chechik, V.; Crooks, R. M.; Stirling, C. J. M., Reactions and reactivity in self-assembled monolayers. *Advanced Materials* **2000,** 12, (16), 1161-1171.

2. Guang, C.; Hong, H. G.; Mallouk, T. E., Layered metal phosphates and phosphonates - from crystals to monolayers. *Accounts of Chemical Research* **1992,** 25, (9), 420-427.

3. Heimel, G.; Romaner, L.; Zojer, E.; Bredas, J. L., The interface energetics of self-assembled monolayers on metals. *Accounts of Chemical Research* **2008,** 41, (6), 721-729.

4. Love, J. C.; Estroff, L. A.; Kriebel, J. K.; Nuzzo, R. G.; Whitesides, G. M., Self-assembled monolayers of thiolates on metals as a form of nanotechnology. *Chemical Reviews* **2005,** 105, (4), 1103-1169.

5. Ulman, A., Formation and structure of self-assembled monolayers. *Chemical Reviews* **1996,** 96, (4), 1533-1554.

6. Veinot, J. G. C.; Marks, T. J., Toward the ideal organic light-emitting diode. The versatility and utility of interfacial tailoring by cross-linked siloxane interlayers. *Accounts of Chemical Research* **2005,** 38, (8), 632-643.

7. Schwartz, D. K., Mechanisms and kinetics of self-assembled monolayer formation. *Annual Review of Physical Chemistry* **2001,** 52, 107-137.

8. Badia, A.; Lennox, R. B.; Reven, L., A dynamic view of self-assembled monolayers. *Accounts of Chemical Research* **2000,** 33, (7), 475-481.

9. Templeton, A. C.; Wuelfing, M. P.; Murray, R. W., Monolayer protected cluster molecules. *Accounts of Chemical Research* **2000,** 33, (1), 27-36.

10. Aswal, D. K.; Lenfant, S.; Guerin, D.; Yakhmi, J. V.; Vuillaume, D., Self assembled monolayers on silicon for molecular electronics. *Analytica Chimica Acta* **2006,** 568, (1-2), 84-108.

11. Langmuir, I., The mechanism of the surface phenomena of flotation. *Transactions of the Faraday Society* **1920,** 15, (3), 62-74.

12. Bigelow, W. C.; Pickett, D. L.; Zisman, W. A., Oleophobic monolayers .1. Films adsorbed from solution in non-polar liquids. *Journal of Colloid Science* **1946,** 1, (6), 513-538.

13. Maoz, R.; Sagiv, J., On the formation and structure of self-assembling monolayers .1. A comparative ATR-wetability study of Langmuir-Blodgett and adsorbed films on flat substrates and glass microbeads. *Journal of Colloid and Interface Science* **1984,** 100, (2), 465-496.

14. Nuzzo, R. G.; Allara, D. L., Adsorption of bifunctional organic disulfides on gold surfaces. *Journal of the American Chemical Society* **1983,** 105, (13), 4481-4483.

15. Duke, C. B., The birth and evolution of surface science: child of the union of science and technology. *Proceedings of the National Academy of Sciences of the United States of America* **2003,** 100, (7), 3858-3864.

16. Nie, H. Y.; Walzak, M. J.; McIntyre, N. S., Delivering octadecylphosphonic acid self-assembled monolayers on a Si wafer and other oxide surfaces. *Journal of Physical Chemistry B* **2006,** 110, (42), 21101-21108.

17. Nie, H. Y.; Walzak, M. J.; McIntyre, N. S., Bilayer and odd-numbered multilayers of octadecylphosphonic acid formed on a Si substrate studied by atomic force microscopy. *Langmuir* **2002,** 18, (7), 2955-2958.

18. Ulman, A., *An Introduction to Ultrathin Organic Films: From Langmuir-Blodgett to Self-Assembly*. Academic: New York, 1991.

19. Dubey, M.; Gouzman, I.; Bernasek, S. L.; Schwartz, J., Characterization of self-assembled organic films using differential charging in X-ray photoelectron spectroscopy. *Langmuir* **2006,** 22, (10), 4649-4653.

20. Gouzman, I.; Dubey, M.; Carolus, M. D.; Schwartz, J.; Bernasek, S. L., Monolayer vs. multilayer self-assembled alkylphosphonate films: X-ray photoelectron spectroscopy studies. *Surface Science* **2006,** 600, (4), 773-781.

21. Klauk, H.; Zschieschang, U.; Halik, M., Low-voltage organic thin-film transistors with large transconductance. *Journal of Applied Physics* **2007,** 102, (7), 074514.

22. Klauk, H.; Zschieschang, U.; Pflaum, J.; Halik, M., Ultralow-power organic complementary circuits. *Nature* **2007,** 445, (7129), 745-748.

23. Byrne, P. D.; Facchetti, A.; Marks, T. J., High-performance thin-film transistors from solution-processed cadmium selenide and a self-assembled multilayer gate dieletric. *Advanced Materials* **2008,** 20, (12), 2319-2324.

24. DiBenedetto, S. A.; Frattarelli, D.; Ratner, M. A.; Facchetti, A.; Marks, T. J., Vapor phase self-assembly of molecular gate dielectrics for thin film transistors. *Journal of the American Chemical Society* **2008,** 130, (24), 7528-7529.

25. Facchetti, A.; Yoon, M. H.; Marks, T. J., Gate dielectrics for organic field-effect transistors: New opportunities for organic electronics. *Advanced Materials* **2005,** 17, (14), 1705-1725.

26. Gawalt, E. S.; Avaltroni, M. J.; Danahy, M. P.; Silverman, B. M.; Hanson, E. L.; Midwood, K. S.; Schwarzbauer, J. E.; Schwartz, J., Bonding organics to Ti alloys: Facilitating human osteoblast attachment and spreading on surgical implant materials corrections (vol 19, pg 200, 2003). *Langmuir* **2003,** 19, (17), 7147-7147.

27. Wang, L.; Yoon, M. H.; Facchetti, A.; Marks, T. J., Flexible inorganic/organic hybrid thin-film transistors using all-transparent component materials. *Advanced Materials* **2007,** 19, (20), 3252-3256.

28. Felhosi, I.; Telegdi, J.; Palinkas, G.; Kalman, E., Kinetics of self-assembled layer formation on iron. *Electrochimica Acta* **2002,** 47, (13-14), 2335-2340.

29. Yip, H. L.; Hau, S. K.; Baek, N. S.; Ma, H.; Jen, A. K. Y., Polymer solar cells that use self-assembled-monolayer-modified ZnO/metals as cathodes. *Advanced Materials* **2008,** 20, (12), 2376-2382.

30. Paniagua, S. A.; Hotchkiss, P. J.; Jones, S. C.; Marder, S. R.; Mudalige, A.; Marrikar, F. S.; Pemberton, J. E.; Armstrong, N. R., Phosphonic acid modification of indium-tin oxide electrodes: Combined XPS/UPS/contact angle studies. *Journal of Physical Chemistry C* **2008,** 112, (21), 7809-7817.

31. Koh, S. E.; McDonald, K. D.; Holt, D. H.; Dulcey, C. S.; Chaney, J. A.; Pehrsson, P. E., Phenylphosphonic acid functionalization of indium tin oxide: Surface chemistry and work functions. *Langmuir* **2006,** 22, (14), 6249-6255.

32. Ashkenasy, G.; Cahen, D.; Cohen, R.; Shanzer, A.; Vilan, A., Molecular engineering of semiconductor surfaces and devices. *Accounts of Chemical Research* **2002,** 35, (2), 121-128.

33. Kumar, A.; Abbott, N. L.; Kim, E.; Biebuyck, H. A.; Whitesides, G. M., Patterned self-assembled monolayers and mesoscale phenomena. *Accounts of Chemical Research* **1995,** 28, (5), 219-226.

34. Mirkin, C. A., The power of the pen: development of massively parallel dip-pen nanolithography. *Acs Nano* **2007,** 1, (2), 79-83.

35. Bietsch, A.; Hegner, M.; Lang, H. P.; Gerber, C., Inkjet deposition of alkanethiolate monolayers and DNA oligonucleotides on gold: Evaluation of spot uniformity by wet etching. *Langmuir* **2004,** 20, (12), 5119-5122.

36. Pardo, L.; Wilson, W. C.; Boland, T. J., Characterization of patterned self-assembled monolayers and protein arrays generated by the ink-jet method. *Langmuir* **2003,** 19, (5), 1462-1466.

37. Behm, J. M.; Lykke, K. R.; Pellin, M. J.; Hemminger, J. C., Projection photolithography utilizing a Schwarzschild microscope and self-assembled alkanethiol monolayers as simple photoresists. *Langmuir* **1996,** 12, (8), 2121-2124.

38. Ryan, D.; Parviz, B. A.; Linder, V.; Semetey, V.; Sia, S. K.; Su, J.; Mrksich, M.; Whitesides, G. M., Patterning multiple aligned self-assembled monolayers using light. *Langmuir* **2004,** 20, (21), 9080-9088.

39. Mutin, P. H.; Lafond, V.; Popa, A. F.; Granier, M.; Markey, L.; Dereux, A., Selective surface modification of SiO2-TiO2 supports with phosphonic acids. *Chemistry of Materials* **2004,** 16, (26), 5670-5675.

40. Gardner, T. J.; Frisbie, C. D.; Wrighton, M. S., Systems for orthogonal self-assembly of electroactive monolayers on Au and ITO - an approach to molecular electronics. *Journal of the American Chemical Society* **1995,** 117, (26), 6927-6933.

41. Edmondson, S.; Osborne, V. L.; Huck, W. T. S., Polymer brushes via surface-initiated polymerizations. *Chemical Society Reviews* **2004,** 33, (1), 14-22.

42. Dyer, D. J., Patterning of gold substrates by surface-initiated polymerization. *Advanced Functional Materials* **2003,** 13, (9), 667-670.

43. Radhakrishnan, B.; Ranjan, R.; Brittain, W. J., Surface initiated polymerizations from silica nanoparticles. *Soft Matter* **2006,** 2, (5), 386-396.

44. Rouhi, A. M., Contemporary biomaterials. *Chemical & Engineering News* **1999,** 77, (3), 51-59.

45. Langer, R., Biomaterials in drug delivery and tissue engineering: One laboratory's experience. *Accounts of Chemical Research* **2000,** 33, (2), 94-101.

46. Santini, J. T.; Richards, A. C.; Scheidt, R.; Cima, M. J.; Langer, R., Microchips as controlled drug-delivery devices. *Angewandte Chemie-International Edition* **2000,** 39, (14), 2397-2407.

47. Ishaug-Riley, S. L.; Okun, L. E.; Prado, G.; Applegate, M. A.; Ratcliffe, A., Human articular chondrocyte adhesion and proliferation on synthetic biodegradable polymer films. *Biomaterials* **1999,** 20, (23-24), 2245-2256.

48. Tidwell, C. D.; Ertel, S. I.; Ratner, B. D.; Tarasevich, B. J.; Atre, S.; Allara, D. L., Endothelial cell growth and protein adsorption on terminally functionalized, self-assembled monolayers of alkanethiolates on gold. *Langmuir* **1997,** 13, (13), 3404-3413.

49. Kataoka, D. E.; Troian, S. M., Patterning liquid flow on the microscopic scale. *Nature* **1999,** 402, (6763), 794-797.

50. Black, F. E.; Hartshorne, M.; Davies, M. C.; Roberts, C. J.; Tendler, S. J. B.; Williams, P. M.; Shakesheff, K. M., Surface engineering and surface analysis of a biodegradable polymer with biotinylated end groups. *Langmuir* **1999,** 15, (9), 3157-3161.

51. Kricka, L. J., Microchips, microarrays, biochips and nanochips: personal laboratories for the 21st century. *Clinica Chimica Acta* **2001,** 307, (1-2), 219-223.

52. Lahiri, J.; Isaacs, L.; Grzybowski, B.; Carbeck, J. D.; Whitesides, G. M., Biospecific binding of carbonic anhydrase to mixed SAMs presenting benzenesulfonamide ligands: A model system for studying lateral steric effects. *Langmuir* **1999,** 15, (21), 7186-7198.

53. Meyyappan, S.; Shadnam, M. R.; Amirfazli, A., Fabrication of surface energy/chemical gradients using self-assembled monolayer surfaces. *Langmuir* **2008,** 24, (6), 2892-2899.

54. Arima, Y.; Iwata, H., Effect of wettability and surface functional groups on protein adsorption and cell adhesion using well-defined mixed self-assembled monolayers. *Biomaterials* **2007,** 28, (20), 3074-3082.

55. Feng, X. J.; Jiang, L., Design and creation of superwetting/antiwetting surfaces. *Advanced Materials* **2006,** 18, (23), 3063-3078.

56. Balss, K. M.; Avedisian, C. T.; Cavicchi, R. E.; Tarlov, M. J., Nanosecond imaging of microboiling behavior on pulsed-heated Au films modified with hydrophilic and hydrophobic self-assembled monolayers. *Langmuir* **2005,** 21, (23), 10459-10467.

57. Critchley, K.; Jeyadevan, J. P.; Fukushima, H.; Ishida, M.; Shimoda, T.; Bushby, R. J.; Evans, S. D., A mild photoactivated hydrophilic/hydrophobic switch. *Langmuir* **2005,** 21, (10), 4554-4561.

58. Takai, K.; Takagi, T.; Baba, T.; Kanamori, T., Highly fluorinated C_{18} fatty acids: synthesis and interfacial properties. *Journal of Fluorine Chemistry* **2004,** 125, (12), 1959-1964.

59. Shafrin, E. G.; Zisman, W. A., The adsorption on platinum and wettability of monolayers of terminally fluorinated octadecyl derivatives. *Journal of Physical Chemistry* **1957,** 61, (8), 1046-1053.

60. Bain, C. D.; Troughton, E. B.; Tao, Y. T.; Evall, J.; Whitesides, G. M.; Nuzzo, R. G., Formation of monolayer films by the spontaneous assembly of organic thiols from solution onto gold. *Journal of the American Chemical Society* **1989,** 111, (1), 321-335.

61. Yang, Y.; Wang, W.; Li, J. R.; Mu, J.; Rong, H. L., Manipulating the solubility of gold nanoparticles reversibly and preparation of water-soluble sphere nanostructure through micellar-like solubilization. *Journal of Physical Chemistry B* **2006,** 110, (34), 16867-16873.

62. Cahen, D.; Kahn, A., Electron energetics at surfaces and interfaces: concepts and experiments. *Advanced Materials* **2003,** 15, (4), 271-277.

63. Shaw, J. M.; Seidler, P. F., Organic electronics: Introduction. *IBM Journal of Research and Development* **2001,** 45, (1), 3-9.

64. Chiang, C. K.; Druy, M. A.; Gau, S. C.; Heeger, A. J.; Louis, E. J.; Macdiarmid, A. G.; Park, Y. W.; Shirakawa, H., Synthesis of highly conducting films of derivatives of polyacetylene, (CH)X. *Journal of the American Chemical Society* **1978,** 100, (3), 1013-1015.

65. Chiang, C. K.; Fincher, C. R.; Park, Y. W.; Heeger, A. J.; Shirakawa, H.; Louis, E. J.; Gau, S. C.; Macdiarmid, A. G., Electrical conductivity in doped polyacetylene. *Physical Review Letters* **1977,** 39, (17), 1098-1101.

66. Aviram, A.; Ratner, M. A., Molecular rectifiers. *Chemical Physics Letters* **1974,** 29, (2), 277-283.

67. Mann, B.; Kuhn, H., Tunneling through fatty acid salt monolayers. *Journal of Applied Physics* **1971,** 42, (11), 4398-4405.

68. Coffey, D. C.; Ginger, D. S., Patterning phase separation in polymer films with dip-pen nanolithography. *Journal of the American Chemical Society* **2005,** 127, (13), 4564-4565.

69. Park, L. Ginger, D., Unpublished Results.

70. Braun, S.; de Jong, M. P.; Osikowicz, W.; Salaneck, W. R., Influence of the electrode work function on the energy level alignment at organic-organic interfaces. *Applied Physics Letters* **2007,** 91, (20), 202108/1-202108/3.

71. de Boer, B.; Hadipour, A.; Mandoc, M. M.; van Woudenbergh, T.; Blom, P. W. M., Tuning of metal work functions with self-assembled monolayers. *Advanced Materials* **2005,** 17, (5), 621-625.

72. Ishii, H.; Sugiyama, K.; Ito, E.; Seki, K., Energy level alignment and interfacial electronic structures at organic-metal and organic-organic interfaces. *Advanced Materials* **1999,** 11, (8), 605-625.

73. Medina, B. M.; Anthony, J. E.; Gierschner, J., Independent tuning of electronic levels in pentacene by site-specific substitution. *Chemphyschem* **2008,** 9, (11), 1519-1523.

74. Liang, Y. Y.; Xiao, S. Q.; Feng, D. Q.; Yu, L. P., Control in energy levels of conjugated polymers for photovoltaic application. *Journal of Physical Chemistry C* **2008,** 112, (21), 7866-7871.

75. Vaynzof, Y.; Dennes, T. J.; Schwartz, J.; Kahn, A., Enhancement of electron injection into a light-emitting polymer from an aluminum oxide cathode modified by a self-assembled monolayer. *Applied Physics Letters* **2008,** 93, (10), 103305/1-103305/3.

76. Yip, H. L.; Hau, S. K.; Baek, N. S.; Jen, A. K. Y., Self-assembled monolayer modified ZnO/metal bilayer cathodes for polymer/fullerene bulk-heterojunction solar cells. *Applied Physics Letters* **2008,** 92, (19), 193313/1-193313/3.

77. Armstrong, N. R.; Carter, C.; Donley, C.; Simmonds, A.; Lee, P.; Brumbach, M.; Kippelen, B.; Domercq, B.; Yoo, S. Y., Interface modification of ITO thin films: organic photovoltaic cells. *Thin Solid Films* **2003,** 445, (2), 342-352.

78. Lee, J.; Jung, B. J.; Lee, J. I.; Chu, H. Y.; Do, L. M.; Shim, H. K., Modification of an ITO anode with a hole-transporting SAM for improved OLED device characteristics. *Journal of Materials Chemistry* **2002,** 12, (12), 3494-3498.

79. Kim, J. S.; Friend, R. H.; Cacialli, F., Surface wetting properties of treated indium tin oxide anodes for polymer light-emitting diodes. *Synthetic Metals* **2000,** 111, 369-372.

80. You, Z. Z.; Dong, J. Y., Oxygen plasma treatment effects of indium-tin oxide in organic light-emitting devices. *Vacuum* **2007,** 81, (7), 819-825.

81. Ma, K. X.; Ho, C. H.; Zhu, F. R.; Chung, T. S., Investigation of surface energy for organic light emitting polymers and indium tin oxide. *Thin Solid Films* **2000,** 371, (1-2), 140-147.

82. Kim, J. S.; Friend, R. H.; Cacialli, F., Surface energy and polarity of treated indium-tin-oxide anodes for polymer light-emitting diodes studied by contact-angle measurements. *Journal of Applied Physics* **1999,** 86, (5), 2774-2778.

83. Strom, G.; Fredriksson, M.; Stenius, P., Contact angles, work of adhesion, and interfacial tensions at a dissolving hydrocarbon surface. *Journal of Colloid and Interface Science* **1987,** 119, (2), 352-361.

84. Zaumseil, J.; Sirringhaus, H., Electron and ambipolar transport in organic field-effect transistors. *Chemical Reviews* **2007,** 107, (4), 1296-1323.

85. Kumaki, D.; Yahiro, M.; Inoue, Y.; Tokito, S., Improvement of mobility and stability in pentacene-TFT by chemical surface treatment. *Journal of Photopolymer Science and Technology* **2006,** 19, (1), 41-44.

86. Kumaki, D.; Yahiro, M.; Inoue, Y.; Tokito, S., Air stable, high performance pentacene thin-film transistor fabricated on SiO_2 gate insulator treated with beta-phenethyltrichlorosilane. *Applied Physics Letters* **2007,** 90, (13), 133511.

87. Halik, M.; Klauk, H.; Zschieschang, U.; Schmid, G.; Dehm, C.; Schutz, M.; Maisch, S.; Effenberger, F.; Brunnbauer, M.; Stellacci, F., Low-voltage organic transistors with an amorphous molecular gate dielectric. *Nature* **2004,** 431, (7011), 963-966.

88. Alberti, G.; Costantino, U.; Dionigi, C.; MurciaMascaros, S.; Vivani, R., Layered and pillared zirconium phosphate-phosphonates and their inclusion chemistry. *Supramolecular Chemistry* **1995,** 6, (1-2), 29-40.

89. Corriu, R. J. P.; Leclercq, D.; Mutin, P. H.; Sarlin, L.; Vioux, A., Nonhydrolytic sol-gel routes to layered metal(IV) and silicon phosphonates. *Journal of Materials Chemistry* **1998,** 8, (8), 1827-1833.

90. Rickard, D. A., Review of phosphorus acid and its salts as fertilizer materials. *Journal of Plant Nutrition* **2000,** 23, (2), 161-180.

91. Ikemura, K.; Tay, F. R.; Nishiyama, N.; Pashley, D. H.; Endo, T., Multi-purpose bonding performance of newly synthesized phosphonic acid monomers. *Dental Materials Journal* **2007,** 26, (1), 105-115.

92. Yeniad, B.; Albayrak, A. Z.; Olcum, N. C.; Avci, D., Synthesis and photopolymerizations of new phosphonated monomers for dental applications. *Journal of Polymer Science Part A-Polymer Chemistry* **2008,** 46, (6), 2290-2299.

93. Ostermayer, B.; Albrecht, O.; Vogt, W., Polymerizable lipid analogs of diacetylenic phosphonic acids - synthesis, spreading behavior and polymerization at the gas-water interface. *Chemistry and Physics of Lipids* **1986,** 41, (3-4), 265-291.

94. Mutin, P. H.; Guerrero, G.; Vioux, A., Hybrid materials from organophosphorus coupling molecules. *Journal of Materials Chemistry* **2005,** 15, (35-36), 3761-3768.

95. Pawsey, S.; Yach, K.; Halla, J.; Reven, L., Self-assembled monolayers of alkanoic acids: A solid-state NMR study. *Langmuir* **2000,** 16, (7), 3294-3303.

96. Taylor, C. E.; Schwartz, D. K., Octadecanoic acid self-assembled monolayer growth at sapphire surfaces. *Langmuir* **2003,** 19, (7), 2665-2672.

97. Mutin, P. H.; Guerrero, G.; Vioux, A., Organic-inorganic hybrid materials based on organophosphorus coupling molecules: from metal phosphonates to surface modification of oxides. *Comptes Rendus Chimie* **2003,** 6, (8-10), 1153-1164.

Chapter 2

Synthesis and Characterization of Novel Phosphonic Acids

2.1 General Synthetic Techniques

There are numerous synthetic pathways to make phosphonic acids. For many, the corresponding dialkylphosphonate is a key intermediate, while others utilize phosphorus tri– or pentachloride precursors. The C–P bond formation routes that have been used to synthesize the compounds within (Michaelis–Arbuzov and related reactions, catalytic P–C bond formation), as well as some of the other common routes, such as the Friedel–Crafts and Michaelis–Becker reactions will be discussed. For a more in depth look at C–P bond formation, the reader is referred to several books and review articles in the literature.[1-4]

2.1.1 The Michaelis – Arbuzov Reaction

The most well–known of the P–C bond–forming reactions is the Michaelis–Arbuzov reaction (hereto referred to as Arbuzov reaction). The Arbuzov reaction is a S_N2 reaction, where a neutral trivalent phosphorus reagent substitutes for a leaving group on carbon. The mechanism of this reaction can be described as having two steps. Step 1 is a S_N2 reaction where the lone pair on the trivalent phosphorus attacks a carbon attached to

a good leaving group (oftentimes a halide) and the leaving group is displaced. This generates an intermediate quasiphosphonium ion (Figure 2.1, Step 1).

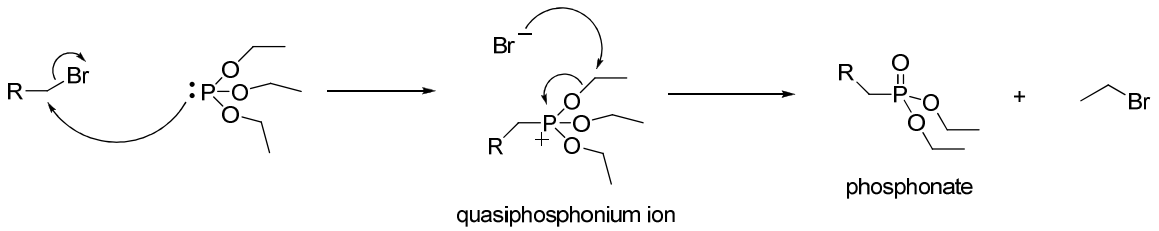

Figure 2.1 Mechanism of the Michaelis – Arbuzov reaction using triethylphosphite.

Step 2 can be generally described as a S_N2 displacement at carbon where the counterion of the positively charged phosphorus (the earlier displaced leaving group) attacks an atom attached to the phosphorus through oxygen. This results in the bond between oxygen and this atom being broken, and the electron pair being shared with the phosphorus to create a phosphoryl group (Figure 2.1, Step 2).

Experimentally, the halide and trivalent phosphite are often combined in a reaction flask and heated to reflux or just below (~140 °C). The phosphite is often used in excess and therefore also acts as the solvent for the reaction. While the yields of Arbuzov reactions are generally high, there is an important side product which must be taken into account. After the second step, and the formation of the phosphonate, the created side–product, usually an alkyl halide (depending on the starting materials) can itself undergo an Arbuzov transformation (Figure 2.2). Therefore, it is necessary to either remove this unwanted side product during the reaction or to add an excess of the trivalent phosphite.

Oftentimes a trimethyl or triethylphosphite is used and the resulting methyl– or ethylbromide can be evaporated from the reaction if desired.

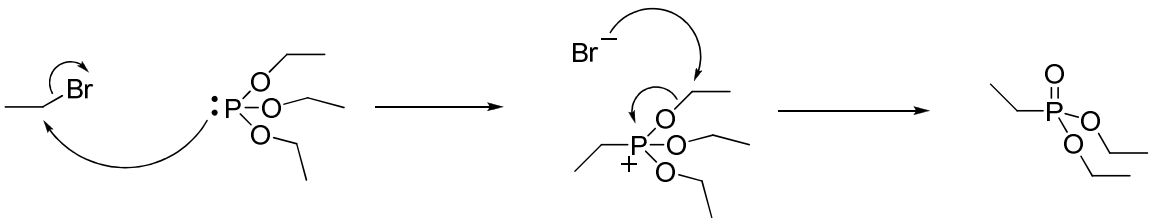

Figure 2.2 Mechanism for the formation of ethyl diethylphosphonate, a common side product of Arbuzov reactions utilizing triethylphosphite.

The Arbuzov reaction results in the very stable and energetically favorable tetracoordinate phosphorus, and this plays a role in the stability of the resulting phosphonate, which can withstand a wide range of synthetic conditions if further reactions are necessary. This reaction can also be classified as an oxidation–reduction reaction, where the phosphorus is oxidized from the +3 to the +5 state, and the newly bonded carbon reduced from the -1 to the -3 state.

The Arbuzov reaction is often performed using a trialkylphosphite and an alkyl halide, where the reactivities of halides increase in the normal fashion (I > Br > Cl). Being an S_N2 reaction, it is not often employed for the formation of aryl or vinyl phosphonates, though these can sometimes work if appropriate electron acceptor groups are present. The presence of an alkyl chain on the carbon β to the phosphorus has been shown to retard the reaction.[5]

Lastly, it should be noted that the Arbuzov reaction can be performed with the use of microwave heating.[6, 7] This has been shown to dramatically reduce reaction time (from

several hours or longer to several minutes) while maintaining high yields.

2.1.2 Photoinitiated Arbuzov Reaction

While the Arbuzov reaction is a very powerful and easy way to create phosphonates, it is not clearly as useful when an S_N2 pathway is not available. Therefore alternative methods have been employed for the formation of arylphosphonates. One such method is what could be described as a photoinitiated Arbuzov reaction, where the first step of the mechanism is different, but the same S_N2 displacement step is seen.

An aryl iodide can, under the presence of UV light, dissociate to form two radical species.[8] The aryl radical can then be trapped by a trialkylphosphite to form a radical, neutral phosphorus species in the +4 oxidation state (Figure 2.3).[9]

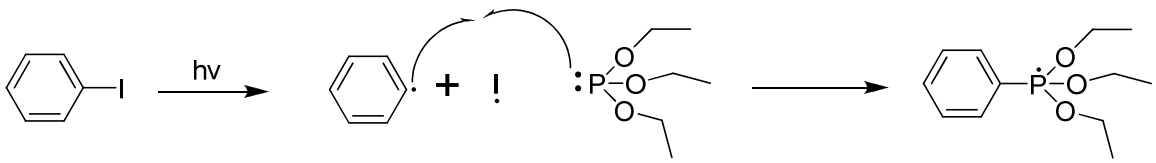

Figure 2.3 First part in the mechanism of a photoinitiated Arbuzov reaction: Homolytic cleavage of the aryl–iodide bond and formation of the neutral radical phosphorus species.

The formation of the quasiphosphonium salt can then form by a one–electron transfer from the phosphorus species to the iodine atom. This is probably at least partially due to the increased stability of the +5 phosphorus species relative to that of the +4 state.

Once the quasiphosphonium salt is formed, the same S_N2 displacement reaction as seen in the standard Arbuzov reaction can occur (Figure 2.4).

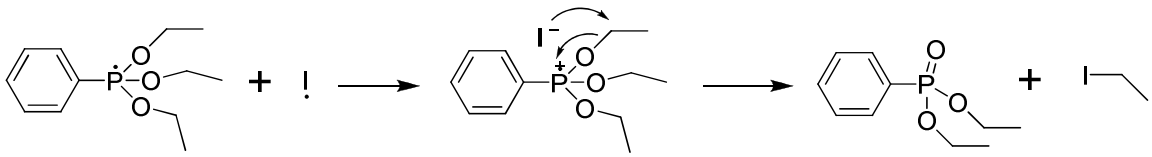

Figure 2.4 Second part in the mechanism of a photoinitiated Arbuzov reaction: formation of the quasiphosphonium salt and then formation of the arylphosphonates.

There are several important side reactions that must be considered. The first is the formation of an alkyl iodide which, like for a standard Arbuzov reaction, can react to yield the dialkyl alkylphosphonate. Additionally, trialkylphosphite, when subjected to ultraviolet irradiation can isomerize to the same dialkyl alkylphosphonate. Therefore, it can be important to keep the temperature low and/or use an excess of the trialkylphosphite to maximize desired product yield.

The photoinitiated Arbuzov reaction appears to be very general, allowing for the incorporation of many photostable substituents off the ring,[10, 11] however the utility of this reaction will always be limited by the availability of aryl iodides.

2.1.3 Transition Metal–Assisted Reactions

Transition metal catalysts can be used effectively in aryl C–P bond formation. The first such report involved the use of $NiCl_2$ at elevated temperatures,[12] though since

then a number of transition metal catalysts, including copper[13, 14] and palladium,[15] have been used in aryl C–P bond formation.

There are two different approaches, each following different mechanisms, to aryl C–P bond formation using a transition metal catalyst. These can be divided into nickel and copper halides, where the nickel forms a trialkyl phosphite complex first, and the palladium salts, where the aryl halide initially undergoes an oxidative addition to the Pd(0) system.

The first reported reaction of the formation of aryl C–P bonds involving transition metal halides was in the early 70's by Tavs.[12] The transition metal is initially reduced to Ni(0) by the trialkylphosphite. This species then reacts with the aryl halide, resulting in the transitionary phosphonium salt, which then dissociates to the arylphosphonates. The Ni(0) complex is then regenerated and can react with another aryl halide (Figure 2.5).[1, 5, 16]

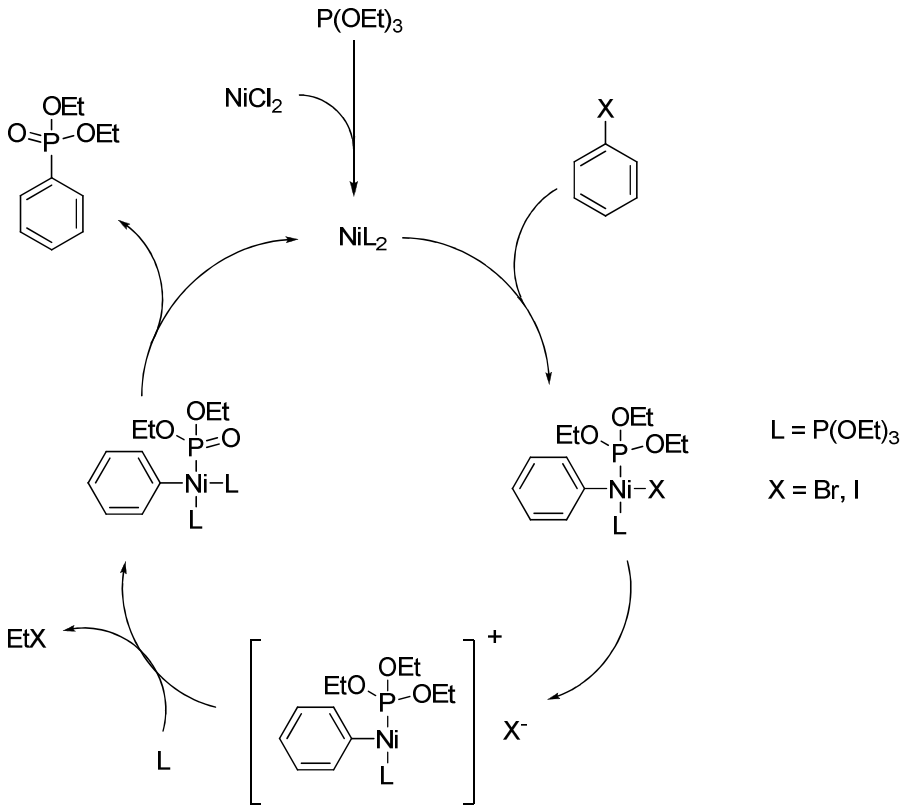

Figure 2.5 Catalytic cycle showing how $NiCl_2$ can be used to form aryl C–P bonds.

Experimentally, reactions of aryl bromides and iodides proceed in the highest yields, and the phosphorus species is often a trialkylphosphite, although recent advances show that triarylphosphites can also be used.[5] Various groups on the aryl ring can be tolerated as well.[17] The transition metal is often a nickel chloride (or bromide), but copper salts can also be used.[13, 14, 18] As the transition metal functions as a catalyst, 5 mole % of the metal halide is often sufficient for the reaction.

The disadvantage of this reaction is the high temperature necessary. Temperatures of ~160 °C are necessary for high yields, and product will not be produced at temperatures lower than ~ 130 °C.[16] These harsh conditions can limit the scope of the

reaction depending on which additional functional groups are present.

The use of palladium salts in lieu of nickel was first investigated in the early 80's by Hirao *et al.*[15, 19] The palladium species undergoes an oxidative addition with an aryl halide to give the aryl–palladium complex. The attack of the dialkylphosphite on the complex leads to the arylphosphonate. An amine is necessary to regenerate the Pd(0) species (Figure 2.6).

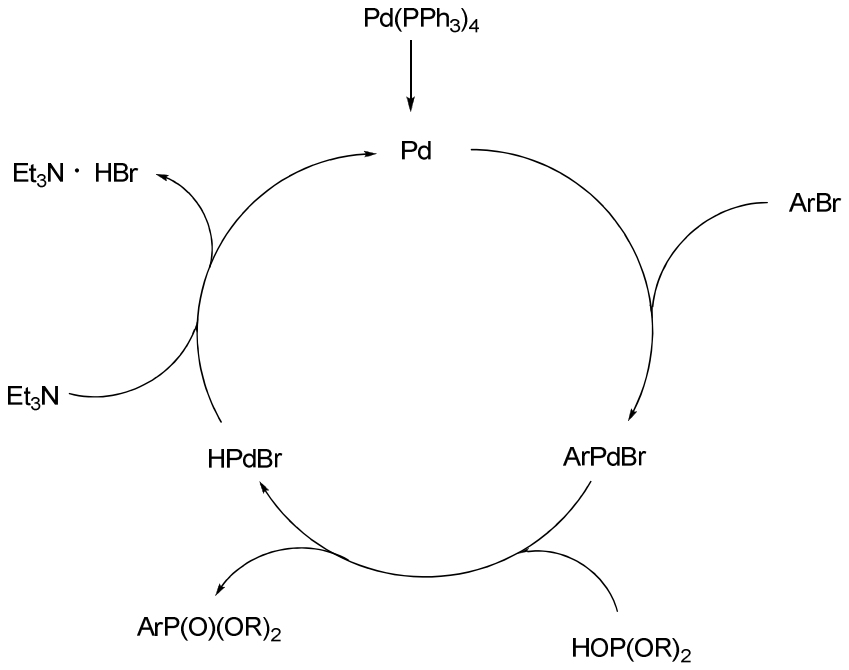

Figure 2.6 Catalytic cycle showing how a palladium salt can be used to form aryl C–P bonds.

Early efforts utilizing this pathway used tetrakis(triphenylphosphine)palladium ($Pd(PPh_3)_4$) as the catalyst and simple amines. Aryl bromides and iodides can be used, and the reaction can be run at much lower temperatures than that of the nickel catalyst – around 90 °C being sufficient for high (above 90%) yields.[20] It has been noted that

strongly electron–donating groups can retard or inhibit the reaction.

An excellent paper appeared in 2005 where the authors optimized the conditions of the palladium–catalyzed aryl C–P bond formation.[21] They note that polar solvents, such as ethanol, are extremely beneficial to the reaction. Palladium acetate was found to be the best yielding palladium source, and tertiary amines with low nucleophilicity and sufficient bulkiness increased reaction yields (Figure 2.7). Yields ranged from 80 to 95 % on a number of various substituted bromobenzenes.

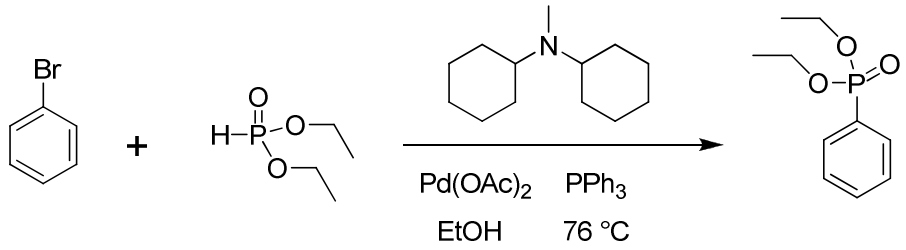

Figure 2.7 Optimized conditions used for a palladium – catalyzed aryl C–P bond formation reaction.[21]

These transition metal mediated reactions can also be completed using microwave conditions, where reaction times and temperatures can be significantly decreased.[22] Various substituted aryl iodides and bromides were shown to be converted to the analogous phosphonates in high (~80%) yields after only 5 minutes at 100 W in a microwave. Both $NiCl_2$ and $PdCl_2$ were used as catalysts.

2.1.4 Other Synthetic Techniques

The Michaelis–Becker reaction was developed simultaneously with the Michaelis–Arbuzov reaction.[1] It involves the reaction of the salts of trivalent phosphorus–centered oxyacids with the same types of alkyl halides that are used in the Arbuzov reaction. Classically, the sodium salt of the oxyacid has been used (Figure 2.8).

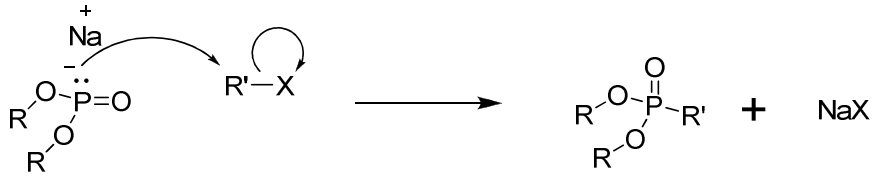

Figure 2.8 Mechanism of the Michaelis – Becker reaction.

This reaction is not utilized as often as the Arbuzov reaction because the sodium salt of the oxyacid has poor solubility in a number of solvents and as such, the method is not as convenient for a number of systems.

A Friedel–Crafts type reaction can also be used to arylate phosphorous trihalides (Figure 2.9).[23, 24] The resultant arylphosphorus dihalide is another popular precursor to phosphonic acids. While the reaction can succeed using the classic aluminum trichloride ($AlCl_3$) as the Lewis acid, other Lewis acids, such as stannic chloride ($SnCl_4$) have been shown to give superior yields while decreasing side products, such as diarylation of the phosphorus.[25]

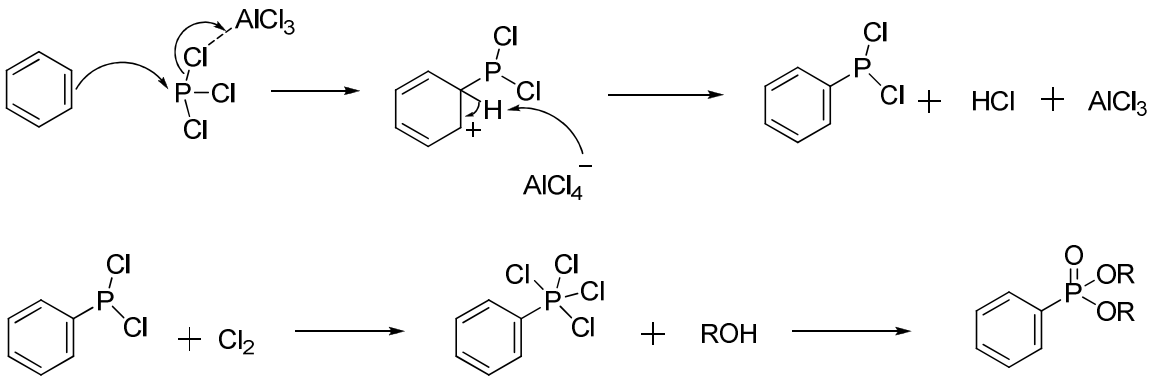

Figure 2.9 Mechanism of a Friedel–Crafts reaction to form an aryl C–P bond.

A radical–initiated reaction forms either dialkyl phosphonates by addition of dialkyl phosphites or phosphonic acids by addition of phosphorous acids to olefins.[26, 27] Even though the mechanism of this reaction is not fully understood, it supposedly follows a normal radical initiated mechanism where a radical generator homolytically breaks the P–H bond, producing a radical phosphorus species. This species can then react with an olefin and the formed radical reacts with a proton on another phosphorus species, continuing the reaction (Figure 2.10).[28]

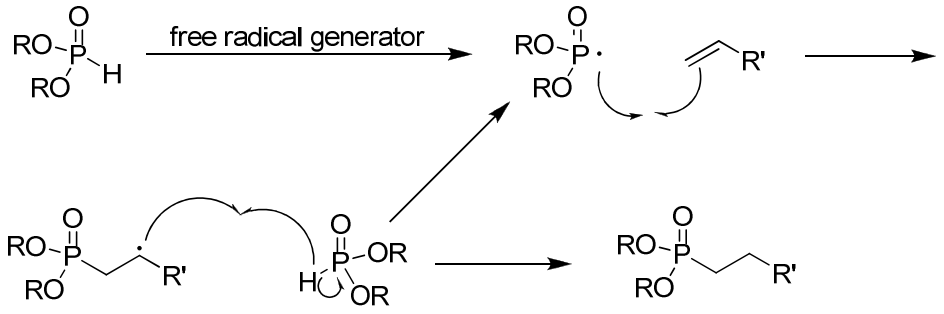

Figure 2.10 Mechanism of a radical initiated C–P bond formation.

This form of C–P bond formation has not seen widespread use due to the generally low yields produced (~20 to 30 %),[26, 29] though increased yields (~ 40 to 70 %) have been obtained with modified reaction conditions.[30] Additionally, the availability of olefins tends to be lower than terminal halides, and as such the reaction has not been frequently used in the literature.

2.1.5 Hydrolysis of Phosphonates to Form Phosphonic Acids

Once the appropriate precursor to the phosphonic acid has been obtained, there are several ways by which the acid can be isolated.

The hydrolysis of phosphonic acid dialkyl esters is the most common way to synthesize phosphonic acids and can be achieved by several methods. Perhaps the most straightforward and popular route, and certainly the least expensive, has been the acid–catalyzed hydrolytic dealkylation by hydrochloric acid. This usually involves refluxing the phosphonate in an excess of HCl (concentration varies, but usually 6 M or higher is used) for several hours, where the phosphonic acid often precipitates upon cooling. However, these conditions are not applicable for compounds that contain functional groups sensitive to strongly acidic conditions, and so for these molecules other conditions must be used.

A milder approach involves the use of a trimethylsilylhalide.[31] Bis(trimethylsilyl) phosphonates have been shown to hydrolyze to their respective acids upon contact with water and/or a low boiling point alcohol at room temperature. Chlorotrimethylsilane can

be used to convert the phosphonates alkyl groups to the necessary trimethylsilyl groups, but this can take a long time (days to weeks) at refluxing conditions.[32] More recent results have shown the ability to hydrolyze with chlorotrimethylsilane at increased pressures and temperatures, thereby decreasing reaction time (8–24 hours).[33] However these results could not be reproduced in our labs. Considering that the halide will partake as both the leaving group and the nucleophile, the use of bromotrimethylsilane greatly reduces reaction time, and can convert the alkyl groups to trimethylsilyl groups in a matter of hours at room temperature.

The mechanism for this hydrolysis is analogous to the Arbuzov reaction, where the phosphoryl oxygen starts by attacking the partially positively charged silicon. The displaced halide ion then attacks one of the alkoxy groups, and the mixed alkyl trimethylsilyl phosphonate is formed. Repetition of this cycle results in the desired bis(trimethylsilyl)phosphonate (Figure 2.11).

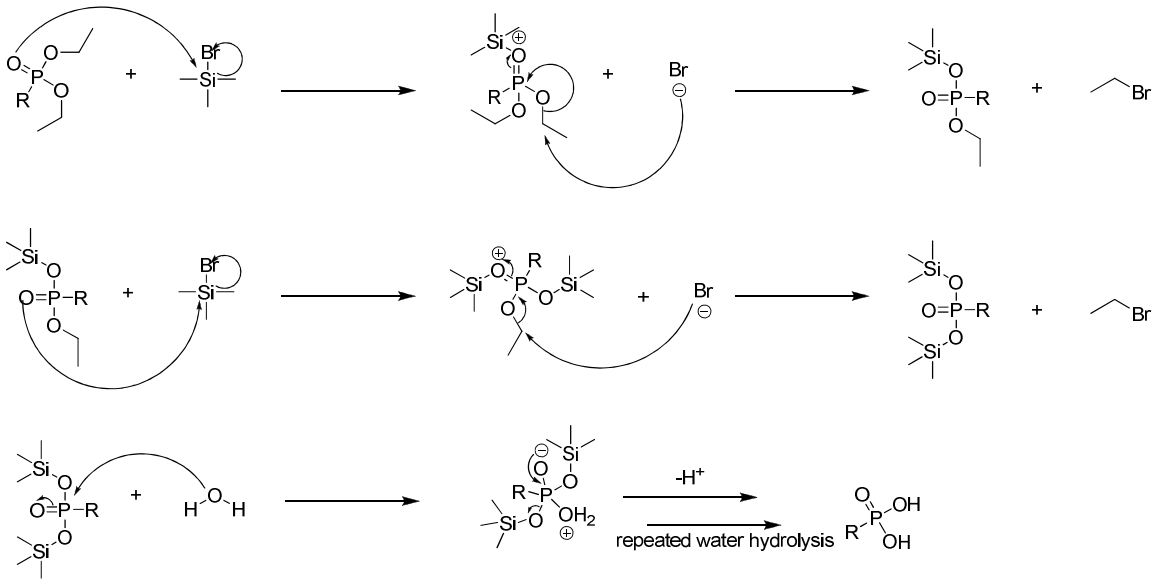

Figure 2.11 Mechanism of hydrolysis of a dialkylphosphonate with bromotrimethylsilane.

2.1.6 Synthetic Considerations and Challenges

Despite the general ease with which phosphonic acids can be synthesized, the preceding phosphonate is often easier to purify and stable towards more conditions than the acid form. Phosphonates tend to be soluble in a myriad of solvents, such as hexanes, ether, dichloromethane, chloroform, ethyl acetate, acetonitrile, and acetone. They can be purified using column chromatography (stationary phase: silica) and often have low R_f values, even for polar solvents such as ethyl acetate, which is oftentimes the solvent of choice as the mobile phase. While the phosphonate moiety is stable on silica gel, the compound cannot be visualized with a standard handheld UV lamp in the absence of other chromophoric groups. Therefore staining agents such as permanganate or iodine

are often employed to view spots on silica thin layer chromatography (TLC) plates. Iodine tends to be the preferred choice as the staining process is more convenient, although somewhat slower. Another important point when performing TLC on phosphonates is that, though they can be seen with a stain, heavier spotting is necessary.

Phosphonic acids are soluble in polar, protic solvents, though usually not water unless the R–group on the phosphonic acid is also polar and/or protic. The acidity of the phosphonic acids and their high degree of polarity effectively precludes purification on silica gel. Hence, recrystallization is the method often used to purify phosphonic acids. However, if a suitable solvent system is not found and the recrystallization is not successful, rehydrolysis of the reaction mixture to convert any remaining phosphonate to the phosphonic acid can sometimes be used to affect purification.

Additionally, further chemistry on phosphonic acids can be difficult due to their very low pK_a (pK_1 ~ 2), so the hydrolysis is often the last step in a given synthesis. Additionally, other functional groups present on the molecule have to be compatible with the phosphonic acid. The acidity of phosphonic acids means that any groups sensitive to acids might not survive on the same molecule. This was an issue when attempting to hydrolyze an epoxide–functionalized phosphonate to the acid in our lab. The desired product could not be isolated as the acid group initiated polymerization/crosslinking of the epoxide group.

It is also important to note under what conditions the C–P bond can be weakened. The presence of strongly electron donating groups in the ortho or para positions of the ring can weaken the C–P bond in arylphosphonic acids. Conversely, electron

withdrawing groups in close proximity of the phosphono group in alkylphosphonic acids can weaken the C–P bond.[2]

2.2 Properties of Phosphonic Acids

This section outlines some of the different properties of phosphonic acids, including their physical, chemical, and common spectroscopic properties.

2.2.1 Physical Properties

Phosphonic acids are usually white crystalline solids. However, this may not be the case for compounds with large molecular weight or a long chain substituent. For example, octylphosphonic acid is a white, crystalline solid. So too is octadecylphosphonic acid, but there is a certain waxiness to the compound. In the case of an oligomeric phosphonic acid based on ethylene glycol units, the acid is a highly viscous oil. Phosphonates are almost always viscous colorless oils. Exceptions are small aromatic phosphonates that have strong intermolecular interactions, such as biphenylmethylphosphonate, which are often solids.

The phosphonic acid group itself is odorless, though the compound can certainly have an odor, as in the case of 10–mercaptodecylphosphonic acid.

Phosphonic acids tend to be soluble in polar solvents, such as dimethylsulfoxide,

tetrahydrofuran, and ethanol. They are sometimes soluble in water, however this is highly dependent on the R–group attached to the phosphonic acid. Most of the phosphonic acids synthesized herein have been recrystallized from acetonitrile with or without a small amount of water.

2.2.2 Chemical Properties

The acid dissociation characteristics of phosphonic acids are well documented.[2, 34] Alkylphosphonic acids tend to have a pK_1 ~ 2.5 and a pK_2 ~ 8, although the pK_a values increase with either increasing chain length or degree of branching as the increasingly saturated carbon atom becomes more electron repelling.[2] The pK_a values of non–alkyl substituted phosphonic acids vary depending on substitution from just over 1 to almost 4, and tend to have a $pK_2 - pK_1$ difference ~ 5, except for the stronger acids, for which the pK difference is smaller.

2.2.3 Spectroscopic Properties – IR

There has been some disagreement in the literature as to the exact assignment and scope of the frequencies of the different P–O vibrational modes. Table 2.1 summarizes the most commonly accepted values for this functional group.[35-39] Observations regarding some of these bands are presented below.

2.2.3.1 Phosphonic Acids

The P=O stretching frequency is in the range 1150 – 1220 cm^{-1} for phosphonic acids, and this vibrational mode shifts to a higher frequency range when the acidic groups are replaced with aliphatic ones (as in the diethyl phosphonate). The lower P=O band frequency when hydroxyl groups are present is due to intermolecular hydrogen bonding between these groups which also broadens the peak as well as decreasing its intensity.[36, 39]

The P=O, or phosphoryl bond, has been widely studied, and has been characterized to the point where predictions can be made, based on the atoms surrounding the phosphorus atom, as to where the P=O stretching frequency will be located.[36] This is possible because the P=O bond does not lie in the same plane as the multiple bonds of other substituents attached to the phosphorus atom. Thus the P=O bond frequency is largely independent of any conjugation effects from the adjoining atoms. Therefore, the inductive effects of substituents on the phosphorus atom have the strongest influence on the frequency of the P=O stretching mode.[36]

Less is known about the P–O–H bands as the P–O and O–H modes can couple easily with other modes and thus their absorptions are "spread out" over the spectrum. Bands resulting from P–O–(H) and (P)–O–H stretches, and visible combinations between the stretching modes are located over a large range of frequencies (Table 2.1). While there are many bands characteristic of this group, there are few generalities that apply to phosphonic acids. One given, however, is that in phosphonic acids the three highest energy bands (2525 – 2725, 2080 – 2350, and 1600 – 1740 cm^{-1}) should all have

comparable intensities.[38]

Table 2.1 List of the various IR assignments and frequencies of different functional groups in phosphonic acids and phosphonates

Mode	Frequency (cm^{-1})
P=O (acid)	1150–1220
P=O (ester)	1200–1320
(P)–O–H	2525–2725
(P)–O–H	2080–2350
P–O–H	1600–1740
P–O–(H)	917–950
P–O–(H)	972–1030
P–O–C2H5	1008–1042
P–C	680–785
P–Ph	1420–1450
P–O–(H)	450–540

The identification of characteristic frequencies of the various vibrational modes in phosphonic acids is useful not only in characterizing the compounds, but also in determining whether they have bound to a metal oxide surface. By examining the signature IR frequencies of P–O–M bands, where M is a metal atom, in phosphonic acids on surfaces and comparing these to the unbound phosphonic acids, insight can be obtained as to the nature of the binding.

2.2.3.2 Mono– and Di–Salts of Phosphonic Acids

It can also be of use to examine the mono and dibasic salts of phosphonic acids. It could be expected that the shifts in the frequencies of the P–O vibrational modes might correspond roughly to the frequencies in resulting P–O–M bonds once the molecule is attached to a metal oxide surface and so some insight might be obtained by looking at the various salts of phosphonic acids.

The PO_2^- anion, when corresponding to a monobasic phosphonic acid salt, usually shows a strong P–O–(H) absorption band at 898 – 921 cm^{-1}, as well as complex symmetric and asymmetric P–O stretching bands between 990 – 1251 cm^{-1}.[38] The exact absorption frequencies depend on the nature of the anion and the cation in question. It has been found that the group directly attached to the phosphorus atom has a strong influence on the actual value of the asymmetric PO_2^- vibration frequency.[39] It has also been observed that the frequencies usually decrease as the size of the cation increases,[40] but there are exceptions.[41]

The PO_3^{2-} anion of a phosphonic acid is also of interest. Due to the absence of any hydroxyl group the vibrational absorption bands related to it are simpler than for the other phosphorous–containing group described above. However, due to the limited amount of data on this class of compounds, band assignments are difficult. It is known that the asymmetric P–O stretching band is observed between 970 and 1124 cm^{-1} and the symmetric band between 962 and 1000 cm^{-1}.[38] Another important note is that the asymmetric band is generally more pronounced in relation to the symmetric band, and in some cases the symmetric band cannot even be distinguished.[39]

2.2.3.3 P–O–M Bonds

While the data in the literature is scarce, there are some general observations. The P–O–M bands are usually broad (indicative of the delocalization of electrons) and generally fall with 900 – 1200 cm^{-1} range. P–O–M interactions can be divided into two types.[38] The first is the formation of a coordinate (dative) bond between the metal and the phosphoryl group. These types of vibrational frequencies fall between 1167 and 1132 cm^{-1}. The second type of bond is a covalent bond with an oxygen atom singly bound to both the phosphorus and the metal (P–O–M). In the analysis of spectra of phosphonic acids bound to a surface, it should be kept in mind that the formation of a P–O–M bond may be accompanied by the disappearance of the P=O and P–O–H bonds, depending on the mode of binding, which can be mono–, bi–, or tridentate. More information on the types of binding modes available for phosphonic acids bound to metal oxides is presented in Chapter 3. These three binding modes are a combination of the two types of coordination to the surface that is possible: the coordination of the phosphoryl oxygen to Lewis acid sites on the metal oxide surface and the condensation between surface hydroxyl groups and hydroxyl groups on the phosphonic acid. Additionally, there could be hydrogen bonding between the phosphonic acid and the metal oxide surface. However, equally as important as the appearance of this broad band is the disappearance of the phosphoryl band at around 1200 cm^{-1} and of the symmetric and asymmetric P–O–H bands. By looking at a combination of these indicators, a clearer picture of what type of bonding (mono, bi, or tridentate) and the nature of this bonding can be obtained. For instance, a phosphonic acid bound in tridentate form should result in just a broad band

from 900 – 1200 cm^{-1}, and the total disappearance of the normal P=O and P–O–H bands.[42-44] The presence of either the P=O band or the P–O–H bands indicates the presence of mono– or bidentate binding, or a mixture of the two.

2.2.4 Spectroscopic Properties – NMR

Due to the fact that the Phosphorus atom has spin = ½, the ^{31}P NMR spectra of phosphonic acids and their phosphonate precursors can be used as a characterization tool. The natural abundance of ^{31}P is 100%, and this results in splitting of peaks in both the ^{1}H and ^{13}C NMR experiments. Coupling to the phosphorus is usually only observed in ^{1}H NMR for the hydrogens on carbons 1–3 bonds away from the phosphorus. However, in ^{13}C NMR the splitting caused by the phosphorus can actually carry as far away as 5 bonds, sometimes resulting in very intricate spectra. However, an advantage of phosphorus–containing compounds is that ^{31}P spectra can be measured, allowing for another analytical technique by which to judge compound purity and properties. The NMR spectra of most phosphonates can be obtained in $CDCl_3$ while the spectra of phosphonic acids are often measured in DMSO–d_6. The following assignments for NMR peak positions are a combination of knowledge from the literature and from personal experience.[38, 45]

2.2.4.1 ^{1}H NMR

^{1}H NMR spectra of the phosphonic acid and phosphonate moieties are themselves not difficult to interpret, but there are several trends to point out. For instance, the protons on the carbon α to the phosphorus are split into a doublet (J ~ 18 – 20 Hz). In the case of an alkyl chain, these protons appear at ~ 1.7 ppm (referenced to the protons in tetramethylsilane) in the phosphonate and shift to ~ 1.4 ppm in the phosphonic acid (Figure 2.12). Benzyl protons are shifted downfield to ~ 3 ppm in both the ester and acid form. For diethylphosphonates, the protons on the carbon α to oxygen on the ethoxy groups are also split into a doublet (J ~ 10 Hz) and appear at ~ 4.0 ppm, and occasionally the terminal CH_3 protons on the ethoxy groups is split, though the coupling is very small (J < 1 Hz) and not always visible in the NMR spectrum. These protons appear ~ 1.2 ppm. The position and shape of the two acidic protons in the phosphonic acid are highly dependent on the amount of water present in the sample. If low amounts of water are present then the protons will oftentimes appear as a broad hump somewhere in the range of 8 – 10 ppm. However, this is not always the case, and differing amounts of water and sample concentration can shift of the peak width.

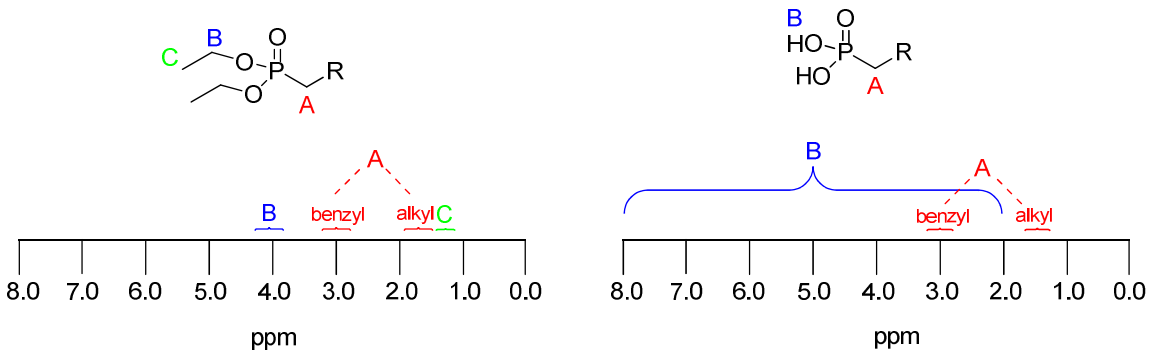

Figure 2.12 Relative peak positions of protons connected to atoms 1 – 3 bonds from the phosphorus in ^{1}H NMR spectrum.

2.2.4.2 ^{13}C NMR

The ^{13}C NMR spectra can show a number of P–C couplings. As phosphorus has spin ½, assuming the presence of only one phosphorous atom, all of the carbons to which it is coupled are split into doublets. For alkyl phosphonates, the carbon on the ethoxy β to the oxygen will appear ~16 ppm as a doublet (J ~ 6 Hz) (Figure 2.13). This doublet comprises two carbons, as does the doublet at ~ 61 ppm (J ~ 6 Hz), which corresponds to the carbon α to the oxygen on the ethoxy group. The carbon connected to the phosphorus has a large coupling constant (J ~ 140 Hz) and is seen as a doublet at ~ 26 ppm. The carbon β to the phosphorus appears as a doublet at ~ 23 ppm (J ~ 5 Hz) and the carbon γ to the phosphorus appears as a doublet at ~ 31 ppm (J ~ 16 Hz). The coupling constant for the coupling between the phosphorus and the δ carbon is often too small (~ 1 Hz) to be resolvable as a doublet in routine spectra.

For alkyl phosphonic acids, the carbons close to the phosphorus are shifted with

respect to the corresponding peaks of the phosphonate. The carbon connected to the phosphorus is split by the phosphorus (J ~ 137 Hz) and is seen as a doublet at ~ 27 ppm. The carbon β to the phosphorus appears as a doublet at ~ 22 ppm (J ~ 5 Hz) and the carbon γ to the phosphorus appears as a doublet at ~ 30 ppm (J ~ 16 Hz). As with the phosphonates, the coupling constant for the coupling between the phosphorus and the δ carbon is often too small (~ 1 Hz) to be resolvable as a doublet in routine spectra.

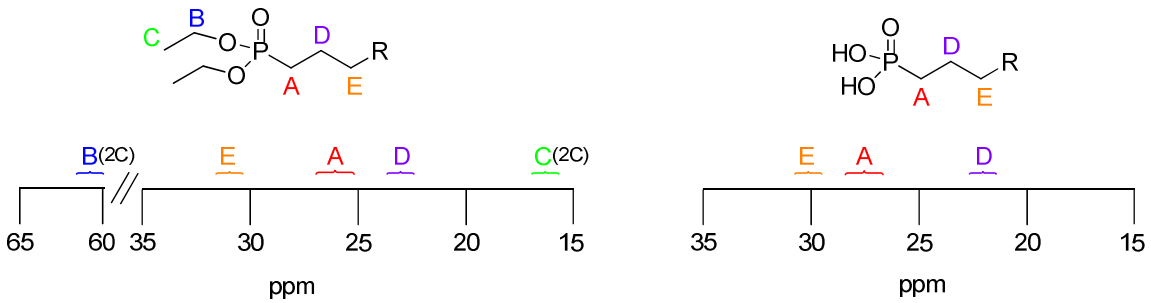

Figure 2.13 Positions of peaks in ^{13}C NMR spectra of phosphonates and phosphonic acids, depending on the carbon interaction and proximity to the phosphorus atom.

As the carbon *s* character in the C–P bond increases, so does the coupling constant. Thus, the coupling seen between the phosphorus and the attached α carbon for a phenylphosphonate increases to ~ 195 Hz and for a phenylphosphonic acid to ~ 180 Hz from the ~ 135 Hz usually seen for sp^3 attached carbons (Figure 2.14). Interestingly, while the carbon–phosphorus coupling for the α carbon in benzylphosphonate is ~ 141 Hz, similar to that seen in an alkylphosphonate, the coupling constant of the analogous carbon in a benzylphosphonic decreases to ~ 131 Hz.

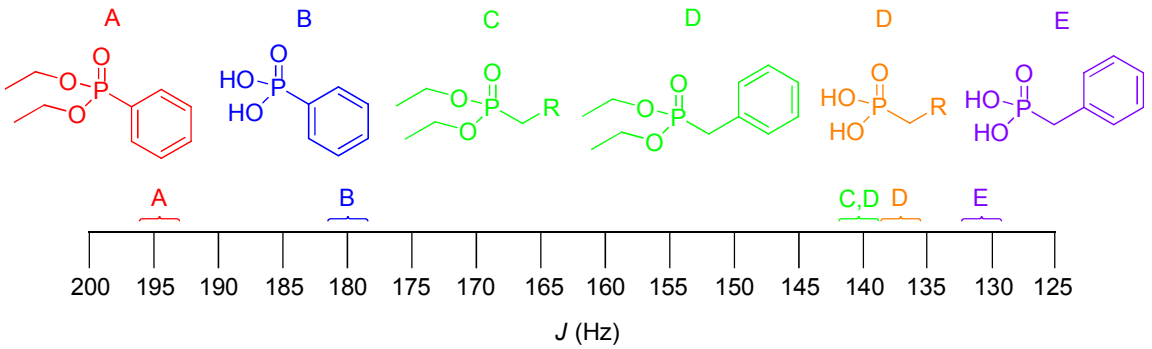

Figure 2.14 Coupling constants for the α carbon depending on the type of carbon and type of phosphorus group.

In addition to the changes in the size of the coupling constants, the benzyl and phenyl phosphonates and phosphonic acids can show carbon–phosphorus couplings up to 5 bonds away and with J ~ 4 Hz. While phosphorus coupling carbon atoms up to 4 bonds away in the phenyl species can be explained considering how couplings can carry further through aromatic regions, the 5–bond coupling seen in some benzyl species is surprising.

2.2.4.3 ^{31}P NMR

^{31}P NMR, as previously mentioned, is a useful tool to further validate the purity of phosphorus–containing compounds. This is especially useful when compounds differ only by their phosphorus oxidation state (for instance, from phosphine to phosphine oxide). In the case of phosphonate synthesis, ^{31}P NMR helps to ensure that other phosphorus impurities and side–products (mainly triethylphosphite and ethyl diethylphosphonate) have been successfully removed upon workup. In the case of phosphonic acid syntheses, it is useful to show that all of the phosphonate has reacted.

While the known ^{31}P chemical shifts range from about -460 ppm (P_4) to +225 ppm (PBr_3), and the known range of chemical shifts for tetravalent phosphorus compounds range from about -115 ppm to +130 ppm, most of the compounds synthesized and discussed herein exhibit ^{31}P chemical shifts in the range from only -3 ppm to +35 ppm.

The phosphonic acids almost always have a ^{31}P position more upfield than the corresponding phosphonates (Table 2.2).

Table 2.2 Range of placement of the phosphorus peak of different phosphonate and phosphonic acids in ^{31P} NMR.

compound	ppm range
aliphatic phosphonate	28 – 34
aliphatic phosphonic acid	26 – 31
benzyl phosphonate	22 – 31
benzyl phosphonic acid	17 – 23
aryl phosphonate	7 – 20
aryl phosphonic acid	-3 – 14

Electronegative substituents and their proximity to the phosphorus atom will also affect the ^{31}P shift. As can be seen in Figure 2.15, our own experiments show that as the number and proximity of fluorines to the phosphorus increases in this series of fluorinated benzylphosphonic acids, the ppm shift of the phosphorus peak moves more upfield. A shift of 4.7 ppm can be seen between 4–fluorobenzylphosphonic acid and pentafluorobenzylphosphonic acid.

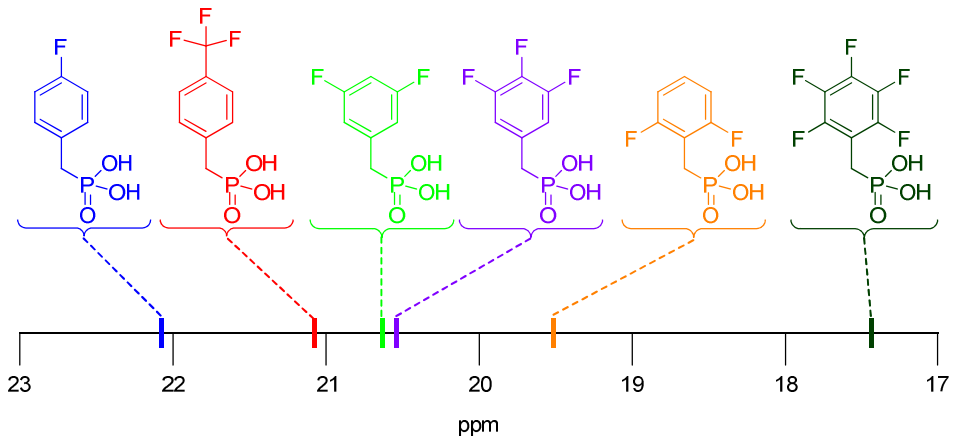

Figure 2.15 Relative shifts of the phosphorus peak in benzylphosphonic acids due to the degree and position of fluorine substitution.

A similar relation can be seen in the shifts due to fluorine substitution in phenylphosphonic acids, except the influence of the fluorines is even greater as the phosphorus is now directly coupled to the ring system (Figure 2.16). Here a shift of 13.5 ppm can be seen between 4–fluorophenylphosphonic acid and pentafluorophenylphosphonic acid.

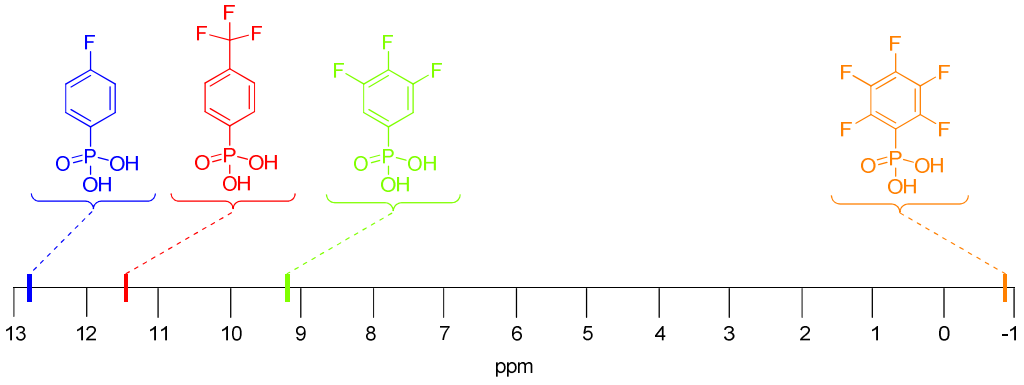

Figure 2.16 Relative shifts of the phosphorus peak in phenylphosphonic acids due to the degree and position of fluorine substitution.

2.3 Design and Synthesis of Phosphonic Acids

As mentioned previously, there are very few commercially available phosphonic acids (~50) and they are often only available in small amounts and at high costs. Therefore, many of the phosphonic acids which are used herein were synthesized. This section will detail the design and synthesis of these specific phosphonic acids. The synthetic procedures for each are mostly common organic transformations and have been well–documented in the literature. No details will be given in this section unless there are specific peculiarities.

This section is divided into three parts. First, the design and synthesis of phosphonic acids for use in changing the physical properties of surfaces will be described. Next, the design and synthesis of phosphonic acids which were synthesized in order to impart various functional groups on the surface will be discussed. Finally, the rationale and synthesis of phosphonic acids which were synthesized to change the work function of surfaces will be described. It should be noted that many of these compounds can and have been used for a number of different applications and thus are included in more than one section. Compounds will be divided into groups based on the original thinking behind their design as well as any application they have been used for.

2.3.1 Phosphonic Acids Designed to Change Physical Properties of Surfaces

The interactions between one material and another are often defined by their respective surface properties. Unfortunately, most materials have only one type of naturally occurring surface chemistry, and this may or may not have the correct properties in order to physically interact well with other materials. This interaction can be regarded as a combination of the forces of adhesion and cohesion present at the interface of two materials. Cohesion is a physical property of a substance caused by intermolecular attraction between like–molecules. Adhesion, which can be broken up into different types, is the tendency of different molecules to be attracted to each other. Metal oxides tend to have surface hydroxyl groups, resulting in a high surface energy that can make the surface physically incompatible with nonpolar organic species. As was discussed in Chapter 1, the properties of surfaces can be tuned by attaching monolayers of organic molecules. Each of the phosphonic acids discussed in this section was designed in order to impart a specific physical property to the surface of the material they modify (Figure 2.17).

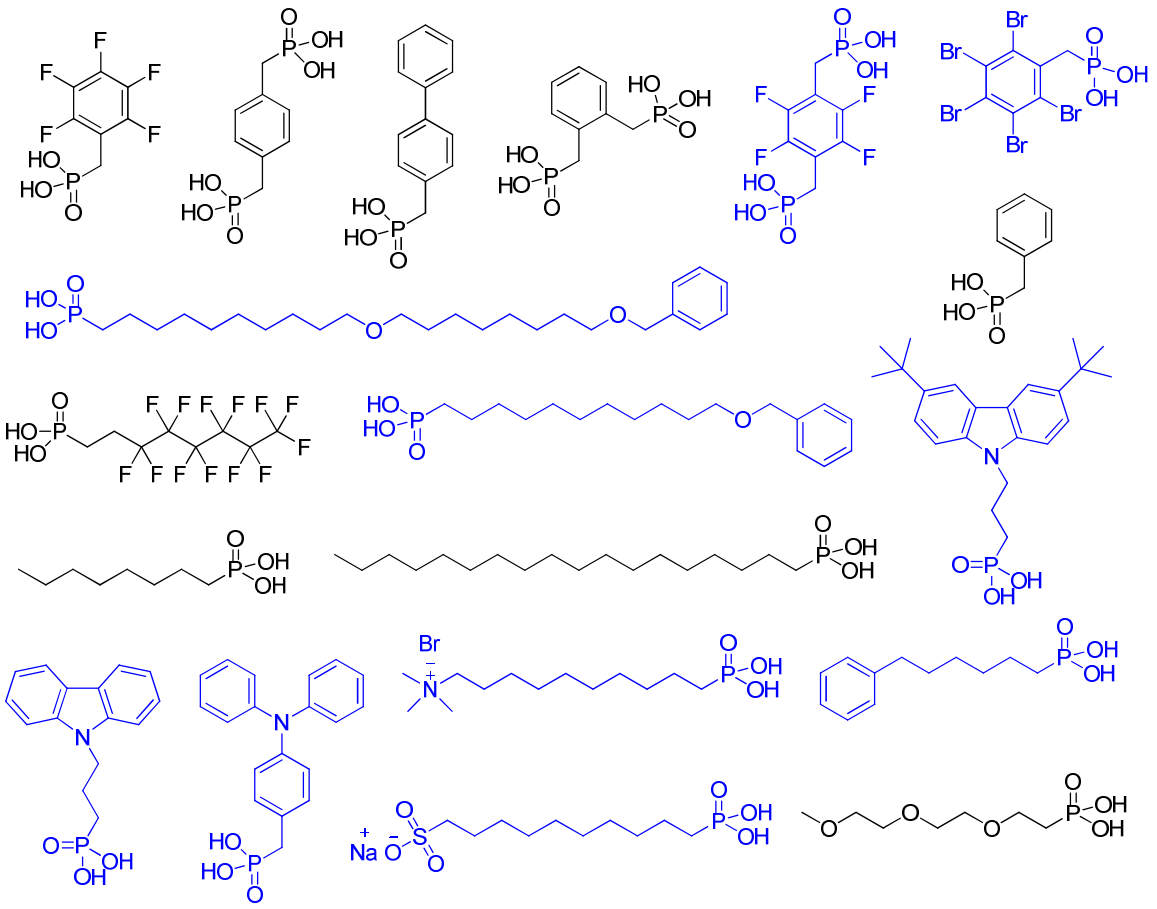

Figure 2.17 Chemical structures of phosphonic acids which have been synthesized for use in altering the physical properties of the metal oxide surface to which they are bound. Compounds in blue have not been previously reported in the literature.

Compatibilization is a broad term, and in the context of this research it mainly refers to the attempts at improving interfacial properties of surfaces. In terms of flat substrates, such as ITO, phosphonic acids can be designed to match surface energies of the materials they modify with other organic compounds by increasing the adhesion force. Or instead of changing merely the surface energy, molecules which have similar functional groups to those of the ensuing organic layer can be made, thereby increasing the interfacial interaction between the layers by tuning the cohesion force between the materials.[46] Additionally, molecules can be designed that will either pack well to form

ordered, dense monolayers, or, that will induce molecules deposited on top to order themselves in a particular fashion.[47]

In terms of nanoparticles, molecules can be synthesized which can allow for better dispersion of the nanoparticles in solvents, or better dispersion of the nanoparticles in polymer matrices.[48]

2.3.1.1 Changing the Wetting Behavior of Planar Substrates for Subsequent Organic Deposition

As mentioned in Chapter 1, ITO is often used as the transparent electrode in organic electronic applications. In these devices, organic molecules and polymers are often deposited on top of the ITO electrode. The surface energies of these species are often low because they are generally non–polar and as such do not have strong permanent or induced dipoles. Metal oxide substrates, on the other hand, are often terminated with hydroxyl groups that greatly increase the polarity and therefore surface energy of the material.[49] It can be the case then, that, when polymers and small molecules are deposited onto the ITO surface, the wetting of the organic on the metal oxide is not optimal, and at some later point the mechanical integrity of the interface could degrade and hinder device performance.

Phosphonic acids that can decrease the surface energy of the metal oxide surface would therefore contain a terminal functional group which is overall fairly non–polar and does not contain any hydrogen bonding groups. Fluorinated compounds tend to have low

surface energies and so two fluorinated phosphonic acids were prepared from their respective halides by means of the aforementioned Arbuzov reactions and subsequent hydrolysis (Figure 2.18).

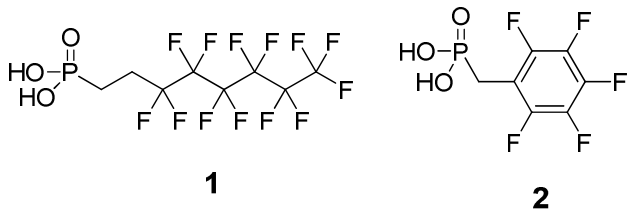

1 **2**

Figure 2.18 Chemical structures of 3,3,4,4,5,5,6,6,7,7,8,8,8–tridecafluorooctyl phosphonic acid (**1**) and 2,3,4,5,6–pentafluorobenzylphosphonic acid (**2**)**.** These phosphonic acids should decrease the surface energies of the metal oxides they modify.

Similar to decreasing the surface energy, attaching organic moieties that mimic the functional groups present in a subsequently applied organic layer may increase the robustness of the interface between the two materials.[46] Specifically for organic electronic applications, attaching aromatic, carbazole, and triphenylamine units to the ITO surface may improve the interfacial interaction with hole–transport materials, which often contain these types of functional groups (Figure 2.19).

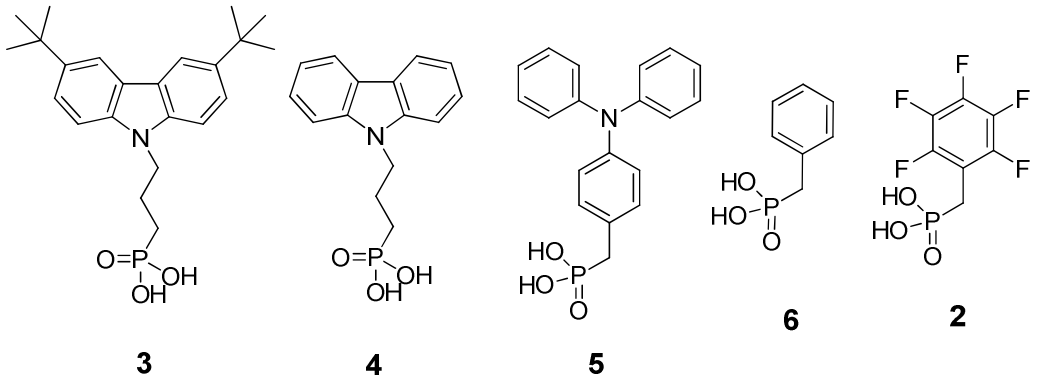

Figure 2.19 Chemical structures of 3–(3,6–di–*tert*–butyl–9H–carbazol–9–yl)propylphosphonic acid (**3**), 3–(9H–carbazol–9–yl)propylphosphonic acid (**4**), 4–(diphenylamino)benzylphosphonic acid (**5**), benzylphosphonic acid (**6**), and 2,3,4,5,6–pentafluorobenzylphosphonic acid (**2**). These phosphonic acids have been designed to increase the robustness of the interface between the metal oxide and organic materials.

Compounds **2** and **6** were synthesized in two steps from their bromide precursors utilizing the Arbuzov reaction. **5** was synthesized from the starting phosphonate[b] in a similar manner.

The carbazole–functionalized phosphonic acids were synthesized by first alkylation of the amine of the carbazole with dibromopropane. The remaining bromine was then utilized in an Arbuzov reaction followed by hydrolysis to obtain **4** (Figure 2.20).

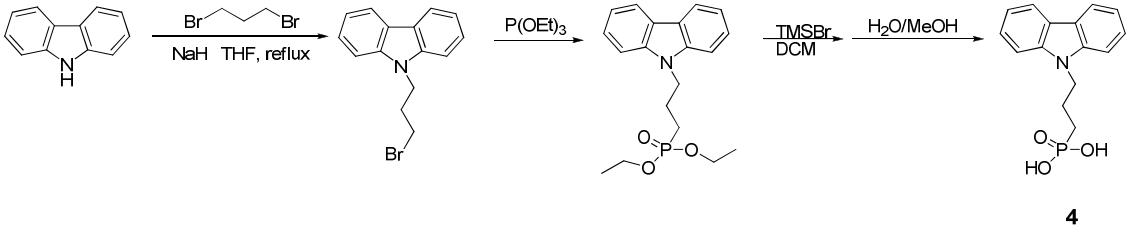

Figure 2.20 Synthetic scheme for the synthesis of 3–(9H–carbazol–9–yl)propylphosphonic acid (**4**).

[b] Obtained from Shijun Zheng (Marder Group)

The synthesis of the *t*–butylcarbazole analogue was obtained *via* a Friedel–Crafts reaction of the carbazole functionalized phosphonate with *t*–butyl chloride in a typical electrophilic aromatic substitution reaction. This was followed by hydrolysis of the phosphonate as normal to obtain **3** (Figure 2.21).

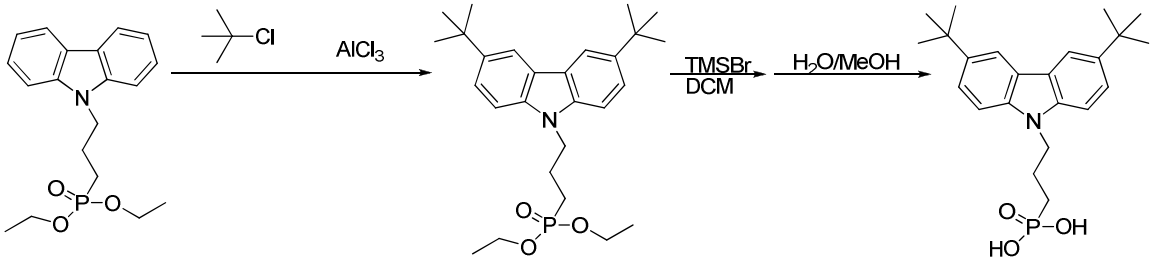

3

Figure 2.21 Synthetic scheme for the synthesis of 3–(3,6–di–*tert*–butyl–9H–carbazol–9–yl)propylphosphonic acid (**3**).

2.3.1.2 Molecules Designed to Form Ordered Monolayers or Induce Order of Other Molecules

As the packing of organic molecules can affect their charge transport characteristics, being able to template the packing of organic materials in OLEDs, OPVs, or transistors would allow for increased device performance. π–π stacking of aromatic rings is a sought after packing motif in the previously mentioned applications as increased orbital overlap between molecules can result in larger mobility of the material. To this end, various long and short chain phosphonic acids incorporating benzyl or pentafluorobenzyl groups were synthesized (Figure 2.22).

While the packing of aromatic groups in charge transport materials can be affected by a monolayer, improved packing order/density of the monolayer can also result in increased device performance. By forming a tightly packed monolayer of material, migration of small molecule semiconductor materials, such as pentacene, to the gate electrode can be minimized.[47]

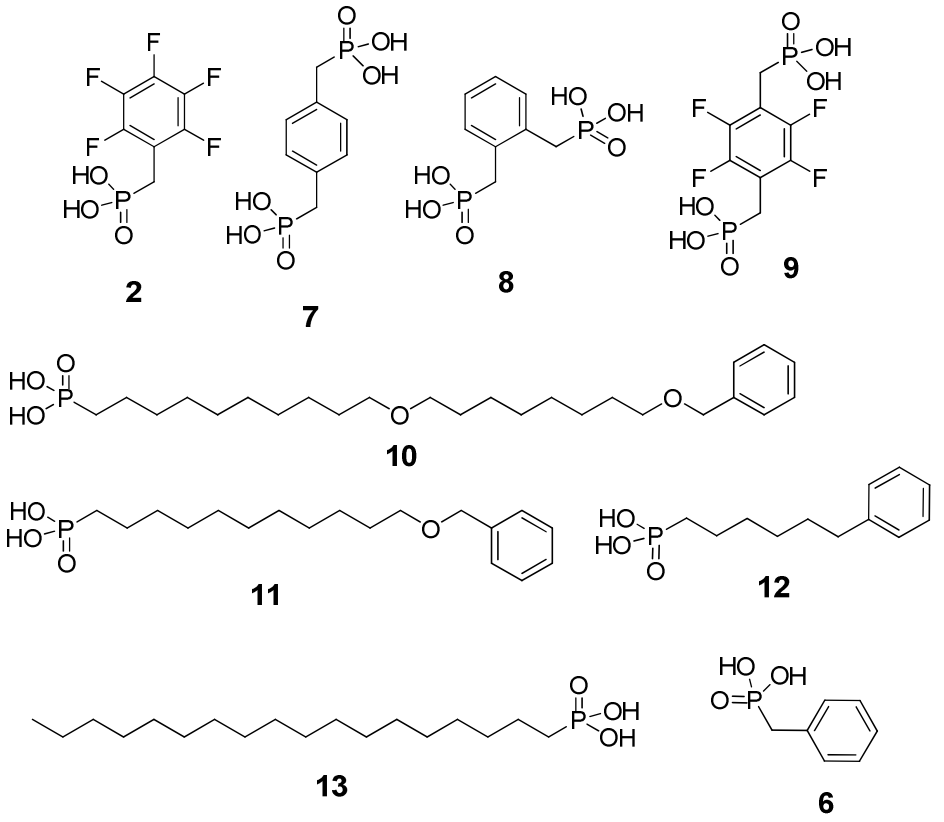

Figure 2.22 Chemical structures of 2,3,4,5,6–pentafluorobenzylphosphonic acid (**2**), 1,4–phenylenebis(methylene)diphosphonic acid (**7**), 1,2–phenylenebis(methylene) diphosphonic acid (**8**), (perfluoro–1,4–phenylene)bis(methylene)diphosphonic acid (**9**), benzylphosphonic acid (**6**), 6–phenylhexylphosphonic acid (**12**), octadecylphosphonic acid (**13**), 11–(benzyloxy)undecylphosphonic acid (**11**), and 10–(8–(benzyloxy)octyloxy)decylphosphonic acid (**10**). These phosphonic acids have the potential to form densely packed monolayers and/or induce packing of organic materials deposited on top of them.

The synthesis of **9** proceeded through a free–radical bromination of the methyl groups on the benzene ring, which is specific to the benzyl positions, followed by an Arbuzov reaction and then hydrolysis (Figure 2.23). The hydrolysis step was allowed to react longer than usual (4 hours instead of 2) in order to ensure that all 4 of the ester groups were hydrolyzed.

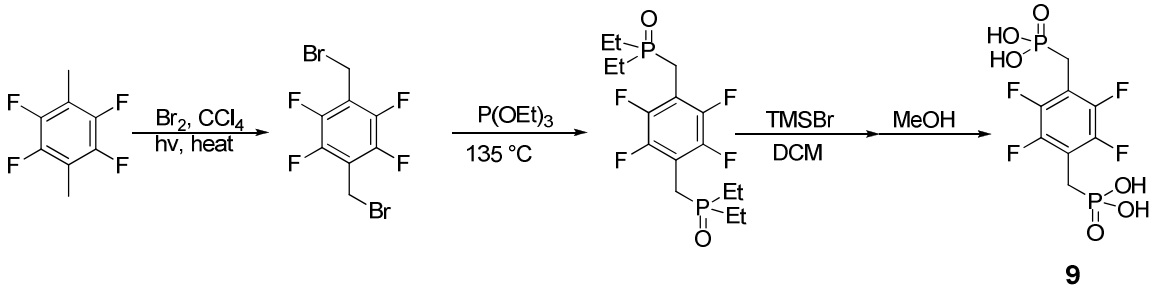

9

Figure 2.23 Synthetic scheme for the synthesis of (perfluoro–1,4–phenylene)bis(methylene)diphosphonic acid (**9**).

The synthesis of **12** consisted of three steps. The initial step involved the formation of the phenyl lithium intermediate by reacting butyl lithium with iodobenzene, followed by coupling with one end of 1,6–dibromohexane. This was followed by an Arbuzov reaction and then hydrolysis with bromotrimethylsilane. (Figure 2.24).

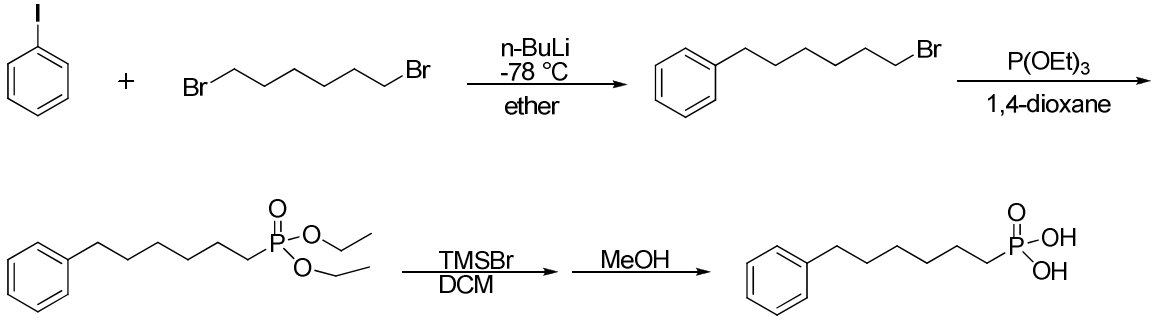

12

Figure 2.24 Synthetic scheme for the synthesis of 6–phenylhexylphosphonic acid (**12**).

Compounds **10** and **11** were designed specifically for use as the dielectric layer in OFETs. Our expectation is that the presence of the long chain should allow for better packing of the monolayer and the presence of the terminal benzene could allow for a preferred orientation of a deposited organic aromatic semiconductor on top.[47]

While larger acenes may be desirable, benzene was chosen for these exploratory studies as it is the simplest to introduce at the end of the molecule. Compound **11** was synthesized by a Williamson ether synthesis between benzyl bromide and an alkylphosphonate with a terminal hydroxyl group. This compound was then hydrolyzed as usual (Figure 2.25).

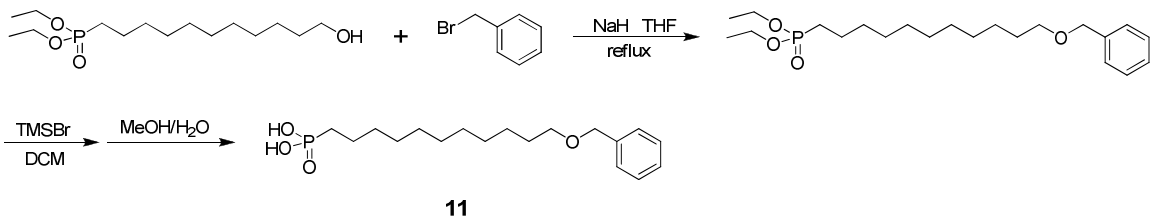

11

Figure 2.25 Synthetic scheme for the synthesis of 11–(benzyloxy)undecylphosphonic acid (**11**).

Whereas the synthesis of **11** was straightforward, the synthesis of **10** was not. An ether synthesis to form the 8–(benzyloxy)octan–1–ol proceeded normally. A second ether synthesis to combine this and a bromodecylphosphonate proved problematic. The reaction conditions resulted in an unidentifiable side–product that could not be separated from the desired product. So this reaction was divided into two separate steps, by first coupling the dibromide to the alcohol followed by formation of the phosphonate, to synthesize **10** (Figure 2.26).

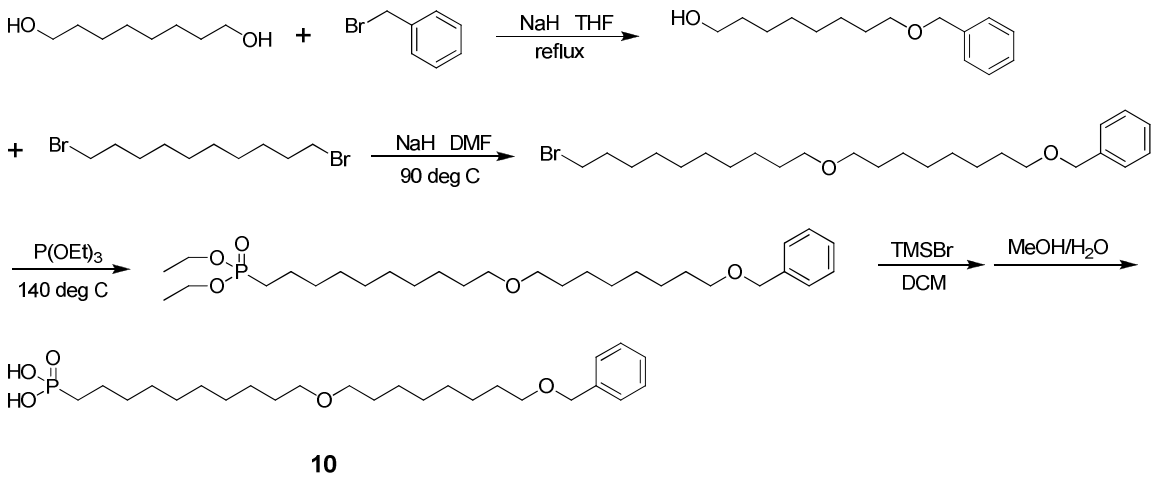

10

Figure 2.26 Synthetic scheme for the synthesis of 10–(8–(benzyloxy)octyloxy)decylphosphonic acid (**10**).

2.3.1.3 Molecules that can be Used to Change the Dispersibility of Nanoparticles in Solvents

Phosphonic acids were designed and synthesized to change the dispersibility/solubility of nanoparticles in solvents. While alkyl–based ligands, such as **16**, have been known to increase the dispersibility of nanoparticles in non–polar media,[50] **14** and **15** were synthesized with the expectation that they would increase the dispersibility of metal oxide nanoparticles in water (Figure 2.27).

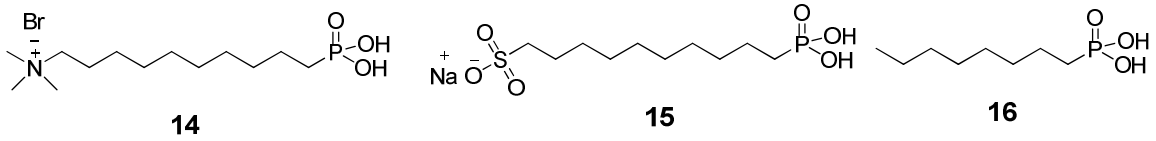

14 **15** **16**

Figure 2.27 Chemical structures of *N,N,N*–Trimethyl–10–phosphonodecan–1–aminium bromide (**14**), sodium 10–phosphonodecane–1–sulfonate (**15**), and octylphosphonic acid (**16**).

The synthesis of **14** was achieved through a standard S_N2 reaction to form the quaternary ammonium salt, followed by hydrolysis to yield the acid (Figure 2.28).

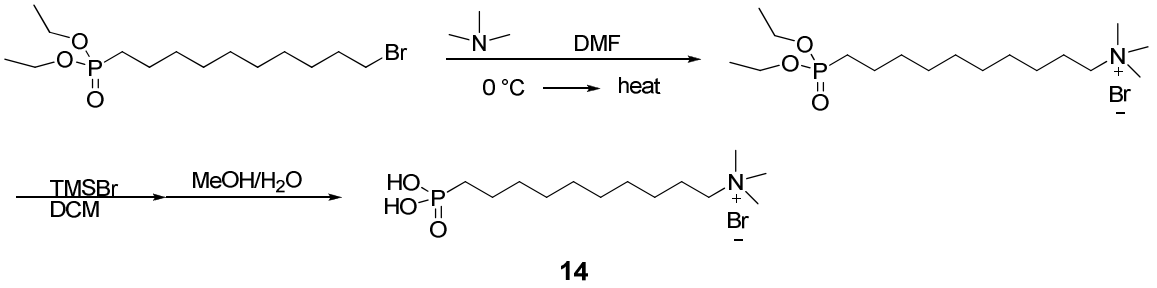

Figure 2.28 Synthetic scheme for the synthesis of *N,N,N*–Trimethyl–10–phosphonodecan–1–aminium bromide (**14**).

The synthesis of **15** was achieved *via* a standard Strecker sulfite alkylation of an alkyl bromide,[51] followed by hydrolysis of the phosphonate to yield the acid (Figure 2.29). Both the sulfonic acid and the sulfonic acid sodium salt were isolated.

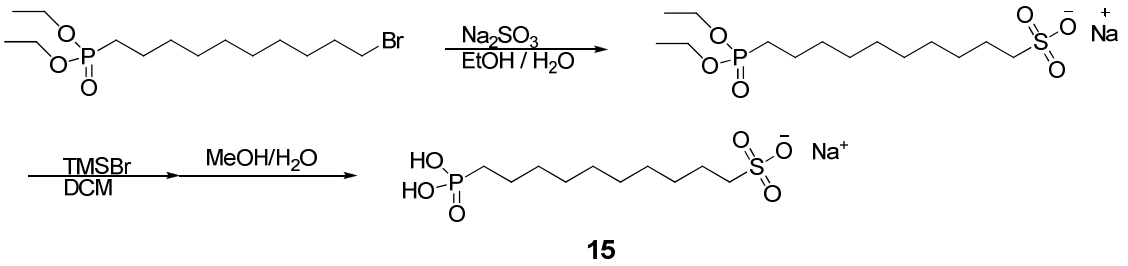

Figure 2.29 Synthetic scheme for the synthesis of sodium 10–phosphonodecane–1–sulfonate (**15**).

As **14** and **15** are both salts, purification was difficult and was usually accomplished *via* extractions to and from various solvents and/or recrystallizations (in the case of the acids).

2.3.1.4 Molecules Designed to Change the Dispersibility of Nanoparticles in Polymers

In addition to controlling dispersibility in solvents such as water, we were interested in tuning the compatibility of nanoparticles in polymer matrices. Phosphonic acids **2** and **18** had previously been successfully used to modify barium titanate nanoparticles in order to produce homogenous films of nanoparticles dispersed in Viton™, a fluorinated polymer, and polycarbonate, respectively.[48]

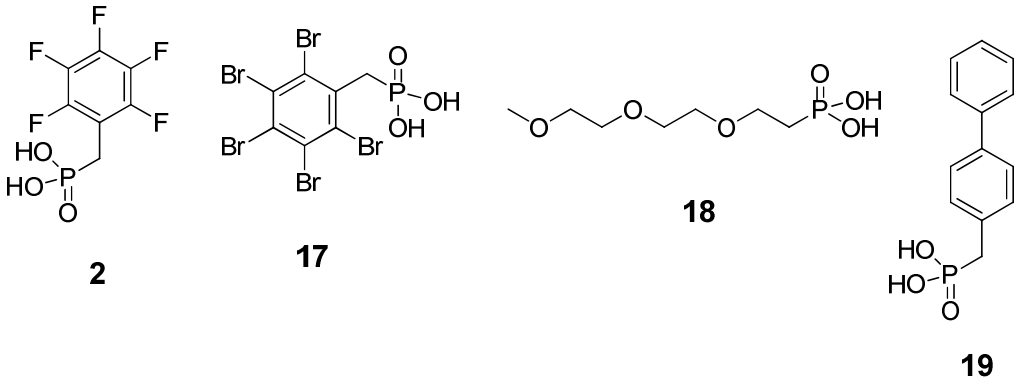

Figure 2.30 Chemical structures of 2,3,4,5,6–pentafluorobenzylphosphonic acid (**2**), 2,3,4,5,6–pentabromobenzylphosphonic acid (**17**), 2–(2–(2–methoxyethoxy)ethoxy) ethylphosphonic acid (**18**), and biphenyl–4–ylmethylphosphonic acid (**19**).

The syntheses of these compounds proceeded in high yield, through the formation of phosphonate and then the phosphonic acids from the starting bromides (or iodide in the case of **18**), and will not be reported in detail.

2.3.2 Phosphonic Acids Designed to Impart Specific Chemical Properties to Surfaces

As mentioned in Chapter 1, the ability to control a surface's chemistry is a powerful tool. The terminal functional group not only helps to control the overall surface properties of the substrate, but is also the means by which further chemical reactions can take place. Therefore, having a specific functional group can allow for further chemistry to be carried out on the surface of the metal oxide. A series of phosphonic acids were synthesized in order to provide a means to do further chemistry off of the surface of metal oxides (Figure 2.31).

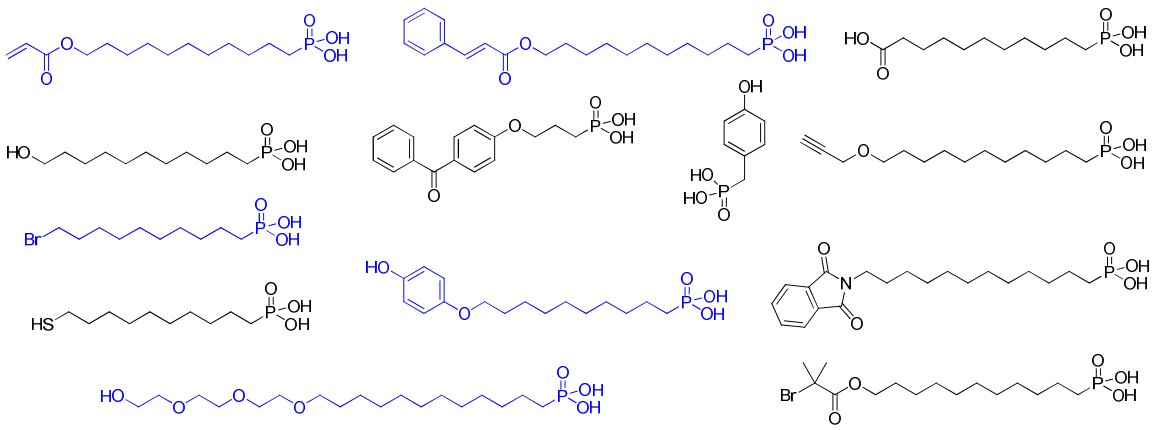

Figure 2.31 Chemical structures of phosphonic acids that have been synthesized for use in altering the chemical properties of the metal oxides they modify. Compounds in blue have not been previously reported in the literature.

The compounds listed are divided into three sections. The 1st is the group of compounds which can partake in a polymerization reaction, either as one of the monomers or as the initiator. The 2nd grouping consists of molecules that can in some

way bind, or crosslink, to other functional moieties or polymers. The 3rd section consists of the remaining molecules, many of which contain functional groups that are ubiquitous in standard organic and bio chemistry.

2.3.2.1 Phosphonic Acids with Polymerizable Groups

The molecules in this group can all partake in polymerization processes, whether as monomers or as initiators (Figure 2.32).

Compound **21** has a terminal acrylate group, a common functionality that can undergo radical or anionic polymerization. Phosphonic acids **20** and **22** are both polymer initiators and the initiating groups have been used to polymerize off of surfaces before.[52] Compound **22** has been reported before as an initiator to synthesize polystyrene where, after polymerization, the polymer chains were grafted to titania nanoparticles via the phosphonic acid group.[53]

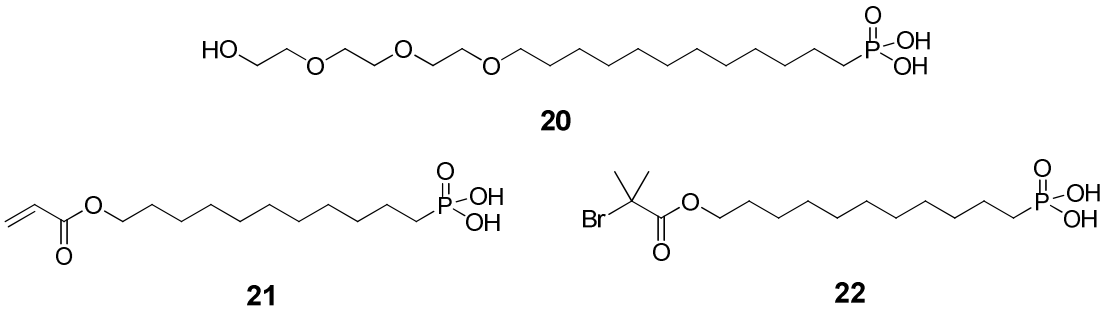

Figure 2.32 Chemical structures of 12–(2–(2–(2–hydroxyethoxy)ethoxy) ethoxy)dodecylphosphonic acid (**20**), 11–(acryloyloxy)undecylphosphonic acid (**21**), and 11–(2–bromo–2–methylpropanoyloxy)undecylphosphonic acid (**22**).

Compound **20** was synthesized in five steps. The extended alkyl chain was included to impart both an ability to form dense, well–packed monolayers through Van der Waals interactions amongst the alkyl chains as well as to promote solubility in more polar solvents, *via* the triethylene glycol portion. The triethylene glycol and dibromododecane were coupled by a Williamson ether synthesis, followed by protection of the alcohol by the nucleophilic attack of acetyl chloride on the alcohol, an Arbuzov reaction, deacetylation, and then hydrolysis (Figure 2.33).

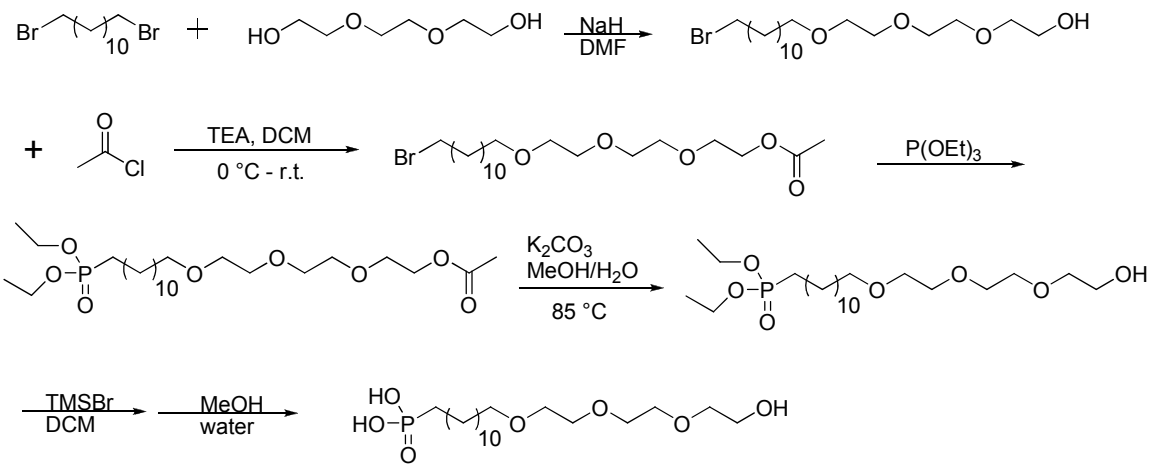

20

Figure 2.33 Synthetic scheme for the synthesis of 12–(2–(2–(2–hydroxyethoxy)ethoxy) ethoxy)dodecylphosphonic acid (**20**).

Compound **21** was synthesized from the hydroxyalkylphosphonate precursor via an esterification with acryloyl chloride, followed by hydrolysis of the phosphonate (Figure 2.34).

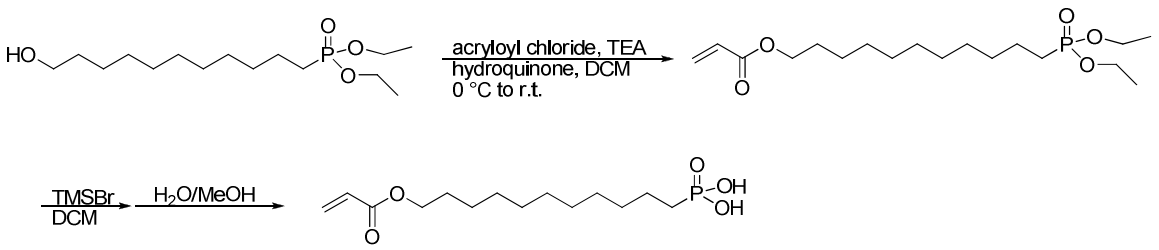

Figure 2.34 Synthetic scheme for the synthesis of 11–(acryloyloxy)undecylphosphonic acid (**21**).

2.3.2.2 Phosphonic Acids with Crosslinking Functionalities

The ability to covalently crosslink polymers to the surface of a metal oxide can be advantageous in the development of robust polymer coatings and layers for various technologies. This can be achieved by either functionalizing the surface with functional groups that are known to react with each other by means of a basic external stimulus, such as light or heat, or by attaching a functional group that can form bonds in a more universal fashion.

Compound **23** contains a cinnamate group that can react by a [2 + 2] cyclo addition with other cinnamate groups in the presence of UV light.[54] Compound **26** has a benzophenone group that has been used to react with C–H groups in alkyl chains of a number of polymers,[55, 56] thus tethering them to the surface (Figure 2.35).

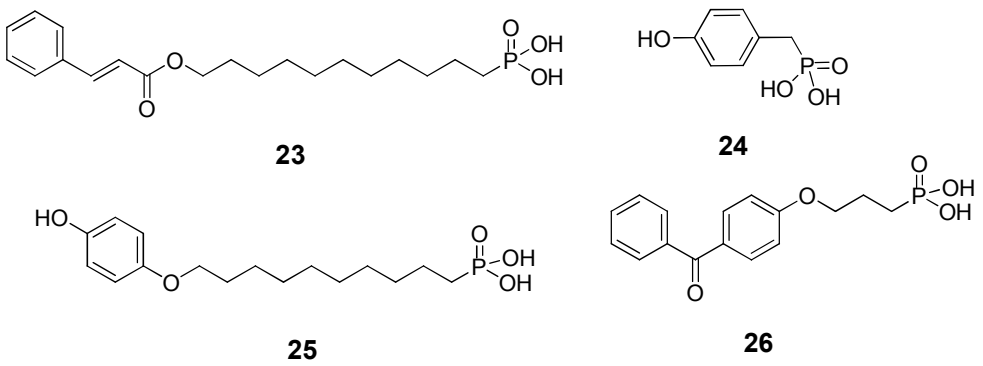

Figure 2.35 Chemical structures of (E)–11–(cinnamoyloxy)undecylphosphonic acid (**23**), 4–hydroxybenzylphosphonic acid (**24**), 10–(4–hydroxyphenoxy)decylphosphonic acid (**25**), and 3–(4–benzoylphenoxy)propylphosphonic acid (**26**).

Phosphonic acids **24** and **25** were both synthesized in order to crosslink nanoparticles modified with these compounds to polymer films. Phenoxy groups are known to react with hexamethoxymethylmelamine (HMMM) in the presence of a catalyst, such as *p*–toluenesulfonic acid and heat, in order to form ether linkages. This method is often used to crosslink poly(vinylphenol) (PVP).[57] Compound **24** was synthesized following a literature procedure where an aminobenzylphosphonate was converted to the hydroxybenzylphosphonate followed by hydrolysis to the acid.[58] However, tests utilizing this modifier showed that it was not efficient in crosslinking the polymer to the surface *vide infra*. It was hypothesized that perhaps the functional group was too close to the surface, thus retarding the reaction. Compound **25** was then synthesized to increase the distance between the substrate surface and the phenoxy group (Figure 2.36). The synthesis, though low–yielding mostly due to the first step with the hydroquinone, proceeded without difficulty.

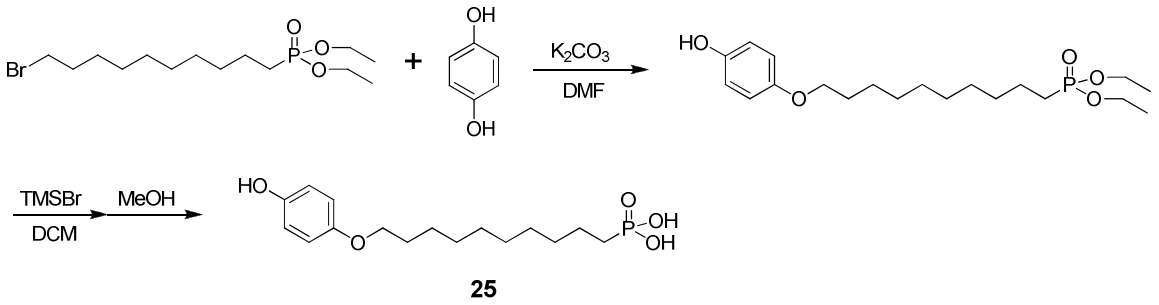

Figure 2.36 Synthetic scheme for the synthesis of 10–(4–hydroxyphenoxy)decylphosphonic acid (**25**).

Compound **23** was synthesized in an analogous way to **22**. An esterification using a cinnamoyl chloride was performed followed by hydrolysis to the acid (Figure 2.37).

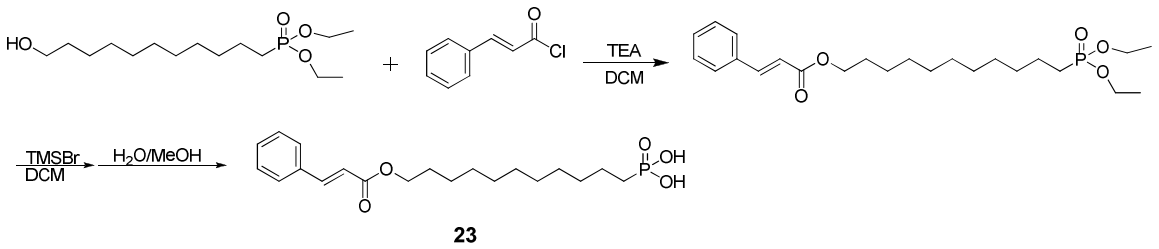

Figure 2.37 Synthetic scheme for the synthesis of (E)–11–(cinnamoyloxy)undecylphosphonic acid (**23**).

Compound **26** has been reported in the literature and was synthesized accordingly.[55, 56]

2.3.2.3 Phosphonic Acids with General Chemical Functionalities

We have been interested in being able to perform many different types of chemistries off of metal oxide substrates, depending on the application. Thus a number of phosphonic acids were synthesized which have common terminal functionalities, such as a halogen, carboxylic acid, alcohol, thiol, and alkyne (Figure 2.38).

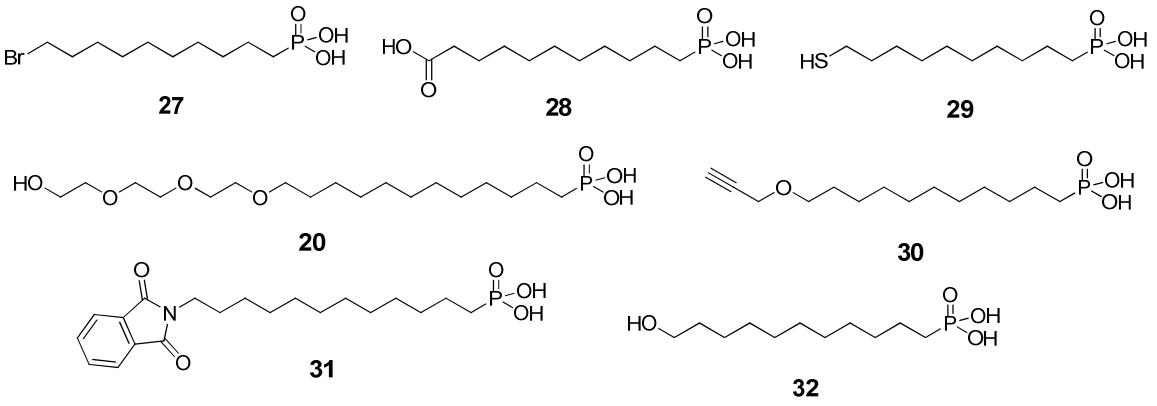

Figure 2.38 Chemical structures of 10–bromodecylphosphonic acid (**27**), 11–phosphonoundecanoic acid (**28**), 10–mercaptodecylphosphonic acid (**29**), 12–(2–(2–(2–hydroxyethoxy)ethoxy)ethoxy)dodecylphosphonic acid (**20**), 11–(prop–2–ynyloxy)undecylphosphonic acid (**30**), 12–(1,3–dioxoisoindolin–2–yl)dodecylphosphonic acid (**31**), and11–hydroxyundecylphosphonic acid (**32**).

Compound **32** was synthesized by the aforementioned acetylation the hydroxyl group on bromoundecanol followed by an Arbuzov reaction and then deprotection (Figure 2.39).

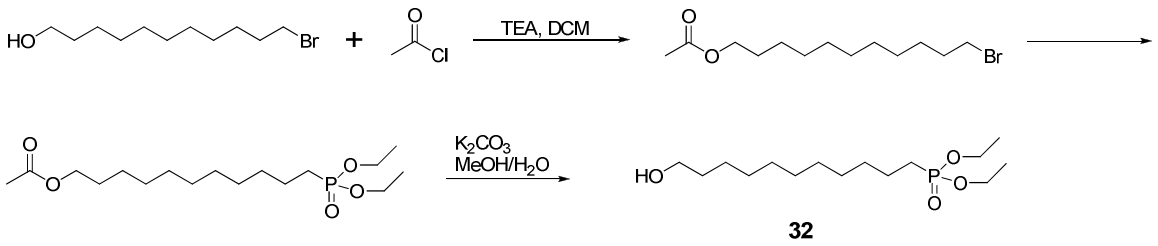

Figure 2.39 Synthetic scheme for the synthesis of 11–hydroxyundecylphosphonic acid (**32**).

Compound **30** was synthesized in two steps from the phosphonate derivative of **32** (which is also the precursor to a number of other compounds described in this chapter). An ether synthesis to attach an alkyne to **32,** followed by hydrolysis, yields **30** (Figure 2.40).

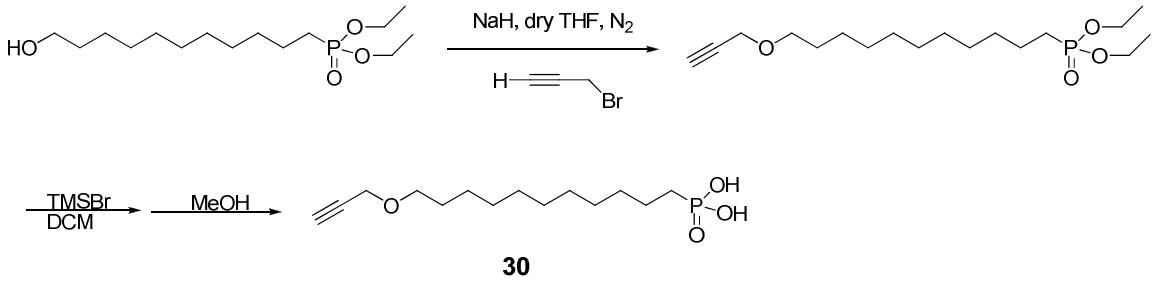

Figure 2.40 Synthetic scheme for the synthesis of 11–(prop–2–ynyloxy)undecylphosphonic acid (**30**).

Compound **29** was synthesized by reaction of bromodecylphosphonate with thiourea in basic aqueous conditions forming the isothiuronium salt intermediate, which is then cleaved to yield the thiol. This yields the mercaptodecylphosphonate which was then hydrolyzed to give **29** (Figure 2.41).

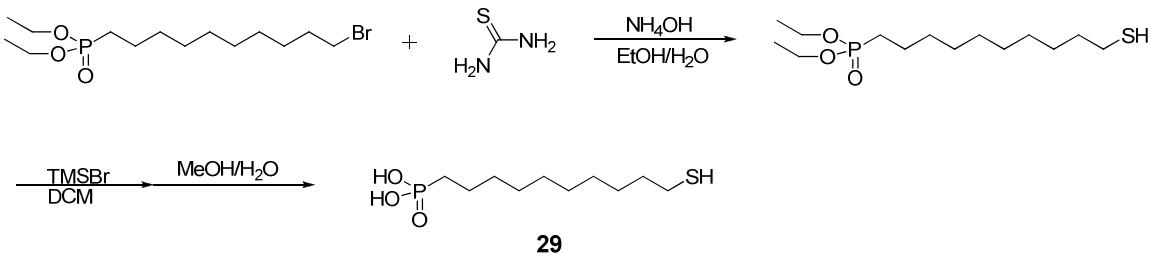

Figure 2.41 Synthetic scheme for the synthesis of 10–mercaptodecylphosphonic acid (**29**).

Compound **31** was synthesized by first following the first step of a Gabriel synthesis where the alkyl bromide was treated with potassium phthalimide. The product was isolated and it was used in an Arbuzov reaction, followed by hydrolysis to the phosphonic acid (Figure 2.42).

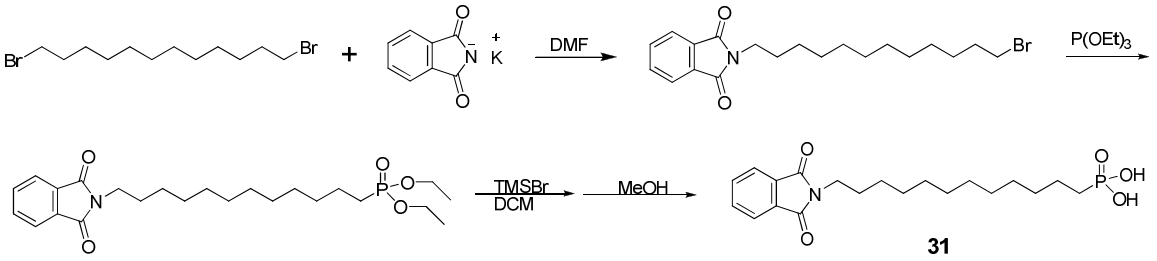

Figure 2.42 Synthetic scheme for the synthesis of 12–(1,3–dioxoisoindolin–2–yl)dodecylphosphonic acid (**31**).

While **31** is inherently useful, the original target was 12–aminododecylphosphonic acid. This could be obtained by subjecting the phthalimide phosphonate to hydrazine to undergo an exchange reaction, followed by hydrolysis of the phosphonate (Figure 2.43).

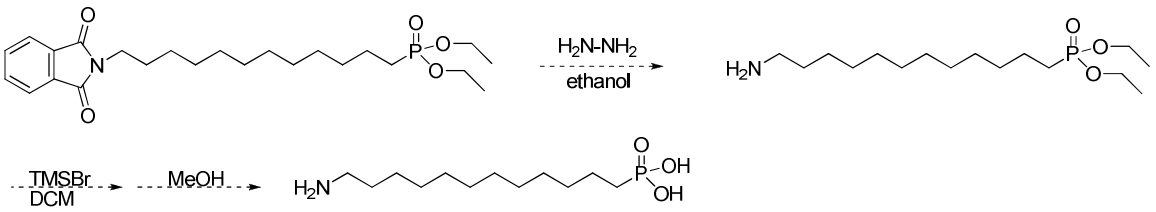

Figure 2.43 Proposed synthetic scheme for the synthesis of 12–aminododecylphosphonic acid.

The exchange reaction with hydrazine was attempted several times, however the desired aminophosphonate could not be isolated.

2.3.3 Phosphonic Acids that can Change the Work Function of Surfaces

If the molecules in a monolayer possess dipoles with a non–zero component normal to the surface the potential generated by this changed double layer can affect the work function of the substrate. This concept was outlined in Chapter 1. The presence of the electronegative fluorine in positions such that the resultant dipole would have its negative end pointing outward of the surface would increase the work function of the substrate. A series of alkyl and benzyl, and fluoroalkyl and fluorobenzyl phosphonic acids were synthesized (Figure 2.45). Except for the synthesis of **9**, all were synthesized in two steps from the corresponding halides. For some of the arylphosphonic acids a photoinitiated Arbuzov reaction was used in one of the steps, while the other phosphonic acids were synthesized *via* a palladium–catalyzed Arbuzov reaction. The use of these PAs to tune the work function of ITO is discussed in Chapter 4.

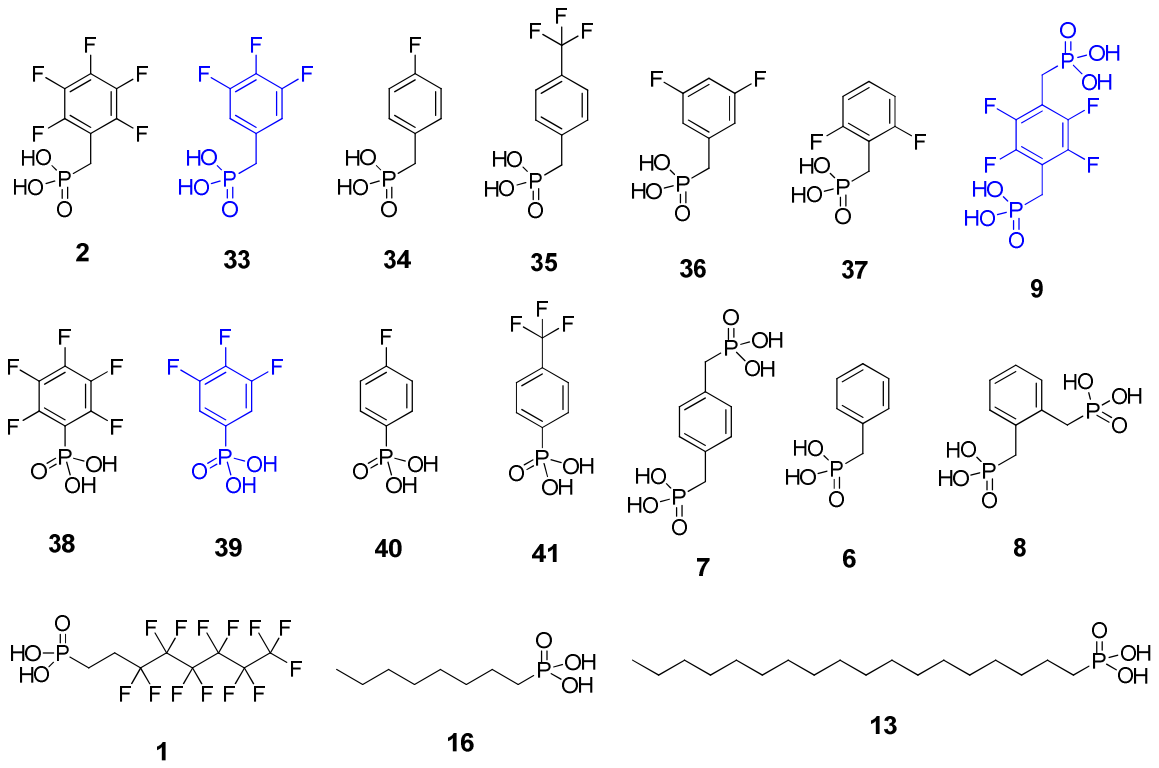

Figure 2.44. Chemical structures of 2,3,4,5,6–pentafluorobenzylphosphonic acid (**2**), 3,4,5–trifluorobenzylphosphonic acid (**33**), 4–fluorobenzylphosphonic acid (**34**), 4–(trifluoromethyl)benzylphosphonic acid (**35**), 3,5–difluorobenzylphosphonic acid (**36**), 2,6–difluorobenzylphosphonic acid (**37**), (perfluoro–1,4–phenylene)bis(methylene) diphosphonic acid (**9**), perfluorophenylphosphonic acid (**38**), 3,4,5–trifluorophenylphosphonic acid (**39**), 4–fluorophenylphosphonic acid (**40**), 4–(trifluoromethyl)phenylphosphonic acid (**41**), 1,4–phenylenebis(methylene)diphosphonic acid (**7**), benzylphosphonic acid (**6**), 1,2–phenylenebis(methylene)diphosphonic acid (**8**), 3,3,4,4,5,5,6,6,7,7,8,8,8–tridecafluorooctylphosphonic acid (**1**), octylphosphonic acid (**16**), and octadecylphosphonic acid (**13**). These phosphonic acids have been synthesized for use in altering the chemical properties of the metal oxides they modify. Compounds in blue have not been previously reported in the literature.

2.4 Conclusions and Future Direction

The most common synthetic techniques used in C–P bond formation for the ultimate synthesis of phosphonic acids have been discussed. The most popular and

additionally most used technique for the compounds in this thesis is the Arbuzov reaction, which transforms a primary or secondary alkyl halide to a dialkylphosphonate. However, other important C–P bond forming reaction were discussed, specifically those which can transform tertiary and aryl halides to the corresponding phosphonates as this cannot be achieved using the Michaelis – Arbuzov reaction. Also, the methods for hydrolysis of phosphonates to phosphonic acids were discussed. While HCl is the least expensive method of hydrolysis, the use of bromotrimethylsilane to form the intermediate bis(trimethylsilyl)phosphonate is a milder approach and has been the method of choice for the compounds in this thesis.

A large variety of phosphonic acids which are not commercially available have been synthesized. Many functional groups are tolerant of the phosphonic acid moiety and many have been attached as the terminal functional group in a number of compounds. Phosphonic acids have been synthesized that are tailored to specific needs and applications, and these will be discussed in further detail in subsequent chapters. Additionally, there exist a number of phosphonic acids which have not yet been used for specific applications, but which possess many useful properties and/or functional groups.

It is reasonable to expect that any functional group that is tolerable of strong acids can be combined with a phosphonic acid moiety. Phosphonic acids which would be interesting to investigate and which have not yet been synthesized include those with thiophene, pyrrole, dithienopyrole, or dithienothiophene groups. Additionally, trifluorovinylidene, 4–iodobenzyl, maleimide, and of course amine phosphonic acids could be useful as well.

In total, 18 phosphonic acids were synthesized that have not been previously

reported in the literature. These, along with various precursors that have not been reported in the literature, have been fully characterized. The synthetic details and characterization data are reported in the Experimental Section.

2.5 Experimental

Unless otherwise specified, all reactions were completed at room temperature using reagent grade chemicals.

^{1}H and ^{13}C NMR spectra were measured on a Varian Mercury 300 MHz or Bruker 400 or 500 MHz spectrometer using tetramethylsilane (TMS; $\delta = 0$ ppm) as a reference.

^{31}P NMR spectra were measured with proton decoupling on a Bruker 400 or 500 MHz spectrometer using 85% H_3PO_4 in a capillary tube as an external reference. While the use of external references can cause some shift in the overall location of the phosphorus peak, this was not corrected and results in a similar shift for all samples meaning that the relative shifts are not affected.

Mass Spectra were measured on a VG Instruments 70–SE using either electron impact (EI) of fast atom bombardment (FAB) mode, or a Applied Biosystems QSTAR-XL using electrospray ionization (ESI) mode.

Elemental analyses were carried out by Atlantic Microlabs using a LECO 932 CHNS elemental analyzer.

Compounds that have not been previously reported in the literature were characterized by ^{1}H, ^{13}C, and ^{31}P (where applicable) NMR, high-resolution mass

spectrometry, and elemental analysis (limits for deviation are 0.4 %). The new compounds are shown in blue in Figures 2.17, 2.31, and 2.44. Any compounds that did not pass elemental analysis have their respective NMR spectra shown in Appendix A.

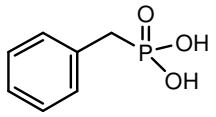

Benzylphosphonic acid

Benzyl bromide (4.00 g, 23.4 mmol) and triethylphosphite (4.663 g, 28.1 mmol) were combined with 1,4–dioxane (20 mL) and refluxed for 16 hours. The resulting liquid was distilled under vacuum (0.1 torr). The product, diethyl benzylphosphonate, was boiled at 98–100° C at 0.1 torr. The product is a colorless oil (PJH–I–17, 3.902 g, 73 % yield). The ^{1}H NMR spectrum is consistent with the desired product.[59]

Diethyl benzylphosphonate (3.902 g, 17.1 mmol) was dissolved in dry dichloromethane (40 mL). Bromotrimethylsilane (8.87 mL, 68.4 mmol) was added and the flask capped with a greased glass stopper. After 3 hours of stirring the volatiles were removed under reduced pressure to yield a dark brown oil which was redissolved in methanol and allowed to stir for 2 hours. The solvent was removed under reduced pressure and the product recrystallized from acetonitrile to yield a white crystalline powder (PJH–I–19a,b,c; 2.814 g, 96 % yield). The ^{1}H NMR spectrum is consistent with the desired product.[60]

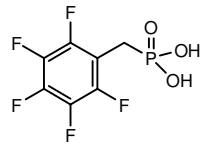

2,3,4,5,6–pentafluorobenzylphosphonic acid

Diethyl perfluorobenzylphosphonate (having been prepared as stated in the literature[61]) (57.0 g, 179.3 mmol) was dissolved in dry dichloromethane (200 mL). Bromotrimethylsilane (75 mL, 574 mmol) was added and the flask capped with a greased glass stopper. After 3 hours of stirring the volatiles were removed under reduced pressure to yield an oil which was redissolved in methanol: water (20: 1) and allowed to stir for 2 hours. The solvent was removed under reduced pressure to give a white solid and the product recrystallized from acetonitrile to yield a white crystalline solid (PJH–II–65a,b; 43.419 g, 93 % yield). The ^{1}H NMR spectrum is consistent with the desired product.[61]

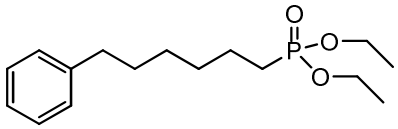

Diethyl 6–phenylhexylphosphonate

An oven–dried 1 L round bottom flask, with a stir bar, was fitted with a Schlenk adapter (greased joints) and put under vacuum. It was then pump–filled with nitrogen twice more. Ether (anhydrous, 500 mL) was added to the vessel *via* cannula. Iodobenzene (15 g, 73.5 mmol) was then added *via* syringe. The system was cooled to –78 ºC and *n*–butyl lithium (30 mL, 2.5M in hexane) was added dropwise *via* syringe. The system was allowed to stir for 45 minutes under nitrogen pressure. A second system, prepared exactly as the first was set up. Dry ether (~100 mL) was added to this second system, followed by addition of 1,6–dibromohexane (53.8 g, 202.5 mmol). This was then cooled to 0 ºC

and the phenyl lithium complex was transferred *via* cannula to the second system at a fast drop–wise rate. The second system was then fitted with a glass stopper and allowed to warm to room temperature and stir overnight. The final solution was a pale yellow color. The solvent was removed under reduced pressure leaving an orange liquid with a white precipitate. An extraction was performed with hexanes and water. The organic layer was kept and the solvent removed under reduced pressure. A distillation of the reaction material (0.3 torr) was completed and the last fraction (82 °C) was found to be the desired product (85 % pure by GCMS). This was not purified further and was used in the next step as ^{1}H NMR spectrum was consistent with the desired product.[62]

1–bromo–6–phenylhexane (~7.3 g, ~30 mmol) was added to triethyl phosphite (25 mL, 143.7 mmol) in a round bottom flask fixed with a condenser under inert atmosphere. This was allowed to reflux overnight until all the starting bromide was gone (GCMS). Excess triethylphosphite and other side products were removed under vacuum (approximately 0.1 torr) and with heating at 40 °C for 6 hours. This was followed by purification using column chromatography (stationary phase: silica, mobile phase: 2: 1 hexanes: ethyl acetate). The desired product had an R_f = 0.55 and was isolated as an oil (PJH–I–37, 6.481 g, 30 % yield over 2 steps). ^{1}H NMR (400.14 MHz, $CDCl_3$) δ 7.28–7.22 (m, 2H), 7.19 – 7.14 (m, 3H), 4.07 – 3.98 (m, 4H), 2.59 (t, J = 7.74 Hz, 2H), 1.71 – 1.52 (m, 6H), 1.50 – 1.32 (m, 4H), 1.29 (t, J = 7.05 Hz, 6H) ^{13}C{^{1}H} NMR (100.61 MHz, $CDCl_3$) δ 142.2, 128.0 (2H), 127.9 (2H), 125.3, 61.05 (d, J = 6.5 Hz, 2C), 35.53, 30.89, 30.11 (d, J = 6.8 Hz), 28.39, 25.31 (d, J = 140.5 Hz), 22.03 (d, J = 5.1 Hz), 16.17 (d, J = 5.9 Hz). ^{31}P{^{1}H} NMR (161.97 MHz, CD_2Cl_2): δ 32.68. Analysis calculated (found) %: C 64.41 (63.46), H 9.12 (9.03). MS (FAB, m/z): 299.1 ([M^+], 100 %). Exact mass

calculated (found) for $[M+H]^+$, m/z): 299.17761 (299.17533).[c]

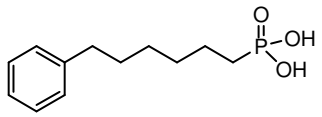

6–phenylhexylphosphonic acid

6–phenyl hexylphosphonate (2.00 g, 6.71 mmol) was dissolved in dry dichloromethane (20 mL) in a round bottom flask. Bromotrimethylsilane (3.05 mL, 23.49 mmol) was added and the flask was capped with a grease stopper and allowed to stir for 2 hours. The volatiles were removed under reduced pressure, methanol was added, and the reaction was stirred. After one hour the solvent was removed under reduced pressure and the product recrystallized from acetonitrile to yield a white solid (PJH–I–40a,b,c,d,e; 1.294 g (80 % yield). ^{1}H NMR (300 MHz, DMSO) δ 7.28–7.10 (m, 5H), 2.54 (t, J = 7.64 Hz, 2H), 1.60–1.15 (m, 10H). ^{13}C{^{1}H} NMR (125.77 MHz, $CDCl_3$) δ 142.59, 128.36 (2H), 128.24 (2H), 125.62, 35.80, 31.13, 30.21 (d, J = 8.18 Hz), 28.63, 25.08 (d, J = 144.63 Hz), 21.91 (d, J = 4.5 Hz). ^{31}P{^{1}H} NMR (161.97 MHz, DMSO): δ 37.88. Analysis calculated (found) %: C 59.50 (59.64), H 7.91 (7.93). MS (FAB, m/z): 243 ($[M^+]$, 100 %). Exact mass calculated (found) for $[M+H]^+$, m/z): 243.11501 (243.11314).

[c] As the elemental analysis did not pass, the appropriate NMR spectra are shown in Appendix A.

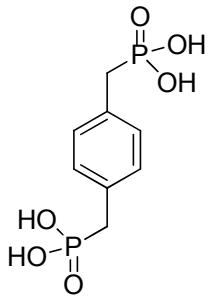

1,4–phenylenebis(methylene)diphosphonic acid

1,4–bis(bromomethyl)benzene (10.00 g, 37.9 mmol) was added to triethyl phosphite (39 mL, 227.3 mmol) in a round bottom flask and the mixture heated to 130 °C overnight while stirring. Excess triethylphosphite and other side products were removed under vacuum (approximately 0.1 torr) and with heating at 50 °C for 6 hours to yield a waxy white crystalline solid (PJH–II–37a, 14.17 g, 99 % yield). ^{1}H NMR spectrum is consistent for tetraethyl 1,4–phenylenebis(methylene)diphosphonate.[63]

Tetraethyl 1,4–phenylenebis(methylene)diphosphonate (4.00 g, 10.5 mmol) was dissolved in anhydrous dichloromethane (50 mL) in a round bottom flask and stirred. Bromotrimethylsilane (8.9 mL, 68.7 mmol) was added *via* syringe. The flask was capped with a greased glass stopper and allowed to stir for 4 hours. The volatiles were removed under reduced pressure and methanol (35 mL) was added and this was stirred 4 hours more. The solvent was removed under reduced pressure and the resulting white solid recrystallized in acetonitrile to yield a white powder (PJH–II–41a, 2.75 g, 99 % yield). ^{1}H NMR spectrum is consistent with the desired product.[64]

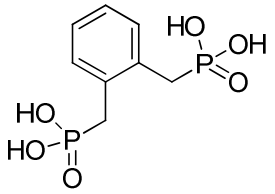

1,2–phenylenebis(methylene)diphosphonic acid

1,2–bis(bromomethyl)benzene (10.00 g, 37.9 mmol) was added to triethyl phosphite (39 mL, 227.3 mmol) in a round bottom flask and the mixture heated to 130 °C overnight while stirring. Excess triethylphosphite and other side products were removed under vacuum (approximately 0.1 torr) and with heating at 50 °C for 6 hours to yield a waxy white crystalline solid (PJH–II–36a, 14.00 g, 98 % yield). ^{1}H NMR spectrum is consistent for tetraethyl 1,2–phenylenebis(methylene)diphosphonate.[65, 66]

Tetraethyl 1,2–phenylenebis(methylene)diphosphonate (4.00 g, 10.5 mmol) was dissolved in anhydrous dichloromethane (50 mL) in a round bottom flask and stirred. Bromotrimethylsilane (8.9 mL, 68.7 mmol) was added *via* syringe. The flask was capped with a greased glass stopper and allowed to stir for 4 hours. The volatiles were removed under reduced pressure and methanol (35 mL) was added and this was stirred 4 hours more. The solvent was removed under reduced pressure and the resulting white solid recrystallized in acetonitrile to yield a white powder (PJH–II–40a, 2.80 g, 100 % yield). ^{1}H NMR spectrum is consistent with the desired product.[65]

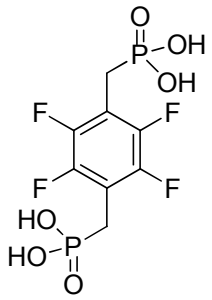

(perfluoro–1,4–phenylene)bis(methylene)diphosphonic acid

1,2,4,5–tetrafluoro–3,6–dimethylbenzene (5.00 g, 28.1 mmol) was dissolved in carbon tetrachloride (50 mL) in a 2–necked round bottom flask. The solution was stirred and heated under two 120 W tungsten lamps. After heating for 20 minutes, bromine (3.08 mL, 60.2 mmol) was added slowly over 4 hours *via* an addition funnel. After 5 hours the reaction was stopped and any excess bromine neutralized with sodium thiosulfate. Dichloromethane was added and the mixture washed twice with water (25 mL). The organic layer was kept and the solvent removed under reduced pressure. The resulting white solid was redissolved in a minimum amount of dichloromethane and passed through a syringe filter. The solvent was removed under reduced pressure and the product recrystallized from ethanol to yield a white crystalline solid (PJH–II–38a, 6.45 g, 68 % yield). ^{1}H NMR (500 MHz, $CDCl_3$) δ 4.50 (4H). ^{1}H NMR spectrum is consistent with the desired product (1,4–bis(bromomethyl)–2,3,5,6–tetrafluorobenzene).[67, 68]

1,4–bis(bromomethyl)–2,3,5,6–tetrafluorobenzene (3.00 g, 8.93 mmol) and triethylphosphite (9.2 mL, 53.6 mmol) were combined in a round bottom flask, heated to 125 °C, and stirred overnight. Upon cooling a white precipitate formed. This was filtered and washed with cold hexanes to yield a white solid (PJH–II–39a, 3.185 g, 79 % yield). ^{1}H NMR (400 MHz, $CDCl_3$) δ 4.15 – 4.07 (m, 8H), 3.25 (d, J = 20.2 Hz, 4H), 1.29 (t, J =

7.0 Hz, 12H). ^{1}H NMR spectrum is consistent with the desired product (tetraethyl (perfluoro–1,4–phenylene)bis(methylene)diphosphonate).[69]

Tetraethyl (perfluoro–1,4–phenylene)bis(methylene)diphosphonate (2.00 g, 4.44 mmol) was dissolved in dry methylene chloride (25 mL). To this was added bromotrimethylsilane (3.5 mL, 26.6 mmol) *via* syringe. The flask was capped with a greased glass stopper and allowed to stir for 4 hours. The solvent was removed under reduced pressure and methanol (20 mL) was added. The reaction was allowed to stir for 3 hours. The solvent was removed under reduced pressure to yield a white solid which was washed multiple times with acetonitrile and dichloromethane, recovering the product each time by centrifugation. The desired product was obtained as a white solid (PJH–II–44p, 1.04 g, 69 % yield). ^{1}H NMR (d_6–DMSO, 400 MHz): δ 3.05 (d, J = 19.2 Hz, 4H). ^{13}C{^{1}H} NMR (d_6–DMSO, 100 MHz): δ 146 – 145 (m, 2C), 143 – 142 (m, 2C), 112 – 111 (m, 2C), 23.62 (d, J = 133.5 Hz, 2C). ^{31}P{^{1}H} NMR (d_6–DMSO, 162 MHz): δ 17.98. Analysis calculated (found) %: C 28.42 (28.61), H 2.39 (2.23). MS (FAB, m/z): 338.9 ([M+H]$^{+}$, 93 %). Exact mass calculated (found) for [M+H]$^{+}$, m/z): 338.98105 (338.98119).

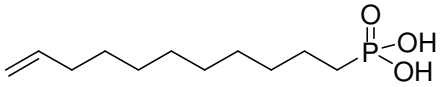

Undec–10–enylphosphonic acid

11–bromo–1–undecene (10.73 g, 46 mmol) was combined with triethyl phosphite (19.11 g, 115 mmol) in a round bottom flask and the mixture was refluxed at 130 °C for 25 hours. Excess triethylphosphite and other side products were removed under vacuum

(approximately 0.1 torr) and with heating at 45 °C for 6 hours to yield a colorless liquid (PJH–I–73g, 10.26 g, 81 % yield). GCMS trace and ^{1}H NMR spectrum are consistent with the desired product.[70]

The phosphonate (1.5 g, 5.17 mmol) was dissolved in dichloromethane (15 mL) in a round bottom flask. Bromotrimethylsilane (1.98 g, 12.92 mmol) was added and the flask capped with a greased cap. After 2 hours the solvent was removed under reduced pressure and methanol (25 mL) was added and the reaction allowed stirred for 1 hour longer. The solvent was removed under reduced pressure and the product recrystallized twice from acetonitrile to yield a white crystalline solid (PJH–I–75c,e; 0.911 g, 75 % yield). ^{1}H NMR (400 MHz, DMSO) δ 5.84 – 5.72 (m), 4.98 (dd, *J* = 17.15, 1.33 Hz), 4.92 (dd, *J* = 10.17, 1.07 Hz), 2.03 – 1.96 (m, 2H), 1.50 – 1.21 (m, 16H). ^{13}C{^{1}H} NMR (100.61 MHz, DMSO) δ 138.8, 114.6, 33.22, 30.08 (d, *J* = 16.0 Hz), 28.88 (2C), 28.71, 28.55, 28.31, 27.47 (d, *J* = 136.7 Hz), 22.69 (d, *J* = 4.4 Hz). ^{31}P{^{1}H} NMR (161.97 MHz, DMSO): δ 27.70. Analysis calculated (found) %: C 56.39 (55.94), H 9.90 (9.81). MS (FAB, m/z): 235.1 ([M+H]$^{+}$, 34%). Exact mass calculated (found) for [M+H]$^{+}$, m/z: 235.14631 (235.14699).[d]

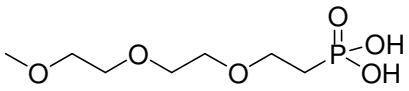

2–(2–(2–methoxyethoxy)ethoxy)ethylphosphonic acid

The synthesis for this molecule was followed from the literature;[48] the only modification being the absence of dioxane from the Arbuzov reaction. The total yield

[d] As the elemental analysis did not pass, the appropriate NMR spectra are shown in Appendix A.

over 3 steps was 28 %. ^{1}H NMR spectrum was consistent with the desired product.

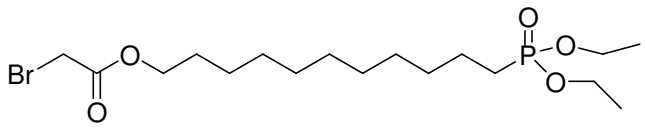

11–(diethoxyphosphoryl)undecyl 2–bromoacetate

This compound was synthesized in a manner analogous to a procedure found in the literature.[53] Diethyl 11–hydroxyundecylphosphonate (1.00 g, 3.24 mmol) and triethylamine (0.328 g, 3.24 mmol) were dissolved in dry dichloromethane (20 mL) in a round bottom flask under inert atmosphere. The reaction mixture was cooled to 0 °C and bromo–isobutyryl bromide (0.719 g, 3.56 mmol) was added dropwise *via* syringe. The reaction was stopped after 3.5 hours and the product isolated using column chromatography (silica) using ethyl acetate as the eluent. The product (R_f = 0.54) was isolated as an orange oil (PJH–I–120a, 1.050 g, 75 % yield). ^{1}H NMR spectrum (consistent with the desired product) missing elemental analysis were obtained. Analysis calculated (found) %: C 47.65 (47.56), H 7.86 (7.98).[e]

[e] This molecule was previously synthesized (Simon Jones, Marder Group) and only elemental analysis was needed to complete the characterization.

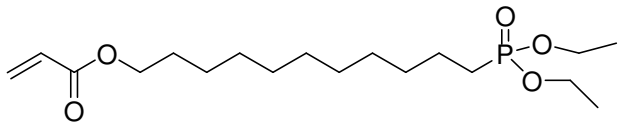

11–(diethoxyphosphoryl)undecyl acrylate

Diethyl 11–hydroxyundecylphosphonate (5.00 g, 16.2 mmol), triethylamine (2.26 mL, 16.2 mmol) and hydroquinone (spatula tip) were dissolved in dry toluene (100 mL) in a round bottom flask under inert atmosphere. The reaction mixture was stirred and cooled to 0 °C in an ice bath and acryloyl chloride (1.54 g, 17.0 mmol) was added dropwise *via* syringe. The reaction was stopped after 90 minutes and filtered. The organic layer was washed with brine and water and then dried over magnesium sulfate, filtered and the solvent removed under reduced pressure to yield a brown oil. The desired product was isolated *via* column chromatography (stationary phase: silica gel, mobile phase: ethyl acetate) (R_f = 0.56) as a yellow oil (PJH–II–58a, 4.21 g, 72 % yield). ^{1}H NMR (300 MHz, $CDCl_3$) δ 6.40 (dd, *J* = 17.32, 1.54 Hz), 6.12 (dd, *J* = 17.32, 10.40 Hz), 5.81 (dd, *J* = 10.36, 1.54 Hz), 4.17 – 4.02 (m, 4H), 4.14 (t, *J* = 6.75 Hz, 2H), 1.80 – 1.50 (m, 6H), 1.42 – 1.22 (m, 20H). ^{13}C{^{1}H} NMR (75.45 MHz, $CDCl_3$) δ 166.55, 130.66, 128.88, 64.91, 61.61 (d, *J* = 6.88 Hz, 2C), 30.82 (d, *J* = 17.21 Hz), 29.69 (2C), 29.55, 29.44, 29.31, 28.84, 26.13, 25.89 (d, *J* = 139.97 Hz), 22.62 (d, *J* = 4.59 Hz), 16.71 (d, *J* = 5.74 Hz, 2C). ^{31}P{^{1}H} NMR (161.97 MHz, C_6D_6): δ 32.43. Analysis calculated (found) %: C 59.65 (58.95), H 9.73 (9.66). MS (FAB, m/z): 363.2 ($[M+H]^+$, 100 %). Exact mass calculated (found) for $[M+H]^+$, m/z: 363.23004 (363.23106).[f]

[f] As the elemental analysis did not pass, the appropriate NMR spectra are shown in Appendix A.

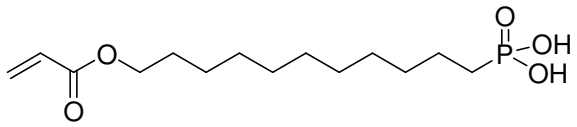

11–(acryloyloxy)undecylphosphonic acid

11–(diethoxyphosphoryl)undecyl acrylate (4.00 g, 11.0 mmol) was dissolved in dry dichloromethane (40 mL). Bromotrimethylsilane (4.3 mL, 33.0 mmol) was added *via* syringe and the flask was capped with a greased stopper and allowed to stir for 2 hours. The volatiles were removed under reduced pressure and water (25 mL) added to the product mixture upon which a white precipitate appeared. This was allowed to stir for 2 hours. Filtration afforded a white solid (PJH–II–60a,c; 3.275 g, 97 % yield). ^{1}H NMR (300 MHz, $CDCl_3$) δ 9.82 (br, s, 2H), 6.40 (dd, *J* = 17.32, 1.61 Hz), 6.12 (dd, *J* = 17.32, 10.41 Hz), 5.81 (dd, *J* = 10.40, 1.60 Hz), 4.15 (t, *J* = 6.73 Hz, 2H), 1.82 – 1.50 (m, 6H), 1.42 – 1.18 (m, 14H). ^{13}C{^{1}H} NMR (125.77 MHz, $CDCl_3$) δ 166.76, 130.85, 129.05, 65.12, 30.87 (d, *J* = 17.38 Hz), 29.89, 29.88, 29.76, 29.65, 29.46, 29.01, 26.33, 25.76 (d, *J* = 143.86 Hz), 22.45 (d, *J* = 4.85 Hz). ^{31}P{^{1}H} NMR (161.97 MHz, $CDCl_3$): δ 38.76. Analysis calculated (found) %: C 54.89 (55.09), H 8.88 (8.79). MS (FAB, m/z): 307.2 ($[M+H]^+$, 100 %). Exact mass calculated (found) for $[M+H]^+$, m/z: 307.16744 (307.16770).

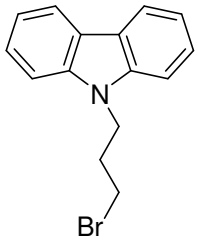

9–(3–bromopropyl)–9*H*–carbazole

Carbazole (15.00 g, 89.71 mmol) and 1,3–dibromopropane (45.5 mL, 450 mmol) were dissolved in dry tetrahydrofuran (200 mL) in a round bottom flask and stirred under inert atmosphere. Sodium hydride (3.23 g, 134.56 mmol) was added and the mixture was brought to reflux and allowed to stir for 40 hours. After cooling to room temperature the mixture was diluted in water (800 mL) and extracted with ethyl acetate. The organic layer was dried over magnesium sulfate and the solvent removed under reduced pressure to yield an orange oil and light brown solid. Excess dibromopropane was removed under high vacuum (0.05 torr) while heating to 100 °C for 2 hours. The product was purified using column chromatography (stationary phase: silica, mobile phase: 30: 1 hexanes: ethyl acetate) (R_f = 0.45) and was isolated as a viscous yellow oil. This oil was dissolved in hot ethanol and put in a freezer (–20 °C) overnight to yield a white solid (PJH–I–144c, 7.70 g, 30 % yield). The ^{1}H NMR spectrum is consistent with the desired product.[71]

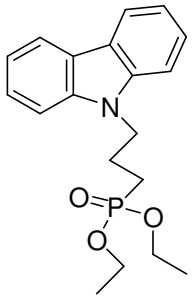

Diethyl 3–(9*H*–carbazol–9–yl)propylphosphonate

Triethylphosphite (13.4 mL, 80.1 mmol) was added *via* syringe to 9–(3–bromopropyl)–9*H*–carbazole (7.70 g, 26.7 mmol) in a round bottom flask. The reaction was heated and stirred under inert atmosphere at 130 °C for 18 hours. Excess triethylphosphite and other side–products were removed under vacuum (approximately 0.1 torr) and with heating at 100 °C for 6 hours to yield a viscous yellow oil (PJH–I–147e, 8.50 g, 92 % yield). ^{1}H NMR (400.14 MHz, CD_2Cl_2) δ 8.10 (dt, *J* = 7.73, 2.00 Hz, 2H), 7.50–7.44 (m, 4H), 7.27–7.19, m, 2H), 4.43 (t, *J* = 7.00 Hz, 2H), 4.10–3.95 (m, 4H), 2.23–2.09 (m, 2H), 1.74 (dt, *J* = 18.41, 7.80 Hz, 2H), 1.26 (t, *J* = 7.00 Hz, 6H). ^{13}C{^{1}H} NMR (100.62 MHz, CD_2Cl_2) δ 139.99 (2C), 125.36 (2C), 122.42 (2C), 119.88 (2C), 118.56 (2C), 108.37 (2C), 61.18 (d, *J* = 6.44 Hz), 42.52 (d, *J* = 15.39 Hz), 22.59 (d, *J* = 141.97 Hz), 21.75 (*J* = 4.83 Hz), 15.91 (d, *J* = 5.84 Hz). ^{31}P{^{1}H} NMR (161.97 MHz, CD_2Cl_2): δ 31.22. Analysis calculated (found) %: C 65.67 (66.07), H 7.01 (7.00), N 4.05 (4.06). MS (EI, m/z): 345.2 ([M], 100 %). Exact mass calculated (found) for [M], m/z: 345.14938 (345.14264).

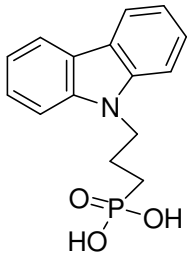

3–(9*H*–carbazol–9–yl)propylphosphonic acid

Diethyl 3–(9*H*–carbazol–9–yl)propylphosphonate (1.00 g, 2.89 mmol) was dissolved in anhydrous dichloromethane (20 mL) in a round bottom flask. Bromotrimethylsilane (1.12 mL, 8.67 mmol) was added *via* syringe. The flask was capped with a greased glass stopper and allowed to stir for 90 minutes. The volatiles were removed under reduced pressure and 1: 1 methanol: water (30 mL) was added. The solution turned a cloudy whitish/grey. The solvent was removed under reduced pressure and the product recrystallized from 2: 1 water: acetone (PJH–II–5a, grey powder, 612 mg) and 1: 1 water: methanol (PJH–II–5c, glassy grey solid, 42 mg). Both recrystallization solvents yielded pure product. Total yield was 78 %. ^{1}H NMR (400.14 MHz, DMSO) δ 8.15 (d, *J* = 8.00 Hz, 2H), 7.65 (d, *J* = 8.00 Hz, 2H), 7.45 (dt, *J* = 15.41, 1.00 Hz, 2H), 7.19 (t, *J* = 14.81 Hz, 2H), 4.48 (t, *J* = 13.60 Hz, 2H), 2.03 – 1.89 (m, 2H), 1.59 – 1.46 (m, 2H). ^{13}C{^{1}H} NMR (100.62 MHz, DMSO) δ 140.01 (2C), 125.76 (2C), 122.07 (2C), 120.33 (2C), 118.78 (2C), 108.33 (2C), 42.48 (d, *J* = 17.31 Hz), 25.00 (d, *J* = 137.35 Hz), 22.67 (d, *J* = 4.13 Hz). ^{31}P{^{1}H} NMR (161.97 MHz, DMSO): δ 26.78. Analysis calculated (found) %: C 62.28 (62.27), H 5.58 (5.56), N 4.84 (4.73). MS (FAB, m/z): 290 ([M+H]$^{+}$, 100 %). Exact mass calculated (found) for [M+H]$^{+}$, m/z): 290.09461 (290.09405)

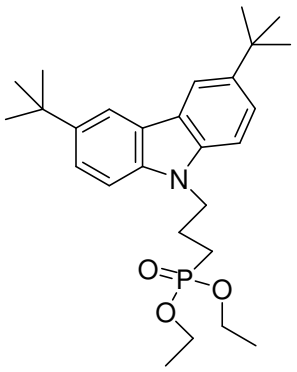

Diethyl 3–(3,6–di–tert–butyl–9*H*–carbazol–9–yl)propylphosphonate

Diethyl 3–(9*H*–carbazol–9–yl)propylphosphonate (1.00 g, 2.89 mmol) was dissolved in 2–chloro–2–methylpropane (5.0 mL) and flushed with N_2 for 5 minutes. Aluminum chloride (1.16 g, 8.67 mmol) was added slowly to the solution while stirring. The solution black, bubbled, and a precipitate formed. The reaction was allowed to stir for 25 minutes after adding all the aluminum chloride. It was then quenched with 25 mL water and the organic separated and washed with water followed by 1 M NaOH (2 × 20 mL), then another water washing. The yellow organic layer was kept, dried over magnesium sulfate and the solvent removed under vacuum. Column chromatography (stationary phase: silica, mobile phase: ethyl acetate) was used to isolate the desired product (R_f = 0.37) as a viscous yellow oil (PJH–II–4a, 447 mg, 34 % yield). ^{1}H NMR (400.14 MHz, CD_2Cl_2) δ 8.10 (d, *J* = 1.6 Hz, 2H), 7.52 (dd, *J* = 8.80, 2.00 Hz, 2H), 7.35 (d, 8.40 Hz, 2H), 4.36 (t, *J* = 7.00 Hz, 2H), 4.08 – 3.93 (m, 4H), 2.21 – 2.07 (m, 2H), 1.71 (dt, *J* = 18.14 Hz, 6.00 Hz, 2H), 1.45 (18H), 1.25 (t, *J* = 7.00 Hz, 6H). ^{13}C{^{1}H} NMR (100.61 MHz, CD_2Cl_2) δ 142.14 (2C), 139.26 (2C), 123.80 (2C), 123.06 (2C), 116.68 (2C), 108.50 (2C), 61.89 (d, *J* = 6.4 Hz, 2C), 43.36 (d, *J* = 15.8 Hz), 34.92 (2C), 32.19 (6C), 23.35 (d, 142.2 Hz), 22.59 (d, *J* = 4.9 Hz), 16.64 (d, *J* = 5.8 Hz, 2C). ^{31}P{^{1}H} NMR

(161.97 MHz, CD_2Cl_2): δ 31.34. Analysis calculated (found) %: C 70.87 (70.59), H 8.81 (8.91), N 3.06 (2.98). MS (FAB, m/z): 457.2 ([M], 100 %). Exact mass calculated (found) for [M], m/z: 457.27458 (457.27546).

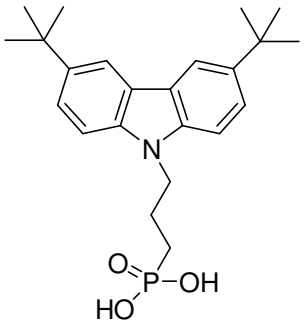

Diethyl 3–(3,6–di–tert–butyl–9*H*–carbazol–9–yl)propylphosphonic acid

Diethyl 3–(3,6–di–tert–butyl–9*H*–carbazol–9–yl)propylphosphonate (420 mg, 0.92 mmol) was dissolved in dichloromethane (10 mL) and stirred. Bromotrimethylsilane (0.36 mL, 2.75 mmol) was added *via* syringe and the solution turned dark purple. The flask was then capped with a greased glass stopper and allowed to stir for 2 hours. The volatiles were removed under reduced pressure and the mixture redissolved in a 1:1 methanol: dichloromethane mixture and allowed to stir for 2 more hours. The solvents were removed under reduced pressure and the reaction residue redissolved in 1: 1 methanol: water mixture and the solvent was again removed under reduced pressure to yield a grey solid (PJH–II–6c, 165 mg, 45 % yield). Alternatively, acetonitrile was used in a later reaction to recrystallize the compound to yield a beige solid. ^{1}H NMR (400.14 MHz, DMSO) δ 8.17 (2H), 7.52–7.45 (m, 4H), 4.39 (t, *J* = 6.67 Hz, 2H), 2.00–1.86 (m, 2H), 1.53–1.43 (m, 2H), 1.40 (18H). ^{13}C{^{1}H} NMR (125.77 MHz, DMSO) δ 140.97

(2C), 138.53 (2C), 123.18 (2C), 122.00 (2C), 116.34 (2C), 108.60 (2C), 42.51 (d, J = 17.36 Hz), 34.41 (2C), 31.92 (6C), 25.07 (d, 137.22 Hz), 22.73 (d, J = 4.02 Hz). $^{31}P\{^{1}H\}$ NMR (161.98 MHz, DMSO): δ 26.79. Analysis calculated (found) %: C 68.81 (67.08), H 8.03 (7.91), N 3.49 (3.61). MS (ESI, m/z): 402 ($[M+H]^+$, 78 %). Exact mass calculated (found) for $[M+H]^+$, m/z): 402.219259 (402.220000).[g]

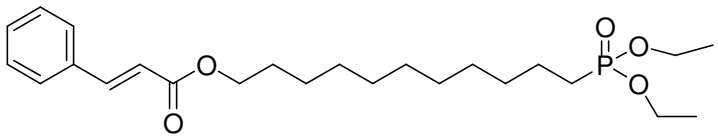

11–(diethoxyphosphoryl)undecyl cinnamate

Diethyl 11–hydroxyundecylphosphonate (1.00 g, 3.24 mmol) was combined with triethylamine (0.48 mL, 3.40 mmol) in anhydrous dichloromethane (15 mL) in a round bottom flask. The reaction mixture was cooled to 0° C and cinnamoyl chloride (566 mg, 3.40 mmol) was added dropwise. The reaction was stirred for 2 hours. Several new spots were visible on TLC (ethyl acetate). The reaction mixture was washed with 1 M NaOH (3 × 20 mL), saturated sodium thiosulfate, and water. The organic layer was kept, dried over magnesium sulfate, filtered, and the solvent removed under reduced pressure. Column chromatography (stationary phase: silica, mobile phase: ethyl acetate) was used to isolate the desired product (R_f = 0.60) as a yellow–tinted oil (PJH–II–11a, 580 mg, 41 % yield). ^{1}H NMR (400.13 MHz, $CDCl_3$) δ 7.68 (d, J = 16.02 Hz), 7.53 (m, 2H), 7.38 (m, 3H), 6.44 (d, J = 16.02 Hz), 4.20 (t, J = 6.74 Hz, 2H), 4.08 (m, 4H), 1.79–1.49 (m, 6H), 1.43–1.22 (m, 20H). $^{13}C\{^{1}H\}$ NMR (100.61 MHz, $CDCl_3$) δ 167.02, 144.48, 134.39, 130.14,

[g] As the elemental analysis did not pass, the appropriate NMR spectra are shown in Appendix A.

128.79 (2C), 127.97 (2C), 118.21, 64.65, 61.28 (d, J = 6.54 Hz, 2C), 30.54 (d, J = 16.94), 29.42 (2C), 29.28, 29.20, 29.02, 28.65, 25.90, 25.62 (d, J = 140.40 Hz), 22.33 (d, J = 5.21 Hz), 16.42 (d, J = 5.92 Hz, 2C). $^{31}P\{^{1}H\}$ NMR (161.98 MHz, $CDCl_3$): δ 33.32. Analysis calculated (found) %: C 65.73 (65.39), H 8.96 (9.05). MS (ESI, m/z): 439 ($[M+H]^+$, 100 %). Exact mass calculated (found) for $[M+H]^+$, m/z): 439.26079 (439.25720).

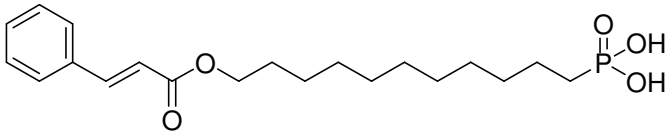

(*E*)–11–(cinnamoyloxy)undecylphosphonic acid

11–(diethoxyphosphoryl)undecyl cinnamate (545 mg, 1.24 mmol) was dissolved in anhydrous dichloromethane (15 mL) in a round bottom flask and stirred. Bromotrimethylsilane (609 mg, 3.98 mmol) was added *via* syringe. The flask was capped with a greased glass stopper and allowed to stir for 90 minutes. The volatiles were removed under reduced pressure and a 1: 3 mixture of methanol: water (20 mL) was added. The solvents were removed under reduced pressure and the product recrystallized from acetonitrile to yield a white crystalline solid (PJH–II–13a, 425 mg, 90 % yield). ^{1}H NMR (500.13 MHz, $CDCl_3$) δ 7.70 (m, 2H), 7.63 (d, J = 16.00 Hz), 7.41 (m, 3H), 6.62 (d, J = 16.00 Hz), 4.12 (t, J = 6.50 Hz, 2H), 1.66–1.57 (m, 2H), 1.51–1.38 (m, 4H), 1.37–1.18 (m, 14H). $^{13}C\{^{1}H\}$ NMR (125.76 MHz, DMSO) δ 166.25, 144.38, 134.01, 130.44, 128.90 (2C), 128.34 (2C), 118.12, 64.03, 30.09 (d, J = 15.94 Hz), 28.97, 28.95, 28.88, 28.71, 28.69, 28.21, 27.54 (d, J = 136.52 Hz), 25.43, 22.73 (d, J = 4.65 Hz). $^{31}P\{^{1}H\}$

NMR (161.98 MHz, DMSO): δ 27.72. Analysis calculated (found) %: C 62.81 (62.51), H 8.17 (8.21). MS (ESI): Exact mass calculated (found) for $[M+H]^+$, m/z):383.198189 (383.197378).

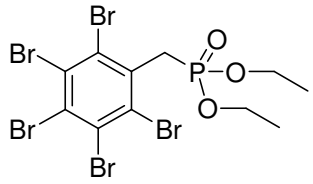

Diethyl perbromobenzylphosphonate

Perbromobenzylbromide (4.50 g, 7.96 mmol) was combined with triethylphosphite (4.36 g, 26.3 mmol) in a round bottom flask and heated at 135° C for 15 hours. A solid precipitated upon cooling and was filtered and washed with hexanes to yield a beige powder (PJH–II–49a, 4.237 g, 85 % yield) ^{1}H NMR (500.13 MHz, $CDCl_3$) δ 4.16–4.10 (m, 4H), 4.01 (d, *J* = 22.5 Hz, 2H), 1.32 (t, *J* = 7.00 Hz, 6H). $^{31}P\{^1H\}$ NMR (202.46 MHz, $CDCl_3$): δ 22.76. ^{1}H and ^{31}P NMR spectra are consistent with the desired product.[72]

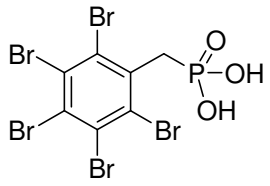

Perbromobenzylphosphonic acid

Diethyl perbromobenzylphosphonate (4.00 g, 6.42 mmol) was dissolved in anhydrous dichloromethane (20 mL) in a round bottom flask and stirred. Bromotrimethylsilane (3.44 g, 22.5 mmol) was added *via* syringe. The flask was capped with a greased glass stopper and allowed to stir for 4 hours. The volatiles were removed under reduced pressure, methanol (25 mL) was added and this was heated at 85° C for 4 hours. A precipitate formed upon cooling. This was filtered and washed with acetonitrile to yield a white powder (PJH–II–51e, 3.19 g, 88 % yield). ^{1}H NMR (400.14 MHz, DMSO) δ 3.77 (d, J = 21.72 Hz, 2H). ^{13}C{^{1}H} NMR (100.61 MHz, DMF) δ 139.10, 129.09 (d, J = 3.90 Hz, 2C), 128.33 (d, J = 6.64 Hz, 2C), 127.11, 42.87 (d, J = 130.5 Hz). ^{31}P{^{1}H} NMR (161.97 MHz, DMSO): δ 17.59. Analysis calculated (found) (calculated) %: C 14.84 (15.05), H 0.71 (0.77), Br 70.51 (70.63). MS (FAB, m/z): 566.5 ([M+H]$^{+}$, 15%). Exact mass calculated (found) for [M+H]$^{+}$, m/z): 566.58522 (566.58498).

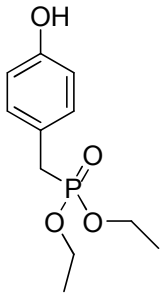

Diethyl 4–hydroxybenzylphosphonate

Diethyl 4–aminobenzylphosphonate (5.00 g, 20.56 mmol) was dissolved in 2 N HCl to yield a dark brown solution. This was cooled in an ice/salt bath and sodium nitrite (1.42 g, 20.56 mmol), dissolved in water (25 mL), was added dropwise over 10 minutes. After stirring for another 20 minutes the solution was heated at 70 °C for 90 minutes. After cooling to room temperature, the flask contained a brown clear layer and a dark–brown oil. The organic layer was extracted with ether (3 × 35 mL) and dried over magnesium sulfate. The solution was filtered and the solvent removed under reduced pressure to yield a reddish–brown oil. Column chromatography (stationary phase: silica, mobile phase: ethyl acetate, iodine stain used for TLC) was used to isolate the desired product (R_f = 0.46) as a glassy yellow solid which was then recrystallized in toluene (3 ×) to yield a white solid (PJH–II–81l, 2.55 g, 51 % yield). ^{1}H NMR (500.13 MHz, $CDCl_3$) δ 7.02 (dd, *J* = 8.50, 2.50 Hz, 2H), 6.60 (d, *J* = 8.5 Hz, 2H), 4.06 – 3.97 (4H), 3.04 (d, *J* = 20.5 Hz, 2H), 1.25 (t, *J* = 7.00 Hz, 6H). ^{31}P{^{1}H} NMR (161.98 MHz, $CDCl_3$): δ 28.18. NMR spectra are consistent with the desired product.[58]

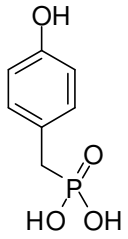

4–hydroxybenzylphosphonic acid

Diethyl 4–hydroxybenzylphosphonate (2.55 g, 10.44 mmol) was dissolved in anhydrous dichloromethane (20 mL). Bromotrimethylsilane (4.75 mL, 36.6 mmol) was added *via* syringe and the flask was capped with a greased glass stopper and the reaction allowed to stir for 2.5 hours. The volatiles were removed under reduced pressure and 50: 1 mixture of methanol: water (20 mL) was added. The reaction was allowed to stir overnight. The solvents were removed under reduced pressure and the remaining solid washed/recrystallized from hot acetonitrile to yield a white powdery solid (PJH–II–83d, 1.495 g, 76 % yield). ^{1}H NMR (500.13 MHz, DMSO) δ 7.01 (dd, *J* = 8.50, 2.00 Hz, 2H), 6.64 (d, *J* = 8.5 Hz, 2H), 2.81 (d, *J* = 20.5 Hz, 2H). ^{31}P{^{1}H} NMR (161.98 MHz, DMSO): δ 23.07. NMR spectra are consistent with the desired product.[73]

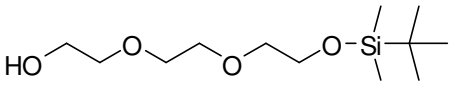

2,2,3,3–tetramethyl–4,7,10–trioxa–3–siladodecan–12–ol

Triethylene glycol (8.9 mL, 66.6 mmol), *t*–butyldimethylchlorosilane (5.02 g, 33.3 mmol), and imidazole (4.53 g, 66.6 mmol) were combined with dimethylformamide (10 mL) in a round bottom flask and stirred for 10 hours. The reaction mixture was

diluted with ether (40mL) and washed with aqueous potassium carbonate. The aqueous portion was then back extracted with ether (2 × 25 mL). All organic layers were combined, washed with brine, dried over magnesium sulfate, and concentrated under reduced pressure. A silica plug, eluting first with 1: 1 ethyl acetate: hexanes, followed by pure ethyl acetate was used to isolate the desired product (R_f = 0.24, 1: 1 ethyl acetate: hexanes, iodine stain used for TLC) as a clear oil (PJH–II–87c, 3.77 g, 43 % yield). ^{1}H NMR spectrum is consistent with the desired product.[74]

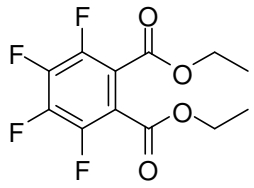

Diethyl 3,4,5,6–tetrafluorophthalate

Tetrafluorophthalic acid (5.00 g, 21 mmol), fuming H_2SO_4 (4.0 mL), and ethanol (50 mL) were all combined in a round bottom flask and refluxed overnight. Upon cooling to room temperature, water (130 mL) was added and the reaction mixture extracted with ether (3 × 30 mL). The desired product (R_f = 0.95, ethyl acetate) was isolated using a silica plug, eluting first with hexanes, then increasing the polarity with ethyl acetate and finally methanol. The final product was isolated as a clear oil (PJH–II–89a, 2.61 g, 42 % yield). ^{1}H NMR spectrum is consistent with the desired product.[75]

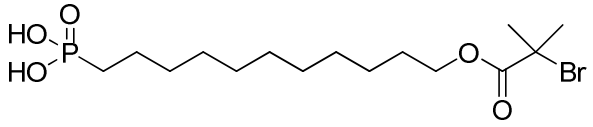

11–(2–bromo–2–methylpropanoyloxy)undecylphosphonic acid

11–(diethoxyphosphoryl)undecyl 2–bromo–2–methylpropanoate (1.00 g, 2.19 mmol) was dissolved in anhydrous dichloromethane (20 mL) and stirred. Bromotrimethylsilane (0.94 mL, 7.22 mmol) was then added *via* syringe and the reaction was capped with a greased glass stopper and allowed to stir for 2 hours. The volatiles were removed under reduced pressure and a 3: 1 water: methanol mixture (20 mL) was added. The reaction was allowed to stir for 2 hours. The solvents were removed under reduced pressure and the crude product was recrystallized in mixture of 5: 1 acetonitrile: water to yield a white solid (PJH–II–94b,c; 790 mg, 90 % yield). ^{1}H NMR and ^{31}P NMR spectra are consistent with desired product.[53]

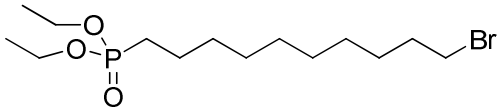

Diethyl 10–bromoodecylphosphonate

1,10–dibromodecane (20.0 g, 66.65 mmol) was combined with triethylphosphite (10.85 mL, 63 mmol) in a round bottom flask, the system purged with N_2, and then the mixture refluxed at 140 °C overnight under inert atmosphere. Excess triethylphosphite and other side products were removed under vacuum (approximately 0.1 torr) and with heating at 90 °C for 4 hours. The desired product (R_f = 0.48, ethyl acetate, iodine stain

used for TLC) was purified using a silica plug, eluting first with hexanes then increasing the solvent polarity with ethyl acetate and then methanol. 8.99 g of starting material (R_f = 0.98, ethyl acetate, iodine stain on TLC) was recovered. A clear oil was isolated (PJH–II–104b, 12.77 g, 97 % yield). ^{1}H NMR spectrum is consistent with the desired product.[76]

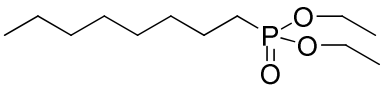

Diethyl octylphosphonate

1–bromooctane (30.0 g, 155 mmol) was combined with triethylphosphite (61 mL, 357 mmol) and the mixture allowed to stir at 140 °C overnight. Excess triethylphosphite and other side products were removed under vacuum (approximately 0.1 torr) and with heating at 65 °C for 7 hours to yield an oil (PJH–II–105a, 38.8 g, 100 % yield). ^{1}H NMR spectrum is consistent with the desired product.[77]

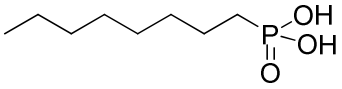

Octylphosphonic acid

Octylphosphonate (38.8 g, 155 mmol) was dissolved in anhydrous dichloromethane (100 mL) and stirred. Bromotrimethylsilane (55 mL, 418 mmol) was added *via* syringe and the reaction capped with a greased glass stopper and stirred for 2 hours. The volatiles were removed under reduced pressure and a mixture of 12: 1

methanol: water was added and the reaction mixture stirred for 3 hours. The solvents were removed under reduced pressure and the product recrystallized from 4: 1 acetonitrile: water to yield a white crystalline solid (PJH–II–111a,b; 20.376 g, 68 % yield). ^{1}H NMR shows a trace impurity of ethylphosphonic acid. Desired product is over 99.5 % pure based on the ^{1}H NMR integrations. ^{1}H NMR spectrum is consistent with desired product.[78]

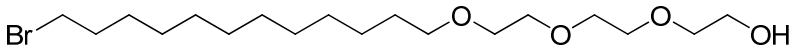

2–(2–(2–(12–bromododecyloxy)ethoxy)ethoxy)ethanol

Triethylene glycol (80.0 mL, 600 mmol) was dissolved in dry dimethylformamide (150 mL) under inert atmosphere. Sodium hydride (2.88 g, 120 mmol) was added to the reaction mixture in small portions. After addition the solution was stirred for 30 minutes followed by the addition of 1,12–dibromododecane (39.2 g, 120 mmol). The reaction mixture was stirred for 4 hours and then diluted with water (200 mL). The product was extracted into ether (3 × 75 mL), washed with 10% potassium carbonate, dried over magnesium sulfate, filtered, and concentrated under reduced pressure. Column chromatography (stationary phase: silica, mobile phase: ethyl acetate) was used to isolated the desired product (R_f = 0.45, ethyl acetate, iodine stain needed for TLC) as a yellow oil (PJH–II–98b, 17.3 g, 52.6 % yield). ^{1}H NMR (400.14 MHz, $CDCl_3$) δ 3.75 – 3.56 (m, 12 H), 3.45 (t, *J* = 6.84 Hz, 2H), 3.40 (t, *J* = 6.88 Hz, 2H), 2.35 (br), 1.85 (quint, *J* = 7.39 Hz, 2H), 1.58 (quint, *J* = 7.06 Hz, 2H), 1.46 – 1.22 (m, 16H). ^{13}C{^{1}H} NMR (100.62 MHz, $CDCl_3$) δ 72.49, 71.49, 70.50, 70.48, 70.23, 69.91, 61.60, 33.98, 32.74,

29.47, 29.45, 29.42, 29.37, 29.33, 28.83, 28.67, 28.08, 25.96. Analysis calculated (found) %: C 54.40 (54.30), H 9.38 (9.55). MS (ESI, m/z): 397.2 (M^+, 97%). Exact mass calculated (found) for $[M+H]^+$, m/z): 397.194798 (397.195700).

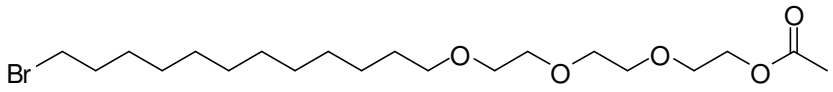

2–(2–(2–(12–bromododecyloxy)ethoxy)ethoxy)ethyl acetate

2–(2–(2–(12–bromododecyloxy)ethoxy)ethoxy)ethanol (17.0 g, 42.8 mmol) was dissolved in anhydrous dichloromethane (100 mL) and the solution cooled to 0 °C. Triethylamine (6.27 mL, 45.0 mmol) was added *via* syringe followed by the dropwise addition of acetyl chloride (3.65 mL, 51.35 mmol) in dichloromethane (25 mL) *via* an addition funnel. The reaction was then allowed to warm up to room temperature and stir for 5 hours more. The formed precipitate was filtered and the filtrate washed with water, dilute HCl, saturated sodium bicarbonate, brine, and then water again. The organic was dried over magnesium sulfate, filtered, and the solvent removed under reduced pressure to yield a yellow oil (PJH–II–99a, 17.86 g, 95 % yield (crude)). A small fraction of this was further purified using column chromatography (stationary phase: silica, mobile phase: ethyl acetate) to isolate the desired product (R_f = 0.80,ethyl acetate, iodine stain needed for TLC). ^{1}H NMR (400.14 MHz, $CDCl_3$) δ 4.22 (t, *J* = 4.78 Hz, 2H), 3.70 (t, *J* = 4.79 Hz, 2H), 3.68 – 3.62 (m, 8H), 3.61 – 3.56 (2H), 3.45 (t, *J* = 6.86 Hz, 2H), 3.41 (t, *J* = 6.94 Hz, 2H), 2.08 (3H), 1.85 (quintet, *J* = 7.20 Hz, 2H), 1.57 (quintet, *J* = 6.92 Hz, 2H), 1.47 – 1.20 (m, 16H). ^{13}C{^{1}H} NMR (100.62 MHz, $CDCl_3$) δ 170.9, 71.43, 70.59, 70.50

(2C), 69.96, 69.03, 63.52, 33.95, 32.74, 29.54, 29.47, 29.44, 29.42, 29.38, 29.33, 28.67, 28.07, 25.99, 20.89. Analysis calculated (found) %: C 54.67 (55.14), H 8.95 (9.03). MS (ESI, m/z): 439.2 (M^+, 100%). Exact mass calculated (found) for $[M+H]^+$, m/z): 439.205362 (439.208300).[h]

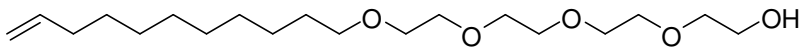

3,6,9,12–tetraoxatricos–22–en–1–ol

Sodium hydride (1.203 g, 50.1 mmol) was added to a solution of tetraethylene glycol (47 mL, 274 mmol) in anhydrous tetrahydrofuran (170 mL) at 0 °C. After stirring for 30 minutes the solution was heated to 80 °C for 2 hours. After the solution turned an orange–brown color, 11–bromoundecene (10.0 mL, 45.6 mmol) was added *via* syringe to the solution and this was stirred at 80 °C for an additional 12 hours. The solution was then cooled to room temperature and extracted with hexanes. This was washed with water and the organic concentrated under reduced pressure. Column chromatography (stationary phase: silica, mobile phase: ethyl acetate) was used to isolate the desired product (R_f = 0.31, ethyl acetate, iodine stain needed for TLC) as a yellow oil (PJH–II–101d, 9.796 g, 62 % yield). ^{1}H NMR (400.14 MHz, $CDCl_3$) δ 5.86 – 5.74 (m, 1H), 4.99 (dd, *J* = 17.12, 1.41 Hz, 1H), 4.93 (dd, *J* = 10.16, 1.48 Hz, 1H), 3.75 – 3.56 (m, 16H), 3.45 (t, *J* = 6.84 Hz, 2H), 2.30 (br), 2.04 (q, 7.06 Hz, 2H), 1.57 (quintet, *J* = 6.91 Hz, 2H), 1.43 – 1.22 (m, 12H). ^{13}C{^{1}H} NMR (100.62 MHz, $CDCl_3$) δ 139.0, 114.0, 72.56, 71.39, 70.46 (2H), 70.42, 70.40, 70.12, 69.89, 61.46, 33.67, 29.42 (2H), 29.31, 29.30, 28.98,

[h] As the elemental analysis did not pass, the appropriate NMR spectra are shown in Appendix A.

28.78, 25.92. Analysis calculated (found) %: C 65.86 (65.57), H 11.05 (11.31). MS (ESI, m/z): 347.3 (M^+, 100%). Exact mass calculated (found) for $[M+H]^+$, m/z): 347.279201 (347.279600).

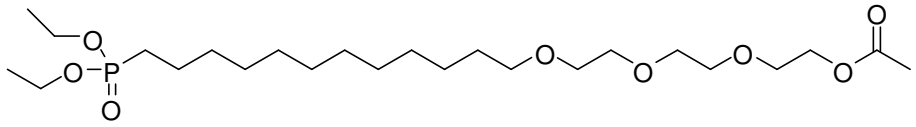

Diethyl 12–(2–(2–(2–acetyloxyethoxy)ethoxy)ethoxy)dodecylphosphonate

2–(2–(2–(12–bromododecyloxy)ethoxy)ethoxy)ethyl acetate (17.5 g, 39.84 mmol) was combined with triethylphosphite (24 mL, 139.4 mmol) in a round bottom flask and the reaction stirred at 140 °C overnight. Excess triethylphosphite and other side products were removed under vacuum (approximately 0.12 torr) and with heating at 100 °C for 5 hours. The product was a yellow oil (PJH–II–100a, 22.43 g (crude)). Column chromatography (stationary phase: silica, mobile phase: ethyl acetate) was used to purify a small portion of the compound (R_f = 0.20, ethyl acetate, iodine stain needed for TLC). ^{1}H NMR (400.14 MHz, $CDCl_3$) δ 4.22 (t, *J* = 4.78 Hz, 2H), 4.16 – 4.01 (m, 4H), 3.70 (t, *J* = 4.78 Hz, 2H), 3.68 – 3.62 (m, 6H), 3.61 – 3.55 (m, 2H), 3.45 (t, *J* = 6.81 Hz, 2H), 2.08 (3H), 1.77 – 1.51 (m, 6H), 1.41 – 1.19 (m, 22H). ^{13}C{^{1}H} NMR (100.62 MHz, $CDCl_3$) δ 170.9, 71.42, 70.57, 70.48 (2), 69.94, 69.01, 63.50, 61.23 (d, *J* =6.49 Hz, 2H), 30.50 (d, *J* = 16.99 Hz), 29.52, 29.46, 29.44 (2H), 29.37, 29.25, 28.98, 25.97, 25.56 (d, *J* = 140.21 Hz), 22.29 (d, *J* = 5.07 Hz), 20.86, 16.38 (d, *J* = 6.13 Hz, 2H). ^{31}P{^{1}H} NMR (161.97 MHz, $CDCl_3$): δ 33.31. Analysis calculated (found) %: C 58.04 (57.88), H 9.95

(10.15). MS (ESI, m/z): 497.3 (M^+, 100%). Exact mass calculated (found) for $[M+H]^+$, m/z): 497.323784 (497.324300).

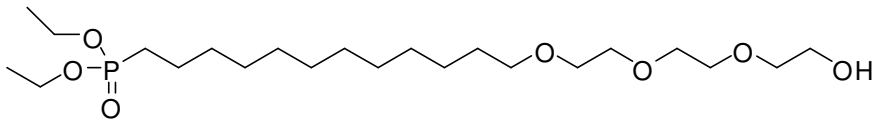

Diethyl 12–(2–(2–(2–hydroxyethoxy)ethoxy)ethoxy)dodecylphosphonate

Diethyl 12–(2–(2–(2–acetyloxyethoxy)ethoxy)ethoxy)dodecylphosphonate (22.00 g, 44.3 mmol) was dissolved in methanol (30 mL) in a round bottom flask. Potassium carbonate (7.8 g, 56.3 mmol), dissolved in water (40 mL) was added and the reaction was stirred at 85 °C overnight. The product was extracted into ether and washed with water. The aqueous layer was then washed with dichloromethane (1 ×) and ether (1 ×) and these washings were combined and added to the prior organic layer. The organic layer was dried over magnesium sulfate, filtered, then concentrated under reduced pressure. Column chromatography (stationary phase: silica, mobile phase: ethyl acetate) was used to isolate the desired product (R_f = 0.1, ethyl acetate, iodine stain needed for TLC) as an oil (PJH–II–103c,d; 12.56 g, 45 % yield (over 3 steps)). ^{1}H NMR (400.14 MHz, $CDCl_3$) δ 4.16 – 4.00 (m, 4H), 3.76 – 3.56 (m, 12H), 3.45 (t, *J* = 6.83 Hz, 2H), 2.07 (br), 1.77 – 1.64 (m, 2H), 1.64 – 1.51 (m, 4H), 1.41 – 1.20 (m, 22H). ^{13}C{^{1}H} NMR (100.62 MHz, $CDCl_3$) δ 72.42, 71.37, 70.46, 70.44, 70.21, 69.86, 61.44, 61.21 (d, *J* = 6.46 Hz, 2C), 30.43 (d, *J* = 16.91 Hz), 29.42, 29.41 (2C), 29.38, 29.30, 29.20, 28.92, 25.90, 25.48 (d, *J* = 140.26 Hz), 22.22 (d, *J* = 5.34 Hz), 16.33 (d, *J* = 5.88 Hz, 2C). ^{31}P{^{1}H} NMR (161.97 MHz, $CDCl_3$): δ 33.31. Analysis calculated (found) %: C 58.13 (58.21), H 10.42 (10.71).

MS (ESI, m/z): 455.3 (M^+, 100%). Exact mass calculated (found) for $[M+H]^+$, m/z): 455.313219 (455.312338).

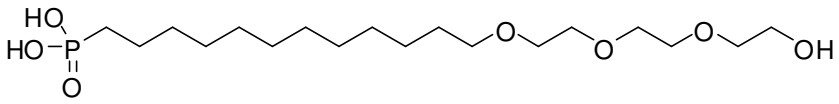

12–(2–(2–(2–hydroxyethoxy)ethoxy)ethoxy)dodecylphosphonic acid

Diethyl 12–(2–(2–(2–hydroxyethoxy)ethoxy)ethoxy)dodecylphosphonate (1.00 g, 2.2 mmol) was dissolved in dry dichloromethane (20 mL) and stirred. Bromotrimethylsilane (0.95 mL, 7.2 mmol) was added *via* syringe. The flask was capped with a greased glass stopper and allowed to stir for 2 hours. The volatiles were removed under reduced pressure and a 1: 1 methanol: water mixture (20 mL) was added. The reaction was allowed to stir for 2 hours. Upon removal of the solvents the final product was recrystallized from acetonitrile to yield a white powder (PJH–II–107a,b; 669 mg, 76 % yield). ^{1}H NMR (400.14 MHz, DMSO) δ 3.49 – 3.37 (m, 12H), 3.34 (t, J = 6.6 Hz, 2H), 1.52 – 1.35 (m, 6H), 1.34 – 1.16 (m, 16H). ^{13}C{^{1}H} NMR (100.62 MHz, DMSO) δ 72.37, 70.33, 69.86, 69.82, 69.79, 69.50, 60.22, 30.11 (d, J =16.1 Hz), 29.23, 29.06 (3C), 28.93 (2C), 28.74, 27.53 (d, J = 136.6 Hz), 25.69, 22.73 (d, J = 4.75 Hz). ^{31}P{^{1}H} NMR (161.97 MHz, DMSO): δ 27.74. Analysis calculated (found) %: C 54.26 (53.96), H 9.87 (9.96). MS (ESI, m/z): 399.25 (M^+, 100%). Exact mass calculated (found) for $[M+H]^+$, m/z): 399.250619 (399.254300).

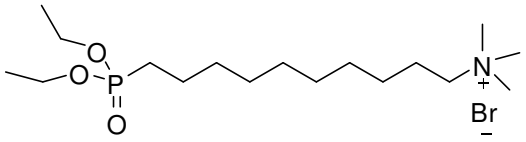

10–(diethoxyphosphoryl)–*N,N,N*–trimethyldecan–1–aminium bromide

Diethyl 10–bromodecylphosphonate (3.00 g, 8.40 mmol) was dissolved in anhydrous dimethylformamide (10 mL) and purged with nitrogen. After cooling to 0 °C, trimethylamine (2.1 mL, 33% in ethanol (4.2 M)) was added and the reaction was heated to 65 °C and stirred overnight. After cooling, methanol (40 mL) was added to the mixture, along with water (20 mL), and the reaction mixture was washed with hexanes (15 × 20 mL). The methanol layer was evaporated to yield a viscous oil (PJH–II–123j, 2.605 g, 75% yield). ^{1}H NMR (400.14 MHz, DMSO) δ 4.00 – 3.88 (m, 4H), 3.27 – 3.22 (m, 2H), 3.02 (9H), 1.72 – 1.62 (m, 4H), 1.45 – 1.17 (m, 20H). ^{13}C{^{1}H} NMR (125.77 MHz, DMSO) δ 65.26, 60.73 (d, J = 6.29 Hz, 2C), 52.12 (2C), 29.72 (d, J = 15.1 Hz), 28.69 (3C), 28.45 (2C), 25.73, 24.45 (d, J = 138.3 Hz), 22.03 (d, J = 5.03 Hz), 22.01, 16.31 (d, J = 5.03 Hz, 2C). ^{31}P{^{1}H} NMR (161.97 MHz, DMSO): δ 33.16. Analysis calculated (found) %: C 49.04 (47.93), H 9.44 (9.54), N 3.36 (3.07). MS (ESI, m/z): 336.27 ([M+H]$^{+}$, 100%). Exact mass calculated (found) for [M+H]$^{+}$, m/z): 336.266209 (336.269000).[i]

[i] As the elemental analysis did not pass, the appropriate NMR spectra are shown in Appendix A.

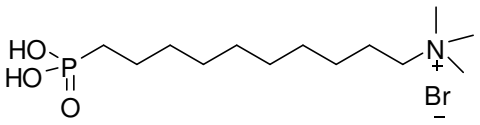

***N,N,N*–Trimethyl–10–phosphonodecan–1–aminium bromide**

10–(Diethoxyphosphoryl)–*N,N,N*–trimethyldecan–1–aminium bromide (2.54 g, 6.1 mmol) was dissolved in anhydrous dichloromethane (30 mL). Bromotrimethylsilane (2.5 mL, 19.5 mmol) was added *via* syringe. The reaction was capped with a greased glass stopper and allowed to stir for 2 hours. The volatiles were evaporated and methanol (30 mL) with a few drops of water was added and the reaction was allowed to stir for 2 more hours. The solvents were removed under reduced pressure and the final product recrystallized in acetonitrile to yield a white crystalline solid (PJH–II–127a, 1.818 g, 83 % yield). ^{1}H NMR (400.14 MHz, DMSO) δ 3.27 – 3.21 (m, 2H), 3.01 (9H), 1.68 – 1.60 (m, 2H), 1.53 – 1.18 (m, 16H). ^{13}C{^{1}H} NMR (100.62 MHz, DMSO) δ 65.2, 52.1 (3C), 30.0 (d, J = 16.0 Hz), 28.8 (2C), 28.6, 28.5, 27.5 (d, J = 136.4 Hz), 25.7, 22.7 (d, J = 4.5 Hz), 22.0. ^{31}P{^{1}H} NMR (161.97 MHz, DMSO): δ 27.67. Analysis calculated (found) %: C 43.34 (43.27), H 8.67 (8.77), N 3.89 (3.92). MS (ESI, m/z): 280.2 ([M+H]$^{+}$, 100 %). Exact mass calculated (found) for [M+H]$^{+}$, m/z): 280.20361 (280.20455).

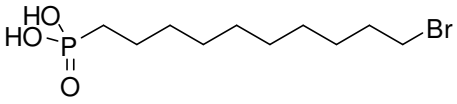

10–Bromodecylphosphonic acid

Diethyl 10–bromodecylphosphonate (1.00 g, 2.8 mmol) was dissolved in

anhydrous dichloromethane (20 mL). Bromotrimethylsilane (1.1 mL, 8.7 mmol) was added *via* syringe. The reaction was capped with a greased glass stopper and allowed to stir for 14 hours. The volatiles were removed under reduced pressure and a 3: 1 methanol: water mixture (20 mL) was added. The reaction was allowed to stir for 12 more hours. The solvents were evaporated and the final product recrystallized in acetonitrile to yield a white solid (PJH–II–124q, 140 mg, 39% yield). ^{1}H NMR (400.14 MHz, DMSO) δ 3.51 (t, *J* = 6.70 Hz, 2H), 1.78 (quint, *J* = 6.80 Hz, 2H), 1.52 – 1.15 (m, 16H). ^{13}C{^{1}H} NMR (100.62 MHz, DMSO) δ 35.21, 32.29, 30.10 (d, *J* = 16.0 Hz), 28.92, 28.84, 28.70, 28.16, 27.57, 27.48 (d, *J* = 136.5 Hz), 22.71 (d, *J* = 4.68 Hz). ^{31}P{^{1}H} NMR (161.97 MHz, DMSO): δ 28.03. Analysis calculated (found) %: C 39.88 (39.83), H 7.36 (7.30). MS (FAB, m/z): 301 ([M+H]$^{+}$, 98 %). Exact mass calculated (found) for [M+H]$^{+}$, m/z): 301.05682 (301.05726).

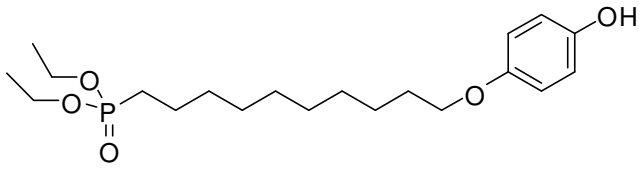

Diethyl 10–(4–hydroxyphenoxy)decylphosphonate

Hydroquinone (2.20 g, 19.6 mmol) was added to a round bottom flask under inert atmosphere. Anhydrous dimethylformamide (15 mL) was added *via* syringe. After stirring a few minutes potassium carbonate (775 mg, 5.6 mmol) was added. After 30 minutes diethyl 10–bromodecylphosphonate (1.00 g, 2.8 mmol) was added. The solution was stirred at room temperature for 8 hours and then at 120 °C overnight. After cooling,

water (50 mL) was added and the reaction mixture extracted with dichloromethane (5 × 20 mL). The organic layer was washed with water (20 mL) and the solvent evaporated to leave a dark red/brown oil. Column chromatography (stationary phase: silica, mobile phase: ethyl acetate) was used to isolate the desired product (R_f = 0.40, ethyl acetate) as an oil (PJH–II–128c, 147 mg, 14 % yield). ^{1}H NMR (400.14 MHz, $CDCl_3$) δ 6.77 (s, 4H), 4.14 – 4.05 (m, 4H), 3.91 (t, *J* = 6.50 Hz, 2H), 1.81 – 1.15 (m, 24H). $^{13}C\{^{1}H\}$ NMR (125.77 MHz, $CDCl_3$) δ 152.5, 150.6, 116.0 (2C), 115.5 (2C), 68.65, 61.68 (d, *J* = 7.5 Hz, 2C), 30.47 (d, *J* = 17.6 Hz), 29.36, 29.29, 29.20, 29.16, 28.95, 25.90, 25.46 (d, *J* = 139.6 Hz), 22.20 (d, *J* = 5.03 Hz), 16.37 (d, *J* = 6.29 Hz, 2C). $^{31}P\{^{1}H\}$ NMR (161.97 MHz, $CDCl_3$): δ 33.50. Analysis calculated (found) %: C 62.16 (62.20), H 9.13 (9.22). MS (FAB, m/z): 387.2 ($[M+H]^+$, 100 %). Exact mass calculated (found) for $[M+H]^+$, m/z): 387.23004 (387.22862).

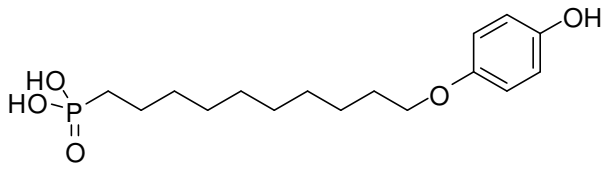

10–(4–hydroxyphenoxy)decylphosphonic acid

Diethyl 10–(4–hydroxyphenoxy)decylphosphonate (140 mg, 0.36 mmol) was dissolved in dry dichloromethane (4 mL). Bromotrimethylsilane (0.15 mL, 1.2 mmol) was added *via* syringe. The reaction was capped with a greased glass stopper and allowed to stir for 2 hours. The volatiles were removed under reduced pressure and methanol (3 mL) with a few drops of water was added. The reaction was allowed to stir for 2 more

hours. The solvents were evaporated and the final product recrystallized twice in acetonitrile (with a few drops of water) to yield a translucent white crystalline solid (PJH–II–139a, 100 mg, 84 % yield). ^{1}H NMR (400.14 MHz, DMSO) δ 6.81 – 6.60 (m, 4H), 3.81 (t, J = 6.43 Hz, 2H), 1.68 – 1.18 (m, 18H). ^{13}C{^{1}H} NMR (125.77 MHz, DMSO) δ 151.5, 151.0, 115.7 (2C), 115.3 (2C), 67.82, 30.06 (d, J = 15.09 Hz), 28.99, 28.85, 28.83, 28.81, 28.68, 27.50 (d, J = 135.8 Hz), 25.56, 22.70 (d, J = 5.03 Hz). ^{31}P{^{1}H} NMR (161.97 MHz, DMSO): δ 27.79. Analysis calculated (found) %: C 58.17 (58.00), H 8.24 (8.31). MS (ESI, m/z): 329.15 ([M-H]$^{-}$, 100 %). Exact mass calculated (found) for [M–H]$^{-}$, m/z): 329.152336 (329.154800).

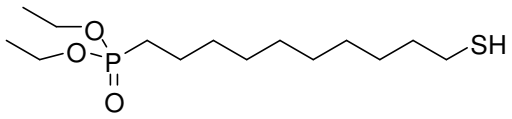

Diethyl 10–mercaptodecylphosphonate

Diethyl 10–bromoodecylphosphonate (6.00 g, 16.8 mmol) was dissolved in ethanol (20 mL) in a round bottom flask. Thiourea (5.11 g, 67.2 mmol) was dissolved in water (20 mL) and this mixture was added to the round bottom flask *via* pipette. The reaction mixture was stirred and heated to 95 °C for 6 hours. Concentrated ammonium hydroxide (4 mL, excess) was then added and the reaction allowed to stir at 75 °C for 2 hours more. Upon cooling to room temperature, the reaction mixture was acidified with HCl and then extracted with ethyl acetate, the organic kept and concentrated under reduced pressure. Column chromatography (stationary phase: silica, mobile phase: ethyl acetate) was used to isolate the desired compound (R_f = 0.41, ethyl acetate) as a clear oil

(PJH–II–143a, 3.64 g, 69.8 % yield. ^{1}H NMR spectrum shows desired compound with ~10% disulfide, but is consistent with the structure.[76]

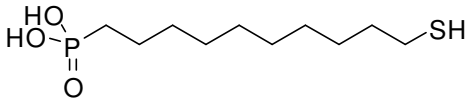

10–mercaptodecylphosphonic acid

Diethyl 10–mercaptodecylphosphonate (1.84 g, 5.93 mmol) was dissolved in anhydrous dichloromethane (25 mL). Bromotrimethylsilane (3.08 mL, 23.7 mmol) was added *via* syringe. The reaction was capped with a greased glass stopper and allowed to stir overnight. The volatiles were removed under reduced pressure and methanol (25 mL) with a few drops of water was added. The reaction was allowed to stir for 4 more hours. The solvents were removed under reduced pressure and the final product recrystallized twice in acetonitrile to yield a white crystalline solid (PJH–II–146a,b; 1.411 g, 94 % yield). ^{1}H NMR (in $CDCl_3$ and DMSO) and ^{31}P NMR ($CDCl_3$) spectra all appear clean and consistent with the desired product.[79]

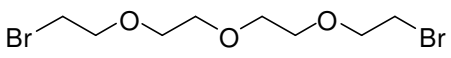

1–Bromo–2–(2–(2–(2–bromoethoxy)ethoxy)ethoxy)ethane

Triphenylphosphine (246.19 g, 938.6 mmol) was suspended in acetonitrile in an ice bath under inert atmosphere. Bromine (150.0 g, 938.6 mmol) was added dropwise

followed by the dropwise addition of tetraethylene glycol (91.1 g, 469.3 mmol). The reaction was allowed to warm up to room temperature and stir for 2 days. The reaction mixture was washed with sodium thiosulfate followed by extractions with hexanes and ether. The volatiles were removed under reduced pressure and the desired product was distilled off from the remaining impurities to yield a yellow oil (PJH–II–144j, 74.00 g, 49 % yield). ^{1}H NMR spectrum is consistent with the desired product.[80]

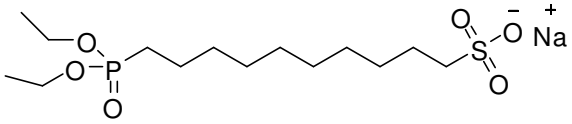

Sodium 10–(diethoxyphosphoryl)decane–1–sulfonate

Diethyl 10–bromoodecylphosphonate (2.00 g, 5.6 mmol) was dissolved in ethanol (20 mL) in a round bottom flask. Sodium sulfite (1.27 g, 10.1 mmol) was dissolved in water (25 mL) and added to the flask. The mixture was refluxed for 1 hour. The mixture was dried under vacuum and a Soxhlet extraction performed with ethanol for 17 hours. The ethanol was removed under reduced pressure to yield a white sticky solid which was precipitated/recrystallized in a 5: 1 ethanol: ether solution in a freezer (–20 °C) overnight. The white solid was filtered and washed with copious amounts of ether (PJH–II–147c, 831 mg, 39 % yield). ^{1}H NMR (400.14 MHz, DMSO) δ 4.00 – 3.86 (m, 4H), 2.34 (t, J = 7.88 Hz, 2H), 1.73 – 1.60 (m, 2H), 1.55 – 1.15 (m, 22H). Analysis calculated (found) %: C 44.20 (35.30), H 7.95 (6.54) MS (ESI, m/z): 357 ([M–Na]$^{-}$, 100 %).: Exact mass

calculated (found) for [M–Na]$^-$, m/z): 357.150623 (357.149300).[j]

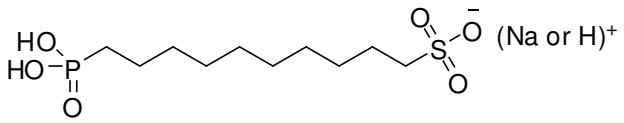

Sodium 10–phosphonodecane–1–sulfonate (PJH–II–150b) and/or **10–phosphonodecane–1–sulfonic acid (PJH–II–150a)**

Sodium 10–(diethoxyphosphoryl)decane–1–sulfonate (500 mg, 1.3 mmol) was dissolved in anhydrous dichloromethane (20 mL). Bromotrimethylsilane (0.61 mL, 4.7 mmol) was added *via* syringe. The reaction was capped with a greased glass stopper and allowed to stir for 2 hours. The solution was a cloudy white color. It was filtered and the white precipitate washed with dichloromethane and then acetonitrile. The solvents were removed from the filtrate under reduced pressure to yield a cloudy oil. This was dissolved in methanol (with a few drops of water) and allowed to stir for 3 hours. After removing the solvents, recrystallization from acetonitrile/water yielded a white powder (PJH–II–150a, 156 mg). ^{1}H NMR (400.14 MHz, D_2O): δ 2.75–2.63 (m, 2H), 1.65 – 1.42 (m, 4H), 1.42 – 1.28 (m, 2H), 1.28 – 1.05, (12H). ^{13}C{^{1}H} NMR (125.77 MHz, DMSO): δ 52.71, 31.35 (d, *J* = 16.7 Hz), 30.05 (2C), 29.84, 29.76, 29.33, 27.91 (d, *J* = 133.3 Hz), 25.60, 23.67 (d, *J* = 4.9 Hz). ^{31}P{^{1}H} NMR (161.97 MHz, D_2O): δ 33.62. Analysis calculated (found) %: C 39.73 (39.29), H 7.67 (7.56). (ESI, m/z): 301 ([M–H]$^-$, 100 %).: Exact mass calculated (found) for [M–H]$^-$, m/z): 301.088022 (301.087000).

[j] This compound could not be adequately purified due to an inability to separate the desired product from excess sodium sulfite. The reaction needs to be redone with less than an equivalent of sodium sulfite.

The white precipitate from the filtration was dissolved in a 1: 1 methanol: water mixture and allowed to stir for 3 hours. The solvents were evaporated and the final product recrystallized from acetonitrile/water to yield a white solid (PJH–II–150b, 71 mg). Analysis calculated (found) %: C 37.04 (36.92), H 6.84 (6.86). This corresponds to the sodium salt.

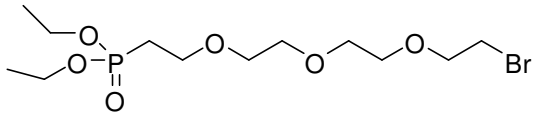

Diethyl 2–(2–(2–(2–bromoethoxy)ethoxy)ethoxy)ethylphosphonate

1–Bromo–2–(2–(2–(2–bromoethoxy)ethoxy)ethoxy)ethane (74.00 g, 231.2 mmol) was combined with triethylphosphite (30.9 mL, 185 mmol) in a round bottom flask and the mixture was stirred and heated to 145 °C overnight. Excess triethylphosphite and other side products were removed under vacuum (approximately 0.1 torr) and with heating at 90 °C for 5 hours. The desired product (R_f = 0.15, ethyl acetate, iodine stain used for TLC) was purified using a silica plug, eluting first with hexanes then increasing the solvent polarity with ethyl acetate. Leftover starting material (R_f = 0.80, ethyl acetate, iodine stain used for TLC) was combined with more triethylphosphite and the reaction and plug performed again. The two products were combined to give a clear oil (PJH–II–153g, 33.13 g, 45 % yield). ^{1}H NMR (500.13 MHz, $CDCl_3$) δ 4.14 – 4.01 (m, 4H), 3.79 (t, J = 12.50 Hz, 2H), 3.76 – 3.57 (m, 10H), 3.45 (t, J = 12.50 Hz, 2H), 2.11 (dt, J = 18.50, 5.00 Hz, 2H), ^{13}C{^{1}H} NMR (100.62 MHz, $CDCl_3$): δ 70.80, 70.17, 70.13, 71.11, 69.79, 64.70, 61.28 (d, J = 6.4 Hz, 2C), 30.01, 26.54 (d, J = 139.4 Hz), 16.06 (d, J = 6.0

Hz, 2C). $^{31}P\{^{1}H\}$ NMR (161.97 MHz, $CDCl_3$): δ 29.16. Analysis calculated (found) %: C 38.21 (37.85), H 6.95 (6.92). MS (FAB, m/z): 377 ($[M+H]^+$, 100 %).: Exact mass calculated (found) for $[M+H]^+$, m/z): 377.07286 (377.07230).

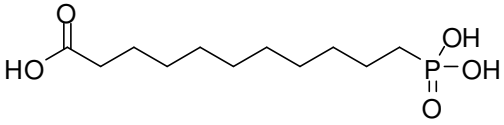

11–phosphonoundecanoic acid

11–methoxy–11–oxoundecylphosphonic acid (1.72 g, 6.136 mmol) was dissolved in 8M HCl (25 mL, excess) and the mixture refluxed overnight. Upon cooling, a white crystalline solid precipitated. This was filtered and washed with cold acetonitrile. (PJH–III–28a,c; 1.156 g, 71 % yield). ^{1}H NMR spectrum was consistent with the desired product.[81]

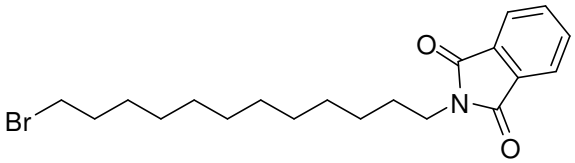

2–(12–bromododecyl)isoindoline–1,3–dione

1,12–dibromododecane (32.22 g, 98.2 mmol) was dissolved in acetone (300 mL) and the mixture brought to reflux. Potassium phthalimide (10.0 g, 53.5 mmol) was added over 4 hours and the reaction left to reflux overnight. Upon cooling to room temperature, the reaction mixture was filtered followed by removal of the acetone under reduced

pressure. Column chromatography (stationary phase: silica, mobile phase: 1: 1 ethyl acetate: hexanes) was used to isolate the desired product (R_f = 0.70, 1: 1 ethyl acetate: hexanes) as a white solid (PJH–III–27e, 9.30 g, 44 % yield). The ^{1}H NMR spectrum was consistent with the desired product.[82]

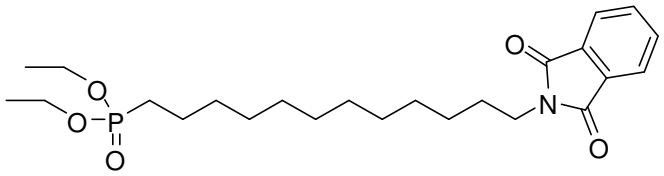

Diethyl 12–(1,3–dioxoisoindolin–2–yl)dodecylphosphonate

2–(12–bromododecyl)isoindoline–1,3–dione (9.30 g, 23.6 mmol) was combined with triethylphosphite (11.76 g, 70.7 mmol) in a round bottom flask and the mixture heated and stirred at 135 °C for 16 hours. Excess triethylphosphite and other side products were removed under vacuum (approximately 0.1 torr) and with heating at 90 °C for 4 hours. Column chromatography (stationary phase: silica, mobile phase: ethyl acetate) was used to isolate the desired product (R_f = 0.60, ethyl acetate) as a clear oil (PJH–III–30a, 8.96 g, 84 % yield). ^{1}H NMR (400.14 MHz, $CDCl_3$) δ 7.80 (dd, *J* = 5.4, 3.0 Hz, 2H), 7.67 (dd, *J* = 5.5, 3.0 Hz, 2H), 4.09 – 4.01 (m, 4H), 3.63 (t, *J* = 7.3 Hz), 1.72 – 1.45 (m, 6H), 1.32 – 1.05 (m, 22H). ^{13}C{^{1}H} NMR (100.62 MHz, $CDCl_3$) δ 168.4 (2C), 133.7 (2C), 132.1 (2C), 123.0 (2C), 61.29 (d, *J* = 6.5 Hz, 2C), 37.96, 30.51 (d, *J* = 17.0 Hz), 29.41 (2C), 29.35, 29.25, 29.07, 28.98, 28.49, 26.75, 25.55 (d, *J* = 140.1 Hz), 22.29 (d, *J* = 5.0 Hz), 16.39 (d, *J* = 6.1 Hz, 2C). ^{31}P{^{1}H} NMR (161.97 MHz, $CDCl_3$): δ 33.38. Analysis calculated (found) %: C 63.84 (63.41), H 8.48 (8.53). MS (ESI, m/z): 452.2

(M^+, 100%). Exact mass calculated (found) for $[M+H]^+$, m/z): 452.2560 (452.2548).[k]

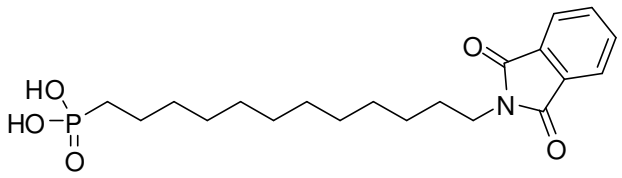

12–(1,3–dioxoisoindolin–2–yl)dodecylphosphonic acid

Diethyl 12–(1,3–dioxoisoindolin–2–yl)dodecylphosphonate (2.00 g, 4.43 mmol) was dissolved in anhydrous dichloromethane (25 mL). Bromotrimethylsilane (1.8 mL, 14.2 mmol) was added *via* syringe. The reaction was capped with a greased glass stopper and allowed to stir overnight. The volatiles were removed under reduced pressure to yield a yellow oil. This was dissolved in 10: 1 methanol: water mixture (20 mL) and allowed to stir overnight. After removal of the solvents under reduced pressure, recrystallization from acetonitrile yielded a white powdery solid (PJH–III–91a, 1.709 g, 98 % yield). ^{1}H NMR (400.14 MHz, DMSO) δ 7.86 – 7.81 (m, 4H), 3.54 (t, J = 7.1 Hz, 2H), 1.58 – 1.53 (m, 2H), 1.50 – 1.31 (m, 4H), 1.30 – 1.20 (m, 16H). ^{13}C{^{1}H} NMR (100.62 MHz, DMSO) δ 167.9 (2C), 134.4 (2C), 131.6 (2C), 123.0 (2C), 37.36, 30.08 (d, J = 16.0 Hz), 28.99, 28.95, 28.87 (2C), 28.70, 28.53, 27.85, 27.54 (d, J = 136.5 Hz), 22.72 (d, J = 4.6 Hz). ^{31}P{^{1}H} NMR (161.97 MHz, DMSO): δ 27.74. Analysis calculated (found) %: C 60.75 (60.64), H 7.65 (7.80). MS (FAB, m/z): 396.2 (M^+, 100%). Exact mass calculated (found) for $[M+H]^+$, m/z): 396.19399 (396.19445).

[k] As the elemental analysis did not pass, the appropriate NMR spectra are shown in Appendix A.

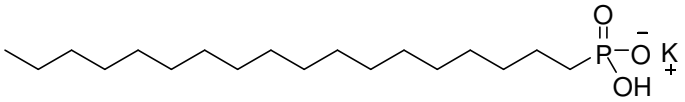

Potassium hydrogenoctadecylphosphonate (octadecylphosphonic acid monobasic potassium salt)

A 100 mM solution of KOH (3.0 mL) was titrated into a dispersed solution of octadecylphosphonic acid (100 mg, 0.3 mmol) in water (30 mL) while stirring. The mixture was then heated to 60 °C while stirring until all the water had evaporated (about 3 hours). The resulting white solid was then dried under vacuum. ^{1}H NMR (D_2O, 400 MHz, 353 K): δ 2.24 – 2.02 (br, 4H), 2.02 – 1.73 (br, 30H), 1.55 – 1.33 (br, 3H). ^{31}P{^{1}H} NMR (D_2O, 162 MHz, 353 K): δ 27.34. Analysis calculated (found) %: C 58.03 (58.42), H 10.28 (10.57).

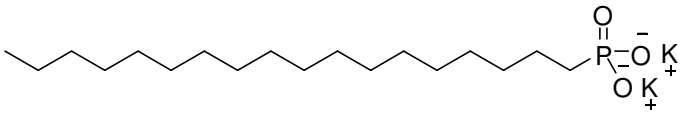

Potassium octadecylphosphonate (octadecylphosphonic acid dibasic potassium salt)

A 100 mM solution of KOH (6.0 mL) was titrated into a dispersed solution of octadecylphosphonic acid (100 mg, 0.3 mmol) in water (30 mL) while stirring. The mixture was then heated to 60 °C while stirring until all the water had evaporated (about 3 hours). The resulting white solid was then dried under vacuum. ^{1}H NMR (D_2O, 400 MHz, 353 K): δ 2.17 – 1.96 (m, 4H), 1.96 – 1.83 (m, br, 30H), 1.43 (t, J = 6.6 Hz, 3H).

$^{31}P\{^{1}H\}$ NMR (D_2O, 162 MHz, 353 K): δ 25.83. Analysis calculated (found, for · $(H_2O)_{1.5}$) %: C 49.40 (49.61), H 9.21 (9.23).

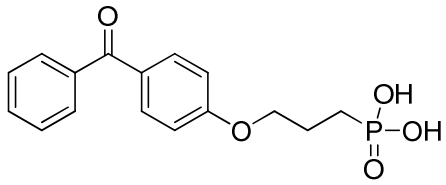

3–(4–benzoylphenoxy)propylphosphonic acid

The synthesis of 3–(4–benzoylphenoxy)propylphosphonic acid was followed as outlined in the literature and all ^{1}H NMR spectra are consistent with the various intermediates and final product.[55]

(4–hydroxyphenyl)(phenyl)methanone (2.00 g, 10.1 mmol) was added to dimethylsulfoxide (20 mL) in a round bottom flask under inert atmosphere and stirred. Sodium hydroxide (600 mg, 15.1 mg) was added (at which point the reaction turned dark brown) and the reaction allowed to stir for 1 hour. 1,3–dibromopropane (5.1 mL, 50.5 mmol) was then added and the reaction allowed to stir overnight. The reaction mixture was diluted with dichloromethane (30 mL), filtered, and the filtrate washed with dilute HCl and then water. The organic layer was dried over magnesium sulfate, filtered, then concentrated under reduced pressure. Column chromatography (stationary phase: silica, mobile phase: dichloromethane) was used to isolate the desired product (R_f = 0.77, dichloromethane) as a yellowish–white viscous oil (PJH–III–98a, 1.20 g, 37 % yield).

(4–(3–bromopropoxy)phenyl)(phenyl)methanone (1.20 g, 3.76 mmol) was combined with triethylphosphite (2.1 mL, 12.0 mmol) and the reaction mixture allowed

to stir at 140 °C overnight. Excess triethylphosphite and other side products were removed under vacuum (approximately 0.1 torr) and with heating at 60 °C for 6 hours to yield a clear oil (PJH–III–99a, 680 mg, 48 % yield).

Diethyl 3–(4–benzoylphenoxy)propylphosphonate (680 mg, 1.8 mmol) was dissolved in anhydrous dichloromethane (10 mL). Bromotrimethylsilane (0.80 mL, 6.1 mmol) was added *via* syringe. The reaction was capped with a greased glass stopper and allowed to stir overnight. The volatiles were removed under reduced pressure to yield a yellow oil. This was dissolved in 1: 1 methanol: water mixture (10 mL) and allowed to stir overnight. After removal of the solvents under reduced pressure, the resulting solid was filtered and washed with water to yield a yellow solid (PJH–III–11a, 280 mg, 49 % yield).

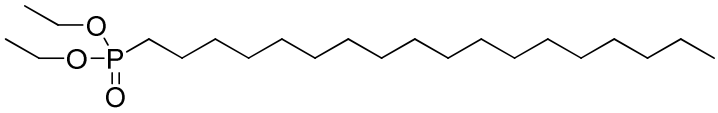

Diethyl octadecylphosphonate

1–bromooctadecane (100.0 g, 300 mmol) was combined with triethylphosphite (180 mL, 1050 mmol) in a round bottom flask and the mixture heated to 140 °C and stirred overnight. Excess triethylphosphite and other side products were removed under vacuum (approximately 0.04 torr) and with heating at 85 °C for 12 hours. A silica plug was run (eluting first with hexanes then gradually increasing the ratio of ethyl acetate until pure ethyl acetate was used) to isolated the desired product (0.05, hexanes, iodine stain needed for TLC) as a soft white crystalline solid (PJH–111–92a, 104 g, 99 % yield

(after recovery of 10.3 g of starting material). ^{1}H NMR is consistent with the desired product.[83]

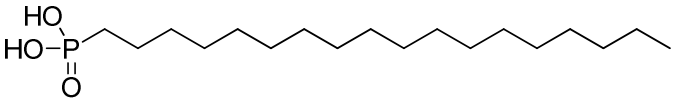

Octadecylphosphonic acid

Diethyl Octadecylphosphonate (30.0 g, 76.8 mmol) was dissolved in anhydrous dichloromethane (200 mL). Bromotrimethylsilane (30 mL, 230.4 mmol) was added *via* syringe. The reaction was capped with a greased glass stopper and allowed to stir overnight. The volatiles were removed under reduced pressure to yield a yellow oil. This was dissolved in 10: 1 methanol: water mixture (200 mL) and allowed to stir overnight. After removing the solvents, cold water was added and the mixture filtered. The white solid was washed with cold acetone (PJH–III–104a, 23.00 g, 89 % yield). ^{1}H NMR is consistent with the desired product.[83]

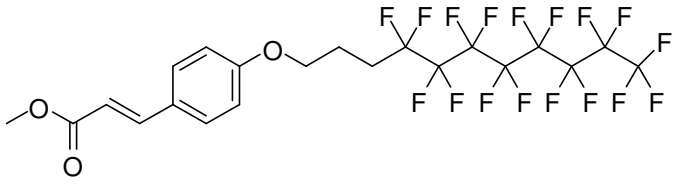

(E)–Methyl 3–(4–(4,4,5,5,6,6,7,7,8,8,9,9,10,10,11,11,11–heptadecafluoroundecyloxy) phenyl) acrylate

(E)–Methyl 3–(4–hydroxyphenyl)acrylate (166 mg, 0.93 mmol (from Yadong Zhang, Marder Group)) was added to anhydrous dimethylsulfoxide (10 mL) and stirred in a round bottom flask under inert atmosphere. Sodium hydroxide (44 mg, 1.1 mmol) was then added. After 30 minutes, 1,1,1,2,2,3,3,4,4,5,5,6,6,7,7,8,8–heptadecafluoro–11–iodoundecane (500 mg, 0.85 mmol) was added and the reaction was allowed to stir overnight. Water and dichloromethane were added and the organic layer was separated and concentrated to yield an oil. Column chromatography (stationary phase: silica, mobile phase: hexanes followed by increasing amounts of ethyl acetate) was used to isolate the desired product (R_f = 0.53, 1: 1 hexanes: ethyl acetate) as a white solid (PJH–III–47a, 418 mg, 77 % yield). ^{1}H NMR (400.14 MHz, $CDCl_3$) δ 7.65 (d, *J* = 16.0 Hz), 7.48 (d, *J* = 8.75 Hz, 2H), 6.90 (d, *J* = 8.75 Hz, 2H), 6.32 (d, *J* = 16.0 Hz), 4.07 (t, *J* = 5.90 Hz, 2H), 3.80 (3H), 2.40 – 2.20 (m, 2H), 2.18 – 2.05 (m, 2H). $^{13}C\{^1H\}$ NMR (100.62 MHz, $CDCl_3$) δ 167.7, 160.3, 144.4, 129.7 (2C), 127.5, 121.5 – 105.0 (8C), 115.5, 114.7 (2C), 66.4, 51.6, 27.9 (t, *J* = 22.4 Hz), 20.5. Analysis calculated (found) %: C 39.51 (39.51), H 2.37 (2.30). MS (ESI, m/z): 307.2 ($[M+H]^+$, 20 %). Exact mass calculated (found) for $[M+H]^+$, m/z: 639.0823 (639.0812).

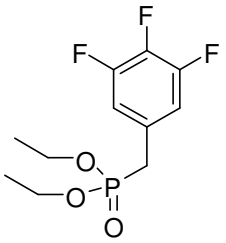

Diethyl 3,4,5–trifluorobenzylphosphonate

3,4,5–trifluorobenzyl bromide (5.075 g, 22.55 mmol) was combined with triethylphosphite (11.6 mL, 67.7 mmol) and the mixture heated and stirred at 135 °C overnight. Excess triethylphosphite and other side products were removed under vacuum (approximately 0.1 torr) and with heating at 70 °C for 12 hours. The final product was a clear oil (PJH–III–40c, 6.10 g, 96 % yield). ^{1}H NMR (400.14 MHz, $CDCl_3$) δ 6.93 (m, 2H), 4.07 (quint, *J* = 7.10 Hz, 4H), 3.06 (d, *J* = 21.7 Hz, 2H), 1.28 (t, *J* = 7.05 Hz, 6H). ^{13}C{^{1}H} NMR (100.62 MHz, $CDCl_3$) δ 150.8 (dddd, *J* = 249.7, 9.8, 3.8, 3.8 Hz, 2C), 138.74 (dtd, *J* = 250.6, 15.2, 3.9 Hz), 128.2 – 127.9 (m), 113.9 – 113.6 (m, 2C), 62.30 (d, *J* = 6.74 Hz, 2C), 32.93 (d, *J* = 139.8 Hz), 16.20 (d, *J* = 6.01 Hz, 2C). ^{31}P{^{1}H} NMR (202.45 MHz, $CDCl_3$): δ 24.96. Analysis calculated (found) %: C 46.82 (46.72), H 5.00 (4.96). MS (FAB, m/z): 269 (M^+, 100%). Exact mass calculated (found) for $[M+H]^+$, m/z): 269.05544 (269.05616).

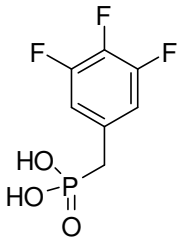

3,4,5–Trifluorobenzylphosphonic acid

Diethyl 3,4,5–trifluorobenzylphosphonate (2.80 g, 9.92 mmol) was dissolved in dry dichloromethane (30 mL). Bromotrimethylsilane (4.1 mL, 31.7 mmol) was added *via* syringe. The reaction was capped with a greased glass stopper and allowed to stir for 6 hours. The volatiles were removed under reduced pressure to yield a yellow oil. This was dissolved in 10:1 methanol: water (20 mL) and allowed to stir overnight. After removing the solvents, recrystallization from acetonitrile yielded white needle–shaped crystals (PJH–III–43a,b,c; 2.00 g, 89% yield). ^{1}H NMR (400.14 MHz, DMSO) δ 7.16 (m, 2H), 2.99 (d, J = 21.4 Hz, 2H). ^{13}C{^{1}H} NMR (100.62 MHz, DMSO) δ 149.9 (dddd, J = 246, 9.6, 3.6, 3.6 Hz, 2C), 137.5 (dtd, J = 247, 15.4, 3.7), 132.1 – 131.8 (m), 114.4 – 114.1 (m, 2C), 34.42 (d, J = 132 Hz). ^{31}P{^{1}H} NMR (161.97 MHz, DMSO): δ 20.54. Analysis calculated (found) %: C 37.19 (37.17), H 2.67 (2.63). MS (FAB, m/z): 227 (M^{+}, 100%). Exact mass calculated (found) for $[M+H]^{+}$, m/z): 227.00849 (227.00670).

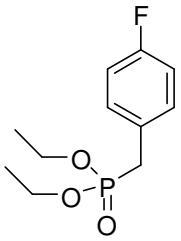

Diethyl 4–fluorobenzylphosphonate

4–Fluorobenzyl bromide (3.30 mL, 26.45 mmol) was combined with triethylphosphite (13.6 mL, 79.4 mmol) and the reaction mixture was refluxed at 135 °C overnight. Excess triethylphosphite and other side products were removed under vacuum (approximately 0.1 torr) and with heating at 40 °C for 6 hours. Column chromatography (stationary phase: silica, mobile phase: ethyl acetate) was used to isolate the desired product (R_f = 0.55, ethyl acetate) as a clear oil (PJH–III–68d, 5.55 g, 85 % yield). ^{1}H NMR spectrum is consistent with desired product.[84]

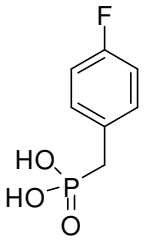

4–Fluorobenzylphosphonic acid

Diethyl 4–fluorobenzylphosphonate (2.426 g, 9.85 mmol) was dissolved in dry dichloromethane (25 mL). Bromotrimethylsilane (4.1 mL, 31.5 mmol) was added *via* syringe. The reaction was capped with a greased glass stopper and allowed to stir for 6 hours. The volatiles were removed under reduced pressure to yield a yellow oil. This was

dissolved in 10:1 methanol: water (20 mL) and allowed to stir overnight. After removing the solvents, recrystallization from acetonitrile yielded a white crystalline solid (PJH–III–72a,d; 767 mg, 46 % yield). ^{1}H NMR (400.14 MHz, DMSO) δ 7.28 – 7.23 (m, 2H), 7.12 – 7.07 (m, 2H), 2.94 (d, J = 21.2 Hz, 2H). ^{31}P{^{1}H} NMR (202.5 MHz, DMSO): δ 22.07. Analysis calculated (found) %: C 44.22 (43.99), H 4.24 (4.03). Spectra and analyses are consistent with the desired product as reported in the literature.[85]

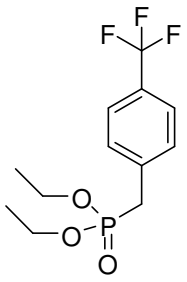

Diethyl 4–(trifluoromethyl)benzylphosphonate

Trifluoromethylbenzyl bromide (4.00 g, 16.7 mmol) was combined with triethylphosphite (8.6 mL, 50.2 mmol) and the reaction mixture refluxed at 135 °C overnight. Excess triethylphosphite and other side products were removed under vacuum (approximately 0.1 torr) and with heating at 40 °C for 6 hours. Column chromatography (stationary phase: silica, mobile phase: ethyl acetate) was used to isolate the desired product (R_f = 0.60, ethyl acetate) as a clear oil (PJH–III–71a, 4.02 g, 81 % yield). ^{1}H NMR spectrum is consistent with the desired product.[86]

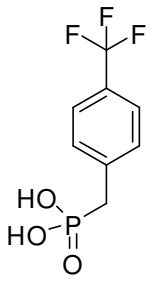

4–(Trifluoromethyl)benzylphosphonic acid

Diethyl 4–(trifluoromethyl)benzylphosphonate (1.250 g, 4.20 mmol) was dissolved in dry dichloromethane (25 mL). Bromotrimethylsilane (1.6 mL, 13.5 mmol) was added *via* syringe. The reaction was capped with a greased glass stopper and allowed to stir for 6 hours. The volatiles were removed under reduced pressure to yield a yellow oil. This was dissolved in 10:1 methanol: water (20 mL) and allowed to stir overnight. After removing the solvents, recrystallization from acetonitrile yielded a white crystalline solid (PJH–III–73a,d; 866 mg, 86 % yield). ^{1}H NMR (400.14 MHz, DMSO) δ 7.64 (d, *J* = 8.1 Hz, 2H), 7.45 (d, *J* = 6.7 Hz, 2H), 3.07 (d, *J* = 21.7 Hz, 2H). ^{31}P{^{1}H} NMR (202.5 MHz, DMSO): δ 21.07. Analysis calculated (found) %: C 40.02 (40.07), H 3.36 (3.25). Spectra and analyses are consistent with those found in the literature.[87]

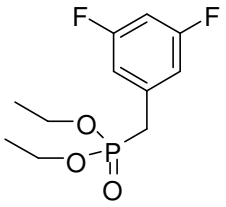

Diethyl 3,5–difluorobenzylphosphonate

3,5–difluorobenzyl bromide (3.0 mL, 23.2 mmol) was combined with triethylphosphite (9.1 mL, 53.3 mmol) and the mixture heated and stirred at 135 °C overnight. Excess triethylphosphite and other side products were removed under vacuum (approximately 0.1 torr) and with heating at 70 °C for 12 hours. The final product was a clear oil (PJH–III–126a, 5.78 g, 94 % yield). ^{1}H NMR (400.14 MHz, $CDCl_3$) δ 6.83 (m, 2H), 6.71 (dt, *J* = 9.00, 2.28 Hz), 4.06 (m, 4H), 3.12 (d, *J* = 21.94 Hz, 2H), 1.28 (t, *J* = 7.09 Hz, 6H). ^{31}P{^{1}H} NMR (161.97 MHz, $CDCl_3$): δ 25.22. Spectra are consistent with those reported in the literature.[88]

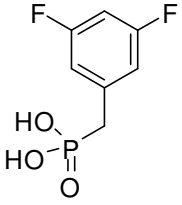

3,5–Difluorobenzylphosphonic acid

Diethyl 3,5–difluorobenzylphosphonate (3.00 g, 11.4 mmol) was dissolved in dry dichloromethane (25 mL). Bromotrimethylsilane (4.9 mL, 37 mmol) was added *via* syringe. The reaction was capped with a greased glass stopper and allowed to stir for 6 hours. The volatiles were removed under reduced pressure to yield a yellow oil. This was

dissolved in 8:1 methanol: water (25 mL) and allowed to stir overnight. After removing the solvents, recrystallization from acetonitrile yielded a white crystalline solid (PJH–III–127a,d; 1.98 g, 91 % yield). ^{1}H NMR (400.14 MHz, DMSO) δ 7.05 (dt, *J* = 9.49, 2.09 Hz), 6.95 (d, *J* = 8.54 Hz, 2H), 3.02 (d, *J* = 21.57 Hz, 2H). ^{31}P{^{1}H} NMR (161.97 MHz, DMSO): δ 20.63. Analysis calculated (found) %: C 40.40 (40.67), H 3.39 (3.39). Spectra and analyses are consistent with those reported in the literature.[89]

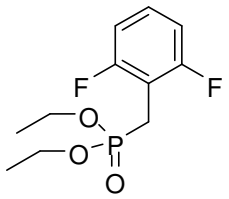

Diethyl 2,6–difluorobenzylphosphonate

2,6–difluorobenzyl bromide (3.0 g, 14.5 mmol) was combined with triethylphosphite (6.2 mL, 36.2 mmol) and the mixture heated and stirred at 135 °C overnight. Excess triethylphosphite and other side products were removed under vacuum (approximately 0.1 torr) and with heating at 80 °C for 10 hours. The final product was a slightly yellow–tinted oil (PJH–III–129c, 3.30 g, 86 % yield). ^{1}H NMR (400.14 MHz, DMSO) δ 7.36 (m), 7.10 (m, 2H), 3.96 (m, 4H), 3.20 (d, *J* = 21.08 Hz, 2H), 1.16 (t, *J* =7.05 Hz, 6H). ^{13}C{^{1}H} NMR (100.62 MHz, $CDCl_3$) δ 161.0 (ddd, *J* = 249.0, 7.3, 6.2 Hz, 2C), 128.4 (dt, *J* = 10.2, 3.82 Hz), 111.0 (ddd, *J* = 18.9, 6.0, 3.5 Hz, 2C), 108.5 (dt, *J* = 19.8, 10.5 Hz), 62.1 (d, *J* = 6.5 Hz, 2C), 20.6 (dt, *J* =142.1, 2.3 Hz), 16.0 (d, *J* = 6.2 Hz, 2C). ^{31}P{^{1}H} NMR (161.97 MHz, DMSO): δ 24.68. Analysis calculated (found) %: C 50.01 (49.71), H 5.72 (5.78). MS (FAB, m/z): 265 (M^+, 100%). Exact mass calculated

(found) for $[M+H]^+$, m/z): 265.08051 (265.08278).

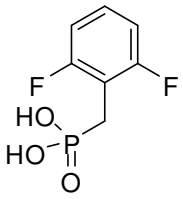

2,6–Difluorobenzylphosphonic acid

Diethyl 2,6–difluorobenzylphosphonate (2.00 g, 7.57 mmol) was dissolved in dry dichloromethane (20 mL). Bromotrimethylsilane (3.3 mL, 25 mmol) was added *via* syringe. The reaction was capped with a greased glass stopper and allowed to stir for 6 hours. The volatiles were removed under reduced pressure to yield a yellow oil. This was dissolved in 10:1 methanol: water (20 mL) and allowed to stir overnight. After removing the solvents, recrystallization from acetonitrile yielded a white crystalline solid (PJH–III–132a,d; 1.199 g, 76 % yield). ^{1}H NMR (400.14 MHz, DMSO) δ 7.29 (m), 7.04 (m, 2H), 2.96 (d, J = 20.99 Hz, 2H). ^{31}P{^{1}H} NMR (161.97 MHz, DMSO): δ 19.51. Analysis calculated (found) %: C 40.40 (40.64), H 3.39 (3.34). Spectra and analyses are consistent with those reported in the literature.[89]

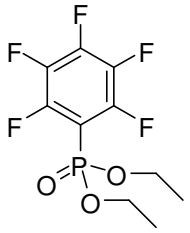

Diethyl perfluorophenylphosphonate

Pentafluoroiodobenzene (0.45 mL, 3.4 mmol) was combined with triethylphosphite (2.9 mL, 17.0 mmol) in a pressure vessel which had been flushed with nitrogen. The vessel was sealed and rotated in a Rayonet photoreactor (8 bulbs – 419 nm, 8 bulbs – 350 nm) for 24 hours. The reaction mixture was put under high vacuum (0.08 Torr) at 40 °C for several hours. Column chromatography (stationary phase: silica, mobile phase: hexanes with increasing amounts of ethyl acetate) was used to isolate the desired product (R_f = 0.72, hexanes) as a clear liquid (PJH–III–39a, 446 mg, 43 % yield). ^{1}H NMR Spectrum is consistent with desired product.[90]

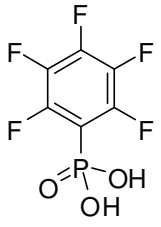

Perfluorophenylphosphonic acid

Diethyl perfluorophenylphosphonate (1060 mg, 3.48 mmol) was combined with 8M HCl (10 mL, excess) and the mixture refluxed overnight. The reaction was cooled and filtered to remove any insoluble impurities. The solvent was removed under vacuum

until a solid began to form. The mixture was then put in the refrigerator (–15 °C) for several hours. The solid was dried to yield an off–white powder (PJH–III–131a,c; 860 mg, 99 % yield). ^{1}H NMR showed no signal other than the DMSO. ^{31}P{^{1}H} NMR (161.97 MHz, DMSO): δ –0.93. Analysis calculated (found) %: C 29.05 (29.33), H 0.81 (0.95). Spectra and analyses are consistent with the desired product.[91]

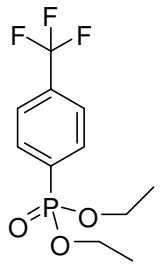

Diethyl 4–(trifluoromethyl)phenylphosphonate

4–iodobenzotrifluoride (2.0 mL, 13.6 mmol) was combined with triethylphosphite (7.0 mL, 40.8 mmol) in a pressure vessel which had been flushed with nitrogen. The vessel was sealed and rotated in a Rayonet photoreactor (16 bulbs – 350 nm) for 24 hours. Excess triethylphosphite and other side products were removed under vacuum (approximately 0.08 torr) and with heating at 40 °C for several hours. Column chromatography (stationary phase: silica, mobile phase: hexanes with increasing amounts of ethyl acetate) was used to isolate the desired product (R_f = 0.67, hexanes) as a yellow liquid (PJH–III–65a, 1.292 g, 34% yield). Spectra are consistent with the literature.[86]

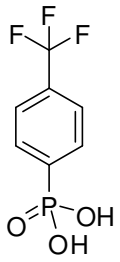

4–(Trifluoromethyl)phenylphosphonic acid

8 M HCl (15 mL, excess) was added to diethyl 4–(trifluoromethyl)phenylphosphonate (725 mg. 2.57 mmol) in a round bottom flask. The reaction mixture was refluxed for 12 hours. A white solid crashed out upon cooling (PJH–III–67a, 377 mg. 65% yield). ^{1}H NMR (400.14 MHz, DMSO) δ 7.90 – 7.80 (m, 4H). ^{31}P{^{1}H} NMR (202.5 MHz, DMSO): δ 11.42. Analysis calculated (found) %: C 37.19 (37.30), H 2.67 (2.59). Spectra and analyses are consistent with desired product.[92, 93]

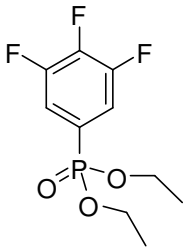

Diethyl 3,4,5–trifluorophenylphosphonate

Trifluorobromobenzene (1.70 mL, 14.2 mmol), diethyl phosphite (2.20 mL, 17.1 mmol), *N,N*–dicyclohexylmethylamine (4.60 mL, 21.3 mmol) and ethanol (50 mL) were all combined in a nitrogen purged round bottom flask. After stirring for 5 minutes,

triphenylphosphine (223 mg, 0.85 mmol) and palladium acetate (64 mg, 0.28 mmol) were added to the flask as one. The solution was heated to 76 °C and allowed to stir overnight. The solution started as a translucent brown color but was clearer by morning. The solvent was removed under reduced pressure and a silica plug using hexanes with increasing amounts of ethyl acetate as the eluent was run to isolate the desired product (R_f = 0.35, 1: 1 hexanes: ethyl acetate) as a clear oil (PJH–III–80a, 3.477 g, 91 % yield). ^{1}H NMR (400.14 MHz, $CDCl_3$) δ 7.44 (dt, *J* = 14.4, 6.50 Hz 2H), 4.19 – 4.07 (m, 4H), 1.34 (t, *J* = 7.07 Hz, 6H). $^{13}C\{^{1}H\}$ NMR (100.62 MHz, $CDCl_3$) δ 151.1 (dddd, *J* = 254.7, 25.4, 10.1, 2.9 Hz, 2C), 142.5 (dtd, *J* = 258.6, 15.1, 3.3 Hz), 125.0 (dtd, *J* = 194.5, 5.8, 5.2 Hz), 116.3 – 116 (m, 2C), 62.72 (d, *J* = 5.63 Hz, 2C), 16.16 (d, *J* = 6.34 Hz, 2C). $^{31}P\{^{1}H\}$ NMR (161.97 MHz, $CDCl_3$): δ 14.94. Analysis calculated (found) %: C 44.79 (44.51), H 4.51 (4.65). MS (FAB, m/z): 283 (M^+, 100%). Exact mass calculated (found) for $[M+H]^+$, m/z): 283.07109 (283.07135).

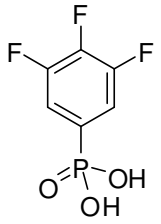

3,4,5–Trifluorophenylphosphonic acid

12 M HCl (12 mL, excess) was added to diethyl 3,4,5–trifluorophenylphosphonate (320 mg) in a round bottom flask. The reaction mixture was refluxed for 12 hours. A brown oil was obtained after cooling and removal of the solvent.

^{1}H NMR showed the presence of unreacted starting material. 12 mL of 8 M HCl were added and the reaction mixture refluxed again for several days. The mixture was allowed to cool and stood undisturbed for several weeks. An off–white solid was obtained after removal of the solvent (PJH–III–86a,b; 356 mg, 76 % yield). ^{1}H NMR (400.14 MHz, DMSO) δ 7.49 – 7.42 (m, 2H). ^{13}C{^{1}H} NMR (100.62 MHz, DMSO) δ 150.1 (dddd, *J* = 251.0, 23.7, 7.3, 2.6 Hz, 2C), 140.5 (dtd, *J* = 253.1, 15.3, 2.6 Hz), 131.8 (dm, *J* = 178.4 Hz), 115.3 – 114.9 (m, 2C). ^{31}P{^{1}H} NMR (161.97 MHz, DMSO): δ 9.22. Analysis calculated (found) %: C 33.98 (33.94), H 1.90 (1.80). MS (FAB, m/z): 213 (M^{+}, 100%). Exact mass calculated (found) for $[M+H]^{+}$, m/z): 212.99284 (212.99418).

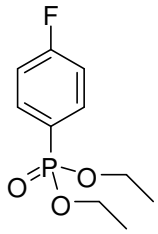

Diethyl 4–fluorophenylphosphonate

4–Fluoroiodobenzene (1.03 mL, 9.0 mmol) was combined with triethylphosphite (6.2 mL, 36.0 mmol) in a pressure vessel which had been flushed with nitrogen. The vessel was sealed and rotated in a Rayonet photoreactor (16 bulbs – 350 nm) for 24 hours. Excess triethylphosphite and other side products were removed under vacuum (approximately 0.08 torr) and with heating at 40 °C for 3 hours. Column chromatography (stationary phase: silica, mobile phase: hexanes with increasing amounts of ethyl acetate) was used to isolate the desired product (R_f = 0.65, 1: 1 hexanes: ethyl acetate) as a clear

liquid (PJH–III–45a, 1.088 g, 52 % yield). ^{1}H NMR is consistent with the desired product.[94]

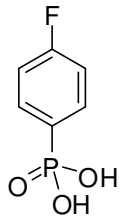

4–Fluorophenylphosphonic acid

Diethyl 4–fluorophenylphosphonate (600 mg, 2.55 mmol) was combined with 8M HCl (10 mL, excess) and the mixture refluxed overnight. The reaction was cooled and filtered to remove dark particulate. The solvent was removed under vacuum until a solid began to form. The mixture was then put in the refrigerator (5 °C) for several hours. The solid was dried to yield an off–white powder (PJH–III–128a,d; 330 mg, 73 % yield). ^{1}H NMR (400.14 MHz, DMSO) δ 7.71 (ddd, *J* = 12.49, 8.52, 5.99 Hz, 2H), 7.28 (ddd, *J* = 9.02, 9.02, 2.65 Hz, 2H). ^{31}P{^{1}H} NMR (161.97 MHz, DMSO): δ 12.81. Analysis calculated (found) %: C 40.93 (40.33), H 3.43 (3.49). ^{1}H NMR is consistent with desired product.[95]

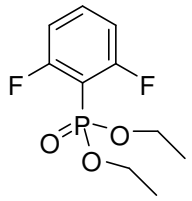

Diethyl 2,6–difluorophenylphosphonate

2,6–difluoroiodobenzene (3.0 g, 12.5 mmol) was combined with triethylphosphite (10.7 mL, 62.5 mmol) in a pressure vessel which had been flushed with nitrogen. The vessel was sealed and rotated in a Rayonet photoreactor (16 bulbs – 350 nm) for 20 hours. Excess triethylphosphite and other side products were removed under vacuum (approximately 0.08 torr) and with heating at 50 °C for 5 hours. Column chromatography (stationary phase: silica, mobile phase: hexanes with increasing amounts of ethyl acetate) was used to isolate the desired product (R_f = 0.70) as a yellow–tinted liquid (PJH–III–141a, 2.30 g, 74% yield). ^{1}H NMR (400.14 MHz, DMSO) δ 7.72 (m), 7.21 (m, 2H), 4.10 (m, 4H), 1.25 (t, *J* =7.04 Hz). ^{13}C{^{1}H} NMR (100.62 MHz, $CDCl_3$) δ 163.4 (ddd, *J* = 255.8, 7.8, 2.1 Hz, 2C), 134.7 (t, *J* = 11.0 Hz), 112.0 (ddd, *J* = 24.4, 7.2, 3.4 Hz, 2C), 106.0 (dt, *J* = 185.5, 20.7 Hz), 62.56 (d, *J* = 5.8 Hz, 2C), 15.89 (d, *J* = 6.7 Hz, 2C). ^{31}P{^{1}H} NMR (161.97 MHz, DMSO): δ 8.23. Analysis calculated (found) %: C 48.01 (47.76), H 5.24 (5.24). MS (FAB, m/z): 251 (M^+, 100%). Exact mass calculated (found) for $[M+H]^+$, m/z): 251.06486 (251.06645).

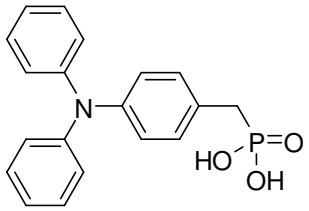

4–(diphenylamino)benzylphosphonic acid

Diethyl 4–(diphenylamino)benzylphosphonate (186 mg (not pure, from SJZ–4–9), 0.47 mmol) was dissolved in dry dichloromethane (10 mL). Bromotrimethylsilane (0.21 mL, 1.65 mmol) was added *via* syringe. The reaction was capped with a greased glass stopper and allowed to stir overnight. The volatiles were removed under reduced pressure to yield a yellow oil. This was dissolved in 4: 1 methanol: water (10 mL) and allowed to stir 4 hours more. After concentration of the organic layer, precipitation in cold water yielded a slightly green–white powdery solid (PJH–III–163a, 144 mg, 90 % yield). ^{1}H NMR (400.14 MHz, DMSO) δ 7.26 (t, *J* = 7.4 Hz, 4H), 7.17 (dd, *J* = 8.6, 2.3 Hz, 2H), 6.99 (t, *J* = 7.3 Hz, 2H), 6.95 (d, *J* = 7.5 Hz, 4H), 6.92 (d, *J* = 8.4 Hz, 2H), 2.90 (d, *J* = 21.3 Hz, 2H). ^{13}C{^{1}H} NMR (100.62 MHz, $CDCl_3$) δ 147.39 (2C), 125.24 (d, *J* = 3.2 Hz), 130.89 (d, *J* = 5.8 Hz), 129.46 (4C), 128.99 (d, *J* = 8.8 Hz), 124.04, 123.34 (4C), 122.61 (2C), 34.68 (d, *J* = 132.6 Hz). ^{31}P{^{1}H} NMR (161.97 MHz, DMSO): δ 22.29. Analysis calculated (found) %: C 67.25 (67.31), H 5.35 (5.34), N 4.13 (4.13). MS (FAB, m/z): 339 (M^+, 30%). Exact mass calculated (found) for $[M]^+$, m/z): 339.10243 (339.10165).

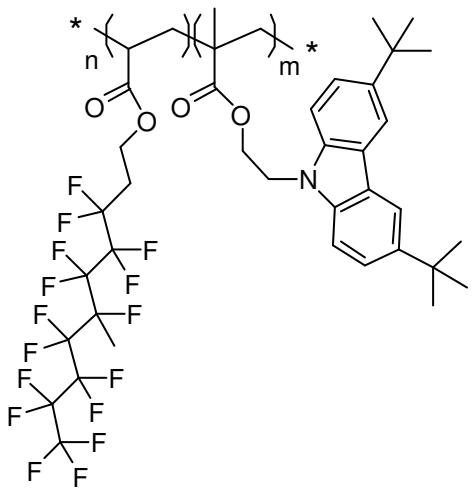

Poly(2–(3,6–di–tert–butyl–9H–carbazol–9–yl)ethyl methacrylate)–co–(3,3,4,4,5,5,6,7,7,8,8,9,9,10,10,10–hexadecafluoro–6–methyldecyl acrylate), 75:25 (m:n) ratio

2–(3,6–di–tert–butyl–9H–carbazol–9–yl)ethyl methacrylate (150 mg, 0.38 mmol) and 3,3,4,4,5,5,6,7,7,8,8,9,9,10,10,10–hexadecafluoro–6–methyldecyl acrylate (75 mg, 0.145 mmol) were combined with anhydrous tetrahydrofuran (1.0 mL) and acetonitrile (1.0 mL) in a pressure vessel purged with nitrogen. Azobisisobutyronitrile (2 mg, catalytic amount) was added and the pressure vessel was sealed and heated and stirred at 75 °C for 24 hours. The reaction was cooled to room temperature and the reaction mixture precipitated into cold methanol (150 mL). A white solid formed which was dissolved in a minimum amount of dichloromethane and precipitated into cold methanol (150 mL). This was repeated a 3rd time to finally yield a white powder (PJH–III–193a, 120 mg, 53 % yield). ^{1}H NMR (400.14 MHz, CD_2Cl_2) δ 8.15 – 7.85 (br, 2H), 7.50 – 7.0 (br, 4H), 4.60 – 3.80 (br, m, 4.6H), 2.5 – 2.0 (br, 0.6H), 1.9 – 1.0 (br, m, 20.9H), 1.0 – 0.3 (br, 3H). ^{1}H is indicative of a m:n ratio of 76:24. Analysis calculated (for a m:n ratio of 74:26) (found) %: C 64.00 (63.39), H 6.23 (6.22), F 19.78 (19.55), N 2.44 (2.39).

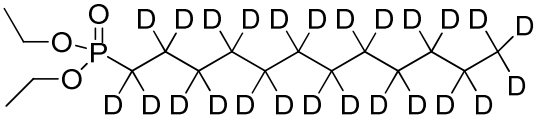

Diethyl dodecylphosphonate–d_{25}

Bromododecane–d_{25} (600 mg, 2.19 mmol) was combined with triethylphosphite (1.3 mL, 7.65 mmol) and the mixture heated and stirred at 135 °C overnight. Excess triethylphosphite and other side products were removed under vacuum (approximately 0.1 torr) and with heating at 60 °C for 5 hours. Column chromatography (stationary phase: silica, mobile phase: ethyl acetate) was used to isolate the desired product (R_f = 0.70, ethyl acetate) as a yellow – tinged liquid (PJH–III–194a, 500 mg, 69 % yield). ^{1}H NMR (400.14 MHz, $CDCl_3$) δ 4.18 – 4.00 (m, 4H), 1.32 (t, *J* = 7.06 Hz, 6H). ^{2}H NMR (76.77 MHz, CH_2Cl_2) δ 1.63 (br, 2D), 1.49 (br, 2D), 1.5 – 0.9 (m, 18D), 0.82 (br, 3D). ^{13}C{^{1}H} NMR (100.62 MHz, CD_2Cl_2) δ 139.4, 128.6 (2C), 127.9 (2C), 127.7, 73.03, 70.88, 61.57 (d, *J* = 6.4 Hz, 2C), 30.95 (d, *J* = 16.8 Hz), 30.17, 29.94, 29.91, 29.85, 29.75, 29.48, 26.58, 25.91 (d, *J* = 139.8 Hz), 22.78 (d, *J* = 5.3 Hz), 16.68 (d, *J* = 5.9 Hz, 2C). ^{13}C{^{1}H} NMR (100.62 MHz, $CDCl_2$) δ 61.53 (d, *J* = 6.4 Hz, 2C), 30.92 (quint, *J* = 18.8 Hz), 29.73 (quint, *J* = 18.5 Hz), 29.4 – 27.5 (m, 6C), 25.06 (dquint, *J* = 139.7, 19.3 Hz), 22.3 – 21.2 (m, 2C), 16.68 (d, *J* = 5.3 Hz, 2C), 13.29 (sept, *J* = 18.9 Hz). ^{31}P{^{1}H} NMR (161.98 MHz, $CDCl_3$): δ 33.56. Analysis calculated (found) %: C 57.96 (57.40), H 10.64 (10.68). MS (ESI). Exact mass calculated (found) for $[M+H]^+$, m/z): 331.3893 (331.3837).[1]

[1] As the elemental analysis did not pass, the appropriate NMR spectra are shown in Appendix A.

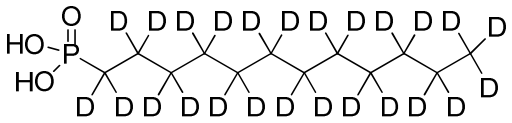

Dodecylphosphonic acid–d_{25}

Diethyl dodecylphosphonate–d_{25} (250 mg, 0.754 mmol) was dissolved in dry dichloromethane (10 mL). Bromotrimethylsilane (0.40 mL, 3.0 mmol) was added *via* syringe. The reaction was capped with a greased glass stopper and allowed to stir overnight. The volatiles were removed under reduced pressure to yield a yellow oil. This was dissolved in 10:1 methanol: water (10 mL) and allowed to stir overnight. After removing the solvents, recrystallization from acetonitrile yielded a white crystalline solid (PJH–III–210a,h, 82 mg, 40 % yield). (PJH–III–215e, 2.173 g, 42 % yield). ^{2}H NMR (76.77 MHz, DMSO) δ 1.65 – 0.65 (m, 22D), 0.73 (br, 3D). ^{13}C{^{1}H} NMR (125.77 MHz, DMSO) δ 30.79 (quint, *J* = 18.7 Hz), 30.0 – 29.1 (m), 29.0 – 27.5 (m, 6C), 27.31 (dm, *J* = 135.8 Hz), 22.8 – 21.9 (m), 21.66 (quint, *J* = 18.7 Hz), 13.61 (sept, *J* = 18.7 Hz). ^{31}P{^{1}H} NMR (161.98 MHz, DMSO): δ 28.03. Analysis calculated (found) %: C 52.32 (52.52), H 9.88 (9.99). MS (ESI, m/z): 276 (M^{+}, 85%). Exact mass calculated (found) for $[M+H]^{+}$, m/z): 276.3340 (276.3305).

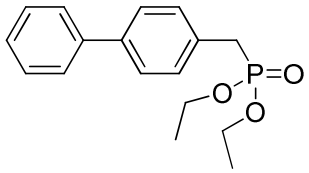

Diethyl biphenyl–4–ylmethylphosphonate

4–bromobiphenyl (5.0 g, 20.2 mmol) was combined with triethylphosphite (12 mL, 70.8 mmol) and the reaction mixture stirred at 135 °C overnight. Excess triethylphosphite and other side products were removed under vacuum (approximately 0.1 torr) and with heating at 60 °C for 5 hours. Upon cooling a white solid formed. This was filtered and washed copiously with cold hexanes. The final product was isolated as a waxy white solid (PJH–III–198a, 5.49 g, 89 % yield). ^{1}H NMR is consistent with the desired produc.[96]

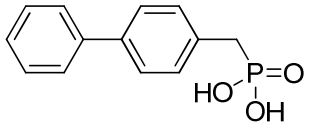

Biphenyl–4–ylmethylphosphonic acid

Diethyl biphenyl–4–ylmethylphosphonate (4.0 g, 13.14 mmol) was dissolved in dry dichloromethane (70 mL). Bromotrimethylsilane (6.0 mL, 46 mmol) was added *via* syringe. The reaction was capped with a greased glass stopper and allowed to stir overnight. The volatiles were removed under reduced pressure to yield a yellow oil. This was dissolved in 10:1 methanol: water (60 mL) and allowed to stir overnight. After removing the solvents, recrystallization from acetonitrile yielded a white crystalline solid

(PJH–III–201a, 2.915 g, 89 % yield). Analysis calculated (found) %: C 62.90 (62.87), H 5.28 (5.39). ^{1}H NMR is consistent with the desired product.[97, 98]

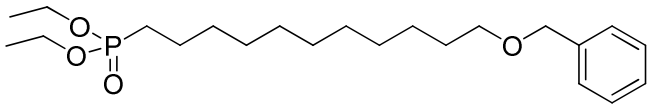

Diethyl 11–(benzyloxy)undecylphosphonate

Diethyl 11–hydroxyundecylphosphonate (4.0 g, 13.0 mmol) and 18–crown–6 (spatula tip) were added to anhydrous tetrahydrofuran under inert atmosphere. Sodium hydride (312 mg, 13.0 mmol) was added and the solution allowed to stir for 10 minutes. Benzyl bromide (2.4 mL, 19.5 mmol) was then added and the reaction stirred at reflux for 4 hours. After cooling to room temperature, dichloromethane was added and the mixture washed with water and brine. The organic layer was collected, dried over magnesium sulfate, and concentrated under reduced pressure to yield a liquid. Column chromatography (stationary phase: silica, mobile phase: ethyl acetate) was used to isolate the desired product (R_f = 0.70, ethyl acetate) as a clear oil (PJH–III–215e, 2.173 g, 42 % yield). ^{1}H NMR (500.13 MHz, CD_2Cl_2) δ 7.36 – 7.29 (m, 4H), 7.29 – 7.23 (m), 4.47 (2H), 4.10 – 3.97 (m, 4H), 3.45 (t, *J* = 6.62 Hz, 2H), 1.72 – 1.62 (m, 2H), 1.62 – 1.48 (m, 4H), 1.40 – 1.20 (m, 20H). ^{13}C{^{1}H} NMR (100.62 MHz, CD_2Cl_2) δ 139.4, 128.6 (2C), 127.9 (2C), 127.7, 73.03, 70.88, 61.57 (d, *J* = 6.4 Hz, 2C), 30.95 (d, *J* = 16.8 Hz), 30.17, 29.94, 29.91, 29.85, 29.75, 29.48, 26.58, 25.91 (d, *J* = 139.8 Hz), 22.78 (d, *J* = 5.3 Hz), 16.68 (d, *J* = 5.9 Hz, 2C). ^{31}P{^{1}H} NMR (202.45 MHz, CD_2Cl_2): δ 32.83. Analysis calculated (found) %: C 66.30 (65.66), H 9.86 (9.95). MS (ESI, m/z): 399 (M^+, 100%).

Exact mass calculated (found) for $[M+H]^+$, m/z): 399.2659 (399.2671).[m]

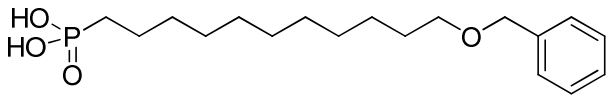

11–(benzyloxy)undecylphosphonic acid

Diethyl 11–(benzyloxy)undecylphosphonate (1.00 g, 2.51 mmol) was dissolved in dry dichloromethane (20 mL). Bromotrimethylsilane (1.1 mL, 8.28 mmol) was added *via* syringe. The reaction was capped with a greased glass stopper and allowed to stir overnight. The volatiles were removed under reduced pressure to yield a yellow oil. This was dissolved in 5: 1 methanol: water (20 mL) and allowed to stir 4 hours more. After concentration of the organic, the viscous yellow oil was dissolved in hot acetonitrile and a white crystalline solid was obtained (PJH–III–218a, 806 mg, 94 % yield). ^{1}H NMR (400.14 MHz, DMSO) δ 7.40 – 7.20 (m, 5H), 4.43 (2H), 3.39 (t, J = 6.49 Hz, 2H), 1.60 – 1.33 (m, 6H), 1.33 – 1.15 (m, 14H). ^{13}C{^{1}H} NMR (100.62 MHz, DMSO) δ 138.7, 128.2 (2C), 127.4 (2C), 127.3, 71.79, 69.59, 30.09 (d, J = 15.9 Hz), 29.21, 29.04, 29.01, 28.89, 28.87, 28.73, 27.53 (d, J = 136.6 Hz), 25.72, 22.72 (d, J = 4.6 Hz). ^{31}P{^{1}H} NMR (161.97 MHz, DMSO): δ 27.71. Analysis calculated (found) %: C 63.14 (62.87), H 9.13 (9.13). MS (ESI, m/z): 341 (M^-, 100%). Exact mass calculated (found) for $[M–H]^-$, m/z): 341.188722 (341.189600).

[m] As the elemental analysis did not pass, the appropriate NMR spectra are shown in Appendix A.

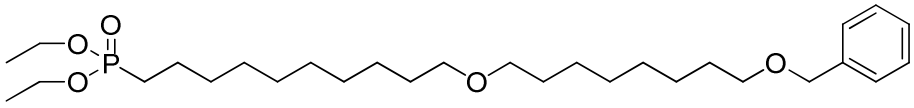

Diethyl 10–(8–(benzyloxy)octyloxy)decylphosphonate

1,8–octanediol (5.0 g, 34.2 mmol) and 18–crown–6 (spatula tip) were added to anhydrous tetrahydrofuran under inert atmosphere. Sodium hydride (820 mg, 34.2 mmol) was added and the solution stirred for 10 minutes. Benzyl bromide (4.1 mL, 34.2mmol) was then added and the reaction stirred at reflux for 4 hours and then overnight at room temperature. A white precipitate formed and this was filtered off. The filtrate was concentrated under reduced pressure. Column chromatography (stationary phase: silica, mobile phase: 1: 1 hexanes: ethyl acetate) was used to isolate the desired product (R_f = 0.40, 1: 1hexanes: ethyl acetate) as a yellow oil (PJH–III–216a, 3.914 g, 48 % yield). ^{1}H NMR is consistent with 8–(benzyloxy)octan–1–ol. [99]

8–(benzyloxy)octan–1–ol (1.15 g, 4.86 mmol) was added to anhydrous dimethylformamide in a round bottom flask under inert atmosphere. Sodium hydride (175 mg, 7.3 mmol) was added and the solution allowed to stir for 30 minutes. 1,10–dibromodecane (11.7 g, 38.9 mmol) was then added and the reaction stirred at 90 °C for 4 hours and then cooled to room temperature. The solvent was removed under reduced pressure. Column chromatography (stationary phase: silica, mobile phase: hexanes with increasing amounts of ethyl acetate) was used to isolate the desired product (R_f = 0.65, 9: 1 hexanes: ethyl acetate) as a viscous oil. The resulting oil contained some desired product (((8–(10–bromodecyloxy)octyloxy)methyl)benzene**,** as evidenced by ^{1}H NMR), though impure (tlc), and used in the next reaction without further purification.

((8–(10–bromodecyloxy)octyloxy)methyl)benzene (900 mg, 2.0 mmol) was

combined with triethylphosphite (5 mL, 30 mmol) and the reaction mixture stirred at 135 °C for 2 days. Excess triethylphosphite and other side products were removed under vacuum (approximately 0.1 torr) and with heating at 80 °C for 5 hours to yield a viscous oil (PJH–III–225a, 760 mg, 74 % yield). ^{1}H NMR (400.14 MHz, CD_2Cl_2) δ 7.35 – 7.29 (m, 4H), 7.29 – 7.21 (m), 4.46 (2H), 4.13 – 3.92 (m, 4H), 3.45 (t, *J* = 6.60 Hz, 2H), 3.35 (t, *J* = 6.66 Hz, 4H), 1.73 – 1.62 (m, 2H), 1.62 – 1.41 (m, 8H), 1.41 – 1.18 (m, 26H). ^{13}C{^{1}H} NMR (100.62 MHz, CD_2Cl_2) δ 139.4, 128.6 (2C), 127.9 (2C), 127.7, 73.02, 71.13 (2C), 70.87, 61.61 (d, *J* = 6.4 Hz, 2C), 30.94 (d, *J* = 16.8 Hz), 30.17 (2C), 30.14, 29.91, 29.84, 29.81 (2C), 29.72, 29.45, 26.57, 26.53 (2C), 25.87 (d, *J* = 140.3 Hz), 22.76 (d, *J* = 5.2 Hz), 16.65 (d, *J* = 5.9 Hz, 2C). ^{31}P{^{1}H} NMR (161.97 MHz, CD_2Cl_2): δ 32.94. Analysis calculated (found) %: C 67.94 (67.08), H 10.42 (10.50). MS (ESI, m/z): 513 (M^+, 100%). Exact mass calculated (found) for $[M+H]^+$, m/z): 513.3703 (513.3674).[n]

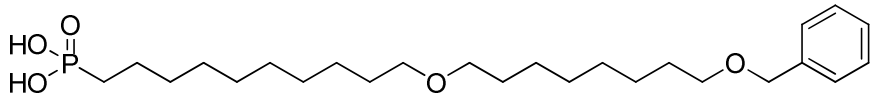

10–(8–(Benzyloxy)octyloxy)decylphosphonic acid

Diethyl 10–(8–(benzyloxy)octyloxy)decylphosphonate (680 mg, 1.33 mmol) was dissolved in dry dichloromethane (15 mL). Bromotrimethylsilane (0.53 mL, 4.05 mmol) was added *via* syringe. The reaction was capped with a greased glass stopper and stirred overnight. The volatiles were removed under reduced pressure to yield a yellow oil. This was dissolved in 5: 1 methanol: water (10 mL) and stirred 4 hours more. After

[n] As the elemental analysis did not pass, the appropriate NMR spectra are shown in Appendix A.

concentration of the organic, the viscous yellow oil was recrystallized in acetonitrile to yield a white crystalline solid (PJH–III–229a,e; 590 mg, 98 % yield). ^{1}H NMR (400.14 MHz, DMSO) δ 7.40 – 7.19 (m, 5H), 4.42 (2H), 3.39 (t, *J* = 6.48 Hz, 2H), 3.29 (t, *J* = 6.46 Hz, 4H), 1.58 – 1.34 (m, 10H), 1.34 – 1.10 (m, 20H). ^{13}C{^{1}H} NMR (100.62 MHz, DMSO) δ 138.7, 128.2 (2C), 127.3 (2C), 127.3, 71.79, 69.91 (2C), 69.59, 30.11 (d, *J* = 16.0 Hz), 29.25, 29.21, 29.20, 29.05, 28.89 (2C), 28.84 (2C), 28.73, 27.55 (d, *J* = 136.5 Hz), 25.76, 25.69, 25.67, 22.74 (d, *J* = 4.5 Hz). ^{31}P{^{1}H} NMR (161.97 MHz, DMSO): δ 27.74. Analysis calculated (found) %: C 65.76 (65.79), H 9.93 (10.00). MS (ESI, m/z): 455 (M^-, 100%). Exact mass calculated (found) for $[M–H]^-$, m/z): 455.2932 (455.2932).

2.5.1 Scale–Up of Phosphonate Precursors and Often–Used Phosphonic Acids

Many of the following phosphonic acids which will be discussed derive from a smaller set of compounds. As such, some of their phosphonate precursors were scaled up so as to ensure sufficient quantities for further reactions. Additionally, they will aid others in the group who are looking to synthesize phosphonic acids or derivatives thereof. Some phosphonic acids which are heavily used were also synthesized in large amounts (Figure 2.45).

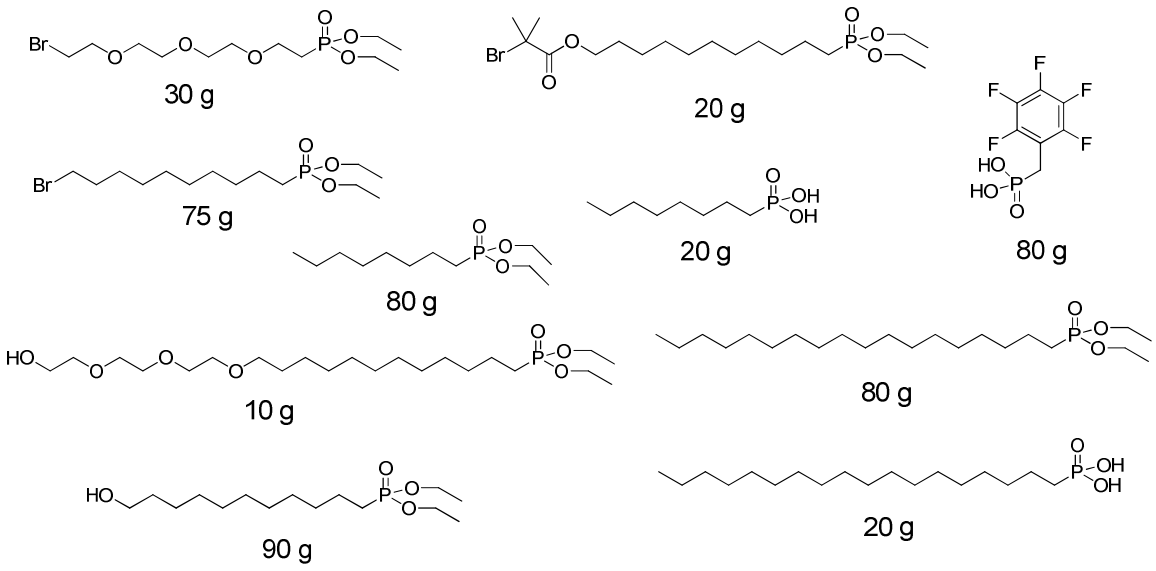

Figure 2.45 Phosphonates and phosphonic acids which have been synthesized in large quantities.

The precursors shown above were for the most part synthesized from commercially available starting materials in 1–3 steps.

2.6 References

1. Engel, R.; Lee, J.; Cohen, I., *Synthesis of Carbon-Phosphorus Bonds*. 2nd ed.; CRC Press: New York, 2004.

2. Freedman, L. D.; Doak, G. O., The preparation and properties of phosphonic acids. *Chemical Reviews* **1957,** 57, (3), 479-523.

3. Kosolapoff, G. M.; Maier, L., *Organic Phosphorus Compounds*. John Wiley & Sons: New York, 1976; Vol. 7.

4. Petrov, K. A.; Chizhov, V. M.; Pokatun, V. P.; Agafonov, S. V., Methods of synthesis of arylphosphonic and arylphosphonothioic acids and their derivatives. *Russian Chemical Reviews* **1986,** 55, (11), 1042 - 1053.

5. Yao, Q.; Levchik, S., A concise method for synthesis of diaryl aryl- or alkylphosphonates. *Tetrahedron Letters* **2006,** 47, (3), 277-281.

6. Kiddle, J. J.; Gurley, A. F., Microwave irradiation in organophosphorus chemistry 1: The Michaelis-Arbuzov reaction. *Phosphorus Sulfur and Silicon and the Related Elements* **2000,** 160, 195-205.

7. Villemin, D.; Simeon, F.; Decreus, H.; Jaffres, P. A., Rapid and efficient Arbuzov reaction under microwave irradiation. *Phosphorus Sulfur and Silicon and the Related Elements* **1998,** 133, 209-213.

8. Wolf, W.; Kharasch, N., Photolysis of iodoaromatic compounds in benzene. *Journal of Organic Chemistry* **1965,** 30, (8), 2493-2498.

9. Plumb, J. B.; Obrycki, R.; Griffin, C. E., Phosphonic acids and esters. 16. Formation of dialkyl phenylphosphonates by photoinitiated phenylation of trialkyl phosphites. *Journal of Organic Chemistry* **1966,** 31, (8), 2455-2458.

10. Obrycki, R.; Griffin, C. E., Phosphonic acids and esters.19. Syntheses of substituted phenyl- and arylphosphonates by photoinitiated arylation of trialkyl phosphites. *Journal of Organic Chemistry* **1968,** 33, (2), 632-636.

11. Burton, D. J.; Flynn, R. M., Facile synthesis of trifluoromethane-phosphonates and pentafluorobenzenephosphonates. *Synthesis-Stuttgart* **1979**, (8), 615-615.

12. Tavs, P., Reaction of aryl halides with trialkyl phosphites and dialkyl benzenephosphonites to aromatic phosphonates and phosphinates by nickel salt catalysed arylation. *Chemische Berichte* **1970,** 103, (8), 2428-2436.

13. Connor, J. A.; Jones, A. C.; Price, R., Copper(II) ethanoate-assisted phosphonation of aryl halides. *Journal of the Chemical Society-Chemical Communications* **1980**, (4), 137-138.

14. Hall, N.; Price, R., Copper-promoted reaction of ortho-halogenodiarylazo-compounds with nucleophiles.1. Copper-promoted reaction of ortho-bromodiarylazo-compounds with trialkyl phosphites - novel method for the preparation of dialkyl arylphosphonates. *Journal of the Chemical Society-Perkin Transactions 1* **1979**, (11), 2634-2641.

15. Hirao, T.; Masunaga, T.; Yamada, N.; Ohshiro, Y.; Agawa, T., Palladium-catalyzed new carbon-phosphorus bond formation. *Bulletin of the Chemical Society of Japan* **1982,** 55, (3), 909-913.

16. Balthazor, T. M.; Grabiak, R. C., Nickel-catalyzed Arbuzov reaction - mechanistic observations. *Journal of Organic Chemistry* **1980,** 45, (26), 5425-5426.

17. Grabiak, R. C.; Miles, J. A.; Schwenzer, G. M., Synthesis of phosphonic dichlorides and correlation of their P-31 chemical shifts. *Phosphorus Sulfur and Silicon and the Related Elements* **1980,** 9, (2), 197-202.

18. Kukhar, V. P.; Sagina, E. I., Reaction of iodoarenes with triethyl phosphite in presence of copper monochloride. *Zhurnal Obshchei Khimii* **1977,** 47, (7), 1662-1662.

19. Hirao, T.; Masunaga, T.; Ohshiro, Y.; Agawa, T., A novel synthesis of dialkyl arenephosphonates. *Synthesis-Stuttgart* **1981**, (1), 56-57.

20. Kabacknik, M. M.; Solntseva, M. D.; Izmer, V. V.; Novikova, Z. S.; Beletskaya, I. P., Palladium-catalyzed phase-transfer arylation of dialkyl phosphonates. *Russian Journal of Organic Chemistry* **1998,** 34, (1), 93 - 97.

21. Goossen, L. J.; Dezfuli, M. K., Practical protocol for the palladium-catalyzed synthesis of arylphosphonates from bromoarenes and diethyl phosphite. *Synlett* **2005**, (3), 445-448.

22. Villemin, D.; Elbilali, A.; Simeon, F.; Jaffres, P. A.; Maheut, G.; Mosaddak, M.; Hakiki, A., Nickel and palladium catalysed reaction of triethyl phosphite with aryl halides under microwave irradiation. *Journal of Chemical Research-S* **2003**, (7), 436-437.

23. Buchner, B.; Lockhart, L. B., An improved method of synthesis of aromatic dichlorophosphines. *Journal of the American Chemical Society* **1951,** 73, (2), 755-756.

24. Kosolapoff, G. M.; Huber, W. F., Synthesis of aromatic phosphonic acids and their derivatives.1. The derivatives of benzene, toluene and chlorobenzenes. *Journal of the American Chemical Society* **1947,** 69, (8), 2020-2021.

25. Miles, J. A.; Beeny, M. T.; Ratts, K. W., General route to methoxy-substituted arylphosphonous dichlorides via mild Lewis acid catalysts. *Journal of Organic Chemistry* **1975,** 40, (3), 343-347.

26. Griffin, C. E.; Wells, H. J., Phosphonic acids and esters.1. Radical initiated addition of phosphorous acid to olefins. *Journal of Organic Chemistry* **1959,** 24, (12), 2049-2051.

27. Stiles, A. R.; Vaughan, W. E.; Rust, F. F., The preparation of dialkyl alkylphosphonates by addition of dialkyl phosphites to olefins. *Journal of the American Chemical Society* **1958,** 80, (3), 714-716.

28. Stiles, A. R.; Rust, F. F.; Vaughan, W. E., The preparation of organo-phosphines by the addition of phosphine to unsaturated compounds. *Journal of the American Chemical Society* **1952,** 74, (13), 3282-3284.

29. Crofts, P. C., Compounds containing carbon phosphorus bonds. *Quarterly Reviews* **1958,** 12, (4), 341-366.

30. Balczewski, P.; Mikolajczyk, M., Phosphorus containing radicals.1. Free-radical reaction of alpha-haloalkylphosphonates with alkenes and alkynes - a new approach to modified phosphonates. *Synthesis-Stuttgart* **1995**, (4), 392-396.

31. McKenna, C. E.; Higa, M. T.; Cheung, N. H.; Mckenna, M. C., Facile dealkylation of phosphonic acid dialkyl esters by bromotrimethylsilane. *Tetrahedron Letters* **1977**, (2), 155-158.

32. Rabinowitz, R., Reactions of phosphonic acid esters with acid chlorides - a very mild hydrolytic route. *Journal of Organic Chemistry* **1963,** 28, (11), 2975-2978.

33. Gutierrez, A. J.; Prisbe, E. J.; Rohloff, J. C., Dealkylation of phosphonate esters with chlorotrimethylsilane. *Nucleosides Nucleotides & Nucleic Acids* **2001,** 20, (4-7), 1299-1302.

34. Bohmer, V.; Vogt, W.; Chafaa, S.; Meullemeestre, J.; Schwing, M. J.; Vierling, F., (O-hydroxyphenyl)Methylphosphonic acids - synthesis and potentiometric determinations of their pka values. *Helvetica Chimica Acta* **1993,** 76, (1), 139-149.

35. Bellamy, L. J., *The Infrared Spectra of Complex Molecules*. John Wiley & Sons: New York, 1975.

36. Bellamy, L. J., *Advances in Infrared Group Frequencies: the Infrared Spectra of Complex Molecules*. Chapman and Hall: London, 1980; Vol. 2.

37. Corbridge, D. E. C., *Topics in Phosphorus Chemistry*. Interscience Publishers: New York, 1969; Vol. 6.

38. Thomas, L. C., *The Identification of Functional Groups in Organophosphorus Compounds*. Academic Press: New York, 1974.

39. Thomas, L. C., *Interpretation of the Infrared Spectra of Organophosphorus Compounds*. Heyden Sons Ltd.: New York, 1974.

40. Corbridge, D. E. C.; Lowe, E. J., The infrared spectra of inorganic phosphorus compounds.2. Some salts of phosphorus oxy-acids. *Journal of the Chemical Society* **1954**, (Dec), 4555-4564.

41. Daasch, L. W., The structures of the dialkyl phosphonates and some of their salts. *Journal of the American Chemical Society* **1958,** 80, (19), 5301-5303.

42. Gao, W.; Dickinson, L.; Grozinger, C.; Morin, F. G.; Reven, L., Self-assembled monolayers of alkylphosphonic acids on metal oxides. *Langmuir* **1996,** 12, (26), 6429-6435.

43. Giza, M.; Thissen, P.; Grundmeier, G., Adsorption kinetics of organ-ophosphonic acids on plasma-modified oxide-covered aluminum surfaces. *Langmuir* **2008,** 24, (16), 8688-8694.

44. Guerrero, G.; Mutin, P. H.; Vioux, A., Anchoring of phosphonate and phosphinate coupling molecules on titania particles. *Chemistry of Materials* **2001,** 13, (11), 4367-4373.

45. Crutchfield, M. M.; Dungan, C. H.; Letcher, J. H.; Mark, V.; Van Wazer, J. R., *Topics in Phosphorus Chemistry*. John Wiley & Sons: New York, 1967; Vol. 5.

46. Lee, J.; Jung, B. J.; Lee, J. I.; Chu, H. Y.; Do, L. M.; Shim, H. K., Modification of an ITO anode with a hole-transporting SAM for improved OLED device characteristics. *Journal of Materials Chemistry* **2002,** 12, (12), 3494-3498.

47. Halik, M.; Klauk, H.; Zschieschang, U.; Schmid, G.; Dehm, C.; Schutz, M.; Maisch, S.; Effenberger, F.; Brunnbauer, M.; Stellacci, F., Low-voltage organic transistors with an amorphous molecular gate dielectric. *Nature* **2004,** 431, (7011), 963-966.

48. Kim, P.; Jones, S. C.; Hotchkiss, P. J.; Haddock, J. N.; Kippelen, B.; Marder, S. R.; Perry, J. W., Phosphonic acid-modified barium titanate polymer nanocomposites with high permittivity and dielectric strength. *Advanced Materials* **2007,** 19, (7), 1001-1005.

49. Veinot, J. G. C.; Marks, T. J., Toward the ideal organic light-emitting diode. The versatility and utility of interfacial tailoring by cross-linked siloxane interlayers. *Accounts of Chemical Research* **2005,** 38, (8), 632-643.

50. Traina, C. A.; Schwartz, J., Surface modification of Y_2O_3 nanoparticles. *Langmuir* **2007,** 23, (18), 9158-9161.

51. Finn, P. W.; Bandara, M.; Butcher, C.; Finn, A.; Hollinshead, R.; Khan, N.; Law, N.; Murthy, S.; Romero, R.; Watkins, C.; Andrianov, V.; Bokaldere, R. M.; Dikovska, K.; Gailite, V.; Loza, E.; Piskunova, I.; Starchenkov, I.; Vorona, M.; Kalvinsh, I., Novel sulfonamide derivatives as inhibitors of histone deacetylase. *Helvetica Chimica Acta* **2005,** 88, (7), 1630-1657.

52. Radhakrishnan, B.; Ranjan, R.; Brittain, W. J., Surface initiated polymerizations from silica nanoparticles. *Soft Matter* **2006,** 2, (5), 386-396.

53. Maliakal, A.; Katz, H.; Cotts, P. M.; Subramoney, S.; Mirau, P., Inorganic oxide core, polymer shell nanocomposite as a high K gate dielectric for flexible electronics applications. *Journal of the American Chemical Society* **2005,** 127, (42), 14655-14662.

54. Sung, S. J.; Cho, K. Y.; Hah, H.; Lee, J.; Shim, H. K.; Park, J. K., Two different reaction mechanisms of cinnamate side groups attached to the various polymer backbones. *Polymer* **2006,** 47, (7), 2314-2321.

55. Griep-Raming, N.; Karger, M.; Menzel, H., Using benzophenone-functionalized phosphonic acid to attach thin polymer films to titanium surfaces. *Langmuir* **2004,** 20, (26), 11811-11814.

56. Pahnke, J.; Ruhe, J., Attachment of polymer films to aluminium surfaces by photochemically active monolayers of phosphonic acids. *Macromolecular Rapid Communications* **2004,** 25, (15), 1396-1401.

57. Kim, P.; Zhang, X. H.; Domercq, B.; Jones, S. C.; Hotchkiss, P. J.; Marder, S. R.; Kippelen, B.; Perry, J. W., Solution-processible high-permittivity nanocomposite gate insulators for organic field-effect transistors. *Applied Physics Letters* **2008,** 93, (1), 013302/1-013302/3.

58. Bellucci, C.; Gualtieri, F.; Chiarini, A., Negative inotropic activity of para-substituted diethyl benzylphosphonates related to Fostedil.3. *European Journal of Medicinal Chemistry* **1987,** 22, (5), 473-477.

59. Vugts, D. J.; Koningstein, M. M.; Schmitz, R. F.; de Kanter, F. J. J.; Groen, M. B.; Orru, R. V. A., Multicomponent synthesis of dihydropyrimidines and thiazines. *Chemistry-a European Journal* **2006,** 12, (27), 7178-7189.

60. Blackburn, G. M.; Ingleson, D., The dealkylation of phosphate and phosphonate esters by iodotrimethylsilane - a mild and selective procedure. *Journal of the Chemical Society-Perkin Transactions 1* **1980**, (5), 1150-1153.

61. Rice, B. L.; Guo, C. Y.; Kirchmeier, R. L., Perfluorocarbon phosphonic and sulfonic acids containing discretely varying terminal functional groups. *Inorganic Chemistry* **1991,** 30, (24), 4635-4638.

62. Spencer, T. A.; Onofrey, T. J.; Cann, R. O.; Russel, J. S.; Lee, L. E.; Blanchard, D. E.; Castro, A.; Gu, P.; Jiang, G. J.; Shechter, I., Zwitterionic sulfobetaine inhibitors of squalene synthase. *Journal of Organic Chemistry* **1999,** 64, (3), 807-818.

63. Plater, M. J.; Jackson, T., Polyaromatic amines. Part 3: Synthesis of poly(diarylamino)styrenes and related compounds. *Tetrahedron* **2003,** 59, (25), 4673-4685.

64. Mayer, C. R.; Herve, M.; Lavanant, W.; Blais, J. C.; Secheresse, F., Hybrid cyclic dimers of divacant heteropolyanions: synthesis, mass spectrometry (MALDI-TOF and ESI-MS) and NMR multinuclear characterisation. *European Journal of Inorganic Chemistry* **2004**, (5), 973-977.

65. Maier, L.; Crutchfield, M. M., Organic phosphorus compounds.70. Preparation and properties of new phosphorus containing chelating agents for calcium and magnesium ions. *Phosphorus Sulfur and Silicon and the Related Elements* **1978,** 5, (1), 45-51.

66. Ernst, L., C-13 NMR spectroscopy of diethyl alkyl-phosphonates and benzyl-phosphonates - study of phosphorus-carbon spin-spin coupling constants over one to 7 Bonds. *Organic Magnetic Resonance* **1977,** 9, (1), 35-43.

67. Filler, R.; Cantrell, G. L.; Wolanin, D.; Naqvi, S. M., Synthesis of polyfluoroaryl [2.2] cyclophanes. *Journal of Fluorine Chemistry* **1986,** 30, (4), 399-414.

68. Flaherty, D. P.; Walsh, S. M.; Kiyota, T.; Dong, Y.; Ikezu, T.; Vennerstrom, J. L., Polyfluorinated bis-styrylbenzene beta-Amyloid plaque binding ligands. *Journal of Medicinal Chemistry* **2007,** 50, (20), 4986-4992.

69. Krebs, F. C.; Jensen, T., Fluorinated molecules relevant to conducting polymer research. *Journal of Fluorine Chemistry* **2003,** 120, (1), 77-84.

70. Lee, T. R.; Carey, R. I.; Biebuyck, H. A.; Whitesides, G. M., The wetting of monolayer films exposing ionizable acids and bases. *Langmuir* **1994,** 10, (3), 741-749.

71. Woo, H. Y.; Hong, J. W.; Liu, B.; Mikhailovsky, A.; Korystov, D.; Bazan, G. C., Water-soluble [2.2]paracyclophane chromophores with large two-photon action cross sections. *Journal of the American Chemical Society* **2005,** 127, (3), 820-821.

72. Liaw, B. R.; Guo, W. J., Synthesis of Some Dialkyl Bromo-Substituted Benzyl Phosphonates. *Journal of the Chinese Chemical Society* **1984,** 31, (3), 311-314.

73. Bentouhami, E.; Bouet, G. M.; Khan, M. A., Acidity and complexation of (O-hydroxyphenyl) mono-methylenephosphonic acids towards lanthanide (III) ions. *Phosphorus Sulfur and Silicon and the Related Elements* **2003,** 178, (4), 903-921.

74. Corey, E. J.; Venkates.A, Protection of hydroxyl groups as tert-butyldimethylsilyl derivatives. *Journal of the American Chemical Society* **1972,** 94, (17), 6190-6191.

75. Coe, P. L.; Croll, B. T.; Patrick, C. R., Aromatic polyfluoro-compounds.35. 1,2,3,4-Tetrafluoroanthraquinone and some reactions of tetrafluorophthalic acid derivatives. *Tetrahedron* **1967,** 23, (1), 505-508.

76. Wang, X. J.; Lieberman, M., Zirconium-phosphonate monolayers with embedded disulfide bonds. *Langmuir* **2003,** 19, (18), 7346-7353.

77. Wu, S. Y.; Casida, J. E., Stereospecific intramolecular cyclization for asymmetric synthesis of (Rp)- and (Sp)-enantiomers of 2-octyl- and 2-phenyl-4H-1,3,2-benzodioxaphosphorin 2-oxides. *Phosphorus Sulfur and Silicon and the Related Elements* **1995,** 102, (1-4), 177-184.

78. Bravo-Altamirano, K.; Montchamp, J. L., A novel approach to phosphonic acids from hypophosphorous acid. *Tetrahedron Letters* **2007,** 48, (33), 5755-5759.

79. Tsai, M. Y.; Lin, J. C., Surface characterization and platelet adhesion studies of self-assembled monolayer with phosphonate ester and phosphonic acid functionalities. *Journal of Biomedical Materials Research* **2001,** 55, (4), 554-565.

80. Biron, E.; Otis, F.; Meillon, J. C.; Robitaille, M.; Lamothe, J.; Van Hove, P.; Cormier, M. E.; Voyer, N., Design, synthesis, and characterization of peptide

nanostructures having ion channel activity. *Bioorganic & Medicinal Chemistry* **2004,** 12, (6), 1279-1290.

81. Gawalt, E. S.; Avaltroni, M. J.; Danahy, M. P.; Silverman, B. M.; Hanson, E. L.; Midwood, K. S.; Schwarzbauer, J. E.; Schwartz, J., Bonding organics to Ti alloys: Facilitating human osteoblast attachment and spreading on surgical implant materials corrections (vol 19, pg 200, 2003). *Langmuir* **2003,** 19, (17), 7147-7147.

82. Apelt, J.; Ligneau, X.; Pertz, H. H.; Arrang, J. M.; Ganellin, C. R.; Schwartz, J. C.; Schunack, W.; Stark, H., Development of a new class of nonimidazole histamine H-3 receptor ligands with combined inhibitory histamine N-methyltransferase activity. *Journal of Medicinal Chemistry* **2002,** 45, (5), 1128-1141.

83. Gaboyard, M.; Hervaud, Y.; Boutevin, B., Synthesis and structural analysis of alkylphosphonic acids with a long hydrocarbon chain. *Phosphorus Sulfur and Silicon and the Related Elements* **2002,** 177, (4), 877-891.

84. Iorga, B.; Eymery, F.; Savignac, P., Controlled monohalogenation of phosphonates: A new route to pure alpha-monohalogenated diethyl benzylphosphonates. *Tetrahedron* **1999,** 55, (9), 2671-2686.

85. Woo, H. Y.; Liu, B.; Kohler, B.; Korystov, D.; Mikhailovsky, A.; Bazan, G. C., Solvent effects on the two-photon absorption of distyrylbenzene chromophores. *Journal of the American Chemical Society* **2005,** 127, (42), 14721-14729.

86. Shim, H. K.; Kang, I. N.; Jang, M. S.; Zyung, T.; Jung, S. D., Electroluminescence of polymer blend composed of conjugated and nonconjugated polymers. White-light-emitting Diode. *Macromolecules* **1997,** 30, (25), 7749-7752.

87. Pogorelova, S. P.; Kharitonov, A. B.; Willner, I.; Sukenik, C. N.; Pizem, H.; Bayer, T., Development of ion-sensitive field-effect transistor-based sensors for benzylphosphonic acids and thiophenols using molecularly imprinted TiO_2 films. *Analytica Chimica Acta* **2004,** 504, (1), 113-122.

88. Weis, U.; Andersson, J. T., Synthesis of fluorinated polycyclic aromatic hydrocarbons through a photochemical cyclization. *Polycyclic Aromatic Compounds* **2002,** 22, (1), 71-85.

89. Montoneri, E.; Savarino, P.; Quagliotto, P.; Adani, F.; Ricca, G., Organosulphur phosphorus acid compounds. Part 7. Preparation and analytical identification of difluorobenzylphosphono-sulfonic acids. *Phosphorus Sulfur and Silicon and the Related Elements* **1998,** 134, 99-108.

90. Nair, H. K.; Burton, D. J., Facile synthesis of fluorinated phosphonates via photochemical and thermal reactions. *Journal of the American Chemical Society* **1997,** 119, (39), 9137-9143.

91. Furin, G. G.; Krupoder, S. A.; Rezvukhin, A. I.; Kilina, T. M.; Yakobson, G. G., Aromatic Fluoroderivatives.95. The Investigation of the Behavior of the Polyfluoroaromatic Compounds Containing Group Va Elements in Acid-Media. *Journal of Fluorine Chemistry* **1983,** 22, (4), 345-375.

92. Grabiak, R. C.; Miles, J. A.; Schwenzer, G. M., Synthesis of Phosphonic Dichlorides and Correlation of Their P-31 Chemical-Shifts. *Phosphorus Sulfur and Silicon and the Related Elements* **1980,** 9, (2), 197-202.

93. Yagupolskii, L. M.; Ivanova, Z. M., p-Trifluoromethylphenyltetrafluorophosphorus and its derivatives. *Zhurnal Obshchei Khimii* **1960,** 30, (12), 4026-4030.

94. Bunnett, J. F.; Traber, R. P., Observations concerning scope and mechanism of photostimulated reactions of aryl iodides with diethyl phosphite ion - remarkable difference in behavior between meta-chloroiodobenzene and para-chloroiodobenzene. *Journal of Organic Chemistry* **1978,** 43, (10), 1867-1872.

95. Bost, R. W.; Quin, L. D.; Roe, A., The synthesis of dimethylaminoethyl esters of aromatic phosphonic acids. *Journal of Organic Chemistry* **1953,** 18, (4), 362-366.

96. Zimmerman, H. E.; Heydinger, J. A., Rearrangement of 1,3-diradicals - arylcyclopropane photochemistry. *Journal of Organic Chemistry* **1991,** 56, (5), 1747-1758.

97. Kosolapoff, G. M., Isomerization of alkyl phosphites.4. The synthesis of some alkaryl phosphonic acids and esters. *Journal of the American Chemical Society* **1945,** 67, (12), 2259-2260.

98. Okamoto, Y.; Iwamoto, N.; Shikata, T.; Takamuku, S., Photochemical C-P bond cleavage of some (substituted benzyl)phosphonic acid derivatives. *Nippon Kagaku Kaishi* **1987**, (7), 1255-1261.

99. Gao, X.; Hall, D. G., Catalytic asymmetric synthesis of a potent thiomarinol antibiotic. *Journal of the American Chemical Society* **2005,** 127, (6), 1628-1629.

Chapter 3

Binding and Coverage of Phosphonic Acids on Metal Oxides

This chapter focuses on how and to what extent phosphonic acids can bind to various metal oxide substrates. The first section focuses on a discussion of the different possible binding modes of phosphonic acids adsorbed onto metal oxides and those most commonly seen. Several characterization techniques utilized for this assessment are briefly described.

The second section discusses the types of coverages that can be expected from phosphonic acids bound to different metal oxide substrates, and how this can be controlled. The evolution of surface coverage with respect to treatment time with phosphonic acids will also be discussed, as will the issue of monolayers and multilayers of phosphonic acids. Characterization techniques routinely used to characterize surfaces with monolayers and multilayers will be presented.

3.1 Binding Modes and Energies of Bond Formation

It can be important to know how strongly a molecule, or group of molecules, is/are bound to a surface. While the energies of bond formation of molecules to surfaces can be determined, it is generally difficult to do so and data analysis relies upon a number of simplifications and approximations.[1] However, relative strengths can be related by

determining the types of bonds present. Monolayers based on thiols on gold form very easily, but the gold–thiol bond is easily broken, and so thiols adsorb and desorb on and off the surface when in solution.[2] Similarly, the manner in which carboxylic acids, silanes and phosphonic acids attach to metal oxides will ultimately play a role in how strong the attachment is and consequently the robustness of the resulting monolayer. Information about the stability of monolayers is vital if they are to be used in high–stress or long–term applications. Insight about the stability of monolayer–forming molecules can be deduced from a knowledge about how they bind to the surface.

Experiments characterizing the surface of planar ITO substrates were done in collaboration with Sergio Paniagua (Chemistry, University of Arizona). Experiments characterizing the surface of planar $BaTiO_3$ were performed by Professor Neal Armstrong and coworkers (Chemistry, University of Arizona) and those characterizing the surface of $BaTiO_3$ nanoparticles were performed by Philseok Kim (Chemistry, Georgia Institute of Technology). Theoretical calculations were performed by Pavel Paramonov (Chemistry, Georgia Institute of Technology). Isothermal calorimetry experiments were performed in collaboration with Nathan Hankins and Philseok Kim (Chemistry, Georgia Institute of Technology).

3.1.1 Binding Modes Available

There are three oxygen atoms in the phosphonic acid moiety – one phosphoryl oxygen and two hydroxyl oxygen atoms. Up to three oxygen atoms can bind to a surface,

thus to a first approximation phosphonic acids can bind to an oxide surface in either a monodentate, bidentate, or tridentate fashion. There can also be various degrees of chemisorption and/or hydrogen bonding involved. Additionally, the bonds can be either bridging (where each acid oxygen binds to a different metal atom) or chelating (where two or three of the acid oxygen atoms bind to the same metal atom.[3] All of these possibilities lead to a large variety of possible binding configurations (Figure 3.1)

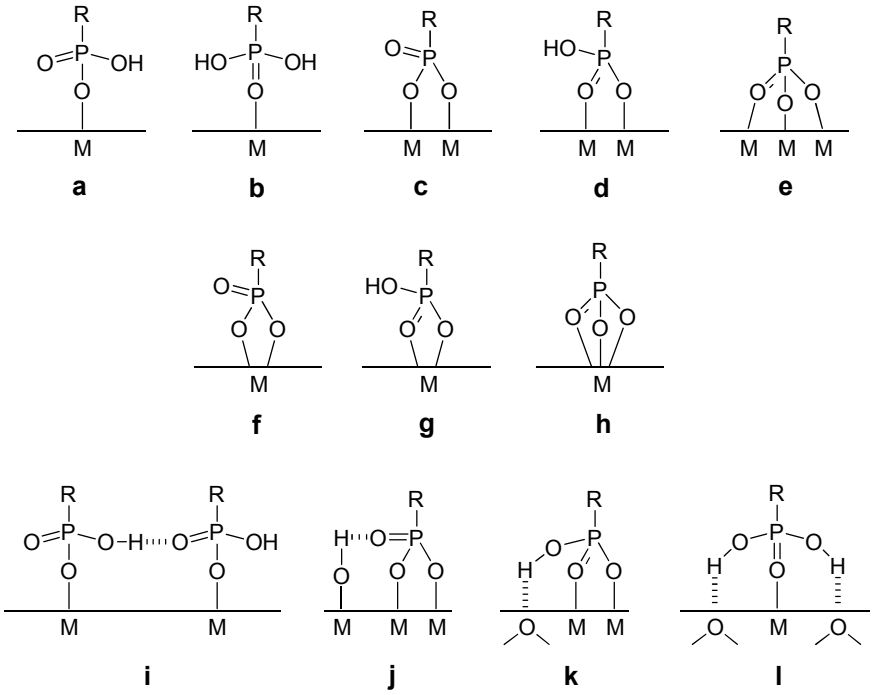

Figure 3.1 Some possible binding modes of phosphonic acids to a metal oxide surface, where M = metal: Monodentate (a and b), bridging bidentate (c and d), bridging tridentate (e), chelating bidentate (f and g), chelating tridentate (h), and some possible additional hydrogen bonding interactions (i – l). Adapted from Brodard–Severac *et al.*[3]

While it may be experimentally difficult to identify any single one of these binding modes present in a particular system, it is possible to distinguish the presence or absence of some of the binding modes and to give an overall indication of mono–, bi–,

and tridentate binding.

3.1.2 Proposed Mechanisms of Binding

The mechanisms by which phosphonic acids bind can differ depending on the nature of the metal oxide surface, and several mechanisms exist depending on the surface chemistry of the metal oxide. For Lewis acidic (electron pair accepting) metal oxide surfaces, it is widely believed that the first step in the binding of phosphonic acids to the surface proceeds first *via* coordination of the phosphoryl oxygen to a Lewis acidic site on the surface, followed by heterocondensation with surface hydroxyl groups (Figure 3.2).[3-7] The heterocondensation is accelerated by the increased electrophilicity of the phosphorus atom after coordination of the phosphoryl group with the surface. At any point hydrogen bonding may take place instead of heterocondensation; this can depend largely on the surface hydroxyl content as well as the experimental conditions.

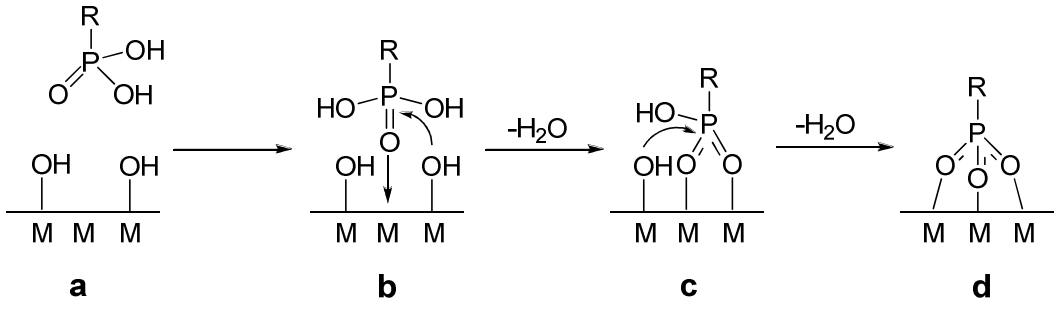

Figure 3.2 Mechanism of phosphonic acid attachment to metal oxides with a phosphoryl coordinated intermediate.

Another potential mechanism by which phosphonic acids can bind to the surface is similar to the previous one discussed, but without the initial coordination of the phosphoryl group to the surface.[8] This may be the case if the surface has poor Lewis acidity, or if it is even basic. One of two heterocondensations may occur, and the phosphoryl group may or may not hydrogen bond with a hydroxyl group located on the oxide surface or present in an adjacent molecule (Figure 3.3). This mechanism of binding is also extremely sensitive to the surface hydroxyl amount as well as the experimental conditions.

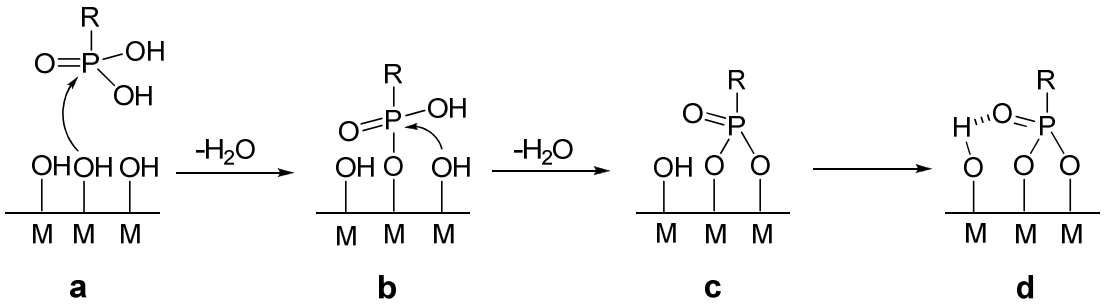

Figure 3.3 Heterocondensation–mediated binding of phosphonic acids to metal oxide surfaces.

As mentioned, the mechanism of phosphonic binding to metal oxide surfaces is dependent on the nature of the surface (ratios of hydroxyl and Lewis acidic sites) and the experimental conditions. While there have been reports of hydroxyl–independent mechanisms,[9] it is widely accepted that the surface hydroxyl content is important. The experimental conditions are also important, as heat will increase the extent of heterocondensation and can turn mostly hydrogen–bond interactions into covalent bonds.

3.1.3 Techniques Used to Study Binding Modes

A brief overview of some of the techniques used to study the binding modes of phosphonic acid on metal oxides is presented.

3.1.3.1 Infrared Spectroscopy

Infrared (IR) spectroscopy is a very useful tool to probe binding modes of phosphonic acids on both planar and nanoparticle metal oxide substrates. The phosphonic acid moiety has several IR–active modes. By looking for the presence or absence of a number of stretches associated with free phosphonic acids and P–O–M bonds it is possible to determine the types of binding modes present. The binding modes expected and the frequencies at which the corresponding P–O–H stretches are expected are discussed in Chapter 2.

Infrared reflectance absorption spectroscopy (IRRAS) relies upon the same principles as the more familiar transmission mode IR, but allows for the analysis of planar substrates.[10] In IRRAS, infrared radiation is polarized and then directed at the sample of interest at a grazing angle (often $\theta \sim 82°$). The incoming electric field is comprised of two components: the vector of light in the incident plane (*p* polarized) and normal to the incident plane (*s* polarized). Due to surface selection rules, only the *p* component of the incident light can interact with the adsorbate on the surface (Figure 3.4). Additionally, only molecular vibrations that contain a finite component of their

dynamic dipole perpendicular to the surface are observed. As the signal is proportional to the amount of reflected light from the surface, only highly reflective surfaces can be used.

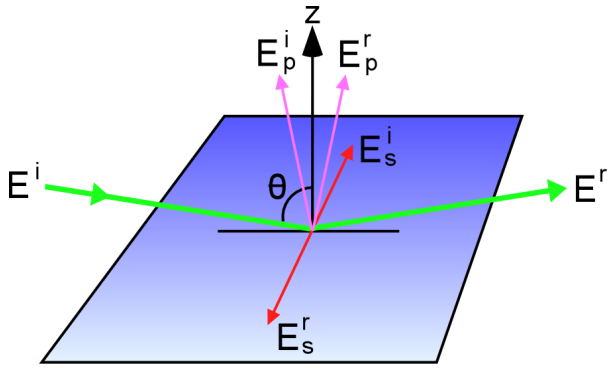

Figure 3.4 Illustration of the interaction of incoming infrared radiation (E^i) with a highly reflective surface as a grazing angle (θ), where E^r is the reflected radiation, and E_s^i, E_s^r, E_p^i, and E_p^r the *s* and *p* components, respectively, of the electric fields of incident and reflected radiation. Figure adapted from Hayden.[10]

3.1.3.2 X–Ray Photoelectron Spectroscopy

The photoelectric effect arises when electrons are emitted from a substance after the absorption of energy from electromagnetic radiation. During the process, if an atom or molecule absorbs the energy of a photon and has more energy than the material's work function, an electron will escape from the material. Some of the energy of the absorbed photon will be used to liberate the electron from the atom (allowing it to escape from its orbital) and the material (overcoming the work function), and any excess energy will contribute to the electron's kinetic energy (Figure 3.5).

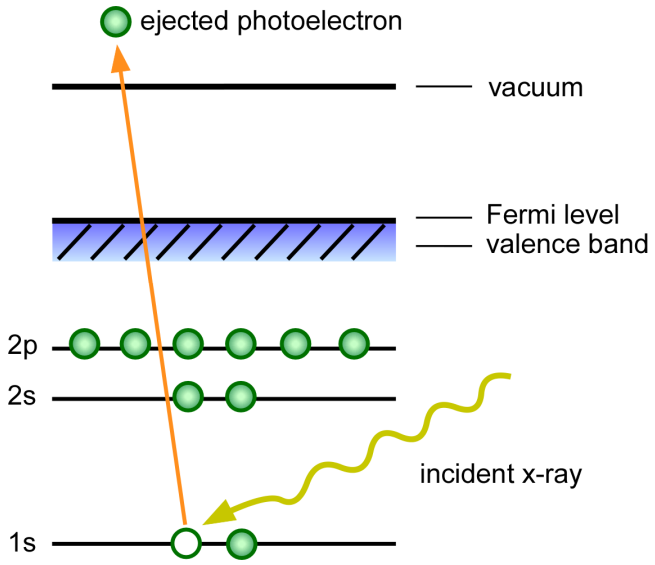

Figure 3.5. Diagram of how an electron can be ejected from its orbital after absorption of an x–ray.

The photoelectric effect gives rise to several types of photoelectron spectroscopy, most notably X–ray Photoelectron Spectroscopy (XPS), Ultraviolet Photoelectron Spectroscopy (UPS), and Auger Electron Spectroscopy (AES). AES will not be described herein, but the reader is referred to several books on the topic.[11, 12]

X–ray Photoelectron Spectroscopy (XPS) concerns primarily the photoemission of an electron from a core level by an X–ray photon. The kinetic energy of the emitted photoelectrons are then analyzed by a spectrometer and the data is presented as a graph of intensity versus electron energy. The kinetic energy of the electron is dependent on the energy of the X–ray used as well as the work function of the spectrometer. This information, along with the knowledge of the energy of the X–rays used, can be used to determine the binding energy of the ejected electrons, as in the equation below:

$$E_B = h\nu - E_K - W \quad \text{(Equation 3.1)}$$

Where E_B is the binding energy of the electron, hν is the energy of the X–ray photons, E_K is the kinetic energy of the emitted electron, and W is the work function of the spectrometer.[11] As the binding energy of electrons depends on the details of their chemical environment, information pertaining to chemical bonding can be obtained with XPS.

Currently most of the X–ray sources can provide monochromated light with a narrow X–ray line width (for example, the full width half maximum is 0.9 eV for Al$K\alpha$ X–rays), allowing for narrower XPS peaks and better chemical state information vs. X–ray sources with larger peak widths. In addition, satellite peaks and inherent Bremsstrahlung continuum (background signal from secondary electrons) prevalent in non–monochromated sources are reduced, and smaller spot sizes on the sample can be analyzed.

XPS can be particularly useful in determining binding modes on surfaces. By looking at the binding energies of the elements involved in the surface binding, it is possible to determine the interactions that are occurring. For instance, in the case of phosphonic acids on metal oxides, it is possible to look at the difference between unbound, solid phosphonic acid and phosphonic acids that have been used to modify a surface. The modified surface can also be compared to a bare, unmodified surface. For metal oxides, the best element to examine is oxygen. The O(1s) binding energies and ratios will change in both the phosphonic acid and in the surface if the two are covalently connected to each other. Binding energies associated with P–O–M, P–O–H, M–O–H, and

P=O bonding can all be investigated and compared to determine how the phosphonic acid is bound to a given surface. Another advantage of XPS is that it is a surface sensitive technique, often yielding information from the top 10 nm or less of samples.[11]

3.1.3.3 Solid State Nuclear Magnetic Resonance

Solid–State Magic Angle Spinning Nuclear Magnetic Resonance (MAS NMR) can provide chemical shift information analogous to solution NMR. Metal oxide nanoparticles are often too large to be dissolved or suspended and can only be analyzed with solid–state NMR. In much the same way as XPS can give information on the binding *via* the elements that partake in the binding, solid–state NMR can give information on the types of bonds present. Hence, looking at differences in the ^{17}O MAS NMR and ^{31}P MAS NMR can give insight on the binding mode(s) present. ^{17}O MAS NMR analysis of nanoparticles modified with phosphonic acids has only been occasionally carried out due to the low natural abundance of ^{17}O, but has been performed.[3, 13] ^{31}P NMR is often used, however, to help determine possible binding modes of phosphonic acids to metal oxides.[6, 14]

By examining at the shift and width of peaks in the ^{31}P MAS NMR spectrum, and combining the information from both cross–polarization (CP) and direct–polarization (DP) spectra it can be possible to relate the types of binding modes present. CP spectra in ^{31}P MAS NMR tends to enhance the signal from more crystalline, or rigid phosphorus species, whereas DP tends to enhance the signal from more fluid, or easily moveable

species. A large sharp peak in the CP can indicate tridentate–bound phosphorus as the phosphorus is rigidly held by three bonds to the surface. Conversely, a large broad peak in the DP can correspond to mono– and bidentate phosphorus species which have more degrees of freedom. Examples of this concept can be seen in Section 3.1.4.2.2.

3.1.2.4 Isothermal Calorimetry

Isothermal calorimetry (ITC) is a characterization method usually found in biochemical applications allowing for the binding energies of macromolecular interactions (proteins and peptides) to be precisely measured. The enthalpy change (ΔH) of an interaction between two or more molecules in solution can be directly measured.

Experimentally, an ITC is composed of two identical cells in an adiabatic jacket (Figure 3.6). Sensitive thermocouple circuits are used to detect temperature differences between the reference cell and the sample cell. Before any ligand (titrant) is added to the sample cell, a constant power is applied to the reference cell. This directs a feedback circuit which activates a heater on the sample cell.

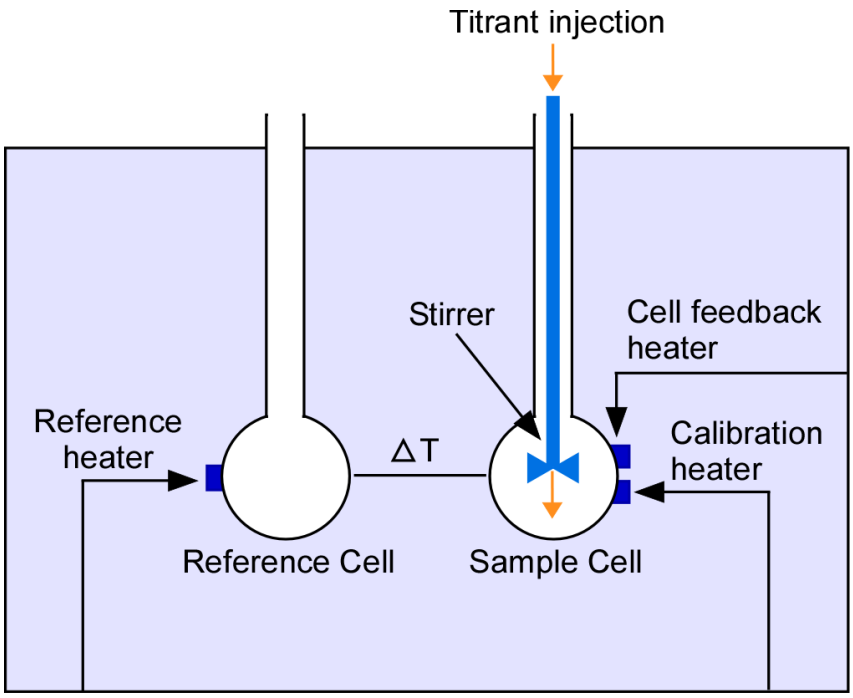

Figure 3.6 Drawing of the main components of an ITC.

A typical experiment requires the titration of a known concentration of ligand into the sample cell (while stirring) that contains a solution of another molecule or entity to which the titrant ligand can bind. If the reaction that takes place is exothermic, then the temperature in the sample cell will increase upon addition of the titrant. This results in the feedback power to the sample cell to be decreased in order to keep the same temperature as the reference cell, and results in a negative peak (plotted as μcal/sec) in the graph. Conversely, if the reaction is endothermic then the feedback power to the sample cell will be increased resulting in a positive peak in the graph. The raw graph for an ITC experiment consists of a series of spikes of heat flow corresponding to injections of the titrant into the sample cell (Figure 3.7). In many cases, though dependent on the types of interactions measured, the intensity of the peaks will decrease over time as the available

binding units for the titrant are depleted. By knowing the concentration of the injectant and the concentration of the material in the sample cell, the aforementioned information can be determined.

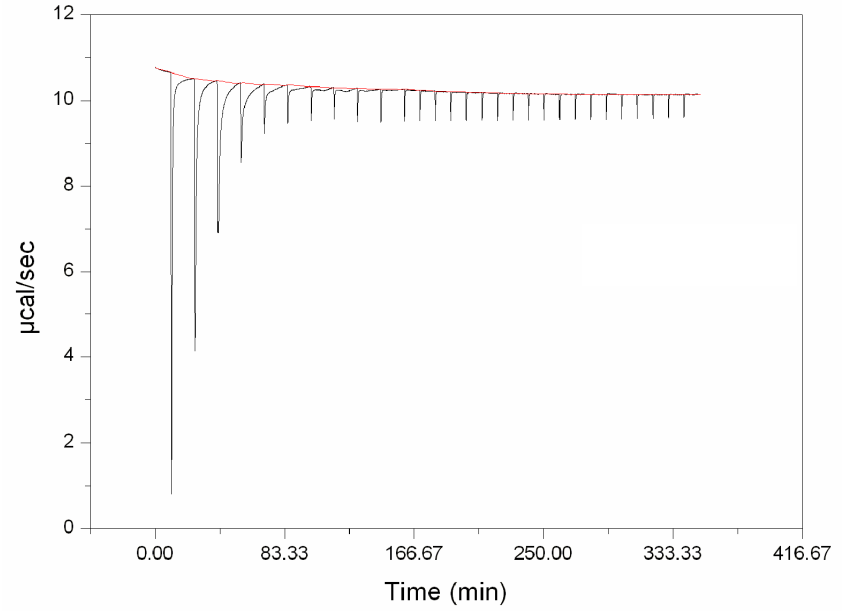

Figure 3.7 Example graph of the raw data from an ITC run. The reaction is exothermic as evidenced by the negative peaks.

Each peak in the raw ITC file can then be integrated with respect to time. The energies for each peak are then normalized by dividing by the number of moles of titrant for the injection, and the resultant isotherm shows the amount of heat evolved as a function of titration and/or reaction completion (Figure 3.8)

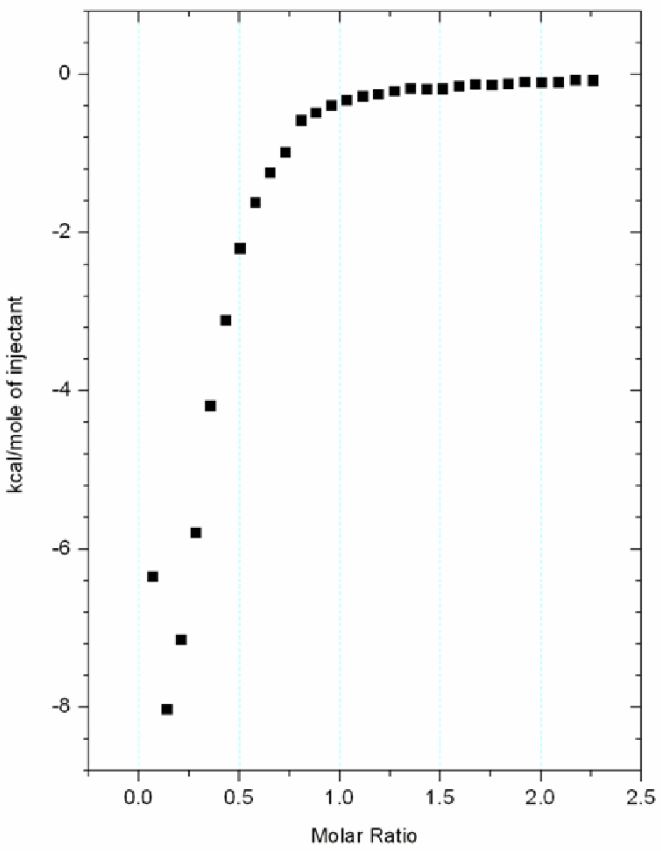

Figure 3.8 Typical isotherm of an ITC experiment. The first peak will often be discarded as evaporation and/or leaking of the titrant solution into the sample cell prior to starting the experiment can result in a decreased heat flow.

It should be noted that ITC experiments can also yield the binding affinity (K_a), and binding stoichiometry (n) of an interaction between two or more molecules in solution. From these measurements and data the Gibbs free energy changes (ΔG) and change in entropy (ΔS) can be calculated using the equation:

$$\Delta G^\circ = -RT\ln K = \Delta H^\circ - T\,\Delta S^\circ \qquad \text{(Equation 3.2)}$$

where R is the gas constant and T is the temperature.

3.1.4 Binding Modes on Metal Oxide Substrates

This section outlines the types of binding modes seen from the attachment of phosphonic acids to various different metal oxide substrates. While an overview of the literature includes all types of metal oxides, our own experimental data focuses on binding interactions of phosphonic acids on ITO, barium titanate, and zinc oxide.

3.1.4.1 Binding modes on ITO

The modification of ITO has been a central theme in our research. As was introduced in Chapter 1, the ability to control the surface properties of ITO can have a large impact on device characteristics involving ITO as the anode. Understanding the binding modes of phosphonic acids to ITO will allow for a better understanding of the robustness of the monolayer and the experimental conditions under which it is stable.

A survey of the literature will be given, followed by our own results on investigating the binding modes of phosphonic acids on ITO using various characterization techniques. IRRAS data were collected on several phosphonic acids bound to ITO and were subsequently compared to XPS and computational investigations. Additionally, ITC measurements have been performed looking at the energies of bond formation of different phosphonic acids to ITO nanoparticles, which have been coupled with SS MAS NMR and FTIR results.

3.1.4.1.1 Survey of the literature

Few studies have been reported in the literature on the binding modes of phosphonic acids to ITO. Koh *et al.* attempted to identify the P–O–M and P–O–H bonds in IRRAS of nitrophenylphosphonic acids on ITO, but considered the signal to noise too high for any reliable assignments.[15]

3.1.4.1.2 Experimental results

As a precursor to this section, it should be noted that different batches of ITO can have varying properties. The surface of ITO is complex and difficult to characterize. While this thesis does not contain any studies regarding the starting properties and characterization of ITO, these have been performed on the ITO used herein and some of the characterization data has been included in the experimental section of this chapter.[o]

Our efforts to understand the binding modes with which phosphonic acids bind to ITO were aided by several studies. IRRAS studies of octadecylphosphonic acid (ODPA) and (perfluoro–1,4–phenylene)bis(methylene)diphosphonic acid (TFBdiPA) bound to the ITO surface have been performed. Additionally, computational chemistry has been used to assist in deconvolution of the O(1s) XPS peak of a free octylphosphonic acid (OPA) powder and an ITO surface modified with OPA. Also, we have examined the enthalpies of reaction of some phosphonic acids with ITO nanoparticles and have coupled these to ^{31}P MAS NMR and FTIR data in order to approximate energies of bond formation of

[o] The characterization data also applies to ITO used in Chapter 4.

phosphonic acids onto ITO.

3.1.4.1.2.1 IRRAS Measurements

While ITO is not sufficiently reflective to obtain IRRAS data with the necessary signal to noise, polarization modulation (PM)–IRRAS can be used, where the signals from ambient contamination, such as carbon dioxide and water, can be all but eliminated allowing for more precise spectra with better signal. Additionally, the higher resolution and better signal to noise aids in obtaining quality spectra. The binding of ODPA and TFBidiPA on ITO were probed with PM–IRRAS (Figure 3.9)

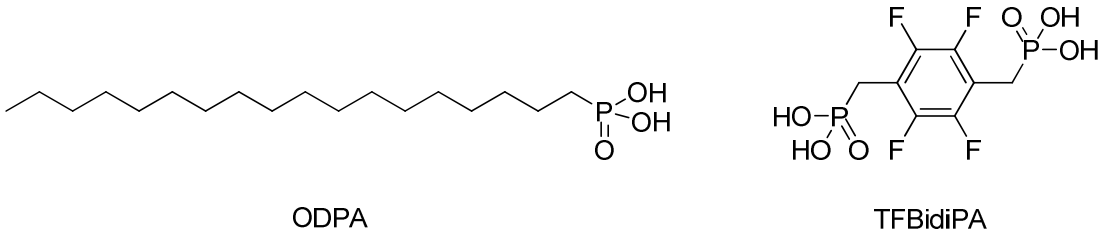

ODPA TFBidiPA

Figure 3.9 Chemical structures of octadecylphosphonic acid (ODPA) and (perfluoro–1,4–phenylene)bis(methylene)diphosphonic acid (TFBdiPA)

The PM–IRRAS spectrum of ODPA–modified ITO was compared with the transmission FTIR spectrum of ODPA powder (Figure 3.10).[16, 17] Peaks corresponding to ν(P=O) vibrations in the 1230 cm^{-1} region are seen in both spectra.[18] Peaks between ca. 955 cm^{-1} and 930 cm^{-1} are assigned to P–O–(H) stretching vibrations, and are clearly different for the surface–bound versus the bulk material.[17] Weak absorption features are

seen at 1160 cm^{-1} (assigned to an asymmetric $\nu_a(PO_2^-)$ vibration[16]) along with unresolved bands from 1000–1070 cm^{-1} (which are believed to arise from symmetric $\nu_s(PO_2^-)$ vibrations, and small amounts of unbound P–O–H groups[16]). The relative intensities and energies of the peaks (particularly the large ν(P=O) absorption) of the ODPA modified ITO in the PM–IRRAS spectra surface suggest mainly bidentate binding of the phosphonic acid with free, unattached P=O moieties.[19] Tridentate attachment may be present but appears to account for a small fraction of the binding events, since only very small peaks are present in the region where $\nu_a(PO_3^{2-})$ (970–1124 cm^{-1}) and $\nu_s(PO_3^{2-})$ (962–1000 cm^{-1}) stretching vibrations would be expected. Small amounts of monodentate and/or bidentate attachment with a free P–O–H group may also be present since a small signal from free P–O–H moieties is observed.

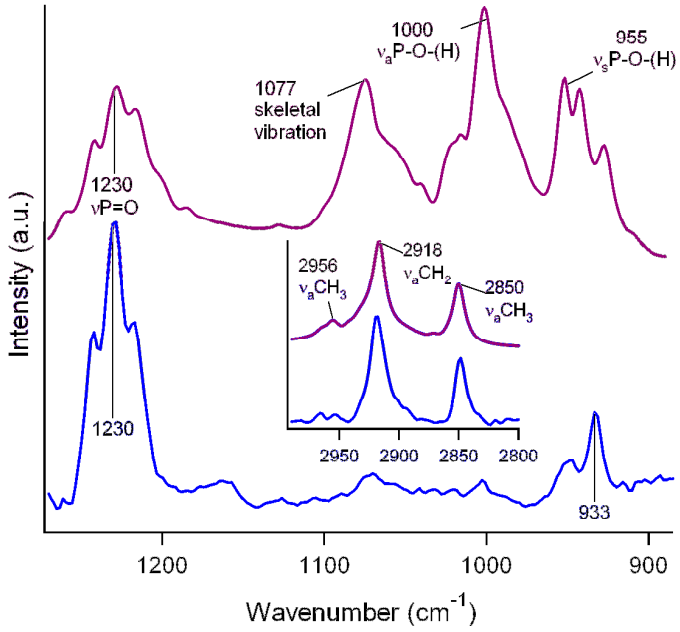

Figure 3.10 Comparison of the ODPA transmission FT–IR spectrum (top spectrum) and the PM–IRRAS spectrum for an ODPA modified DSC/OP–treated ITO surface (bottom spectrum) in the ν(P–O) region. Inset: Same spectral comparisons for the ν(C–H) region. (Data collected and figure prepared by S. Paniagua)

The PM–IRRAS spectra was also taken for ITO modified with TFBdiPA and compared to the free acid in a KBr pellet (Figure 3.11).

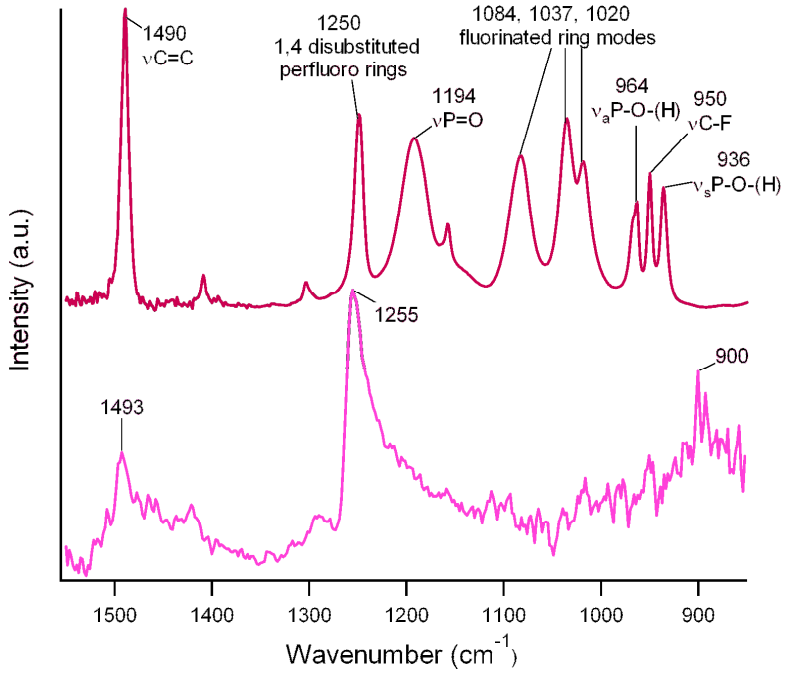

Figure 3.11Comparison of the powder/KBr TFBdiPA transmission FT–IR spectrum (top spectrum) and the PM–IRRAS spectrum for a TFBdiPA modified DSC/OP treated ITO surface (bottom spectrum). (Data collected and figure prepared by S. Paniagua)

It was unclear *a priori* whether TFBdiPA will attach to the ITO surface with one or both phosphonic groups, and several reasonable conformations can be hypothesized (Figure 3.12). Assignments were aided by data found in literature reports of related molecules.[17, 20, 21] The vibrational modes that are not expected to be perpendicular to the surface, in a "flat–lying" TFBdiPA orientation, appear greatly diminished in intensity relative to the randomly oriented molecule in the powder spectrum. It appears that after modification, the P=O stretch is shifted to higher frequency in comparison to the powder (in which the bond is believed to be weakened by hydrogen bonding), and is probably

overlapping with a ring mode absorption (which should be weakened due to the surface selection rule). Below 1100 cm^{-1}, the PM–IRRAS spectrum has a poor signal to noise ratio, however some peaks can be clearly seen near 900 cm^{-1}, which could correspond to P–O–(H) vibrations when a PO_2^- species is present, and some small peaks can be seen from 1000–1150 cm^{-1} which may be attributed to PO_2^- stretching vibrations.[17] These results are consistent with either of the "flat–lying" orientations shown in Figure 3.12a or 3.12b, but are not consistent with those shown in Figure 3.12c or 3.12d.

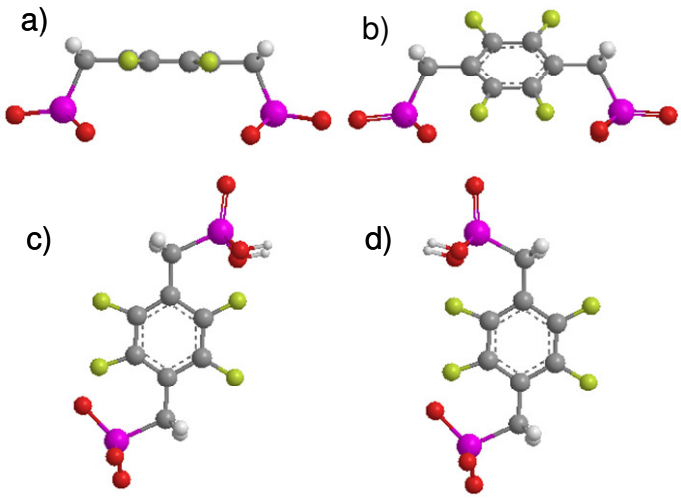

Figure 3.12 Most probable conformations for TFBdiPA bonded to ITO. (a) shows a flat–lying orientation, with both phosphonic head groups involved in binding to the surface; (b) is similar to (a) but with the ring tilted 45° in order to achieve some π–π interaction with adjacent molecules (a greater degree of tilt would be hindered by the ITO surface); (c) and (d) represent binding of only one phosphonic head group to the ITO surface, with different orientations of the unbound head group. (Figure prepared by S. Paniagua (in Chem3D))

3.1.4.1.2.2 XPS /Computational Results

There is still uncertainty in the reported spectroscopic, in particular XPS, studies in attempting to discern among the different binding modes of phosphonic acids in ITO because of a lack of precise knowledge of the features specific to each binding mode. As was seen in the IRRAS studies, it is believed that phosphonic acid adsorption on ITO can be described to occur *via* multiple modes, with a predominance of bidentate and tridentate modes.

In order to determine more concretely the core–level energies of various atom types that could be used to determine the binding of phosphonic acids to ITO (as well as other metal oxide surfaces), a theoretical study, based on density functional theory (DFT), of a model indium tin oxide surface and of the nature of the binding sites that determine the adsorption of phosphonic acid monolayers was performed (P. Paramonov). The validity of the theoretical description was assessed by comparing the first–principles results to XPS data on the ITO surface modified by phosphonic acid monolayers. The goal of this approach was to use core–level energies calculated at the quantum–mechanical level for specific atom types to assist in making unambiguous assignments of the various peak components in the XPS spectra on the experimental side.

A number of assumptions, although reasonable, had to be made about the nature of the ITO surface, which is invariably different from batch to batch and vendor to vendor. Despite these assumptions, good correlation was achieved with the experimental data (Figure 3.13). In order to characterize various adsorption possibilities, a large number (>20) of initial geometries were generated, sampling the under–coordinated

metal sites and surface hydroxyl groups expected to participate in OPA binding. Geometry optimizations were then performed for each initial configuration, allowing elimination of up to two water molecules to accompany OPA chemisorption.

Adsorption modes corresponding to bidentate (with and without hydrogen bonding of the unbound oxygen species) and tridentate binding were most commonly obtained as a result of structural optimizations. Since the core level energies of the oxygen atoms belonging to the phosphonic/phosphonate moiety are sensitive to their chemical environment, the DFT binding energies of the O(1s) levels were calculated.

In order to better identify experimentally which binding mode(s) is (are) predominant under realistic adsorption conditions, monolayers of OPA were prepared on ITO and their XPS spectra recorded. The ITO surface was modified *via* a modified T–BAG (Tethering by Aggregation) procedure (explained in Chapter 4). The O(1s) XPS spectrum of ITO modified with OPA, at 70° takeoff angle (the angle vs. the surface normal at which electrons are detected. Increasing the takeoff angle reduces the information depth to *ca.* 3 nm instead of the usual 9 nm), was recorded with high–resolution (0.1 eV) (Figure 3.13). The best fit for the spectrum was achieved with three simulated components based on the *calculated* O(1s) core level energies, and an additional adjusted low–intensity component was considered. The XPS spectrum of isolated OPA was recorded separately and calibrated using the C(1s) level at 284.9 eV; it displays O(1s) peaks at significantly higher binding energies, similar to the calculated oxygen core levels in the P–OH$^{\cdots}$O(ITO) mode. Importantly, using the procedure described above, the comparison between the simulated and experimental XPS spectra indicates the absence of hydrogen bonding and P–OH groups in the phosphonic acid

monolayers formed on ITO. Thus, these results allow us to unambiguously identify bidentate modes, with and without the phosphoryl oxygen hydrogen bonded to the ITO surface, as well as a tridentate binding mode as the main products of phosphonic acid adsorption.

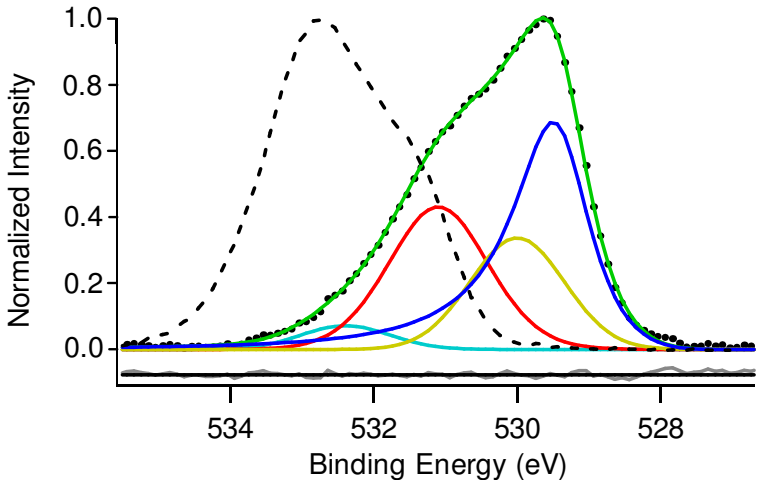

Figure 3.13 Experimental O(1s) core level XPS spectrum for *n*–octylphosphonic acid adsorbed on the ITO surface (dots), fitted with components calculated at the DFT level (colored lines); the fit error is indicated by the gray baseline. The three main components of the fit are at 529.5 eV (bulk O, with asymmetry due to energy–loss processes); 530.0 eV (surface In–O–In); and 531.1 eV (P–O–In, P=O···In, and surface In–OH). An additional peak at 532.6 eV was used to complete the fit (not accounted in the model OPA/ITO system). Sn–O species are also included in the 530.0 eV component. The XPS spectrum of the isolated OPA powder (dashed line) is shown for comparison. H–bonded configurations (POH···O(ITO), have a calculated O(1s) peak at *ca*. 534 eV (similar to core levels in isolated OPA); they are absent in the XPS spectrum of the OPA/ITO system, indicating that modes bi– and tridentate binding modes are the main products of OPA adsorption on ITO.

3.1.4.1.2.3 ITC results

While the other studies probed the types of binding modes phosphonic acids adopt when attached to an ITO surface, this study attempted to quantify the strength of the attachment, regardless of the binding mode. While the binding modes give a qualitative idea of the strength of the interaction (tridentate is stronger than bidentate which is stronger than monodentate), ITC experiments can provide quantitative information regarding the strength of the interaction by providing enthalpies of reactions which can be used to calculate binding energies.

While ITC is often used to measure thermodynamic properties of protein and macromolecular interactions, its use to study ligand–nanoparticle interactions has been minimal. Fadeev and coworkers reported the binding of phosphonic acids of various alkyl lengths to titania and zirconia nanoparticles.[1] They developed a model to determine the binding energy of the phosphonic acid group onto the two different metal oxides. Herein we present a similar study where we measure the enthalpies of reaction of the binding of three different phosphonic acids to ITO nanoparticles. The binding energies are then calculated using the same model as was previously reported, and these results are coupled with ^{31}P MAS NMR, TGA, and FTIR measurements to obtain an overall picture of the binding events.

Fadeev and coworkers developed a thermodynamic equation to relate all the factors involved in determining the net enthalpy as a result of the formation of monolayers of an organic ligand on a solid support:

$$\Delta H_r = -D - (\Delta H_{sol} + \Delta H_{dil}) - (E_S - E_{SAM}) \quad \text{(Equation 3.3)}$$

Where ΔH_r is the reaction enthalpy, D is the binding energy, ΔH_{sol} and ΔH_{dil} are the enthalpies of dissolution and dilution, respectively, and E_S and E_{SAM} are the surface energies of bare solid and monolayer, respectively. By approximating values for E_S and E_{SAM}, and measuring ΔH_r, ΔH_{sol} and ΔH_{dil} with an ITC, they calculated the binding energies of the reaction of a phosphonic acid group with both titania and zirconia nanoparticles, which were found to be 58 ± 7 kJ/mol and 55 ± 5 kJ/mol, respectively.[1]

The model they developed to determine the contributions of different energies in the enthalpy of monolayer self–assembly at a solid–liquid interface is presented in Figure 3.14. They determined that five discrete thermodynamic states that are involved in the overall formation of monolayers onto a solid substrate from solution. State 1 has the solid dispersed in or solvated by the solvent, with a solution of the monolayer forming molecules (ligands) separate. State 2 is the system directly after addition and reaction of the ligands with the substrate to form a monolayer. The energy difference between State 1 and 2 can be described as the reaction enthalpy. An imaginary State 3 can be achieved by breaking the monolayer–solvent interface and creating two new interfaces: a solvent–vacuum interface and a monolayer–vacuum interface. The energy required to create State 3 from State 2 can be given as a sum of the total surface energies of the new interfaces: E_{SAM} (the surface energy of the monolayer) and E_L (the surface energy of the solvent). State 4 can be achieved by removal of the ligands from the surface and dissolving them back in the solvent. This process requires breaking the bonds between the ligands and the solid surface (D) and the enthalpy of dissolution of the ligands into the solvent (ΔH_{sol}).

State 5 is achieved by concentration of the ligands back into a small, separate solution, and this process is equal to the enthalpy of dilution with the opposite sign ($-\Delta H_{dil}$). Completing the cycle requires recreating the solid–solvent interface from the solid–vacuum and solvent–vacuum interfaces. The energy to do this is given by $-(E_S + E_L)$. Due to the conservation of energy, the individual factors must all add up to zero, and Equation 3.3 is obtained.

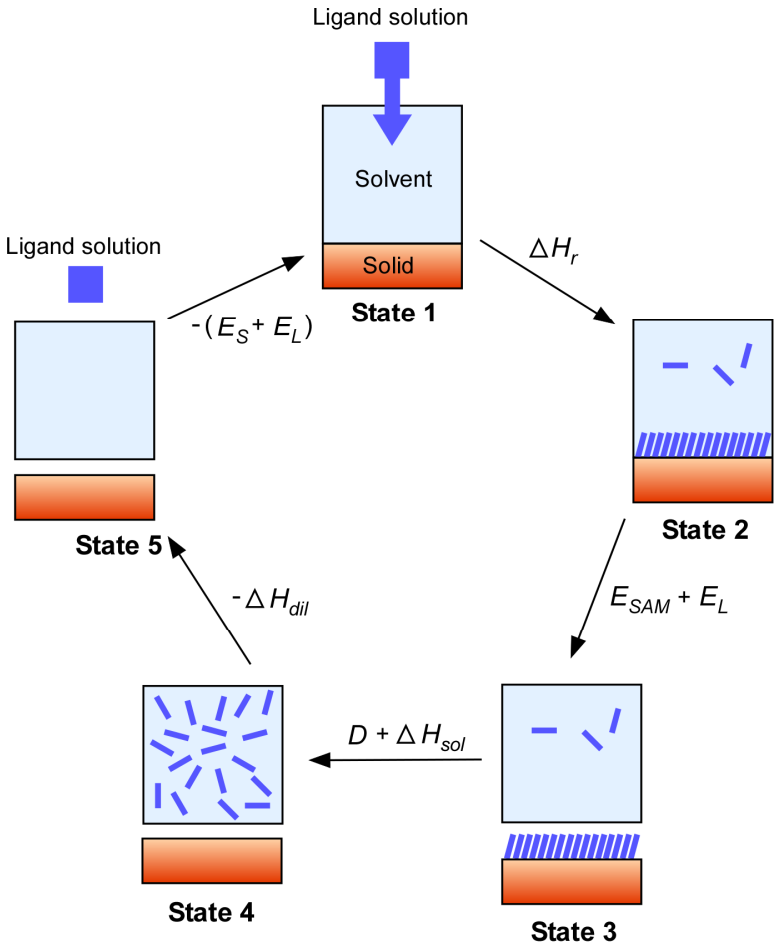

Figure 3.14 Thermodynamic states involved in the formation of monolayers on a solid substrate at the liquid–solid interface.

We decided to study the binding of three different phosphonic acids to the ITO surface: phenylphosphonic acid (PhPA), octylphosphonic acid (OPA), and octadecylphosphonic acid (ODPA). E_{SAM} was approximated from the surface energies of films from materials with similar organic constituents. Hence, the surface energy of paraffin,[22] 25 mJ/m^2, was used for OPA and ODPA, and the surface energy of polystyrene,[23] 32.4 mJ/m^2, was used for PhPA. E_S has been reported before for planar ITO and is equal to 55 mJ/m^2.[24] ΔH_{dil} was measured in the ITC but the values were sufficiently small enough that they can be ignored. ΔH_{sol} was approximated by measuring the enthalpies of dissolution of each of the phosphonic acids in a simple solution calorimeter. ΔH_r was measured in the ITC.

The enthalpies of dissolution of the different phosphonic acids in a 95:5 ethanol: water mixture (chosen due to the success of prior nanoparticle modification experiments) were determined with a simple solution calorimeter. Fadeev and coworkers note that their equation takes into account several assumptions, one of which being that the lateral interactions in the formed monolayer are the same as those in the pure phosphonic acid reagent. This approximation allows for the use of the enthalpy of dissolution (a measurable quantity) as an estimate for ΔH_{sol}. The enthalpies of dissolution for the three different phosphonic acids were determined by measuring the heat change when a known amount of the compound is dissolved into a known volume of solvent. By measuring the heat change of several different molar amounts of each phosphonic acid, a trendline can be determined that equals the change in temperature per mole of phosphonic acid (Figure 3.15). Calibration of the calorimeter to determine the amount of energy that a 1 °C change in temperature constitutes then allows for the final determination of the heats of

dissolution for the different phosphonic acids (Table 3.1).[p]

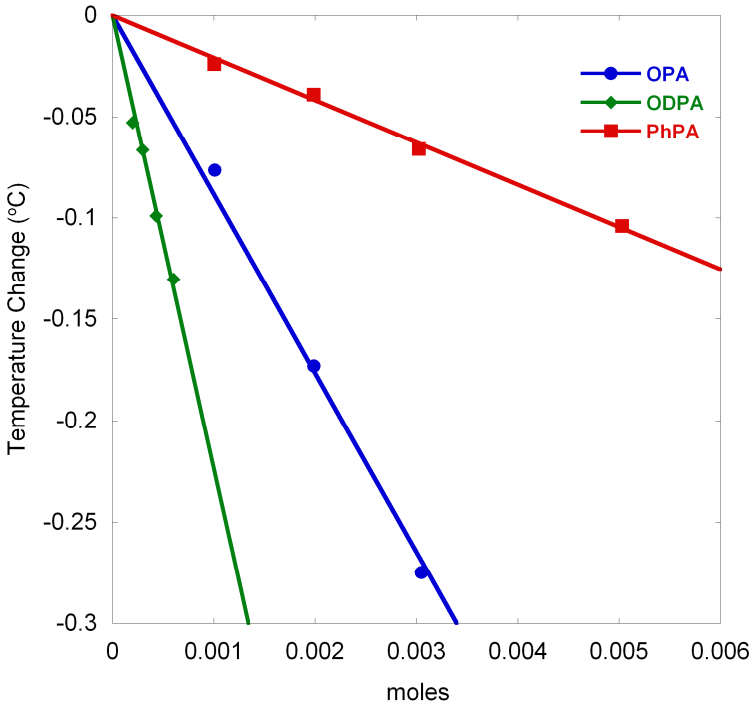

Figure 3.15 Plots of the temperature change vs. moles of phosphonic acid added and the trendlines for each set of data.

The enthalpies of reaction were measured by ITC (Table 3.1). Substituting all the parameters into Equation 3.3, the binding energies for each of the phosphonic acids can be computed (Table 3.1).

[p] Calibration details are outlined in the experimental section

Table 3.1 Values obtained for ΔH_{sol} and ΔH_r and the computed binding energies for each phosphonic acid.

	ΔH_{sol} (kJ/mol)	ΔH_r (kJ/mol)	D (kJ/mol)
PhPA	- 10.8 ± 0.5	- 44 ± 0.6	52 ± 1
OPA	- 45.3 ± 3.0	- 41 ± 0.5	82 ± 4
ODPA	- 114.8 ± 7.0	- 49 ± 1.0	159 ± 8

Fadeev and coworkers measured the enthalpies of reaction and dissolution of three different alkylphosphonic acids: methyl–, octyl–, and octadecylphosphonic acid. The three binding energies were similar in nature, as expected considering the same binding group for each. However, our results are differ from theirs. The values for PhPA (52 ± 1 kJ/mol) and OPA (82 ± 4 kJ/mol) are somewhat similar to those found by the authors. The difference can be explained by the different nature of the phosphonic acid moiety for each: PhPA and OPA are expected to have different acidities and this may change the manner in which they bind to ITO. Additionally, a different solvent system was used and a different metal oxide was studied.

The strange difference is in regards to the ODPA. Our results indicate a binding energy of 159 ± 8 for this molecule onto ITO. We believe the discrepancy arises from the inadequacy of the developed model to account for additional interactions in the solid state of the compound which manifest themselves in the dissolution of ODPA. ODPA is amphiphilic by nature, containing a long non–polar alkyl chain on one end and a polar, protic phosphonic acid moiety on the other end. Due to the strong Van der Waals interactions present in adjacent long alkyl chains, it is conceivable that the molecules interact with each other differently in their bare, solid state as opposed to OPA or PhPA.

The stabilizing forces involved in this interaction are comprised of the Van der Waals forces as well as an enhanced degree of hydrogen bonding between molecules. Therefore, the lateral interactions of the monolayer cannot be approximated as merely ΔH_{sol}. The presence of these additional stabilizing forces can be seen in the much larger ΔH_{sol} of ODPA in comparison to OPA and PhPA, carrying through to a much larger resulting binding energy of ODPA to the ITO surface. FTIR and ^{31}P MAS NMR were used to test this hypothesis as well as to further characterize the interaction between the different phosphonic acids and ITO.

In order to test our hypothesis, ITO nanoparticles were stirred with a 5 fold excess of each phosphonic acid at room temperature for 24 hours. Though many reports indicate the presence of heat as critical to good coverage of nanoparticles with phosphonic acids, these sample were reacted at room temperature to mimic the reaction conditions in the ITC.

FTIR was used to characterize the different phosphonic acids before and after their binding to ITO (Figure 3.16). Due to the broad absorption of ITO over most of the spectral region, the IR spectra of the various modified ITO samples are of limited use. C–H stretching can be seen in the nanoparticles modified with OPA and ODPA, and a peak at ~3500 cm^{-1} in the unmodified ITO nanoparticles, associated with surface hydroxyl groups, is greatly diminished in all the samples post–modification (Figure 3.16, upper right).

Analysis of the IR spectra of the different phosphonic acids is consistent with our hypothesis. The $\nu_a CH_2$ stretching band is located at 2917 cm^{-1} in ODPA, shifted from 2930 cm^{-1} in OPA (Figure 3.16, lower left). This frequency is consistent with highly

ordered alkyl chains.[25] Additionally, a the broad band overlapping with the C–H stretching bands associated with P–O stretching in P–OH and the broad peak at ~2350 cm^{-1} associated with O–H out of phase deformation show greatly reduced absorption in ODPA vs. OPA, consistent with increased hydrogen bonding (Figure 3.16, upper left). The region from 1150 – 1300 cm^{-1}, where the ν(P=O) band for phosphonic acids is located, is also very different between OPA and ODPA (Figure 3.16, lower right).

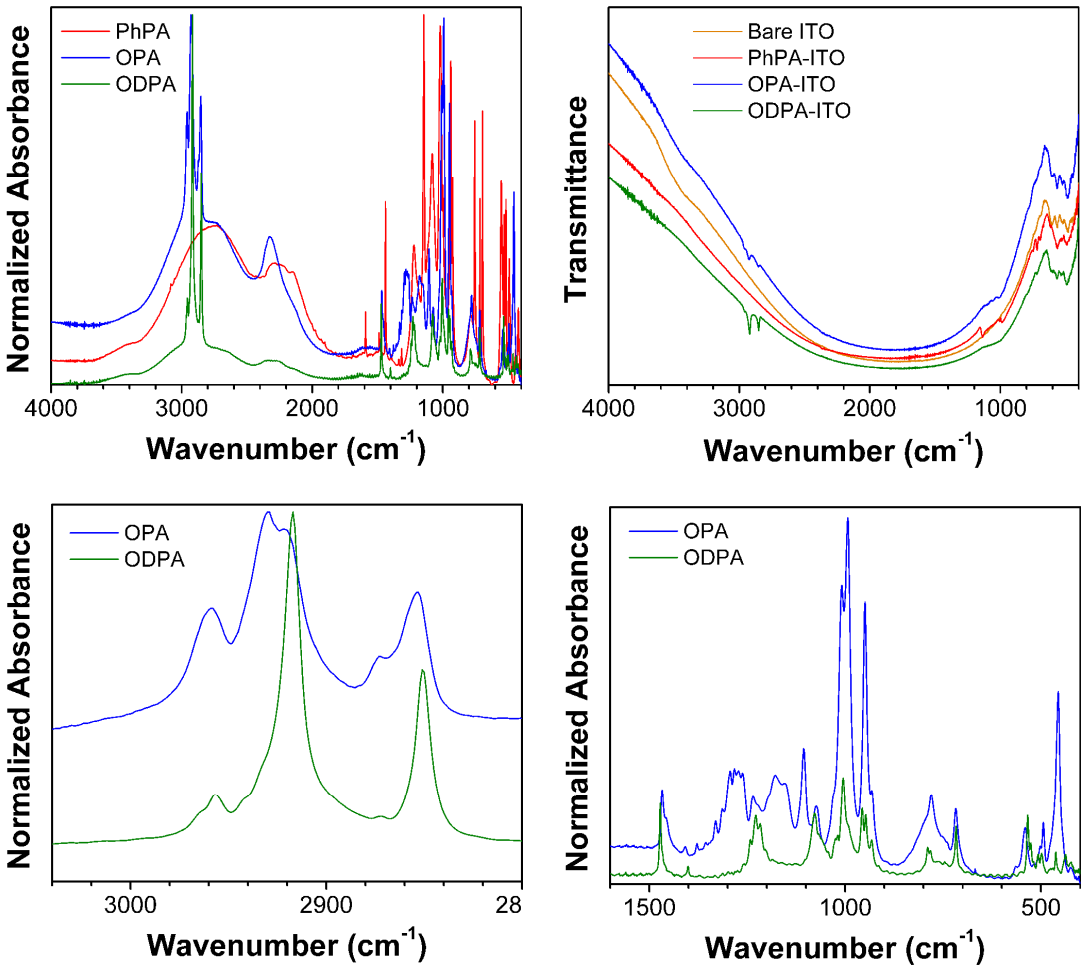

Figure 3.16 FTIR spectra of PhPA (red), OPA (blue) and ODPA (green) for the free, unbound phosphonic acids, and for the nanoparticles bound with these ligands. Unmodified ITO (orange) is also shown for comparison. (Data collected and graphs prepared by P. Kim)

In addition to the differences seen in the FTIR, differences can be seen in the ^{31}P MAS NMR spectra (Figure 3.17). The chemical shifts of OPA and PhPA are 36 and 20 ppm, respectively. These peaks broaden and shift upfield by 8 ppm once both of these phosphonic acids are bound to the ITO surface. However, while the phosphorus peak for ODPA–modified ITO appears qualitatively similar to that of OPA–modified ITO, also appearing at 28 ppm, the peak of the unbound ODPA is located at 30 ppm. This peak position for ODPA is 6 ppm upfield from OPA. This is also consistent with increased hydrogen bonding throughout the material.

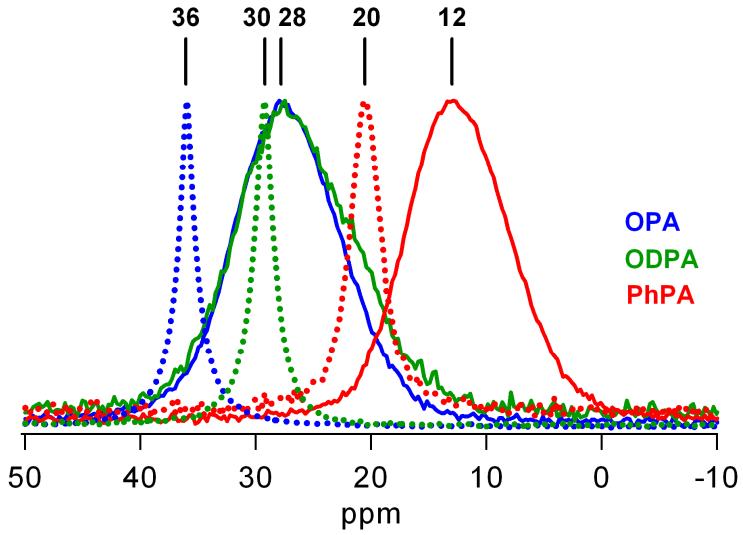

Figure 3.17 ^{31}P MAS NMR spectra of PhPA (red), OPA (blue) and ODPA (green) before (dotted lines) and after (solid lines) binding with ITO nanoparticles.

TG analyses were also conducted to ensure that the appropriate amount of phosphonic acid was binding to the nanoparticles in each of the sample (Figure 3.18). Mass losses of 1.2, 2.2, and 5.2% were seen, corresponding to surface coverages that are 41, 61, and 87% that of theoretical monolayers for PhPA, OPA, and ODPA, respectively.

It is interesting, though not surprising, that the coverage increases with an increase in alkyl chain length. This is likely due to the stabilizing effects of the interchain Van der Waals forces, resulting in increased surface coverage.

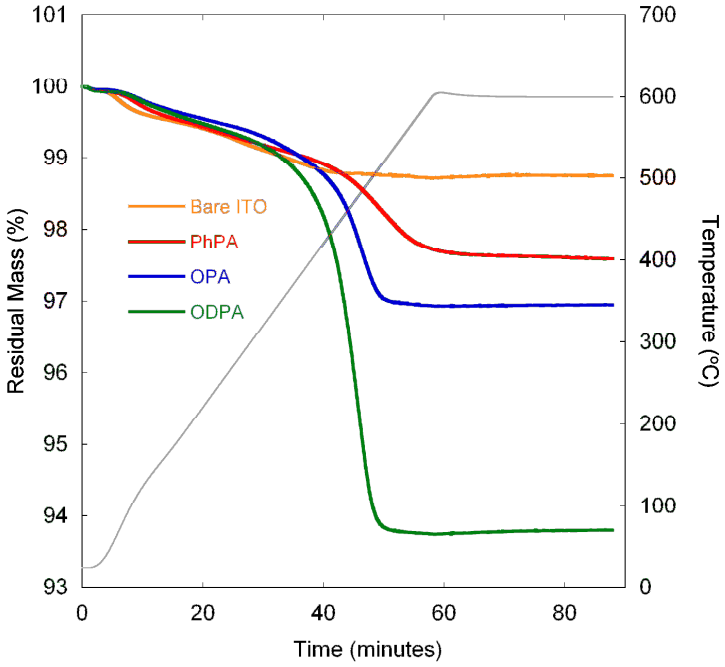

Figure 3.18 TGA traces of bare ITO nanoparticles (orange), and ITO nanoparticles modified with PhPA (red), OPA (blue), and ODPA (green). The temperature program is shown in grey.

In summary, the calculated binding energies differed depending on the phosphonic acid, with PhPA ~52 ± 1 kJ/mol, OPA ~82 ± 4 kJ/mol, and ODPA ~159 ± 8 kJ/mol. Although a different solvent media was used vs. the earlier report (tetrahydrofuran), the values differ greatly to the results reported by Fadeev, where the binding energy of alkylphosphonic acids on ZrO_2 ~ 55 +/– 5 kJ/mol, and on TiO_2 ~ 58 +/– 7 kJ/mol. The difference in PhPA and OPA can be explained by a difference in the

nature of the phosphonic acid group for each. The binding energy calculated for OPA on ITO is ~25 kJ/mol higher than that seen for alkylphosphonic acids on TiO_2 and ZrO_2, indicative of a stronger P–O–M bond when binding alkylphosphonic acids to ITO.

The binding energy for ODPA differs greatly from the other two, seemingly too high. This can be explained by the thermodynamic model developed by Fadeev and coworkers not accounting for a greater degree of intermolecular hydrogen–bonding present in ODPA vs. OPA, as evidenced by FTIR and ^{31}P MAS NMR measurements. Lastly, TGA analysis indicates a higher degree of coverage as the length of the alkyl chain increases.

3.1.4.2 Binding Modes on Other Metal Oxides

This section outlines the literature and our results on the binding of phosphonic acids to metal oxide surfaces other than ITO.

3.1.4.2.1 Survey of the Literature

While relatively little has been reported on the binding modes of phosphonic acids to ITO, there is more information detailing the binding modes of phosphonic acids to other metal oxides.

Extensive studies have been performed on the binding of phosphonic acids to

aluminum oxide, or the native oxide layer on aluminum. As there are different types of aluminum oxide surfaces, there may be binding modes that are preferred depending on the surface modified and its hydroxyl content.[26] This may partly account for contradictory conclusions in the work of different groups. Giza *et al.* used FT–IRRAS to show that ODPA bound to the oxide coating on aluminum surfaces in a tridentate fashion, as both the phosphoryl and hydroxyl bands were absent when bound to the surface, and a single broad peak at 1100 cm^{-1} was seen, corresponding to the stretching vibrations of $\nu_a(PO_3^{2-})$.[8] Theoretical calculations by Hector *et al.* also suggest a tridentate binding,[27] while other theoretical studies suggest that the mode of binding is more surface dependent and can differ between different types of aluminum oxides, such as corundum, bayerite and boehmite.[26] Ramsier *et al.* also performed spectroscopic measurements, though rather than using IRRAS they used inelastic electron tunneling spectroscopy (IETS), to show that smaller phosphonic acids bind in a tridentate fashion while large phosphonic acids, with larger terminal functional groups, bound in a mixture of bidentate and tridentate modes.[28] Adolphi *et al.* conducted a very detailed XPS study on the binding of phosphonic acids to the native oxides on several metals, and determined that a bidentate binding scheme was seen for aluminum oxide.[29]

Titanium/titanium dioxide has received a similar amount of attention as to Al_2O_3. A large amount of the literature comes from Mutin *et al.* They have conducted extensive studies on the binding phosphonic acids and phosphonates on the surfaces of different metal oxides, though they have focused on titania. Initial FTIR and ^{31}P MAS NMR studies indicated a mainly tridentate binding of phosphonic acids, as well as the diethylphosphonates, to titania nanoparticles.[4] More recent ^{17}O MAS NMR results

support this finding, although they indicate a small amount of bidentate, and perhaps monodentate, species,[13] and support the idea of bridging binding modes instead of chelating ones.[3] Adolphi *et al.* also report a tridentate binding of ω–(thiophene–3–yl alkyl) phosphonic acids to planar titanium surfaces, as evidenced by high resolution XPS studies.[29]

The surfaces of silica and Si/SiO_x have also been widely studied. Early studies by Lukeš *et al.* indicate a monodentate binding of phenyl and methylphosphonic acids to the surface of silica particles.[30] Schwartz *et al.* have shown that phosphonic acids bind in a tridentate fashion to the native oxide on silicon by both IRRAS experiments, where the typical $\nu_a(PO_3^{2-})$ absorbance was seen,[9] and XPS, where analysis of the O(1s) peak of modified Si/SiO_x did not indicate the presence of any P=O or P–O–H peaks.[31]

Binding modes have been presented for phosphonic acids bound to a number of other metal oxides. Holland *et al.* propose a combination of bi– and tridentate phosphonic acid binding to SnO_2 nanoparticles, as evidenced by ^{31}P and ^{1}H MAS NMR.[32] Traina *et al.* studied the binding of several different phosphonic acids to Y_2O_3 nanoparticles and found evidence of tridentate binding from FTIR measurements.[33] Textor *et al.*[34] report mainly monodentate and chelating bidentate binding of ODPA to planar Ta_2O_5 surfaces and Adolphi *et al.*[29] report the binding of phosphonic acids to be mainly bidentate where the phosphoryl group is unbound. Ago *et al.* reported the binding of ODPA to ZrO_2 nanoparticles as mainly monodentate.[35] The binding of poly(vinylphosphonic acid) onto steel substrates was shown by Beentjes *et al.* to be tridentate.[36]

3.1.4.2.2 Experimental Results

While a large amount of our research has focused on the modification of ITO, we have also studied the modification of barium titanate (both planar substrates and nanoparticles) as well as planar zinc oxide.

Studies on the binding modes of phosphonic acids on $BaTiO_3$ (barium titanate) have been completed for both relatively planar and nanoparticulate surfaces. The FTIR spectra was taken for ODPA (powder) and its monobasic potassium salt and these were compared to the PM–IRRAS data for monolayer films of ODPA on $BaTiO_3$ (Figure 3.19). Capturing both the IR spectra of the neutral molecule, along with the monobasic salt of the phosphonic acid, makes it easier to distinguish between tridentate and bidentate binding modes.

The PM–IRRAS data for ODPA, using the monobasic salt of ODPA as a standard, suggest a predominantly bidentate attachment of the phosphonic acid modifier to the surface, with a remaining free P–O–H group. Tridentate binding of ODPA is expected to produce at least one intense asymmetric stretching band for PO_3^{2-} near 1050 cm^{-1}, with a less intense symmetric stretch for the same moiety near 990 cm^{-1}, bands which are not observed. In the PM–IRRAS measurement, no ν(P=O) absorption band is seen, however, an intense band at 1160 cm^{-1} arises, which can be easily related to the $\nu_a(PO_2^-)$ 1165 cm^{-1} band in the monobasic anion of ODPA ($\nu_s(PO_2^-)$). There is also a band at *ca.* 920 cm^{-1} attributable to νP–O–(H), as also seen for the monobasic anion. A bidentate attachment mode, with a free P–O–H group, is likely to produce a ν(P)–O–H

band that is masked by the ν(C–H) vibrations, just as in the case of the powder of the monobasic potassium salt.

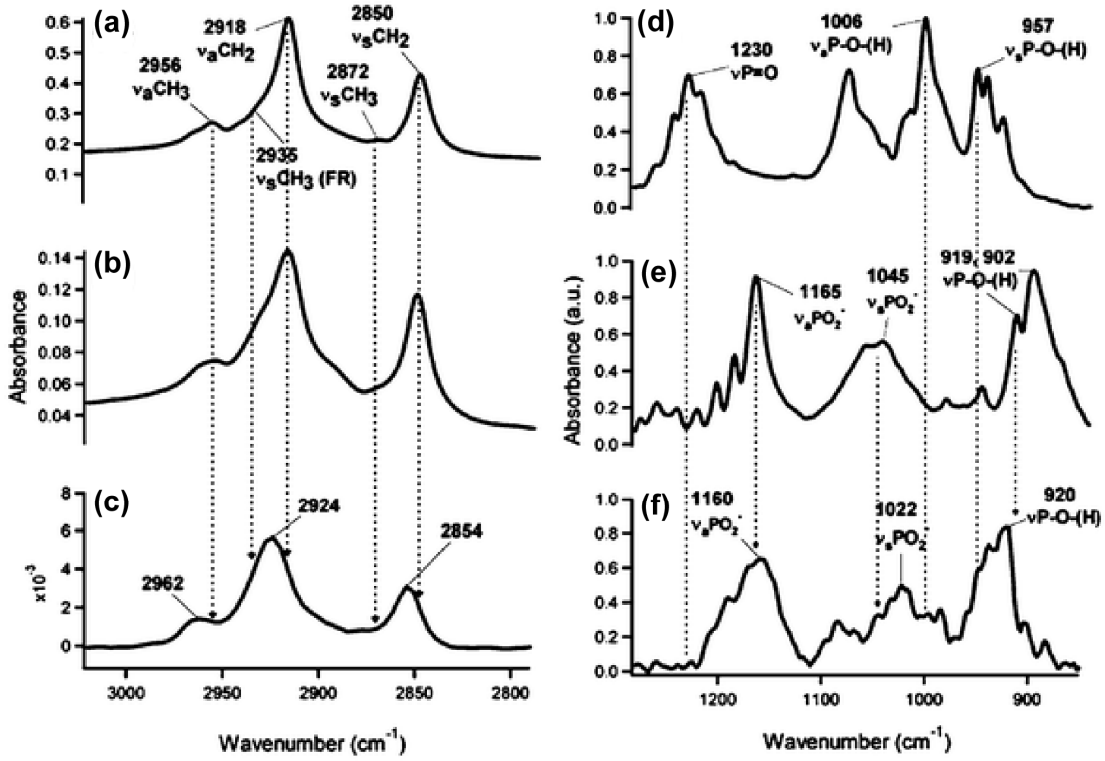

Figure 3.19 (a–c) Comparison between FT–IR spectra of ODPA powder (a), monobasic potassium salt of ODPA (b), and PM–IRRAS of $BaTiO_3$ surface modified by ODPA (c) in the region of C–H stretch absorptions. (d–f) Expansion in the region of P–O stretching absorptions. ODPA peak wavenumbers are followed in (a–f) by dashed lines, and arrows are present when the modified surface retains peaks of either ODPA or its monobasic anion.

A proposed modification scheme of phosphonic acids on nanostructured $BaTiO_3$ is shown in Figure 3.20.

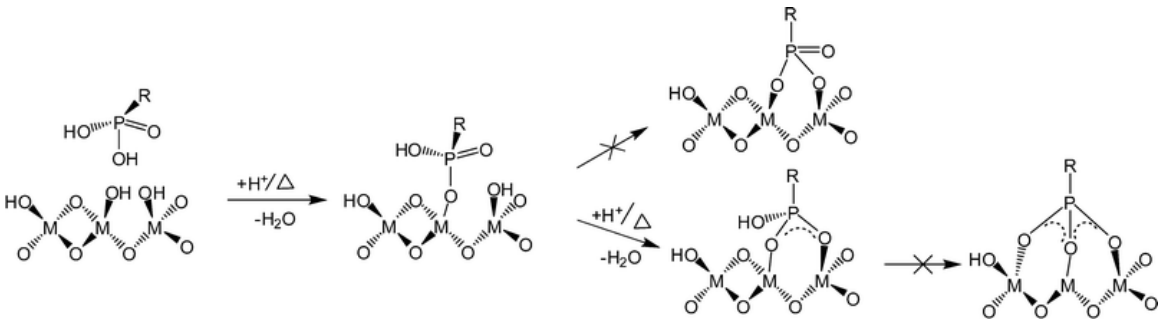

Figure 3.20 Reaction steps for $BaTiO_3$ modification with ODPA: with the experimental procedure followed, condensation stops at bidentate bonding in which the free moiety in the acid is a hydroxyl, due to the acidity of the medium. A crossed arrow indicates that evidence was not obtained for the occurrence of that step.

Studies on the modification of barium titanate (BT) nanoparticles with octylphosphonic acid yielded similar results. Figure 3.21 shows major changes in the number and frequencies of the P–O stretching bands (1106 and 990~1010 cm^{-1} for OPA vs. 1140 and 1057 cm^{-1} for OPA bound to BT (OPA–BT), and the disappearance of P=O stretching (1260~1300 cm^{-1}) and PO–H stretching (2321 cm^{-1}) bands.

The IR and NMR spectra provide insight into the binding of OPA to the surface of BT. As discussed above, the P=O and the P–O stretching peaks are replaced by two peaks of intermediate frequency at 1140 and 1057 cm^{-1}. This indicates an involvement of all three oxygen atoms of OPA in a tridentate form of binding to the BT surface for the majority of the bound phosphonic acid. This is consistent with previous IR spectral results reported for phosphonic acids binding to TiO_2 and ZrO_2 surfaces, which were also interpreted as evidence of tridentate binding.[6, 35]

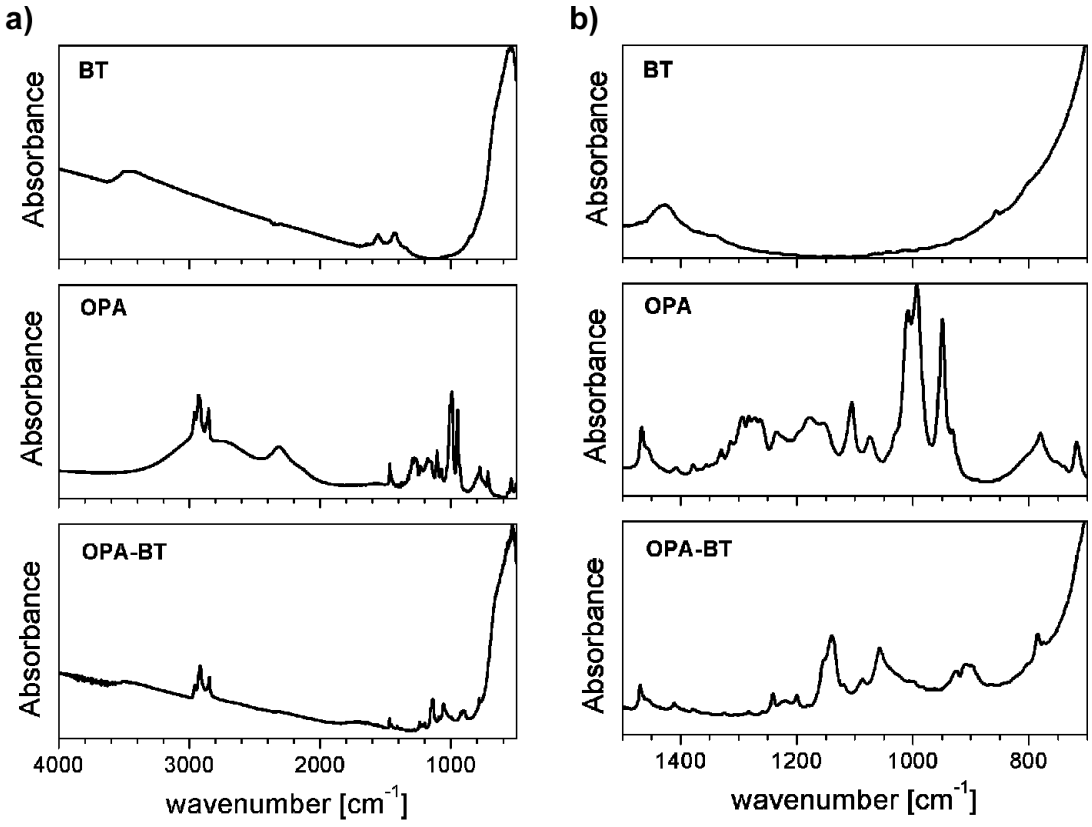

Figure 3.21 (a) FT–IR spectra of BT, OPA, and OPA–BT. (b) Wide–range FT–IR spectra of BT, OPA, and OPA–BT.

Cross polarization ^{31}P MAS NMR show sharp singlets at 36 ppm for free OPA and 23 ppm for OPA–BT; the resonance for OPA–BT indicates the presence of rigidly bound phosphonic acid to BT which could be attributed to densely–packed, strongly–bound tridentate ligand. Direct polarization ^{31}P MAS NMR, which is sensitive to all phosphorus nuclei, of OPA–BT shows an additional broad peak at intermediate chemical shift (~27 ppm), which indicates the presence of at least some disordered phosphonic acid groups on the surface, such as bidentate or monodentate bound forms (Figure 3.22) to bulk metal–phosphonate gel from stripping of surface metal and/or oligophosphonate gel

via homo–condensation is evident (both have $\delta \leq 0$), suggesting these are not formed under the surface modification conditions.

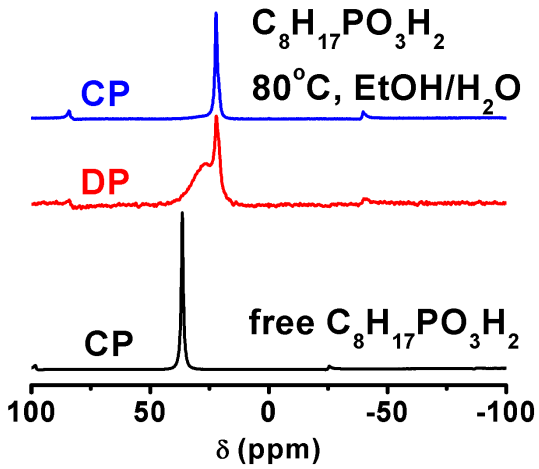

Figure 3.22 Cross–polarization (CP) and direct–polarization (DP) magic angle spinning (MAS) ^{31}P solid state NMR spectra of OPA–modified $BaTiO_3$ nanoparticles with ammonium dihydrogen phosphate, δ = 1 ppm as the reference. The differences between CP and DP spectra show that there are at least two different types of phosphorus environments present on the $BaTiO_3$ surface. (Data collected and figured prepared by P. Kim)

3.2 Surface Coverage

Surface coverage of monolayers is also an important factor in the assessment of the utility of monolayers. An important measure of the robustness and utility of monolayer–forming molecules, besides their binding energies, is the types of surface coverage densities that they produce. Thiols are used extensively for the surface modification of gold because they can form highly ordered, dense monolayers. The adsorption of molecules onto a surface affects the surface properties in two major ways:

firstly, it can add functionality to the surface *via* the monolayer; secondly, the underlying substrate's surface properties can be masked. Therefore, monolayers can be used to either actively change the surface properties by imparting its own functionality onto a surface, or they can passively change the surface properties by covering those of the substrate. Dense, homogeneous coverages of monolayers are important in both instances.

3.2.1 Techniques Used to Study Surface Coverage

There are a wide variety of techniques that can be used to study the extent of surface coverage by phosphonic acids on metal oxides. Some of the techniques are applicable only for nanoparticle species, such as thermogravimetric analysis (TGA) whereas others are only appropriate for planar substrates (quartz crystal microbalance (QCM), ellipsometry, atomic force microscopy (AFM), contact angle (CA)) and other techniques can be used for both media (XPS, IR). Most of the techniques can provide quantitative information (TGA, XPS, QCM, and AFM, IR and CA (to an extent). However, the use of multiple characterization techniques for any given sample greatly increases the reliability of the data, assuming the data corroborate each other.

3.2.1.1 Thermogravimetric analysis (TGA)

TGA is probably the most straightforward of the techniques used to determine surface coverage, and is perhaps one of the most precise. Though it is only applicable for nanoparticle samples, due to detection limits as well as instrument architecture, it is easy to use and provides concrete data on the mass loss of a sample.

The concept is as follows: A pre–weighed amount of sample is placed in a crucible, which is heated at a controlled rate, and the weight loss measured over time. As the monolayers are organic–based they will tend to break down and decompose at far lower temperatures than the inorganic nanoparticles, so by measuring the total weight loss it is a relatively easy calculation to determine the surface coverage of a given sample with a given ligand. Using the equation:

$$\frac{SA_{NP} \times MW_L}{A \times BA_L} = \frac{g_L}{g_{NP}} \qquad \text{(Equation 3.4)}$$

where SA_{NP} is the surface area of the nanoparticles (which can be found using BET analysis, or approximated using the size of the nanoparticles), MW_L the molecular weight of the ligand, A Avogadro's number, BA_L the binding area of the ligand (0.24 nm^2 for phosphonic acids)[35], and g_L/g_{NP} the mass of ligand per gram of nanoparticle corresponding to a complete monolayer on the surface. The mass of the ligand per gram of nanoparticle can then be used to determine the expected % weight loss in TGA:

$$\frac{M_L}{M_L + 1} = \%Mass \qquad \text{(Equation 3.5)}$$

where M_L is the mass of the ligand per gram of nanoparticle.

3.2.1.2 Elemental Analysis

Elemental analysis has been used in much the same way that TGA is used to determine the surface coverages of monolayers on nanoparticles. The technique can provide slightly more information, however, as the composition of the organic species can be determined to an extent. The %C in the elemental analysis, given the size and elemental composition of the nanoparticles, can be related to the amount of ligand in a sample which can then be used to compute the coverage by that ligand.

3.2.1.3 XPS

XPS can also provide valuable information about the surface coverage of monolayers. While in practice this is not always straightforward, it remains a powerful technique for examination of monolayers on surfaces.

Relating surface elemental composition can give an idea of the amount of the monolayer–forming molecules present, but in order to obtain more quantitative information regarding the coverage of the monolayer, angle–resolved (AR) XPS can be

used. ARXPS takes advantage of the fact that the depths from which photoelectrons can be detected will change as the angle of detection increases from the surface normal (Figure 3.23). This is because the limited mean free path changes depth as the angle of detection increases.

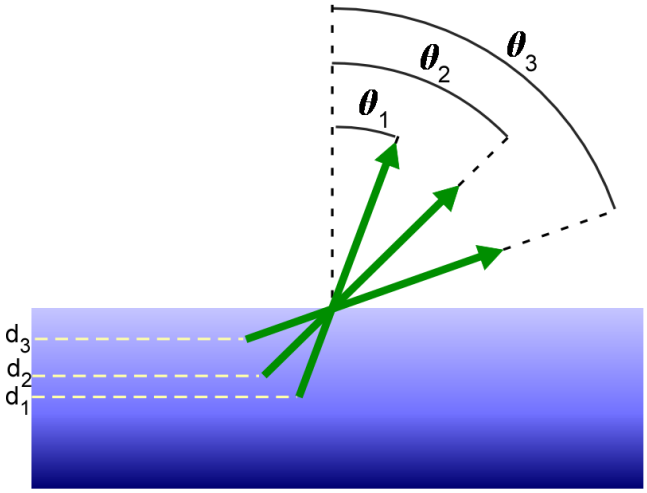

Figure 3.23 Diagram of how increasing the angle of detection (from the surface normal) (for example, from θ_1 to θ_2 to θ_3 can decrease the depth from which photoelectrons will be detected (fro example, from d_1 to d_2 to d_3, effectively making the technique more surface sensitive.

ARXPS allows for depth–profiling of a sample, where relative amounts of the elements can be determined at specific depths. From this, monolayer thicknesses and orientations can be obtained.

3.2.1.4 Atomic Force Microscopy (AFM)

AFM is perhaps one of the more powerful tools with which to look at monolayers. The lateral resolution (on the Angstrom scale) is excellent, and simple topography images

can reveal where and where not monolayer clusters have formed on a surface (Figure 3.24). Additionally, information can be obtained regarding the presence of multilayers, if applicable.

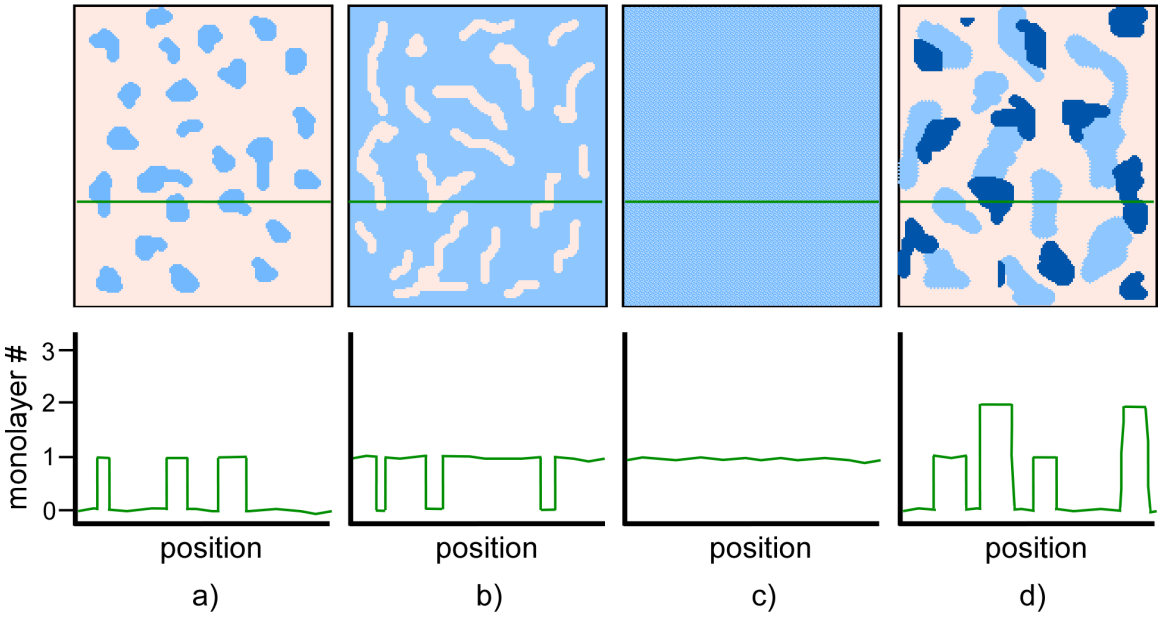

Figure 3.24 Method by which the surface coverage of a monolayer (in blue) on a substrate (pink) can be determined. Depth traces for each image (marked by a green line) are presented below the image. a) relatively low coverage of monolayer. b) much higher, but incomplete coverage by a monolayer. c) complete coverage by a monolayer. No height changes should be seen in the depth trace. d) Presence of an incomplete monolayer and bilayers on the surface.

However, obtaining the type of surface coverage information as presented in Figure 3.24 requires very smooth surfaces. If a surface is not smooth on the Angstrom scale, then it becomes difficult to determine height differences from the presence or absence of molecules vs. the natural height changes in the substrate. Additionally, it should be pointed out that while the homogeneity of a surface can be determined, the density of the monolayer cannot be as easily calculated, though other scanning probe

microscopy techniques, such as scanning tunneling microscopy (STM), have the ability to provide such information.

3.2.1.5 Quartz Crystal Microbalance (QCM)

A QCM measures a mass per unit area by measuring the change in frequency of a quartz crystal resonator. It is easy to measure mass loadings below 1 $\mu g/cm^2$ due to the precision with which frequency measurements can be made. It can be an excellent technique to study not only the total surface coverage of a film but also the kinetics of monolayer formation. The mass change can be measured as a function of time, thus providing kinetic information on the rate of monolayer formation on the surface.

The technique is limited to planar substrates, and even more so to planar substrates which are piezoelectric, such as quartz. Other materials can be deposited on top of the quartz, however.

3.2.1.6 IR

While IR is best known as a qualitative tool to measure the types of chemical bonds on a surface, it can also be used as a quantitative tool for surface coverage in certain situations. It is useful when looking at the binding of alkyl–substituted modifiers, where the C–H stretching frequencies will shift depending on how rigid and crystalline

the chains are.[25] The more rigid and crystalline the alkyl chains, the closer the packing and the higher the surface coverage. KBr pellets can be used for nanoparticle samples whereas IRRAS needs to be used for planar substrates.

3.2.1.7 Ellipsometry

While ellipsometry was not used in any of the research presented in this thesis, it remains an important tool for the study of monolayer systems and as such will be briefly discussed. Ellipsometry is an optical technique that is both non–destructive and contactless. The technique measures the change in polarization upon reflection of light off a sample film. Linearly polarized light of a known orientation is reflected from a surface resulting in elliptical polarization of the reflected light. The relative phase change and amplitude change introduced by reflection from the surface can be calculated. If the surface undergoes a change, such as the thickness of a film on the surface changing, then the reflection properties of the polarized light will also change. Measuring these changes in polarization allows one to deduce the change in the thickness of a film.

The technique has unsurpassed resolution, allowing for the quantification of film thicknesses on the angstrom scale. It is thus well equipped to study monolayers, though it has a dynamic range of a few angstroms to a few microns. It is useful in the study of coverage of monolayers because of its extreme sensitivity. Well–packed monolayers should have a thickness defined by their length and the angle with which they are oriented to the surface. If there is a sub–monolayer, then the packing will be less tight and the molecules will be allowed to fold over more, resulting in a thinner perceived layer.

Conversely, if a multilayer is present then the thickness measured by the ellipsometer will be more than what would be expected for a monolayer. A limitation of ellipsometry is that it is only applicable to planar substrates

3.2.1.8 Contact Angle measurements

Contact angle measurements can yield relative surface coverages of monolayers of planar substrates by relating the contact angle measurement of the sample in question with the contact angle of a substrate modified with a complete monolayer of the molecules in question. Film coverage can be derived with the following equation:[37]

$$\text{Cos } \theta = f_1 \cos \theta_1 + f_2 \cos \theta_2 \qquad \text{(Equation 3.6)}$$

where θ is the measured contact angle for a given film, f_1 the fractional coverage of the ligand in question on the substrate in question, θ_1 the contact angle for a complete coverage of the ligand, f_2 the fractional unmodified substrate coverage $(1 - f_1)$, and θ_2 the contact angle of the bare substrate. Examples of this are presented herein.

3.2.1 Surface coverages of flat substrates

This section outlines the literature and our own results in quantifying the coverage of phosphonic acids on metal oxides.

3.2.2 Kinetics and Surface coverages of planar substrates

The first part of this section will discuss the surface coverages that have been obtained on planar substrates. The importance of pre–cleaning substrates will also be discussed. Lastly, our own experiments quantifying surface coverages of phosphonic acids bound to ITO and ZnO will be discussed.

3.2.2.1 Importance of Pre–Cleaning

As has been discussed in Chapter 1, the surface energy plays an important role in how a surface interacts with other materials. Additionally, as was discussed earlier in this chapter, the presence of hydroxyl groups greatly facilitates and could perhaps even be considered necessary for dense coverages of phosphonic acids on metal oxides. There have been many reports on pre–cleaning treatments of metal oxides trying to optimize these two points. ITO has been heavily researched due to its use in many organic electronic device platforms.

The cleaning of metal oxide surfaces is often characterized with contact angle and XPS measurements. Contact angle measurements (with water) should approach 0° as the number of surface hydroxyl groups increases and the amount of carbonaceous impurities decreases.[38, 39] Surface energies should therefore increase. In the XPS, cleaned surfaces should show decreased carbon content and changed oxygen peak shape corresponding to more hydroxyl groups.

A number of reports on the cleaning of ITO in order to increase its work function have been reported. Kim *et al.* report a modest increase of work function (+ 0.1 – 0.2 eV) after either oxygen plasma treatment, aqua regia treatment, or a combination of the two, as measured by Kelvin Probe and UPS.[40] Sugiyama *et al.* studied the effects of solvent cleaning, UV–ozone cleaning, and Ar^+ sputtering on the surface chemistry and work function of ITO.[41] They found that solvent cleaning did not change the work function and carbon contamination remained on the surface. UV–ozone cleaning reduced the carbon content as well as raised the work function ~ 0.2 eV. Ar^+ sputtering decreased the surface content of both carbon and oxygen, and decreased the work function ~0.2 eV. Chaney *et al.* report a significant decrease of the work function of ITO after base–cleaning (to 4.5 eV from 5.0 eV) and a significant increase upon plasma–cleaning (to 5.4 eV from 5.0 eV).[42]

An extensive study on the surface wetting properties of ITO after various surface treatments was conducted by Kim *et al.*[39] Various rubbing, sonication, acid, base, and plasma treatments were used and the resultant surface energies determined from contact angle measurements with formamide, methylene iodide, and water. Oxygen plasma was found to decrease (from 24 to 18 mJ/m^2) the dispersive component and greatly increase (from 23 to 47 mJ/m^2) the polar component of the surface energy compared to as–received ITO. Argon had the opposite effect, increasing (from 24 to 31 mJ/m^2) the dispersive component and decreasing (from 23 to 4 mJ/m^2) the polar component of the surface energy compared to as–received ITO. Other treatments have various intermediate effects.

Increasing the surface hydroxyl content of ITO by cleaning has also been

investigated. Purvis *et al.* have demonstrated an ability to increase the surface hydroxyl content of ITO by initial Ar^+ sputtering followed by cycles of water exposure followed by desorption at 50 °C.[43]

The importance of pre–cleaning before monolayer deposition has also been investigated. Donley *et al.*[44] report a comprehensive XPS study on the effects of various surface treatments on the ITO surface elemental content, the relative hydroxide concentration, and the amount of ferrocene dicarboxylic acid that subsequently absorbed to the ITO surface. They found that "piranha" (3:1 concentrated sulfuric acid: 30% hydrogen peroxide) treatment of the surface results in the highest surface hydroxyl content, followed by air plasma and then RCA cleaning. However, ~ 9 times as much carboxylic acid absorbed to the air–plasma cleaned ITO vs. the "piranha" cleaned, as evidenced by electrochemical measurements. Koh *et al.*[15] performed a similar study in order to determine the best pre–cleaning procedure for the absorption of phosphonic acids on ITO. Various solvents and combinations of solvent treatments were used, as well as base and oxygen plasma treatments. They adopted a treatment of trichloroethylene/acetone/methanol/KOH in isopropanol for subsequent modification studies over an oxygen plasma cleaning procedure because, while the oxygen plasma resulted in similar hydrophilicity of the ITO surface to the adopted treatment (11° vs. 7°), the percentage of carbon on the surface after plasma treatment was substantially higher (18 % vs. 8 %).

The effects of different pre–cleaning treatments on the surface properties of other metal oxides have also been reported. One example comes from Giza *et al.*, where the effects of water and argon plasma on the surface hydroxyl content and adsorption of

ODPA on the surface of native–oxide–covered aluminum were measured.[8] XPS showed a large increase of surface hydroxyl content after water plasma vs. untreated Al/AlO_x. A more modest increase was seen after water plasma treatment followed by argon plasma treatment. QCM measurements of adsorption of ODPA onto the various treated surfaces showed an increase in the kinetics of monolayer formation as the surface hydroxyl content increased.

Taking the previous and other studies into account, we adopted a pre–cleaning procedure which involves both detergent and solvent cleaning (DSC) and oxygen plasma cleaning (OP). Two small studies were done to study the effects of these treatments on ITO.

The role of oxygen plasma is to both remove surface contamination and "activate" the metal oxide surface by creating surface hydroxyl and other oxygen species on the surface. The differences in both the surface carbon contamination and the ability to adsorb phosphonic acids onto the surface can be seen in Figure 3.25. DSC/OP treatment leads not only to a substantial decrease in the initial carbon contamination on the surface vs. DSC treatment, as evidenced by the C(1s) peak in XPS (Figure 3.25a), but also to increased absorption of phosphonic acid molecules, in this case FHOPA (Figure 3.25b,c). The F(1s)/In($3p_{3/2}$) peak ratio increases by ca. 162% on DSC/OP treated samples vs. samples treated with only DSC. This corresponds to a ca. 65% higher coverage of FHOPA on DSC/OP treated ITO.[45, 46] A similar increase in the coverage can be expected for other phosphonic acids.

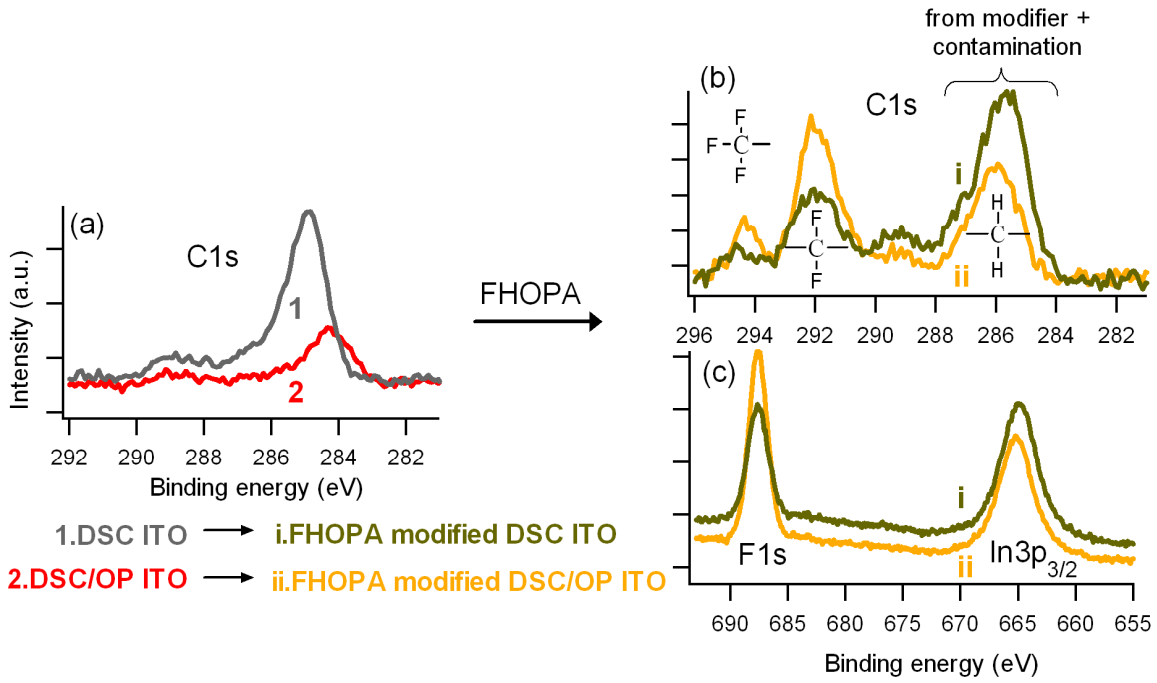

Figure 3.25. XPS C(1s) spectra for DSC and DSC/OP ITO before (a) and after modification with FHOPA (b), and F(1s) and In($3p_{3/2}$) lines after the FHOPA modification (c) –offset for clarity; the surface coverage of the modifier is inversely proportional to the level of carbon contamination both before and after the modification. (Data collected and figure prepared by S. Paniagua).

Another small study on the effects of OP treatment on the adsorption of phosphonic acids to ITO was achieved by studying both the change in F(1s)/In($3p_{3/2}$) peak ratios as well as the work function by the adsorption of two different fluorinated phosphonic acids onto both DSC and DSC/OP ITO (Figure 3.26).

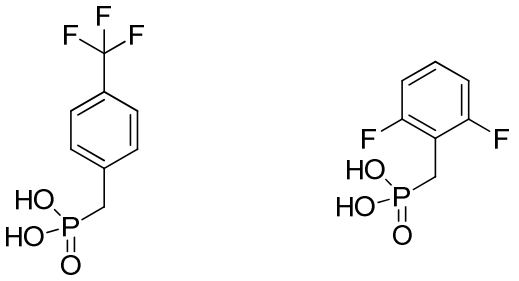

pCF_3BnPA oF_2BnPA

Figure 3.26 The two phosphonic acids, 4–(trifluoromethyl)benzylphosphonic acid (pCF_3BnPA) and 2,6–difluorobenzylphosphonic acid (oF_2BnPA) used to study the influence of oxygen plasma on the subsequent binding of PAs and shifts in work function.

Two phosphonic acids, pCF_3BnPA and oF_2BnPA, were chosen to modify both a DSC ITO surface and a DSC/OP ITO surface. These molecules were chosen because they should either raise or lower the effect work function of ITO, respectively. XPS was used to relate the different treatments to one–another, and Kelvin Probe studies were used to relate the work function changes to each other and to bare ITO.

XPS measurements show that the O_2 plasma indeed increased the coverage of each of the phosphonic acids to the ITO surface. Normalizing the $In(3p_{3/2})$ peaks for each set of samples allows for the relative amount of fluorine to be determined (Figure 3.27). In both cases the modification on DSC/OP ITO (blue trace) results in more fluorine content on the surface than the modification on just DSC ITO (red trace). As fluorine is not a normal contaminant from the atmosphere, this can be readily attributed to more of the phosphonic acid modifier on the surface of DSC/OP ITO, and hence better coverage. By looking at the areas of the F(1s) peaks, it can be determined that DSC/OP treatment vs. DSC treatment results in 16% and 28% more coverage for (pCF_3BnPA) and

(oF_2BnPA), respectively, on the surface of ITO (Table 3.2).

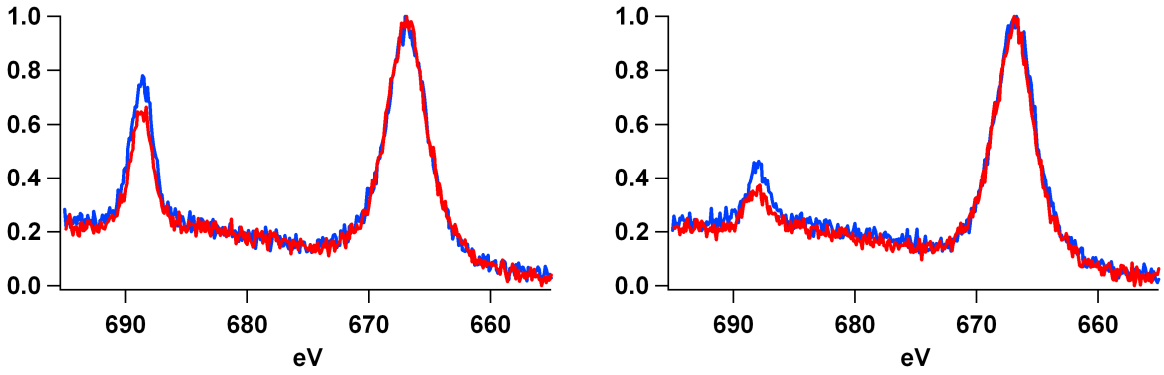

Figure 3.27 XPS spectra of DSC (red) and DSC/OP ITO (blue) modified with pCF_3BnPA (left) and oF_2BnPA (right) The peak at ~688 eV corresponds to the F(1s) electrons, and the peak at ~666 eV corresponds to the $In(3p_{3/2})$ electrons in the sample.

Kelvin Probe measurements also indicate an increased adsorption of the phosphonic acids after DSC/OP treatment. pCF_3BnPA 1 should raise the work function of the ITO by a considerable amount, whereas oF_2BnPA should lower it. This is indeed the case, however the modified DSC/OP ITO samples show an increased absolute change in the work function vs. modified DSC ITO samples, consistent with increased coverage of the phosphonic acid.

Table 3.2 Statistics of the relative F/In ratios detected from the surface of the various samples, and the work function of the surfaces measured with Kelvin Probe. (Kelvin Probe data collected by A. Sharma)

Sample	F/In Ratio	Work Function (eV)
DSC ITO	0	4.8
DSC ITO with pCF_3BnPA	0.54	5.3
DSC/OP ITO with pCF_3BnPA	0.67	5.5
DSC ITO with oF_2BnPA	0.19	4.7
DSC/OP ITO with oF_2BnPA	0.25	4.5

3.2.2.2 Surface Coverages on ITO

There are not many studies in the literature quantifying the surface coverage of ITO by phosphonic acids. Koh *et al.* relate contact angle of ODPA on ITO to contact angle data for the analogous thiol on gold and find that they achieve a coverage slightly smaller (87%, or 4.8 molecules/nm^2) than that of a full monolayer of octadecanethiol on gold.[15]

We used a similar approximation to determine the coverages of some phosphonic acids on ITO. Using Equation 3.6, coverages of FHOPA (2.9 molecules/nm^2), ODPA (5 molecules/nm^2) and HPA (5 molecules/nm^2) were found, indicating that, though the monolayers are not as dense as those of the corresponding thiols on gold, relatively good coverages can be obtained. The lower coverage may be at least partially a result of the larger surface area of the head group of phosphonic acids (~0.24 nm^2)[47] vs. thiols (~0.19 nm^2)[48].

3.2.2.3 Kinetics and Surface Coverages on Other Planar Metal Oxides

There are a number of reports in the literature on the types of coverage that can be achieved with monolayers of phosphonic acids on various metal oxides. These studies range from qualitative assessments based on contact angle[49-52] and/or IR[53] data to in–depth studies incorporating XPS, QCM, AFM and other data.

Hanson *et al.* report an almost (> 95%) full coverage of phosphonic acid on Si/SiO_x substrates as evidenced by AFM images.[9] McIntyre *et al.* report similar coverages of ODPA on Si/SiO_x[54] and mica[55] with quite impressive AFM images. They also show images for partially formed monolayers. Schwartz *et al.* report the surface coverage of various phosphonic acids on the native oxide on titanium.[56-58] They report coverages as low as 1.5 molecules/nm^2 for 1,4–phenylenebis(methylene) diphosphonic acid and as high as 7.2 molecules/nm^2 for OPA. Additionally, an extremely detailed study was performed by Textor *et al.* on the surface modification of tantalum oxide with octadecylphosphoric acid (similar to ODPA). By using AFM, SIMS, and angle–resolved XPS they found a dense coverage of 4.8 molecules/nm^2.

Related to the surface coverage is the kinetics of formation of monolayers of phosphonic acids on metal oxides. There are several reports in the literature quantifying the kinetics of adsorption of phosphonic acids. Giza *et al.* report an increase in kinetics and in overall surface coverage of ODPA on Al/AlO_x surfaces, as measured by QCM.[8] They find that monolayer formation is complete after only 5 minutes when a water plasma is used to treat the surface beforehand, as opposed to ~ 15 minutes when no treatment is used. The water plasma treatment also increases the total coverage by the

ODPA, though no specific numbers were given. Similarly, Tsud *et al.* find that monolayer formation of phenylphosphonic acid on amorphous alumina is complete after 20 minutes vacuum vapor deposition.[59]

Nie *et al.* report the formation of physisorbed monolayers of ODPA on Si/SiO_x after only a few seconds, and their subsequent removal with solvent washing.[60] Felhosi *et al.* report the formation of robust monolayer films based on phosphonic acids on iron substrates over the course of several days.[61] Brovelli *et al.* report the formation of monolayers based on octadecylphosphoric acid in ~ 10 minutes, though the coverage is estimated at a little under 90%.

Additionally, several interesting studies on the formation and detection of multilayers of phosphonic acids have been reported. Nie *et al.* report multilayer formation of ODPA on both mica and Si/SiO_x, as evidence by AFM. Gouzman *et al.* report a technique using differential charging in XPS to distinguish between mono– and multilayer films of ODPA on Si/SiO_x.[31]

For our own studies on the surface modification of ZnO with phosphonic acids, no direct evidence of surface coverage has been acquired. However, as for ITO, the surface coverage of ZnO with several different phosphonic acids was approximated using Equation 3.6. Surface coverages of 3.2, 3.7, and 5.3 molecules/nm^2 were calculated for monolayers of OPA, FHOPA, and ODPA, respectively. Additionally, IRRAS spectrum of an ODPA–modified ZnO surface shows $\nu_a CH_2$ at 2920 cm^{-1} which is indicative of a fairly close–packed system.[62] The characterization for ZnO modification with phosphonic acids is presented fully in Chapter 4.

3.2.3 Kinetics and Surface coverages of nanoparticles

Quantitative analyses of the surfaces coverage of metal oxide nanoparticles by phosphonic acids is most easily and often ascertained by either TG analysis or elemental analysis.

Doussineau *et al.* obtained surface coverages of 50% and 70% of a full monolayer for the modification of alumina (d_{avg} = 13 nm) and titania (d_{avg} = 21 nm) nanoparticles, respectively, with a semicarbazide–functionalized alkylphosphonic acid.[63] Gao *et al.* report decent coverage of 73% for zirconia and 61% for titania nanoparticles with ODPA in methanol/water (from carbon content in elemental analyses), though similar reaction conditions with alumina nanoparticles resulted in the formation of bulk (aluminoalkyl)phosphate.[35] A future study by the same group reports surface modification of similar nanoparticles with carboxyalkylphosphonic acids in refluxing acetone. Elemental analysis indicated excellent surface coverages of ~ 92% and ~ 85% of a full monolayer for zirconia and titania nanoparticles, respectively. Guerrero *et al.* report good coverages of titania nanoparticles with phenylphosphonic acids and even phenylphosphonates under mild conditions (water/methanol, room temperature).[4] When forcing conditions (water or toluene, 120 °C for 24 hours, closed reaction) were used, a number of the samples showed formation of bulk phases.

The kinetics of modification of some types of metal oxide nanoparticles with phosphonic acids have also been reported. Farrow *et al.* report the adsorption of styrylphosphonic acid onto stannic oxide nanoparticles.[64] They measured coverages of the phosphonic acid in solution at pH 5.0 of 80% after 2 hours, 90% after 4 hours, and

full adsorption after 30–40 hours. The reaction is even slower at pH = 3.0, where coverages of 50% after 2 hours, 60% after 4 hours, and full coverage after 50–60 hours are seen. Helmy *et al.* report a uniform mechanism of growth of ODPA monolayers on titania nanoparticles, with relatively fast reactivity, though much less so than octadecyltrichlorosilane.

Our own research on the modification and characterization of metal oxide nanoparticles is fully described in Chapter 5, and as such, will not be discussed here.

3.3 Conclusions

This chapter discussed our efforts on how strongly phosphonic acids bind to ITO and $BaTiO_3$, and what degrees of surface coverage can be obtained. Both IRRAS and XPS (coupled with theory) experiments were used to characterize phosphonic acid–modified ITO substrates. We found that alkylphosphonic acids bind to ITO in a mainly bi– and tri–dentate fashion. The coverage of alkylphosphonic acids on planar ITO substrates was found to be ~ 90% the density of complete alkylthiols on gold, indicating an overall high surface coverage.

In addition to studying the binding modes of phosphonic acids on ITO, we determined the binding energies of several different phosphonic acids on ITO. ITC measurements indicate that the binding energy of PhPA to the ITO (nanoparticle) surface is ~ 50 kJ/mol and the binding energy of OPA to the ITO (nanoparticle) surface is ~ 80 kJ/mol, both stronger than the ~25–30 kJ/mol seen for carboxylic acids on metal oxide

surfaces. Additionally, it should be noted that these binding energies were obtained for the reaction of phosphonic acid with ITO at room temperature. Knowing the importance of heat in driving the heterocondensation reaction between phosphonic acids and a metal oxide surface, these numbers are probably much lower than the true binding energies that could be obtained when using elevated temperatures during or after the reaction.

Like ITO, the binding modes of phosphonic acids to $BaTiO_3$ were determined. It was found that for planar $BaTiO_3$ films, the predominant binding mode is bidentate whereas for $BaTiO_3$ nanoparticles the predominant binding mode is tridentate. For both ITO and $BaTiO_3$ nanoparticles, high surface coverages could be obtained with phosphonic acids.

The ability to measure and know the binding modes and strengths of phosphonic acids to metal oxides is important when considering the use of surface modifiers in specific applications. In some applications, such as protective coatings for materials, as robust a monolayer as possible is important to effectively passivate and protect the surface. In other applications, such as tuning the work function of the surface with a monolayer, the way in which the molecules attach may not be as important, and obtaining as dense a monolayer as possible may not be necessary.

3.4 Experimental

The ITO used herein was obtained from Colorado Concept Coating, LLC. with a sheet resistance of ca. 15 Ω/□ and film thicknesses between 90 and 160 nm depending on

the batch. Commercial ITO was ordered in sheets of 14 in. by 14 in. with good uniformity in transparency, color, and conductivity across each sheet. The outer one inch of an ITO sheet is not suitable for reproducible experiments due to inhomogeneities in the ITO deposition and is thus discarded. The conductivity, transparency, and/or color of ITO can vary, making universal characterization of ITO surfaces in general difficult. Commercial ITO is polycrystalline and typically has an RMS roughness between 1 and 3nm. The data presented below was all collected and the figures prepared by Michael Brumbach.[65, 66] For a more in-depth analysis of the data, the reader is referred to the priormentioned studies by Brumbach.

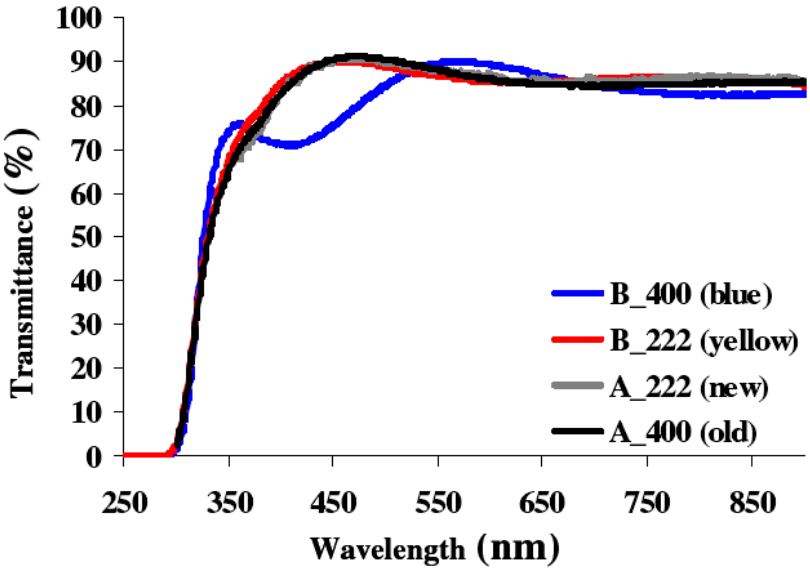

Figure 3.28 UV/Vis transmission spectra for four different ITO samples obtained from Colorado Concepts. All of the samples have similar thicknesses except for B_400 (blue), which is thicker. Figure from Brumbach.[66]

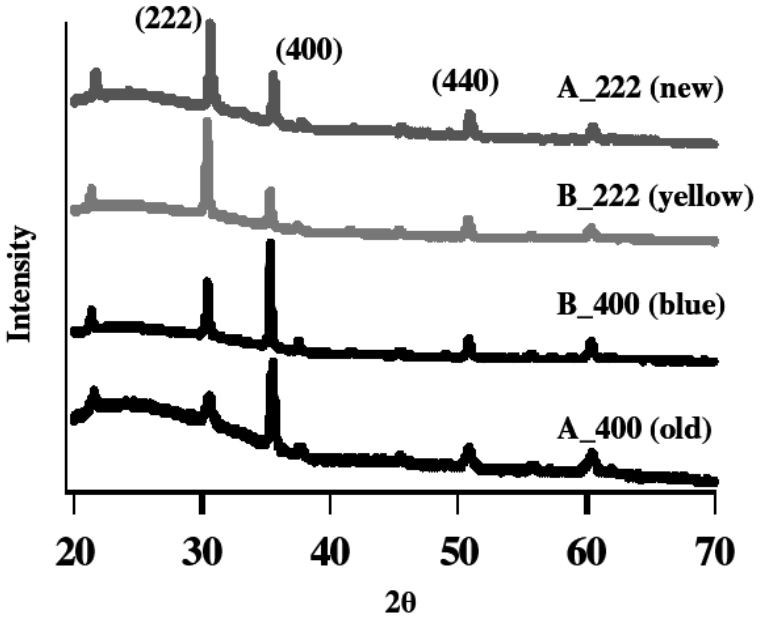

Figure 3.29 XRD patterns for four different batches of ITO from Colorado Concepts. Figure from Brumbach.[66]

Table 3.3 The ratio of tin to indium, calculated over the given sputtering stages, for the four ITO samples. Table adapted from Brumbach.[66]

ITO Sample	Sn/In Ratio	Sputtering stages for ratio analysis
B_222 (yellow)	0.16 ± 0.03	1 to 5
A_222 (new)	0.14 ± 0.01	3 to 10
B_400 (blue)	0.13 ± 0.01	1 to 3
A_400 (old)	0.11 ± 0.01	1 to 6

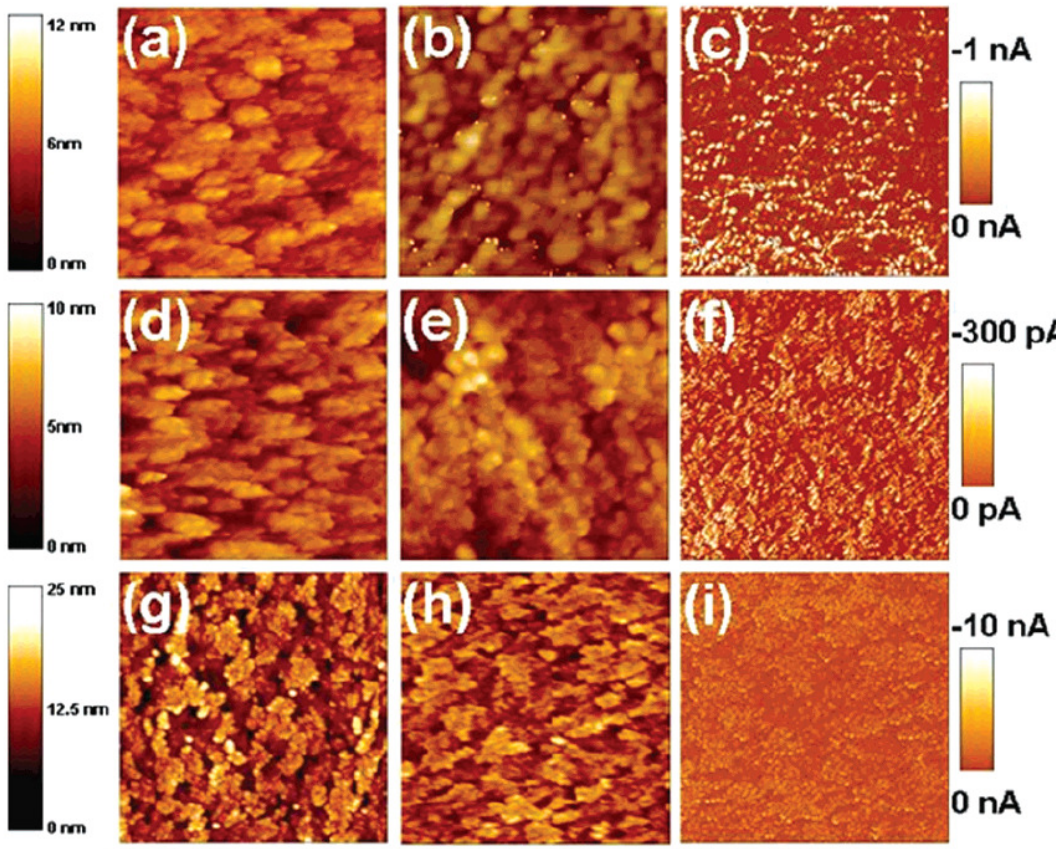

Figure 3.30 Tapping mode height AFM (left-hand column), contact mode height AFM (middle column), and Conductive AFM (right-hand column) characterization of various pretreated ITO samples (all images are 2 μm on a side). (a–c) DSC (detergent/solvent cleaned) ITO, (d–f) air–plasma etched ITO, and (g–i) oxygen-plasma-etched ITO. Figure from Brumbach *et al*.[65]

Details of the PM–IRRAS characterization for phosphonic acid–modified ITO[24] and nanostructure $BaTiO_3$[16] films have been published, as have been the details for the FTIR characterization of $BaTiO_3$ nanoparticles with phosphonic acids.[14] XPS spectra were obtained as outlined in the experimental section of Chapter 4. ^{31}P MAS NMR were obtained in a manner analogous to that published in the literature.[14]

TG analyses of nanoparticle samples were performed in a Netzsch STA 449 C instrument by heating to 600 °C at a rate of 10 °Cmin^{-1} followed by constant heating at

600 °C for 30 minutes.

ITO, $BaTiO_3$, and ZnO substrates were cleaned and modified as described in Chapter 4.

Isothermal titration calorimetry experiments were performed using a Microcal VP–ITC. 10 µL of a known concentration (PhPA = 10 mM, OPA = 7 mM, ODPA = 4 mM) of phosphonic acid was injected into 1.4 mL of a 7.4 mg/mL dispersion of ITO nanoparticles (27.4 m^2/g, Inframat Advanced Materials. The nanoparticles were ultrasonicated for 3 days and then centrifuged to remove large conglomerations prior to use) in 95:5 ethanol: water. Enthalpies of binding were calculated from the integrated heats. The raw data and subsequent isotherms for each of the samples are shown below:

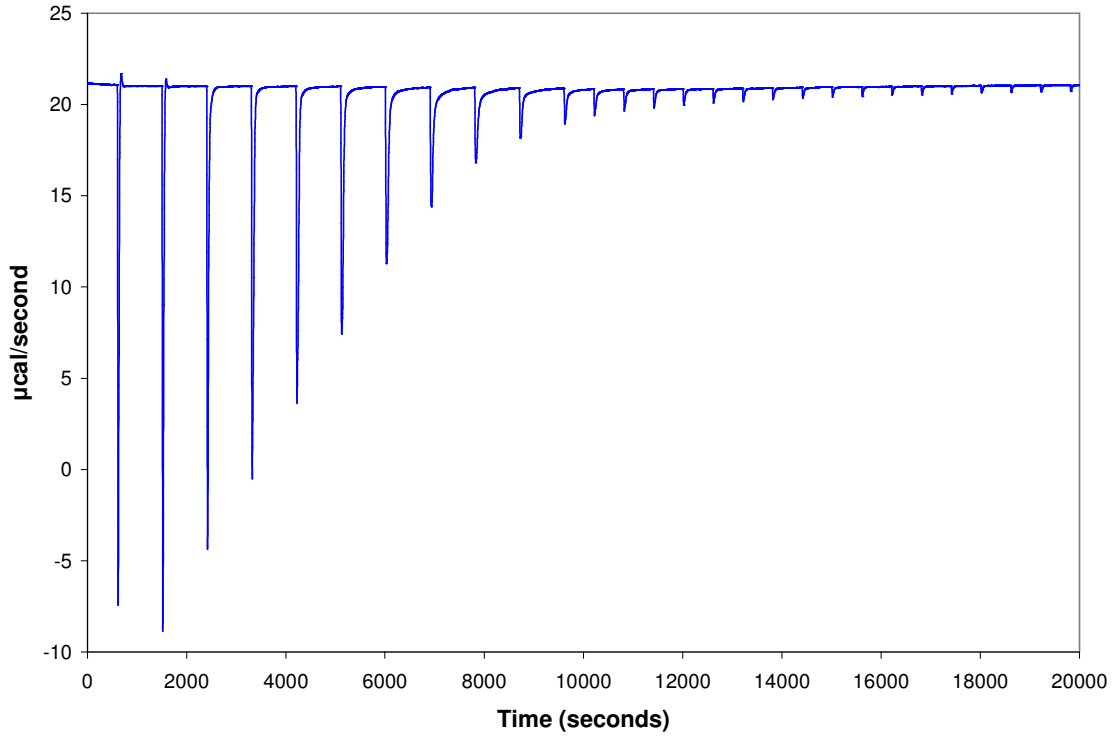

Figure 3.31 Raw ITC data for the addition of 10 mM PhPA to 7.4 mg/mL ITO nanoparticles. (Data collected by N. Hankins)

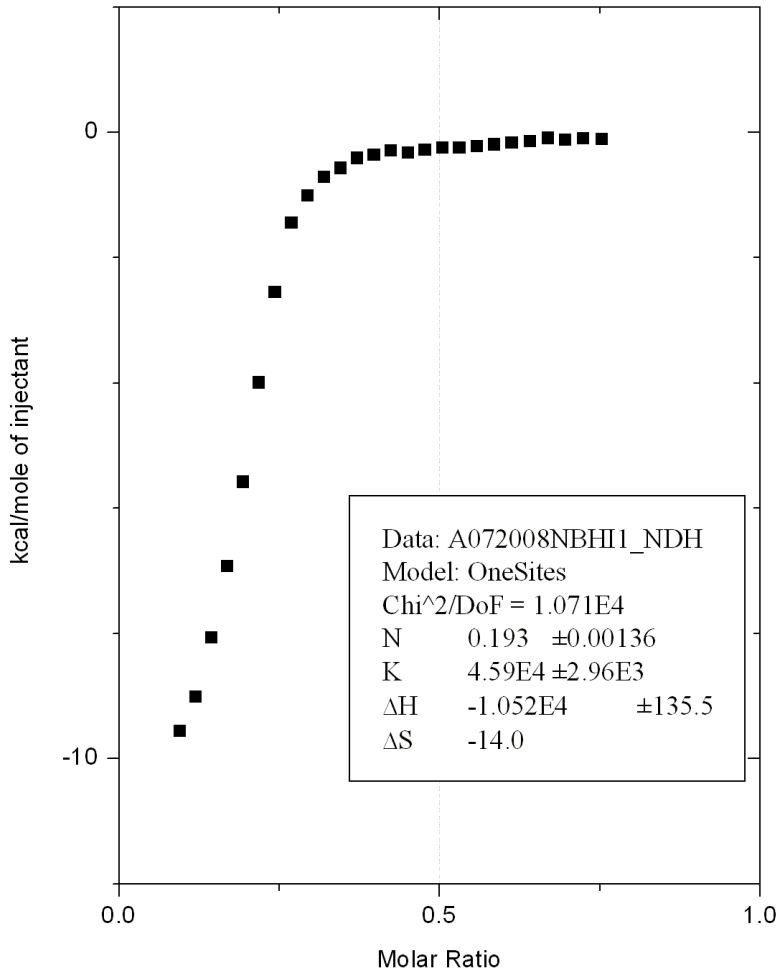

Figure 3.32 Isotherm (obtained from integrating raw data with respect to time) for the addition of 10 mM PhPA to 7.4 mg/mL ITO nanoparticles. (Data collected and graph prepared by N. Hankins)

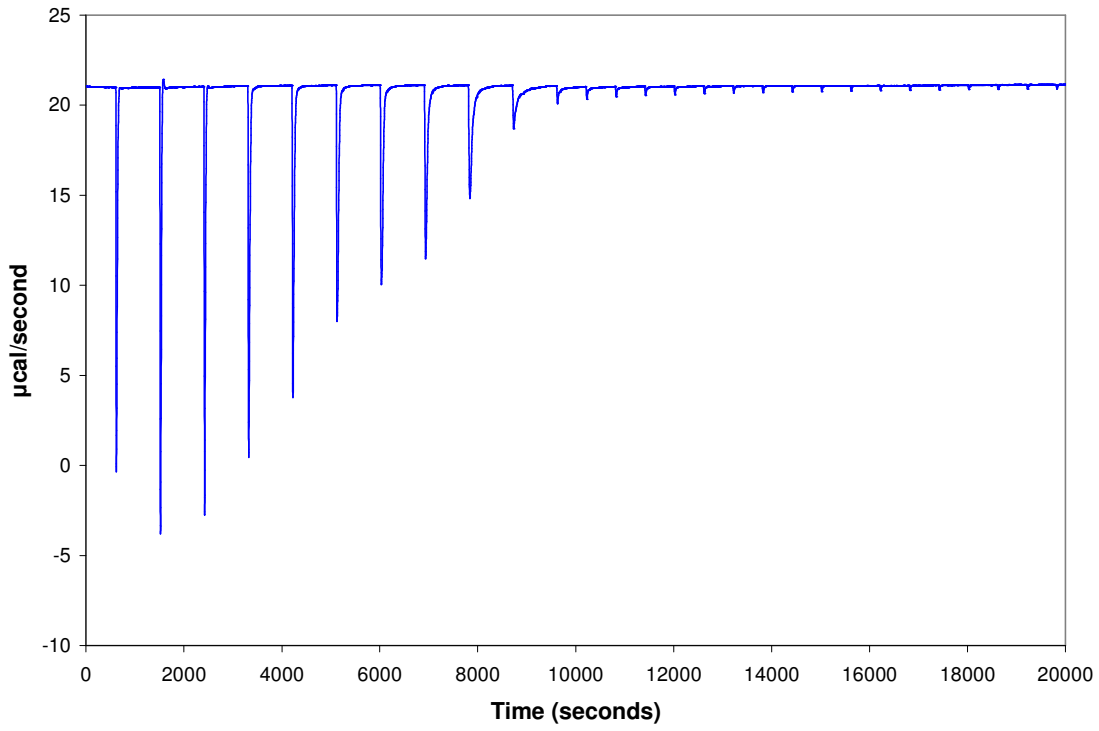

Figure 3.33 Raw ITC data for the addition of 7 mM OPA to 7.4 mg/mL ITO nanoparticles. (Data collected by N. Hankins)

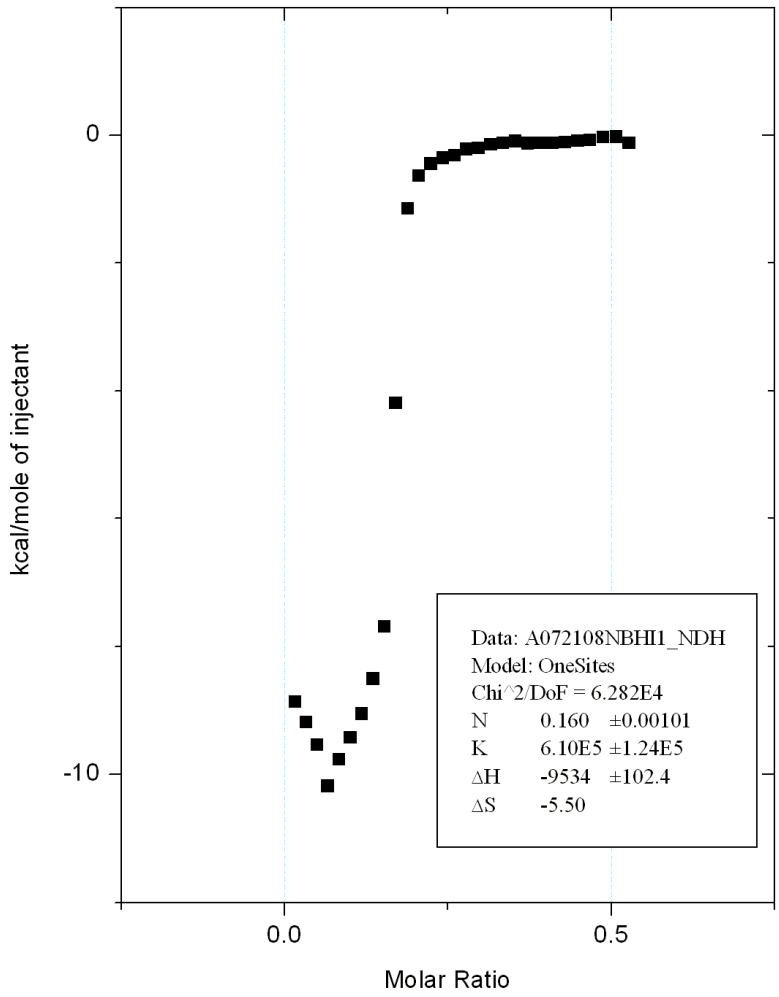

Figure 3.34 Isotherm (obtained from integrating raw data with respect to time) for the addition of 7 mM OPA to 7.4 mg/mL ITO nanoparticles. (Data collected and graph prepared by N. Hankins)

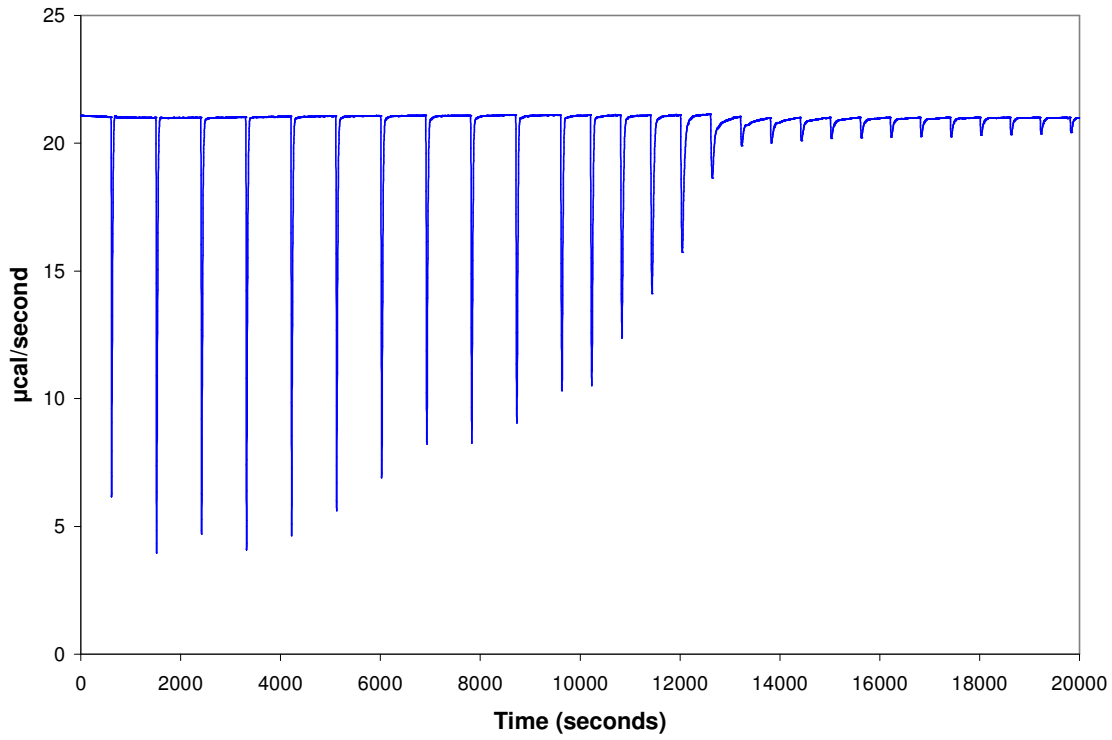

Figure 3.35 Raw ITC data for the addition of 4 mM ODPA to 7.4 mg/mL ITO nanoparticles. (Data collected by N. Hankins)

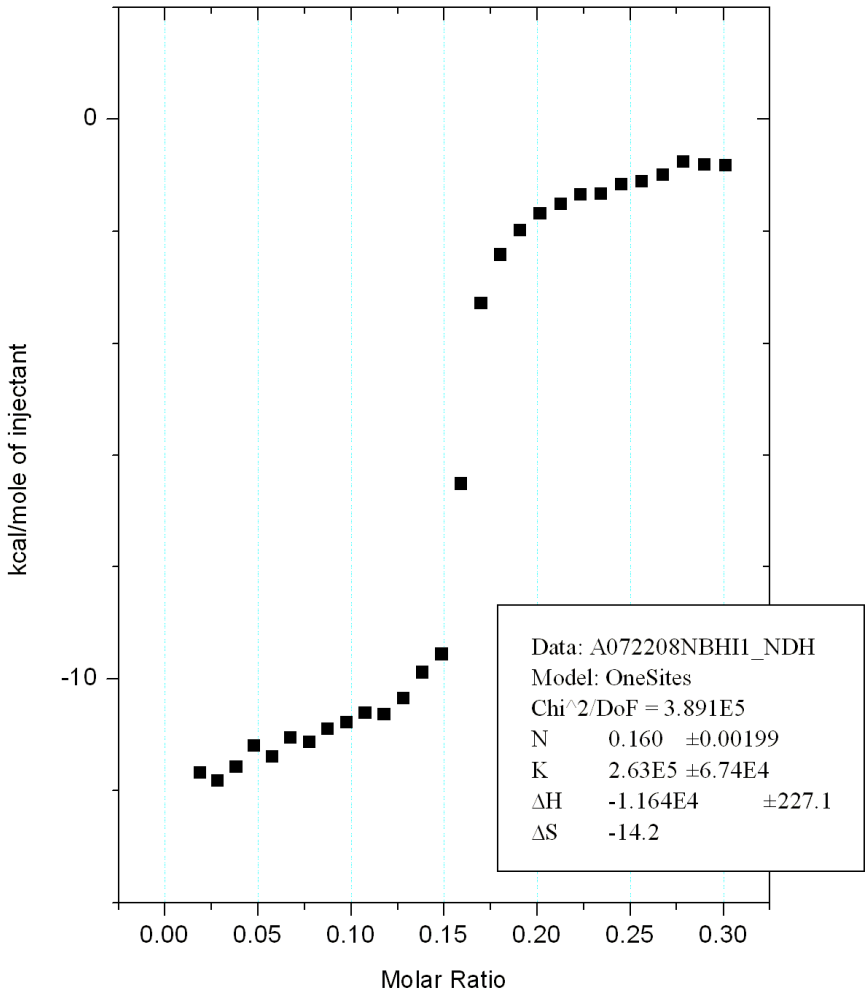

Figure 3.36 Isotherm (obtained from integrating raw data with respect to time) for the addition of 4 mM ODPA to 7.4 mg/mL ITO nanoparticles. (Data collected and graph prepared by N. Hankins)

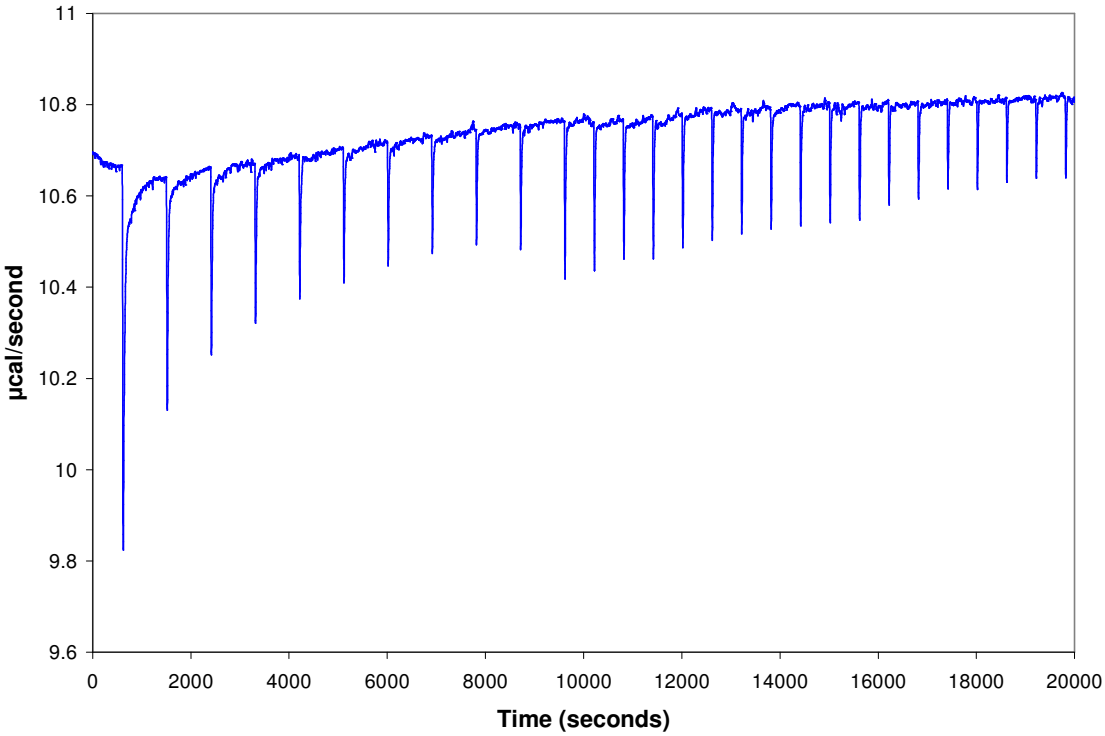

Figure 3.37 Raw ITC data for the addition of 30 mM OPA to pure solvent. (Data collected by N. Hankins)

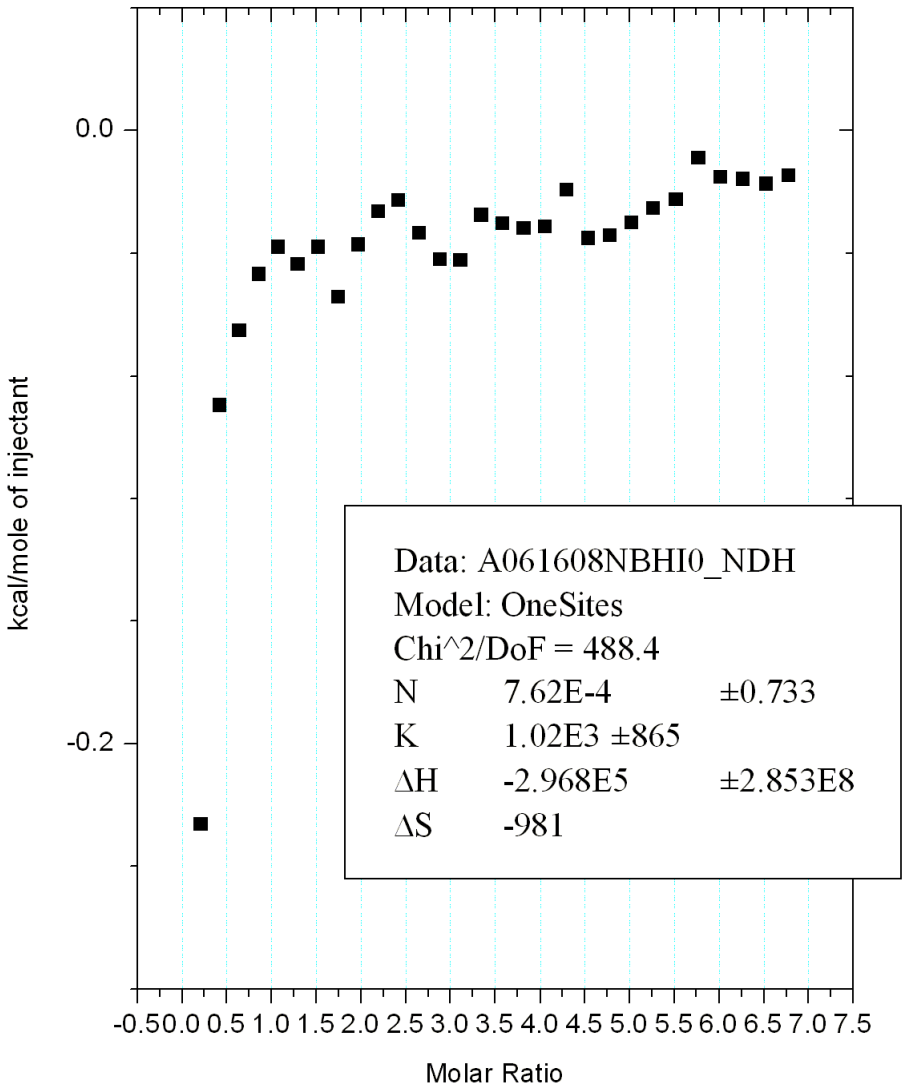

Figure 3.38 Isotherm (obtained from integrating raw data with respect to time) for the addition of 30 mM OPA to pure solvent. (Data collected and graph prepared by N. Hankins)

Solution calorimetry experiments were performed on a Parr Instruments 6755 Solution Calorimeter. The calorimeter was standardized and calibrated using a sample of tris(hydroxymethyl)aminoethane (TRIS). TRIS was dissolved in a dilute solution of HCl in a controlled reaction for which the amount of heat evolved is well established. The

observed temperature change can then be correlated to a specific amount of heat iven off in the reaction. For sample measurements, differing amounts of solid phosphonic acid were dissolved in 100 mL of a 95:5 ethanol: water mixture and the temperature changes measured.

ITO nanoparticles were modified and characterized for TG, ^{31}P MAS NMR, and BET analyses as follows:

ITO nanoparticles (120 mg) were combined with phosphonic acid (5 × molar excess based on surface area of the nanoparticles (27.4 m^2/g) and the binding area of a phosphonic acid (0.24 nm^2)) in 10 mL solvent (95:5 ethanol: water) and allowed to stir at room temperature for 24 hours. After settling of the nanoparticles, the solvent was decanted, and the nanoparticles were then resuspended in tetrahydrofuran and centrifuged (2 ×), then dichloromethane (1 ×). They were then transferred to a vial and dried in an oven (~45 °C, 2 hours) and then under high vacuum.

TG analyses of nanoparticle samples were performed in a Netzsch STA 449 C instrument by heating to 600 °C at a rate of 10 °Cmin^{-1} followed by constant heating at 600 °C for 30 minutes.

Fourier transform infrared (FT-IR, Perkin-Elmer Spectrum 1000) spectra were obtained by using KBr pellets containing 5 wt. % of each treated BT with 1 cm^{-1} resolution.

^{31}P MAS NMR Spectra were recorded on a Bruker DSX 400 (161.98 MHz ^{31}P frequency, 10 kHz MAS frequency, 256 scans, 10 s delay time) for both DP (5 μs 90º pulse length, high power ^{1}H decoupling) and CP (1 ms contact time) experiments.

3.5 References

1. Ferreira, J. M.; Marcinko, S.; Sheardy, R.; Fadeev, A. Y., Calorimetric study of the reactions of n-alkylphosphonic acids with metal oxide surfaces. *Journal of Colloid and Interface Science* **2005,** 286, (1), 258-262.

2. Love, J. C.; Estroff, L. A.; Kriebel, J. K.; Nuzzo, R. G.; Whitesides, G. M., Self-assembled monolayers of thiolates on metals as a form of nanotechnology. *Chemical Reviews* **2005,** 105, (4), 1103-1169.

3. Brodard-Severac, F.; Geuerrero, G.; Maquet, J.; Florian, P.; Gervais, C.; Mutin, P. H., High-field ^{17}O MAS NMR investigation of phosphonic acid monolayers on titania. *Chemistry of Materials* **2008,** 20, 5191-5196.

4. Guerrero, G.; Mutin, P. H.; Vioux, A., Anchoring of phosphonate and phosphinate coupling molecules on titania particles. *Chemistry of Materials* **2001,** 13, (11), 4367-4373.

5. Mingalyov, P. G.; Lisichkin, G. V., Chemical modification of oxide surfaces with organophosphorus(v) acids and their esters. *Uspekhi Khimii* **2006,** 75, (6), 604-624.

6. Mutin, P. H.; Guerrero, G.; Vioux, A., Hybrid materials from organophosphorus coupling molecules. *Journal of Materials Chemistry* **2005,** 15, (35-36), 3761-3768.

7. Rusu, C. N.; Yates, J. T., Adsorption and decomposition of dimethyl methylphosphonate on TiO2. *Journal of Physical Chemistry B* **2000,** 104, (51), 12292-12298.

8. Giza, M.; Thissen, P.; Grundmeier, G., Adsorption kinetics of organ-ophosphonic acids on plasma-modified oxide-covered aluminum surfaces. *Langmuir* **2008,** 24, (16), 8688-8694.

9. Hanson, E. L.; Schwartz, J.; Nickel, B.; Koch, N.; Danisman, M. F., Bonding self-assembled, compact organophosphonate monolayers to the native oxide surface of silicon. *Journal of the American Chemical Society* **2003,** 125, (51), 16074-16080.

10. Hayden, B. E., Reflection Absorption Infrared Spectroscopy. In *Vibrational Spectroscopy of Molecules on Surfaces*, Yates, J. T.; Madey, T. E., Eds. Plenum Press: New York, 1987; pp 267-344.

11. Watts, J. F.; Wolstenholme, J., *An Introduction to Surface Analyses by XPS and AES*. John Wiley & Sons, Inc.: New York, 2003.

12. Bishop, H. E., Auger Electron Spectroscopy. In *Methods of Surface Analysis*, Walls, J. M., Ed. Cambridge University Press: Cambridge, 1989; pp 87-126.

13. Lafond, V.; Gervais, C.; Maquet, J.; Prochnow, D.; Babonneau, F.; Mutin, P. H., O-17 MAS NMR study of the bonding mode of phosphonate coupling molecules in a titanium oxo-alkoxo-phosphonate and in titania-based hybrid materials. *Chemistry of Materials* **2003,** 15, (21), 4098-4103.

14. Kim, P.; Jones, S. C.; Hotchkiss, P. J.; Haddock, J. N.; Kippelen, B.; Marder, S. R.; Perry, J. W., Phosphonic acid-modified barium titanate polymer nanocomposites with high permittivity and dielectric strength. *Advanced Materials* **2007,** 19, (7), 1001-1005.

15. Koh, S. E.; McDonald, K. D.; Holt, D. H.; Dulcey, C. S.; Chaney, J. A.; Pehrsson, P. E., Phenylphosphonic acid functionalization of indium tin oxide: Surface chemistry and work functions. *Langmuir* **2006,** 22, (14), 6249-6255.

16. Schulmeyer, T.; Paniagua, S. A.; Veneman, P. A.; Jones, S. C.; Hotchkiss, P. J.; Mudalige, A.; Pemberton, J. E.; Marder, S. R.; Armstrong, N. R., Modification of $BaTiO_3$ thin films: adjustment of the effective surface work function. *Journal of Materials Chemistry* **2007,** 17, (43), 4563-4570.

17. Thomas, L. C., *Interpretation of the Infrared Spectra of Organophosphorus Compounds*. Heyden Sons Ltd.: New York, 1974.

18. Liakos, I. L.; Newman, R. C.; McAlpine, E.; Alexander, M. R., Comparative study of self-assembly of a range of monofunctional aliphatic molecules on magnetron-sputtered aluminium. *Surface and Interface Analysis* **2004,** 36, (4), 347-354.

19. Barja, B. C.; Tejedor-Tejedor, M. I.; Anderson, M. A., Complexation of methylphosphonic acid with the surface of goethite particles in aqueous solution. *Langmuir* **1999,** 15, (7), 2316-2321.

20. Green, J. H. S.; Harrison, D. J., Vibrational spectra of benzene derivatives .18. Dihalogenotetrafluorobenzenes. *Spectrochimica Acta Part A - Molecular and Biomolecular Spectroscopy* **1977,** 33, (2), 193-197.

21. Long, D. A.; Steele, D., The vibrational spectra and assignments for C_6F_5Cl, C_6F_5Br and C_6F_5I. *Spectrochimica Acta* **1963,** 19, (11), 1955-1961.

22. Janczuk, B.; Bialopiotrowicz, T., Surface free-energy components of liquids and low-energy solids and contact angles. *Journal of Colloid and Interface Science* **1989,** 127, (1), 189-204.

23. Wang, L.; Yan, L. F.; Zhao, P. T.; Torimoto, Y. F.; Sadakata, M.; Li, Q. X., Surface modification of polystyrene with atomic oxygen radical anions-dissolved solution. *Applied Surface Science* **2008,** 254, (13), 4191-4200.

24. Paniagua, S. A.; Hotchkiss, P. J.; Jones, S. C.; Marder, S. R.; Mudalige, A.; Marrikar, F. S.; Pemberton, J. E.; Armstrong, N. R., Phosphonic acid modification of indium-tin oxide electrodes: Combined XPS/UPS/contact angle studies. *Journal of Physical Chemistry C* **2008,** 112, (21), 7809-7817.

25. Laibinis, P. E.; Nuzzo, R. G.; Whitesides, G. M., Structure of monolayers formed by coadsorption of 2 normal alkanethiols of different chain lengths on gold and its relation to wetting. *Journal of Physical Chemistry* **1992,** 96, (12), 5097-5105.

26. Luschtinetz, R.; Oliveira, A. F.; Frenzel, J.; Joswig, J. O.; Seifert, G.; Duarte, H. A., Adsorption of phosphonic and ethylphosphonic acid on aluminum oxide surfaces. *Surface Science* **2008,** 602, (7), 1347-1359.

27. Hector, L. G.; Opalka, S. M.; Nitowski, G. A.; Wieserman, L.; Siegel, D. J.; Yu, H.; Adams, J. B., Investigation of vinyl phosphonic acid/hydroxylated alpha-Al_2O_3(0001) reaction enthalpies. *Surface Science* **2001,** 494, (1), 1-20.

28. Ramsier, R. D.; Henriksen, P. N.; Gent, A. N., Adsorption of phosphorus acids on alumina. *Surface Science* **1988,** 203, (1-2), 72-88.

29. Adolphi, B.; Jahne, E.; Busch, G.; Cai, X. D., Characterization of the adsorption of omega-(thiophene-3-yl alkyl) phosphonic acid on metal oxides with AR-XPS. *Analytical and Bioanalytical Chemistry* **2004,** 379, (4), 646-652.

30. Lukes, I.; Borbaruah, M.; Quin, L. D., Direct reaction of phosphorus acids with hydroxy of a silanol and on the silica-gel surface. *Journal of the American Chemical Society* **1994,** 116, (5), 1737-1741.

31. Gouzman, I.; Dubey, M.; Carolus, M. D.; Schwartz, J.; Bernasek, S. L., Monolayer vs. multilayer self-assembled alkylphosphonate films: X-ray photoelectron spectroscopy studies. *Surface Science* **2006,** 600, (4), 773-781.

32. Holland, G. P.; Sharma, R.; Agola, J. O.; Amin, S.; Solomon, V. C.; Singh, P.; Buttry, D. A.; Yarger, J. L., NMR characterization of phosphonic acid capped SnO_2 nanoparticles. *Chemistry of Materials* **2007,** 19, (10), 2519-2526.

33. Traina, C. A.; Schwartz, J., Surface modification of Y_2O_3 nanoparticles. *Langmuir* **2007,** 23, (18), 9158-9161.

34. Textor, M.; Ruiz, L.; Hofer, R.; Rossi, A.; Feldman, K.; Hahner, G.; Spencer, N. D., Structural chemistry of self-assembled monolayers of octadecylphosphoric acid on tantalum oxide surfaces. *Langmuir* **2000,** 16, (7), 3257-3271.

35. Gao, W.; Dickinson, L.; Grozinger, C.; Morin, F. G.; Reven, L., Self-assembled monolayers of alkylphosphonic acids on metal oxides. *Langmuir* **1996,** 12, (26), 6429-6435.

36. Beentjes, P. C. J.; Van Den Brand, J.; De Wit, J. H. W., Interaction of ester and acid groups containing organic compounds with iron oxide surfaces. *Journal of Adhesion Science and Technology* **2006,** 20, (1), 1-18.

37. Cassie, A. B. D., Contact angles. *Discussions of the Faraday Society* **1948,** 3, 11-16.

38. Kim, J. S.; Friend, R. H.; Cacialli, F., Surface energy and polarity of treated indium-tin-oxide anodes for polymer light-emitting diodes studied by contact-angle measurements. *Journal of Applied Physics* **1999,** 86, (5), 2774-2778.

39. Kim, J. S.; Friend, R. H.; Cacialli, F., Surface wetting properties of treated indium tin oxide anodes for polymer light-emitting diodes. *Synthetic Metals* **2000,** 111, 369-372.

40. Kim, J. S.; Lagel, B.; Moons, E.; Johansson, N.; Baikie, I. D.; Salaneck, W. R.; Friend, R. H.; Cacialli, F., Kelvin probe and ultraviolet photoemission measurements of indium tin oxide work function: a comparison. *Synthetic Metals* **2000,** 111, 311-314.

41. Sugiyama, K.; Ishii, H.; Ouchi, Y.; Seki, K., Dependence of indium-tin-oxide work function on surface cleaning method as studied by ultraviolet and X-ray photoemission spectroscopies. *Journal of Applied Physics* **2000,** 87, (1), 295-298.

42. Chaney, J. A.; Koh, S. E.; Dulcey, C. S.; Pehrsson, P. E., Surface chemistry of carbon removal from indium tin oxide by base and plasma treatment, with implications on hydroxyl termination. *Applied Surface Science* **2003,** 218, (1-4), 258-266.

43. Purvis, K. L.; Lu, G.; Schwartz, J.; Bernasek, S. L., Surface characterization and modification of indium tin oxide in ultrahigh vacuum. *Journal of the American Chemical Society* **2000,** 122, (8), 1808-1809.

44. Donley, C.; Dunphy, D.; Paine, D.; Carter, C.; Nebesny, K.; Lee, P.; Alloway, D.; Armstrong, N. R., Characterization of indium-tin oxide interfaces using X-ray photoelectron spectroscopy and redox processes of a chemisorbed probe molecule: Effect of surface pretreatment conditions. *Langmuir* **2002,** 18, (2), 450-457.

45. Seah, M. P., The quantitative analysis of surfaces by XPS: a review. *Surface and Interface Analysis* **1980,** 2, (6), 222-239.

46. Seah, M. P., Chapter 5: Quantification of AES and XPS. In *Practical Surface Analysis*, Briggs, D.; Seah, M. P., Eds. John Wiley & Sons, Ltd.: New York, 1983.

47. Pawsey, S.; Yach, K.; Reven, L., Self-assembly of carboxyalkylphosphonic acids on metal oxide powders. *Langmuir* **2002,** 18, (13), 5205-5212.

48. Alves, C. A.; Porter, M. D., Atomic-force microscopic characterization of a fluorinated alkanethiolate monolayer at gold and correlations to electrochemical and infrared reflection spectroscopic structural descriptions. *Langmuir* **1993,** 9, (12), 3507-3512.

49. Liakos, I. L.; Newman, R. C.; McAlpine, E.; Alexander, M. R., Study of the resistance of SAMs on aluminium to acidic and basic solutions using dynamic contact angle measurement. *Langmuir* **2007,** 23, (3), 995-999.

50. Li, M.; Xu, J. H.; Lu, Q. H., Creating superhydrophobic surfaces with flowery structures on nickel substrates through a wet-chemical-process. *Journal of Materials Chemistry* **2007,** 17, (45), 4772-4776.

51. Harm, U.; Burgler, R.; Furbeth, W.; Mangold, K. M.; Juttner, K., Novel protective coatings for steel based on a combination of self-assembled monolayers and conducting polymers. *Macromolecular Symposia* **2002,** 187, 65-75.

52. Ma, H.; Acton, O.; Ting, G.; Ka, J. W.; Yip, H. L.; Tucker, N.; Schofield, R.; Jen, A. K. Y., Low-voltage organic thin-film transistors with pi-sigma-phosphonic acid molecular dielectric monolayers. *Applied Physics Letters* **2008,** 92, (11), 113303/1-113303/3.

53. Acton, O.; Ting, G.; Ma, H.; Jen, A. K. Y., Low-voltage high-performance C_{60} thin film transistors via low-surface-energy phosphonic acid monolayer/hafnium oxide hybrid dielectric. *Applied Physics Letters* **2008,** 93, 083302.

54. Nie, H. Y.; McIntyre, N. S.; Lau, W. M., Nanolithography of a full-coverage octadecylphosphonic acid monolayer spin coated on a Si substrate. *Applied Physics Letters* **2007,** 90, (20), 203114/1-203114/3.

55. Francis, J. T.; Nie, H. Y.; McIntyre, N. S.; Briggs, D., ToF-SIMS investigation of octadecylphosphonic acid monolayers on a mica substrate. *Langmuir* **2006,** 22, (22), 9244-9250.

56. Danahy, M. P.; Avaltroni, M. J.; Midwood, K. S.; Schwarzbauer, J. E.; Schwartz, J., Self-assembled monolayers of alpha,omega-diphosphonic acids on Ti enable complete or spatially controlled surface derivatization. *Langmuir* **2004,** 20, (13), 5333-5337.

57. Gawalt, E. S.; Avaltroni, M. J.; Danahy, M. P.; Silverman, B. M.; Hanson, E. L.; Midwood, K. S.; Schwarzbauer, J. E.; Schwartz, J., Bonding organics to Ti alloys: Facilitating human osteoblast attachment and spreading on surgical implant materials corrections (vol 19, pg 200, 2003). *Langmuir* **2003,** 19, (17), 7147-7147.

58. Silverman, B. M.; Wieghaus, K. A.; Schwartz, J., Comparative properties of siloxane vs phosphonate monolayers on a key titanium alloy. *Langmuir* **2005,** 21, (1), 225-228.

59. Tsud, N.; Yoshitake, M., Vacuum vapour deposition of phenylphosphonic acid on amorphous alumina. *Surface Science* **2007,** 601, (14), 3060-3066.

60. Nie, H. Y.; Walzak, M. J.; McIntyre, N. S., Delivering octadecylphosphonic acid self-assembled monolayers on a Si wafer and other oxide surfaces. *Journal of Physical Chemistry B* **2006,** 110, (42), 21101-21108.

61. Felhosi, I.; Telegdi, J.; Palinkas, G.; Kalman, E., Kinetics of self-assembled layer formation on iron. *Electrochimica Acta* **2002,** 47, (13-14), 2335-2340.

62. Nuzzo, R. G.; Dubois, L. H.; Allara, D. L., Fundamental studies of microscopic wetting on organic surfaces. 1. Formation and structural characterization of a self-consistent series of polyfunctional organic monolayers. *Journal of the American Chemical Society* **1990,** 112, (2), 558-569.

63. Doussineau, T.; Durand, J. O.; Granier, M.; Smaihi, M.; Valtchev, V., Synthesis of phosphonic acids with the semicarbazide group for the functionalization of metal oxide and zeolite nanoparticles. *Synlett* **2004**, (10), 1735-1738.

64. Farrow, J. B.; Warren, L. J., Adsorption of short-chained organic acids on stannic oxide. *Colloids and Surfaces* **1989,** 34, (3), 255-269.

65. Brumbach, M.; Veneman, P. A.; Marrikar, F. S.; Schulmeyer, T.; Simmonds, A.; Xia, W.; Lee, P.; Armstrong, N. R., Surface composition and electrical and electrochemical properties of freshly deposited and acid-etched indium tin oxide electrodes. *Langmuir* **2007,** 23, (22), 11089-11099.

66. Brumbach, M., Near Surface Composition and Reactivity of Indium Tin Oxide:An Evaluation Towards Surface Chemical Concepts and Relevance in Titanyl Phthalocyanine Photovoltaic Devices. *Ph.D. Dissertation, University of Arizona* **2007**.

Chapter 4

Modification of Planar Metal Oxide Substrates

This chapter reports on our efforts on the modification of planar surfaces of metal oxides with phosphonic acids. As the mechanism of bond formation and surface coverage of phosphonic acids on these types of substrates were covered in Chapter 3, emphasis will be given here to the properties of these metal oxide substrates that can and have been tuned by modification with phosphonic acids. A brief overview will be given on different metal oxides that have been modified with phosphonic acids, however, focus will be given to zinc oxide (ZnO) and especially indium tin oxide (ITO).

4.1 Background and literature

This first section is a survey of the types of planar metal oxides that have been modified with phosphonic acids. Additionally, an overview of the different methods used to modify surfaces will be given. Finally, a brief overview of the types of technologies and applications in which phosphonic acid–modified planar metal oxides have been used will be presented.

4.1.1 Different Planar Substrates of Metal Oxides That Have Been Modified with Phosphonic Acids

A large variety of metal oxide planar substrates have been modified with phosphonic acids. While ITO,[1-3] the native oxide on titanium,[4, 5] various forms of silica (mica,[6] quartz,[7] Si/SiO_x[7-9]), and aluminum oxide[7, 10, 11] have been studied to a fair extent, there are a number of other metal oxide (or natives oxide on metal) planar surfaces that have been successfully modified. These include, but are not limited to, hafnium oxide,[12-14] copper oxide,[15] tantalum oxide,[16-18] nickel oxide,[19] barium titanate,[20] chromium oxide,[21] iron oxide,[22] niobium oxide,[23] zirconium oxide,[24, 25] and even some common metal alloys such as brass,[15] nitinol (an alloy of nickel),[26] and steel.[21, 27]

4.1.2 Methods of Surface Modification

There are a number of different procedures that have been reported for the modification of planar metal oxides with phosphonic acids. Hanson *et al.* have reported a procedure they call T–BAG (tethering by aggregation and growth), which has been one of the common methods used in the literature.[1, 8] This procedure involves holding the substrate to be modified vertically in a solution of a phosphonic acid and letting the solvent evaporate over time until the solvent level falls below the target substrate (Figure 4.1). The authors postulate that as the solvent evaporates, the phosphonic acid molecules are transferred to the surface in some organized fashion as a result of their amphiphilic

nature at the solvent/air interface.

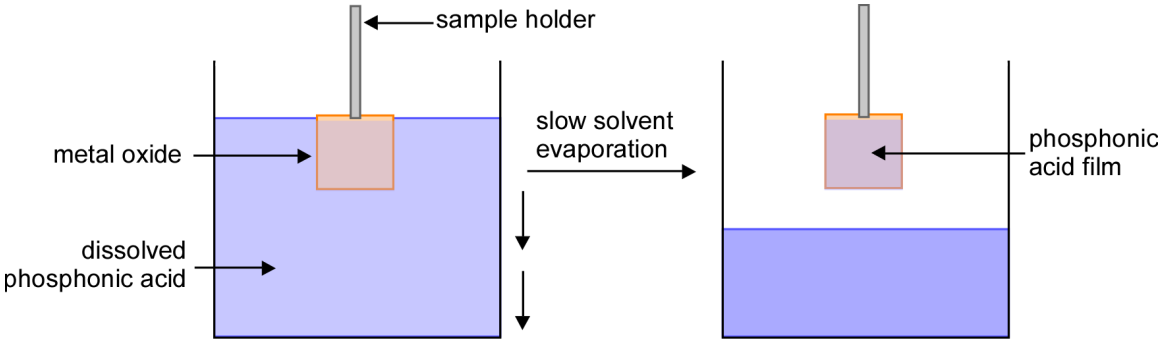

Figure 4.1 Schematic displaying the T–BAG method. Adapted from Hanson *et al.*[8]

After the solvent level reaches below the substrate edge, the substrate can be rinsed and then placed in an oven (~ 140 °C) for anywhere from hours to days. This is thought to complete the heterocondensation reaction of the phosphonic acid to the surface. After heating, the substrate is rinsed in a weak base to remove any unbound or weakly bound phosphonic acid.

While T–BAG has been the most popular method, a number of other methods have been reported, such as dip–coating,[28, 29] spincoating,[7, 30] spray–coating,[26] vacuum depositing,[31] and microcontact printing.[9, 25, 32]

Additionally, there have been several reports, especially in the last few years, regarding which solvents can be used to successfully grow monolayers of phosphonic acids on metal oxides. While polar solvents such as ethanol, 2–propanol and tetrahydrofuran have commonly been used, Nie *et al.*[7, 33] have reported on the use of relatively nonpolar solvents, such as toluene and trichloroethylene, which gave better

monomolecular coverage on mica, Si/SiO_x, and Al/AlO_x with respect to polar solvents such as ethanol. Water has also been used in certain systems.[21]

The planar substrates modified in our work have been done so *via* a modified T–BAG procedure, where the substrates are placed horizontally in the phosphonic acid solution after DSC/OP treatment.[q] The subsequent rinsing and heating steps are the same as for the original T–BAG method; the details are reported in the experimental section of this chapter.

4.1.3 Applications of Surface–Modified Planar Substrates of Metal Oxides

Transparent metal oxides, such as ITO, have been incorporated into organic light emitting diodes (OLEDs) and organic photovoltaics (OPVs). There are a number of reports on the surface modification of ITO with phosphonic acids in order to improve various properties, such as increasing hole injection efficiency and luminance in OLEDs.[1, 34, 35] There exist a number of other metal oxides that play important roles in various technologies. Both silicon and aluminum are ubiquitous substrates in transistor technology, and their native surface oxides have been modified with phosphonic acids resulting in enhanced properties.[9, 32, 36] Hafnium oxide has a high dielectric constant and a wide bandgap making it suitable as a dielectric material when high capacitance and low leakage current are desirable.[14] Titanium and its alloys are often used in biomedical applications, where it is a common material for implants, and their native oxides have

[q] It was found that placing the substrate horizontally rather than vertically did not result in a substantial change in coverage, and being easier experimentally, was the orientation used hencewith.

been better compatibilized with materials, such as bone and tissue, inside the body by surface modification with phosphonic acids.[4, 5, 37, 38] Materials such as steel, iron, and aluminum are important building materials, and protecting the integrity of these materials against corrosion utilizing monolayers of phosphonic acids has been reported.[39-41]

4.2 Modification of ITO with phosphonic acids

ITO can be modified in a number of ways in order to alter the interfacial properties it has with other materials. While wet and plasma etching and cleaning of the surface and/or deposition of thin metallic or polymeric layers have all been explored,[42, 43] another way to alter the surface properties is by using monolayers of organic compounds.[1, 44] In the past, silanes and carboxylic acids have been popular choices for the surface modification of ITO,[45, 46] however recently phosphonic acids have been investigated as a promising alternative.[1, 2, 8]

This section describes our efforts on the modification of ITO with phosphonic acids to tune various surface properties, such as the work function, surface energy, and chemical functionality (specifically, the ability to crosslink molecules and polymers to the surface). Our efforts on the tuning of the work function and surface energies of ITO can be divided into two distinct studies. The initial study was conducted to both gain a better understanding of the binding and coverage of a range of phosphonic acids on ITO and to study the changes they induce in the work function and surface energy. The use of fluorine substitution on benzylphosphonic acids to control the molecular dipole and the

subsequent work function shift in ITO surfaces modified with these compounds was the focus of our second study. Additionally, the theoretical work function for ITO modified with various phosphonic acids was calculated by quantum mechanical methods, to aid in the interpretation of the experimental results. Large changes in the surface energies as a result of the phosphonic acid surface modification were seen in each study, and these are described in detail in the following sections.

This work has been completed in conjunction with a number of collaborators. Characterization of ITO substrates was done in part by Sergio Paniagua[r] (Chemistry, University of Arizona). Theoretical calculations were performed by Hong Li and Pavel Paramonov[s] (Chemistry, Georgia Tech) and the stability of work functions was measured by Asha Sharma[t] (Electrical and Computer Engineering, Georgia Tech).

4.2.1 Tuning the Work Function

This section outlines the success in our efforts directed at tuning the work function of ITO. This success was achieved *via* intelligent design and synthesis of phosphonic acids that can impart dipoles of various magnitude onto the surface of ITO, effectively changing its work function.

[r] While working with Prof. Neal Armstrong
[s] Both work or worked with Prof. Jean-Luc Brédas
[t] While working with Prof. Bernard Kippelen

4.2.1.1 Reasoning and Literature

The work function of ITO is one important characteristic that can be tuned by the attachment of monolayers. The work function can either be increased or decreased by attaching organic ligands such that the negatively charged end of the molecular dipole is directed either away from or towards the structure, respectively.[47]

Several interesting studies have been reported that utilize phosphonic acids specifically to change the work function of ITO. One early study was reported by Appleyard *et al.*[48] In that study, modification of the ITO surface with (trichloromethyl)phosphonic acid, (4–nitrophenyl)phosphonic acid, (2–chloroethyl)phosphonic acid and (aminomethyl)phosphonic acid induced work function changes (measured by Kelvin Probe) of +0.19, +0.30, -0.14, and +0.18 eV, respectively. They then report both reduced turn–on voltages and increased luminance for OLEDs modified with these monolayers with respect to the unmodified versions.

Guo *et al.*[49] report a decrease in the work function of ITO ($\Delta\Phi$ = -0.28 eV, measured by Kelvin Probe)) upon attachment of a monolayer of quarterthiophene–2–phosphonic acid. Upon doping of the monolayer with tetrafluorotetracyanoquinodimethane (F_4–TCNQ), however, they measured an increase in the work function of the substrate with respect to that of bare ITO ($\Delta\Phi$ = +0.35 eV). This doped substrate showed a factor of 4 increase in both the charge carrier density and the luminance with respect to an unmodified ITO electrode in a bilayer OLED device.[1] Koh *et al.*[3] published a study comparing the effects of nitrophenylphosphonic acid and cyanophenylphosphonic acid on the work function of ITO. They report large increases of

+0.77 and +0.60 eV, with respect to bare ITO, for the cyano and nitro–substituted versions, respectively.

4.2.1.2 Tuning the Work Function of ITO – 1st Study

Our initial study focused more on the methods of attachment of some basic phosphonic acids to ITO and their ability to modify the surface energy and work function. Five different phosphonic acids were used in the study (Figure 4.2).

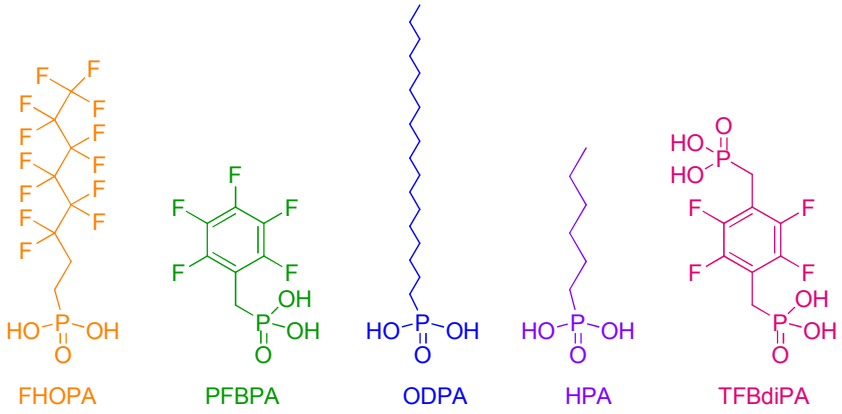

Figure 4.2 Chemical structures of the phosphonic acids used in the 1st study: 3,3,4,4,5,5,6,6,7,7,8,8,8–tridecafluorooctyl phosphonic acid (FHOPA), pentafluorobenzylphosphonic acid (PFBPA), Octadecylphosphonic acid (ODPA), hexylphosphonic acid (HPA), and (perfluoro–1,4–phenylene)bis(methylene)diphosphonic acid (TFBdiPA). The same color scheme will be used in Figures 4.3, 4.4, and 4.11.

The modified T–BAG method was used to deposit the aforementioned phosphonic acids on ITO. XPS and UPS spectra, as well as contact angles, were recorded for each of the samples to understand the effects each of the different modifiers, in

combination with detergent/solvent cleaned (DSC) and detergent/solvent cleaned plus oxygen plasma–etched (DSC/OP) cleaning protocols, had on ITO. XPS was used to ensure that the different PA modifiers bound to the surface. Survey scans (Figure 4.3) as well as high resolution scans (not shown) for the largest peak for each element were recorded.[2]

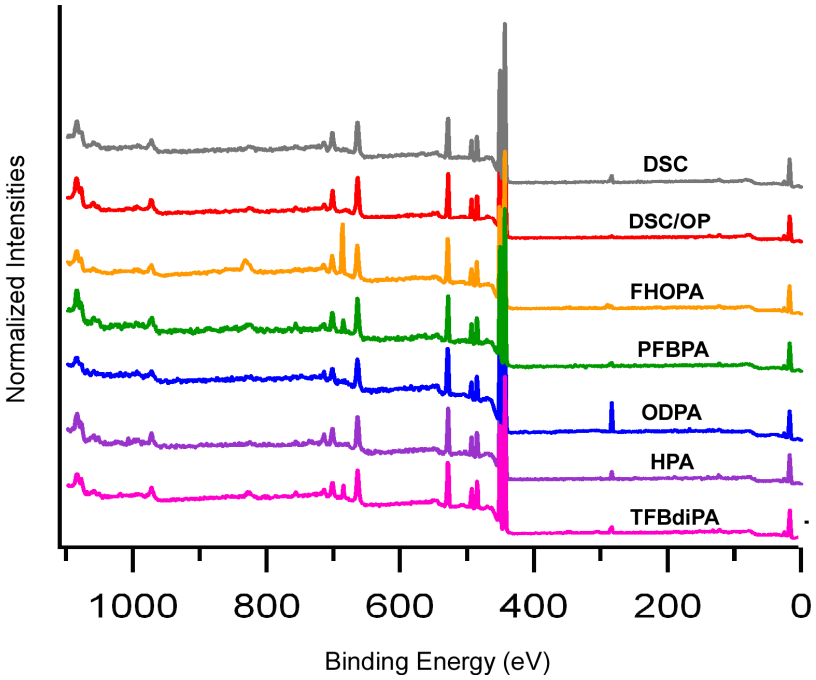

Figure 4.3 XPS survey scans (1 eV resolution) for the various surface treatments. (Data collected and figure prepared by S. Paniagua).

Changes in the surface electronic properties of phosphonic acid modified DSC/OP ITO samples were probed using UPS (Figure 4.4). While both UPS and Kelvin Probe can yield the absolute surface work function, UPS has the advantage of operating under UHV, thereby minimizing the contamination of the surface. UPS can also provide more information than just the work function; it can also show the low kinetic energy edge of

surfaces (corresponding to the valence band maximum (VBM), which can be used to determine the contribution of a surface dipole to variations in surface work function, relative to the unmodified surface). The work function of a surface can be measured with UPS by measuring the kinetic energy of the electrons upon absorption of a photon with known energy (UPS often uses a He(I) source with hν = 21.2 eV) at the onset of photoemission.[47] This can be related by the equation:

$$\Phi_m = E_K^{min} + h\nu - E_K^{max} \qquad \text{(Equation 4.1)}$$

where E_K^{min} is the kinetic energy of electrons excited from the Fermi level, E_K^{max} the kinetic energy of electrons escaping the solid just above the local vacuum level of the sample, $h\nu$ the energy of the photon used for excitation, and Φ_m the work function of the metal. The UPS spectra reported herein have been converted into binding energies, which takes into account the Fermi levels of the different samples. Work functions can therefore be computed by simply subtracting the binding energy measured at the onset of photoemission from the photon energy, or:

$$\Phi_m = 21.2 \text{ eV} - B.E. \qquad \text{(Equation 4.2)}$$

Both the SEE and VBM for the different modified ITO substrates are shown in Figure 4.4. OP–treatment of the DSC–treated ITO surface leads to an increase in the work function (+0.6 eV).

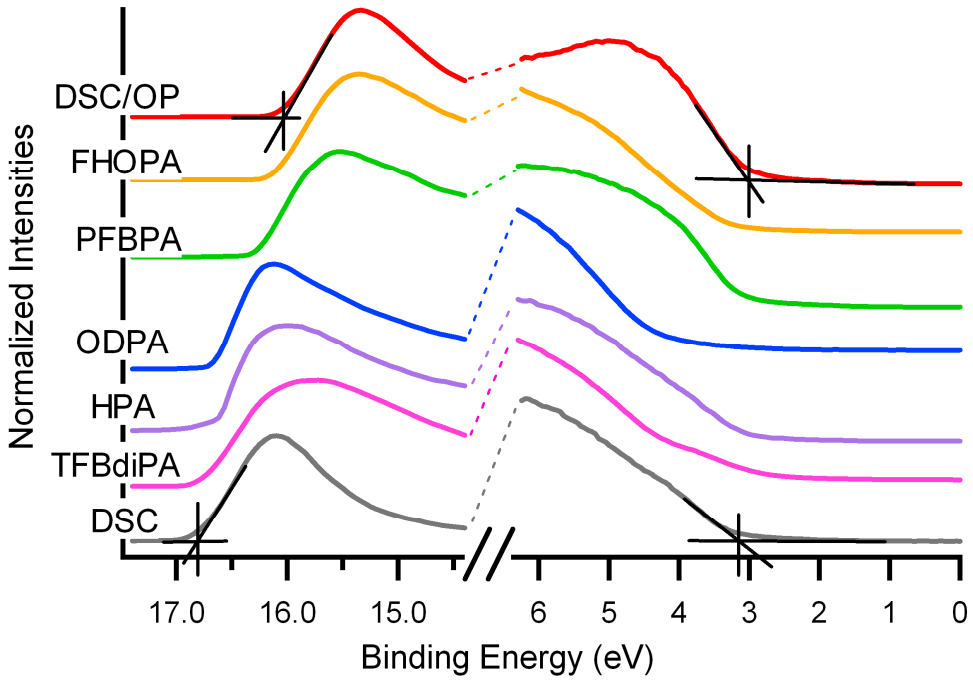

Figure 4.4 UPS data for DSC and DSC/OP treated ITO and surfaces after DSC/OP treatment and modification with phosphonic acid. The left side of these spectra is a view of the secondary electron edge (SEE), while the right hand part of these spectra is a view of the valence band maximum (VBM) region. Shifts in the SEE energy are directly proportional to surface work function change, whereas shifts in the VBM are incorporated into that analysis to account for charge redistribution (band bending) as a result of the modification. (Data collected and figure prepared by S. Paniagua)

In addition to the shifts in SEE brought about by phosphonic acid modification, changes were observed in the VBM features because of new photoemission bands due to the modifiers.[20] For those modified surfaces where the SEE shifts to higher binding energy (BE), there is a decrease in the effective surface work function. Accounting for the VBM allows for the differentiation of the surface dipole contribution from any band bending contribution. We hypothesize that the change in effective surface work function is mostly due to an adlayer–induced interface dipole. It is likely that the interface dipole

arising from OP treatment of ITO is altered or completely removed as a result of the PA modification of these surfaces.

The alkyl phosphonic acids, HPA and ODPA, induce surface dipoles in the opposite direction to those created by FHOPA and PFBPA on the ITO surface. This is due to the relatively nonpolar alkyl chain and the fact that the negative end of the dipole is now directed towards the surface due to the polar phosphonic acid binding group. These factors plus the pushing back of the electron density on the ITO surface upon monolayer attachment result in little to no change in the effective surface work function in comparison to DSC–treated ITO. The partially–fluorinated modifier FHOPA increases the original surface dipole by 0.6 eV compared to DSC–treated ITO. Due to the substitution pattern of the fluorines on the aromatic ring, PFBPA is expected to have only one C–F group whose dipole contribution to the overall molecular dipole is not cancelled by an opposing C–F group on the ring. The effect that this group has on the molecular dipole results in an effective surface work function of 4.9 eV, about 0.4 eV higher than DSC ITO. Both of the fluorinated compounds have their dipoles partially offset by the phosphonic acid binding group polarity. TFBdiPA produced a decrease in the surface dipole (-0.2 eV), which is offset by a decrease in VBM of -0.2 eV, resulting in a work function of 4.5 eV. These work functions are tabulated in Table 4.2.

Fractional coverages of some of the phosphonic acids were estimated from contact angle measurements. Absolute monolayer coverages of 5.5, 5.5, and 3.4 molecules/nm^2 have been reported for hexanethiol, octadecanethiol, and $CF_3(CF_2)_7(CH_2)_2SH$ (a compound close in structure to FHOPA), respectively.[50, 51] Based on water contact angle measurements on ITO substrates modified with phosphonic acids

bearing the same (or similar) R groups as the abovementioned thiols, coverages of 5.0, 5.0, and 2.9 molecules/nm^2 for HPA, ODPA, and FHOPA were found, respectively. As the phosphonic acid moiety has been calculated to need a surface area of 0.24 nm^2 for attachment,[52] these numbers indicate dense monolayers. No monolayer coverage values could be determined for PFBPA and TFBdiPA using the same method, as their analogous thiols have not been studied in detail on gold.

4.2.1.3 Tuning the Work Function of ITO – 2nd Study

While the first study demonstrated a means by which the ITO work function and surface energy could be modified and characterized, the second study focused on optimizing these modifications by tuning the dipoles of the phosphonic acids. Six fluorinated benzylphosphonic acids were synthesized and characterized (Figure 4.5). Fluorine substituents were chosen in order to tune the molecular dipole and resultant work function of ITO because fluorine is very electronegative and as such electron withdrawing. Additionally, a wide number of fluorinated compounds are available commercially and C–F bonds are not particularly sensitive to a variety of reaction conditions. Nitro and cyano groups are more electron withdrawing than fluorine atoms, but the synthesis of a series of compounds employing these functionalities would be more complex. The degree and position of fluorination on these molecules was expected to affect the overall dipole moment of the molecules, therefore also affecting the surface dipole once the molecules are absorbed onto an ITO substrate.

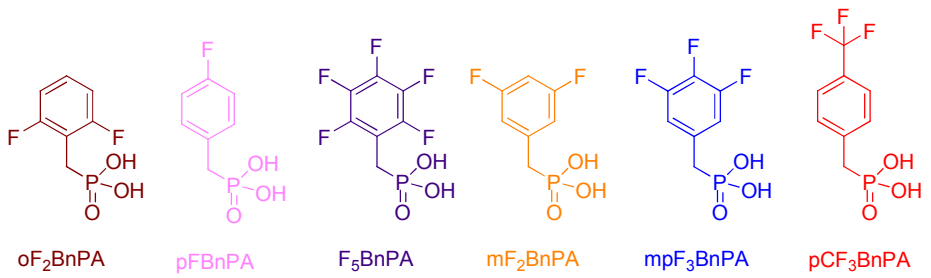

Figure 4.5 Chemical structures of the phosphonic acids used in the 2nd study: 2,6–difluorobenzylphosphonic acid (oF_2BnPA), 4–fluorobenzylphosphonic acid (pFBnPA), pentafluorobenzylphosphonic acid (F_5BnPA), 3,5–difluorobenzylphosphonic acid (mF_2BnPA), 3,4,5–trifluorobenzylphosphonic acid (mpF_3BnPA), and 4–(trifluoromethyl)benzylphosphonic acid (pCF_3BnPA). The same color scheme is used in Figures 4.6, 4.7, and 4.12.

As with the 1st study, XPS data were collected to ensure proper coverage and modification of the ITO surface with the phosphonic acids (Figure 4.6). High resolution spectra of the largest peak for each element were also collected (not shown).

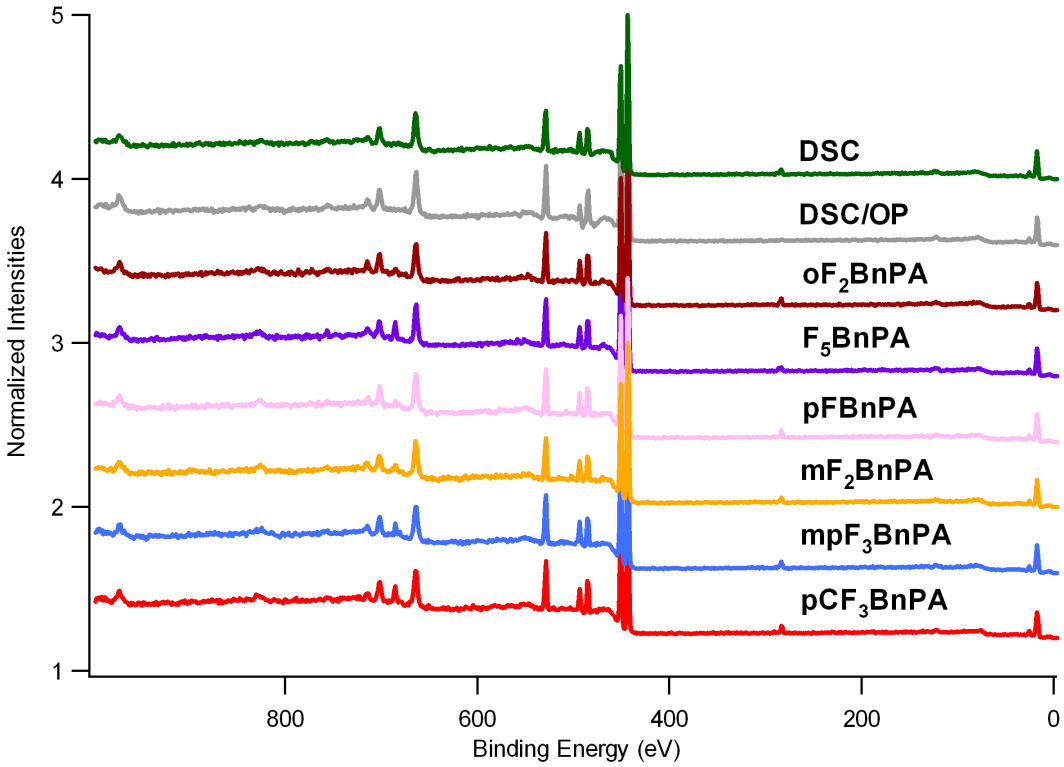

Figure 4.6 XPS survey scans (1 eV resolution) for the various surface treatments.

By comparing the F1s peak area in the XPS spectra, relative amounts of phosphonic acid modifier on the ITO surface could be determined. With the exception of the phosphonic acids containing ortho–substituted fluorines, the F 1s areas, once adjusted for the degree of fluorination, are all similar (Table 4.1). In the case of PAs with ortho–substituted fluorines, a reduced intensity in the F1s peak was observed. It is unclear whether this is due to decreased coverage on the surface or perhaps a decreased signal in the XPS due to a slightly more attenuated path of the ortho–substituted fluorines. Further studies need to be done in order to obtain a satisfactory explanation.

Table 4.1 Fluorine content of phosphonic acid adlayers on ITO, as obtained from UPS data. For each sample, the number of fluorines per molecule, the ratio of the areas of the F1s peak to the In3p peak, the adjusted ratio (taking the number of fluorines on the molecule into account), and the relative ratios (by setting one of the adjusted ratios to 1.00, and adjusting the others in a likewise fashion) are shown.

Sample	# F	ratio F1s / $In3p_{3/2}$	adjusted ratio	relative ratio
F_5BnPA	5	0.19	0.038	0.76
pCF_3BnPA	3	0.16	0.053	1.1
mpF_3BnPA	3	0.16	0.053	1.1
oF_2BnPA	2	0.07	0.035	0.70
pFBnPA	1	0.05	0.050	1.0
mF_2BnPA	2	0.09	0.045	0.90
mpF_3PhPA	3	0.15	0.050	1.0
pCF_3PhPA	3	0.17	0.057	1.1
F_5PhPA	5	0.19	0.038	0.76

Changes in the work function after the various surface modifications were probed with UPS (Figure 4.7). Changes in the secondary electron edge (SEE) can be seen due to the attachment of the phosphonic acids on the ITO surface. As the dipole moment of the phosphonic acids is increased (with the negative end pointing away from the surface), the SEE shifts to lower binding energy. An overall change of 1.2 eV can be realized between ITO modified with oF_2BaPA and pCF_3BnPA. Additionally, various surface work functions in between were seen by the tuning of the surface dipole the various phosphonic acids impart. The VBM are not plotted as the focus of this study was not the various components of and reasoning behind the change in work function, but merely the overall shift.

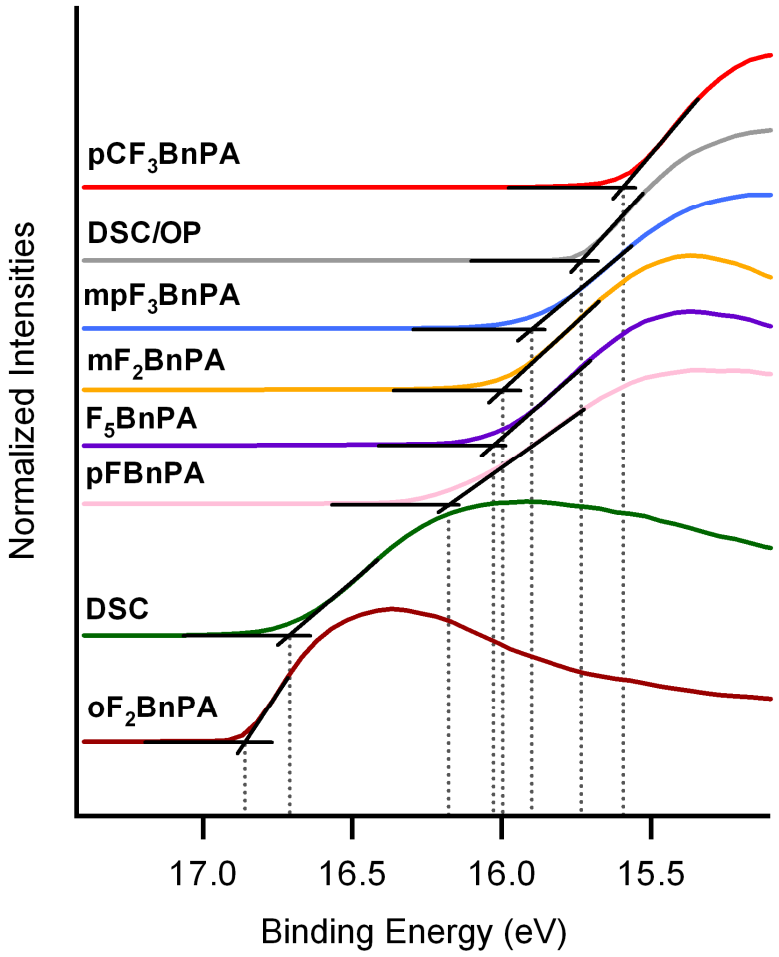

Figure 4.7 UPS data for DSC and DSC/OP treated ITO and after both DSC/OP treatment and modification with benzylphosphonic acids. The secondary electron edge (SEE), which is a direct measurement of the work function, is indicated by a dotted line for each surface.

Work function changes ($\Delta\Phi$) of PA modified ITO surfaces with respect to unmodified ITO were also derived through DFT calculations and compared to the experimental results (Figure 4.8). The calculated $\Delta\Phi$ (using a density of coverage of 7.4×10^{13} molecules/cm^2) are slightly larger than those measured experimentally for ITO modified with the same compounds. In theoretical work on interface systems of gold and

biphenylthiol–based molecules, it is found that, at low coverage, both ΔV_{vac} and bond dipole show good linear correlation with molecule packing density.[53]

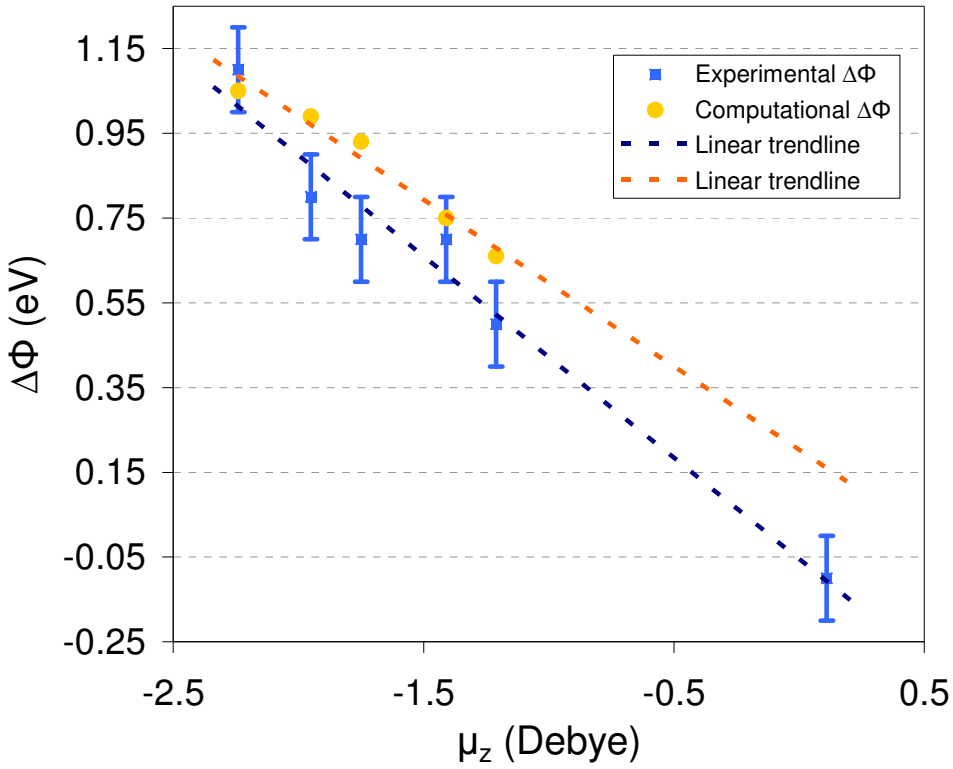

Figure 4.8 Comparison of the changes in work function with respect to DSC ITO (experimental) and bare ITO (theoretical) as measured by UPS (blue) and calculated by First–principles (orange) depending on the dipole normal to the surface created by adsorption of the phosphonic acids. Errors on the experimental values are ± 0.1 eV.

The slopes of the experimental data (-0.48 eV/debye) and the calculated points (-0.39 eV/debye) are in good agreement. The calculations provide the same trend in ΔΦ as seen experimentally, suggesting that the magnitude of the dipole moment of the modifier has the largest influence on the work function. Similar studies have been reported, though using different surface modifiers and/or different surfaces. Schwartz *et al.* report a variation of the work function of ITO by attachment of substituted phenoxy–tin

compounds on ITO.[54] They found a good correlation between the dipole moment of the surface modifiers (in the gas phase) and the subsequent $\Delta\Phi$ of the ITO, resulting in a slope of -0.11 eV/debye. Additionally, Alloway *et al.* report a correlation between the dipole normal to the surface and the change in work function for a series of alkyl and semi–fluorinated alkylthiols on gold.[55] They found a slope of -0.51 eV/debye which is very close to the slope we see in phosphonic acids on ITO.

Several phenyl analogues to the benzylphosphonic acids described above were also synthesized and were used to modify ITO surfaces. The lack of a flexible CH_2 linking group between the phosphonic acid moiety and the phenyl ring could potentially change the tilt of the molecule on the surface, thus affecting the component of dipole moment perpendicular to the surface and subsequent work function. The work function changes of ITO surfaces modified with several of these phenylphosphonic acids were similar to those observed for their benzyl analogues (Table 4.2).

Overall, the work function of ITO can be decreased or increased by judicious choice of the modifying molecule. A maximum shift of 1.2 eV (Figure 4.8) was seen corresponding to the difference in work function of ITO modified with pCF_3BnPA vs. oF_2BnPA (Figure 4.8 and Table 4.2).

4.2.1.4 Tuning the Work Function of ITO: Comparisons and Conclusions

Interestingly, the effects on the work function of ITO upon oxygen plasma treatment were different in the two studies, despite the fact that the same vendor was

used. Work function shifts of + 1.0 eV with respect to DSC–treated ITO are seen in the 2nd study, an increase from a + 0.6 eV shift seen in the 1st study.

The Fermi energy (E_F) at the surface of DSC ITO used in each of the studies is shown in the bandgap in Figure 4.9. After OP treatment the valence band maximum (E_{VBM}) at the surface appears closer to E_F (-0.2 eV in the 1st study, -0.1 in the 2nd study), in agreement with similar observations by Christou *et al.*[56]; however, there is also an important contribution from an interface dipole layer, δ (0.4 eV in the 1st study, 0.9 eV in the 2nd study), that ultimately brings the surface work function to its final value of 5.1 eV and 5.5 eV in the 1st and 2nd studies, respectively. The chemical origins of this surface dipole are still debated;[56] hypotheses include the formation of radical species during OP treatment, and accumulation of excesses of charged species at the surface.[57-60]

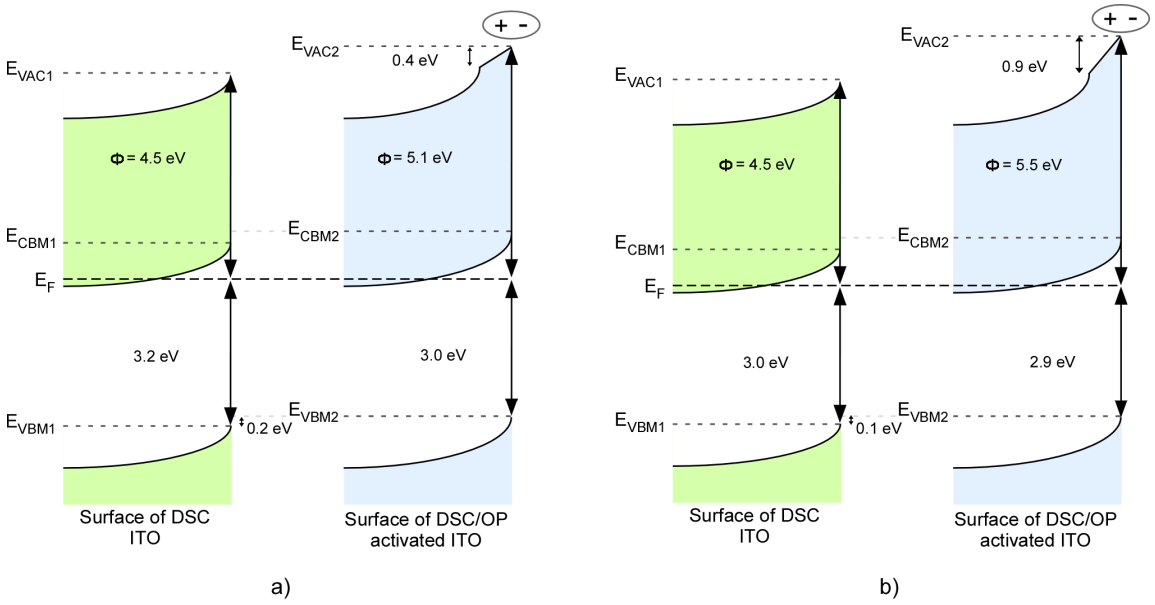

Figure 4.9 Band energy diagrams of DSC vs. DSC/OP cleaned ITO, based on our UPS measurements, for a) the 1st study, and b) the 2nd study, study presented herein.

While a shift of this magnitude in work function upon exposure to oxygen plasma is not unprecedented,[61-63] the effect of binding of several phosphonic acids on the ITO work function studied previously were reexamined to determine whether similar work function differences were seen for a given modifier on ITO in the two studies (Table 4.2). A similar increase of + 0.4 (± 0.1) eV was seen in the relative work functions of ITO modified with HPA, PFBPA, and FHOPA from the 1st to the 2nd study (PFBPA is redesignated as F_5BnPA in the 2nd study). It is hypothesized that less carbonaceous contaminants were present in the uppermost portion of ITO used for the 2nd study, resulting in an increased work function after etching with oxygen plasma, though further studies are necessary to verify this. All of the SEE and VBM for each of the molecules tested are summarized in Table 4.2.

Table 4.2 Work function and valence band results with all treatments / phosphonic acids, determined by the main cutoffs of the region. Errors on the values are ± 0.1 eV.

1st Study			2nd Study		
ITO treatment / molecule used for modification	Φ (eV) UPS	VBM (eV) UPS	ITO treatment / molecule used for modification	Φ (eV) UPS	VBM (eV) UPS
DSC	4.5	3.2	DSC	4.5	3.0
OP/DSC	5.1	3.0	OP/DSC	5.5	2.9
HPA	4.5	3.0	HPA	4.9	2.9
FHOPA	5.1	3.2	FHOPA	5.6	3.1
PFBPA	4.9	3.1	F_5BnPA	5.2	3.1
ODPA	4.5	2.9	pCF_3BnPA	5.6	2.7
TFBdiPA	4.5	2.8	mpF_3BnPA	5.3	2.8
			oF_2BnPA	4.4	3.1
			pFBnPA	5.0	2.9
			mF_2BnPA	5.2	2.9
			mpF_3PhPA	5.4	3.0
			pCF_3PhPA	5.6	3.0
			F_5PhPA	5.1	3.1

4.2.1.5 Work Function Stability Over Time

Further studies have investigated the stability of the change in work function induced by some of these phosphonic acid surface modifiers. Measurements were performed with a Kelvin Probe as a function of time under ambient conditions for differently modified ITO substrates (Figure 4.10). The work function of ITO is increased to 5.5 eV (an increase of 0.8 eV over DSC ITO) after air plasma[u] treatment. The increase in work function by air plasma is generally attributed to the removal of carbon–based residual organic impurities as well as activation of the surface, forming various polar oxygen species.[64] However, when exposed to ambient conditions, the change in work function is reversible and rapidly decreases to its original value, indicating the sensitivity of the surface to ambient absorbents. Conversely, the increase in work function induced by FHOPA does not change after more than 250 hours, and can actually be maintained for over 70 days (not shown). This is due to the formation of a permanent effective dipole moment at the interface resulting from the binding of the phosphonic acids to the ITO surface as well as, perhaps, an increased repelling nature of the surface towards ambient contamination due to the lowered surface energies.

[u] Air plasma was used instead of oxygen plasma for device work due to different availabilities of plasma etchers for use by our collaborators. The effects of both types of plasma on the ITO surface appear to be similar.

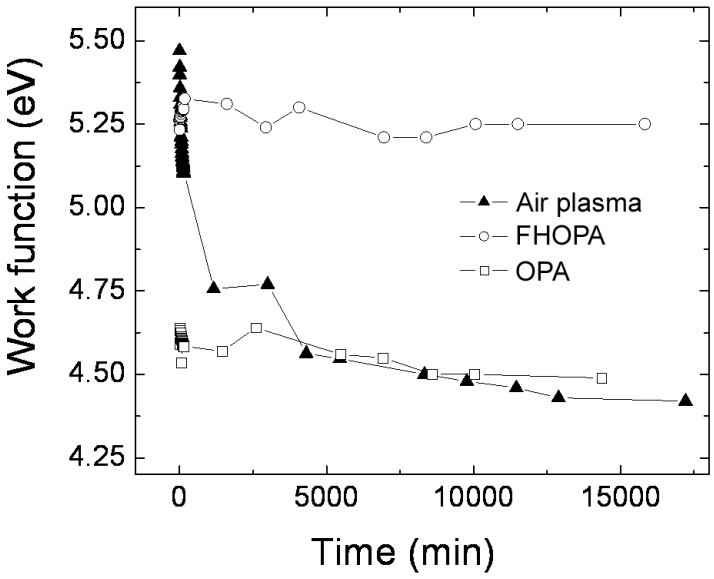

FIG. 4.10 Effect of ambient exposure on the stability of the work function over time in differently modified ITO substrates: air plasma (filled triangles), OPA (open square), and FHOPA (open circles) treated ITO. (Data collected and figure prepared by A. Sharma)

4.2.2 Changing the Surface Energies

This section details the study of the changes in surface energy of ITO as a result of its modification with the series of phosphonic acids introduced above.

4.2.2.1 Background and Literature

Improving the wetting of subsequent organic layers deposited on ITO can help in improving charge transfer and lifetime of optoelectronic devices.[65] As has been mentioned in Chapter 1, the surface energies of surfaces can be affected by use of organic monolayers. While ITO usually has a high surface energy as a result of surface hydroxyl groups, the surface energy of many organic hole–transport materials (both polymer and small molecule) is often much lower. This difference in surface energies can result in poor adhesion characteristics and could ultimately result in delamination of the film from the ITO over time.[66] Hence, phosphonic acids that can decrease the surface energy of ITO become attractive for creating monolayers on ITO.

There have been several studies regarding the issue of interfacial compatibility of materials to ITO. Most of the research to date on this topic has focused on the attachment of silane monolayers with terminal functional groups very similar to the functional groups present in the subsequently deposited hole–transport material. Veinot *et al.* have attached mono, di, tri, and tetra–silane substituted triarylamines and tetraphenylbiphenyldiamines (TPDs) to the surface of ITO to improve interfacial compatibility.[65] Upon heating, common triarylamine–based polymers dewetted on unmodified ITO surfaces whereas the film integrity was maintained on surfaces modified with the aforementioned silanes (see Figure 1.9 in Chapter 1 for an illustration of this). This enhanced film integrity lead to stable OLED performance over time as opposed to devices made from unmodified ITO, for which the performance degraded over time.

A similar study by Lee *et al*. used a triethoxysilane with a terminal triarylamine

functional group to form monolayers on ITO to change not only the work function (an increase of 0.5 eV vs. bare ITO) but also the surface energy (contact angle of 77° vs. 15° on bare ITO (with water)).[66] They demonstrated unequivocally the increased thermal stability of a deposited TPD film on the monolayer–modified surface with respect to the unmodified ITO. After 1 hour of heating (80 °C) the TPD beaded up on the bare ITO surface while no change could be seen on the monolayer–protected surface.

4.2.2.2 Changing the Surface Energy of ITO – 1st Study

In our 1st study, all of the phosphonic acids utilized to modify ITO resulted in a large decrease in the overall surface energy, especially in regards to the polar component (Figure 4.11). This is not surprising, as the binding and essentially replacement of surface hydroxyls by aliphatic and benzylic moieties would be expected to decrease the polar component of the surface energy. The highly fluorinated octylphosphonic acid (FHOPA) resulted in the lowest overall surface energy of the molecules used due to the highly hydrophobic and oleophobic nature of fluorinated hydrocarbons. Of note is the fact that modifying ITO with hexylphosphonic acid (HPA) resulted in an overall lower surface energy than doing so with pentafluorobenzylphosphonic acid (PFBPA). This is probably due to the ability of alkyl chains to form denser monolayers than aromatic groups, thereby creating a more hydrophobic surface.[67]

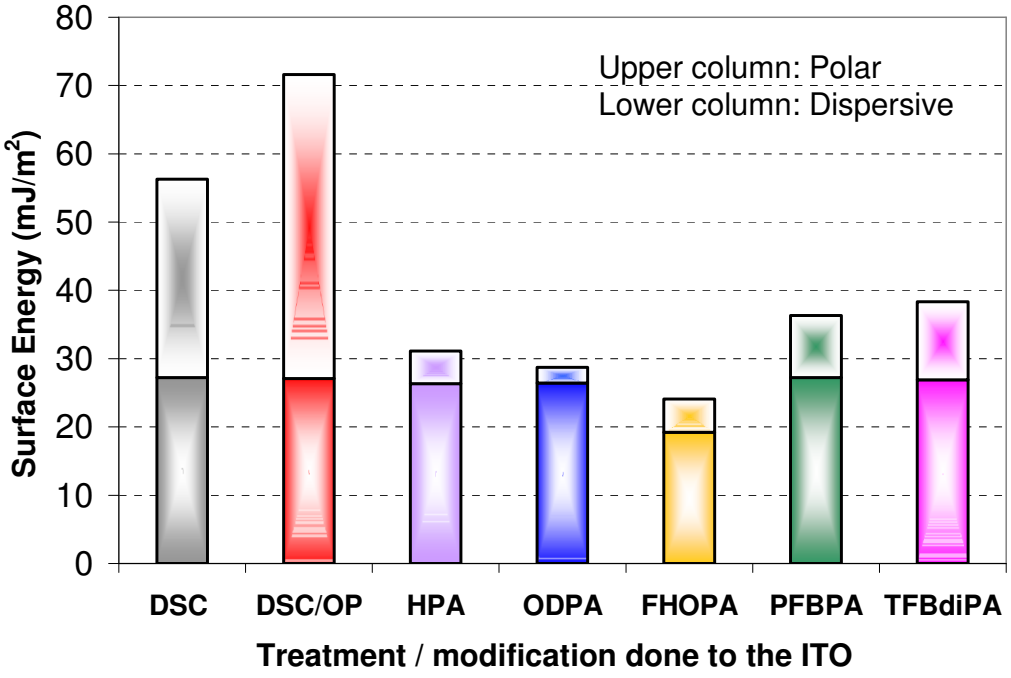

Figure 4.11 Harmonic mean–determined surface energies (γ_s) broken into their polar (γ_s^p) and dispersion (γ_s^d) components for ITO and after DSC/OP activation and modification with the phosphonic acids. The uncertainty on each component of the surface energies is not more than ± 1 mJ/m^2. (Data collected and figure prepared by S. Paniagua)

4.2.2.3 Changing the Surface Energy of ITO – 2nd Study

All the phosphonic acids used in this study also greatly reduced the surface energy of ITO compared to DSC and DSC/OP cleaned ITO. While the surface energies of the DSC and DSC/OP treated ITO substrates were high (56 mJ/m^2 and 72 mJ/m^2, respectively), using any of the benzylphosphonic acids as a surface modifier greatly decreased the surface energy to 35 – 38 mJ/m^2 (Figure 4.12). While the dispersion components were similar regardless of surface treatment, the polar components were greatly decreased after surface modification with a phosphonic acid. While this effect

was seen in the 1st study, the interesting result here is that the surface energy can be kept relatively constant, within a few mJ/m^2, while the work function can be tuned over a range of about 1.2 eV (Figure 4.7). This ability could be beneficial to tune the surface for the specific hole–transport material used in a particular device. It is worth noting that the fact that the surface energies obtained in the first and second study for ITO modified with F_5BnPA are very similar. So, whatever was the origin for the difference in the work function behavior, it did not affect the ability to form a monolayer (probably with similar surface coverage) in the two studies.

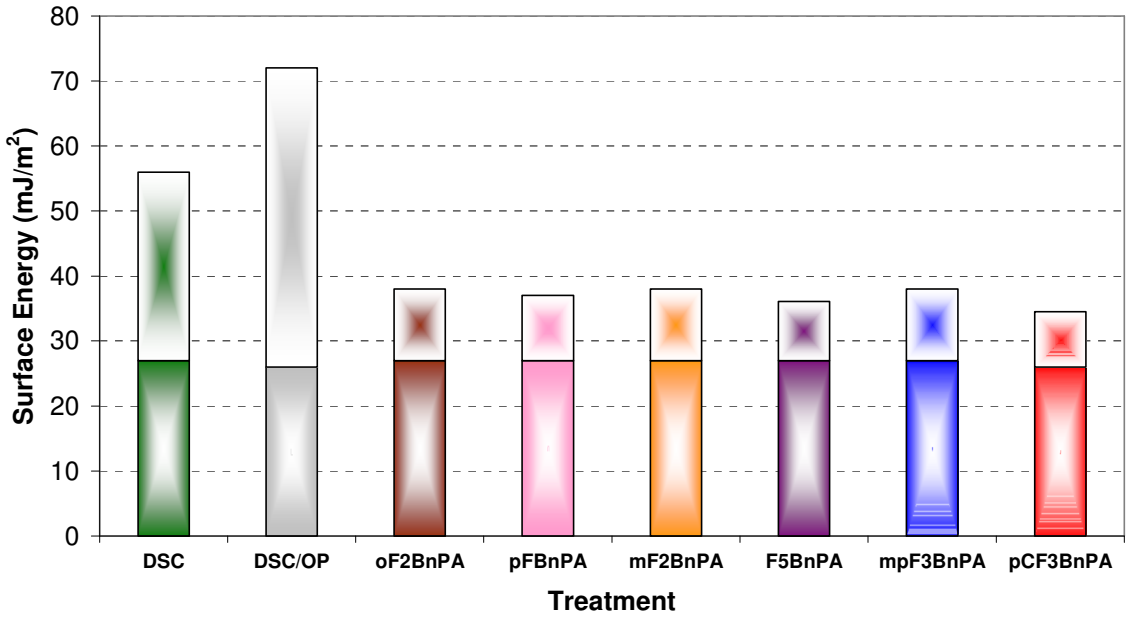

Figure 4.12 Harmonic mean–determined surface energies (γ_s) broken into their polar (γ_s^p) (top column) and dispersion (γ_s^d) (bottom column) components for ITO and after DSC/OP activation and modification with the various benzylphosphonic acids. The uncertainty on each component of the surface energies is not more than ± 1 mJ/m^2. (Data collected by S. Paniagua)

4.2.2.4 Changing the Surface Energy of ITO: Comparisons and Conclusions

The individual contact angle measurements are presented (Table 4.3) and were used in the calculation of the surface energies discussed above, according to Equations 1.3 and 1.4 from Chapter 1. DSC–treated ITO shows an intermediate contact angle with water (~45°), indicative of carbon contaminants that have not been fully removed from the surface during the cleaning. These contaminants can be more completely removed when an oxygen plasma is also used, as can be seen by the complete wetting of a water drop on a DSC/OP ITO surface. All of the phosphonic acid modifications, except for FHOPA, tend to preserve the dispersion component of surface wetting, while decreasing the polar component, the lower limit being the ODPA modification, as expected, since the close packing and long hydrocarbon chain result in a mostly non–polar environment for the probe droplet. Contact angle data for the FHOPA modification is somewhat different than for the rest of modifiers, as it gives a relatively high value (50°) with hexadecane. This may be due to a certain amount of intrinsic hydrocarbon repellent behavior of perfluorinated groups in the tail,[68] which has previously been observed for 3,3,4,4,5,5,6,6,7,7,8,8,8–tridecafluorooctane–1–thiol on gold ($\theta_{HD} = 67°$).[69]

Table 4.3 Contact angle measurements, Θ, and surface energies (γ_s, in mJ/m^2) with their dispersion (γ_s^d) and polar (γ_s^p) components, calculated using the geometric (G) and harmonic (H) mean methods.

ITO treated by / modified with	Θ_{water}/°	$\Theta_{hexadecane}$/°	γ_s^d (mJ/m^2)		γ_s^p (mJ/m^2)		$\gamma_s = \gamma_s^d + \gamma_s^p$	
			H	G	H	G	H	G
DSC/OP	complete wetting 10° or less	18 ± 1	26	26	46	46	72	72
DSC	47 ± 3	10 ± 1	27	27	29	27	56	54
HPA	96 ± 1	18 ± 3	26	26	4.8	1.5	31	28
ODPA	103 ± 1	17 ± 1	26	26	2.3	0.35	29	27
FHOPA	101 ± 1	50 ± 3	19	19	4.9	1.7	24	20
PFBPA	85 ± 1	10 ± 1	27	27	9.1	4.5	36	32
TFBdiPA	80 ± 1	13 ± 1	27	27	11	6.7	38	34
pCF_3BnPA	87 ± 1	20 ± 1	26	26	8.5	4.1	35	30
mpF_3BnPA	81 ± 2	13 ± 2	27	27	11	6.3	38	33
oF_2BnPA	81 ± 1	12 ± 1	27	27	11	6.2	38	33
pFBnPA	82 ± 1	12 ± 1	27	27	10	5.8	37	33
mF_2BnPA	80 ± 1	13 ± 1	27	27	11	6.7	38	34
F_5BnPA	85 ± 1	10 ± 1	27	27	9.1	4.5	36	32
mpF_3PhPA	80 ± 1	13 ± 1	27	27	11	6.7	38	34
pCF_3PhPA	87 ± 1	24 ± 1	25	25	8.7	4.3	34	30
F_5PhPA	79 ± 1	14 ± 1	27	27	12	7.2	39	34

4.2.3 Conclusion

It was experimentally demonstrated that the work function of ITO can be systematically tuned by a total amount of 1.2 eV by forming a monolayer of an appropriately chosen phosphonic acid on the surface. The work function can either be decreased or increased, with respect to bare ITO, by attaching molecules that impart dipoles with their negative ends pointing towards or away from the surface, respectively. Additionally, work function changes on ITO induced by phosphonic acid monolayer were shown to be stable over time, resulting in increased device performance and lifetime of an OLED with respect to an analogous device using air-plasma modified ITO. Controlling the work function of the ITO can allow for better energy level matching with the HOMO of hole–transport materials resulting in decreased barriers and easier charge transport between the materials, potentially resulting in better device performance.

Additionally, the surface energies of ITO can be significantly decreased by attachment of various phosphonic acids. Interestingly, we have identified a series of phosphonic acids that impart similar surface energies to the ITO, while tuning the work function over a wide energy range. This independent modulation of surface energy and work function has not to our knowledge been shown before and could be useful for device design.

4.3 Modification of ZnO

This section details the work that has been done on the modification of planar zinc oxide with phosphonic acids. The work has been done in collaboration with Chris Corso and Tony Dickherber (Electrical and Computer Engineering, Georgia Tech).

4.3.1 Background and Literature

Zinc oxide (ZnO) is a piezoelectric[v] metal oxide and has recently been generating interest as energy generators and in sensor applications,[70] as well as in the general field of molecular electronics.[71, 72] Acoustic–based sensors can potentially be an intriguing alternative to current designs as they can be made simply and cheaply, and could potentially afford better sensitivity than other sensing techniques, such as those based on surface plasmon resonance and electrochemistry.[73] ZnO could be used in film bulk acoustic resonators (FBARs) for biological sensing.[73]

Past studies have mainly focused on the use of silanes to modify the ZnO surface, however with mixed success.[74-76] Additionally, phosphonic acids have been used to successfully modify ZnO nanoparticles.[77, 78] Sinapi *et al.* report on the modification of zinc substrates with alkylphosphonic acids, but they do not discuss the binding modes of the phosphonic acids to the substrate.[79] A detailed study of the binding of phosphonic acids to ZnO and a quantitative assessment of the surface coverage has not yet been

[v] Piezoelectric materials generate an electric potential in response to applied mechanical stress.

reported.

4.3.2 XPS Characterization

The approach to the surface modification of ZnO substrates is similar to that for ITO; that is, a modified T–BAG method was used to form monolayers of phosphonic acids. The substrates were then characterized using a number of techniques, including XPS, IRRAS, AFM, and contact angle measurements.

ZnO substrates were modified with OPA, ODPA, and FHOPA. XPS measurements were performed on these treated substrates as well as on cleaned ZnO and ZnO subjected to oxygen plasma (Figure 4.13). High resolution XPS spectra were recorded for the major peaks for each element. Analysis of these peaks can be used in the determination of the binding mode and surface coverage of the phosphonic acids on ZnO.

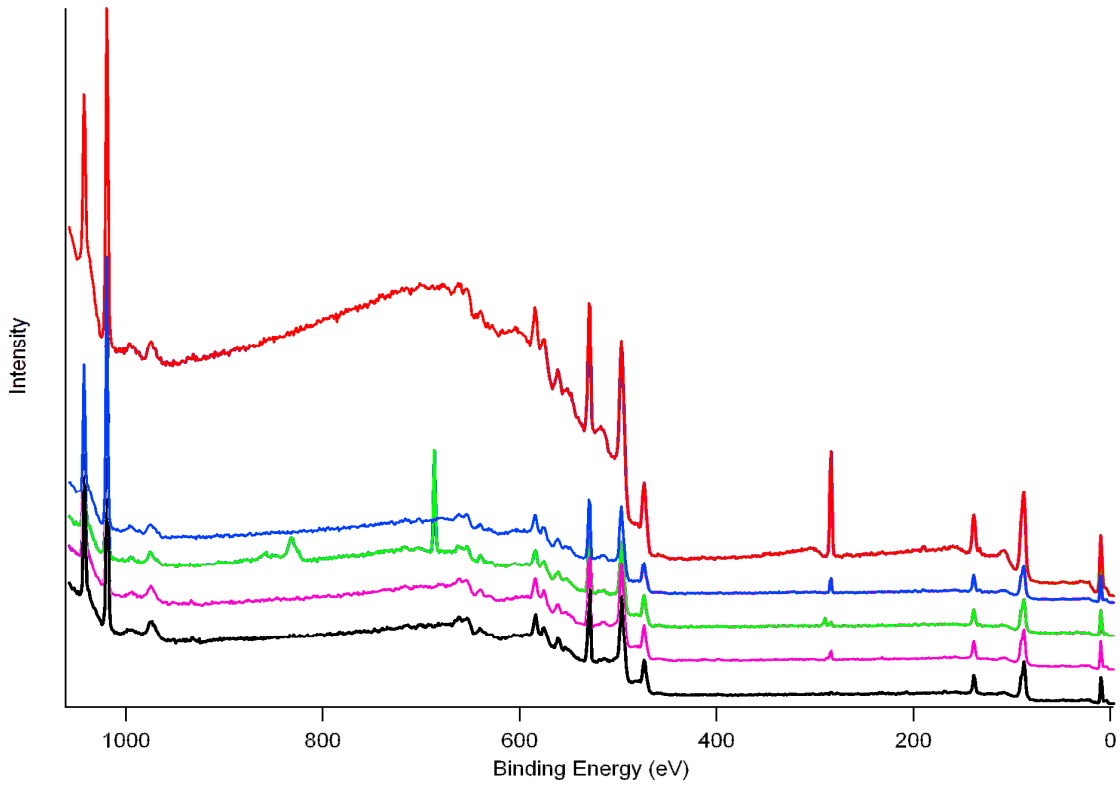

Figure 4.13 XPS survey spectra of ZnO (pink), oxygen plasma etched ZnO (black), OPA–modified ZnO (blue), ODPA–modified ZnO (red), and FHOPA–modified ZnO (green). The spectra have been offset for clarity.

The F(1s) peak in the sample modified with the F_{13}OPA (green trace) appears clearly at 690 eV, the C(1s) peak (~285 eV) increases in relative intensity as the number of carbons on the phosphonic acid modifier increases, and the $Zn2p_{3/2}$ peak (~1020 eV) decreases in relative intensity as the thickness of the monolayer increases. This is expected as the photoelectrons from the substrate are more attenuated when the organic layer is thicker.

The O(1s) peak of ZnO, which has been shown to clearly change in shape and constitution in ITO when modified with phosphonic acids,[2, 80] also appears to change upon modification of ZnO (Figure 4.14).

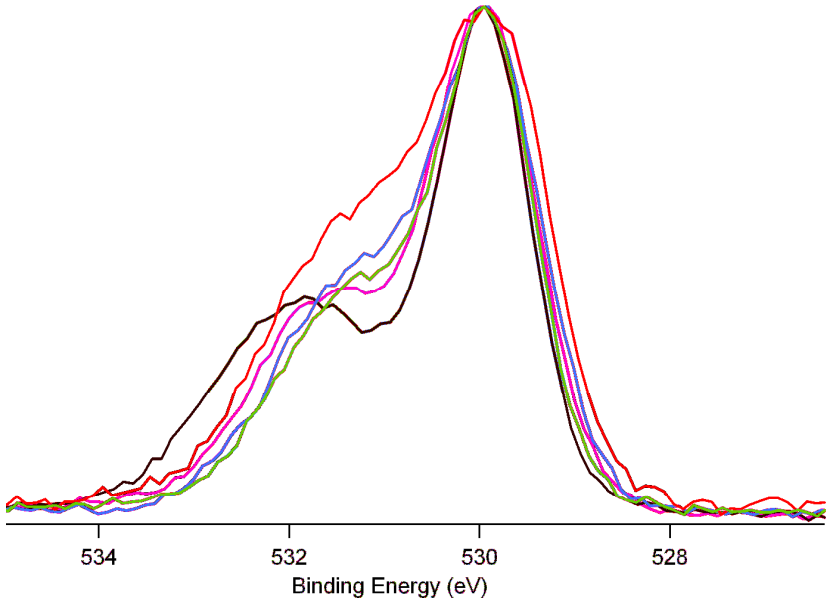

Figure 4.14 XPS O(1s) peaks (normalized) of ZnO (pink), oxygen plasma etched ZnO (black), OPA–modified ZnO (blue), ODPA–modified ZnO (red), and FHOPA–modified ZnO (green). All peaks have been normalized.

In the solvent cleaned ZnO (pink trace), there is a main peak at ~530.0 eV with a shoulder at ~531.5 eV. This shoulder is associated with surface hydroxyl groups.[79] After oxygen plasma (black trace), this peak shifts to higher binding energy. Upon the binding of phosphonic acids (green, blue, and red traces), a new peak ~531.1 eV appears, accompanied by a decrease in the peak associated with surface hydroxyl groups, corresponding to P–O–Zn bonds.[79]

F_{13}OPA–modified ZnO (green trace) shows three peaks in the C(1s) spectrum (Figure 4.15), associated with the various fluorinated carbon species. The other samples show C(1s) intensities relatively similar to what is expected.

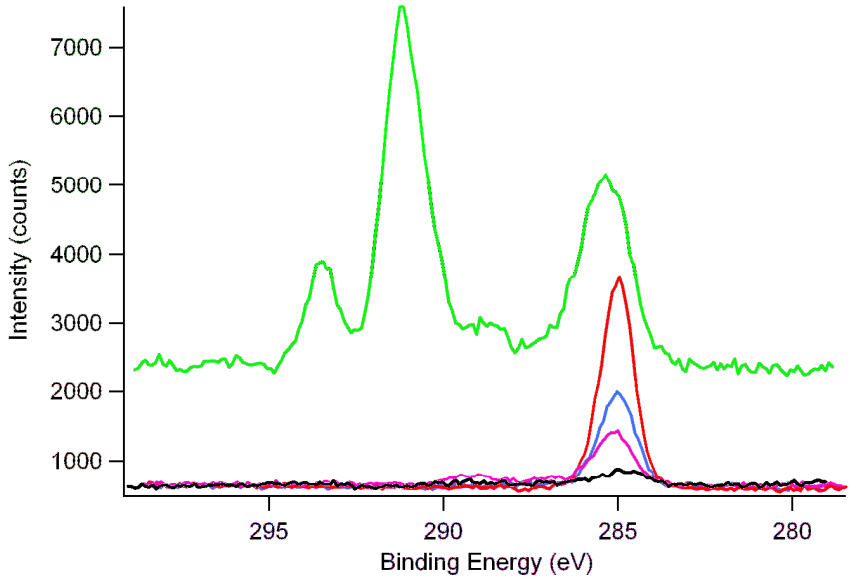

Figure 4.15 XPS C1s peaks of ZnO (pink), oxygen plasma etched ZnO (black), OPA–modified ZnO (blue), ODPA–modified ZnO (red), and FHOPA–modified ZnO (green).

The P(2p) peaks of the three substrates modified with phosphonic acids are shown next to the normalized Zn(3s) peaks (Figure 4.16). The intensity and relative area of the P(2p) peaks is highest for the ODPA–modified ZnO, followed by the OPA–modified ZnO and then the F_{13}OPA–modified ZnO. This implies that more dense monolayers may be seen with ODPA followed by OPA, as might be expected due to the potential of Van der Waals forces to stabilize the ligands during monolayer formation.

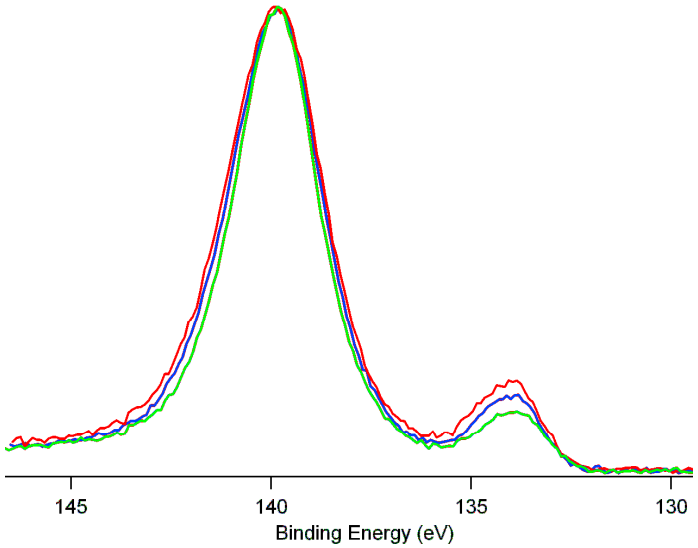

Figure 4.16 XPS P(2p) peaks (~ 134 eV) of OPA–modified ZnO (blue), ODPA–modified ZnO (red), and FHOPA–modified ZnO (green). The Zn(3s) peaks (~140 eV) were normalized.

4.3.3 AFM Characterization

AFM characterization of unmodified ZnO and phosphonic acid modified ZnO was also completed. Topography images using tapping–mode AFM indicate that no change can be seen between unmodified ZnO and ZnO modified with either OPA, ODPA, or FHOPA (Figure 4.17). The images clearly show the grains of the ZnO surface which are still visible after modification with the phosphonic acids. The fact that the grains can still be clearly seen indicates the absence of significant multilayers of the phosphonic acids, as these would tend to blur the grains in the images. Additionally, the rms roughness of the ZnO substrate (~1.5 nm) was the same, within error, after modification with the different phosphonic acids.

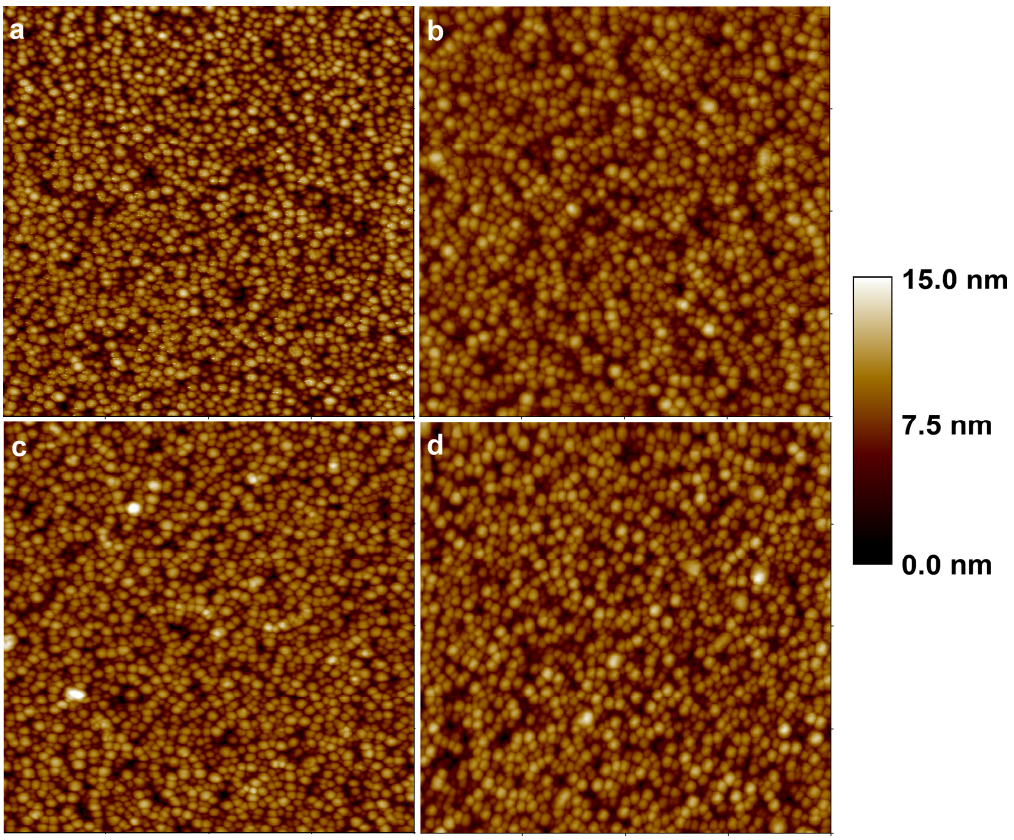

Figure 4.17 AFM topography images of unmodified ZnO (a), and ZnO modified with OPA (b), ODPA (c), and FHOPA (d). Images are 1 μm × 1 μm. (Images collected by A. Giordano)

Lateral force microscopy images were also obtained (Figure 4.18). While no quantitative analysis has been done, qualitatively the images appear different. Bare ZnO appears very uniform (Figure 4.18a), OPA– and FHOPA–modified ZnO have a surface friction which appears different from unmodified ZnO (Figure 4.18b,d), but similar to each other, and ODPA–modified ZnO has a surface friction which qualitatively appears different from that of the others (Figure 4.18c).

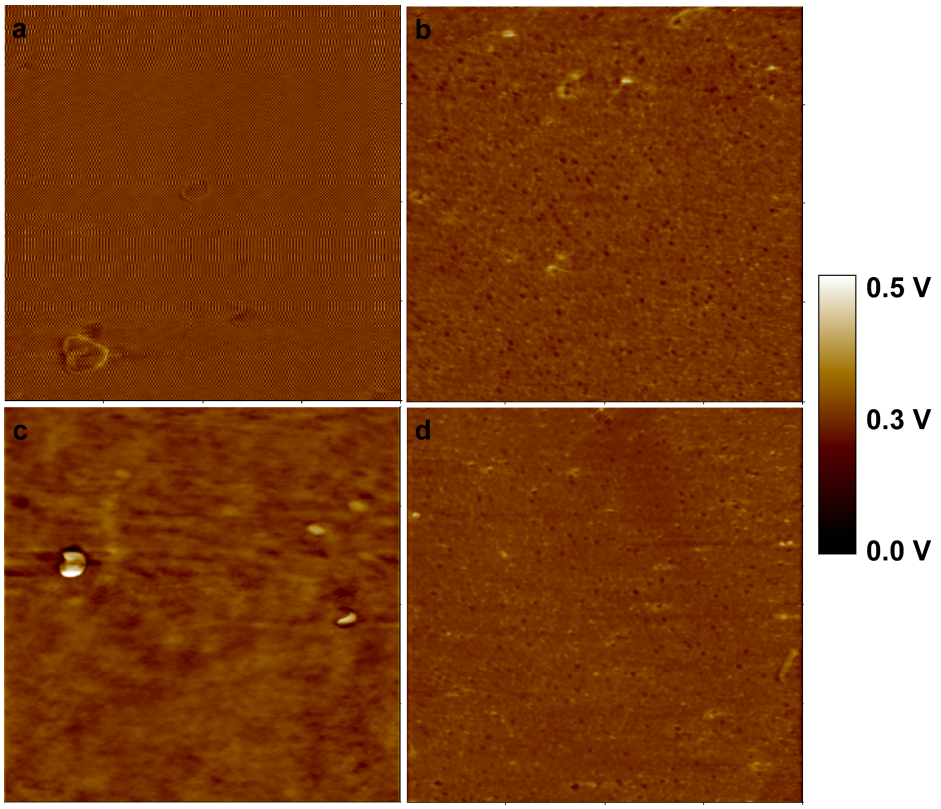

Figure 4.18 Lateral Force Microscopy images of unmodified ZnO (a), and ZnO modified with OPA (b), ODPA (c), and FHOPA (d). Images are10 μm × 10 μm. (Images collected by A. Giordano)

4.3.4 Contact Angle Characterization

Contact angle measurements with water have also been performed (Figure 4.19). As expected, the contact angle of solvent cleaned ZnO is fairly low (33 ± 3°). Oxygen plasma treatment (2 minutes) decreases the contact angle (15 ± 1°). Modification with OPA greatly increases the contact angle (76 ± 3°), while attaching ODPA, which has a much longer alkyl chain, increases the contact angle (108 ± 1°) even further. Modification with FHOPA can increase the hydrophobicity of the ZnO substrate even

further, resulting in a contact angle of 120 ± 1°, which is in fair agreement with the contact angles measured on glass substrates modified with an analogously fluorinated alkylsilane.[81]

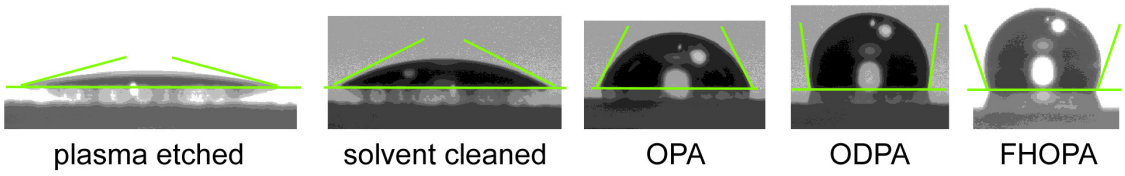

Figure 4.19 Images of water drops on the various treated ZnO surfaces.

Additionally, as was done with phosphonic acid–modified ITO, fractional surface coverages, which can then be related to overall surface coverages, were obtained for each of the modifiers by using Equation 3.6. Surface coverages on ZnO of 3.2, 3.7, and 5.3 molecules/nm^2 were calculated for monolayers of OPA, FHOPA, and ODPA, respectively.

4.3.5 IRRAS Characterization

The IRRAS spectrum of ODPA on a 20 nm ZnO coating on gold substrate has been obtained (Figure 4.20). Spectra were collected with both a bare substrate as well as a substrate modified with a perdeuterated dodecylphosphonic acid. The C–H stretching frequencies are clearly seen (Figure 4.20a, inset) and the absorbance of the $\nu_a CH_2$ band (0.0016) is consistent with that of a dense monolayer.[82] the frequency of the $\nu_a CH_2$ band

(2920 cm^{-1}) is also indicative of a well–packed monolayer.[83] The intensity and frequency of the $\nu_a CD_2$ band in the sample modified with the perdeuterated phosphonic acid is also indicative of a well–packed monolayer (Figure 4.20b, inset). Additionally, the broad peak(s) centered at 1072 cm^{-1} is indicative of tridentate binding of the phosphonic acid. This broad peak (with a shoulder) is strong evidence for the presence of tridentate bonding of the PA moieties to the surface.[11, 84] This broad peak, that corresponds to $\nu(PO_3^{2-})$, as well as the absence of the P=O and P–O–H bands indicates a mainly tridentate binding of the phosphonic acid to the ZnO substrate. The presence of small amounts of other binding modes cannot be ruled out as the spectra indicate a certain amount of absorbed contamination to either the optics or the substrates during data collection that manifests itself in the fingerprint region of the spectra.

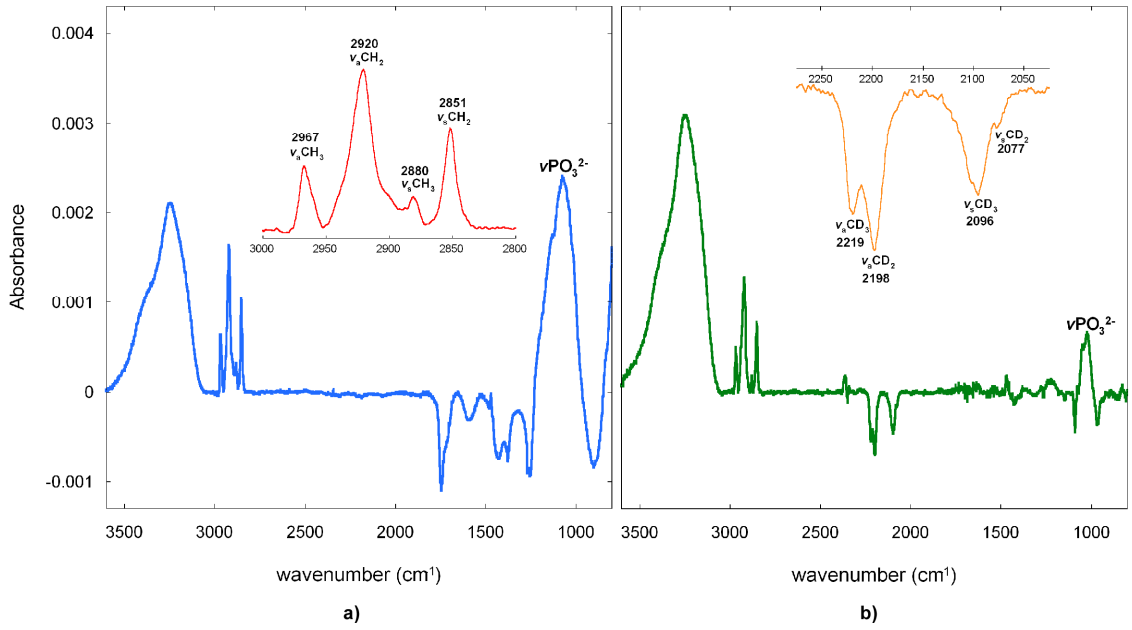

Figure 4.20 IRRAS spectrum of ODPA–modified ZnO/Au/SiO_2 substrate with a) bare ZnO/Au/SiO_2 as the background, and b) d_{25}–dodecylphosphonic acid modified ZnO/Au/SiO_2 as the background. The large broad peak at ~3200 cm^{-1} is from condensed water on the optics.

4.3.6 Conclusions

A detailed study of the attachment of phosphonic acid monolayers on planar zinc oxide was performed. While it has been shown before that phosphonic acids bind to zinc oxide nanoparticles, no in–depth studies had been performed to study the binding modes of phosphonic acids to ZnO. We have shown that phosphonic acids do bind strongly to zinc oxide, with high surface coverages approximated from contact angle and IRRAS measurements, and bind predominantly in a tridentate fashion.

4.4 Experimental

Modification of ITO with phosphonic acids for tuning the work functions and surface energies and resultant characterization:

All commercial ITO films (Colorado Concept Coatings, Loveland CO, 9–15Ω/□) were first cleaned by a detergent/solvent cleaning (DSC) procedure, that consisted of scrubbing with a Triton X–100 solution for 5 minutes, followed by sonication in successive solutions of Triton X–100 in water, nanopure water, and ethanol for 10 min each, followed by drying in a flow of an inert gas. All oxygen plasma (OP) cleaning was performed after the DSC protocol, in an oxygen fed plasma cleaner (Harrick, model PDC–32G) operated at 60 W for 15 min, followed by immediate reaction with the modifier.

The modified T–BAG procedure is as follows: after the activation procedure, the ITO slides were immersed horizontally on top of a clean sample holder in a 1mM ethanol solution of the corresponding phosphonic acid, so that *ca.* 70% of the volume of the modifying solution was underneath the sample. The solvent was allowed to evaporate until the volume fell below the substrate (ca. 3½ h). The ITO substrate was then sonicated in absolute ethanol to remove any multilayer material, and transferred to an oven where it was baked at 140°C for 48h to achieve completion of chemical bonding. After this annealing step a base rinse was performed to ensure no physisorbed molecules remained; this consisted of sonicating for 30 min in a 5% triethylamine/ethanol solution, followed by copious rinsing with ethanol.

XPS with a monochromatic Al(Kα) source (300W) and UPS (He I excitation source) were performed as stated elsewhere using a Kratos Axis–Ultra spectrometer,[55] with the Fermi energy (E_F) calibrated frequently using an atomically clean gold sample. All ITO samples were in electronic equilibrium with the spectrometer, i.e. that the Fermi energy for each sample was known. All XPS spectra were acquired before UPS data acquisition. All measurements were performed at normal takeoff angle (0°).

Contact Angle measurements were conducted on a KRÜSS Drop Shape Analysis System DSA 10Mk2, using water and hexadecane as probe liquids (0.5 µL). Several drops (typically 6 repetitions) were quickly placed on the surface, the needle pulled back, and the drop shape captured immediately with the camera. Images were analyzed with the Drop Shape Analysis software to determine the contact angle by the method most suitable for each given drop, usually circle fitting, and averaging the results.

Modification and Characterization of ZnO substrates:

All ZnO films (500 nm) were deposited onto silicon substrates by rf magnetron sputtering using a Unifilm PVD–300 sputtering system. Substrates were sonicated in acetone (2 ×) and then rinsed with ethanol. This was followed by oxygen plasma (OP) cleaning for 2 minutes (Harrick, model PDC–32G) operated at 60 W followed by immediate reaction with the modifier.

The modified T–BAG procedure is as follows: after the activation procedure, the ZnO slides were immersed horizontally on top of a clean sample holder in a 1mM ethanol solution of the corresponding phosphonic acid, so that *ca.* 70% of the volume of the modifying solution was underneath the sample. The solvent was allowed to evaporate until the volume fell below the substrate (ca. 3½ h). The ZnO substrate was then sonicated in absolute ethanol to remove any multilayer material, and transferred to an oven where it was baked at 140°C for 48h to achieve completion of chemical bonding. After this annealing step a base rinse was performed to ensure no physisorbed molecules remained; this consisted of sonicating for 30 min in a 5% triethylamine/ethanol solution, followed by copious rinsing with ethanol.

XPS with a monochromatic Al(Kα) source (300W) was performed as stated elsewhere using a Kratos Axis–Ultra spectrometer,[55] with the Fermi energy (E_F) calibrated frequently using an atomically clean gold sample. ZnO samples were all referenced to their carbon peaks at 284.6 eV. All measurements were performed at normal takeoff angle (0°).

Contact Angle measurements were conducted using water as the probe liquid (0.5 μL). Several drops (typically 8 repetitions) were quickly placed on the surface (at least 2

different substrates measured for each sample), the needle pulled back, and the drop shape captured immediately with the camera.

IRRAS measurements were performed with a Digilab FTS-7000 FT-IR instrument. A grazing angle accessory (80Spec from Pike) was employed in the studies. The light was *p*-polarized with a gold grid polarizer. The resolution was 2 cm^{-1} and the mirror speed used was 1.28 cm/s. 9000 scans were collected for each sample. In order to check the stability of monolayers two reflection spectra were collected one after another for each sample of interest.

20 nm ZnO was deposited on gold slides with rf magnetron sputtering using a Unifilm PVD–300 sputtering system. Backgrounds of unmodified ZnO/Au and ZnO/Au modified with perdeuterated dodecylphosphonic acid were used. The reflectance spectra were contaminated with either positive or negative signals from water vapor. These could be easily removed by subtracting a prerecorded water vapor spectrum with an appropriate scaling factor. The water vapor free spectrum was baseline corrected using the spline function approach.

4.5 References

1. Hanson, E. L.; Guo, J.; Koch, N.; Schwartz, J.; Bernasek, S. L., Advanced surface modification of indium tin oxide for improved charge injection in organic devices. *Journal of the American Chemical Society* **2005,** 127, (28), 10058-10062.

2. Paniagua, S. A.; Hotchkiss, P. J.; Jones, S. C.; Marder, S. R.; Mudalige, A.; Marrikar, F. S.; Pemberton, J. E.; Armstrong, N. R., Phosphonic acid modification of indium-tin oxide electrodes: Combined XPS/UPS/contact angle studies. *Journal of Physical Chemistry C* **2008,** 112, (21), 7809-7817.

3. Koh, S. E.; McDonald, K. D.; Holt, D. H.; Dulcey, C. S.; Chaney, J. A.; Pehrsson, P. E., Phenylphosphonic acid functionalization of indium tin oxide: Surface chemistry and work functions. *Langmuir* **2006,** 22, (14), 6249-6255.

4. Gawalt, E. S.; Avaltroni, M. J.; Koch, N.; Schwartz, J., Self-assembly and bonding of alkanephosphonic acids on the native oxide surface of titanium. *Langmuir* **2001,** 17, (19), 5736-5738.

5. Gawalt, E. S.; Avaltroni, M. J.; Danahy, M. P.; Silverman, B. M.; Hanson, E. L.; Midwood, K. S.; Schwarzbauer, J. E.; Schwartz, J., Bonding organics to Ti alloys: Facilitating human osteoblast attachment and spreading on surgical implant materials corrections (vol 19, pg 200, 2003). *Langmuir* **2003,** 19, (17), 7147-7147.

6. Nie, H. Y.; Miller, D. J.; Francis, J. T.; Walzak, M. J.; McIntyre, N. S., Robust self-assembled octadecylphosphonic acid monolayers on a mica substrate. *Langmuir* **2005,** 21, (7), 2773-2778.

7. Nie, H. Y.; Walzak, M. J.; McIntyre, N. S., Delivering octadecylphosphonic acid self-assembled monolayers on a Si wafer and other oxide surfaces. *Journal of Physical Chemistry B* **2006,** 110, (42), 21101-21108.

8. Hanson, E. L.; Schwartz, J.; Nickel, B.; Koch, N.; Danisman, M. F., Bonding self-assembled, compact organophosphonate monolayers to the native oxide surface of silicon. *Journal of the American Chemical Society* **2003,** 125, (51), 16074-16080.

9. Zschieschang, U.; Halik, M.; Klauk, H., Microcontact-printed self-assembled monolayers as ultrathin gate dielectrics in organic thin-film transistors and complementary circuits. *Langmuir* **2008,** 24, (5), 1665-1669.

10. Luschtinetz, R.; Oliveira, A. F.; Frenzel, J.; Joswig, J. O.; Seifert, G.; Duarte, H. A., Adsorption of phosphonic and ethylphosphonic acid on aluminum oxide surfaces. *Surface Science* **2008,** 602, (7), 1347-1359.

11. Giza, M.; Thissen, P.; Grundmeier, G., Adsorption kinetics of organ-ophosphonic acids on plasma-modified oxide-covered aluminum surfaces. *Langmuir* **2008,** 24, (16), 8688-8694.

12. Vyklicky, L.; Afzali-Ardakani, A.; Kagan, C. R., Self-assembly and oligomerization of alkyne-terminated molecules on metal and oxide surfaces. *Langmuir* **2005,** 21, (25), 11574-11577.

13. Hannon, J. B.; Afzali, A.; Klinke, C.; Avouris, P., Selective placement of carbon nanotubes on metal-oxide surfaces. *Langmuir* **2005,** 21, (19), 8569-8571.

14. Acton, O.; Ting, G.; Ma, H.; Jen, A. K. Y., Low-voltage high-performance C_{60} thin film transistors via low-surface-energy phosphonic acid monolayer/hafnium oxide hybrid dielectric. *Applied Physics Letters* **2008,** 93, 083302.

15. Van Alsten, J. G., Self-assembled monolayers on engineering metals: structure, derivatization, and utility. *Langmuir* **1999,** 15, 7605-7614.

16. Adolphi, B.; Jahne, E.; Busch, G.; Cai, X. D., Characterization of the adsorption of omega-(thiophene-3-yl alkyl) phosphonic acid on metal oxides with AR-XPS. *Analytical and Bioanalytical Chemistry* **2004,** 379, (4), 646-652.

17. Oberoi, S.; Jahne, E.; Adler, H. J. P., Bifunctional adhesion promoter for grafting polypyrrole films on metal/metal oxide surfaces. *Macromolecular Symposia* **2004,** 217, 147-159.

18. Brovelli, D.; Hahner, G.; Ruiz, L.; Hofer, R.; Kraus, G.; Waldner, A.; Schlosser, J.; Oroszlan, P.; Ehrat, M.; Spencer, N. D., Highly oriented, self-assembled alkanephosphate monolayers on tantalum(V) oxide surfaces. *Langmuir* **1999,** 15, (13), 4324-4327.

19. Li, M.; Xu, J. H.; Lu, Q. H., Creating superhydrophobic surfaces with flowery structures on nickel substrates through a wet-chemical-process. *Journal of Materials Chemistry* **2007,** 17, (45), 4772-4776.

20. Schulmeyer, T.; Paniagua, S. A.; Veneman, P. A.; Jones, S. C.; Hotchkiss, P. J.; Mudalige, A.; Pemberton, J. E.; Marder, S. R.; Armstrong, N. R., Modification of $BaTiO_3$ thin films: adjustment of the effective surface work function. *Journal of Materials Chemistry* **2007,** 17, (43), 4563-4570.

21. Fishbein, I.; Alferiev, I. S.; Nyanguile, O.; Gaster, R.; Vohs, J. M.; Wong, G. S.; Felderman, H.; Chen, I. W.; Choi, H.; Wilensky, R. L.; Levy, R. J., Bisphosphonate-mediated gene vector delivery from the metal surfaces ot stents. *Proceedings of the National Academy of Sciences of the United States of America* **2006,** 103, (1), 159-164.

22. Felhosi, I.; Telegdi, J.; Palinkas, G.; Kalman, E., Kinetics of self-assembled layer formation on iron. *Electrochimica Acta* **2002,** 47, (13-14), 2335-2340.

23. Hahner, G.; Hofer, R.; Klingenfuss, I., Order and orientation in self-assembled long chain alkanephosphate monolayers adsorbed on metal oxide surfaces. *Langmuir* **2001,** 17, (22), 7047-7052.

24. Folkers, J. P.; Gorman, C. B.; Laibinis, P. E.; Buchholz, S.; Whitesides, G. M.; Nuzzo, R. G., Self-assembled monolayers of long-chain hydroxamic acids on the native oxides of metals. *Langmuir* **1995,** 11, (3), 813-824.

25. Kagan, C. R.; Breen, T. L.; Kosbar, L. L., Patterning organic-inorganic thin-film transistors using microcontact printed templates. *Applied Physics Letters* **2001,** 79, (21), 3536-3538.

26. Quinones, R.; Gawalt, E. S., Polystyrene formation on monolayer-modified nitinol effectively controls corrosion. *Langmuir* **2008**, ASAP.

27. Harm, U.; Burgler, R.; Furbeth, W.; Mangold, K. M.; Juttner, K., Novel protective coatings for steel based on a combination of self-assembled monolayers and conducting polymers. *Macromolecular Symposia* **2002,** 187, 65-75.

28. Ma, H.; Acton, O.; Ting, G.; Ka, J. W.; Yip, H. L.; Tucker, N.; Schofield, R.; Jen, A. K. Y., Low-voltage organic thin-film transistors with pi-sigma-phosphonic acid molecular dielectric monolayers. *Applied Physics Letters* **2008,** 92, (11), 113303/1-113303/3.

29. Busch, G.; Jaehne, E.; Cai, X. D.; Oberoi, S.; Adler, H. J. P., Ultrathin layers for adhesion promotion. *Synthetic Metals* **2003,** 137, (1-3), 871-872.

30. Nie, H. Y.; McIntyre, N. S.; Lau, W. M., Nanolithography of a full-coverage octadecylphosphonic acid monolayer spin coated on a Si substrate. *Applied Physics Letters* **2007,** 90, (20), 203114/1-203114/3.

31. Tsud, N.; Yoshitake, M., Vacuum vapour deposition of phenylphosphonic acid on amorphous alumina. *Surface Science* **2007,** 601, (14), 3060-3066.

32. Klauk, H.; Zschieschang, U.; Pflaum, J.; Halik, M., Ultralow-power organic complementary circuits. *Nature* **2007,** 445, (7129), 745-748.

33. Nie, H. Y.; Walzak, M. J.; McIntyre, N. S., Bilayer and odd-numbered multilayers of octadecylphosphonic acid formed on a Si substrate studied by atomic force microscopy. *Langmuir* **2002,** 18, (7), 2955-2958.

34. Besbes, S.; Ltaief, A.; Reybier, K.; Ponsonnet, L.; Jaffrezic, N.; Davenas, J.; Ben Ouada, H., Injection modifications by ITO functionalization with a self-assembled monolayer in OLEDs. *Synthetic Metals* **2003,** 138, (1-2), 197-200.

35. Davenas, J.; Besbes, S.; Abderrahmen, A.; Jaffrezic, N.; Ben Ouada, H., Surface characterisation and functionalisation of indium tin oxide anodes for improvement of charge injection in organic light emitting diodes. *Thin Solid Films* **2008,** 516, (7), 1341-1344.

36. Aswal, D. K.; Lenfant, S.; Guerin, D.; Yakhmi, J. V.; Vuillaume, D., Self assembled monolayers on silicon for molecular electronics. *Analytica Chimica Acta* **2006,** 568, (1-2), 84-108.

37. Adden, N.; Gamble, L. J.; Castner, D. G.; Hoffmann, A.; Gross, G.; Menzel, H., Phosphonic acid monolayers for binding of bioactive molecules to titanium surfaces. *Langmuir* **2006,** 22, (19), 8197-8204.

38. Gawalt, E. S.; Raman, A.; Quinones, R.; Papariella, K., The formation of organic monolayers on alloy oxide surfaces. *Abstracts of Papers of the American Chemical Society* **2006,** 231.

39. Jaehne, E.; Kowalik, T.; Adler, H. J. P.; Plagge, A.; Stratmann, M., Ultra-thin layers of phosphorylated cellulose derivatives on metal surfaces. *Macromolecular Symposia* **2002,** 177, 97-109.

40. Kowalik, T.; Adler, H. J. P.; Plagge, A.; Stratmann, M., Ultrathin layers of phosphorylated cellulose derivatives on aluminium surfaces. *Macromolecular Chemistry and Physics* **2000,** 201, (15), 2064-2069.

41. Fang, J. L.; Li, Y.; Ye, X. R.; Wang, Z. W.; Liu, Q., Passive films and corrosion protection due to phosphonic acid inhibitors. *Corrosion* **1993,** 49, (4), 266-271.

42. Brumbach, M.; Veneman, P. A.; Marrikar, F. S.; Schulmeyer, T.; Simmonds, A.; Xia, W.; Lee, P.; Armstrong, N. R., Surface composition and electrical and electrochemical properties of freshly deposited and acid-etched indium tin oxide electrodes. *Langmuir* **2007,** 23, (22), 11089-11099.

43. Donley, C.; Dunphy, D.; Paine, D.; Carter, C.; Nebesny, K.; Lee, P.; Alloway, D.; Armstrong, N. R., Characterization of indium-tin oxide interfaces using X-ray photoelectron spectroscopy and redox processes of a chemisorbed probe molecule: Effect of surface pretreatment conditions. *Langmuir* **2002,** 18, (2), 450-457.

44. Kim, J. S.; Park, J. H.; Lee, J. H.; Jo, J.; Kim, D. Y.; Cho, K., Control of the electrode work function and active layer morphology via surface modification of indium tin oxide for high efficiency organic photovoltaics. *Applied Physics Letters* **2007,** 91, (11), 112111/1-112111/3.

45. Carrara, M.; Nuesch, F.; Zuppiroli, L., Carboxylic acid anchoring groups for the construction of self-assembled monolayers on organic device electrodes. *Synthetic Metals* **2001,** 121, (1-3), 1633-1634.

46. Luscombe, C. K.; Li, H. W.; Huck, W. T. S.; Holmes, A. B., Fluorinated silane self-assembled monolayers as resists for patterning indium tin oxide. *Langmuir* **2003,** 19, (13), 5273-5278.

47. Cahen, D.; Kahn, A., Electron energetics at surfaces and interfaces: concepts and experiments. *Advanced Materials* **2003,** 15, (4), 271-277.

48. Appleyard, S. F. J.; Day, S. R.; Pickford, R. D.; Willis, M. R., Organic electroluminescent devices: enhanced carrier injection using SAM derivatized ITO electrodes. *Journal of Materials Chemistry* **2000,** 10, (1), 169-173.

49. Guo, J.; Koch, N.; Bernasek, S. L.; Schwartz, J., Enhanced hole injection in a polymer light emitting diode using a small molecule monolayer bound to the anode. *Chemical Physics Letters* **2006,** 426, (4-6), 370-373.

50. Alves, C. A.; Porter, M. D., Atomic-force microscopic characterization of a fluorinated alkanethiolate monolayer at gold and correlations to electrochemical and

infrared reflection spectroscopic structural descriptions. *Langmuir* **1993,** 9, (12), 3507-3512.

51. Widrig, C. A.; Chung, C.; Porter, M. D., The electrochemical desorption of n-alkanethiol monolayers from polycrystalline Au and Ag electrodes. *Journal of Electroanalytical Chemistry* **1991,** 310, (1-2), 335-359.

52. Gao, W.; Dickinson, L.; Grozinger, C.; Morin, F. G.; Reven, L., Self-assembled monolayers of alkylphosphonic acids on metal oxides. *Langmuir* **1996,** 12, (26), 6429-6435.

53. Romaner, L.; Heimel, G.; Zojer, E., Electronic structure of thiol-bonded self-assembled monolayers: impact of coverage. *Physical Review B* **2008,** 77, (4), 045113/1-045113/9.

54. Schwartz, J.; Bruner, E. L.; Koch, N.; Span, A. R.; Bernasek, S. L.; Kahn, A., Controlling the work function of indium tin oxide: differentiating dipolar from local surface effects. *Synthetic Metals* **2003,** 138, (1-2), 223-227.

55. Alloway, D. M.; Hofmann, M.; Smith, D. L.; Gruhn, N. E.; Graham, A. L.; Colorado, R.; Wysocki, V. H.; Lee, T. R.; Lee, P. A.; Armstrong, N. R., Interface dipoles arising from self-assembled monolayers on gold: UV-photoemission studies of alkanethiols and partially fluorinated alkanethiols. *Journal of Physical Chemistry B* **2003,** 107, (42), 11690-11699.

56. Christou, V.; Etchells, M.; Renault, O.; Dobson, P. J.; Salata, O. V.; Beamson, G.; Egdell, R. G., High resolution x-ray photoemission study of plasma oxidation of indium-tin-oxide thin film surfaces. *Journal of Applied Physics* **2000,** 88, (9), 5180-5187.

57. Ding, X. M.; Hung, L. M.; Cheng, L. F.; Deng, Z. B.; Hou, X. Y.; Lee, C. S.; Lee, S. T., Modification of the hole injection barrier in organic light-emitting devices studied by ultraviolet photoelectron spectroscopy. *Applied Physics Letters* **2000,** 76, (19), 2704-2706.

58. Milliron, D. J.; Hill, I. G.; Shen, C.; Kahn, A.; Schwartz, J., Surface oxidation activates indium tin oxide for hole injection. *Journal of Applied Physics* **2000,** 87, (1), 572-576.

59. Wu, C. C.; Wu, C. I.; Sturm, J. C.; Kahn, A., Surface modification of indium tin oxide by plasma treatment: An effective method to improve the efficiency, brightness, and reliability of organic light emitting devices. *Applied Physics Letters* **1997,** 70, (11), 1348-1350.

60. You, Z. Z.; Dong, J. Y., Surface properties of treated ITO anodes for organic light-emitting devices. *Applied Surface Science* **2005,** 249, (1-4), 271-276.

61. Lee, K. H.; Jang, H. W.; Kim, K. B.; Tak, Y. H.; Lee, J. L., Mechanism for the increase of indium-tin-oxide work function by O_2 inductively coupled plasma treatment. *Journal of Applied Physics* **2004,** 95, (2), 586-590.

62. Kim, S. Y.; Hong, K.; Lee, J. L.; Choi, K. H.; Song, K. H.; Ahn, K. C., Enhancement of physical properties of indium tin oxide deposited by super density arc plasma ion plating by O_2 plasma treatment. *Solid-State Electronics* **2008,** 52, (1), 1-6.

63. Ishii, M.; Mori, T.; Fujikawa, H.; Tokito, S.; Taga, Y., Improvement of organic electroluminescent device performance by in situ plasma treatment of indium-tin-oxide surface. *Journal of Luminescence* **2000,** 87-9, 1165-1167.

64. Furukawa, K.; Terasaka, Y.; Ueda, H.; Matsumura, M., Effect of a plasma treatment of ITO on the performance of organic electroluminescent devices. *Synthetic Metals* **1997,** 91, (1-3), 99-101.

65. Veinot, J. G. C.; Marks, T. J., Toward the ideal organic light-emitting diode. The versatility and utility of interfacial tailoring by cross-linked siloxane interlayers. *Accounts of Chemical Research* **2005,** 38, (8), 632-643.

66. Lee, J.; Jung, B. J.; Lee, J. I.; Chu, H. Y.; Do, L. M.; Shim, H. K., Modification of an ITO anode with a hole-transporting SAM for improved OLED device characteristics. *Journal of Materials Chemistry* **2002,** 12, (12), 3494-3498.

67. Lee, S.; Puck, A.; Graupe, M.; Colorado, R.; Shon, Y. S.; Lee, T. R.; Perry, S. S., Structure, wettability, and frictional properties of phenyl-terminated self-assembled monolayers on gold. *Langmuir* **2001,** 17, (23), 7364-7370.

68. Chambers, R. D., *Fluorine in Organic Chemistry*. Blackwell: Oxford, 2004.

69. Laibinis, P. E.; Whitesides, G. M., Omega-terminated alkanethiolate monolayers on surfaces of copper, silver, and gold have similar wettabilities. *Journal of the American Chemical Society* **1992,** 114, (6), 1990-1995.

70. Wang, Z. L.; Song, J. H., Piezoelectric nanogenerators based on zinc oxide nanowire arrays. *Science* **2006,** 312, (5771), 242-246.

71. Song, J. H.; Wang, X. D.; Liu, J.; Liu, H. B.; Li, Y. L.; Wang, Z. L., Piezoelectric potential output from ZnO nanowire functionalized with p-type oligomer. *Nano Letters* **2008,** 8, (1), 203-207.

72. Tomita, Y.; May, C.; Toerker, M.; Amelung, J.; Eritt, M.; Loeffler, F.; Luber, C.; Leo, K.; Walzer, K.; Fehse, K.; Huang, Q., Highly efficient p-i-n-type organic light emitting diodes on ZnO: Al substrates. *Applied Physics Letters* **2007,** 91, (6), 063510/1-063510/3.

73. Corso, C. D.; Dickherber, A.; Hunt, W. D., Lateral field excitation of thickness shear mode waves in a thin film ZnO solidly mounted resonator. *Journal of Applied Physics* **2007,** 101, (5), 054514/1-054514/7.

74. Bourlinos, A. B.; Stassinopoulos, A.; Anglos, D.; Herrera, R.; Anastasiadis, S. H.; Petridis, D.; Giannelis, E. P., Functionalized ZnO nanoparticles with liquidlike behavior and their photoluminescence properties. *Small* **2006,** 2, (4), 513-516.

75. Thomsen, L.; Watts, B.; Dastoor, P. C., A NEXAFS orientation study of gamma-aminopropyltriethoxysilane on zinc oxide surfaces. *Surface and Interface Analysis* **2006,** 38, (7), 1139-1145.

76. Sinapi, F.; Forget, L.; Delhalle, J.; Mekhalif, Z., Self-assembly of (3-mercaptopropyl)trimethoxysilane on polycrystalline zinc substrates towards corrosion protection. *Applied Surface Science* **2003,** 212, 464-471.

77. Chen, Y. F.; Kim, M.; Lian, G.; Johnson, M. B.; Peng, X. G., Side reactions in controlling the quality, yield, and stability of high quality colloidal nanocrystals. *Journal of the American Chemical Society* **2005,** 127, (38), 13331-13337.

78. Demir, M. M.; Koynov, K.; Akbey, U.; Bubeck, C.; Park, I.; Lieberwirth, I.; Wegner, G., Optical properties of composites of PMMA and surface-modified zincite nanoparticles. *Macromolecules* **2007,** 40, (4), 1089-1100.

79. Sinapi, F.; Forget, L.; Delhalle, J.; Mekhalif, Z., Formation and characterization of thin films of $H(CH_2)_xPO(OH)_2$ on polycrystalline zinc substrates. *Surface and Interface Analysis* **2002,** 34, (1), 148-154.

80. Paramonov, P. B.; Paniagua, S. A.; Hotchkiss, P. J.; Jones, S. C.; Armstrong, N. R.; Marder, S. R.; Brédas, J.-L., Theoretical characterization of the indium tin oxide surface and its binding sites for adsorption of phosphonic acid monolayers. *Chemistry of Materials* **2008,** 20, (16), 5131-5133.

81. Kawase, T.; Sawada, H., End-capped fluoroalkyl-functional silanes. Part I: Modification of glass. *Journal of Adhesion Science and Technology* **2002,** 16, (8), 1103-1120.

82. Laibinis, P. E.; Nuzzo, R. G.; Whitesides, G. M., Structure of monolayers formed by coadsorption of 2 normal alkanethiols of different chain lengths on gold and its relation to wetting. *Journal of Physical Chemistry* **1992,** 96, (12), 5097-5105.

83. Nuzzo, R. G.; Dubois, L. H.; Allara, D. L., Fundamental studies of microscopic wetting on organic surfaces. 1. Formation and structural characterization of a self-consistent series of polyfunctional organic monolayers. *Journal of the American Chemical Society* **1990,** 112, (2), 558-569.

84. Kim, P.; Jones, S. C.; Hotchkiss, P. J.; Haddock, J. N.; Kippelen, B.; Marder, S. R.; Perry, J. W., Phosphonic acid-modified barium titanate polymer nanocomposites with high permittivity and dielectric strength. *Advanced Materials* **2007,** 19, (7), 1001-1005.

Chapter 5

Surface Modification of Metal Oxide Nanoparticles with Phosphonic Acids

This chapter focuses on our efforts to modify nanoparticles of various metal oxides with phosphonic acids. Additionally, the modification of zeolites is discussed.

5.1. Background and literature

There are a fair number of reports discussing the modification of metal oxide nanoparticles with phosphonic acids. While we initially became interested in phosphonic acids while attempting to find a suitable surface modifier for barium titanate nanoparticles,[1] there exist many reports of their ability to bind to a number of other metal oxide nanoparticles, including, but not limited to, TiO_2,[2-14] ZnO,[15-18] Fe_2O_3,[19-23] ZrO_2,[2, 3, 5, 6] Al_2O_3,[4, 7, 24] SnO_2,[4, 25, 26] $CoFe_2O_4$,[27] CeO_2,[28] Y_2O_3,[29] CdSe,[30] WO_3,[31] and SiO_2.[32] Additionally, there is a report of the formation of discretely sized rhodium clusters using phosphonic acid binding groups,[33] as well as a report on the use of a large number of metal oxides bound to poly(vinylphosphonic acid) for use in polyelectrolyte cements.[34] In this paper the authors list ZnO, MgO, Cu_2O, CuO, La_2O_3, Bi_2O_3, CaO, CoO, SnO, PbO, Pd_3O_4, HgO, CdO, Y_2O_3, and MoO_3 as all forming hydrolytically stable cements with poly(vinylphosphonic acid).[34] However, no characterization information was given in regards to the binding or coverage of the phosphonic acid on the metal oxides.

5.1.1 Applications of Modified Metal Oxide Nanoparticles

Oftentimes nanoparticles of metal oxides are used to study the binding of ligands to the surface due to the larger surface area of the nanoparticles relative to planar substrates for a given volume of material. This may lead to easier characterization of the surface properties, as in many measurement techniques the signal due to the surface–bound ligands increases with an increase of the surface–to–volume ratio. However, a number of applications have been described for which nanoparticles of metal oxides have been specifically utilized. Magnetic nanoparticles, such as Fe_2O_3 and $CoFe_2O_4$, have been tested as magnetic resonance imaging contrast agents,[23, 35] site–specific drug–delivery carriers,[22, 27, 36] and in magnetic storage devices.[19, 37] Y_2O_3 nanoparticles are promising materials for cellular imaging.[29, 38] ZnO nanoparticles are used in polymer hybrid materials in order to obtain easily–processible materials with tunable optical properties.[17] Al_2O_3 nanoparticles have been used in polymer blends to enhance flame–retardancy.[24] WO_3 nanoparticles have been used as gas sensors[31] and in electrochromic devices.[10] SnO_2 nanostructured materials have been used in photovoltaics,[39] catalysis,[40] in lithium rechargeable batteries,[41] and as gas sensors.[42] TiO_2 nanoparticles and nanocrystalline films are a key material in many dye–sensitized solar cells,[11, 43] can be used as catalysts,[44] and in applications requiring materials with high refractive index or dielectric constant.[8] These are just a handful of the applications for which metal oxide nanoparticles are currently being researched and used.

5.2 Phosphonic Acids as a Universal Ligand

Considering the wide variety of metal oxide materials to which phosphonic acids have been known to bind, perhaps it is reasonable to consider them as universal ligands for metal oxide modification. As the binding of phosphonic acids has been shown to be dependent on the presence of surface hydroxyl groups and/or Lewis acidic sites (see Chapter 3), certain surface functionalities must be present for the chemisorption of phosphonic acids to take place, but nonetheless phosphonic acid are very versatile ligands and the use of surface modified metal oxide nanoparticles is expected to be investigated further.

The potential impact of the use of phosphonic acids as a binding group for most if not all metal oxides is large; libraries of ligands could be greatly reduced, as the need for ligands based on other binding groups, such as carboxylic acids, sulfonic acids, and silanes, could diminish; commercial availability of various substituted phosphonic acids would most likely follow, as was seen for silanes once their utility in the surface modification of glass was demonstrated.

5.2.1 Methodology

Though phosphonic acids have been used to modify a variety of different metal oxides has been reported in the literature, as mentioned above, a complete understanding of the binding of the phosphonic acid to the material has often been lacking. Philseok

Kim (Chemistry, Georgia Institute of Technology) and I undertook a study to try to provide a better understanding of the binding modes and coverages that can be obtained with phosphonic acids on a number of different metal oxides. Nanoparticles were chosen as opposed to planar substrates due to their relative ease of characterization.

A number of metal oxide nanoparticles were purchased and octylphosphonic acid (OPA) and octadecylphosphonic acid (ODPA) were used as the surface modifiers. Unmodified and modified metal oxides were characterized by a combination of FTIR (Fourier Transform Infrared Spectroscopy), TGA (Thermogravimetric Analysis), XPS (X–Ray Photoelectron Spectroscopy), XRD (X–Ray Diffraction (powder)), and SEM (Scanning Electron Microscopy). Three different conditions for the modification procedure were used. Normal conditions refer to modification in 95:5 ethanol: water at 80 °C for 1 hour. Mild conditions refer to modification in 95:5 ethanol: water at room temperature for 1 hour. Forcing conditions refer to modification in 95:5 ethanol: water at heavy reflux (100 °C oil bath) for 5 hours. Normal conditions were used unless otherwise specified. For all conditions, a 5 times excess of phosphonic acid was used based on the surface area of the nanoparticles. Full experimental and characterization procedures are described in the experimental section of this chapter.

All SEM and FTIR data were collected by P. Kim.

5.2.2 Modification of ITO (Indium Tin Oxide) Nanoparticles

While the modification of planar ITO substrates with phosphonic acids has been

reported in the literature,[45-47] a search of the literature using Sci-Finder revealed no reports of the modification of their nanoparticle analogues. Utilizing the inherent advantages of the increased surface energy of nanoparticles with respect to planar surfaces, the binding of phosphonic acids to the ITO surface can be studied in new ways.[w]

SEM images appear to show no change in nanoparticle morphology after surface modification with OPA. Additionally, no excess phosphonic acid can be seen in the images, supporting the fact that the washing steps satisfactorily removed any unbound ligand after the reaction. (Figure 5.1).

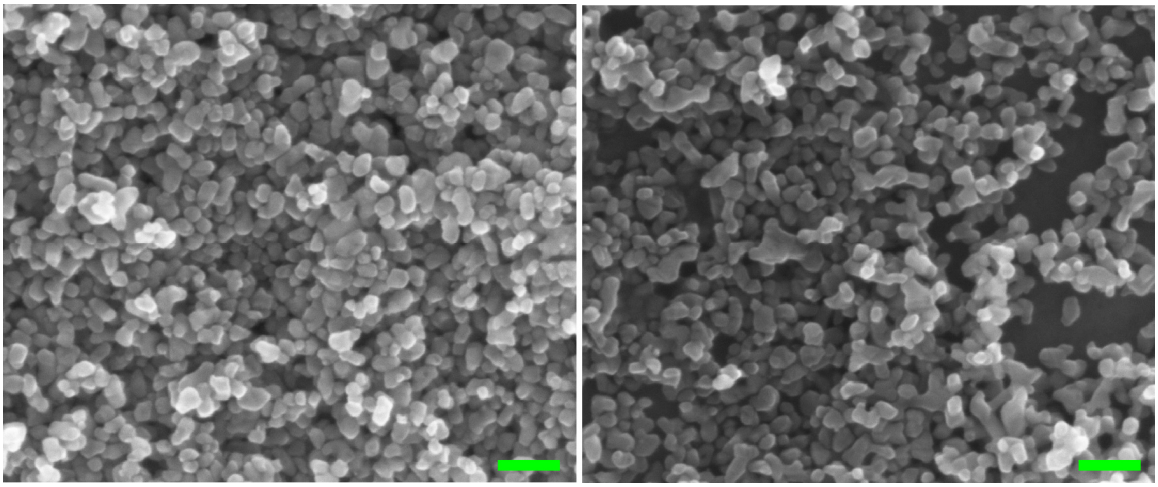

Figure 5.1 SEM images of ITO nanoparticles before (left) and after (right) modification with OPA. Scale bars are equal to 100 nm. (Images taken by P. Kim)

XRD patterns of the nanoparticles prior to and after surface modification (normal conditions) appear identical in line-shapes and relative peak-intensities (Figure 5.2).

[w] It should be noted that additional characterization and results on the modification of ITO nanoparticles with phosphonic acids is reported in Chapter 3.

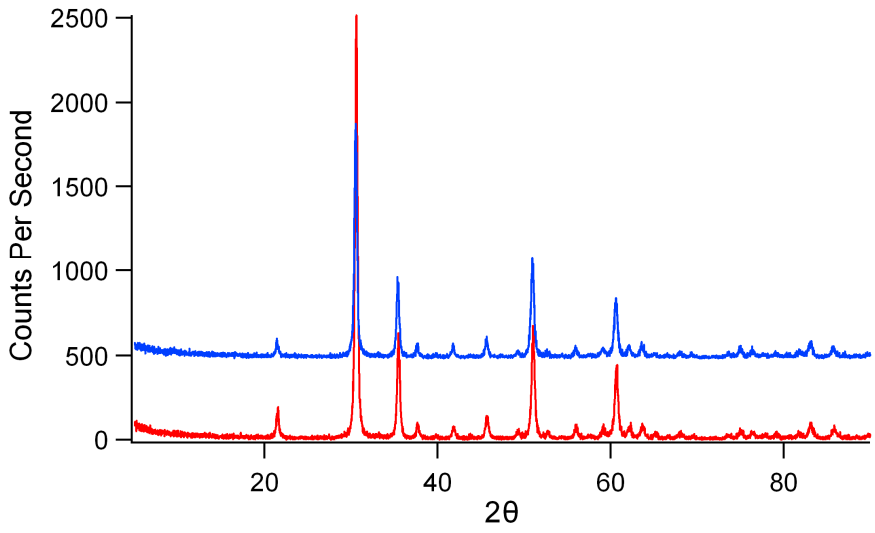

Figure 5.2 XRD patterns of ITO nanoparticles before (red) and after (blue) surface modification with OPA under normal conditions. Patterns are offset for clarity.

FTIR spectra of unmodified ITO nanoparticles, along with those modified with either OPA or ODPA were recorded (Figure 5.3). Unfortunately, the ITO nanoparticles absorb strongly over most of the IR region, making any differences resulting from their modification difficult to assess. However, the appropriate sp^3 C–H stretching bands can be seen in the region around 2900 cm^{-1} (CH_2 asymmetric stretch at about 2920 cm^{-1}, CH_2 symmetric stretch at about 2850 cm^{-1}) for the OPA–modified nanoparticles, and especially for the ODPA–modified nanoparticles (Figure 5.3b). The fingerprint region of the spectra, often useful for the determination of the binding mode of the phosphonic acid moieties to the surface, yields no information in this case due to the strong absorption of the ITO nanoparticles.

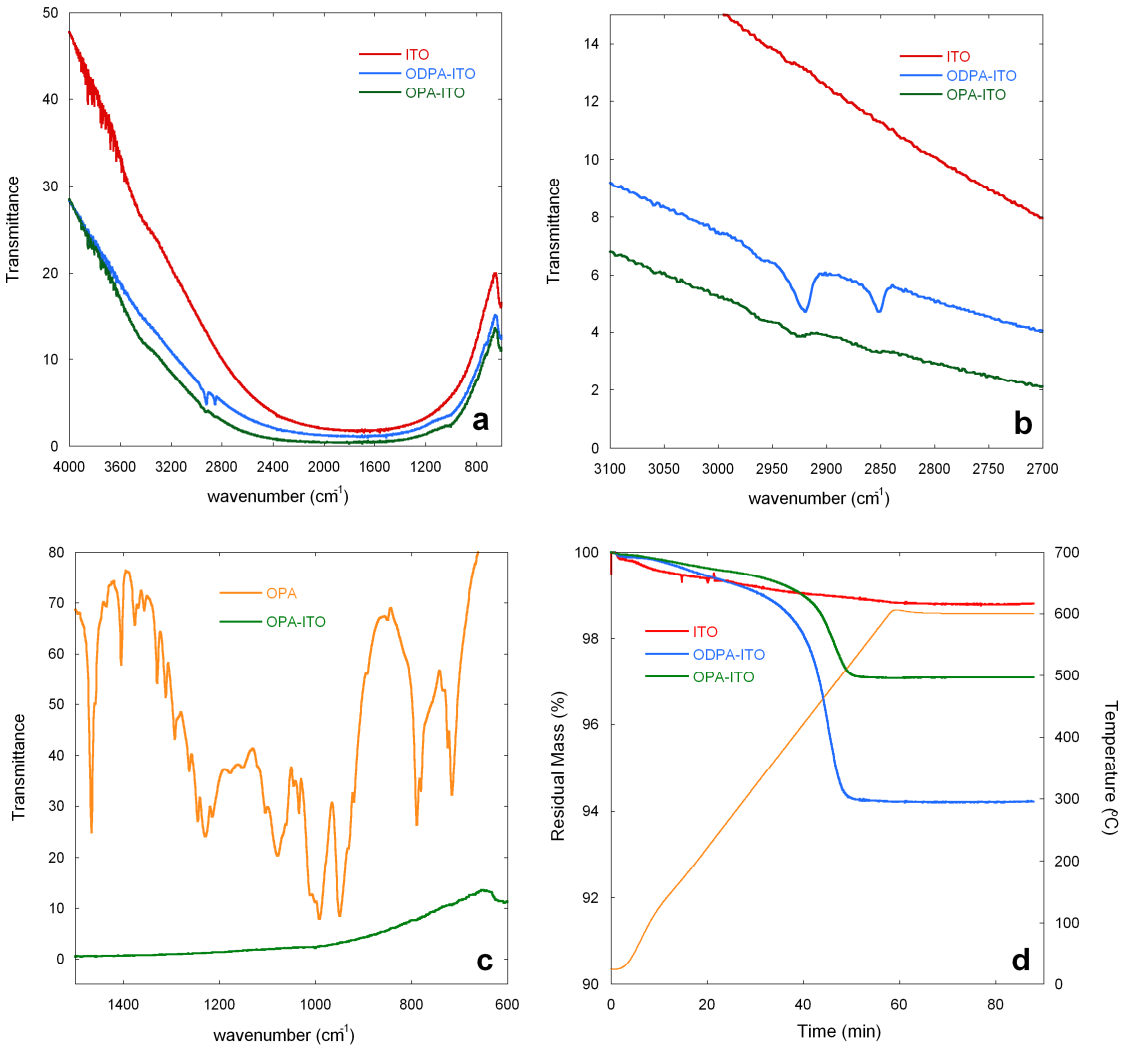

Figure 5.3 a) FTIR spectra of ITO nanoparticles before (red), after reaction with OPA (green), and after reaction with ODPA (blue), b) detail of the C–H stretching region for the same samples, and c) detail of the fingerprint region of OPA–modified nanoparticles (green) and unbound OPA (orange). d) TGA traces for each of the nanoparticle species. The orange trace corresponds to the temperature as a function of time. (IR data collected by P. Kim)

TGA plots of the unmodified and modified nanoparticles are also shown (Figure 5.3d). Nanoparticles modified with OPA show a mass loss of 2.1%, corresponding to a surface coverage of ~72% of a theoretical monolayer. Nanoparticles modified with

ODPA show a mass loss 4.6%, corresponding to a surface coverage ~94% of a theoretical monolayer. The surface coverage values are based on a the surface area of the nanoparticles (23 m^2/g, from the manufacturer) and the footprint of a phosphonic acid group bound to a surface (~0.24 nm^2/g)[5].

XPS spectra were also recorded of the modified and unmodified nanoparticles (Figure 5.4). The carbon signal increases as expected for the OPA and ODPA–modified samples. The O(1s) peaks appear to change in composition once the phosphonic acid is attached, becoming wider on the high binding energy side, which is consistent with the presence of P–O–M bonds.[48] It should be noted that the phosphonic acid–modified nanoparticles showed charging (resulting in a shift of the binding energies) during analysis, consistent with the addition of an insulating layer, such as alkyl chains, on their surface. As such, all spectra were calibrated to the accepted C(1s) binding energy of sp^3 C–H groups (284.6 eV).[49]

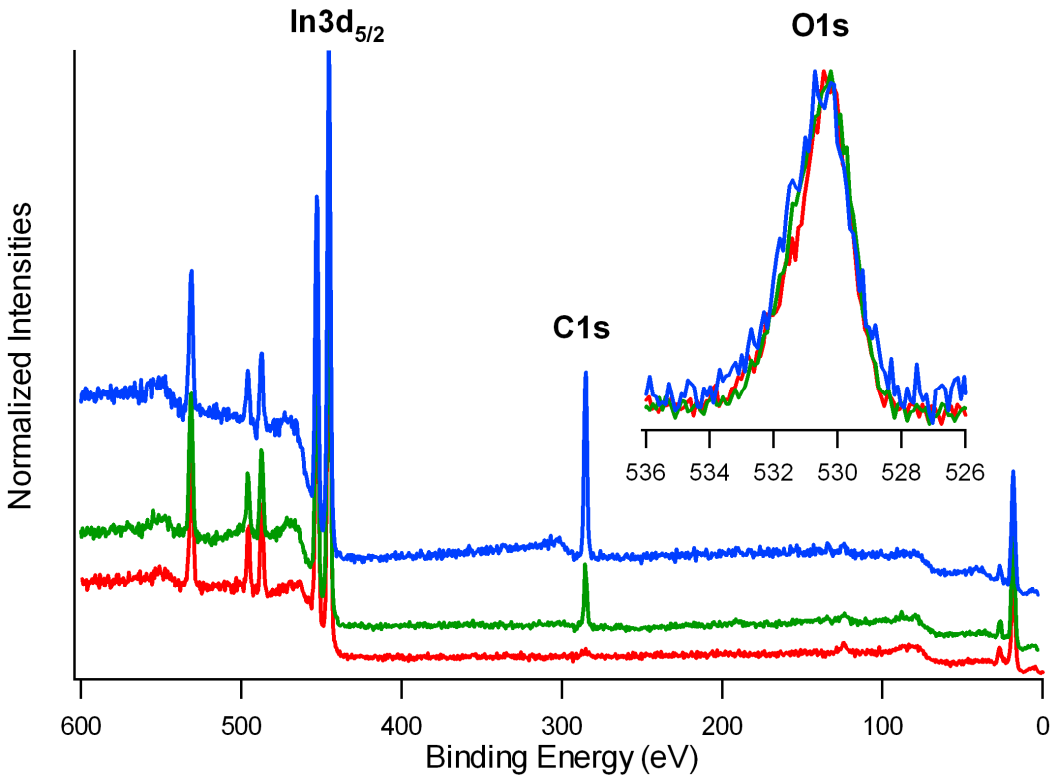

Figure 5.4 XPS survey scans of unmodified ITO nanoparticles (red), OPA–modified nanoparticles (green) and ODPA–modified nanoparticles (blue). The spectra were normalized to the In($3d_{5/2}$) peak of each sample and offset for clarity. High–resolution scans of the O(1s) peak (normalized) for each sample are shown in the inset.

Quantitative XPS results are given in Table 5.1. It can be seen that a signal from phosphorus is present upon modification, and concomitantly the C/In ratio increases significantly, consistent with the addition of alkylphosphonic acids to the nanoparticle surface. In theory, the C/P ratios for nanoparticles modified with OPA or ODPA would be 8/1 or 18/1, respectively, assuming no additional carbon contamination. The C/P ratios obtained for these samples, 11.3 and 30, are relatively consistent with the attachment of OPA and ODPA, respectively. It should be remembered, however, that the alkyl chains should attenuate the phosphorus signal slightly for OPA and more so for ODPA, yielding

ratios higher than would be expected theoretically.

Table 5.1 Detected atomic composition (%) of the different ITO nanoparticle samples.[x]

	% Detected Composition					Ratios		
Sample	In	Sn	O	C	P	O/In	C/In	C/P
Unmodified	36	5.5	49	10	0	1.4	0.3	NA
OPA-modified	24	3.6	35	34	3.0	1.5	1.4	11
ODPA-modified	14	2.3	21	60	2.0	1.5	4.3	30

Unfortunately, due to the rather high absorbance of the ITO nanoparticles across the IR spectrum, it is not possible to determine the binding modes with which the phosphonic acids are binding. However, the TGA results indicate a relatively high degree of coverage, as has been shown for analogous planar substrates of ITO, and the O(1s) peak in the XPS shows a similar change in shape upon binding of OPA or ODPA to the surface.

5.2.3 Modification of Dy_2O_3 (Dysprosium Oxide) Nanoparticles

Dy_2O_3 possesses interesting luminescence properties,[50] and is used in magneto–optical recording materials.[51] No reports have been found in the literature regarding the surface modification of Dy_2O_3, either in nanoparticle or planar form, with phosphonic

[x] Detected atomic composition values have an error of ± 10%. This error also applies for subsequent XPS tables in the chapter.

acids.

SEM images appear to show no change in nanoparticle morphology after surface modification with OPA, though more images need to be seen to verify this (Figure 5.5).

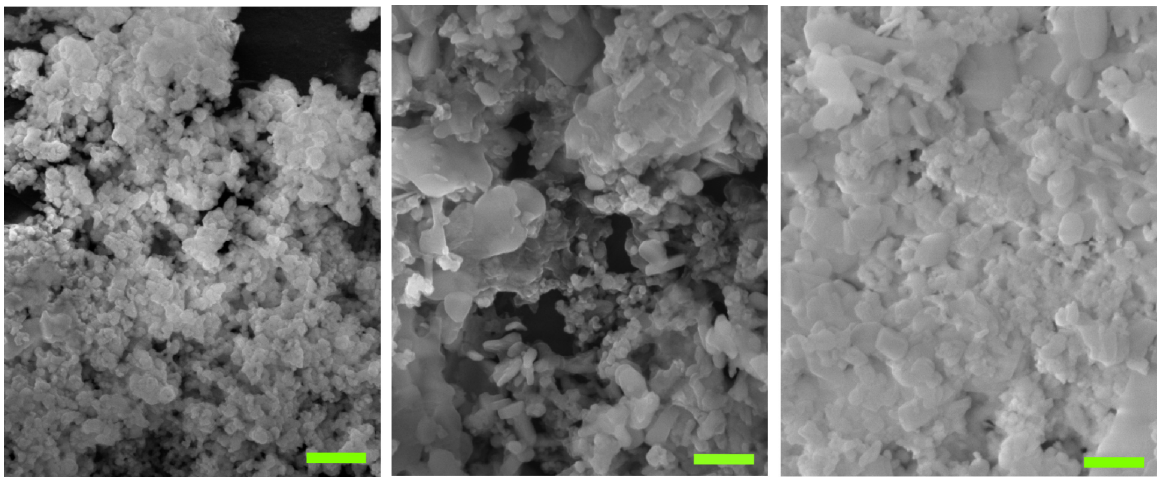

Figure 5.5 SEM images of unmodified (left), OPA–modified (middle), and OPA–modified using mild reaction conditions (right) Dy_2O_3 nanoparticles. Scale bars are equal to 200 nm. (Images taken by P. Kim)

Results from XRD characterization also do not show a difference in the composition of the nanoparticles after modification (Figure 5.6).

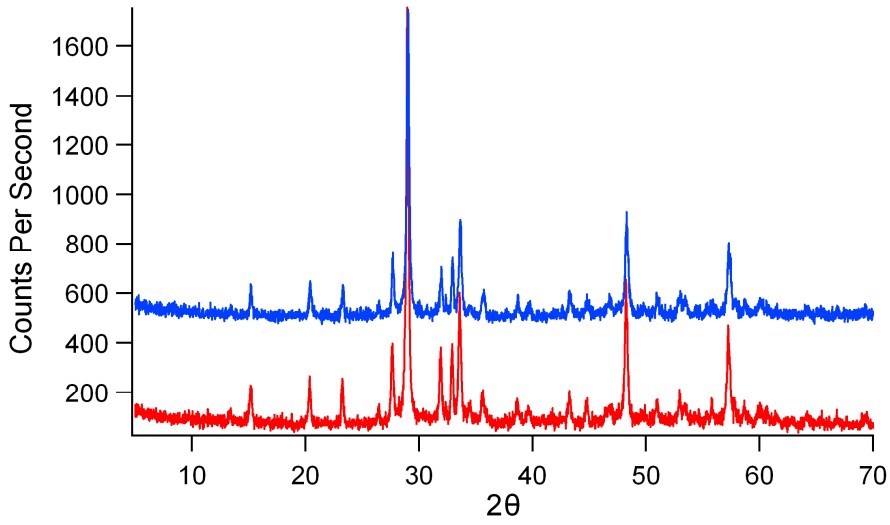

Figure 5.6 XRD patterns of Dy_2O_3 nanoparticles before (red) and after (blue) surface modification with OPA under normal conditions. Patterns are offset for clarity.

FTIR spectra of the different samples show both an apparent decrease in the OH–stretch band upon binding of OPA and ODPA vs. unmodified nanoparticles, and the appearance of C–H stretching modes (Figure 5.7a,b). The fingerprint region shows the disappearance of the P=O band (1230 cm^{-1}) and either the disappearance or shift of the P–O– (H) stretching modes (ν_a(P–O–(H)) at ~1000 cm^{-1} and ν_s(P–O–(H)) at ~950 cm^{-1}). In addition, the C–H bend vibration of the alkyl chain at 1468 cm^{-1} is visible in the modified nanoparticles.

TGA traces show that, while there is a continuous mass loss in the as–received nanoparticles, this is also present the in the surface modified nanoparticles, and is thus considered an inherent thermal property of the nanoparticles (Figure 5.7d). The mass losses in the OPA and ODPA modified nanoparticles are 5.2% and 6.1%, respectively, corresponding to surface coverages of 200% and 140%, respectively, when compared to a

theoretical monolayer. When milder conditions are used for the modification of the nanoparticles with OPA, a mass loss of 1.8% is seen, corresponding to a surface coverage of 69% when compared to a theoretical monolayer. Additionally, the mass loss begins at a higher temperature, implying higher thermal stability and perhaps stronger binding of the OPA to the nanoparticles than to nanoparticles modified under normal conditions. As with ITO, Dy_2O_3 nanoparticle surface coverages were determined by using the surface area of the nanoparticles (20 m^2/g, from the manufacturer).

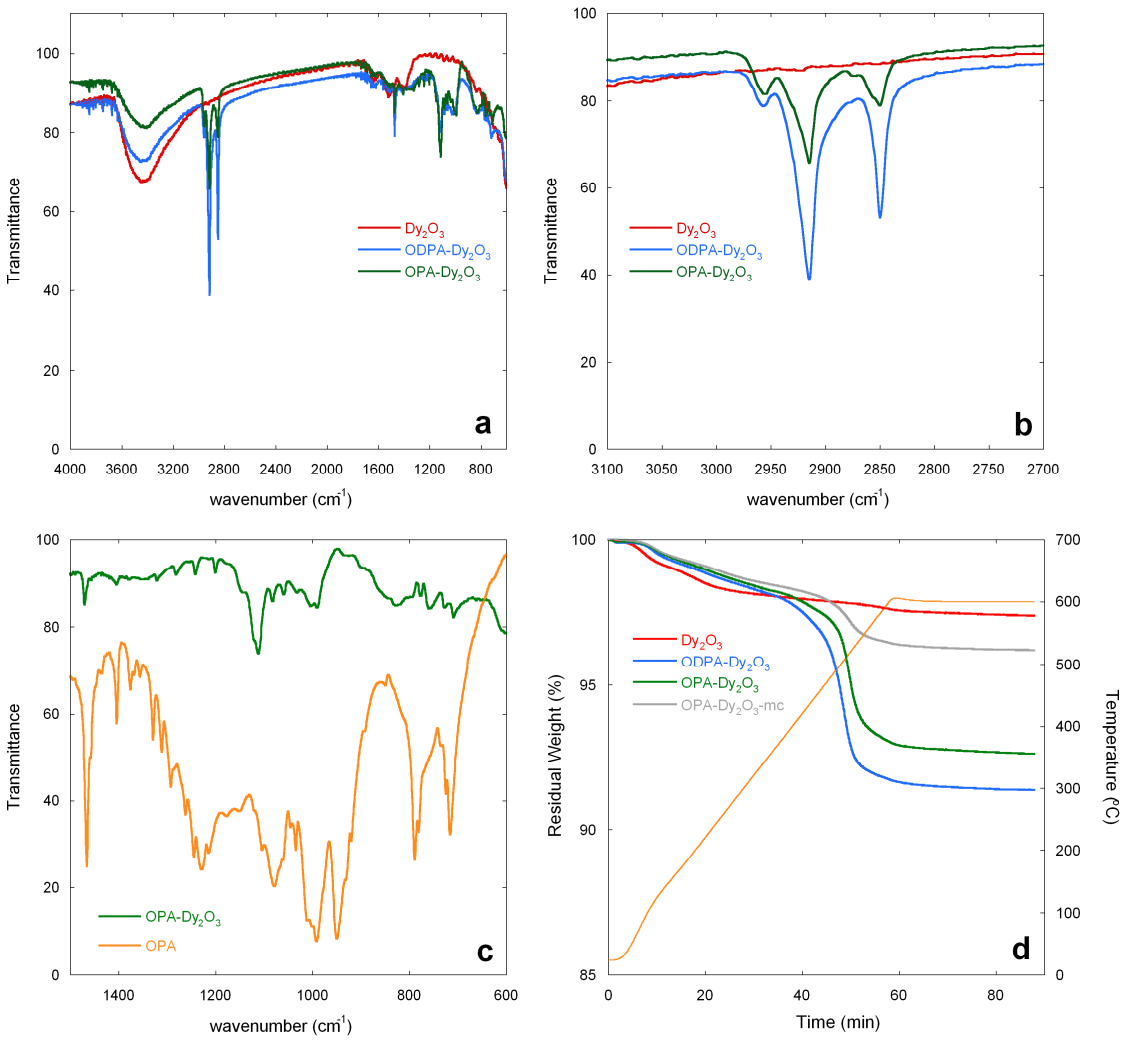

Figure 5.7 a) FTIR spectra of Dy_2O_3 nanoparticles before (red), after reaction with OPA (green), and after reaction with ODPA (blue), b) detail of the C–H stretching region, and c) detail of the fingerprint region of OPA–modified nanoparticles (green) and unbound OPA (orange). d) The TGA traces for each of the nanoparticle species as well as OPA–modified nanoparticles using mild reaction conditions (grey). The orange trace corresponds to the temperature as a function of time. (IR data collected by P. Kim)

XPS survey scans of the various samples indicate that ODPA–modified nanoparticles have the highest carbon content, followed by OPA–modified nanoparticles under normal conditions, and then OPA–modified nanoparticles under mild conditions, as would be expected (Figure 5.8). Unmodified nanoparticles do not show any carbon

content. No changes in the O(1s) peak can be resolved, however, due to the poor signal to noise ratio of the peaks. The phosphonic acid–modified nanoparticles showed charging (resulting in a shift of the binding energies) during analysis, consistent with the addition of an insulating layer, such as alkyl chains, on their surface. As such, all spectra were calibrated to the C(1s) binding energy.

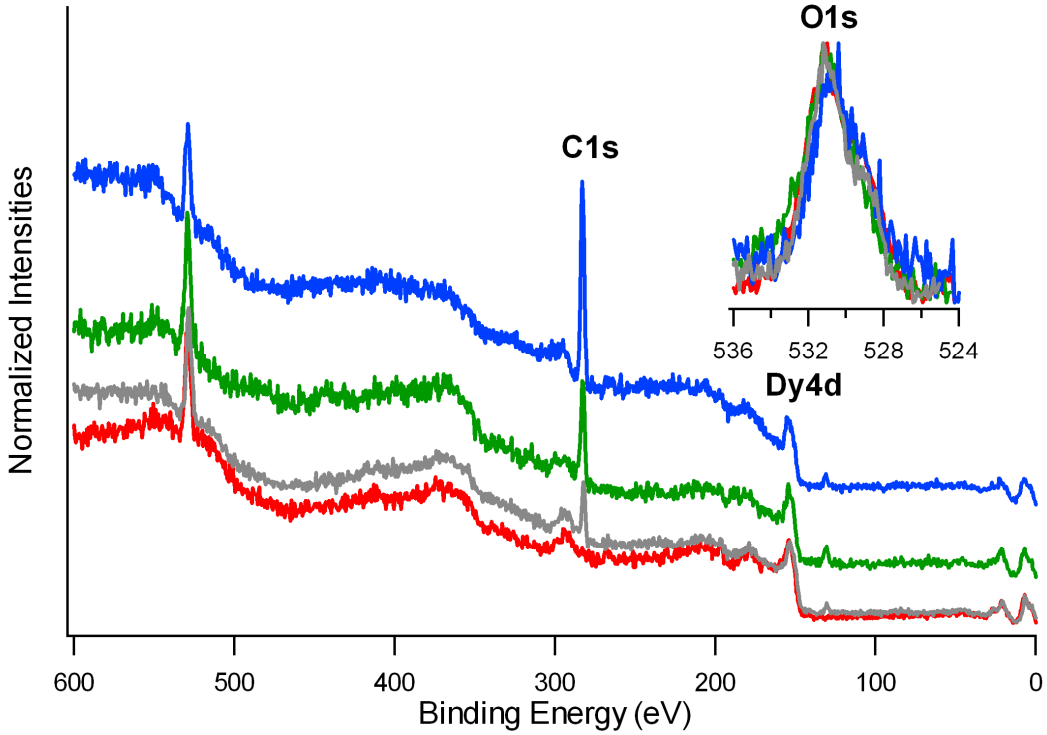

Figure 5.8 XPS survey scans of unmodified Dy_2O_3 nanoparticles (red), OPA–modified nanoparticles under normal (green) and mild (grey) conditions, and ODPA–modified nanoparticles (blue). The spectra were normalized to the Dy(4d) peak of each sample and offset for clarity. High–resolution scans of the O(1s) peak (normalized) for each sample are shown in the inset.

Quantitative XPS results are given in Table 5.2. It can be seen that a signal from phosphorus is present upon modification, as well as a significantly increased C/Dy ratios, consistent with the addition of alkylphosphonic acids to the nanoparticle surface. The C/P

ratios obtained for OPA–modified and ODPA–modified nanoparticles under normal conditions are 8.5 and 37.5, respectively, similar to what was obtained for ITO nanoparticles. The C/P ratio of OPA–modified nanoparticles under mild conditions is 9.8.

Table 5.2 Detected atomic composition (%) of the different Dy_2O_3 nanoparticle samples.

	% Detected Composition				Ratios		
Sample	Dy	O	C	P	C/Dy	O/Dy	C/P
Unmodified	12	88	0	0	0	7.3	NA
OPA-modified	3.8	39	51	6.3	13	9.8	8
OPA-modified (mc)	7.9	49	39	4.0	4.9	6.1	10
ODPA-modified	2.9	20	75	2.4	25	6.7	31

The IR spectra indicate a mixture of binding modes for OPA to Dy_2O_3 nanoparticles. The disappearance of the P=O band as well as the shifts or disappearance of several P–O–H stretches indicate a mixture of binding modes, probably a combinations of all three. TGA indicates a dense coverage of the surface by the phosphonic acid. XPS, while indicating successful surface attachment, did not yield any further information and higher resolution scans are needed.

5.2.4 Modification of HfO_2 (Hafnium Oxide) Nanoparticles

HfO_2 is a high–k dielectric material that has found use in capacitor applications as

well as, potentially, in the replacement of silicon oxide as the gate insulator in field effect transistors.[52] While phosphonic acids have been used to modify planar surfaces of hafnium oxide,[52-54] the modification of HfO_2 nanoparticles has not been reported. Additionally, no studies have been reported on the binding modes of phosphonic acids to hafnium oxide.

SEM images appear to show no change in nanoparticle morphology after surface modification with OPA (Figure 5.9). XRD characterization also does not show a difference in the composition of the nanoparticles after modification (Figure 5.10).

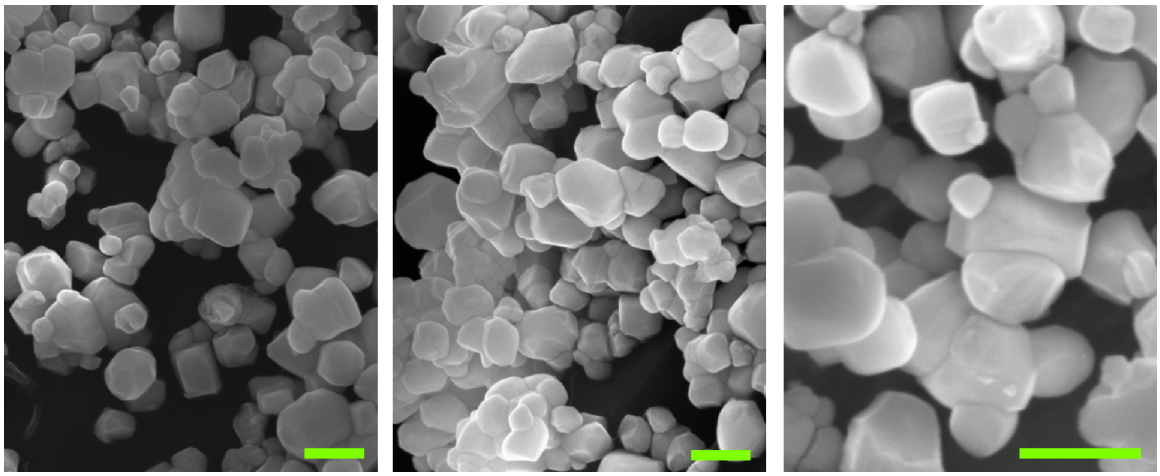

Figure 5.9 SEM images of unmodified (left), OPA–modified (middle), and OPA–modified using forcing reaction conditions (right) HfO_2 nanoparticles. Scale bars are equal to 200 nm. (Images taken by P. Kim)

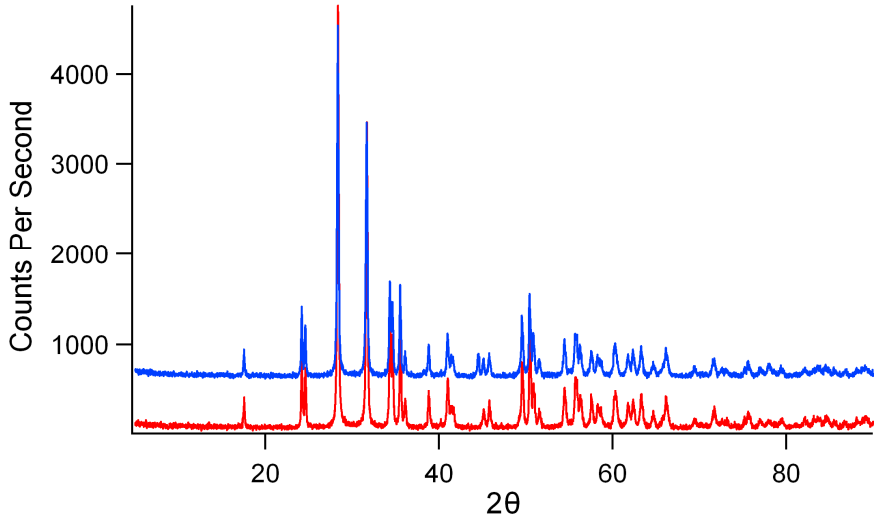

Figure 5.10 XRD patterns of HfO_2 nanoparticles before (red) and after (blue) surface modification with OPA under normal conditions. Patterns are offset for clarity.

TG analysis shows a weight loss in the as-received nanoparticles at around 400 °C (Figure 5.11d). Firing the nanoparticles at 400 °C for 4 hours removed the unknown mass. Fired nanoparticles were subsequently used for all modification experiments. FTIR data show a small O–H stretch vibration present in the fired nanoparticles, whose intensity decreases upon binding of OPA or ODPA (Figure 5.11a). C–H stretching bands are visible, and the absorbance appears larger for the ODPA–modified nanoparticles (Figure 5.11b). Also, there appears to be a small shoulder to the low–energy side of the intense, sharp peak at 800 cm^{-1}, which is consistent with a PO_3^{2-} band (Figure 5.11c). It is difficult to obtain better signal to noise as the nanoparticles are quite large (100 – 200 nm in diameter), thereby resulting in a relatively small signal from the surface–bound phosphonic acids.

OPA and ODPA–modified nanoparticles show mass losses of 0.26% and 0.42%, respectively (Figure 5.11d). This corresponds to a surface coverage of ~ 51% for OPA–

modified nanoparticles, and ~48% for ODPA–modified nanoparticles, relative to a theoretical monolayer (surface area of nanoparticles is 4.8 m^2/g, as measured by BET[y]). Interestingly, the mass loss for OPA–modified nanoparticles prepared under forcing conditions (0.18%) is less than under normal conditions (0.26%), however the TGA curve is substantially less noisy.

[y] BET stands for Brunauer Emmett Teller, the last names of the people who developed the theory of measuring the surface areas of solid surfaces using the adsorption of gas molecules.

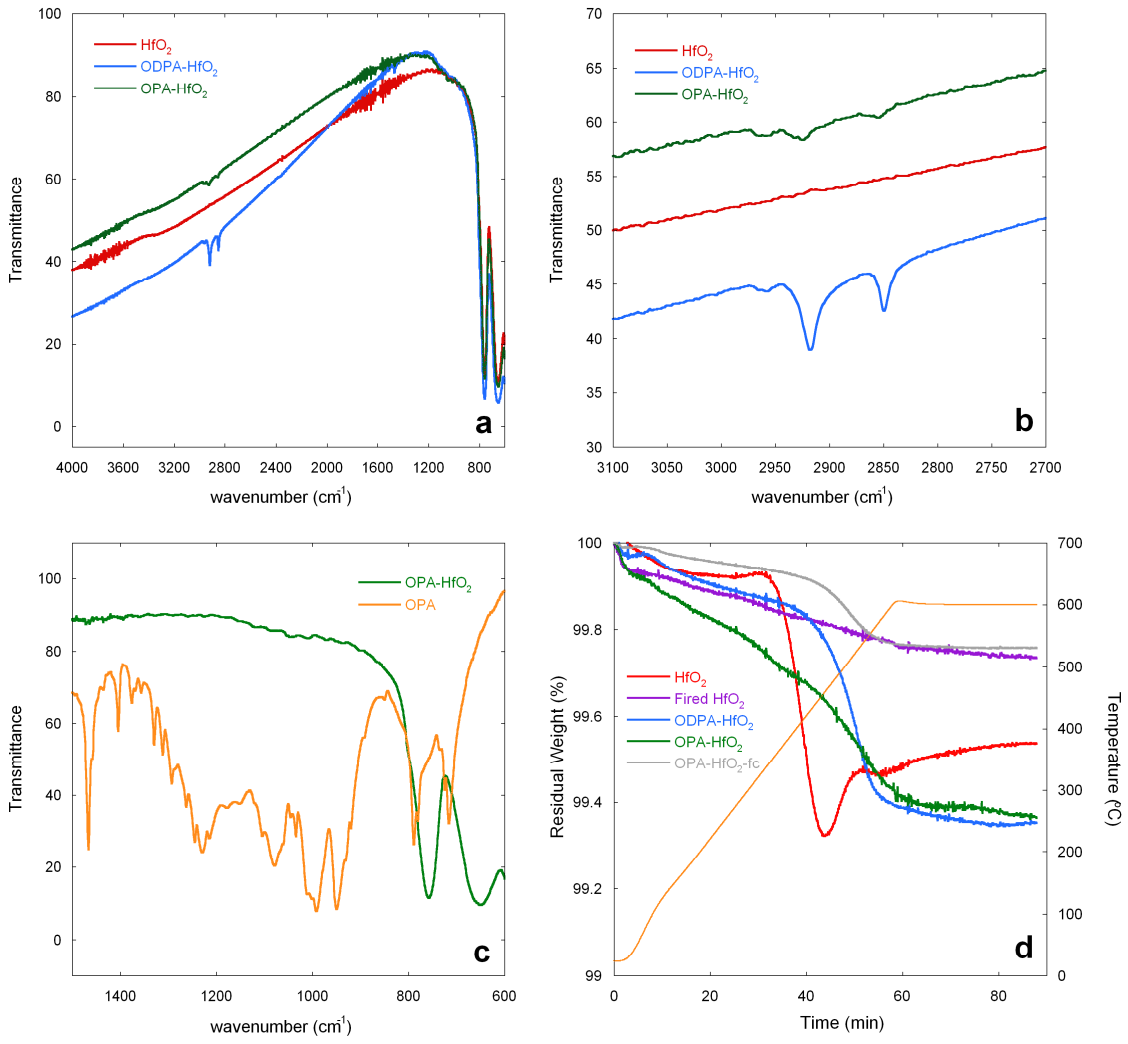

Figure 5.11 a) FTIR spectra of HfO_2 nanoparticles before (red), after reaction with OPA (green), and after reaction with ODPA (blue), b) detail of the C–H stretching region, and c) detail of the fingerprint region of OPA–modified nanoparticles (green) and unbound OPA (orange). d) The TGA traces for as–received nanoparticles (red), fired nanoparticles (purple), OPA–modified under normal (green) and forcing (grey) conditions, and ODPA–modified (blue) nanoparticles. The orange trace corresponds to the temperature as a function of time. (IR data collected by P. Kim)

XPS survey spectra are reported for the unmodified HfO_2 nanoparticles and their modified counterparts in Figure 5.12. The amount of carbon on the surface is greatest for ODPA–modified nanoparticles, as would be expected. The samples modified with OPA also indicate a substantial increase in the carbon content on the surface vs. unmodified

nanoparticles. The O(1s) peaks of the different samples do not show any differences before and after surface modification though this may be due to the fact that the signal originating from the phosphonic acid is small with respect to that due to the O atoms in the underlying HfO_2.

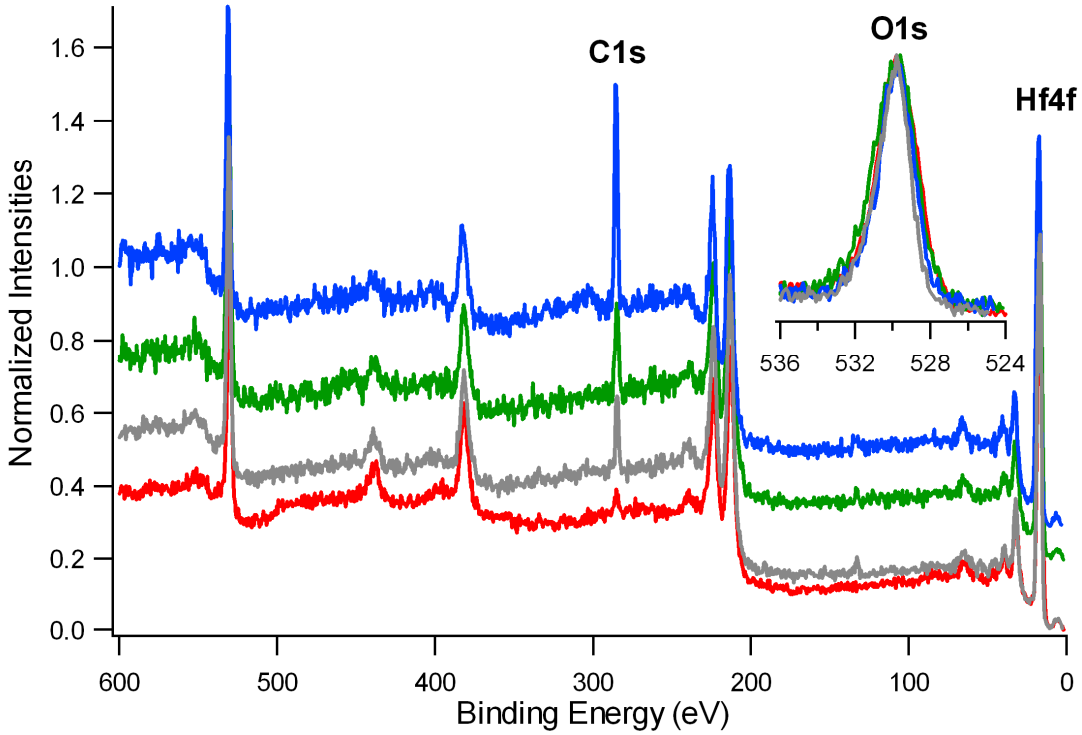

Figure 5.12 XPS survey scans of unmodified HfO_2 nanoparticles (red), OPA–modified nanoparticles under normal (green) and forcing (grey) conditions, and ODPA–modified nanoparticles (blue). The spectra were normalized to the Hf(4f) peak of each sample and offset for clarity. High–resolution scans of the O1s peak (normalized) for each sample are shown in the inset.

Quantitative XPS results are given in Table 5.3. It can be seen that a signal from phosphorus is present upon modification and that the C/Hf ratio increases with increasing length of the alkyl chain of the phosphonic acids attached to the surface. The C/P ratios

obtained for OPA–modified and ODPA–modified nanoparticles under normal conditions are 10.7 and 26, respectively. The C/P ratio of OPA–modified nanoparticles under forcing conditions is 5.8. The ratios are consistent with the expected values.

Table 5.3 Detected atomic composition (%) of the different HfO_2 nanoparticle samples.

	% Detected Composition				Ratios		
Sample	Hf	O	C	P	C/Hf	O/Hf	C/P
Unmodified	26	63	11	0	0.4	2.4	NA
Unmodified (fired)	27	60	13	0	0.5	2.2	NA
OPA-modified	18	47	32	3.0	1.8	2.6	11
OPA-modified (fc)	21	52	23	4.4	1.1	2.5	5
ODPA-modified	14	32	52	2.4	3.7	2.3	22

Due to the relatively large size of the HfO_2 nanoparticles, it is not possible to obtain any binding mode information in the IR due to the weak signal present from the modifier and the attachment interface. TGA indicate a substantial coverage of the nanoparticles. XPS also indicates successful surface modification.

5.2.5 Modification of $NiFe_2O_4$ (Nickel Ferrite) Nanoparticles

$NiFe_2O_4$ nanoparticles are highly ferromagnetic and could thus be used in recording media, as magnets, and as catalysts.[55] While the modification of $NiFe_2O_4$ with phosphonic acids has not been reported, the modification of the similar $CoFe_2O_4$

nanoparticles has been reported.[27] The authors attached alkylphosphonic acids with both terminal CH_3 or OH groups to the nanoparticles. IR analysis indicated a large amount of tridentate species as evidenced by the presence of a broad PO_3^{2-} bond. Additionally, there are a number of reports of the modification of Fe_2O_3 nanoparticles with phosphonic acids.[19-23]

SEM images appear to show no change in nanoparticle morphology after surface modification with OPA (Figure 5.13).

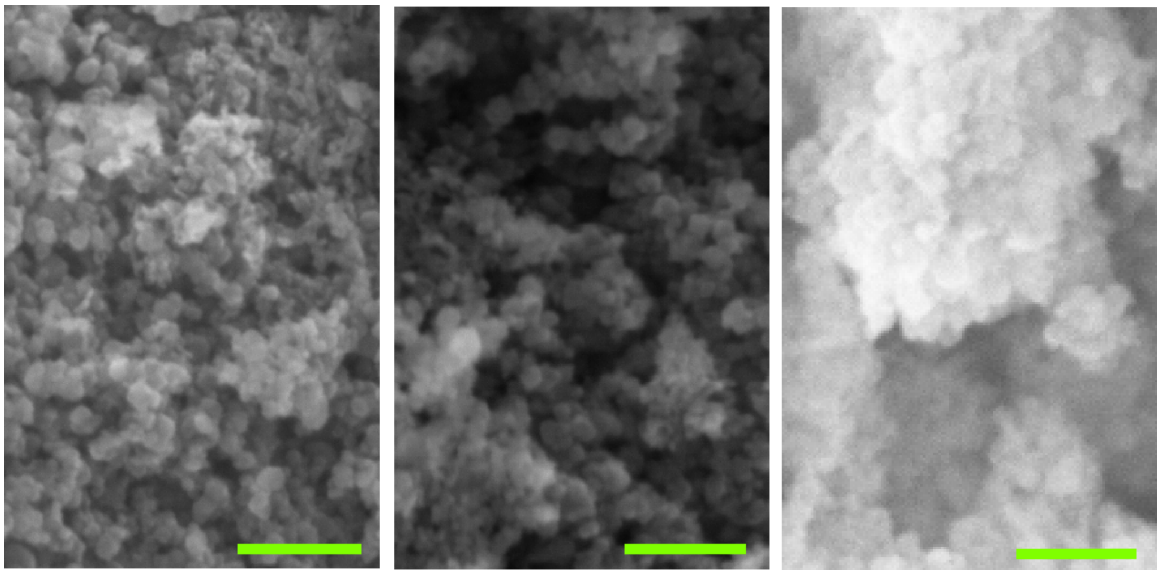

Figure 5.13 SEM images of unmodified (left), OPA–modified (middle), and OPA–modified using mild reaction conditions (right) $NiFe_2O_4$ nanoparticles. Scale bars are equal to 100 nm. (Images taken by P. Kim)

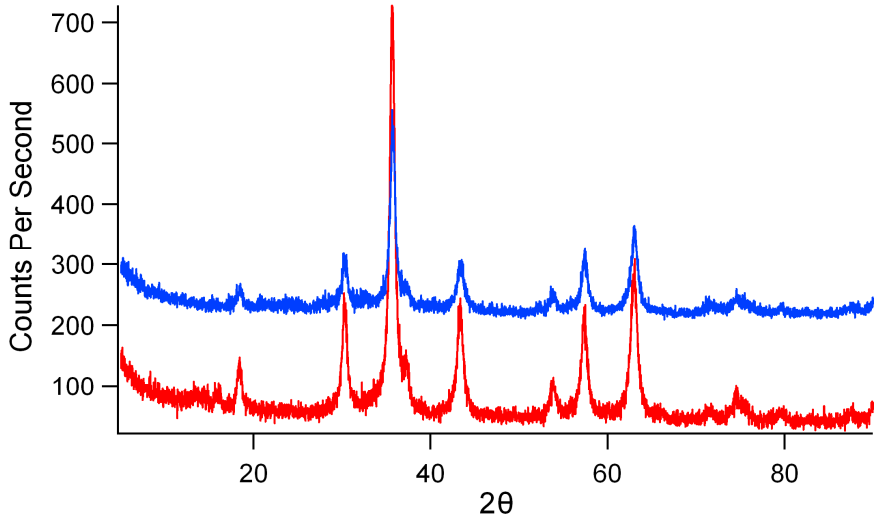

Figure 5.14 XRD patterns of $NiFe_2O_4$ nanoparticles before (red) and after (blue) surface modification with OPA under normal conditions. Patterns are offset for clarity.

FTIR spectra were recorded for nanoparticles before and after modification with OPA (Figure 5.15). Unmodified nanoparticles show a broad peak ~3400 cm^{-1}, indicative of surface hydroxyl groups (Figure 5.15a). After modification with OPA, the hydroxyl band is less intense, and clear C–H stretching bands can be seen in the region from 3000 –2800 cm^{-1} (Figure 5.15a,b). A peak at 1467 cm^{-1}, resulting from C–H bending vibrations in alkanes, as well as two overlapping broad absorptions at ~1030 cm^{-1}, indicative of a tridentate attachment (νPO_3^{2-}) of OPA to the surface, can be seen (Figure 5.15c). It is worth noting that all other P=O and P–O–H modes of OPA can no longer be seen in the spectrum after attachment to the $NiFe_2O_4$ nanoparticles.

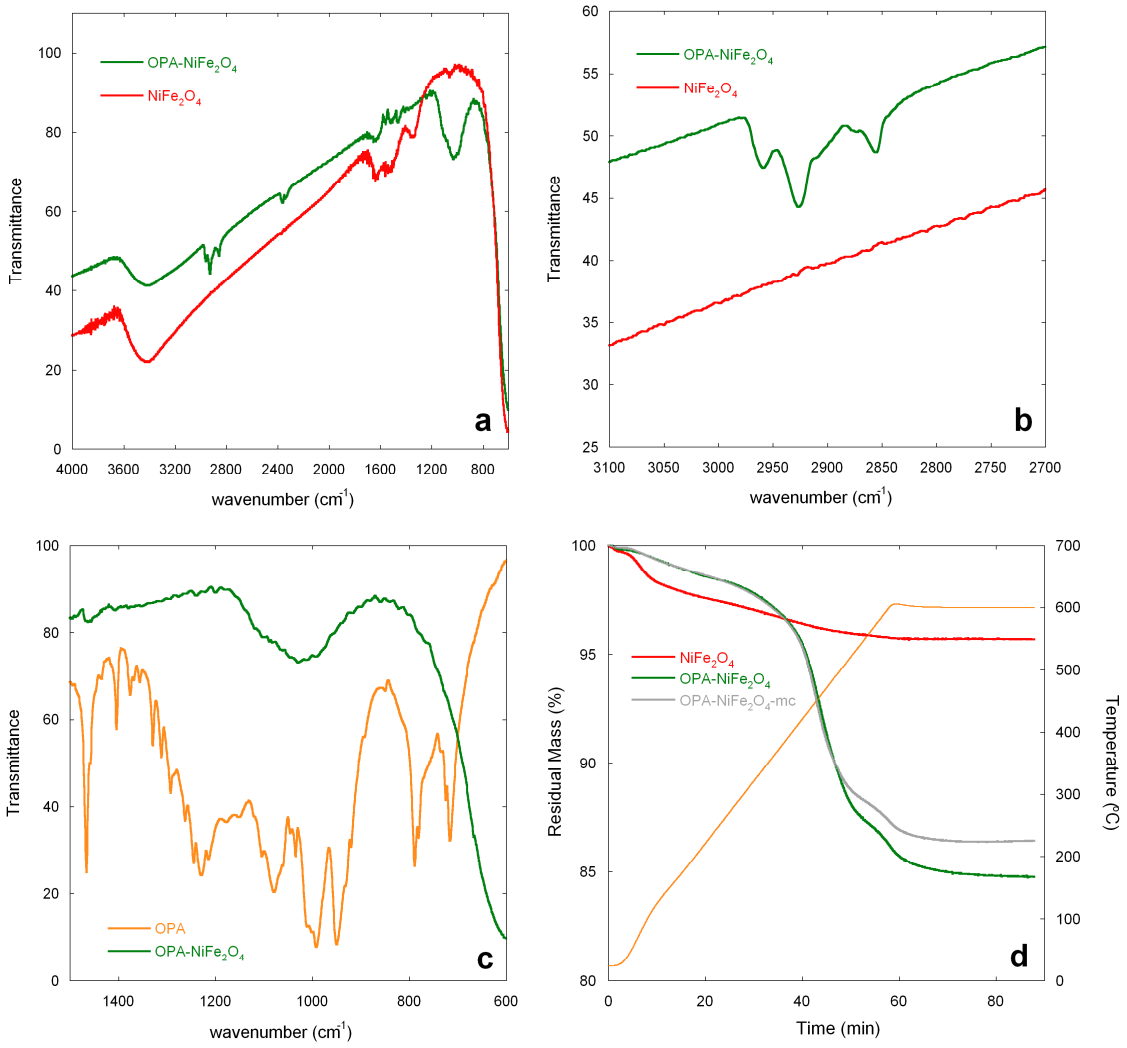

Figure 5.15 a) IR spectra of $NiFe_2O_4$ nanoparticles before (red), after modification with OPA (green), b) the C–H stretching region, and c) the fingerprint region of OPA–modified nanoparticles (green) and unbound OPA (orange). d) The TGA traces for unmodified nanoparticles (red), and nanoparticles modified with OPA under normal (green) and mild (grey) reaction conditions. The orange trace corresponds to the temperature as a function of time. (IR data collected by P. Kim)

TGA traces of OPA–modified nanoparticles under normal and mild conditions show mass losses of 12% and 11%, respectively, corresponding to surface coverages of 170% (normal conditions) and 140% (mild conditions) when compared to a theoretical

monolayer. Interestingly, two distinct mass losses can be seen in the traces for the modified nanoparticles, possibly due to phosphonic acids bound in two different ways. The mass losses are similar to those seen for the modification of $BaTiO_3$ nanoparticles with OPA. Except for the total mass loss, the curves for the nanoparticles modified under normal and mild conditions follow the same course.

XPS spectra of the unmodified and OPA-modified nanoparticles are shown in Figure 5.16. The C(1s) increases substantially after surface modification. The O(1s) appears to narrow slightly after modification, but this is not indicative, specifically, of any surface bound species.

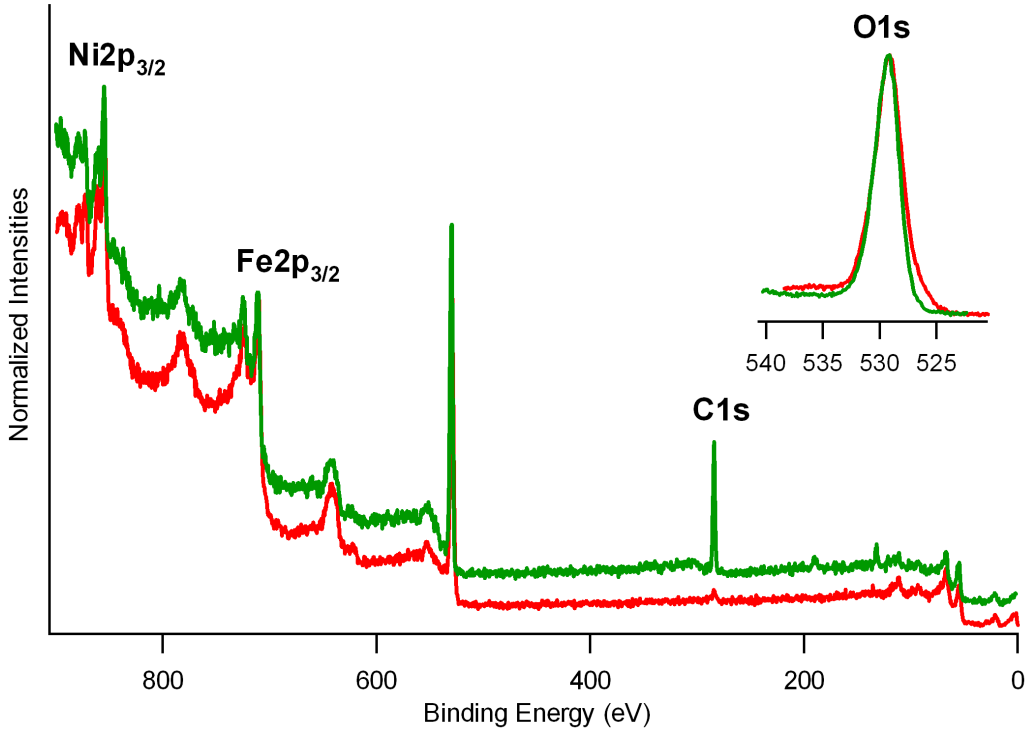

Figure 5.16 XPS survey scans of unmodified $NiFe_2O_4$ nanoparticles (red) and OPA–modified nanoparticles (green). The spectra were normalized to the Ni($2p_{3/2}$) peak of each sample and offset for clarity. High–resolution scans of the O(1s) peak (normalized) for each sample are shown in the inset.

Quantitative XPS results are given in Table 5.4. While very little carbon is detected on the surface of unmodified nanoparticles, this increases greatly upon modification with OPA, resulting in a 9-fold increase in the C/Fe ratio. Additionally, the C/P ratio of 7 is consistent with the attachment of OPA to the surface.

Table 5.4 Detected atomic composition (%) of the different $NiFe_2O_4$ nanoparticle samples.

	% Detected Composition					Ratios		
Sample	Ni	Fe	O	C	P	O/Fe	C/Fe	C/P
Unmodified	10	13	71	6.8	0	5.5	0.5	NA
OPA-modified	4.8	7.7	48	35	4.7	6.0	4.4	7

The IR data clearly indicate a predominately tridentate binding of OPA to $NiFe_2O_4$ nanoparticles. TGA and XPS results also indicate a dense coverage of bound phosphonic acid on the surface. The TGA does show two distinct changes in slope during weight loss, indicative of perhaps phosphonic acid bound in two different ways to the surface.

5.2.6 Modification of ZnO (Zinc Oxide) Nanoparticles

ZnO nanoparticles are used in dental cements[56] and as flame retardants,[57] to name a few of their applications. The modification of ZnO nanoparticles with phosphonic acids has been reported in the literature.[15-18] Of the reported studies, two present evidence for a mainly tridentate binding of phosphonic acids to zinc oxide nanoparticles.[15, 18] Wei *et al.*

have reported the modification of Co/ZnO core/shell nanoparticles with bisphosphonic acids for use in nanocomposite capacitors.[15] They identified a mainly tridentate linkage of the phosphonic acids to the ZnO surface, as evidenced by FTIR spectroscopy. Liu *et al.* also report a tridentate linkage of phosphonic acids to zinc oxide.[18] The authors modified ZnO tetrapods with alkylphosphonic acids and studied them with FTIR. They note the appearance of a broad peak at 1071 cm^{-1}, indicative of a PO_3^{2-} band and therefore tridentate linkage of the phosphonic acid to the surface. They suggest that both or either a chelating and/or bridging tridentate binding mode could be present, as well as small amounts of bidentate binding.

SEM images indicate that the structure of the nanoparticles does not change after modification with OPA (Figure 5.17). This is an important result as it is known that acidic conditions can etch the zinc oxide surface.[58]

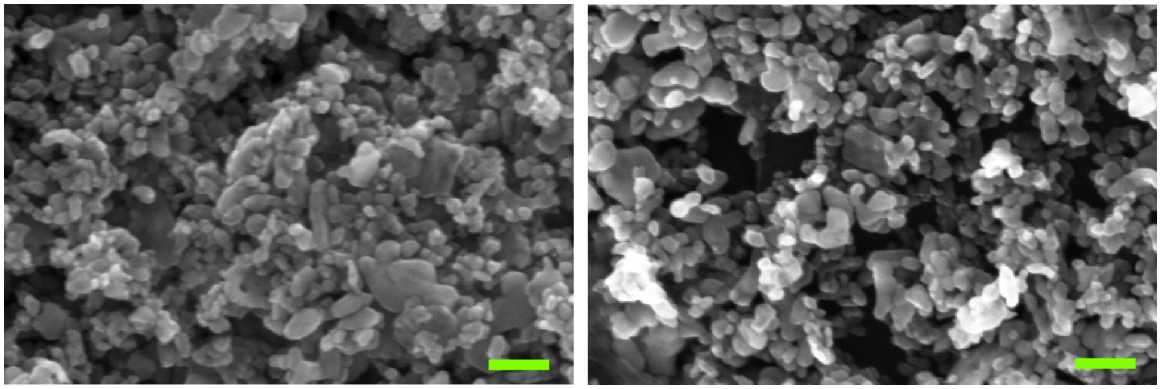

Figure 5.17 SEM images of unmodified (left) and OPA–modified (right) ZnO nanoparticles. Scale bars are equal to 100 nm. (Images taken by P. Kim)

XRD patterns indicate that, although the same composition of ZnO is present after modification, two new peaks at low angle appear (Figure 5.18). These could be indicative

of either excess organic species or perhaps formation of a zinc phosphate gel, however, nothing in the XRD pattern database (Jade) matched the peaks on initial comparison.

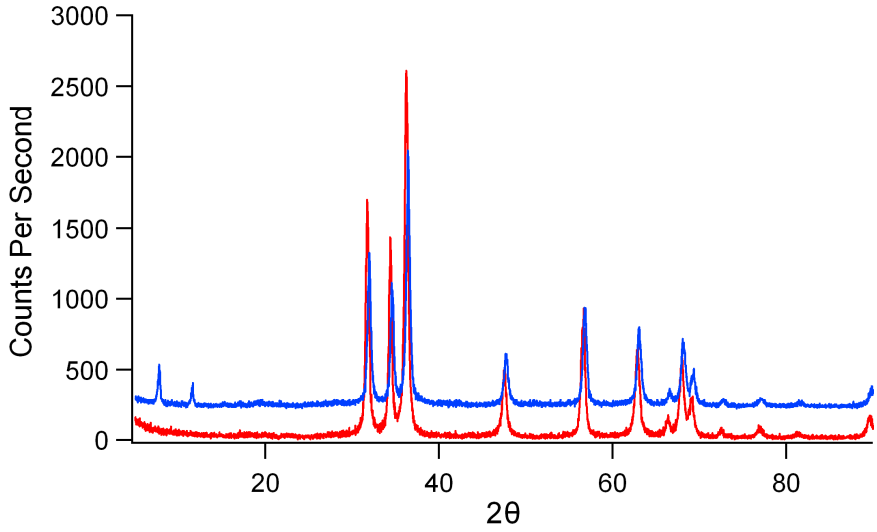

Figure 5.18 XRD patterns of ZnO nanoparticles before (red) and after (blue) surface modification with OPA under normal conditions. Patterns are offset for clarity.

TGA data were also collected on the different samples (Figure 5.19d). Unmodified ZnO nanoparticles show a mass loss at ~250 °C, indicating some sort of loosely bound organic on the surface. After firing the nanoparticles at 300 °C for 6 hours, the mass loss disappears. Hence fired ZnO nanoparticles were used for modification with OPA and ODPA. OPA–modified and ODPA–modified nanoparticles show mass losses of 7.5% and 20.1%, respectively. Interestingly, the onset of the mass loss occurs ~100 °C lower in nanoparticles modified with ODPA versus OPA, perhaps indicating more physisorbed ligand on the surface in the OPDA case. These mass losses correspond to surface coverages of approximately 170% (for OPA) and 270% (for ODPA).

FTIR spectra were measured for the nanoparticle samples and display some interesting traits. First, the O–H stretching band, which is located at ~3500 cm^{-1} in the

unmodified nanoparticles, increases substantially in the OPA–modified nanoparticles, but almost completely disappears in ODPA–modified nanoparticles (Figure 5.19a). The sp^3 C–H stretching modes are more intense in the ODPA–modified nanoparticles, as would be expected due to the longer chain–length (Figure 5.19b). The fingerprint region of the spectra is also interesting. In both samples, the band due to the P=O stretch of the OPA (~1230 cm^{-1}) disappears. The OPA–modified nanoparticles display strong absorptions at 1080 and ~1000 cm^{-1}, which are also present in the free acid (Figure 5.19c). The two peaks at 1002 and 972 cm^{-1} are consistent with ν(P–O–H) bands. However, the peak ~1250 cm^{-1} that is also associated with P-O-(H) stretching has disappeared in the OPA-modified nanoparticles. These data indicate a predominately monodentate/bidentate binding of OPA to ZnO. The spectrum of the ODPA–modified ZnO nanoparticles also shows the same bands in the fingerprint region, but they are less intense, perhaps indicative of more bi– or tridentate binding on the surface.

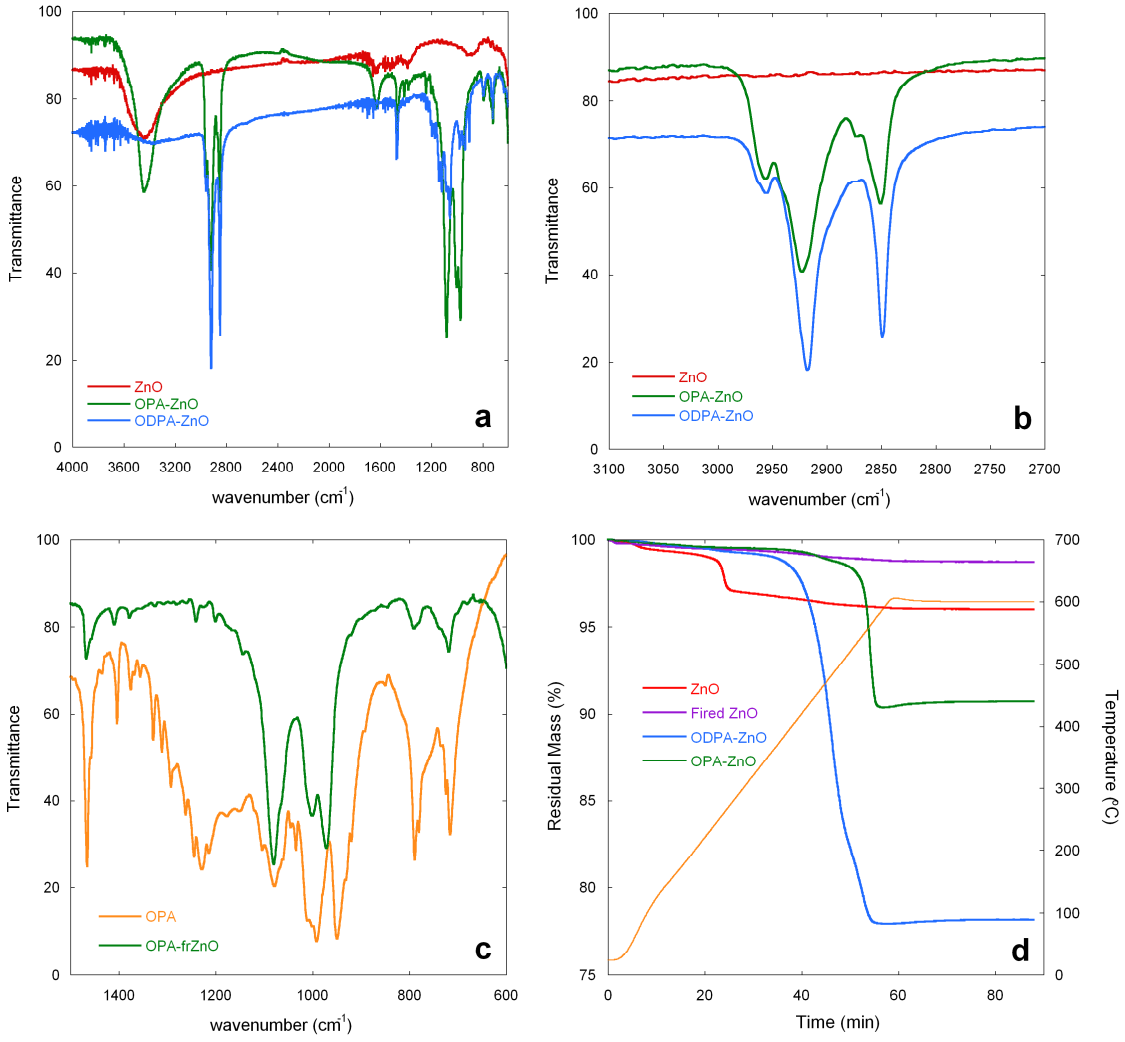

Figure 5.19 a) IR spectra of ZnO nanoparticles before (red) and after modification with OPA (green) and ODPA (blue), b) detail of the C–H stretching region, and c) detail of the fingerprint region of OPA–modified nanoparticles and unbound OPA (orange). d) TGA traces for each of the nanoparticle species. The orange trace corresponds to the temperature as a function of time. (IR data collected by P. Kim)

XPS spectra show a distinct increase in carbon on the surface after OPA– and ODPA–modification of the nanoparticles, as well as a change in the O(1s) peak shape (Figure 5.20). The O(1s) peak of ZnO appears as a combination of a large peak at ~530 eV (corresponding to bulk Zn–O) with a smaller peak at ~531.5 eV (corresponding to surface hydroxyl groups). The hydroxyl–associated peak decreases after modification and

a new peak appears at ~530.8 eV, consistent with the formation of P–O–M bonds (Figure 5.15 inset).[59]

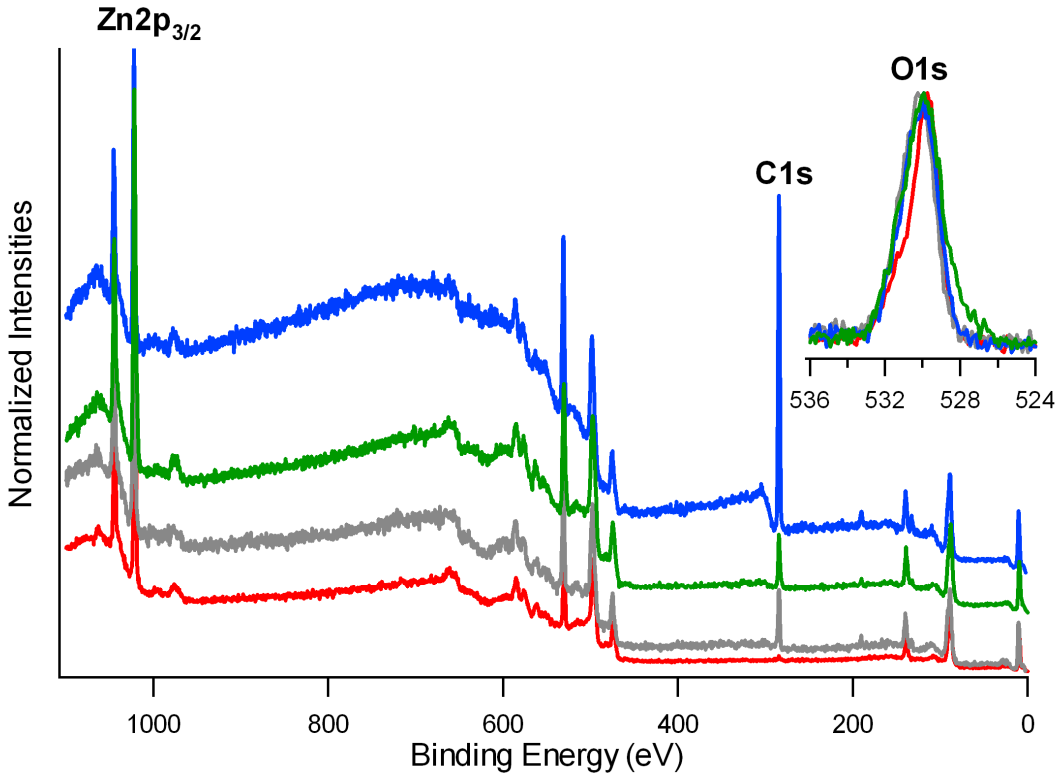

Figure 5.20 XPS survey scans of unmodified ZnO nanoparticles (red), OPA–modified nanoparticles under normal (green) and mild (grey) conditions, and ODPA-modified nanoparticles (blue). The spectra are normalized to the Zn($2p_{3/2}$) peak of each sample and offset for clarity. High–resolution scans of the O(1s) peak for each sample are shown in the inset.

Quantitative XPS results are given in Table 5.5. Signals from phosphorus can be detected after modification, and an increase in C/Zn ratios is observed, consistent with the addition of alkylphosphonic acids to the nanoparticle surface. The C/P ratios obtained for the various phosphonic acid treatments are similar to those obtained with different nanoparticles presented herein.

Table 5.5 Detected atomic composition (%) of the different ZnO nanoparticle samples.

	% Detected Composition				Ratios		
Sample	Zn	O	C	P	C/Zn	O/Zn	C/P
Unmodified	54	41	5.6	0	0.1	0.8	NA
Unmodified (fired)	57	41	2.6	0	0.1	0.7	NA
OPA-modified	29	38	30	3.0	1.0	1.3	10
OPA-modified (mc)	28	33	36	3.3	1.3	1.2	11
ODPA-modified	7.7	17	73	2.7	9.1	2.1	27

While the TGA data indicates an excess of ligand on the nanoparticle surface, especially for ODPA–modified nanoparticles, the FTIR data does not indicate any excess ligand as the P=O band is absent from the spectra of modified nanoparticles. However, hydrogen bonding of the phosphoryl group may shift the band to lower frequency. As such, it is unclear at this point which binding modes are present and how these compare with previous literature reports. Additionally, it is unclear as to why the onset of weight loss of the ODPA–modified ZnO is at considerably lower temperature vs. that of OPA–modified ZnO. Further studies need to be carried out to answer some of these questions.

5.2.7 Modification of CuO (Copper Oxide) Nanoparticles

While CuO has been used in pigments and some other applications,[60] copper, which has a native oxide on its surface, is often used in electrical conduction applications,[61] in pipes, and as a constituent in a number of metal alloys. Therefore,

studying the binding of phosphonic acids to copper oxide is relevant to copper materials as well. While the interaction of phosphonic acids with alloys including copper has been reported,[62] no studies have been found that describe the binding of phosphonic acids to copper–containing nanoparticles.

SEM images of copper oxide nanoparticles were recorded before and after surface modification (Figure 5.21). These images indicate the presence of a large amount of aggregation of the particles, and, perhaps, and increase in aggregation after surface modification, however more images need to be analyzed to verify this.

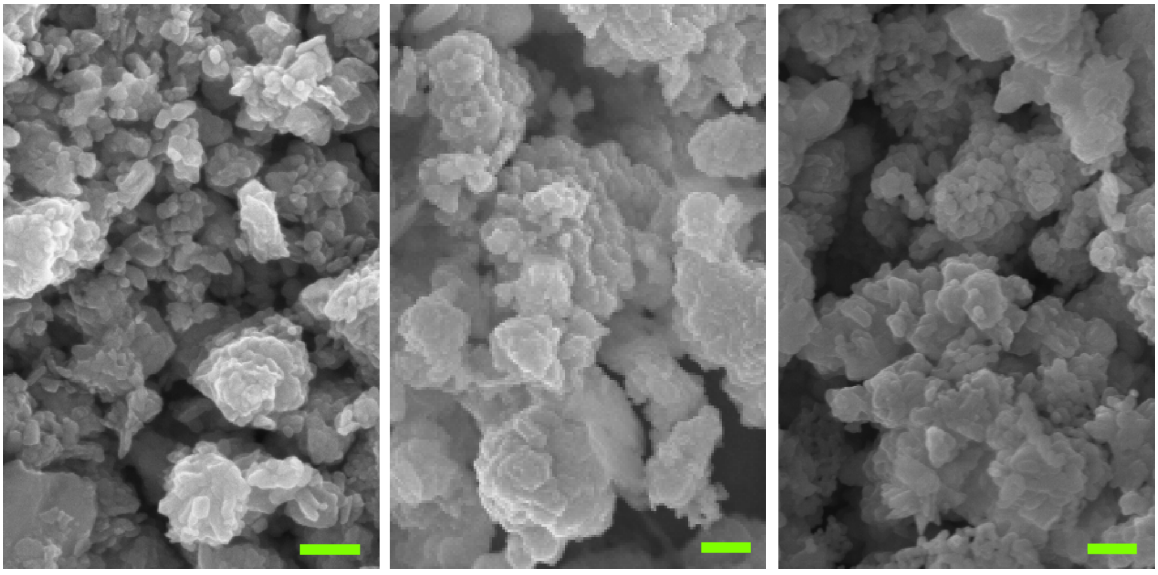

Figure 5.21 SEM images of unmodified (left), OPA–modified (middle), and OPA–modified using mild reaction conditions (right) CuO nanoparticles. Scale bars are equal to 200 nm. (Images taken by P. Kim)

XRD patterns did not show any difference in composition of the CuO nanoparticles after surface modification with OPA.

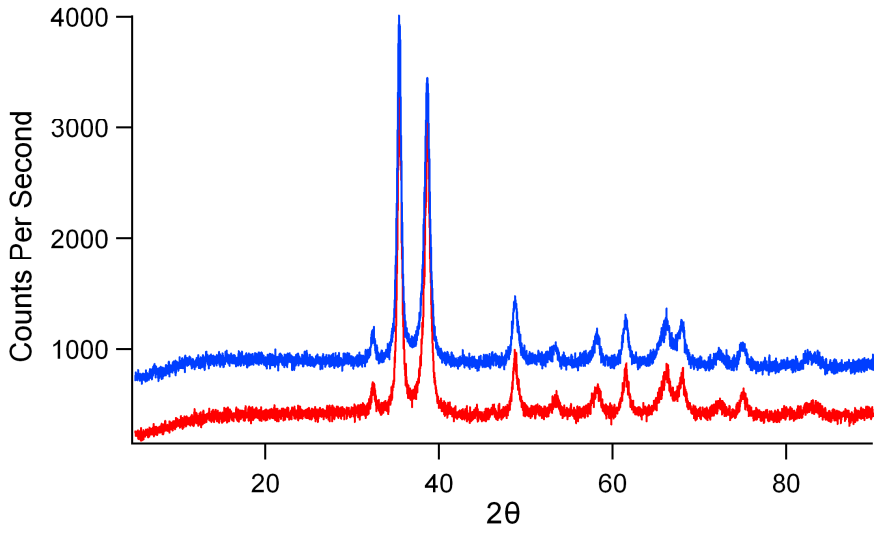

Figure 5.22 XRD patterns of CuO nanoparticles before (red) and after (blue) surface modification with OPA under normal conditions. Patterns are offset for clarity.

The FTIR and TGA data are reported in Figure 5.23, but are contradictory. FTIR data suggest very little, if any, modification by OPA, as evidenced by extremely weak C–H stretching bands as well as very weak P–O–(M or H) bands at lower frequency (Figure 5.23a,b). TGA data, however, suggests the opposite: Large mass losses can be seen for OPA–modified nanoparticles using both normal and mild reaction conditions (Figure 5.23c).

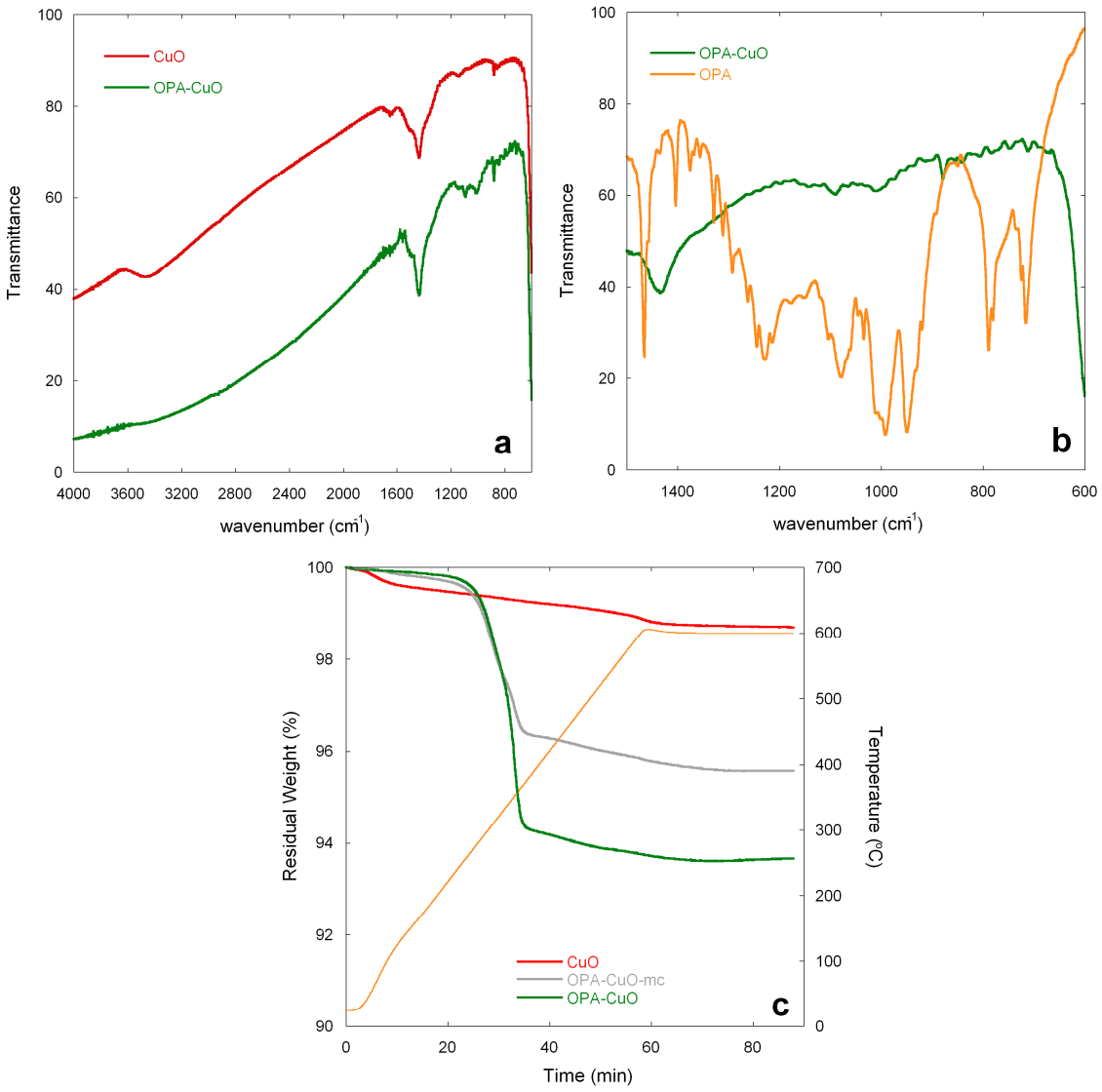

Figure 5.23 a) FTIR spectra of CuO nanoparticles before (red) and after modification with OPA (green), b) detail of the fingerprint region of OPA–modified nanoparticles (green) and unbound OPA (orange). c) TGA traces for each of the nanoparticle species including OPA-modified nanoparticles using mild reaction conditions (grey). The orange trace corresponds to the temperature as a function of time. (IR data collected by P. Kim)

XPS spectra of the different nanoparticle samples show a large increase in the carbon content on the nanoparticles upon OPA–modification, as well as a change in the O(1s) peak (Figure 5.24). The O(1s) peak changes are similar to those seen for

phosphonic acid–modified ZnO nanoparticles; that is, the surface hydroxyl peak ~531.5 eV decreases upon modification while a new peak appears on the high binding energy side of the main peak.

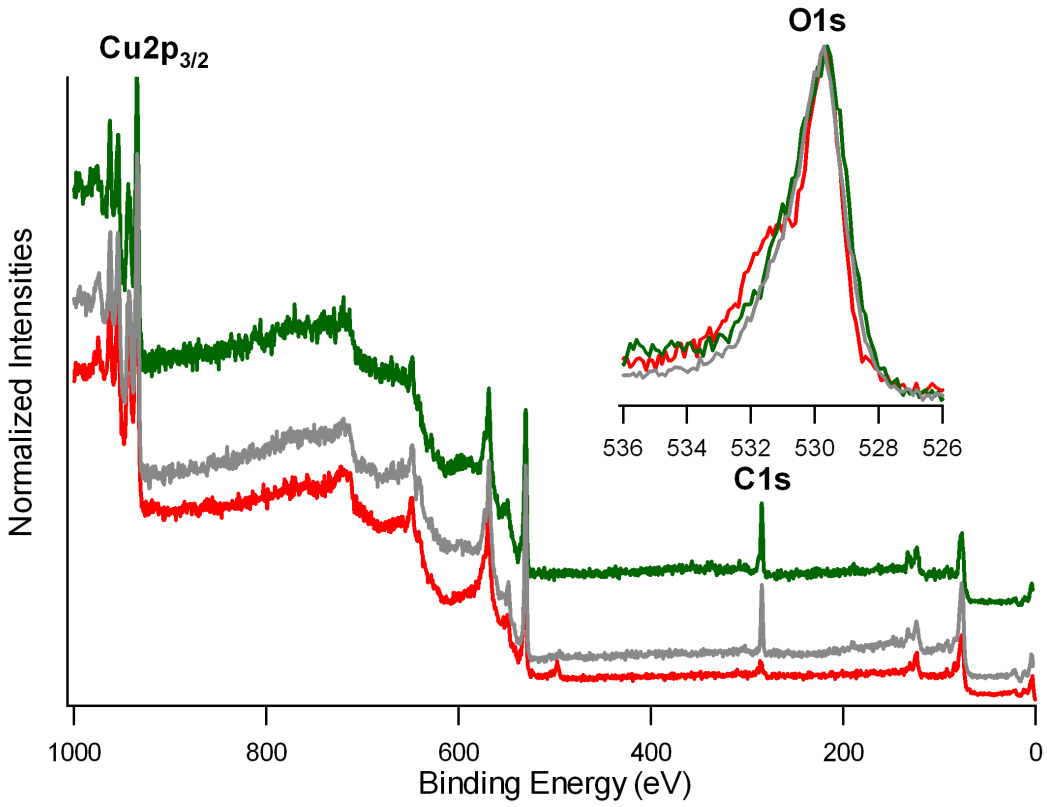

Figure 5.24 XPS survey scans of unmodified CuO nanoparticles (red) and the same nanoparticles modified with OPA under normal (green) and mild (grey) conditions. The spectra were normalized to the Cu($2p_{3/2}$) peak of each sample and offset for clarity. High–resolution scans of the O(1s) peak for each sample are shown in the inset.

Quantitative XPS results are given in Table 5.6 and indicate the presence of phosphorus on the surface after modification, as well as an increase in the C/Cu ratios. The C/P ratios obtained for OPA–modified nanoparticles under normal and mild reaction conditions are 7.4 and 11, respectively, consistent with the theoretical value (8).

Table 5.6 Detected atomic composition (%) of the different CuO nanoparticle samples.

	% Detected Composition				Ratios		
Sample	Cu	O	C	P	C/Cu	O/Cu	C/P
Unmodified	28	53	18	0	0.6	1.9	NA
OPA-modified	18	40	37	5.1	2.1	2.2	7
OPA-modified (mc)	20	44	33	3.3	1.7	2.2	10

It is difficult at this time to make any conclusions about these data. While it may be that the lack of pronounced C-H stretching in the IR is due to a large absorbance of the nanoparticles in that region, TGA and XPS data suggest a significant amount of bound phosphonic acid. The results are not self-consistent and the experiments should be repeated to ensure their validity.

5.2.8 Comparison of Different Modified Metal Oxide Nanoparticles

The different modified nanoparticles can be compared to one–another, in order to obtain a general idea as to the ability of phosphonic acids to bind to them.

TGA results (Table 5.7) show that more than a theoretical monolayer is obtained for many of the metal oxides. While many of the modified nanoparticles, such as that for ODPA–modified ZnO nanoparticles and OPA– and ODPA–modified CuO nanoparticles, showed mass-losses higher than expected from TG analysis, the coverages in the other cases are within reason. Surface areas of the nanoparticles were determined by BET

measurements (most are from the manufacturer). For more accurate surface coverages, BET surface area measurements should be performed ourselves on all the nanoparticles as the surface areas could vary a significant amount from batch to batch, and the manufacturers do not measure the surface areas for each batch.

Table 5.7 Summary of TGA data for each of the PA–modified nanoparticle samples. Surface areas for ZnO, $NiFe_2O_4$, ITO, Dy_2O_3, and CuO nanoparticles were obtained from the vendors.[z] The surface area for HfO_2 nanoparticles was calculated using BET analysis. (mc) and (fc) stand for mild reaction conditions and forcing reaction conditions, respectively. All other samples were reacted under normal conditions.

Sample	Surface Area (m^2/g)	Weight Loss (%)	Theoretical Loss (%)	% of Theoretical
OPA - ZnO	35	7.5	4.5	170
ODPA - ZnO	35	20.1	7.5	270
OPA - $NiFe_2O_4$	59	12.1	7.3	170
OPA - $NiFe_2O_4$ (mc)	59	10.5	7.3	140
OPA - ITO	23	2.1	2.9	72
ODPA - ITO	23	4.6	4.9	94
OPA - Dy_2O_3	20	5.2	2.6	200
OPA - Dy_2O_3 (mc)	20	1.8	2.6	69
ODPA - Dy_2O_3	20	6.1	4.4	140
OPA - HfO_2	3.8	0.26	0.51	51
OPA - HfO_2 (fc)	3.8	0.18	0.51	35
ODPA - HfO_2	3.8	0.42	0.88	48
OPA - CuO	14	6.2	1.7	360
OPA - CuO (mc)	14	4.0	1.7	230

The FTIR spectra (combined in Figure 5.25) indicate that all of the modified nanoparticles display sp^3 C–H stretching bands at similar frequencies to those for the free, unbound OPA. Analysis of the fingerprint region shows that the ν(P=O) band at 1230 cm^{-1} is not present in any of the OPA–modified nanoparticles. This implies that, at

[z] The vendors used BET analysis to determine surface areas.

the very least, OPA is bound in a monodentate fashion in each of the samples. OPA appears to bind to $NiFe_2O_4$ nanoparticles in a mostly tridentate fashion, while its binding to Dy_2O_3, ZnO, and CuO nanoparticles appears to occur through a combination of multiple binding modes. Due to either strong absorption or low signal, we were not able to determine the binding modes present on OPA-modified ITO or HfO_2 nanoparticles, respectively.

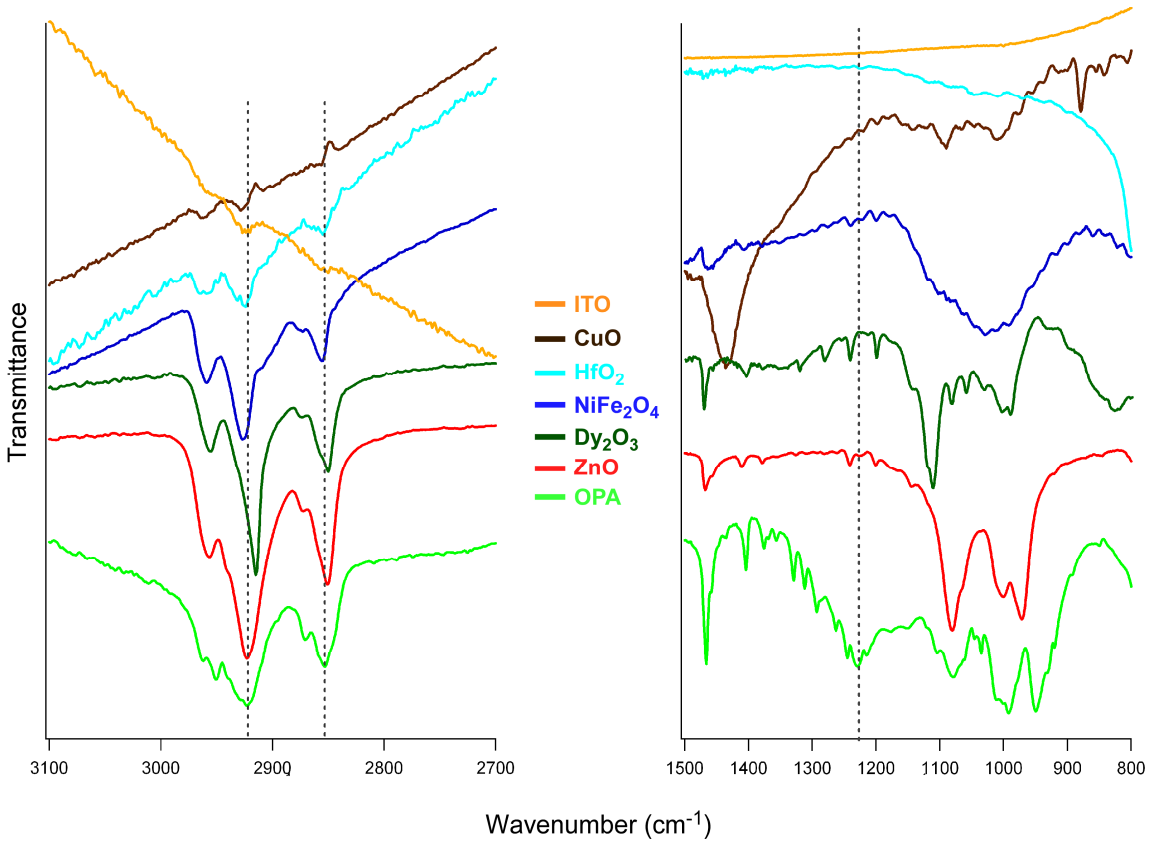

Figure 5.25 FTIR spectra in the C–H stretching region (left) and fingerprint region (right) for each of the OPA–modified nanoparticle samples (under normal reaction conditions). Dotted lines indicate $\nu_a(CH_2)$ at about 2925 cm^{-1}, $\nu_s(CH_2)$ at about 2855 cm^{-1}, and ν(P=O) at about 1230 cm^{-1}.

As was mentioned in Chapter 3, both the amount of Lewis acidic sites and the amount of Bronsted acid sites (hydroxyl groups) will help determine the relative amounts of the different binding modes present upon reaction of phosphonic acid with a metal oxide surface. It may be useful then to consider the relative Lewis and Bronsted acidities of the different metal oxide nanoparticles. To be even more specific, it could be useful to consider the size and charge of uncoordinated metal species in the metal oxide, which will determine how hard or soft the Lewis acid is. Harder Lewis acids would be expected to react more readily with phosphonic acids that contain a fairly hard Lewis basic site (the phosphoryl group). Additionally, it could be useful to factor in the isoelectric points of the different metal oxides as these will determine the number of available hydroxyl sites in the reaction media.

Considering that the pH of pure ethanol is ~7.3, metal oxides with isoelectric points lower than this will tend to have more hydroxyl groups on the surface than those with isoelectric points that are higher (Table 5.8). Therefore, it could be expected that hafnium oxide and dysprosium oxide could partake in more surface heterocondensation reactions due to more surface hydroxyl groups relative to some of the other metal oxides. There does not appear to be any correlation between the extent of surface heterocondensation and the isoelectric point in the IR data presented here. This is not surprising, however, as it could be that the pH of the reaction media is in fact lower than expected due to the excess phosphonic acid present. Additionally, the initial amount of surface hydroxylation varies considerably for the different samples.

Table 5.8 Isoelectric points for different metal oxides. Isoelectric point for ITO from Chen *et al.*[63], the isoelectric point of HfO_2 from Blanc *et al.*[64], and the isoelectric point of Dy_2O_3 from Happy *et al.*[65]. All other isoelectric points from Kung.[66]

Metal Oxide	Isoelectric Point
CuO	~9.5
Fe_2O_3	~6.7
NiO	9.9–11.3
ITO	~7–8
ZnO	8.7–10.3
Dy_2O_3	~6–7
HfO_2	~5

The Lewis acidity, and the relative hardness, of different metal oxides depends on the charge and size of the metal cations. Harder cations would be expected to be smaller, less polarizable, and have higher electronegativities. While it is not possible to determine exactly the relative hardness and acidity of the different metal oxides, as this depends heavily on the charge of the cations and their oxidation number (which is not known for each of the metal oxide species), it may be possible to see a trend. The Pauling electronegativities and ionic radii of each of the relevant metal atoms are shown in Table 5.9.

Table 5.9 Pauling electronegativities and ionic radii of different metal atoms. Ionic radii found at environmentalchemistry.com.[67] Pauling electronegativities found in CRC handbook.[68]

Element	Pauling Electronegativity	Ionic Radius (pm)
Cu	1.90	7.3
Sn	1.96	6.9
In	1.78	8
Ni	1.91	6.9
Fe	1.83	6.5
Zn	1.65	7.4
Hf	1.30	7.1
Dy	1.22	9.1

Considering that none of the OPA–modified metal oxides show a phosphoryl stretch in the IR, it appears as if, regardless of the relative hardness of the Lewis acidic meta cation, the coordination step of the reaction between OPA and the metal oxide proceeded in each of the samples.

Information on the thermal stability of the phosphonic acid–metal oxide bonds can be obtained, in an approximate way, from the TGA results for each sample; specifically, from the derivatives of the traces (Figure 5.26). The minima in the trace derivatives correspond to inflection points of the original TGA traces and can be related to the relative temperature of evaporation of the phosphonic acid in each sample. Interestingly, the range of temperatures over which the inflection points are seen is broad, indicative of different thermal stabilities for the various metal oxide nanoparticles, depending on the strength of the P–O–M bond. All of the OPA– and ODPA–modified inflection points occur at higher temperatures than free OPA or ODPA (~450 °C) except

for OPA–modified CuO nanoparticles, where the inflection point occurs at a significantly lower temperature (~340 °C), indicative of lower thermal stability compared to the other metal oxides.

For OPA-modified nanoparticles, ZnO and Dy_2O_3 appear to form the most hydrothermally stable P–O–M bonds of the nanoparticles tested. P–O–Cu bonds appear to be weak, indicating that perhaps OPA is only physisorbed or hydrogen bonded to the surface of CuO. Additionally, small peaks appearing as shoulders on the low-temperature side for CuO, Dy_2O_3, and ZnO nanoparticles, all of which show abnormally high mass loss in TGA, can be seen. These most likely correspond to weakly bound OPA on the particles. ODPA-modified nanoparticles show similar hydrothermal stabilities for each nanoparticle. HfO_2 nanoparticles appear to form the most stable bonds. ZnO nanoparticles show two peaks when modified with ODPA. Considering the large mass loss seen in the TGA for the ODPA-modified ZnO nanoparticles, it appears likely that the larger, lower temperature peak corresponds to loosely attached ODPA while the smaller peak at higher temperature is indicative of more strongly-bound ODPA.

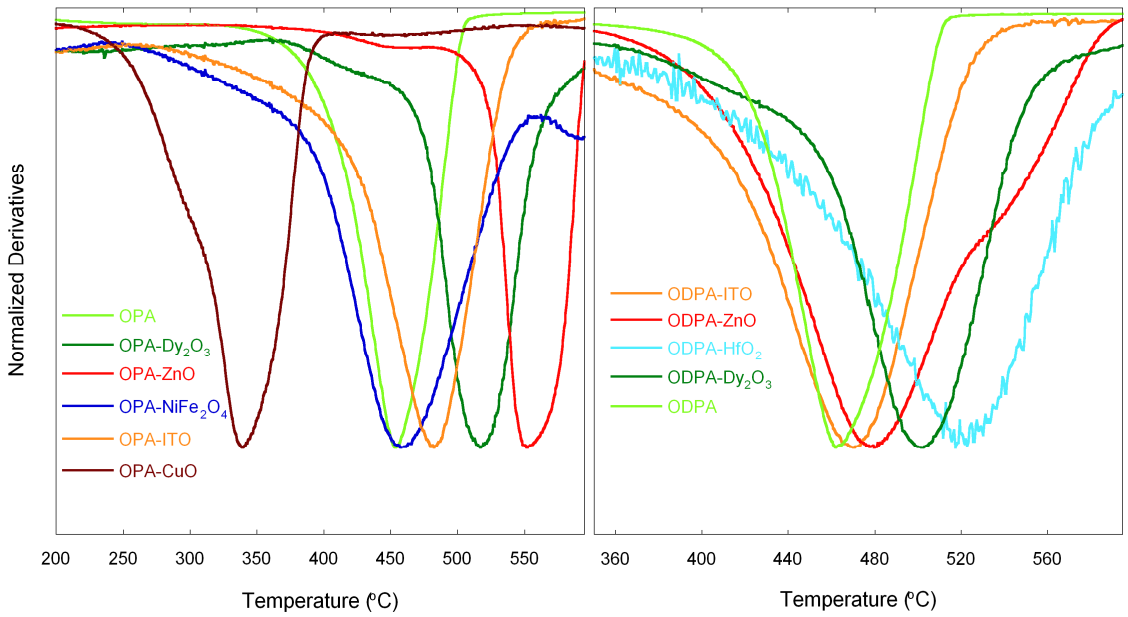

Figure 5.26 Normalized derivatives of the TGA traces for OPA and OPA–modified nanoparticles (left) and ODPA and ODPA–modified nanoparticles (right) all under normal reaction conditions. The curves were smoothed by averaging over 100 points; this broadens the peaks but does not change their relative minima.

As with the IR data, it could be useful to look for trends in the thermal stability of the phosphonic acids attached to different metal oxide species. As the thermal stabilities appear to vary depending on the metal oxide (Table 5.10), it could be useful to compare these data to the bond strengths of the atoms present at the attachment interface. As we are forming P–O–M bonds, and these are the bonds that differ between samples, the P–O and M–O bonds strengths may play an important role in the overall thermal stability. In order to determine this, the diatomic bond strengths of C–P, P–O, and the relevant M–O species are shown in Table 5.11.

Table 5.10 TGA derivative minima, indicative of the thermal stability of the phosphonic acid on each metal oxide.

Sample	Derivative minimum for OPA modified (°C)	Derivative minimum for ODPA modified (°C)
free PA powder	455	465
CuO	340, large shoulder ~300	not measured
$NiFe_2O_4$	460, small peak ~595	not measured
ITO	480	470
ZnO	550, small peak ~450	480, large shoulder ~530
Dy_2O_3	520, small peak ~430	500
HfO_2	not determined	520

Table 5.11 Bond strengths for a number of diatomic molecules relevant to the thermal stability of phosphonic acids bound to various metal oxides. Values from CRC Handbook.[68]

Molecule	Bond strengths in diatomic molecules (kJ/mol)
C–P	513 ± 8
O–P	599 ± 13
Cu–O	269 ± 21
Zn–O	159 ± 4
Ni–O	382 ± 17
Fe–O	390 ± 17
In–O	<320 (no error given)
Sn–O	532 ± 13
Dy–O	607 ± 17
Hf–O	802 ± 13

According to Table 5.11, the weakest bonds are between Cu–O and Zn–O, whereas the strongest bonds are between Dy–O and Hf–O. It would be expected then,

assuming similar coverages and binding modes, that the thermal stability of phosphonic acids attached to HfO_2 and Dy_2O_3 would be higher than that of phosphonic acids attached to CuO or ZnO. This appears to be the case, except for the case of ZnO, which shows a much higher thermal stability than would be expected (Figure 5.27).

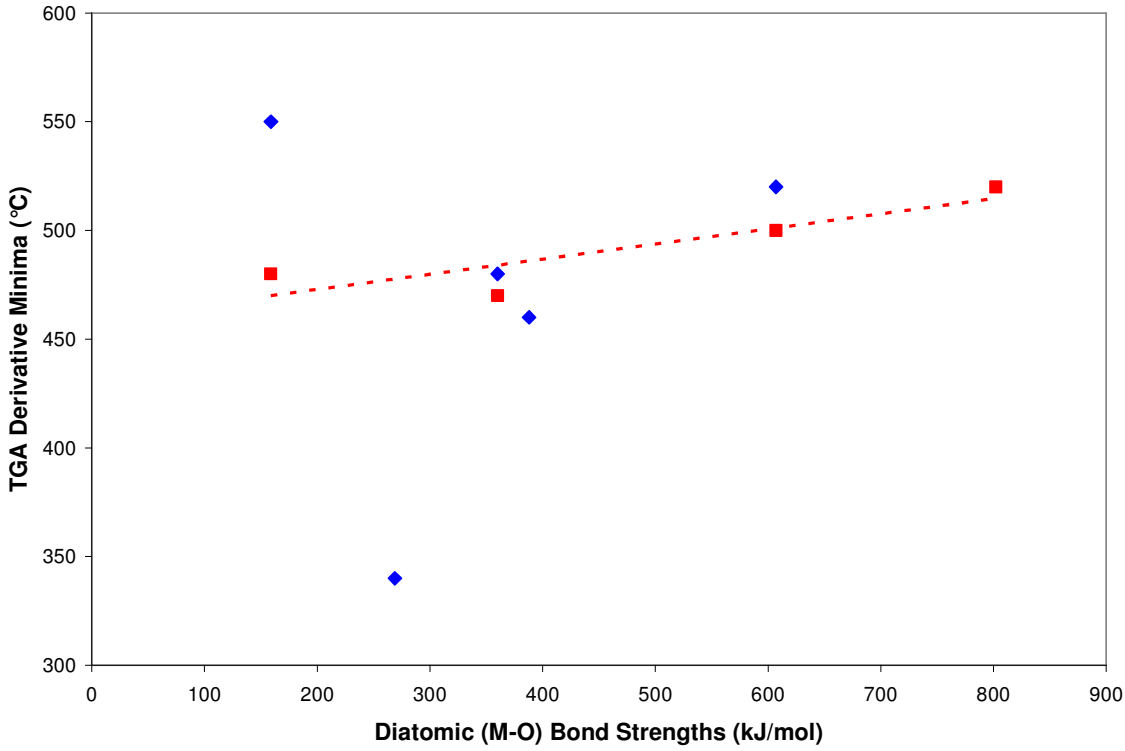

Figure 5.27 Plot of diatomic bond strengths vs. TGA derivative minima for the OPA– and ODPA–modified metal oxides. A trendline is shown for the ODPA data. The diatomic bond strengths for $NiFe_2O_4$ and ITO are taken as an average of the individual M–O bond strengths, taking into account molar relativities.

5.2.9 Conclusions

The data presented and discussed here suggest that all of the metal oxides tested bind to alkylphosphonic acids, but the results currently available are not sufficient to unambiguously identify the type of binding of the phosphonic acid to the surface and their relative strength. Further analyses of the relative P–O–M bond strengths would be interesting. Comparison of the IR and TG data for each of the modified metal oxide species with known properties of the metals and the metal–oxygen bonds do not seem to shown any definitive trends. More data needs to be collected in order to determine whether any trends exist. ITC experiments, where the enthalpies of reaction can be measured, would be useful, as would additional TGA analyses focusing on the hydrothermal stabilities of each sample. Additionally, a wider range of reaction conditions should be tested, to identify those that yield nanoparticles which are modified robustly but do not contain multilayers. BET analyses of the different nanoparticles would also be needed to more quantitative information on the relative surface coverages that can be obtained for the various metal oxides.

5.3 Modification of Zeolites for Membrane Applications

This section details our initial work at modifying zeolites in an effort to improve their compatibility in polymer matrices for use in membrane applications. The work is

done in collaboration with Madhava Kosuri[aa] (Chemical Engineering, Georgia Institute of Technology).

5.3.1 Motivation of the Approach

Zeolites are mesoporous aluminosilicates. They can be synthesized with various additional cationic species in the structure, and can be made to have various shapes, overall sizes and pore sizes. They are used in catalysis,[69] gas sensing and separation,[70] among other applications.

The Koros lab uses polymer matrices incorporating zeolites for advanced membranes.[71] By utilizing both zeolites and polymers, that exhibit different gas permeation properties, they are able to create membranes that have the ability to separate gases, such as O_2 and N_2, from each other. However, one problem with this approach is a lack of control over the interface between the polymer matrix and the zeolite surface (Figure 5.28). Voids, which are larger than the Angstrom-sized pores in zeolites, can seen between the zeolites (small circular species) and the polymer matrix.

[aa] While working with Prof. William Koros

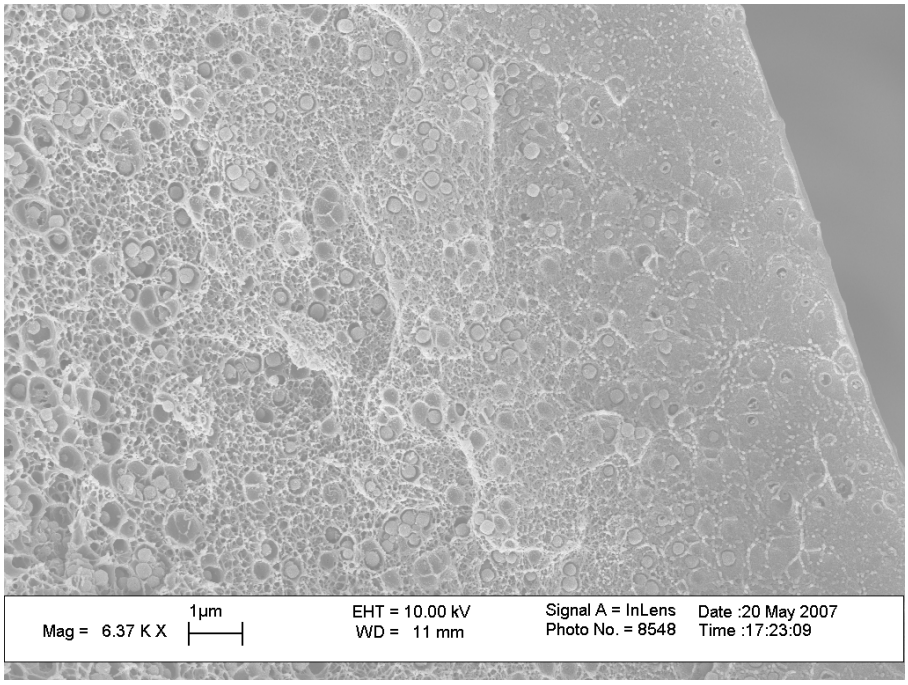

Figure 5.28 Typical SEM micrograph of a membrane incorporating zeolites. The voids surrounding the zeolites from poor interfacial interaction with the polymer are clearly visible. (Image taken by M. Kosuri)

The Koros lab uses Zeolite 4A (with an average edge length of 5 µm) with pore sizes on the order of 4-5 Angstroms in size. If there are gaps between the organic and inorganic that are larger than the pore sizes of the zeolites in a given membrane then it will be the dimensions of these voids that regulate the performance of the resulting membrane, not the zeolite pore size (Figure 5.29). It is therefore important that the wetting between the zeolites and the polymer is excellent, leaving no gaps between the two materials.

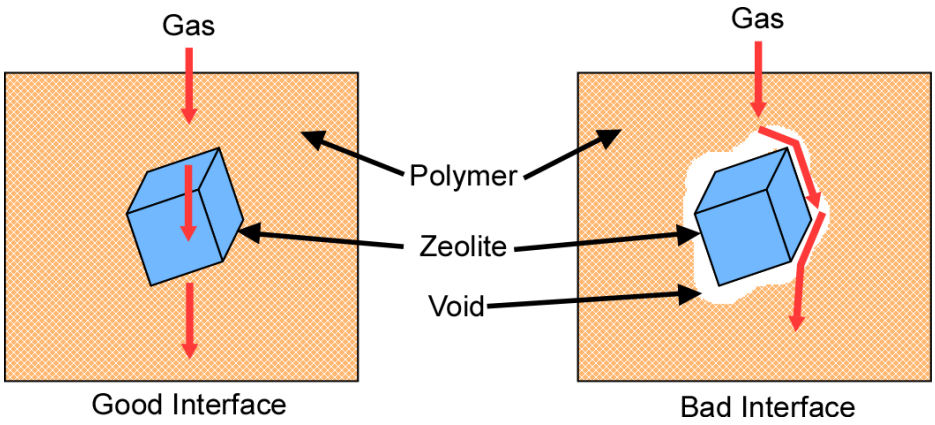

Figure 5.29 Schematic illustrating the difference in gas flow between membranes characterized by good wetting between the zeolites and the polymer matrix (left) and membranes containing zeolites that do not wet the polymer matrix well, resulting in voids.

It is possible that phosphonic acid modification of the zeolites could be used to improve the dispersion and relative interfacial characteristics of the materials. To determine if this approach is feasible, it must first be determined whether phosphonic acids can bind to the zeolite structure. Second, it must be determined whether it is possible to modify only the outside surface of the zeolites, so as to not clog the inner pores, which are needed for enhanced gas separation in the resultant membrane. If these initial concerns can be addressed, then it needs to be determined which substituent groups can be used to improve the wetting of the polymer to the zeolites while maintaining optimal pore integrity.

5.3.2 Literature Background

Little has been reported on the modification of zeolites with phosphonic acids, although a few studies have been reported. Doussineau *et al*. report on the functionalization of zeolites with phosphonic acids in a 1:1 DMSO: water mixture. They obtained a loading of 38 μmol/g and state that the low hydrolytic stability of the P–O–Si bond may be a reason for the low coverage.[7] Phosphonic acids have also been used to template the growth of zeolites off of gold surfaces.[72]

5.3.3 Initial Characterization

As mentioned, it is important to first determine whether phosphonic acids will bind to the zeolite surface. As a first attempt, the same conditions used to modify the metal oxides presented earlier in this chapter were employed: 1 hour reaction time, 5 times excess of phosphonic acid (calculated from the amount of phosphonic acid needed to cover only the outer surface of the zeolites), in a 95:5 ethanol: water solution at 80 °C.

The potential chemical signal from a monolayer on the outer surface of zeolite with 5 micron edges is quite low with any particular instrument, with respect to the signal due to the zeolite itself or to other background signal. The exact chemical formula of the zeolite is $(Na_{96}(H_{20})_{216})(Al_{96}Si_{96}O_{384})$. It has a silicon to aluminum ratio of 1, and the surface is covered with hydroxyl groups, which are necessary for PA attachment. In order to maximize the signal that could be seen by various characterization techniques,

octadecylphosphonic acid (ODPA), with a long alkyl chain, was used to modify the zeolite surface. The modified and unmodified zeolites were then analyzed using FTIR, TGA, and SS MAS NMR.

Unmodified zeolites show a number of intense absorption bands in the IR region, due not only to vibrational modes of the zeolites themselves, but probably also due those of any trapped gases and other species within the pores (TGA data also suggests the presence of trapped species). However, changes between the modified and unmodified zeolites can be seen. In particular, C–H stretching bands appear upon modification with ODPA (Figure 5.30).

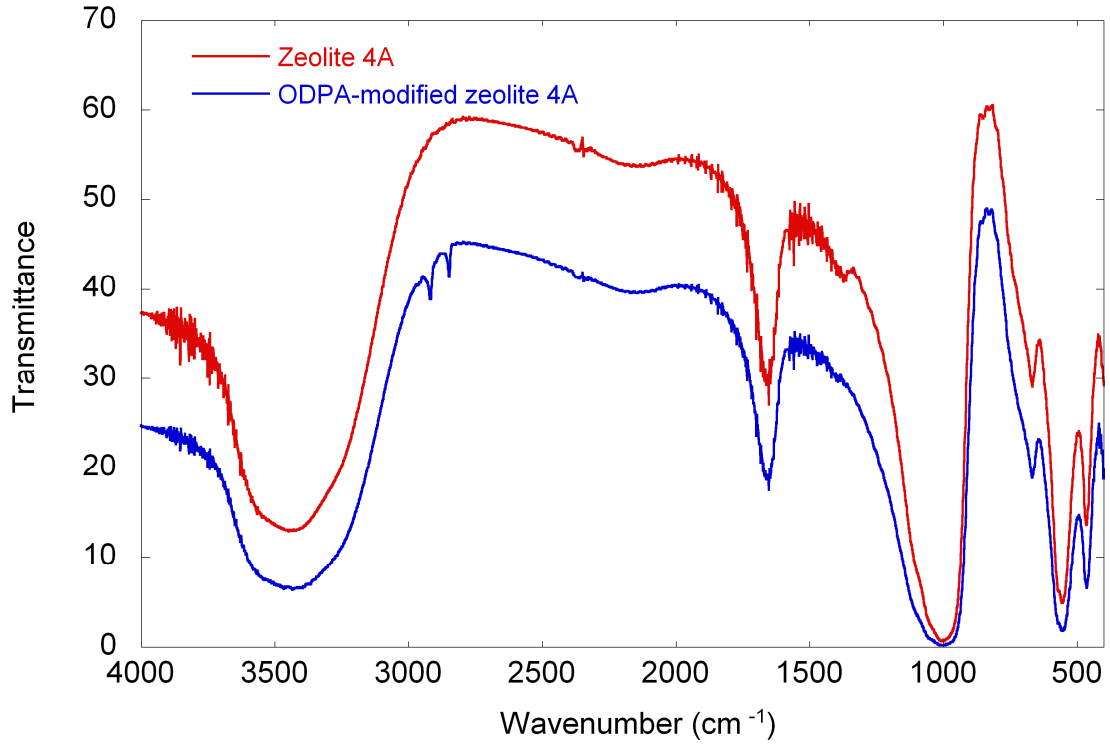

Figure 5.30. FTIR spectra of unmodified (red) and ODPA–modified (blue) Zeolite 4A.

TGA was also used to obtain information on the modified and unmodified zeolites (Figure 5.31). A large mass loss is seen in both samples (~20%) throughout the run, most likely due to adsorbed gases and other species in and on the zeolites. At first glance the two traces appear to be quite similar. However, upon closer inspection a change in the slope of mass loss can be seen at around 500 °C in the ODPA–modified zeolites which is not present in the unmodified zeolites. This experiment was repeated and similar results were obtained.

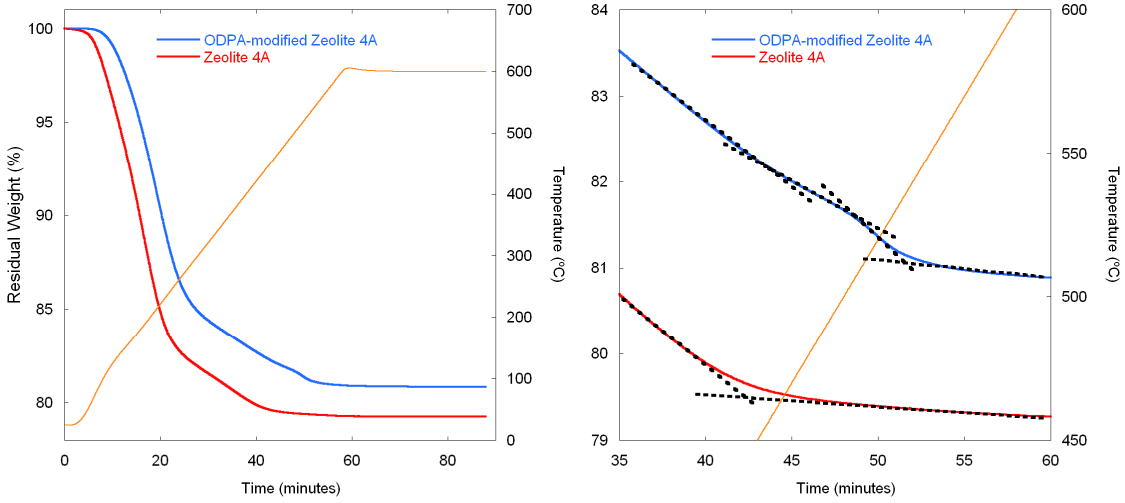

Figure 5.31 TGA of unmodified zeolites (red) and ODPA–modified zeolites (blue). The orange trace corresponds to the temperature as a function of time. The right–hand graph is a magnified portion of interest in the left–hand graph. Tangent lines are drawn to indicate the slope differences.

The mass loss corresponding to this change in slope can be estimated to be about 0.60%, which corresponds to approximately 120% of a theoretical outer–surface monolayer of ODPA on the zeolites.

It is interesting that, despite the fact that a 5–fold excess of ODPA was used, the

amount of ODPA bound to the zeolite is similar to that needed to modify only the outer surface. However, BET measurements show that the surface area of the ODPA–modified zeolites is approximately half that of unmodified zeolites. This indicates some degree of pore blockage in the zeolites. XRD analyses showed no difference in the morphology of the zeolites prior to and after modification with ODPA, indicating that the zeolites were not being degraded under the reaction conditions.

The solid state NMR results are also interesting. ^{31}P MAS NMR shows that, phosphorous species are present in the zeolite structure after modification with ODPA (Figure 5.32). The Direct Polarization spectrum shows a broad peak ~ 18.0 ppm, which is indicative of phosphonic acids loosely bound to the surface of the zeolite. The Cross Polarization spectrum shows this broad peak as well as a sharp peak at ~ 25.7 ppm, indicative of rigid phosphorus species on the surface. Unbound ODPA appears as a sharp peak at 28 ppm.

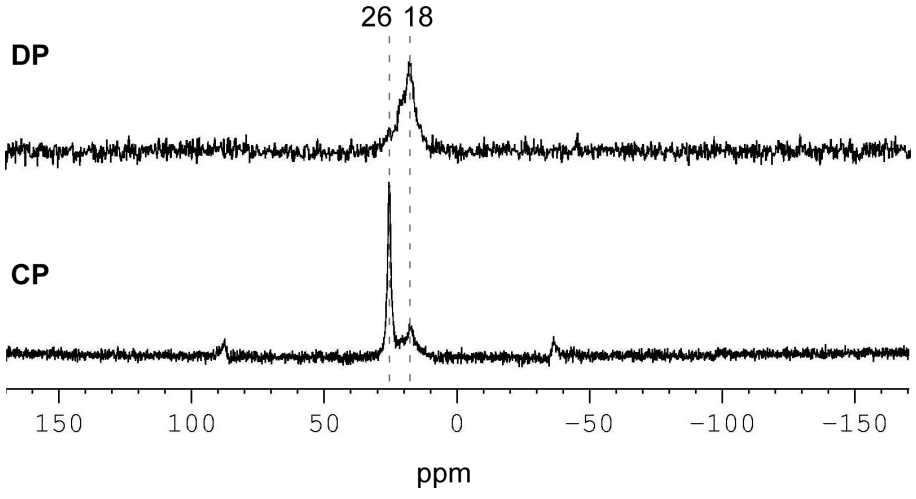

Figure 5.32 DP (top) and CP (bottom) ^{31}P MAS NMR spectra of ODPA–modified zeolites.

^{29}Si MAS NMR spectra of the unmodified and ODPA–modified zeolites are very similar (not shown). This is not surprising considering the amount of bulk silicon versus the amount of outer–surface surface silicon in the zeolites. However, a difference can be seen in the ^{1}H MAS NMR spectra (Figure 5.33). Small peaks can be seen at ~1 and 0.5 ppm in the ODPA–modified zeolites spectrum and these peaks are absent in the spectrum of unmodified zeolites. This is consistent with the presence of an alkyl chain on the zeolite, giving rise to signals for CH_2 (~1 ppm) and CH_3 (~0.7 ppm) protons.

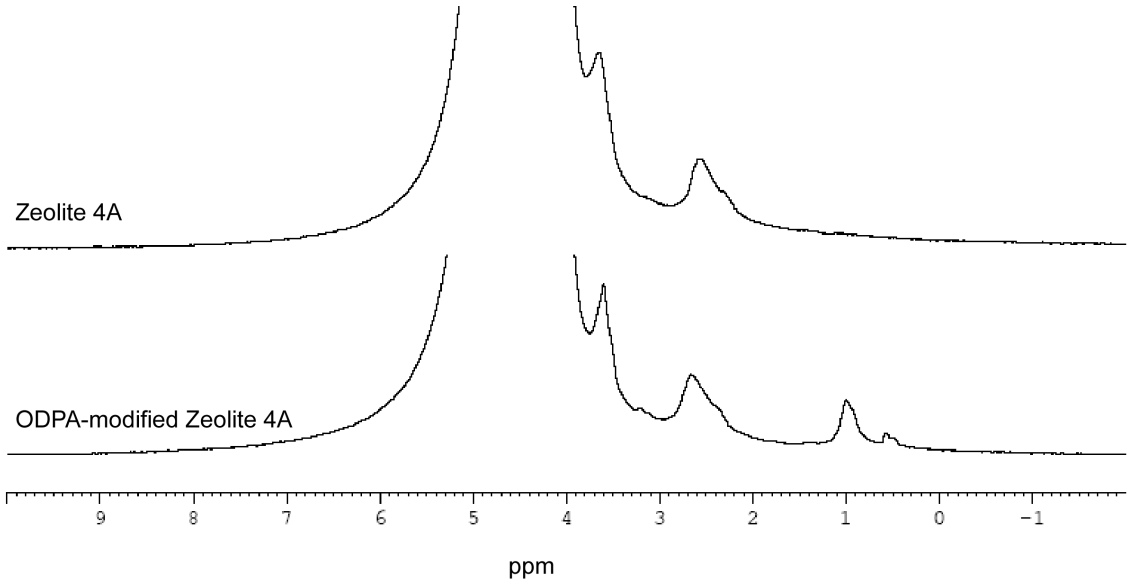

Figure 5.33 ^{1}H MAS spectra of unmodified zeolites (top) and ODPA–modified zeolites (bottom).

XPS spectra also indicate the binding of ODPA, as an increased carbon signal is seen in the ODPA-modified zeolites compared to the unmodified zeolites (Figure 5.34).

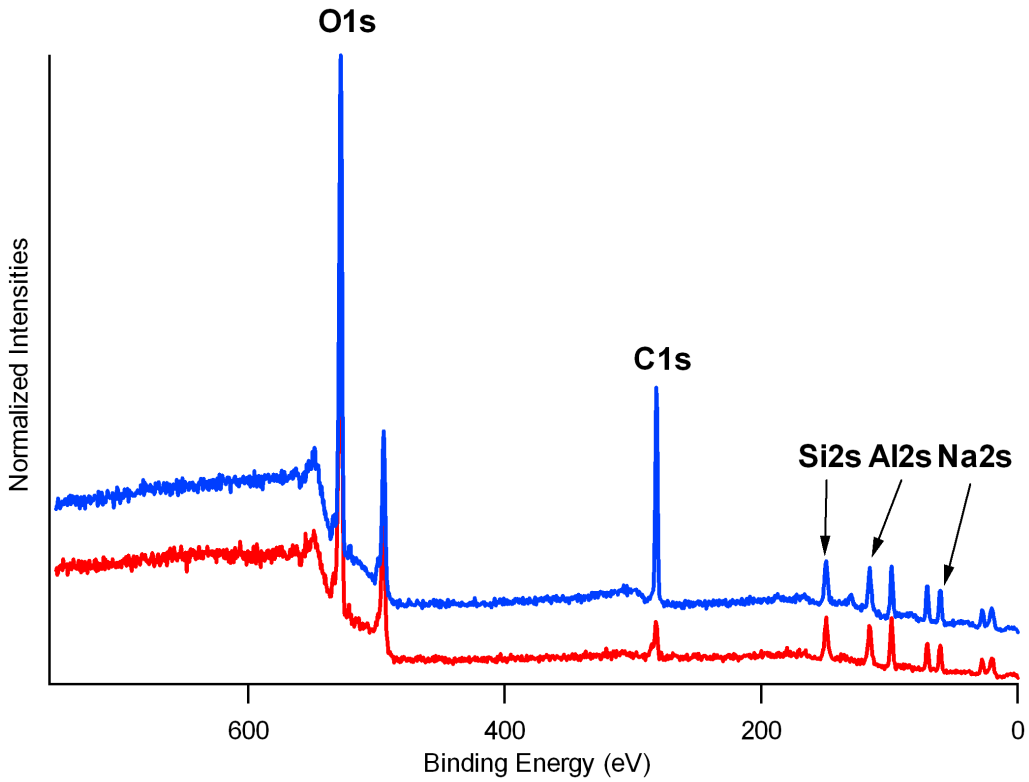

Figure 5.34 XPS spectra of unmodified (red) and ODPA-modified (blue) zeolites. The spectra are normalized at the O(1s) peak in each sample and offset for clarity.

While all evidence indicates that the ODPA–modified zeolites are successfully modified with ODPA, BET analyses indicate that the pores are being blocked to a significant degree. This may be due to the dense packing of ODPA on the surface (as evidenced by CP ^{31}P MAS NMR), effectively blocking a portion of the inner pores. Pore blockage may be decreased by using phosphonic acids which pack in a less ordered or dense fashion on the surface. Shorter alkyl chains may solve the problem.

5.3.4 Results of Surface Modification with Other Phosphonic Acids

The Koros group uses Torlon® in their membranes, which is a polyimide–amide (Figure 5.35).

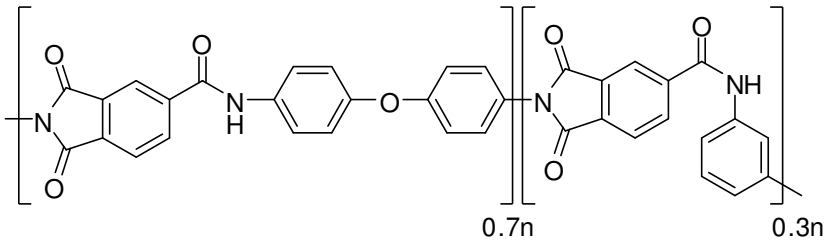

Figure 5.35 Chemical structure of Torlon®.

As it has been shown that phosphonic acids will bind to the zeolite surface, the next challenge is finding a phosphonic acid that will not block the pores but still provide a surface which will interact well with Torlon. As a first attempt, two ligands, pentafluorobenzylphosphonic acid (PFBnPA) and a phthalimide–phosphonic acid (PhthalPA), were chosen to modify the zeolites with the thought that the terminal functional groups on these modifiers would interact well with the polymer resulting in improved interfacial properties (Figure 5.36).

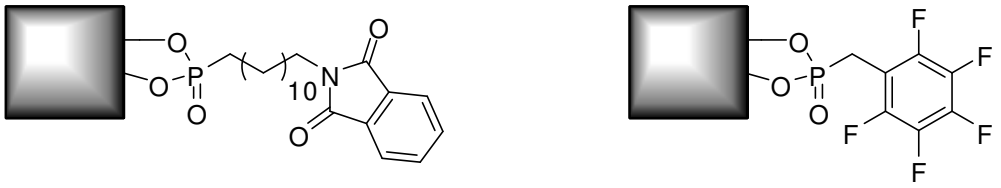

Figure 5.36 Representations of zeolites modified by a phthalimide–phosphonic acid (left) and pentafluorobenzylphosphonic acid (right).

^{31}P MAS NMR of these modified zeolites, show decreased phosphorus signals in comparison to ODPA–modified zeolites. (Figure 5.37). This may be due to that fact that the long alkyl chains in ODPA may result in better packing and subsequent increased coverage of the zeolite surface compared to the other modifiers that have bulkier terminal functional groups.

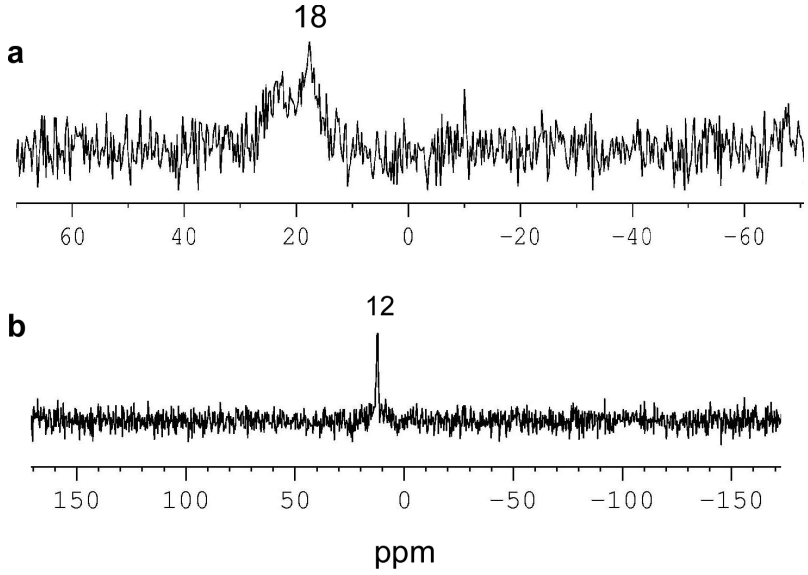

Figure 5.37 DP ^{31}P MAS NMR spectra of zeolites modified with either a) a phthalimide–phosphonic acid or b) a pentafluorobenzylphosphonic acid.

TGA analysis of the PFBnPA–modified zeolites showed no discernable weight loss in the region where a weight loss was seen in the ODPA–modified zeolites. Therefore, XPS measurements were performed on the PFBnPA–modified zeolites. A general survey scan of the PFBnPA–modified zeolites is shown in Figure 5.38. A clear F(1s) peak can be seen, indicating the presence of PFBnPA on the surface.

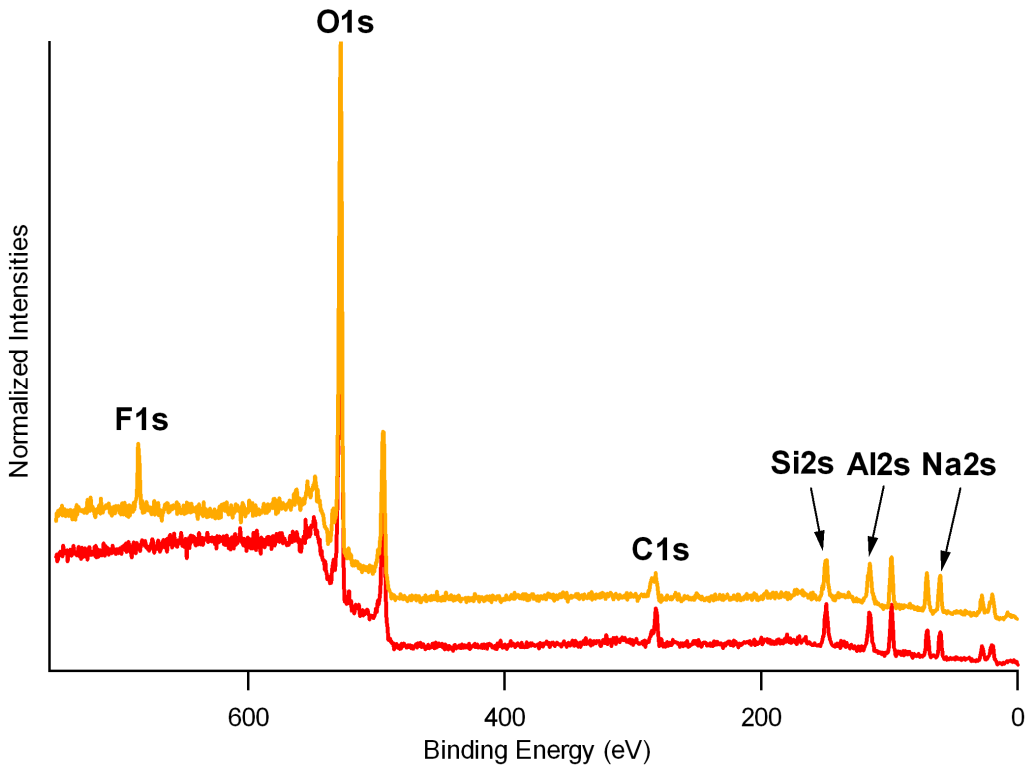

Figure 5.38 XPS spectra of unmodified zeolites (red) and zeolites modified with PFBnPA (orange). The spectra are normalized at the O(1s) peak in each sample and offset for clarity.

BET measurements of zeolites modified with PFBnPA indicate no blockage of the pores as the surface areas are similar before and after modification. Differential scanning calorimetry (DSC) measurements show a glass transition temperature of 289.3

°C, higher than that of pure Torlon (277.7 °C) and Torlon with incorporated unmodified Zeolite 4A (284.9 °C) for Torlon incorporated with PFBnPA-modified Zeolite 4A. This increase in the glass transition temperature is indicative of a strong interaction between the incorporated zeolites and the polymer.

In summary, it has been shown that phosphonic acids can modify the surfaces of zeolites. Further studies are underway to try to optimize the interaction between the zeolites and the polymer by judicious selection of the terminal functional group on the phosphonic acid. Additional studies (M. Kosuri) are being performed utilizing the polymer/zeolite hybrid materials for use as membranes for gas separation.

5.3.5 Conclusions

This chapter has discussed our efforts at the modification of different metal oxide nanoparticles, as well as micron-sized zeolites, with phosphonic acids. In all cases, it appears as if the phosphonic acids interact with the surface, as evidenced by FTIR, TGA, XPS, and SS MAS NMR analyses. Demonstrating the ability of phosphonic acids to bind to most metal oxides may help to support the notion that they can serve as universal ligands for metal oxide modification.

Specifically, detailed studies on the binding and coverage of 6 different types of metal oxide nanoparticles with phosphonic acids have been presented. The purpose of the studies was to gain a better understanding the types of interactions that exist between the

phosphonic acids and the surface, their stability, and the overall degree to which nanoparticles are modified.

The attachment of phosphonic acids to the surface of zeolites has also been studied. Zeolites were successfully modified with ODPA, leading to further studies with other phosphonic acids with different terminal functional groups. The end goal is to attach a phosphonic acid which does not block the pores of the zeolites but does increase the wettibility and interfacial interactions between the zeolites and different polymer matrices for use in membranes for gas separation technologies.

5.4 Experimental

Metal oxide nanoparticles were obtained from either Inframat Advanced Materials (ITO, ZnO) or Nanoamor (HfO_2, Dy_2O_3, $NiFe_2O_4$, CuO).

The normal reaction conditions for the modification of nanoparticles are as follows: Metal oxide nanoparticles (500 mg) were dispersed in a 95:5 ethanol: water mixture (25 mL) and the mixture sonicated for 1 hour utilizing point ultrasonicator with a pulse program (30 seconds on, 5 seconds off, at 35% power). A solution of phosphonic acid ligand (5 × that needed for a theoretical monolayer, based on surface area) dissolved in a minimal amount of solvent is then added and this mixture sonicated in an ultrasonic bath for 10 minutes. The reaction vessel was then submerged in an oil bath (80 °C) and stirred vigorously for 1 hour. Upon cooling and settling of the nanoparticles, the solvent was decanted, and the nanoparticles then resuspended in ethanol and centrifuged (3 ×),

then dichloromethane (1 ×). The nanoparticles were then transferred to a vial and dried in an oven (~ 70 °C, 2 hours) and then under high vacuum (0.1 torr) overnight.

Mild and forcing reaction conditions are identical to those stated above except for the temperature of the bath and the reaction time. Mild conditions refer to stirring the reaction for 1 hour at room temperature. Forcing conditions refer to stirring the reaction for 5 hours in an oil bath (100 °C).

Zeolites were modified as follows: Zeolite 4A microcubes (2.50 g) were added to a 95:5 ethanol: water mixture (150 mL) and the mixture ultrasonicated in a water bath for 30 minutes. Phosphonic acid ligand (5 × that needed for a theoretical monolayer, based on the particle's outer surface area) was dissolved in a minimum amount of ethanol and added to the reaction mixture, followed by 10 minutes additional sonication. The mixture was submerged in a 80 °C oil bath and stirred for a 1 hour. Upon cooling the supernatant was poured off and the zeolites were then resuspended in a solvent that the phosphonic acid is soluble in and centrifuged (4 ×). The zeolites were then transferred to a vial and dried in an oven (~ 70 °C, 2 hours) and then under high vacuum (0.1 torr) overnight.

TG analyses of nanoparticle samples were performed in a Netzsch STA 449 C instrument by heating to 600 °C at a rate of 10 °Cmin^{-1} followed by constant heating at 600 °C for 30 minutes.

XPS scans were taken with a Surface Science Laboratories SSX-100 ESCA Spectrometer using monochromatic Al*K*α radiation (1486.6 eV). A pass energy of 150 eV was used for survey scanes and a pass energy of 50 eV was used for high-resolution scans. All measurements were performed at a takeoff angle 55° to the normal with 200 μm spot sizes.

Fourier transform infrared (FT-IR, Perkin-Elmer Spectrum 1000) spectra were obtained by using KBr pellets containing 5 wt. % of each treated BT with 1 cm^{-1} resolution.

^{31}P MAS NMR Spectra were recorded on a Bruker DSX 400 (161.98 MHz ^{31}P frequency, 10 kHz MAS frequency, 256 scans, 10 s delay time) for both DP (5 μs 90º pulse length, high power ^{1}H decoupling) and CP (1 ms contact time) experiments.

Powder X-ray diffraction data were collected using Cu Kα radiation on a Scintag X1 diffractometer equipped with a Scintag Peltier cooled solid-state detector. Diffraction patterns were recorded (20-70 2, 2.5 2θ /min) for each of the samples.

5.5 References

1. Kim, P.; Jones, S. C.; Hotchkiss, P. J.; Haddock, J. N.; Kippelen, B.; Marder, S. R.; Perry, J. W., Phosphonic acid-modified barium titanate polymer nanocomposites with high permittivity and dielectric strength. *Advanced Materials* **2007,** 19, (7), 1001-1005.

2. Pawsey, S.; McCormick, M.; De Paul, S.; Graf, R.; Lee, Y. S.; Reven, L.; Spiess, H. W., H-1 fast MAS NMR studies of hydrogen-bonding interactions in self-assembled monolayers. *Journal of the American Chemical Society* **2003,** 125, (14), 4174-4184.

3. Pawsey, S.; Yach, K.; Reven, L., Self-assembly of carboxyalkylphosphonic acids on metal oxide powders. *Langmuir* **2002,** 18, (13), 5205-5212.

4. Kar, S.; Durand, J. O.; Granier, M.; Joly, P.; Melnyk, O., COCHO-modified oxides nanoparticles by using phosphonic acid as grafting agent. *Tetrahedron Letters* **2003,** 44, (30), 5617-5619.

5. Gao, W.; Dickinson, L.; Grozinger, C.; Morin, F. G.; Reven, L., Self-assembled monolayers of alkylphosphonic acids on metal oxides. *Langmuir* **1996,** 12, (26), 6429-6435.

6. Ferreira, J. M.; Marcinko, S.; Sheardy, R.; Fadeev, A. Y., Calorimetric study of the reactions of n-alkylphosphonic acids with metal oxide surfaces. *Journal of Colloid and Interface Science* **2005,** 286, (1), 258-262.

7. Doussineau, T.; Durand, J. O.; Granier, M.; Smaihi, M.; Valtchev, V., Synthesis of phosphonic acids with the semicarbazide group for the functionalization of metal oxide and zeolite nanoparticles. *Synlett* **2004**, (10), 1735-1738.

8. Maliakal, A.; Katz, H.; Cotts, P. M.; Subramoney, S.; Mirau, P., Inorganic oxide core, polymer shell nanocomposite as a high K gate dielectric for flexible electronics applications. *Journal of the American Chemical Society* **2005,** 127, (42), 14655-14662.

9. Guerrero, G.; Mutin, P. H.; Vioux, A., Anchoring of phosphonate and phosphinate coupling molecules on titania particles. *Chemistry of Materials* **2001,** 13, (11), 4367-4373.

10. Bonhote, P.; Gogniat, E.; Gratzel, M.; Ashrit, P. V., Novel electrochromic devices based on complementary nanocrystalline TiO2 and WO3 thin films. *Thin Solid Films* **1999,** 350, (1-2), 269-275.

11. Ruhle, S.; Greenshtein, M.; Chen, S. G.; Merson, A.; Pizem, H.; Sukenik, C. S.; Cahen, D.; Zaban, A., Molecular adjustment of the electronic properties of nanoporous electrodes in dye-sensitized solar cells. *Journal of Physical Chemistry B* **2005,** 109, (40), 18907-18913.

12. Helmy, R.; Fadeev, A. Y., Self-assembled monolayers supported on TiO_2: comparison of $C_{18}H_{37}SiX_3$ (X = H, Cl, $OCH_3C_{18}H_{37}Si(CH_3)_2C1$, and $C_{18}H_{37}PO(OH)(2)$. *Langmuir* **2002,** 18, (23), 8924-8928.

13. Rusu, C. N.; Yates, J. T., Adsorption and decomposition of dimethyl methylphosphonate on TiO2. *Journal of Physical Chemistry B* **2000,** 104, (51), 12292-12298.

14. Brodard-Severac, F.; Geuerrero, G.; Maquet, J.; Florian, P.; Gervais, C.; Mutin, P. H., High-field ^{17}O MAS NMR investigation of phosphonic acid monolayers on titania. *Chemistry of Materials* **2008,** 20, 5191-5196.

15. Wei, T.; Jin, C. Q.; Zhong, W.; Liu, J. M., High permittivity polymer embedded with Co/ZnO core/shell nanoparticles modified by organophosphorus acid. *Applied Physics Letters* **2007,** 91, (22), 222907/1-222907/3.

16. Chen, Y. F.; Kim, M.; Lian, G.; Johnson, M. B.; Peng, X. G., Side reactions in controlling the quality, yield, and stability of high quality colloidal nanocrystals. *Journal of the American Chemical Society* **2005,** 127, (38), 13331-13337.

17. Demir, M. M.; Koynov, K.; Akbey, U.; Bubeck, C.; Park, I.; Lieberwirth, I.; Wegner, G., Optical properties of composites of PMMA and surface-modified zincite nanoparticles. *Macromolecules* **2007,** 40, (4), 1089-1100.

18. Liu, D.; Wu, W.; Qiu, Y.; Yang, S.; Xiao, S.; Wang, Q. Q.; Ding, L.; Wang, J., Surface functionalization of ZnO nanotetrapods with photoactive and electroactive organic monolayers. *Langmuir* **2008,** 24, (9), 5052-5059.

19. Yee, C.; Kataby, G.; Ulman, A.; Prozorov, T.; White, H.; King, A.; Rafailovich, M.; Sokolov, J.; Gedanken, A., Self-assembled monolayers of alkanesulfonic and -phosphonic acids on amorphous iron oxide nanoparticles. *Langmuir* **1999,** 15, (21), 7111-7115.

20. Matsuno, R.; Yamamoto, K.; Otsuka, H.; Takahara, A., Polystyrene-grafted magnetite nanoparticles prepared through surface-initiated nitroxyl-mediated radical polymerization. *Chemistry of Materials* **2003,** 15, (1), 3-5.

21. Sahoo, Y.; Pizem, H.; Fried, T.; Golodnitsky, D.; Burstein, L.; Sukenik, C. N.; Markovich, G., Alkyl phosphonate/phosphate coating on magnetite nanoparticles: a comparison with fatty acids. *Langmuir* **2001,** 17, (25), 7907-7911.

22. Mohapatra, S.; Mallick, S. K.; Maiti, T. K.; Ghosh, S. K.; Pramanik, P., Synthesis of highly stable folic acid conjugated magnetite nanoparticles for targeting cancer cells. *Nanotechnology* **2007,** 18, (38), 385102/1-385102/9.

23. Babu, K.; Dhamodharan, R., Grafting of poly(methyl methacrylate) brushes from magnetite nanoparticles using a phosphonic acid based initiator by ambient temperature atom transfer radical polymerization (ATATRP). *Nanoscale Research Letters* **2008,** 3, (3), 109-117.

24. Cinausero, N.; Azema, N.; Cochez, M.; Ferriol, M.; Essahli, M.; Ganachaud, F.; Lopez-Cuesta, J. M., Influence of the surface modification of alumina nanoparticles on the thermal stability and fire reaction of PMMA composites. *Polymers for Advanced Technologies* **2008,** 19, (6), 701-709.

25. Holland, G. P.; Sharma, R.; Agola, J. O.; Amin, S.; Solomon, V. C.; Singh, P.; Buttry, D. A.; Yarger, J. L., NMR characterization of phosphonic acid capped SnO_2 nanoparticles. *Chemistry of Materials* **2007,** 19, (10), 2519-2526.

26. Farrow, J. B.; Warren, L. J., Adsorption of short-chained organic acids on stannic oxide. *Colloids and Surfaces* **1989,** 34, (3), 255-269.

27. Baldi, G.; Bonacchi, D.; Franchini, M. C.; Gentili, D.; Lorenzi, G.; Ricci, A.; Ravagli, C., Synthesis and coating of cobalt ferrite nanoparticles: A first step toward the obtainment of new magnetic nanocarriers. *Langmuir* **2007,** 23, (7), 4026-4028.

28. Pautrot-d'Alencon, L.; Barboux, P.; Boilot, J. P., Synthesis and acid functionalization of cerium oxide nanoparticles. *Journal of Sol-Gel Science and Technology* **2006,** 39, (3), 261-267.

29. Traina, C. A.; Schwartz, J., Surface modification of Y_2O_3 nanoparticles. *Langmuir* **2007,** 23, (18), 9158-9161.

30. Milliron, D. J.; Alivisatos, A. P.; Pitois, C.; Edder, C.; Frechet, J. M. J., Electroactive surfactant designed to mediate electron transfer between CdSe nanocrystals and organic semiconductors. *Advanced Materials* **2003,** 15, (1), 58-61.

31. Kim, C. S.; Lad, R. J.; Tripp, C. P., Interaction of organophosphorous compounds with TiO2 and WO3 surfaces probed by vibrational spectroscopy. *Sensors and Actuators B-Chemical* **2001,** 76, (1-3), 442-448.

32. Lukes, I.; Borbaruah, M.; Quin, L. D., Direct reaction of phosphorus acids with hydroxy of a silanol and on the silica-gel surface. *Journal of the American Chemical Society* **1994,** 116, (5), 1737-1741.

33. Glockler, J.; Klutzke, S.; Meyer-Zaika, W.; Reller, A.; Garcia-Garcia, F. J.; Strehblow, H. H.; Keller, P.; Rentschler, E.; Klaui, W., With phosphinophosphonic acids to nanostructured, water-soluble, and catalytically active rhodium clusters. *Angewandte Chemie-International Edition* **2007,** 46, (7), 1164-1167.

34. Ellis, J.; Wilson, A. D., The formation and properties of metal-oxide poly(vinylphosphonic acid) cements. *Dental Materials* **1992,** 8, (2), 79-84.

35. Kim, D. K.; Mikhaylova, M.; Wang, F. H.; Kehr, J.; Bjelke, B.; Zhang, Y.; Tsakalakos, T.; Muhammed, M., Starch-coated superparamagnetic nanoparticles as MR contrast agents. *Chemistry of Materials* **2003,** 15, (23), 4343-4351.

36. Dobson, J., Magnetic nanoparticles for drug delivery. *Drug Development Research* **2006,** 67, (1), 55-60.

37. Chou, S. Y.; Wei, M. S.; Krauss, P. R.; Fischer, P. B., Single-domain magnetic pillar array of 35-nm diameter and 65-Gbits/in(2) density for ultrahigh density quantum magnetic storage. *Journal of Applied Physics* **1994,** 76, (10), 6673-6675.

38. Lim, S. F.; Riehn, R.; Ryu, W. S.; Khanarian, N.; Tung, C. K.; Tank, D.; Austin, R. H., In vivo and scanning electron microscopy imaging of upconverting nanophosphors in Caenorhabditis elegans. *Nano Letters* **2006,** 6, (2), 169-174.

39. Hasobe, T.; Imahori, H.; Kamat, P. V.; Fukuzumi, S., Quaternary self-organization of porphyrin and fullerene units by clusterization with gold nanoparticles on SnO_2 electrodes for organic solar cells. *Journal of the American Chemical Society* **2003,** 125, (49), 14962-14963.

40. Wang, S. R.; Huang, J.; Zhao, Y. Q.; Wang, S. P.; Wu, S. H.; Zhang, S. M.; Huang, W. P., Nanostructure SnO_2 and supported Au catalysts: synthesis, characterization, and catalytic oxidation of CO. *Materials Letters* **2006,** 60, (13-14), 1706-1709.

41. Ahn, H. J.; Choi, H. C.; Park, K. W.; Kim, S. B.; Sung, Y. E., Investigation of the structural and electrochemical properties of size-controlled SnO_2 nanoparticles. *Journal of Physical Chemistry B* **2004,** 108, (28), 9815-9820.

42. Martinelli, G.; Carotta, M. C.; Traversa, E.; Ghiotti, G., Thick-film gas sensors based on nano-sized semiconducting oxide powders. *Mrs Bulletin* **1999,** 24, (6), 30-36.

43. Bonhote, P.; Moser, J. E.; Humphry-Baker, R.; Vlachopoulos, N.; Zakeeruddin, S. M.; Walder, L.; Gratzel, M., Long-lived photoinduced charge separation and redox-type photochromism on mesoporous oxide films sensitized by molecular dyads. *Journal of the American Chemical Society* **1999,** 121, (6), 1324-1336.

44. Wedel, M.; Walter, A.; Monforts, F. P., Synthesis of metalloporphyrins and metallochlorins for immobilization on electrode surfaces. *European Journal of Organic Chemistry* **2001**, (9), 1681-1687.

45. Appleyard, S. F. J.; Day, S. R.; Pickford, R. D.; Willis, M. R., Organic electroluminescent devices: enhanced carrier injection using SAM derivatized ITO electrodes. *Journal of Materials Chemistry* **2000,** 10, (1), 169-173.

46. Hanson, E. L.; Guo, J.; Koch, N.; Schwartz, J.; Bernasek, S. L., Advanced surface modification of indium tin oxide for improved charge injection in organic devices. *Journal of the American Chemical Society* **2005,** 127, (28), 10058-10062.

47. Koh, S. E.; McDonald, K. D.; Holt, D. H.; Dulcey, C. S.; Chaney, J. A.; Pehrsson, P. E., Phenylphosphonic acid functionalization of indium tin oxide: Surface chemistry and work functions. *Langmuir* **2006,** 22, (14), 6249-6255.

48. Paniagua, S. A.; Hotchkiss, P. J.; Jones, S. C.; Marder, S. R.; Mudalige, A.; Marrikar, F. S.; Pemberton, J. E.; Armstrong, N. R., Phosphonic acid modification of indium-tin oxide electrodes: Combined XPS/UPS/contact angle studies. *Journal of Physical Chemistry C* **2008,** 112, (21), 7809-7817.

49. Wu, C. K.; Yin, M.; O'Brien, S.; Koberstein, J. T., Quantitative analysis of copper oxide nanoparticle composition and structure by X-ray photoelectron spectroscopy. *Chemistry of Materials* **2006,** 18, (25), 6054-6058.

50. Lai, H.; Bao, A.; Yang, Y. M.; Xu, W. W.; Tao, Y. C.; Yang, H., Preparation and luminescence property of Dy3+-doped YPO4 phosphors. *Journal of Luminescence* **2008,** 128, (3), 521-524.

51. Malakhovskii, A. V.; Isachenko, V. A.; Sukhachev, A. L.; Potseluyko, A. M.; Zabluda, V. N.; Zarubina, T. V.; Edelman, I. S., Magneto-optical properties of Dy^{3+} in oxide glasses: The origin of the magneto-optical activity of f-f transitions and its anomalous temperature dependence. *Physics of the Solid State* **2007,** 49, (4), 701-707.

52. Acton, O.; Ting, G.; Ma, H.; Jen, A. K. Y., Low-voltage high-performance C_{60} thin film transistors via low-surface-energy phosphonic acid monolayer/hafnium oxide hybrid dielectric. *Applied Physics Letters* **2008,** 93, 083302.

53. Hannon, J. B.; Afzali, A.; Klinke, C.; Avouris, P., Selective placement of carbon nanotubes on metal-oxide surfaces. *Langmuir* **2005,** 21, (19), 8569-8571.

54. Vyklicky, L.; Afzali-Ardakani, A.; Kagan, C. R., Self-assembly and oligomerization of alkyne-terminated molecules on metal and oxide surfaces. *Langmuir* **2005,** 21, (25), 11574-11577.

55. Sugimoto, M., The past, present, and future of ferrites. *Journal of the American Ceramic Society* **1999,** 82, (2), 269-280.

56. Pawluk, K.; Booth, S. E.; Coleman, N. J.; Nicholson, J. W., The interaction of zinc oxide-based dental cements with aqueous solutions of potassium fluoride. *Journal of Materials Science-Materials in Medicine* **2008,** 19, (9), 3035-3039.

57. Qu, H. Q.; Wu, W. H.; Jiao, Y. H.; Xu, J. Z., Thermal behavior and flame retardancy of flexible poly(vinyl chloride) treated with Al(OH)(3) and ZnO. *Polymer International* **2005,** 54, (11), 1469-1473.

58. Taratula, O.; Galoppini, E.; Wang, D.; Chu, D.; Zhang, Z.; Chen, H. H.; Saraf, G.; Lu, Y. C., Binding studies of molecular linkers to ZnO and MgZnO nanotip films. *Journal of Physical Chemistry B* **2006,** 110, (13), 6506-6515.

59. Sinapi, F.; Forget, L.; Delhalle, J.; Mekhalif, Z., Formation and characterization of thin films of $H(CH_2)(x)PO(OH)(2)$ on polycrystalline zinc substrates. *Surface and Interface Analysis* **2002,** 34, (1), 148-154.

60. Giudice, C. A.; Delamo, B.; Benitez, J. C., Determination of Metallic Copper, Cuprous-Oxide and Cupric Oxide during the Manufacture and Storage of Antifouling Paints. *Journal of the Oil & Colour Chemists Association* **1981,** 64, (1), 12-19.

61. Nolan, M.; Elliott, S. D., Tuning the electronic structure of the transparent conducting oxide Cu_2O. *Thin Solid Films* **2008,** 516, (7), 1468-1472.

62. Van Alsten, J. G., Self-assembled monolayers on engineering metals: structure, derivatization, and utility. *Langmuir* **1999,** 15, 7605-7614.

63. Chen, Q.; Boothroyd, C.; Tan, G. H.; Sutanto, N.; Mcintosh Soutar, A.; Zeng, X. T., Silica coating of nanoparticles by the sonogel process. *Langmuir* **2008,** 24, 650 - 653.

64. Blanc, P.; Larbot, A.; Palmeri, J.; Lopez, M.; Cot, L., Hafnia ceramic nanofiltration membranes. Part I: Preparation and characterization. *Journal of Membrane Science* **1998,** 149, 151 - 161.

65. Happy; Tok, A. I. Y.; Boey, F. Y. C.; Huebner, R.; Ng, S. H., Synthesis of dysprosium oxide by homogeneous precipitation. *Journal of Electroceramics* **2006,** 17, 75 - 78.

66. Kung, H. H., *Transition Metal Oxides: Surface Chemistry and Catalysis*. Elsevier: New York, 1989; Vol. 45.

67. Barbalace, K. Periodic Table of Elements. http://EnvironmentalChemistry.com (10/28/2008),

68. Lide, D. R., *CRC Handbook of Chemistry and Physics*. CRC Press: 2002.

69. Kureshy, R. I.; Singh, S.; Khan, N. U. H.; Abdi, S. H. R.; Suresh, E.; Jasra, R. V., Efficient method for ring opening of epoxides with amines by NaY zeolite under solvent-free conditions. *Journal of Molecular Catalysis a-Chemical* **2007,** 264, (1-2), 162-169.

70. Lin, L.; Guthrie, J. T., Novel oxygen-enhanced membrane assemblies for biosensors. *Journal of Membrane Science* **2006,** 278, (1-2), 173-180.

71. Shu, S.; Husain, S.; Koros, W. J., Formation of nanostructured zeolite particle surfaces via a halide/Grignard route. *Chemistry of Materials* **2007,** 19, (16), 4000-4006.

72. Feng, S.; Bein, T., Growth of oriented molecular-sieve crystals on organophosphonate films. *Nature* **1994,** 368, (6474), 834-836.

Chapter 6

Thesis Conclusions and Future Direction

This thesis has presented a body of work aimed at understanding the synthesis of functionalized phosphonic acids, their attachment to metal oxide surfaces and the properties of those surfaces that can be changed. As was mentioned in the introductory chapter, the discipline of monolayer science can be divided into three main thrusts: design and synthesis of ligands, characterization of formed monolayers on surfaces, and the study of the effects these monolayers have on the surface and their subsequent use in applications. Accordingly, our own study of the modification of metal oxide surfaces with phosphonic acids can be divided into similar thrusts.

The following paragraphs provide an overall summary and conclusions of the work presented in this thesis. This includes the results and summaries of the various reported studies, but more importantly relates a significance to the studies and the effects they can have on future endeavors. While some specific recommendations have been given at the ends of sections throughout the thesis, broader recommendations about projects are given at the end here.

There are few phosphonic acids that are commercially available. The synthesis of a number of interesting, functional phosphonic acids has been reported in this thesis. We attempted to control a number of properties of surfaces, such as work function, surface energy, and reactivity, by the design of phosphonic acids which can be used to impart these properties onto a surface. A number of said phosphonic acids were synthesized, and

expertise was gained in how to synthesize them. The phosphonic acid moiety is amenable to a number of attached functional groups. As such a number of phosphonic acids were synthesized with a variety of functional groups, such as polymerizable groups, fluorinated groups, simple functional groups, complicated functional groups, alkyl groups, and aromatic groups. Additionally, it was demonstrated that many of the precursor phosphonates, as well as several heavily used phosphonic acids, could be synthesized in large scales (~50 g). Having a library of compounds from which to choose allows for a mix and match approach where, depending on the problem and the desired properties wanted on a surface, hopefully a phosphonic acid will exist in our library which can be easily used to modify the surface to obtain the desired properties. This opens the door not only to our own research but to a number of collaborations that can already be seen in the studies presented.

The characterization of monolayers on surfaces has been perhaps the most difficult of the thrusts, as there is not a lot of literature precedent for the study of the binding, stability, and coverage of phosphonic acid monolayers. However, we have been able, in a collaborative effort, to initiate and complete some important studies on the nature and strength of the bonds between phosphonic acids and the surfaces they modify. In particular, a number of interesting and unprecedented studies have been completed on the binding of phosphonic acids to ITO surfaces.[1, 2] ITO has been an important component in organic electronic devices, such as photovoltaics and light-emitting diodes, and it has been demonstrated that ITO can be modified with phosphonic acids. However, only a few detailed studies have been reported on the modification of ITO with phosphonic acids.[3-6]

We have demonstrated that the ITO surface can be modeled using theory, and that these calculations can be coupled with experimental techniques, such as XPS, in order to determine the binding modes phosphonic acids adopt on the surface of ITO.[2] Additional studies using IRRAS further corroborate these studies, and it has been shown that phosphonic acids bind to ITO predominately in a mixture of bi-and tridentate modes.[1] Knowing the number of bonds that phosphonic acids use to attach to a surface allows one to infer the stability of the assembled monolayer. This knowledge is important when deciding which surface modification techniques can be successfully used in technological applications that may demand specific parameters that need to be met, such as lifetime or stability of the monolayer.

Along the same lines as studying the binding modes, though in a more quantitative way, we have studied the binding energies of phosphonic acids on ITO using ITC. The heats of enthalpy of the reaction between phosphonic acids and ITO nanoparticles at room temperature was directly measured with the ITC and was found to be ~ 50kcal/mol and ~80 kcal/mol for the adsorption of phenylphosphonic acid and octylphosphonic acid, respectively. A Sci-Finder search revealed no other studies which report on the bond strengths of phosphonic acids adsorbed to ITO.

However, while our work has focused on the modification and characterization of ITO surfaces, several other substrate types have been examined. Zinc oxide, which can be used as a material in piezoelectric sensors,[7] as well as receiving attention as a potential cathode material in organic electronic device architectures,[8, 9] has also been modified with phosphonic acids and characterized. Few reports exist on the surface modification of planar zinc oxide substrates with phosphonic acids, and the ones that do exist are

incomplete in terms of demonstrating the manner in which phosphonic acids bind to the surface.[10] We used IRRAS measurements to determine that a predominately tridentate binding is seen between phosphonic acids and planar zinc oxide substrates, and further studies using Contact Angle, AFM, and XPS indicate a high degree of coverage using alkylphosphonic acids. The ability of phosphonic acids to bind in a tridentate manner, with high surface coverage to zinc oxide means that they are a promising ligand with which to continue further studies, more on the application side, of their use to bind biomolecules to zinc oxide in biosensor platforms.

We have also studied the ability of phosphonic acids to modify zeolites. The ability to modify zeolites with phosphonic acids has been demonstrated before,[11] but an in depth study has not been reported. Using a combination of SS MAS NMR, TGA, FTIR, and XPS, we have shown an ability to modify the surface, and we think preferentially the outer surface, of zeolites. The end goal is to be able to use phosphonic acids to change the surface wetting properties of the zeolites such that they better interact with polymer matrices. Hopefully a better wetting between the two materials will lead to membranes which can better separate mixes of gases. So far, initial DSC measurements indicate good interfacial properties between the zeolites and a polymer host, and further studies are underway to investigate this.

The third aspect of monolayer science is measuring the ability of the monolayers to affect a change in properties of the materials they modify. While the first two aspects of monolayer science are important, they are studied in order to understand and control the properties they impart on surfaces. We have demonstrated an ability to systematically tune some of these surface parameters. The work function of a surface, determined by a

combination of dipoles located at the surface, can be systematically tuned with the attachment of molecules which add a dipole to the surface. Using this strategy, we have been able to tune to the work function of ITO a maximum of 1.2 eV, which incorporates the ability to not only increase the work function to ~5.6 eV, but also to decrease the work function to ~ 4.4 eV, from that of solvent-cleaned ITO (~4.5 eV). While a similar increase can be obtained with air or oxygen plasma treatment of the ITO, we have also demonstrated that the change in work function of ITO as a result of surface modification with phosphonic acids is quite stable over time, while the work function increase of ITO as a result of plasma treatment is short-lived and rapidly decreases in ambient conditions. This result is important in the sense that one major consideration of any electronic device is its lifetime. Only products which can show lifetimes above a certain threshold, which varies depending on the application, will be produced. Therefore, demonstrating not only the ability to change the work function, but also maintaining that change over time, is significant. Initial studies on OLED luminance lifetimes indicate this. An OLED device using plasma-treated ITO shows a luminance half life (the time it takes for the device to reach half of its initial luminance) is 97 hours. An OLED device using a phosphonic acid monolayer, which imparts a similar increase in work function and a similar starting luminance, shows a half life of 616 hours. These results indicate the advantage of using monolayers over air plasma in device platforms.

The surface energy of a material is also an important property, especially when the material interacts with another material. The ability to form robust interfaces between two materials is also an important ability, especially in organic electronics where layers of materials are combined to form devices. While monolayers cannot be used on all the

layers in an OPV or OLED, they can be used to modify the surface energy of ITO. We have performed two studies which demonstrate the ability to decrease the relatively high surface energy of ITO to a surface energy that should be more like the organic materials that will form interfaces with ITO in these devices. Our first study was the first reported that shows an ability to decrease the surface energy of ITO using phosphonic acid monolayers. We then conducted a second study that was novel in that the surface energy can now be tuned to a relatively constant 35-58 mJ/m^2 while the work functions of the ITO can be tuned the previously stated amount of 1.2 eV. This ability allows for the systematic change of the work function while keeping the surface energy constant, which allows for studies which can directly attribute changes in device performance to a change in work function rather than a difference in wetting of the organic materials on ITO.

Lastly, we have broadened the study of the ability of phosphonic acids to modify metal oxides. It is our belief that phosphonic acids can be considered a universal modifier for hydroxyl terminated metal oxide substrates, and that the recognition of this will play a large role in promoting the use of phosphonic acids for this purpose. We investigated the surface modification of six different metal oxide nanoparticles with phosphonic acids, and found that the phosphonic acids modified these surfaces in all cases. It also seems apparent from TGA derivative curves that the thermal stability of the phosphonic acid-modified surfaces is dependent on the metal oxide. This is not surprising as the bond energies of different metals to oxygen can differ greatly, and this appears to play a role in the thermal stability of phosphonic acids on their surfaces.

While a number of the aforementioned studies are complete and published, some of them are works in progress. There are other additional studies which would be

interesting to undertake in the near future.

The ability of ITC to measure the enthalpies of binding interaction in solution is a powerful one. While there is merit in studying and knowing the binding modes with which phosphonic acids attach to metal oxides, being able to directly measure the enthalpies of bond formation of the interactions is more useful in terms of gaining quantitative insight. It would therefore be interesting to study further the binding interactions of phosphonic acids with different metal oxides and perhaps then determine a new model relating the thermodynamic process which yields more concrete binding energies.

The modification of zeolites with phosphonic acids is an ongoing study, with only the initial results presented herein. However, it is clear that phosphonic acids have the ability to modify the zeolite surface. This ability can be used in further studies to change the wetting behavior of the zeolites towards polymers, in much the same was as we have modified ITO substrates[1] and barium titanate nanoparticles[12] for the same purpose.

Additionally, preliminary results have been obtained on using phosphonic acid–modified ZnO for the attachment of biomolecules and ITO for the crosslinking of small molecules.[bb] Both of these studies can be continued.

Lastly, expanding on the data already collected on the modification of various metal oxide nanoparticles with phosphonic acids would be interesting. While the initial data shows an ability to successfully functionalize all six of the metal oxides tested, further insight can be obtained by more detailed TG analysis studies and surface area studies of the unmodified and modified materials.

[bb] See Appendix B for detailed experimental results.

6.1 References

1. Paniagua, S. A.; Hotchkiss, P. J.; Jones, S. C.; Marder, S. R.; Mudalige, A.; Marrikar, F. S.; Pemberton, J. E.; Armstrong, N. R., Phosphonic acid modification of indium-tin oxide electrodes: Combined XPS/UPS/contact angle studies. *Journal of Physical Chemistry C* **2008,** 112, (21), 7809-7817.

2. Paramonov, P. B.; Paniagua, S. A.; Hotchkiss, P. J.; Jones, S. C.; Armstrong, N. R.; Marder, S. R.; Brédas, J.-L., Theoretical characterization of the indium tin oxide surface and its binding sites for adsorption of phosphonic acid monolayers. *Chemistry of Materials* **2008,** 20, (16), 5131-5133.

3. Koh, S. E.; McDonald, K. D.; Holt, D. H.; Dulcey, C. S.; Chaney, J. A.; Pehrsson, P. E., Phenylphosphonic acid functionalization of indium tin oxide: Surface chemistry and work functions. *Langmuir* **2006,** 22, (14), 6249-6255.

4. Appleyard, S. F. J.; Day, S. R.; Pickford, R. D.; Willis, M. R., Organic electroluminescent devices: enhanced carrier injection using SAM derivatized ITO electrodes. *Journal of Materials Chemistry* **2000,** 10, (1), 169-173.

5. Besbes, S.; Ltaief, A.; Reybier, K.; Ponsonnet, L.; Jaffrezic, N.; Davenas, J.; Ben Ouada, H., Injection modifications by ITO functionalization with a self-assembled monolayer in OLEDs. *Synthetic Metals* **2003,** 138, (1-2), 197-200.

6. Brewer, S. H.; Brown, D. A.; Franzen, S., Formation of thiolate and phosphonate adlayers on indium-tin oxide: Optical and electronic characterization. *Langmuir* **2002,** 18, (18), 6857-6865.

7. Corso, C. D.; Dickherber, A.; Hunt, W. D., Lateral field excitation of thickness shear mode waves in a thin film ZnO solidly mounted resonator. *Journal of Applied Physics* **2007,** 101, (5), 054514/1-054514/7.

8. Yip, H. L.; Hau, S. K.; Baek, N. S.; Jen, A. K. Y., Self-assembled monolayer modified ZnO/metal bilayer cathodes for polymer/fullerene bulk-heterojunction solar cells. *Applied Physics Letters* **2008,** 92, (19), 193313/1-193313/3.

9. Yip, H. L.; Hau, S. K.; Baek, N. S.; Ma, H.; Jen, A. K. Y., Polymer solar cells that use self-assembled-monolayer-modified ZnO/metals as cathodes. *Advanced Materials* **2008,** 20, (12), 2376-2382.

10. Sinapi, F.; Forget, L.; Delhalle, J.; Mekhalif, Z., Formation and characterization of thin films of $H(CH_2)_xPO(OH)_2$ on polycrystalline zinc substrates. *Surface and Interface Analysis* **2002,** 34, (1), 148-154.

11. Doussineau, T.; Durand, J. O.; Granier, M.; Smaihi, M.; Valtchev, V., Synthesis of phosphonic acids with the semicarbazide group for the functionalization of metal oxide and zeolite nanoparticles. *Synlett* **2004**, (10), 1735-1738.

12. Kim, P.; Jones, S. C.; Hotchkiss, P. J.; Haddock, J. N.; Kippelen, B.; Marder, S. R.; Perry, J. W., Phosphonic acid-modified barium titanate polymer nanocomposites with high permittivity and dielectric strength. *Advanced Materials* **2007,** 19, (7), 1001-1005.

Appendix A

^{1}H, ^{13}C, and ^{31}P NMR spectra for the samples which did not pass elemental analysis are shown below. In most cases, the presence of water can be seen in the ^{1}H NMR spectra.

Diethyl 6–phenylhexylphosphonate

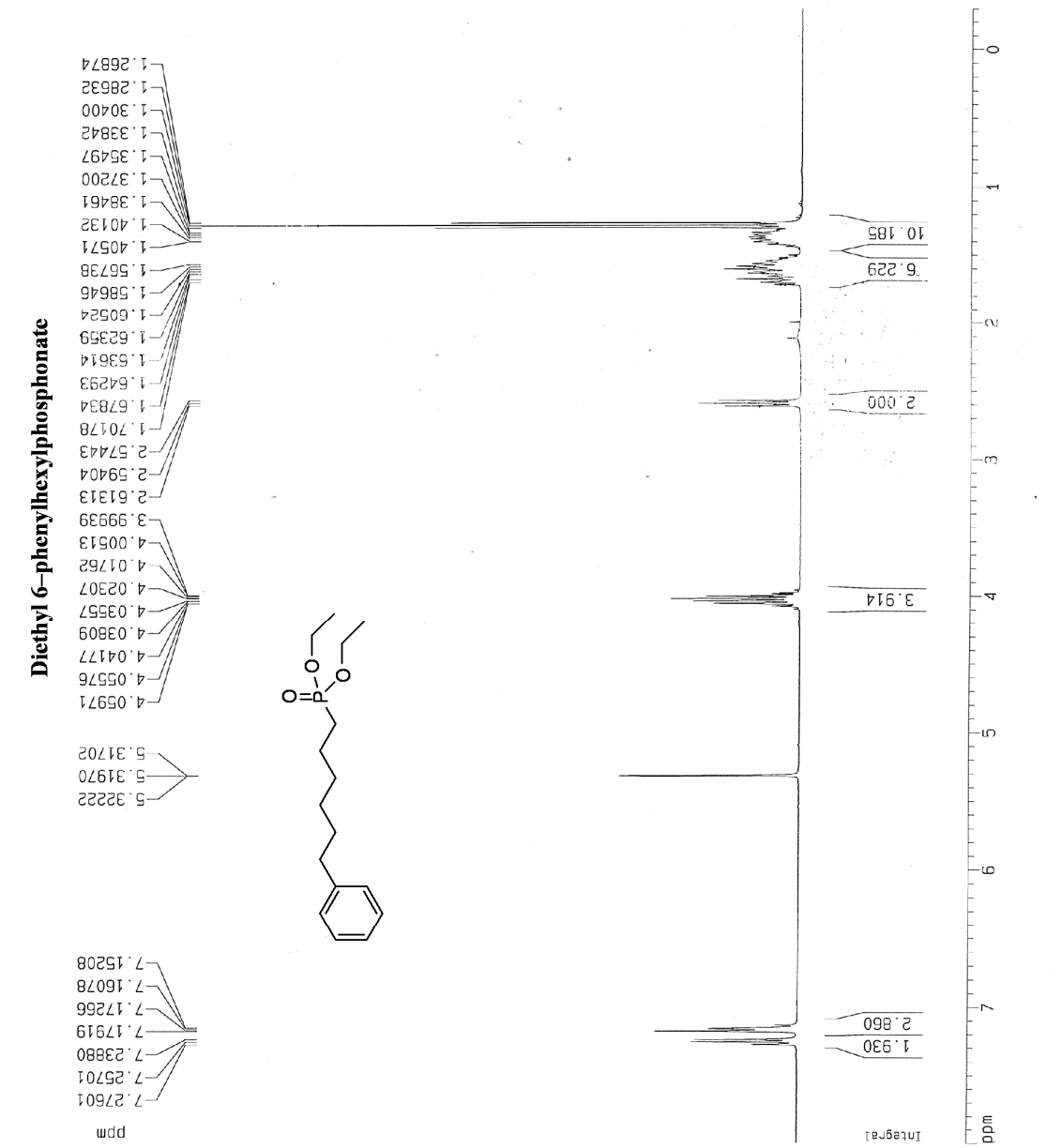

Diethyl 6–phenylhexylphosphonate

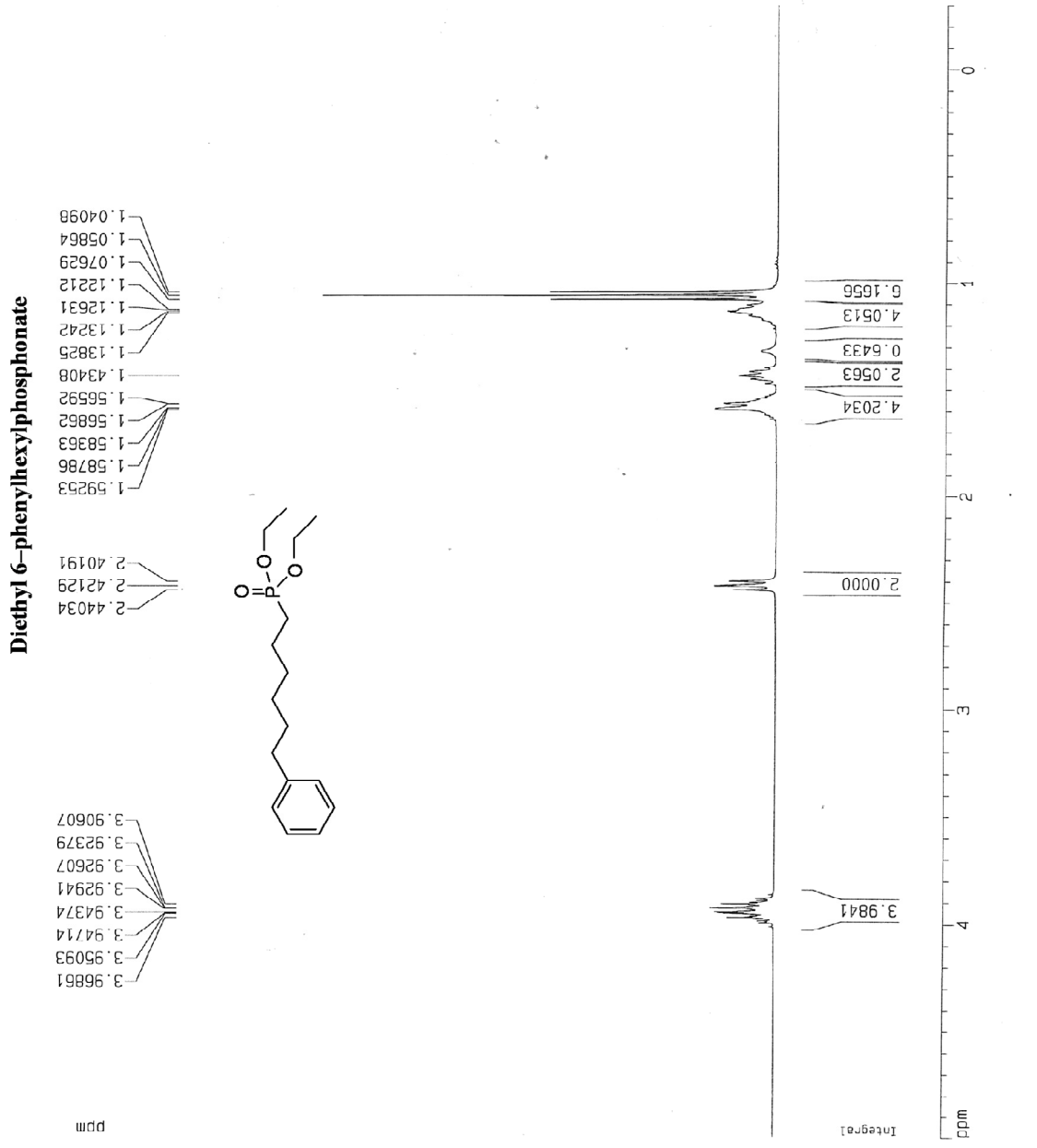

Diethyl 6–phenylhexylphosphonate

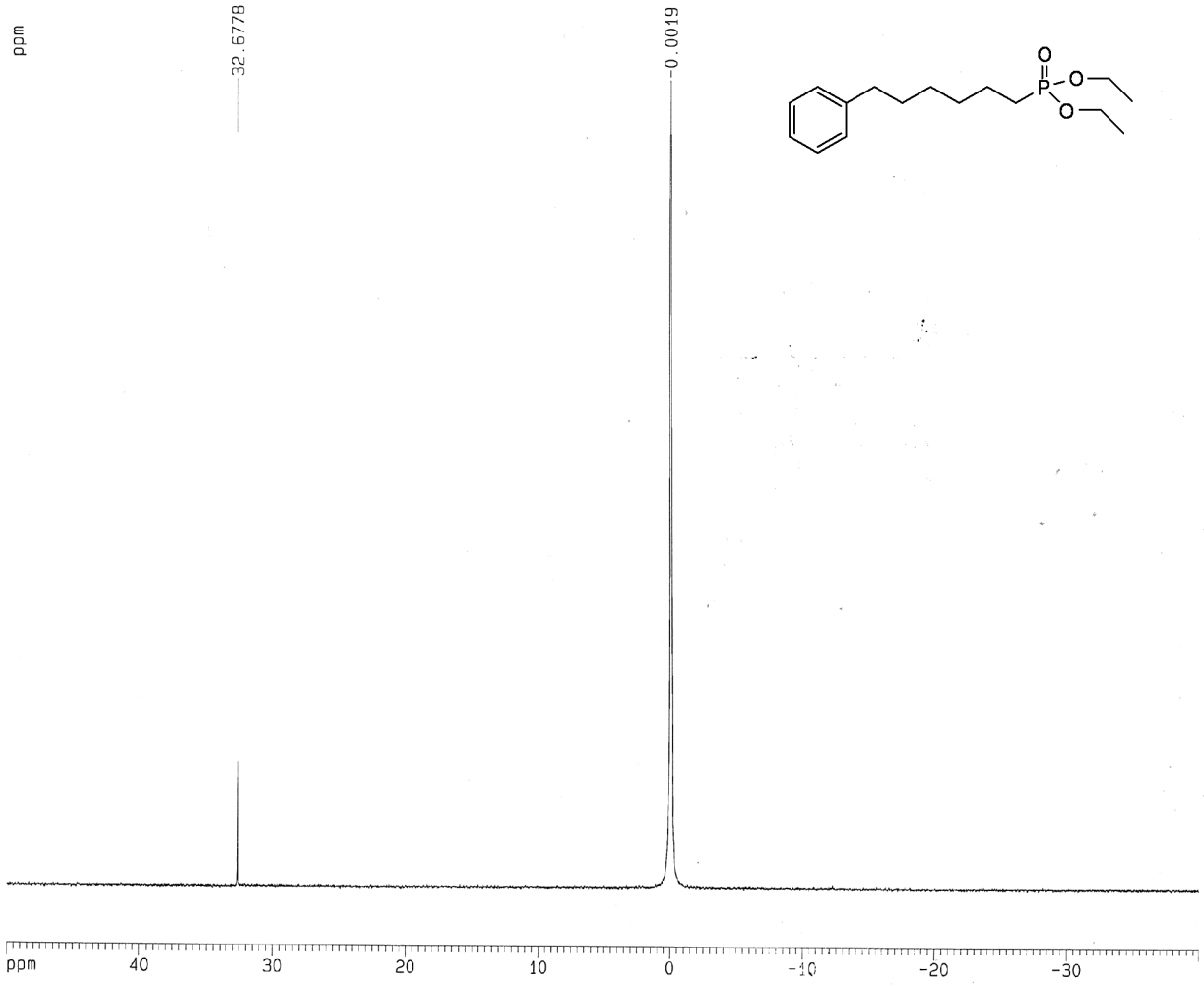


```
Current Data Parameters
NAME                 PJH-I-37m
EXPNO                        1
PROCNO                       1

F2 - Acquisition Parameters
Date_                 20080818
Time                     14.47
INSTRUM                amx400
PROBHD      5 mm Multinu
PULPROG                zgpg30
TD                        65536
SOLVENT                CD2Cl2
NS                           32
DS                            4
SWH                  71428.570 Hz
FIDRES               1.089913 Hz
AQ                   0.4586020 sec
RG                         4096
DW                    7.000 usec
DE                   10.00 usec
TE                   300.0 K
HL1                          0 dB
D1                   2.00000000 sec
CPDPRG                 waltz16
P31                   100.00 usec
S4                           23 dB
D11                  0.03000000 sec
S2                           23 dB
P1                    11.50 usec
SFO1                161.9692445 MHz
NUCLEUS                    31P

F2 - Processing parameters
SI                        32768
SF                  161.9775845 MHz
WDW                          EM
SSB                          0
LB                    1.00 Hz
GB                           0
PC                    1.40

1D NMR plot parameters
CX                   20.00 cm
F1P                  50.000 ppm
F1                   8098.88 Hz
F2P                  -40.000 ppm
F2                   -6479.10 Hz
PPMCM                4.50000 ppm/cm
HZCM                 728.89911 Hz/cm
```

Diethyl 6–phenylhexylphosphonate

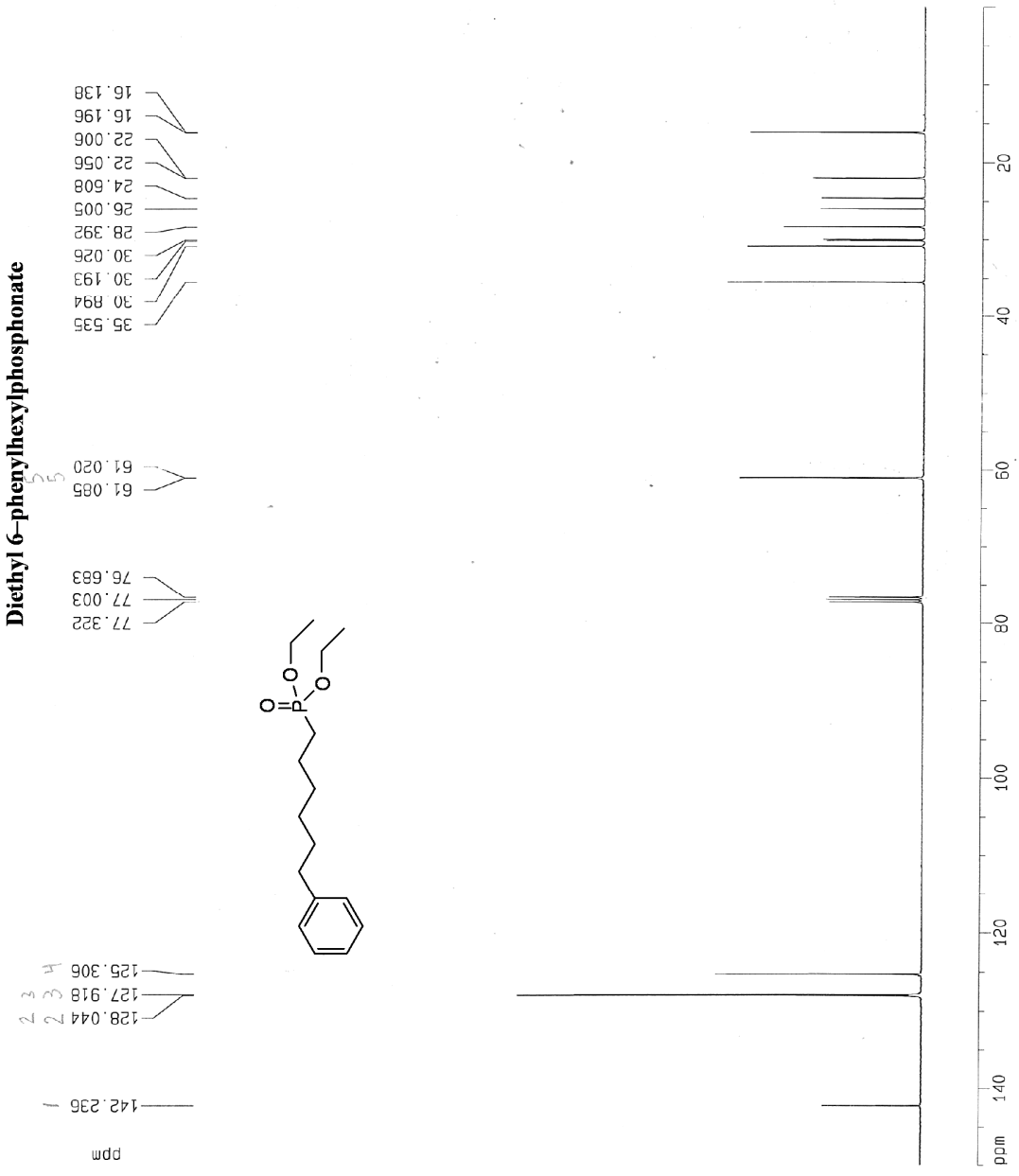

Undec–10–enylphosphonic acid

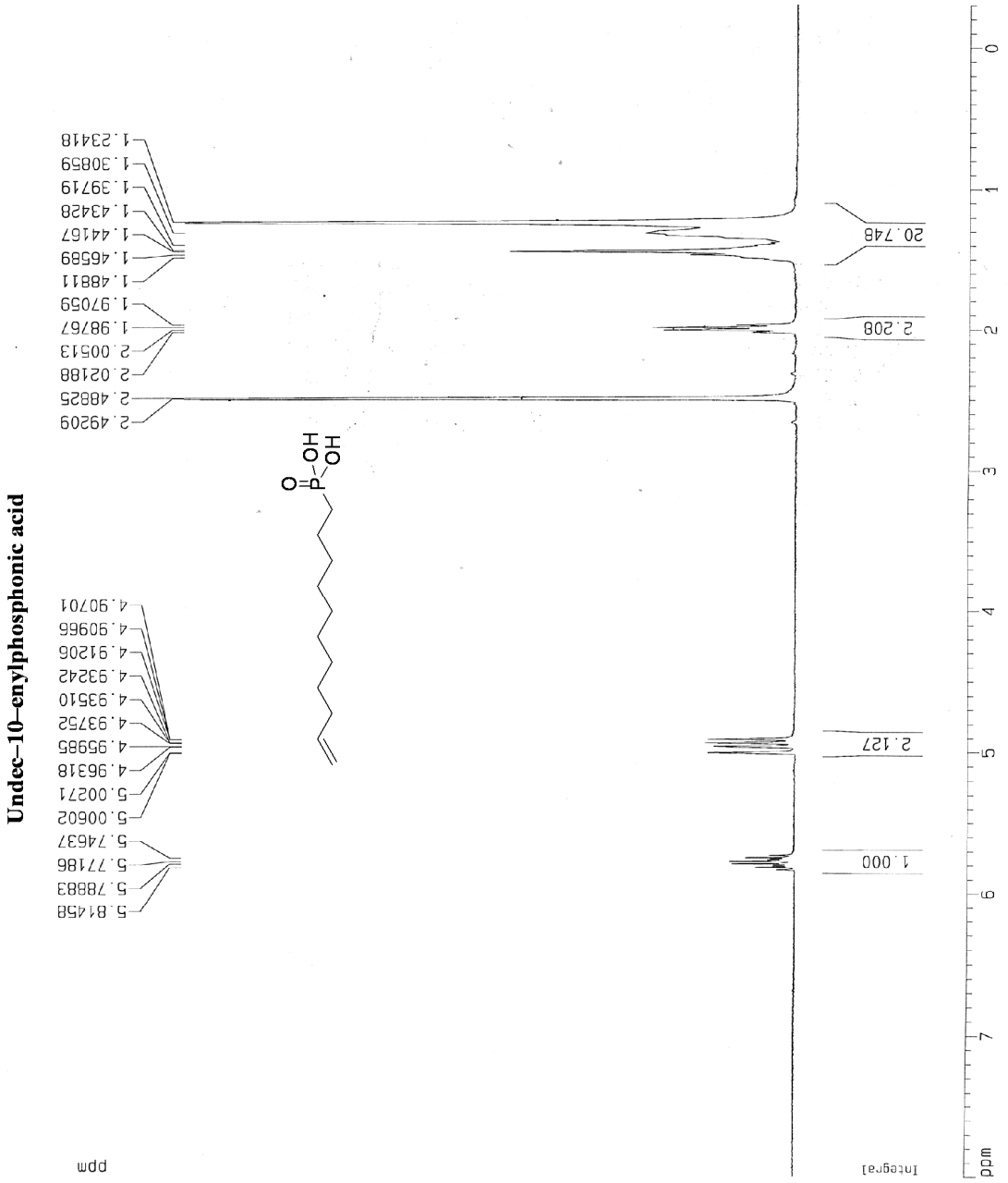

Undec–10–enylphosphonic acid

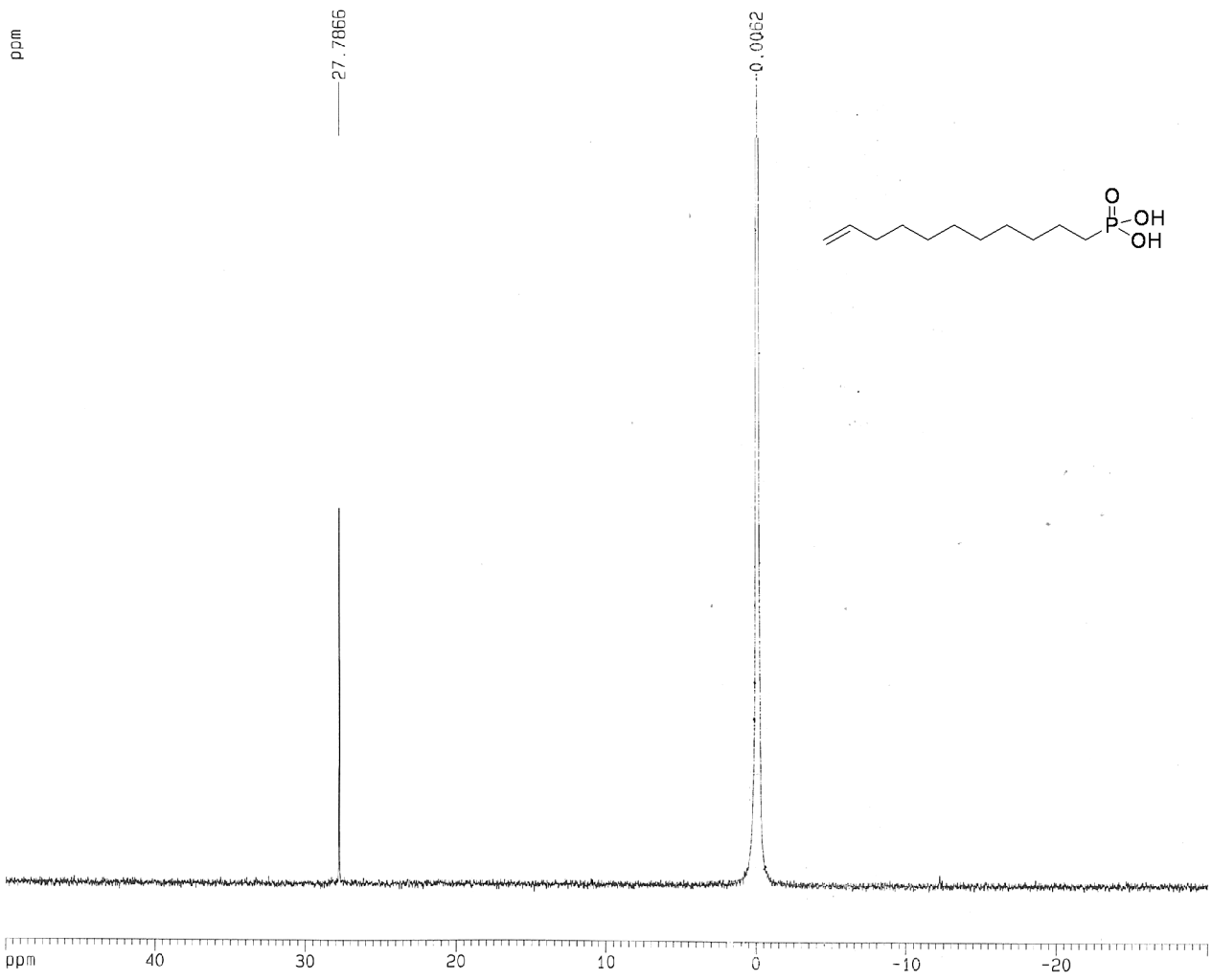


```
Current Data Parameters
NAME          PJH-I-75n
EXPNO                 1
PROCNO                1

F2 - Acquisition Parameters
Date_          20080818
Time              15.02
INSTRUM         amx400
PROBHD     5 mm Multinu
PULPROG         zgpg30
TD               65536
SOLVENT           DMSO
NS                  32
DS                   4
SWH          71428.570 Hz
FIDRES        1.089913 Hz
AQ            0.4588020 sec
RG                4096
DW               7.000 usec
DE              10.00 usec
TE              300.0 K
HL1                 0 dB
D1          2.00000000 sec
CPDPRG          waltz16
P31             100.00 usec
S4                  23 dB
D11         0.03000000 sec
S2                  23 dB
P1              11.50 usec
SFO1       161.9692445 MHz
NUCLEUS            31P

F2 - Processing parameters
SI                32768
SF         161.9779463 MHz
WDW                EM
SSB                 0
LB               1.00 Hz
GB                  0
PC               1.40

1D NMR plot parameters
CX              20.00 cm
F1P             50.000 ppm
F1            8098.90 Hz
F2P            -30.000 ppm
F2           -4859.34 Hz
PPMCM          4.00000 ppm/cm
HZCM         647.91180 Hz/cm
```

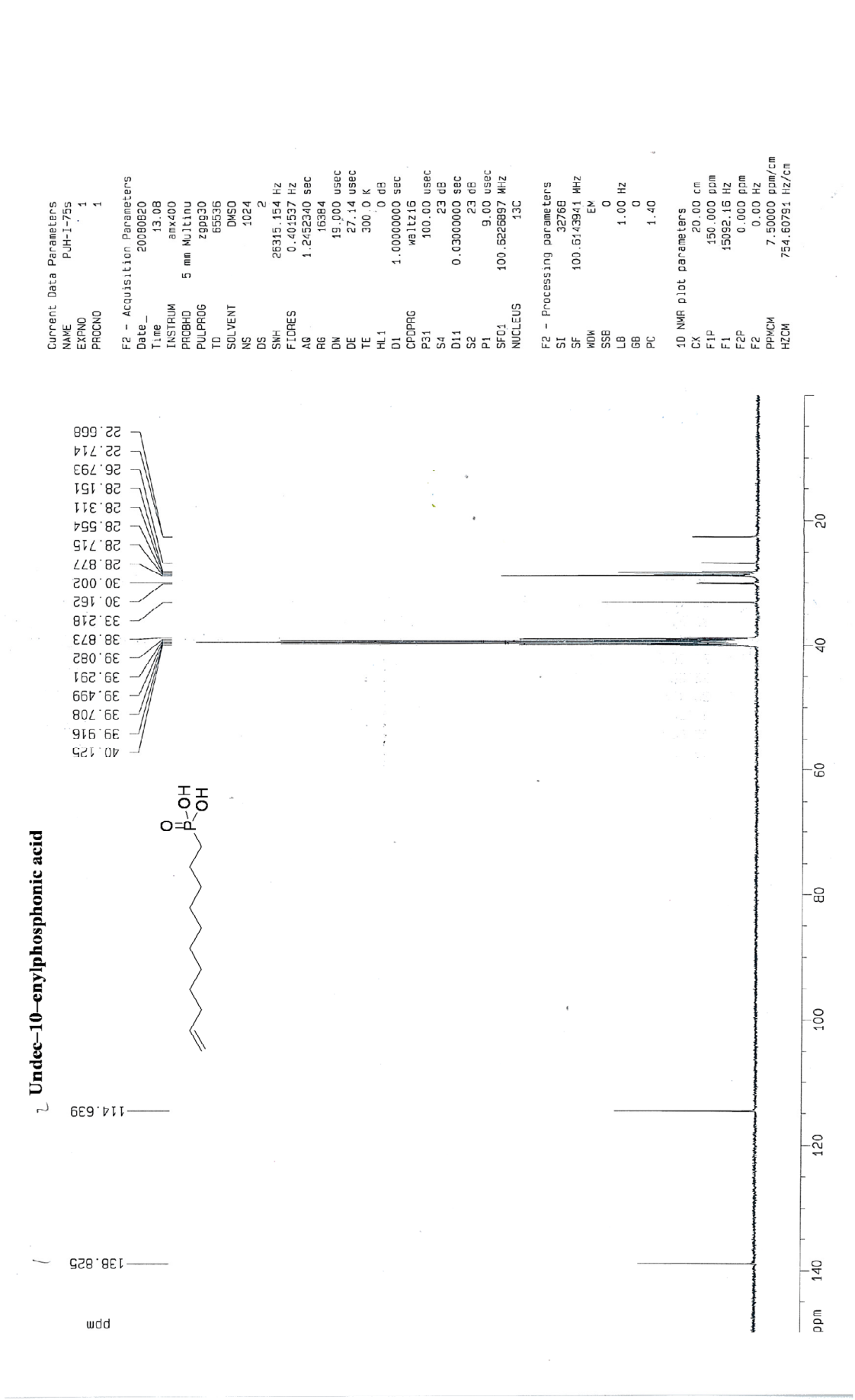
Undec–10–enylphosphonic acid
Current Data Parameters
NAME PJH-1-75s
EXPNO 1
PROCNO 1
F2 - Acquisition Parameters
Date_ 20080820
Time 13.08
INSTRUM amx400
PROBHD 5 mm Multinu
PULPROG zgpg30
TD 65536
SOLVENT DMSO
NS 1024
DS 2
SWH 26315.154 Hz
FIDRES 0.401537 Hz
AQ 1.2452340 sec
RG 16384
DW 19.000 usec
DE 27.14 usec
TE 300.0 K
HL1 0 dB
D1 1.00000000 sec
CPDPRG waltz16
P31 100.00 usec
S4 23 dB
D11 0.03000000 sec
S2 23 dB
P1 9.00 usec
SFO1 100.6228897 MHz
NUCLEUS 13C
F2 - Processing parameters
SI 32768
SF 100.6143941 MHz
WDW EM
SSB 0
LB 1.00 Hz
GB 0
PC 1.40
1D NMR plot parameters
CX 20.00 cm
F1P 150.000 ppm
F1 15092.16 Hz
F2P 0.000 ppm
F2 0.00 Hz
PPMCM 7.50000 ppm/cm
HZCM 754.60791 Hz/cm
ppm
138.825
114.639
40.125
39.916
39.708
39.499
39.291
39.082
38.873
33.218
30.162
30.002
28.877
28.715
28.554
28.311
28.151
26.793
22.714
22.668
O
P
OH
OH
ppm
140
120
100
80
60
40
20

11–(diethoxyphosphoryl)undecyl acrylate

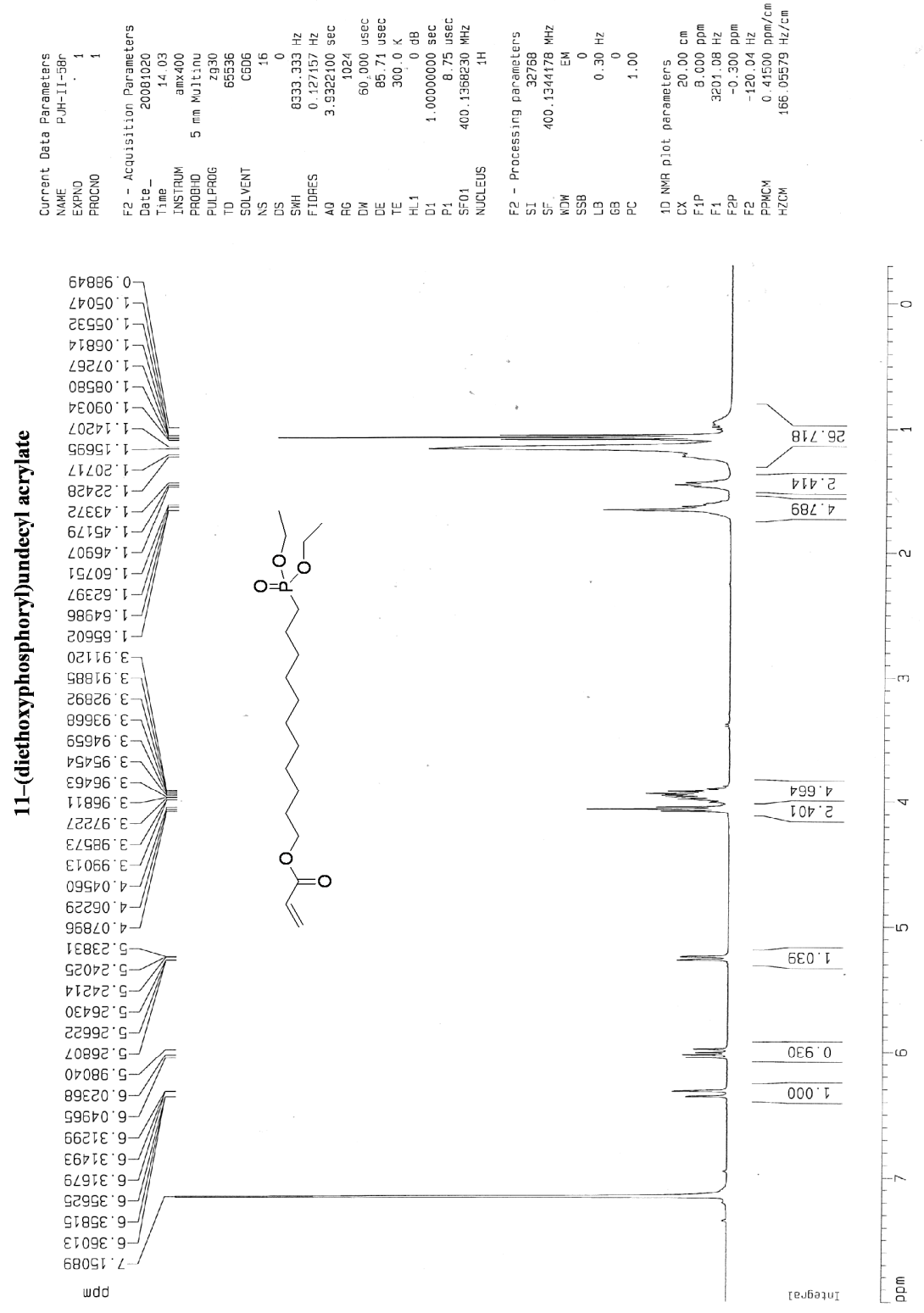

11–(diethoxyphosphoryl)undecyl acrylate

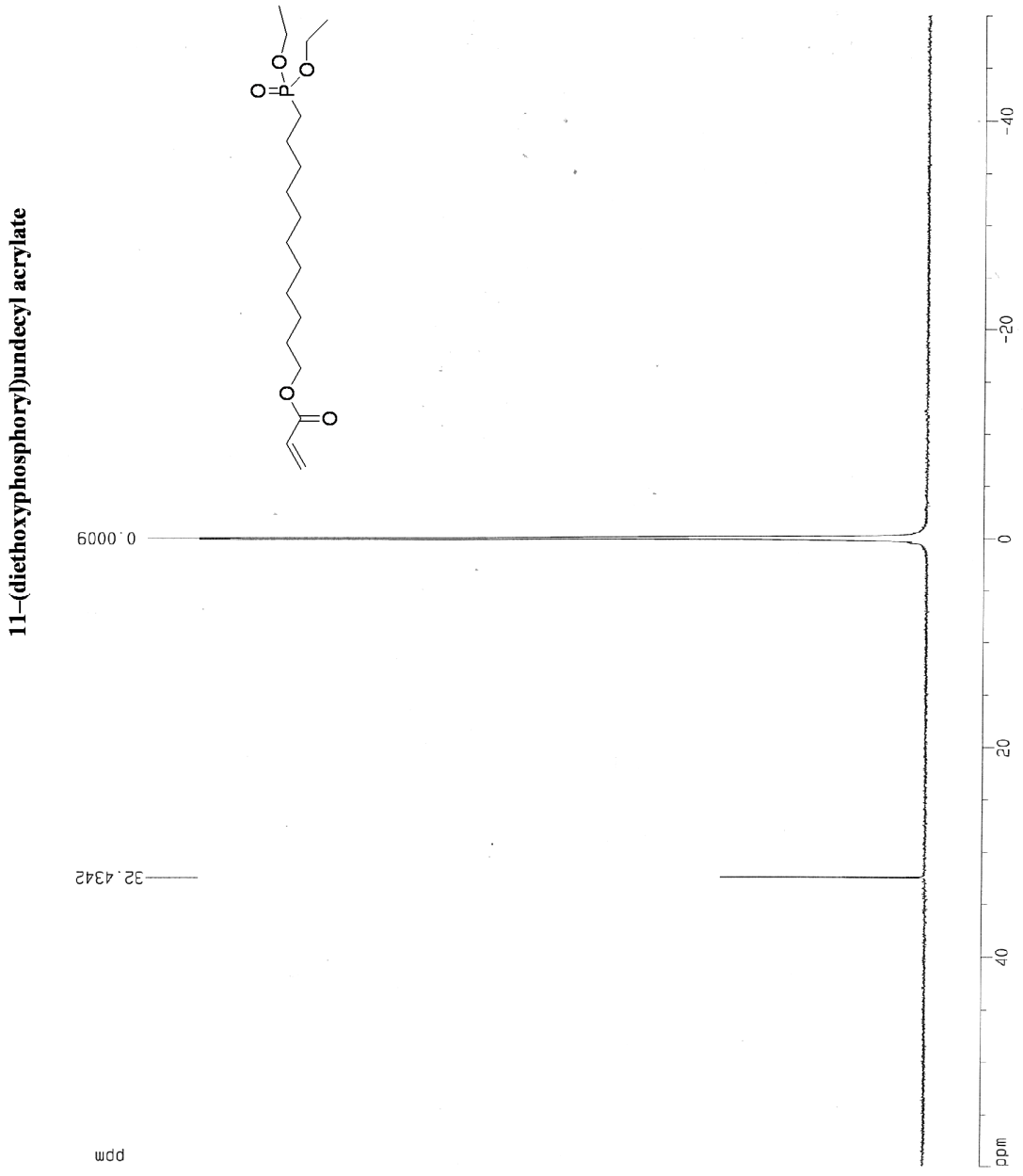

11–(diethoxyphosphoryl)undecyl acrylate

13C OBSERVE

Pulse Sequence: s2pul

USER: hotchkis
DATE: Oct 5 2005
File: exp

Solvent: CDCl3
Ambient temperature
Mercury-300 "r2d2"

PULSE SEQUENCE
Relax. delay 1.000 sec
Pulse 45.0 degrees
Acq. time 0.851 sec
Width 18797.0 Hz
186 repetitions
OBSERVE C13, 75.4466759 MHz
DECOUPLE H1, 300.0477349 MHz
Power 44 dB
continuously on
WALTZ-16 modulated
DATA PROCESSING
Line broadening 1.0 Hz
FT size 32768
Total time 2 hr, 5 min, 44 sec

INDEX	FREQUENCY	PPM	HEIGHT
1	12565.268	166.545	26.5
2	9857.693	130.658	106.2
3	9723.462	128.879	59.1
4	5859.432	77.663	14.6
5	5849.106	77.526	18.8
6	5816.982	77.101	15.0
7	4896.866	64.905	122.6
8	4651.349	61.651	77.5
9	4644.465	61.560	58.9
10	2333.848	30.934	56.5
11	2316.639	30.706	58.9
12	2239.772	29.687	199.2
13	2229.446	29.550	109.8
14	2221.415	29.444	104.2
15	2211.090	29.307	88.8
16	2175.524	28.835	79.3
17	2022.936	26.813	53.2
18	1971.309	26.129	84.8
19	1882.968	24.958	49.0
20	1708.582	22.646	48.3
21	1703.993	22.585	49.1
22	1263.439	16.746	70.1
23	1257.702	16.670	58.1

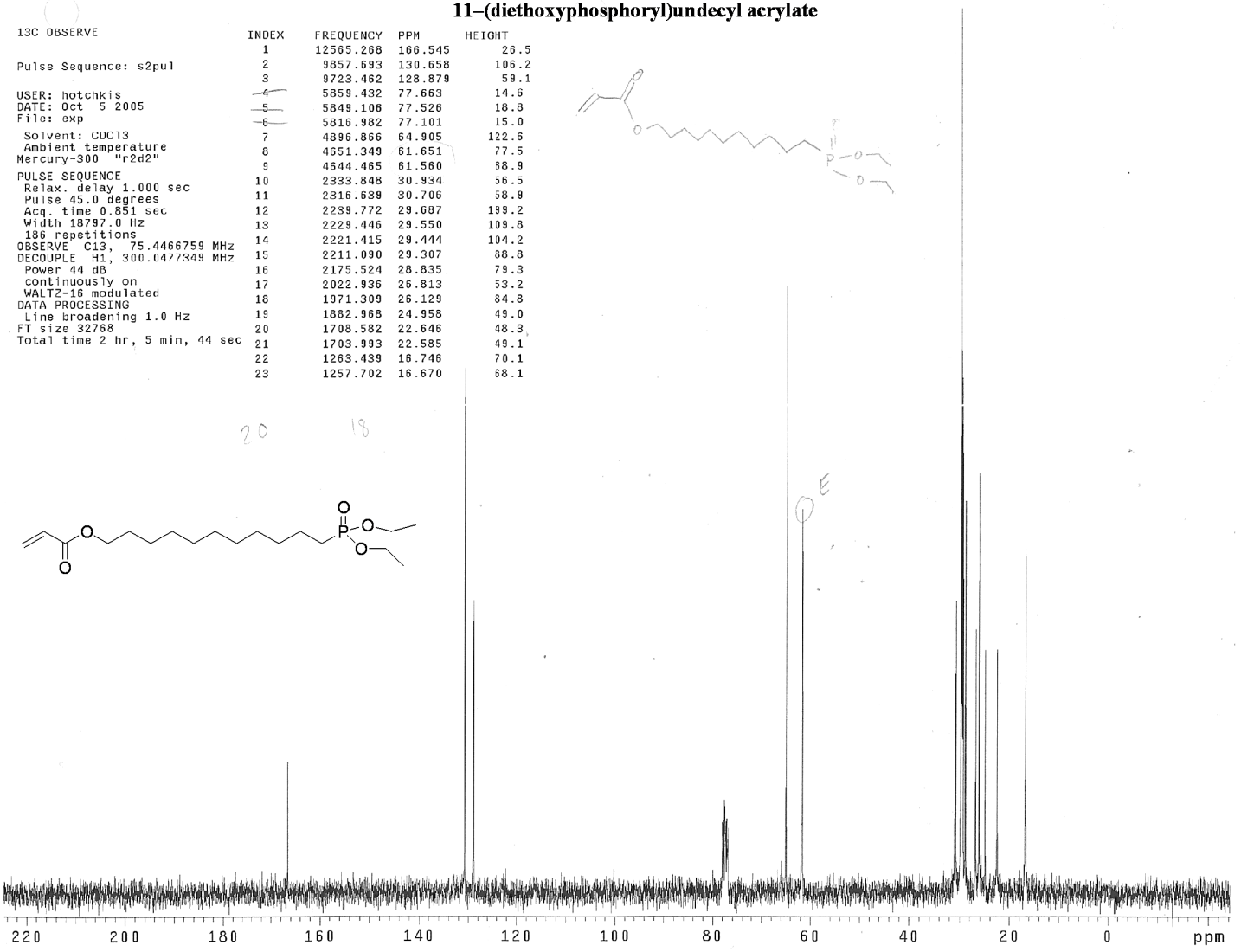

Diethyl 3–(3,6–di–tert–butyl–9*H*–carbazol–9–yl)propylphosphonic acid

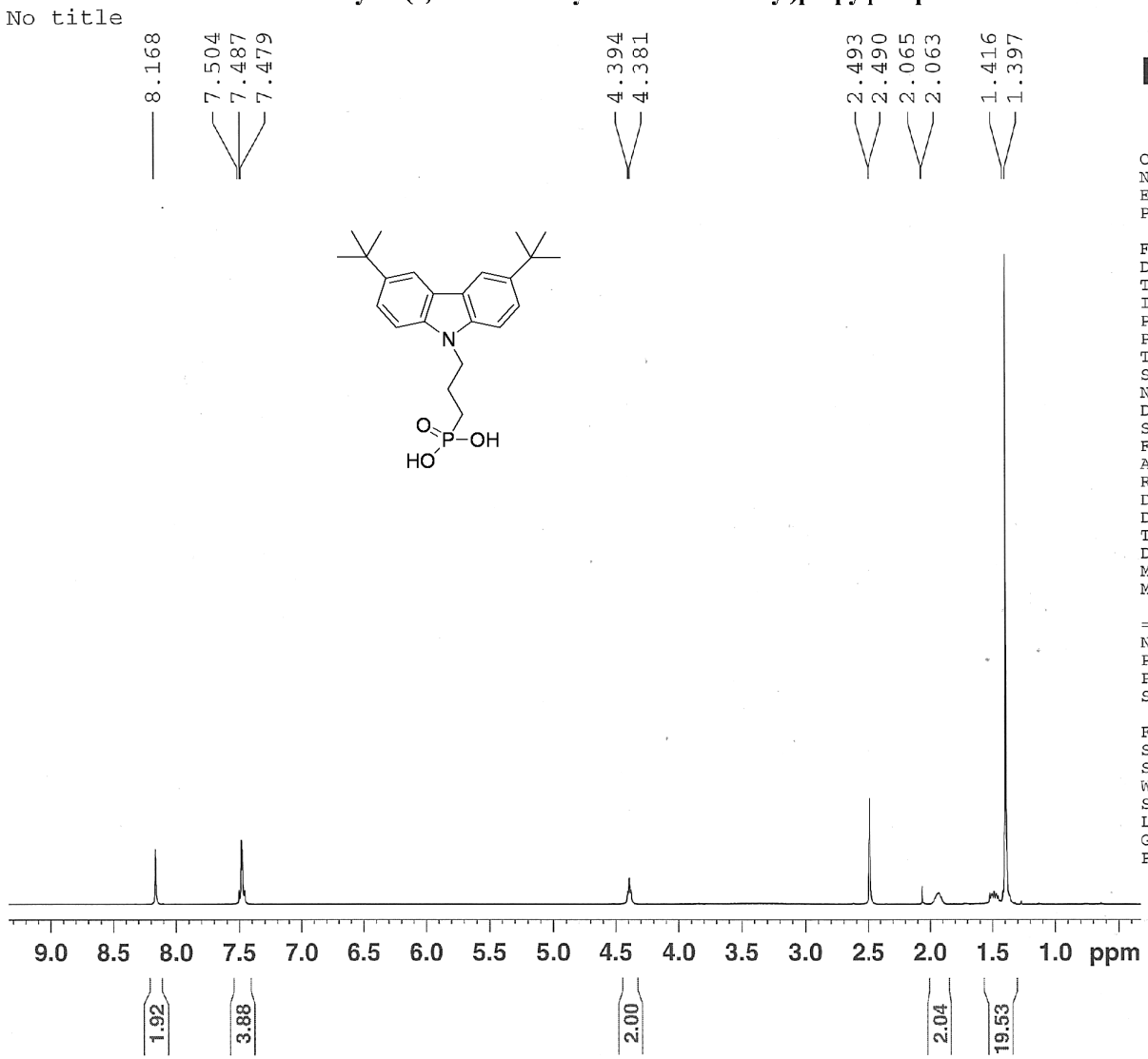

BRUKER

Current Data Parameters
NAME PJH-II-15n
EXPNO 1
PROCNO 1

F2 - Acquisition Parameters
Date_ 20060120
Time 17.23
INSTRUM spect
PROBHD 5 mm Multinucl
PULPROG zg30
TD 65536
SOLVENT DMSO
NS 16
DS 2
SWH 10330.578 Hz
FIDRES 0.157632 Hz
AQ 3.1719923 sec
RG 362
DW 48.400 usec
DE 6.00 usec
TE 298.0 K
D1 1.00000000 sec
MCREST 0.00000000 sec
MCWRK 0.01500000 sec

======== CHANNEL f1 ========
NUC1 1H
P1 8.80 usec
PL1 0.00 dB
SFO1 500.1330885 MHz

F2 - Processing parameters
SI 32768
SF 500.1300109 MHz
WDW EM
SSB 0
LB 0.30 Hz
GB 0
PC 1.00

Diethyl 3–(3,6–di–tert–butyl–9*H*–carbazol–9–yl)propylphosphonic acid

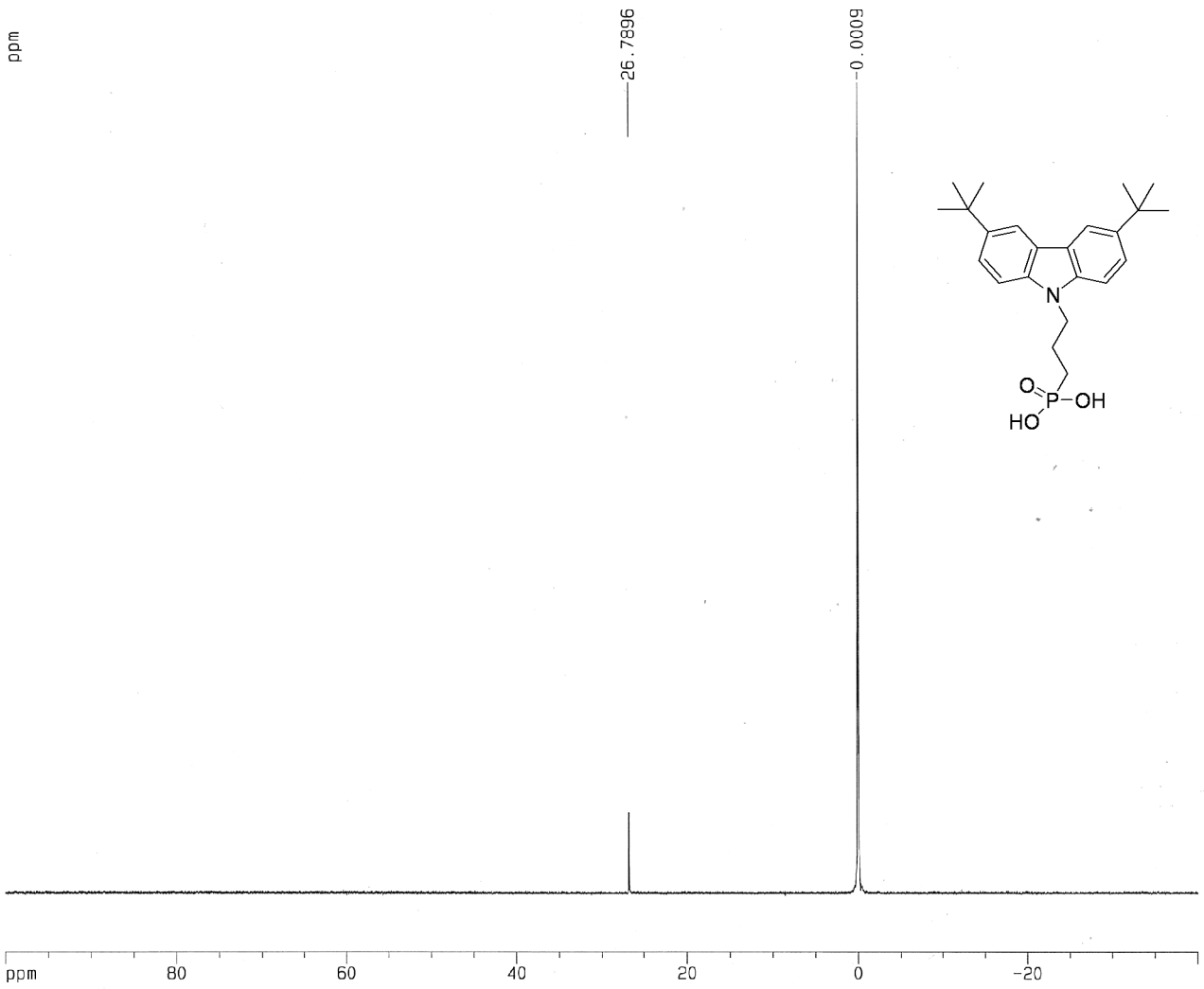


```
Current Data Parameters
NAME                  PJH-II-6e
EXPNO                         1
PROCNO                        1

F2 - Acquisition Parameters
Date_                  20060105
Time                      15.50
INSTRUM                 amx400
PROBHD      5 mm Multinu
PULPROG                 zgpg30
TD                         65536
SOLVENT                   DMSO
NS                            32
DS                             4
SWH                   71428.570 Hz
FIDRES                1.089913 Hz
AQ                    0.4588020 sec
RG                         4096
DW                        7.000 usec
DE                       10.00 usec
TE                        300.0 K
HL1                           0 dB
D1                   2.00000000 sec
CPDPRG                  waltz16
P31                      100.00 usec
S4                           23 dB
D11                  0.03000000 sec
S2                           23 dB
P1                       11.50 usec
SFO1                161.9692445 MHz
NUCLEUS                    31P

F2 - Processing parameters
SI                         32768
SF                  161.9779463 MHz
WDW                           EM
SSB                            0
LB                          1.00 Hz
GB                             0
PC                          1.40

1D NMR plot parameters
CX                         20.00 cm
F1P                       100.000 ppm
F1                      16197.79 Hz
F2P                       -40.000 ppm
F2                      -6479.12 Hz
PPMCM                     7.00000 ppm/cm
HZCM                 1133.84570 Hz/cm
```

PJH-II-6g

Bu$_4$NPf$_6$

Diethyl 3–(3,6–di–tert–butyl–9*H*–carbazol–9–yl)propylphosphonic acid

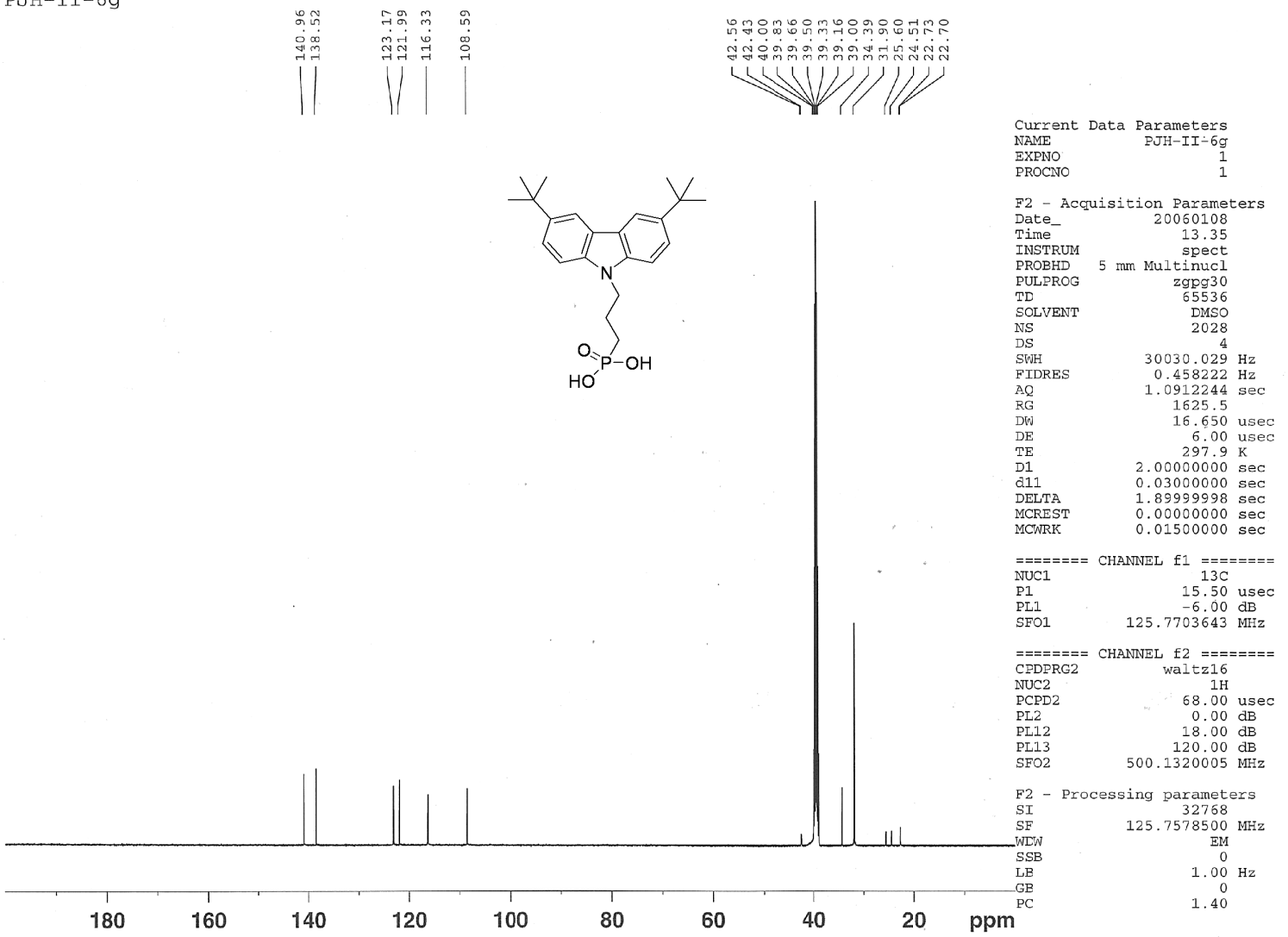


```
Current Data Parameters
NAME                  PJH-II-6g
EXPNO                         1
PROCNO                        1

F2 - Acquisition Parameters
Date_                  20060108
Time                      13.35
INSTRUM                   spect
PROBHD    5 mm Multinucl
PULPROG                  zgpg30
TD                        65536
SOLVENT                    DMSO
NS                         2028
DS                            4
SWH                30030.029 Hz
FIDRES              0.458222 Hz
AQ                  1.0912244 sec
RG                     1625.5
DW                     16.650 usec
DE                      6.00 usec
TE                     297.9 K
D1                2.00000000 sec
d11               0.03000000 sec
DELTA             1.89999998 sec
MCREST            0.00000000 sec
MCWRK             0.01500000 sec

======== CHANNEL f1 ========
NUC1                      13C
P1                     15.50 usec
PL1                    -6.00 dB
SFO1             125.7703643 MHz

======== CHANNEL f2 ========
CPDPRG2                waltz16
NUC2                       1H
PCPD2                  68.00 usec
PL2                     0.00 dB
PL12                   18.00 dB
PL13                  120.00 dB
SFO2             500.1320005 MHz

F2 - Processing parameters
SI                        32768
SF               125.7578500 MHz
WDW                          EM
SSB                           0
LB                     1.00 Hz
GB                            0
PC                     1.40
```

2–(2–(2–(12–bromododecyloxy)ethoxy)ethoxy)ethyl acetate

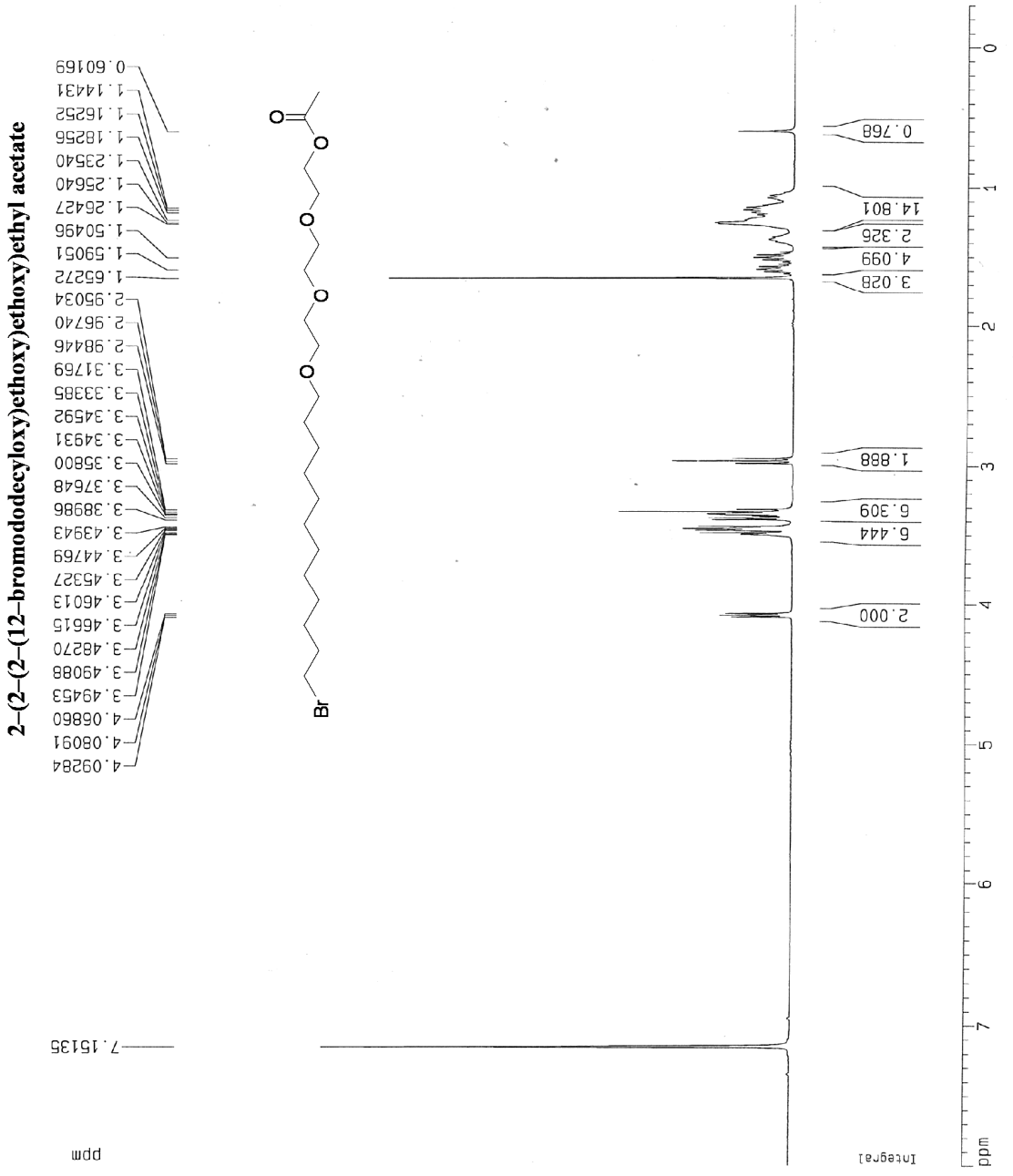

2–(2–(2–(12–bromododecyloxy)ethoxy)ethoxy)ethyl acetate

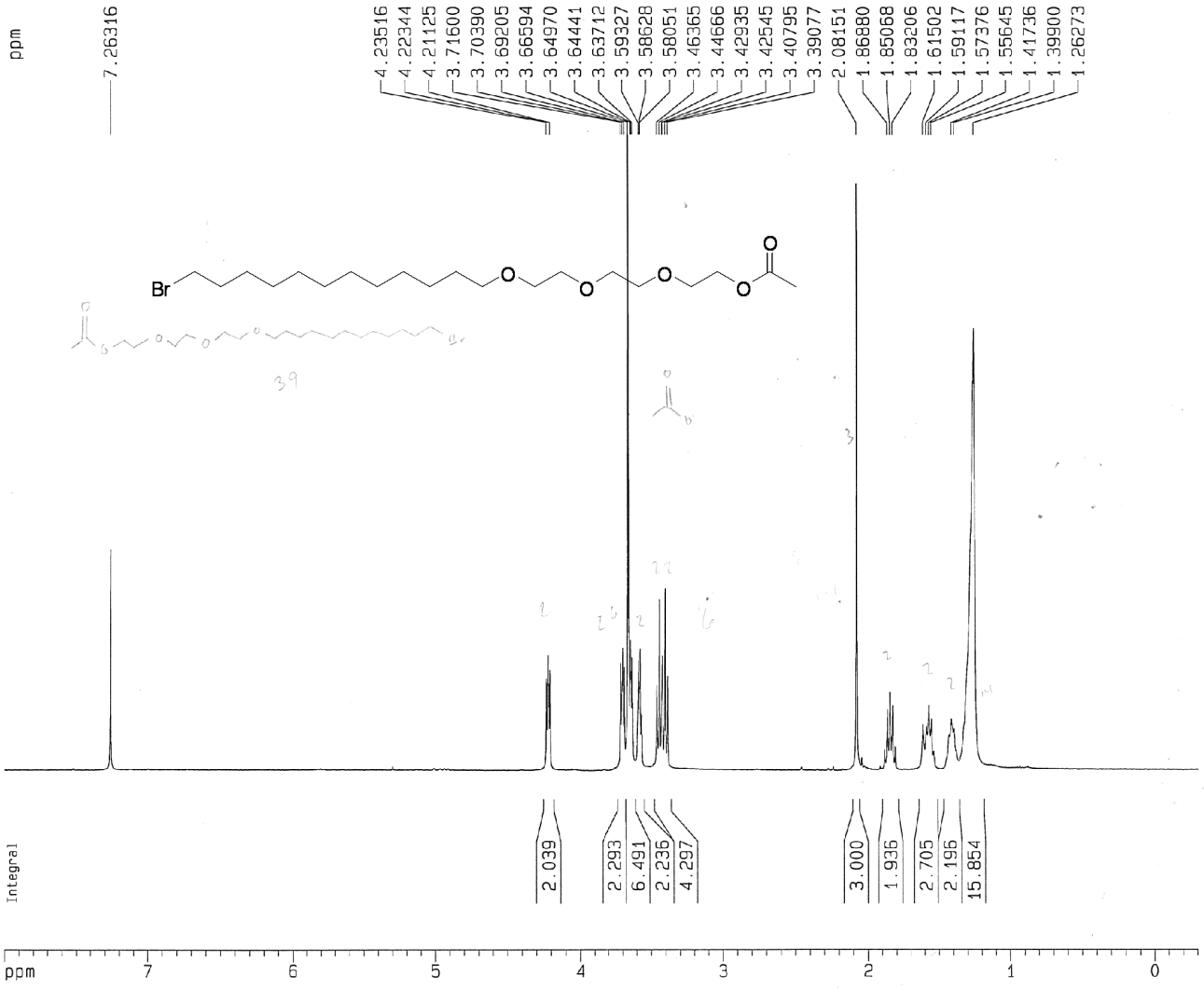

Current Data Parameters

NAME	PJH-II-99h
EXPNO	1
PROCNO	1

F2 - Acquisition Parameters

Date_	20061116
Time	19.15
INSTRUM	amx400
PROBHD	5 mm Multinu
PULPROG	zg30
TD	65536
SOLVENT	CDCl3
NS	16
DS	0
SWH	8333.333 Hz
FIDRES	0.127157 Hz
AQ	3.9322100 sec
RG	1024
DW	60.000 usec
DE	85.71 usec
TE	300.0 K
HL1	0 dB
D1	1.00000000 sec
P1	8.75 usec
SF01	400.1368230 MHz
NUCLEUS	1H

F2 - Processing parameters

SI	32768
SF	400.1343934 MHz
WDW	EM
SSB	0
LB	0.30 Hz
GB	0
PC	1.00

1D NMR plot parameters

CX	20.00 cm
F1P	8.000 ppm
F1	3201.08 Hz
F2P	-0.300 ppm
F2	-120.04 Hz
PPMCM	0.41500 ppm/cm
HZCM	166.05579 Hz/cm

2–(2–(2–(12–bromododecyloxy)ethoxy)ethoxy)ethyl acetate

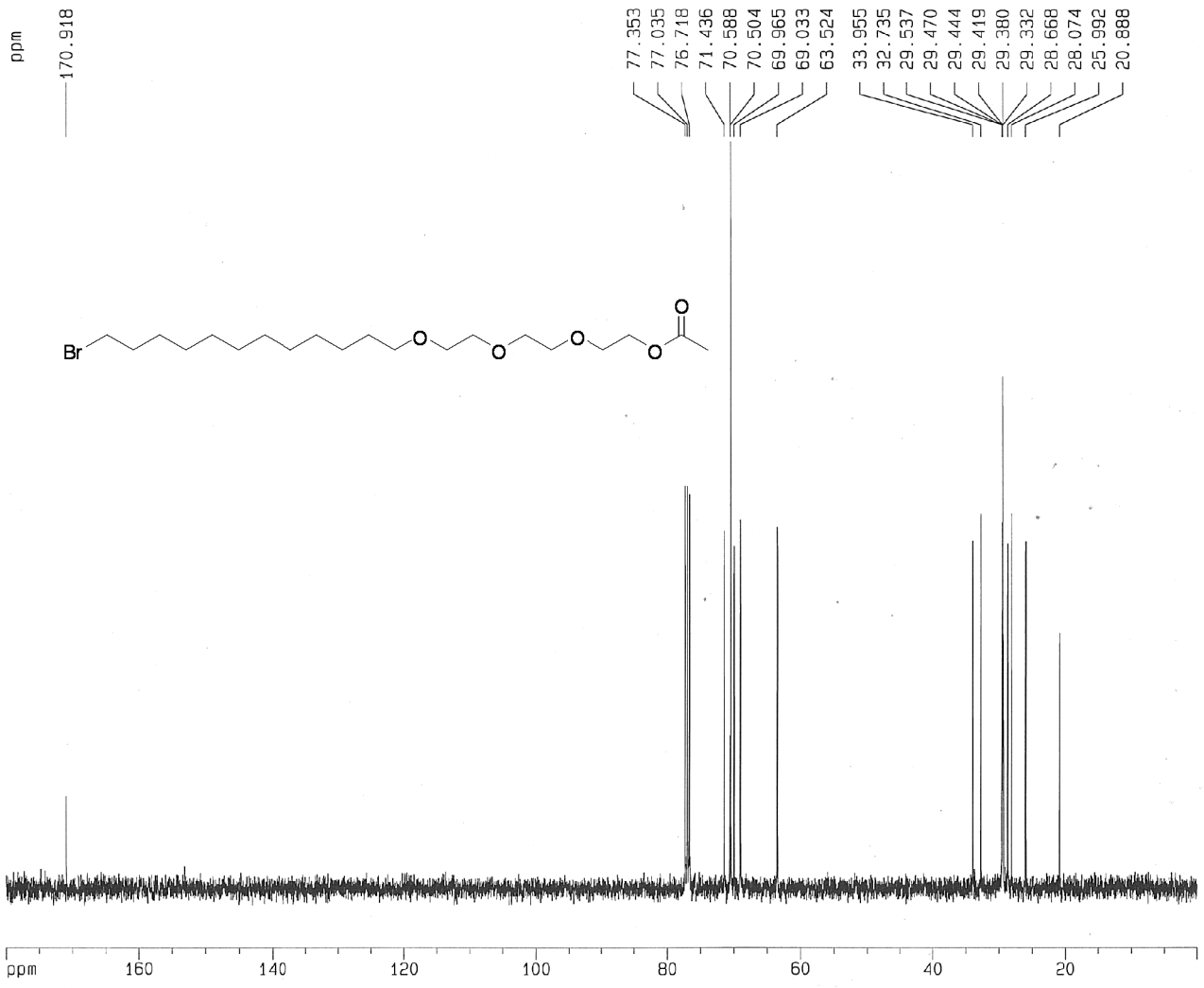


```
Current Data Parameters
NAME          PJH-II-99e
EXPNO                  1
PROCNO                 1

F2 - Acquisition Parameters
Date_           20061115
Time               17.54
INSTRUM          amx400
PROBHD     5 mm Multinu
PULPROG          zgpg30
TD                65536
SOLVENT           CDCl3
NS                   50
DS                    2
SWH           26315.154 Hz
FIDRES        0.401537 Hz
AQ            1.2452340 sec
RG                16384
DW               19.000 usec
DE               27.14 usec
TE               300.0 K
HL1                   0 dB
D1            1.00000000 sec
CPDPRG           waltz16
P31              100.00 usec
S4                   23 dB
D11           0.03000000 sec
S2                   23 dB
P1                9.00 usec
SFO1         100.6226897 MHz
NUCLEUS             13C

F2 - Processing parameters
SI                32768
SF          100.6138792 MHz
WDW                  EM
SSB                   0
LB                 1.00 Hz
GB                    0
PC                 1.40

1D NMR plot parameters
CX                20.00 cm
F1P              180.000 ppm
F1             18110.50 Hz
F2P              0.000 ppm
F2               0.00 Hz
PPMCM          9.00000 ppm/cm
HZCM         905.52490 Hz/cm
```

10–(diethoxyphosphoryl)–*N,N,N*–trimethyldecan–1–aminium bromide

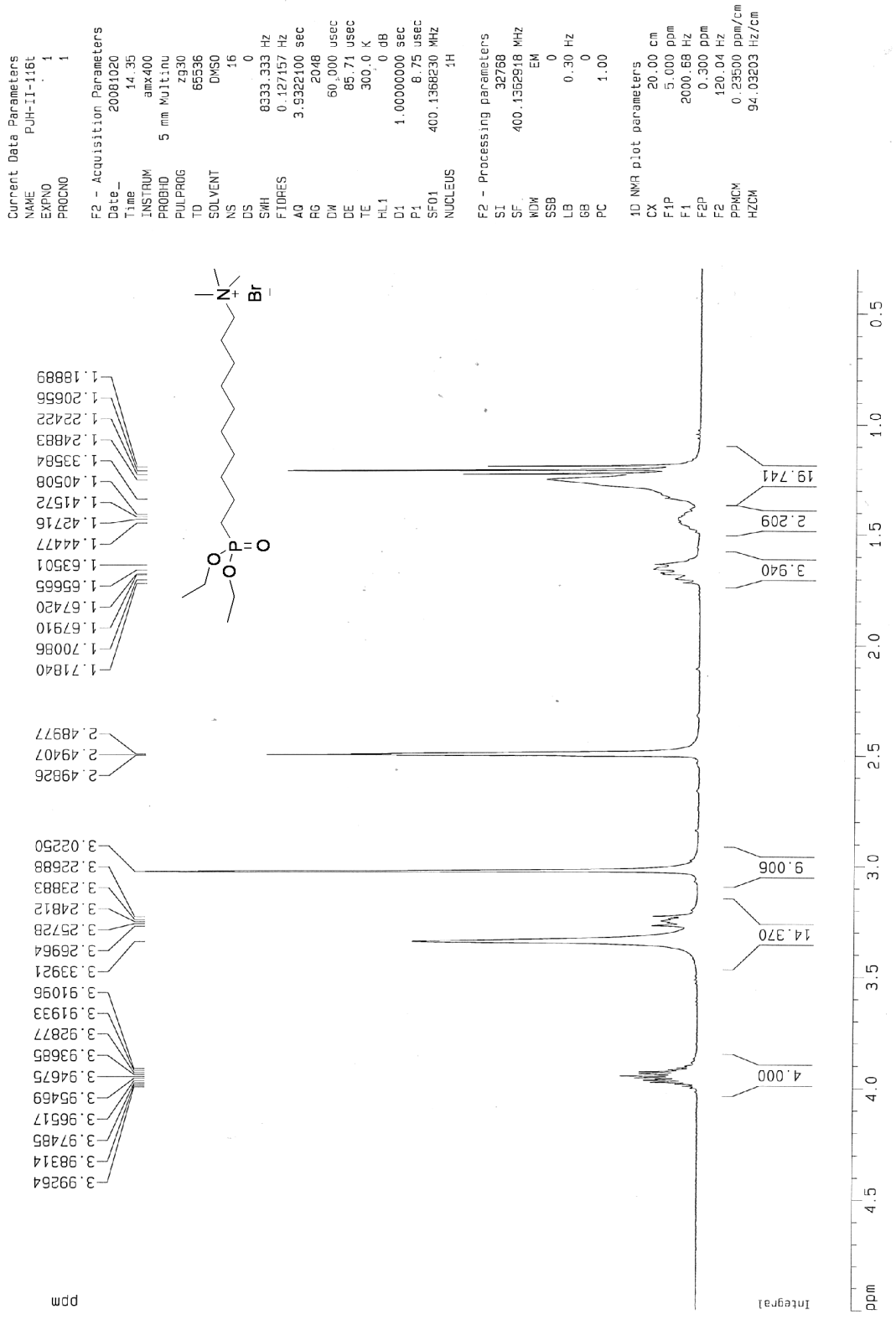

10–(diethoxyphosphoryl)–*N,N,N*–trimethyldecan–1–aminium bromide

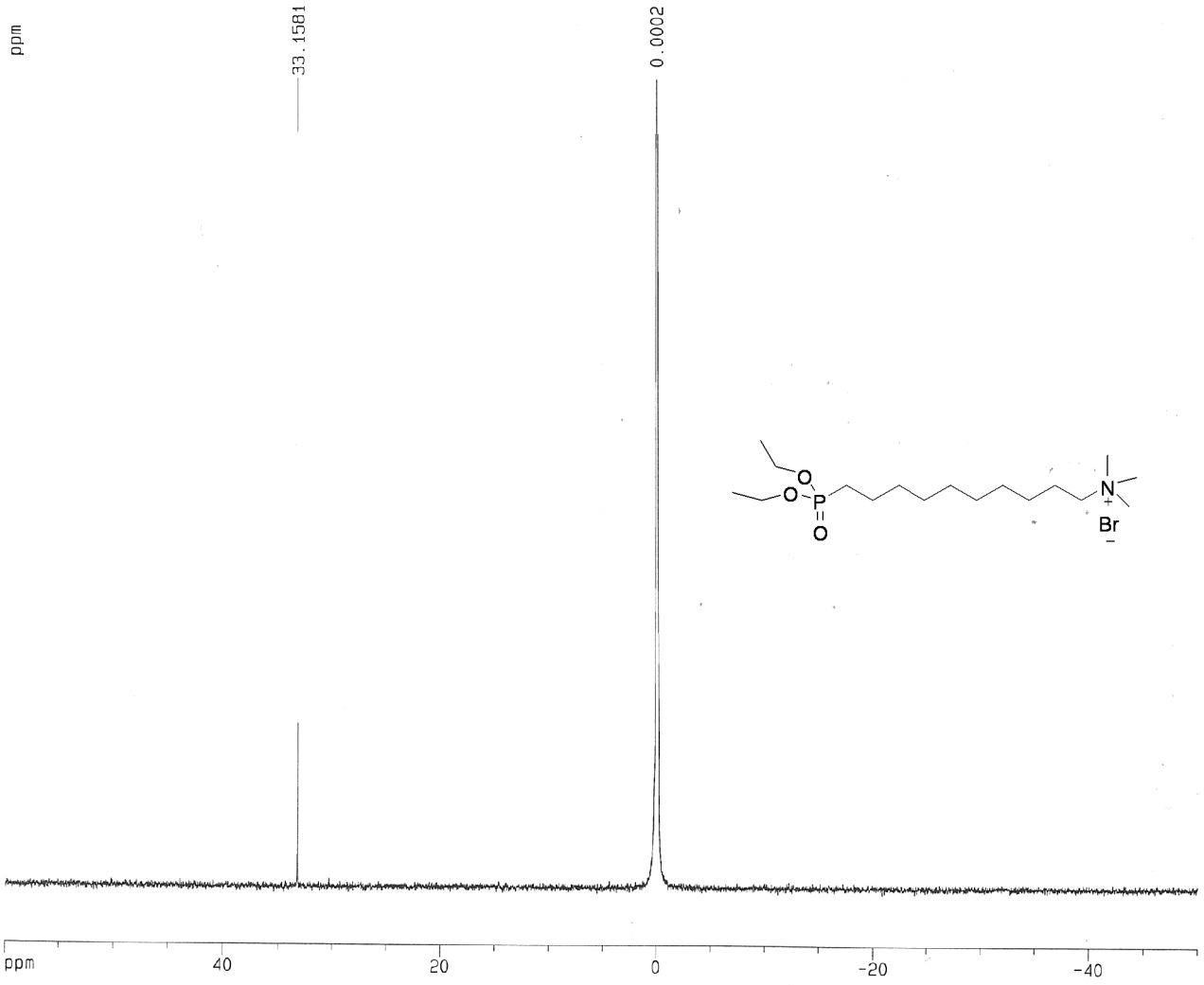


```
Current Data Parameters
NAME          PJH-II-116u
EXPNO                   1
PROCNO                  1

F2 - Acquisition Parameters
Date_           20081020
Time               14.42
INSTRUM          amx400
PROBHD     5 mm Multinu
PULPROG          zgpg30
TD                65536
SOLVENT           CD2Cl2
NS                    32
DS                     4
SWH           71428.570 Hz
FIDRES         1.089913 Hz
AQ             0.4588020 sec
RG                  4096
DW                 7.000 usec
DE                10.00 usec
TE                300.0 K
HL1                    0 dB
D1           2.00000000 sec
CPDPRG           waltz16
P31               100.00 usec
S4                    23 dB
D11          0.03000000 sec
S2                    23 dB
P1                 11.50 usec
SFO1         161.9692445 MHz
NUCLEUS             31P

F2 - Processing parameters
SI                 32768
SF         161.9779463 MHz
WDW                   EM
SSB                    0
LB                  1.00 Hz
GB                     0
PC                  1.40

1D NMR plot parameters
CX                 20.00 cm
F1P                60.000 ppm
F1                 9718.68 Hz
F2P               -50.000 ppm
F2                -8098.90 Hz
PPMCM              5.50000 ppm/cm
HZCM             890.87872 Hz/cm
```

10–(diethoxyphosphoryl)–*N,N,N*–trimethyldecan–1–aminium bromide

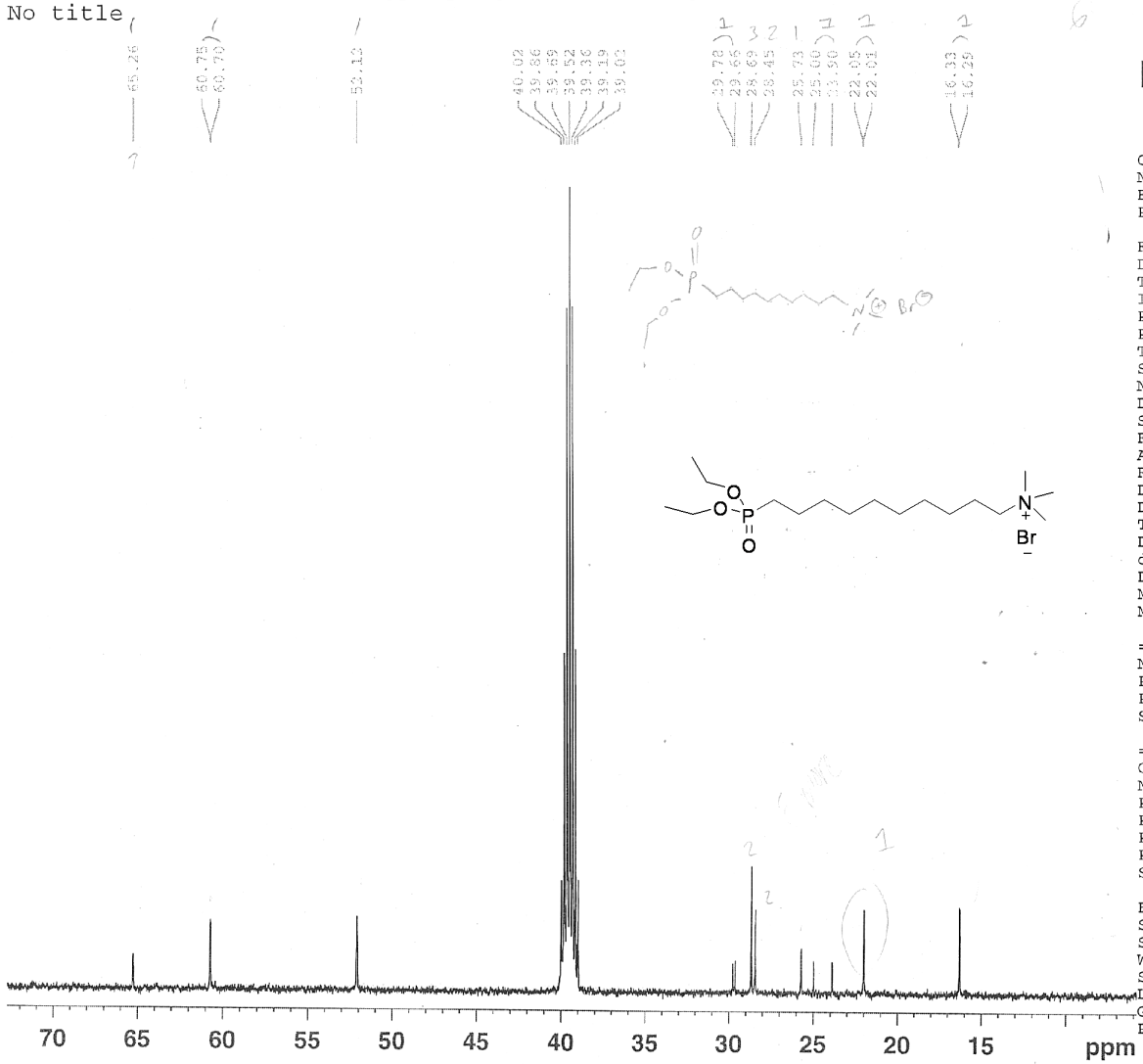

BRUKER

Current Data Parameters

NAME	PJH-II-123g
EXPNO	1
PROCNO	1

F2 - Acquisition Parameters

Date_	20070227
Time	19.14
INSTRUM	spect
PROBHD	5 mm Multinucl
PULPROG	zgpg30
TD	65536
SOLVENT	DMSO
NS	1048
DS	4
SWH	30030.029 Hz
FIDRES	0.458222 Hz
AQ	1.0912244 sec
RG	3649.1
DW	16.650 usec
DE	6.00 usec
TE	298.0 K
D1	2.00000000 sec
d11	0.03000000 sec
DELTA	1.89999998 sec
MCREST	0.00000000 sec
MCWRK	0.01500000 sec

======== CHANNEL f1 ========

NUC1	13C
P1	15.50 usec
PL1	-6.00 dB
SFO1	125.7703643 MHz

======== CHANNEL f2 ========

CPDPRG2	waltz16
NUC2	1H
PCPD2	68.00 usec
PL2	0.00 dB
PL12	18.00 dB
PL13	120.00 dB
SFO2	500.1320005 MHz

F2 - Processing parameters

SI	32768
SF	125.7578490 MHz
WDW	EM
SSB	0
LB	1.00 Hz
GB	0
PC	1.40

Diethyl 12–(1,3–dioxoisoindolin–2–yl)dodecylphosphonate

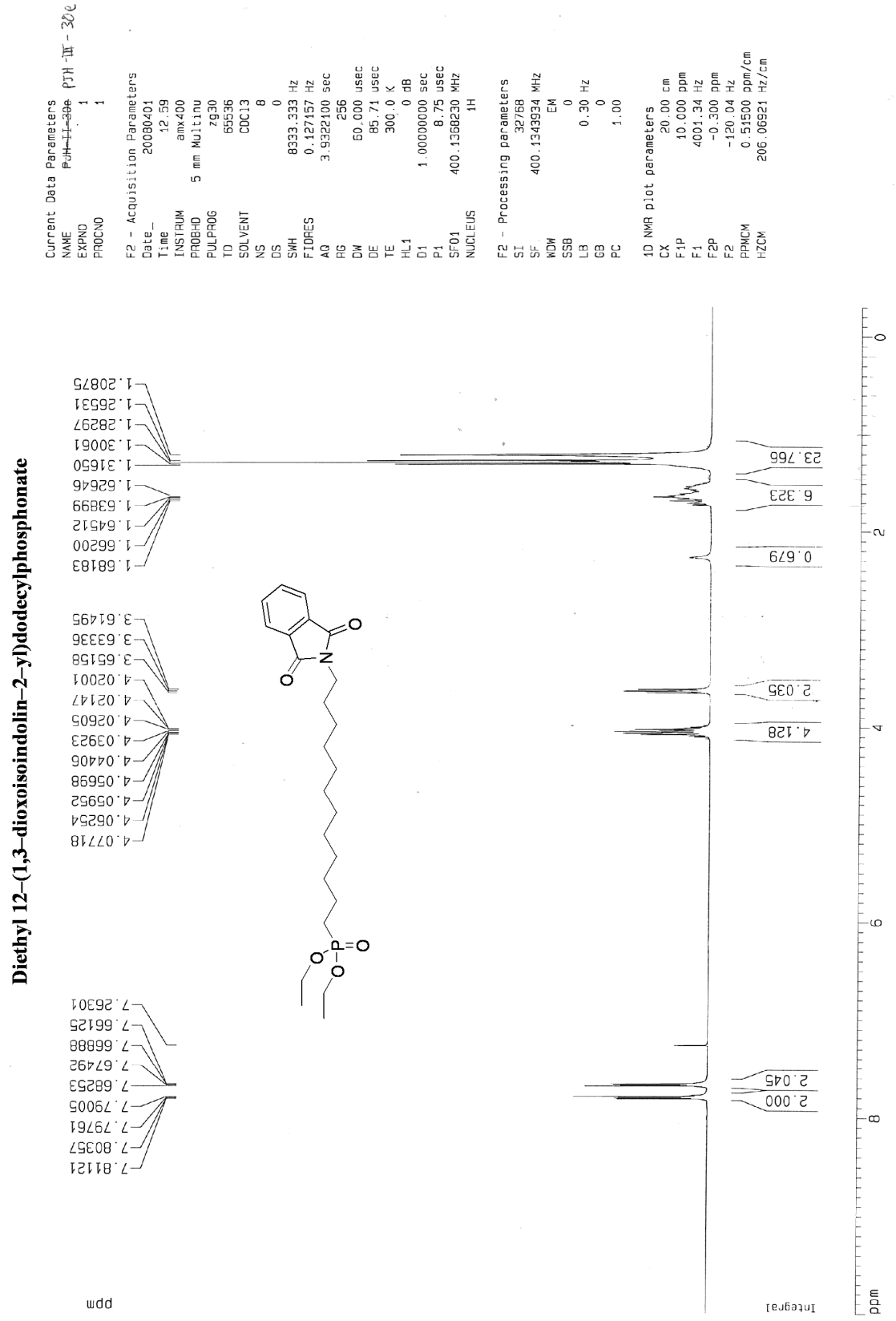

Diethyl 12–(1,3–dioxoisoindolin–2–yl)dodecylphosphonate

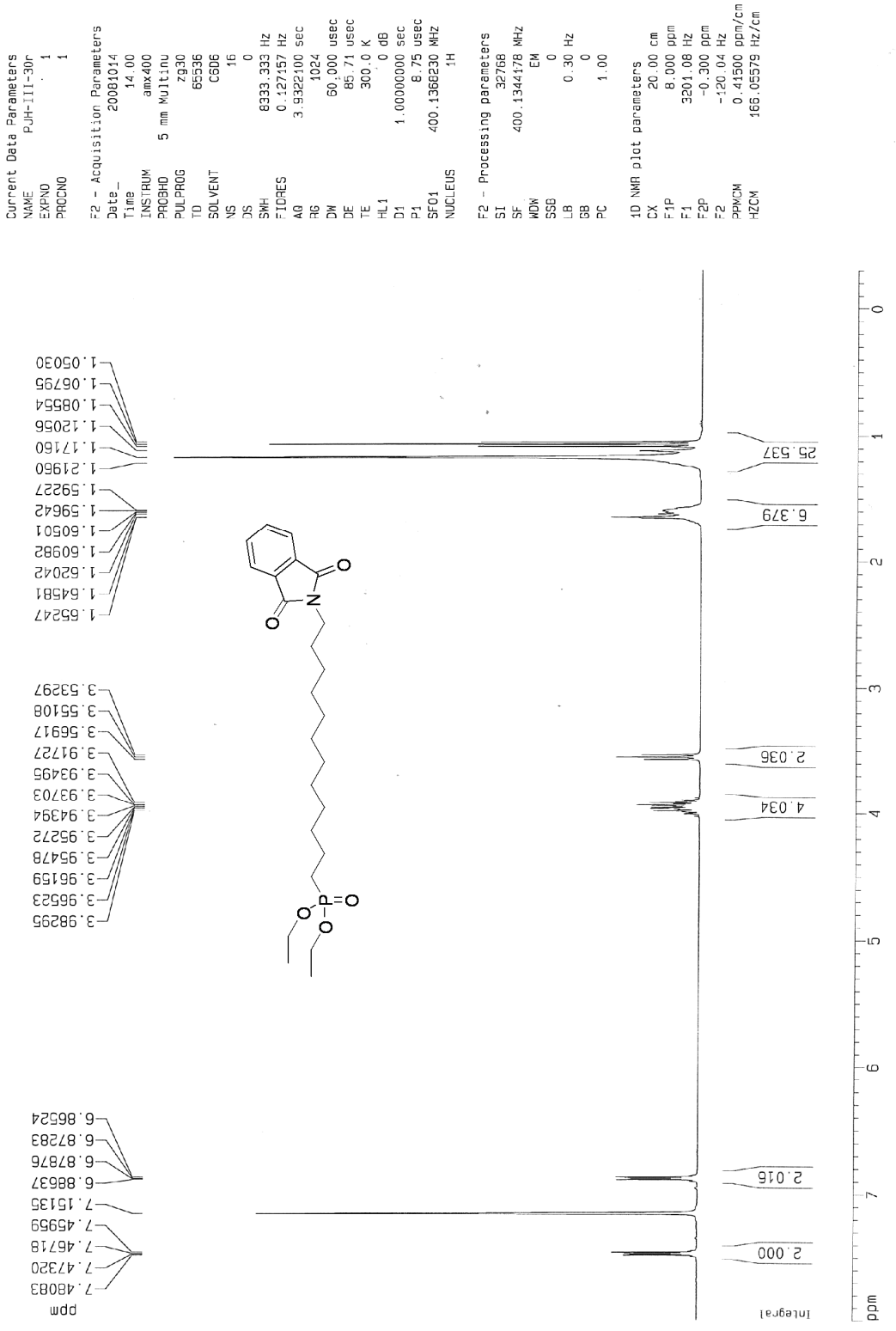

Diethyl 12–(1,3–dioxoisoindolin–2–yl)dodecylphosphonate

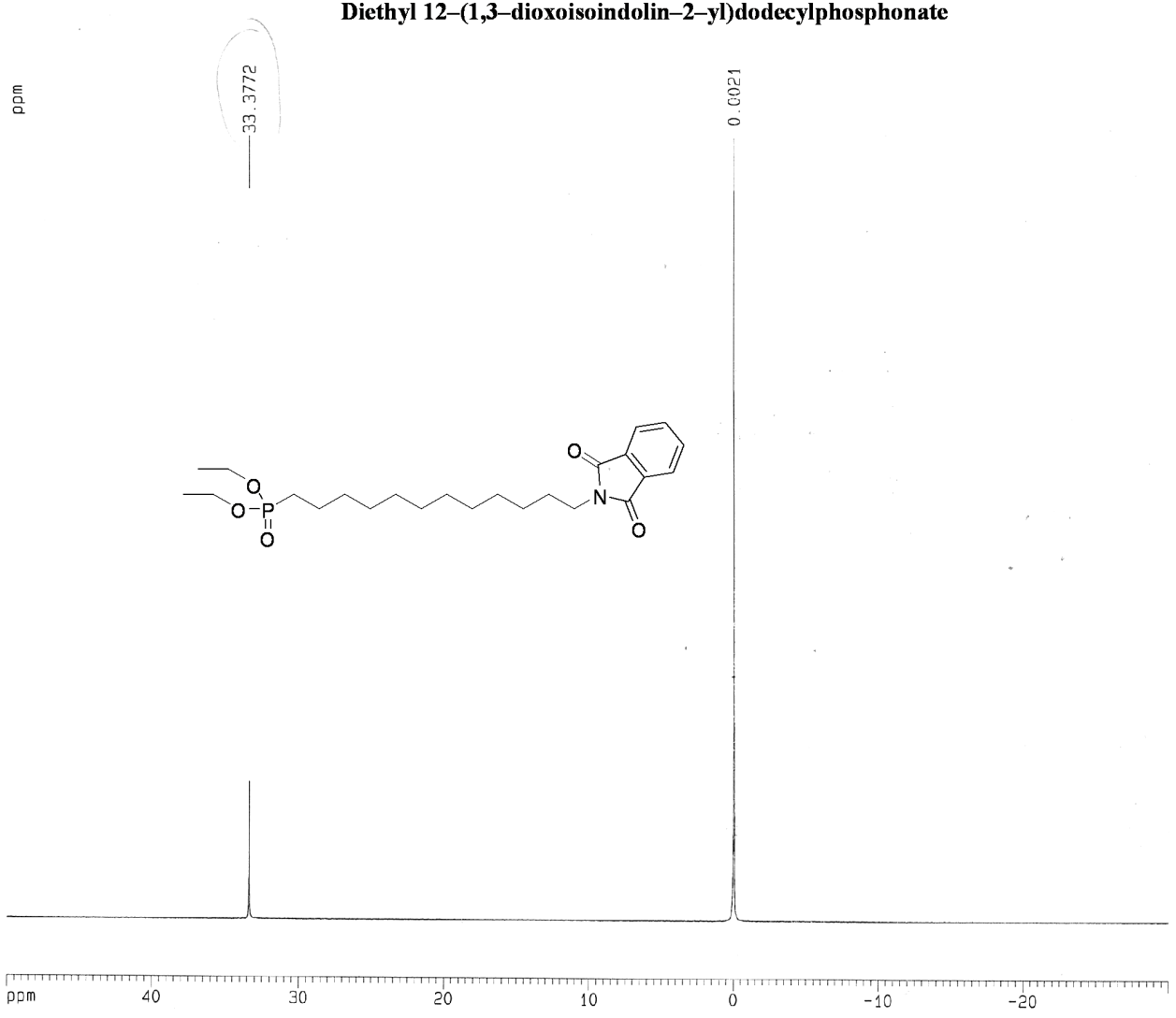

Current Data Parameters

NAME	PJH-III-30f
EXPNO	1
PROCNO	1

F2 - Acquisition Parameters

Date_	20080401
Time	13.08
INSTRUM	amx400
PROBHD	5 mm Multinu
PULPROG	zgpg30
TD	65536
SOLVENT	CDCl3
NS	16
DS	4
SWH	71428.570 Hz
FIDRES	1.089913 Hz
AQ	0.4588020 sec
RG	4096
DW	7.000 usec
DE	10.00 usec
TE	300.0 K
HL1	0 dB
D1	2.00000000 sec
CPDPRG	waltz16
P31	100.00 usec
S4	23 dB
D11	0.03000000 sec
S2	23 dB
P1	11.50 usec
SF01	161.9692445 MHz
NUCLEUS	31P

F2 - Processing parameters

SI	32768
SF	161.9772597 MHz
WDW	EM
SSB	0
LB	1.00 Hz
GB	0
PC	1.40

1D NMR plot parameters

CX	20.00 cm
F1P	50.000 ppm
F1	8098.86 Hz
F2P	-30.000 ppm
F2	-4859.32 Hz
PPMCM	4.00000 ppm/cm
HZCM	647.90906 Hz/cm

Diethyl 12–(1,3–dioxoisoindolin–2–yl)dodecylphosphonate

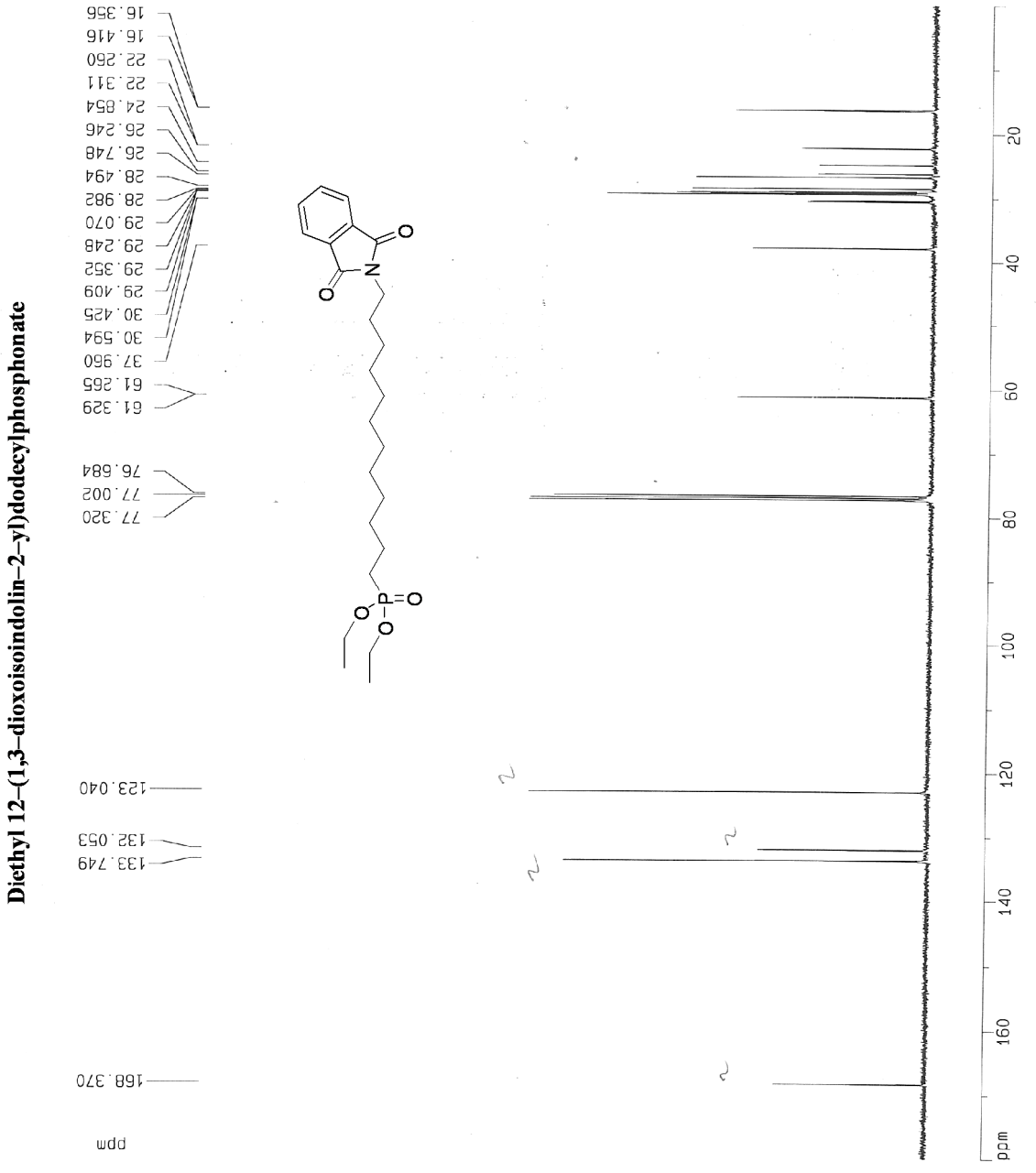

Diethyl dodecylphosphonate–d_{25}

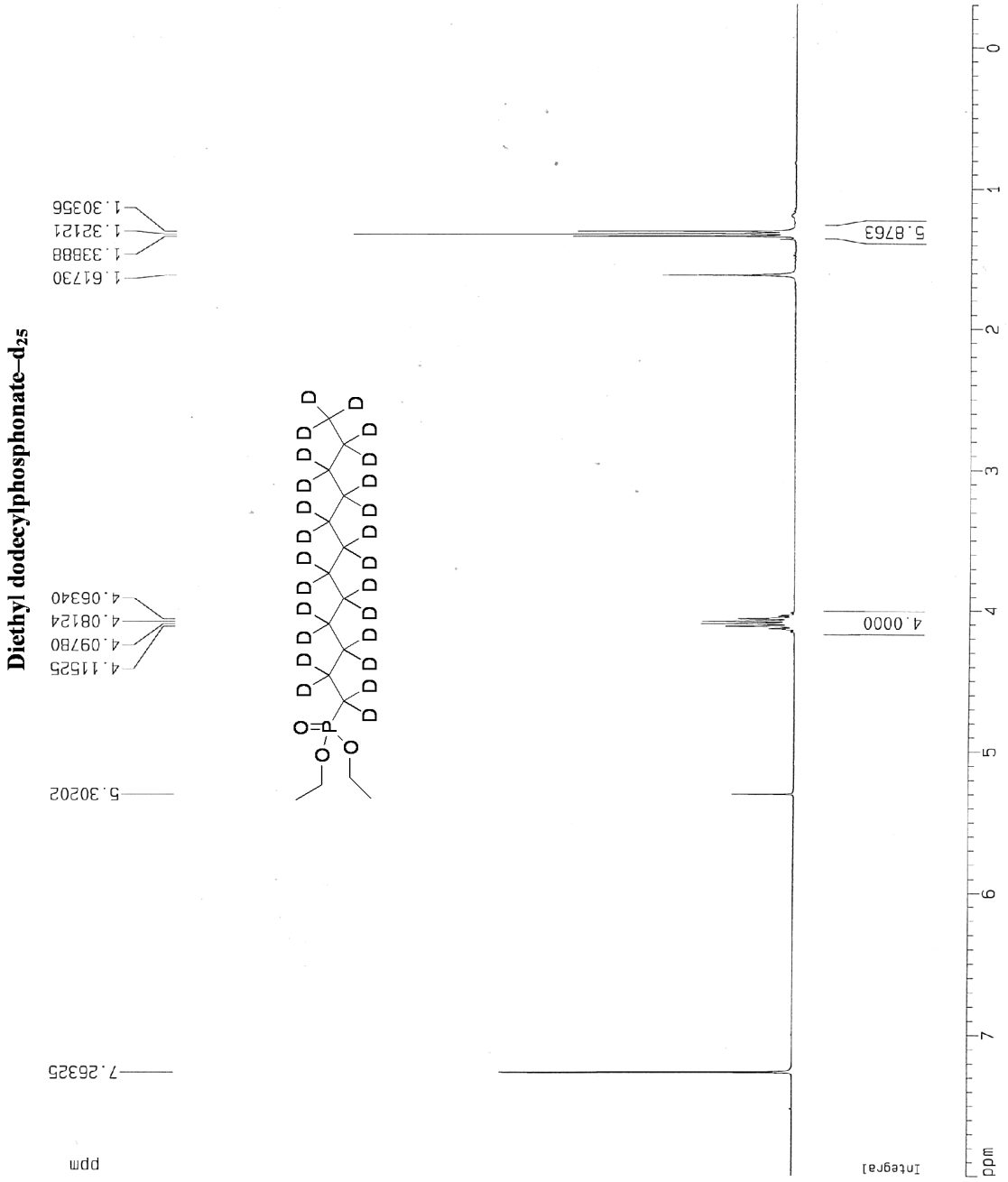

p3919gp

Diethyl dodecylphosphonate–d_{25}

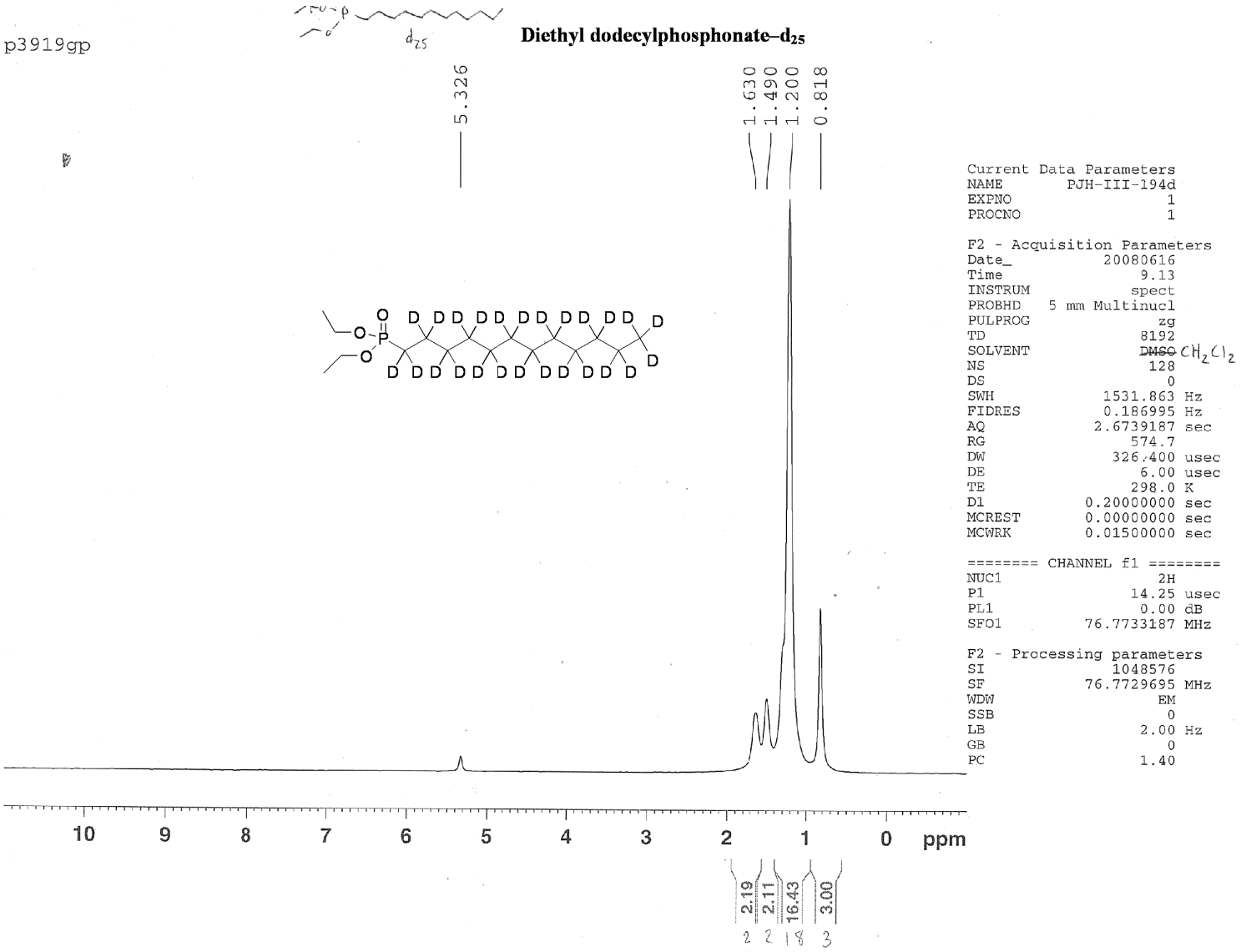


```
Current Data Parameters
NAME        PJH-III-194d
EXPNO                  1
PROCNO                 1

F2 - Acquisition Parameters
Date_           20080616
Time                9.13
INSTRUM            spect
PROBHD   5 mm Multinucl
PULPROG               zg
TD                  8192
SOLVENT             DMSO CH2Cl2
NS                   128
DS                     0
SWH             1531.863 Hz
FIDRES          0.186995 Hz
AQ             2.6739187 sec
RG                 574.7
DW              326.400 usec
DE                6.00 usec
TE                298.0 K
D1           0.20000000 sec
MCREST       0.00000000 sec
MCWRK        0.01500000 sec

======== CHANNEL f1 ========
NUC1                  2H
P1                14.25 usec
PL1                0.00 dB
SFO1          76.7733187 MHz

F2 - Processing parameters
SI                 1048576
SF            76.7729695 MHz
WDW                   EM
SSB                    0
LB                  2.00 Hz
GB                     0
PC                  1.40
```

Diethyl dodecylphosphonate–d_{25}

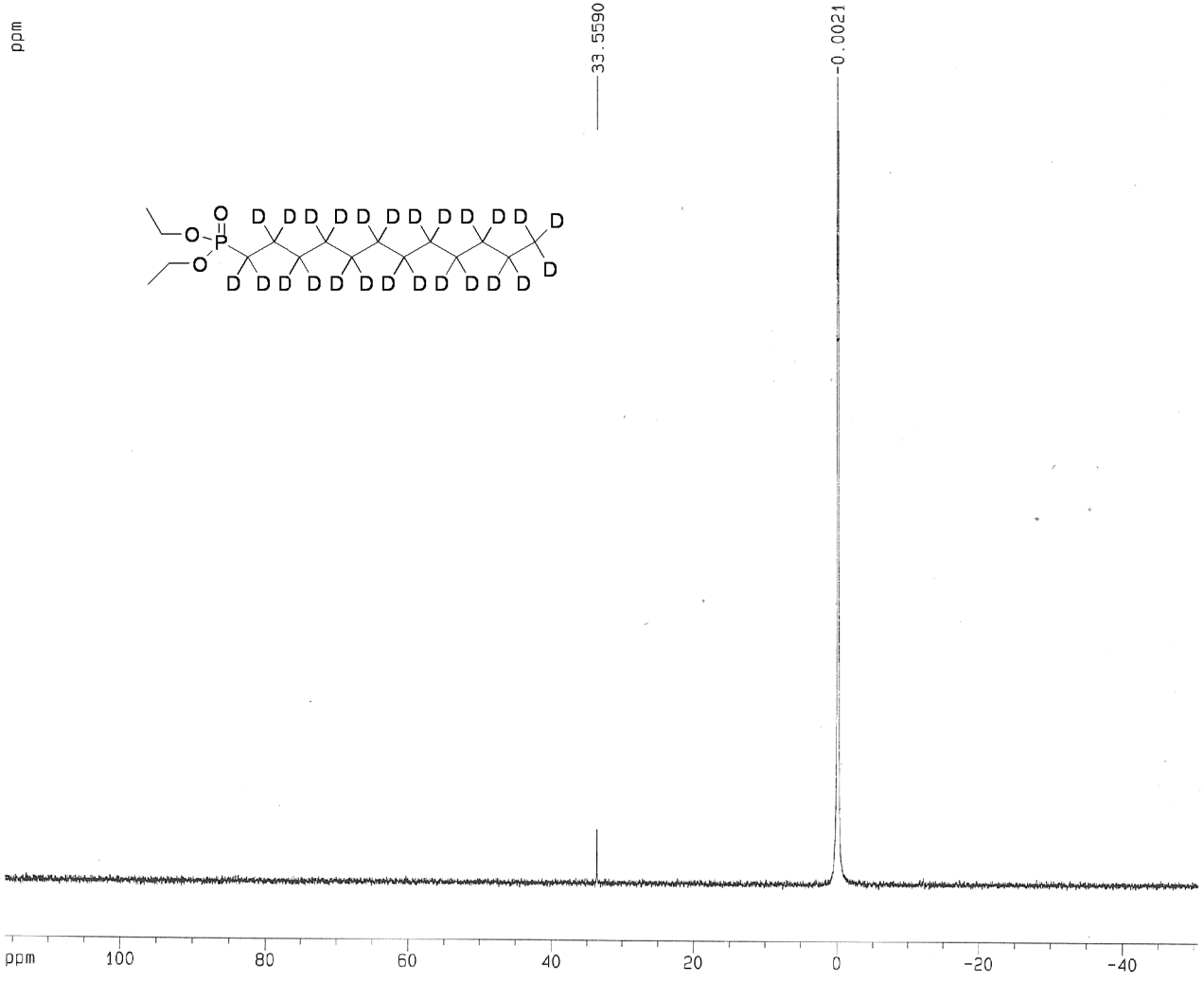


```
Current Data Parameters
NAME        PJH-III-194c
EXPNO                  1
PROCNO                 1

F2 - Acquisition Parameters
Date_           20080613
Time               10.51
INSTRUM          amx400
PROBHD     5 mm Multinu
PULPROG          zgpg30
TD                65536
SOLVENT           CDCl3
NS                   32
DS                    4
SWH           71428.570 Hz
FIDRES         1.089913 Hz
AQ             0.4588020 sec
RG                 4096
DW                7.000 usec
DE               10.00 usec
TE               300.0 K
HL1                   0 dB
D1           2.00000000 sec
CPDPRG           waltz16
P31               100.00 usec
S4                    23 dB
D11          0.03000000 sec
S2                    23 dB
P1                11.50 usec
SF01        161.9692445 MHz
NUCLEUS             31P

F2 - Processing parameters
SI                 32768
SF          161.9772652 MHz
WDW                   EM
SSB                    0
LB                  1.00 Hz
GB                     0
PC                  1.40

1D NMR plot parameters
CX                 20.00 cm
F1P              116.061 ppm
F1             18799.28 Hz
F2P              -50.549 ppm
F2             -8187.87 Hz
PPMCM           8.33053 ppm/cm
HZCM         1349.35718 Hz/cm
```

Diethyl dodecylphosphonate–d_{25}

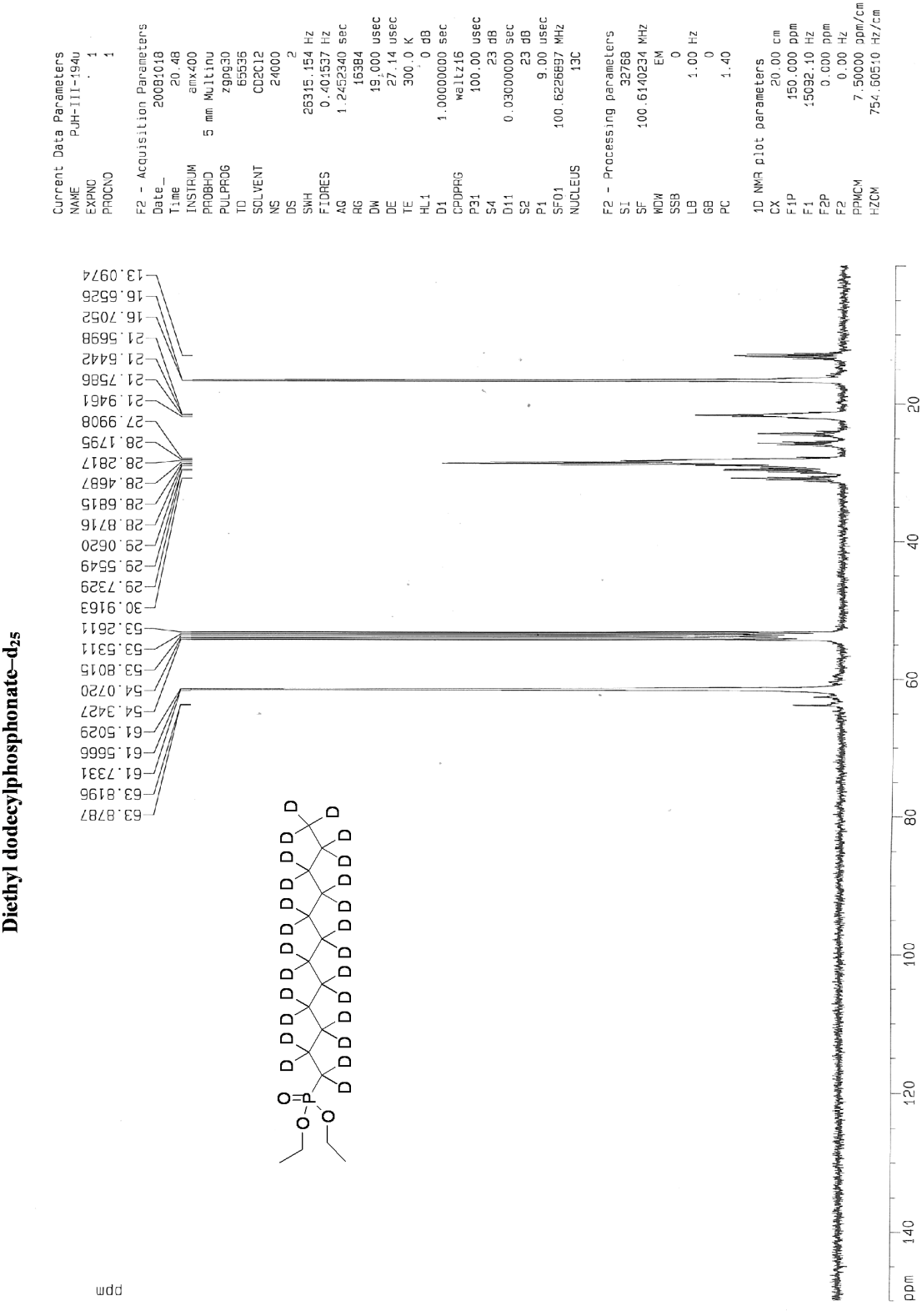

Diethyl dodecylphosphonate–d_{25}

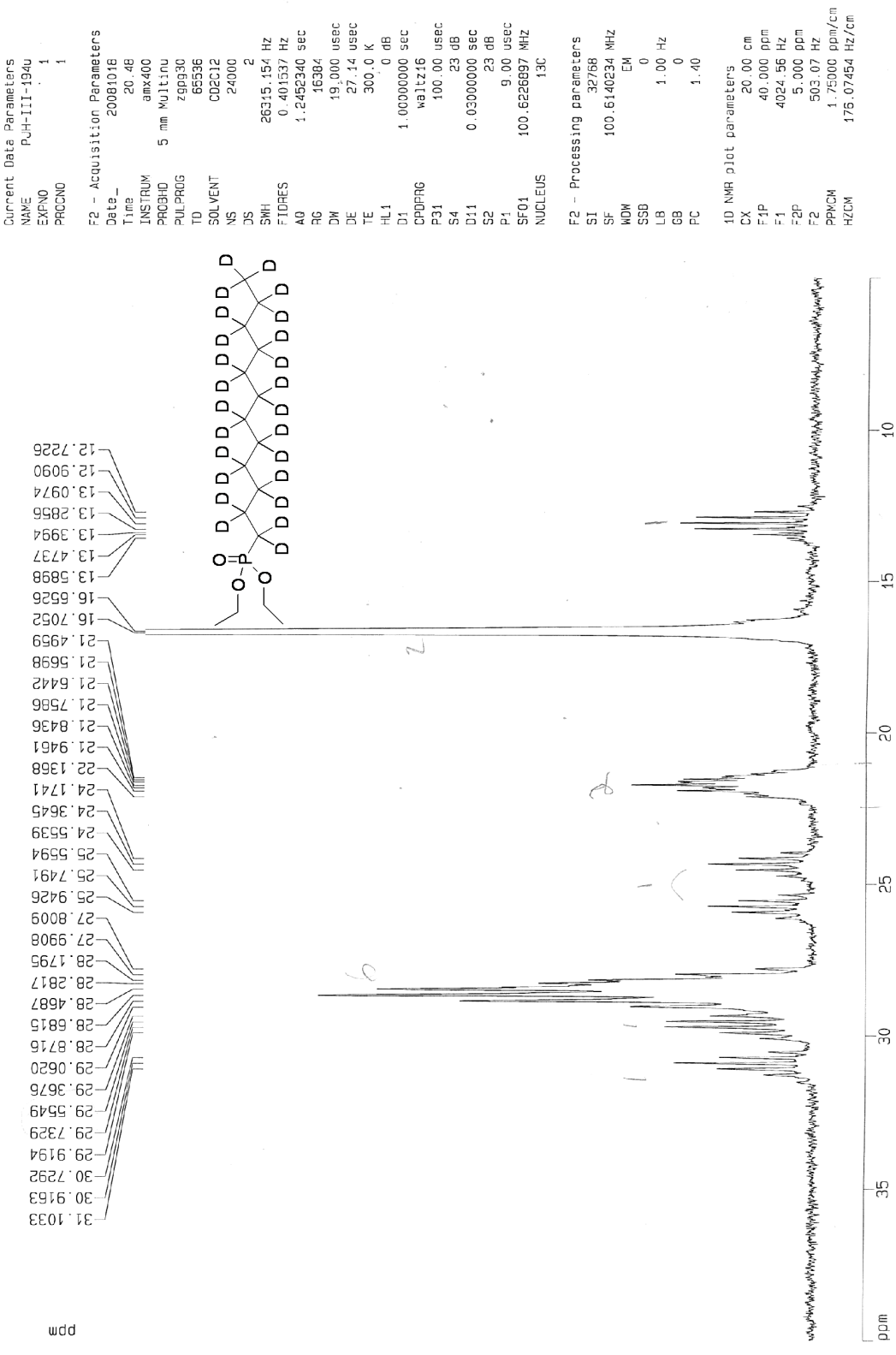

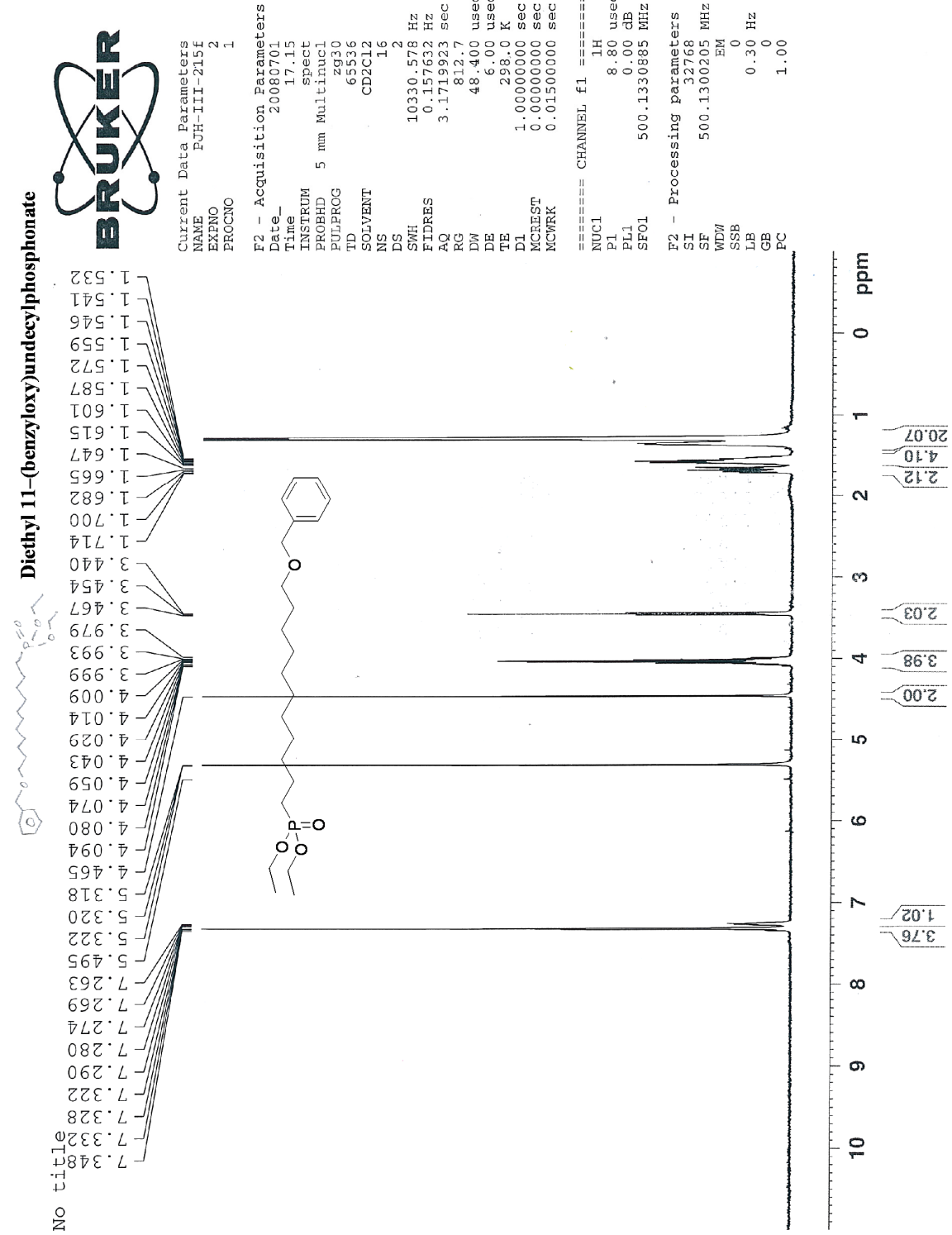
Diethyl 11–(benzyloxy)undecylphosphonate
No title
BRUKER
Current Data Parameters
NAME PUH-III-215f
EXPNO 2
PROCNO 1
F2 - Acquisition Parameters
Date_ 20080701
Time 17.15
INSTRUM spect
PROBHD 5 mm Multinucl
PULPROG zg30
TD 65536
SOLVENT CD2Cl2
NS 16
DS 2
SWH 10330.578 Hz
FIDRES 0.157632 Hz
AQ 3.1719923 sec
RG 812.7
DW 48.400 usec
DE 6.00 usec
TE 298.0 K
D1 1.00000000 sec
MCREST 0.00000000 sec
MCWRK 0.01500000 sec
======== CHANNEL f1 ========
NUC1 1H
P1 8.80 usec
PL1 0.00 dB
SFO1 500.1330885 MHz
F2 - Processing parameters
SI 32768
SF 500.1300205 MHz
WDW EM
SSB 0
LB 0.30 Hz
GB 0
PC 1.00
7.348
7.332
7.328
7.322
7.290
7.280
7.274
7.269
7.263
5.495
5.322
5.320
5.318
4.465
4.094
4.080
4.074
4.059
4.043
4.029
4.014
4.009
3.999
3.993
3.979
3.467
3.454
3.440
1.714
1.700
1.682
1.665
1.647
1.615
1.601
1.587
1.572
1.559
1.546
1.541
1.532
ppm
20.07
4.10
2.12
2.03
3.98
2.00
3.76
1.02

Diethyl 11–(benzyloxy)undecylphosphonate

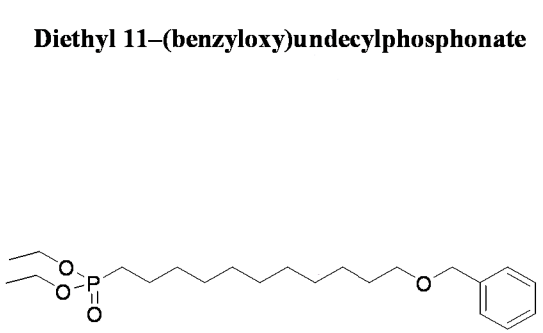

BRUKER

```
Current Data Parameters
NAME        PJH-III-215g
EXPNO                  1
PROCNO                 1

F2 - Acquisition Parameters
Date_           20080701
Time               17.25
INSTRUM            spect
PROBHD   5 mm Multinucl
PULPROG          zgpg30
TD                65536
SOLVENT            DMSO   CD2Cl2
NS                    32
DS                     0
SWH           80645.164 Hz
FIDRES         1.230548 Hz
AQ            0.4063732 sec
RG                  2048
DW                 6.200 usec
DE                 6.00 usec
TE                298.0 K
D1           2.00000000 sec
d11          0.03000000 sec
DELTA        1.89999998 sec
MCREST       0.00000000 sec
MCWRK        0.01500000 sec

======== CHANNEL f1 ========
NUC1                  31P
P1                 10.50 usec
PL1                 0.00 dB
SFO1        202.4562087 MHz

======== CHANNEL f2 ========
CPDPRG2          waltz16
NUC2                  1H
PCPD2              68.00 usec
PL2                 0.00 dB
PL12               13.24 dB
PL13              120.00 dB
SFO2        500.1320005 MHz

F2 - Processing parameters
SI                 32768
SF          202.4562161 MHz
WDW                   EM
SSB                    0
LB                  1.00 Hz
GB                     0
PC                  1.40
```

Diethyl 11–(benzyloxy)undecylphosphonate

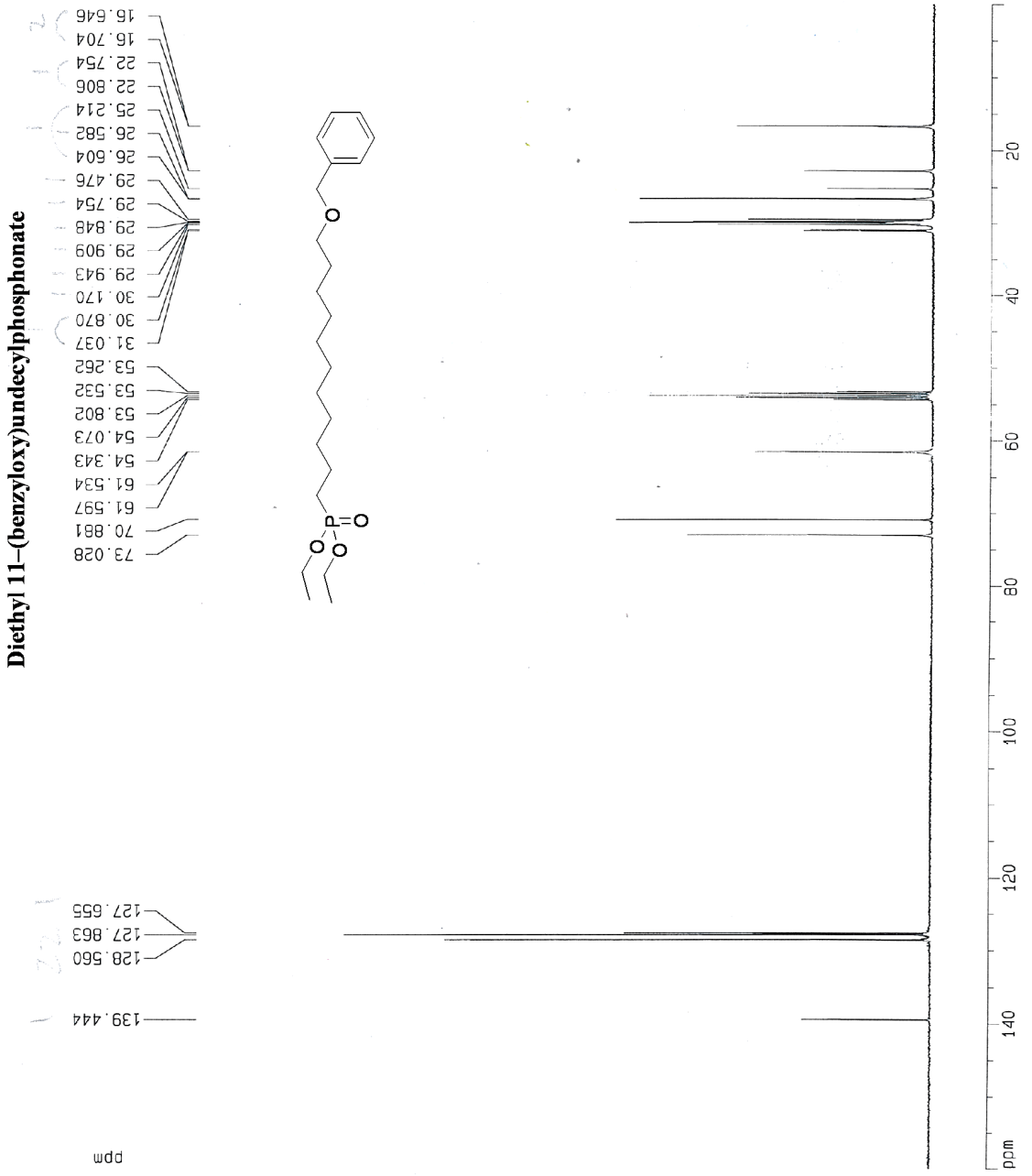

Diethyl 10–(8–(benzyloxy)octyloxy)decylphosphonate

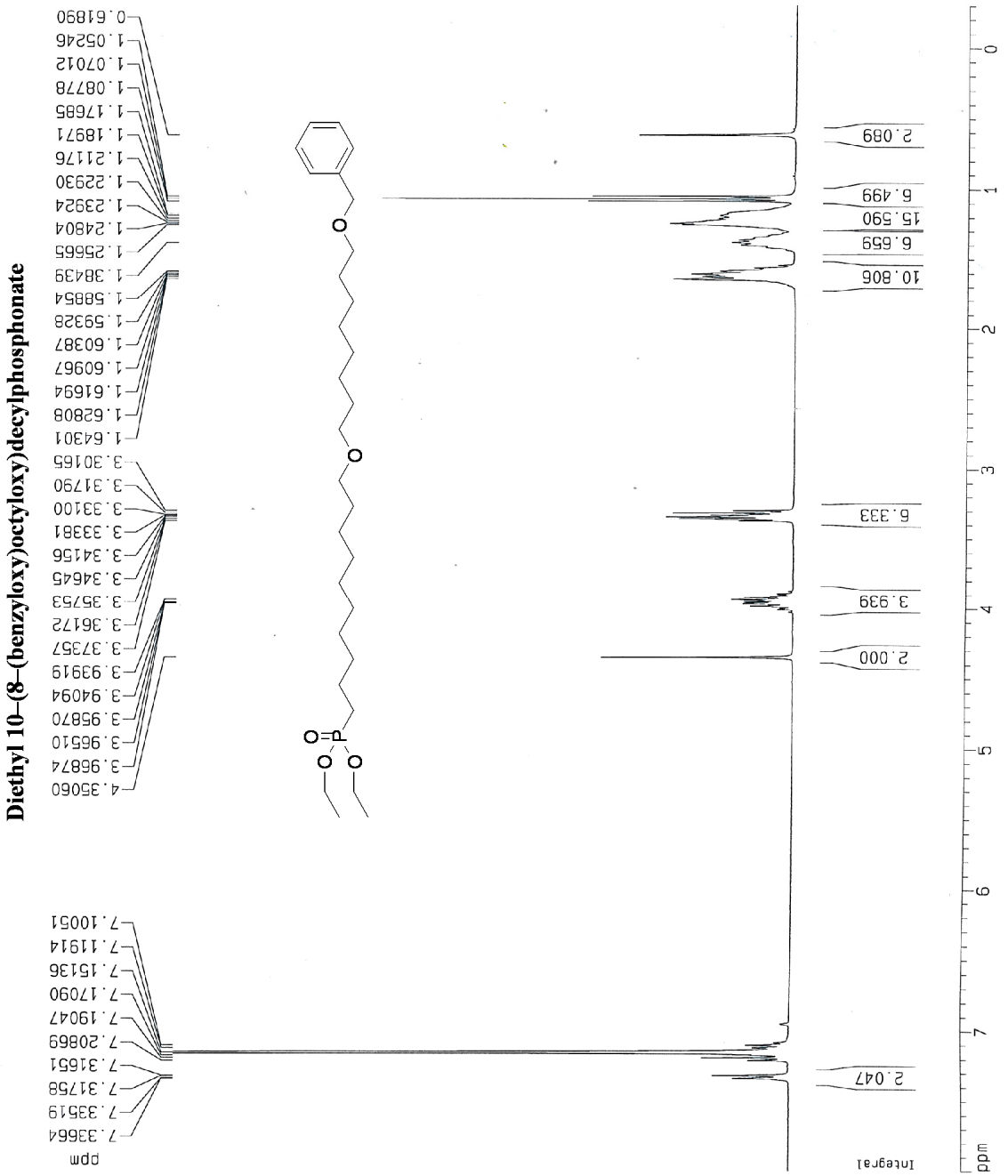

Diethyl 10–(8–(benzyloxy)octyloxy)decylphosphonate

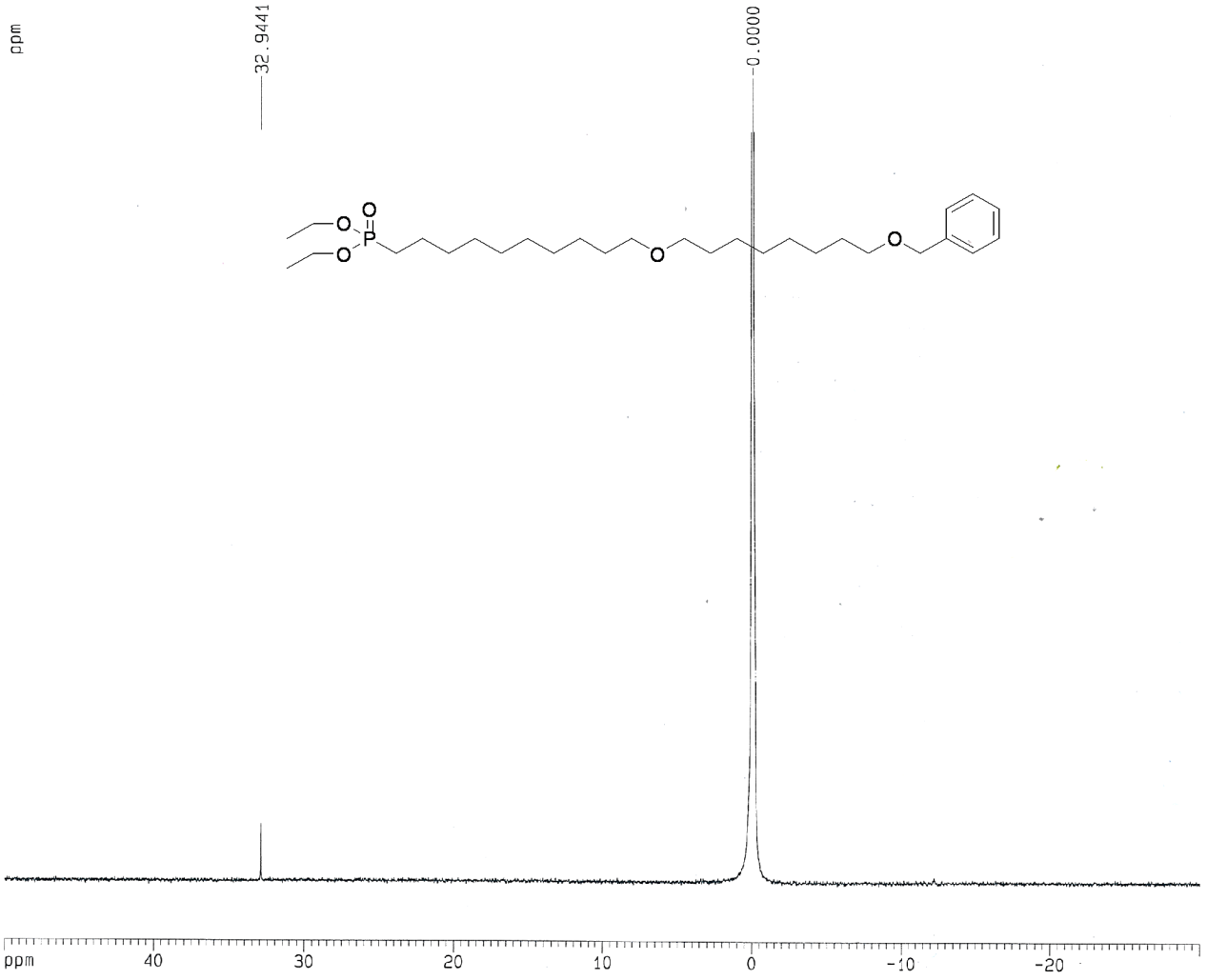

Current Data Parameters
NAME PJH-III-225f
EXPNO 1
PROCNO 1

F2 - Acquisition Parameters
Date_ 20080729
Time 13.56
INSTRUM amx400
PROBHD 5 mm Multinu
PULPROG zgpg30
TD 65536
SOLVENT CD2Cl2
NS 64
DS 4
SWH 71428.570 Hz
FIDRES 1.089913 Hz
AQ 0.4588020 sec
RG 4096
DW 7.000 usec
DE 10.00 usec
TE 300.0 K
HL1 0 dB
D1 2.00000000 sec
CPDPRG waltz16
P31 100.00 usec
S4 23 dB
D11 0.03000000 sec
S2 23 dB
P1 11.50 usec
SFO1 161.9692445 MHz
NUCLEUS 31P

F2 - Processing parameters
SI 32768
SF 161.9775845 MHz
WDW EM
SSB 0
LB 1.00 Hz
GB 0
PC 1.40

1D NMR plot parameters
CX 20.00 cm
F1P 50.000 ppm
F1 8098.88 Hz
F2P -30.000 ppm
F2 -4859.33 Hz
PPMCM 4.00000 ppm/cm
HZCM 647.91034 Hz/cm

Diethyl 10–(8–(benzyloxy)octyloxy)decylphosphonate

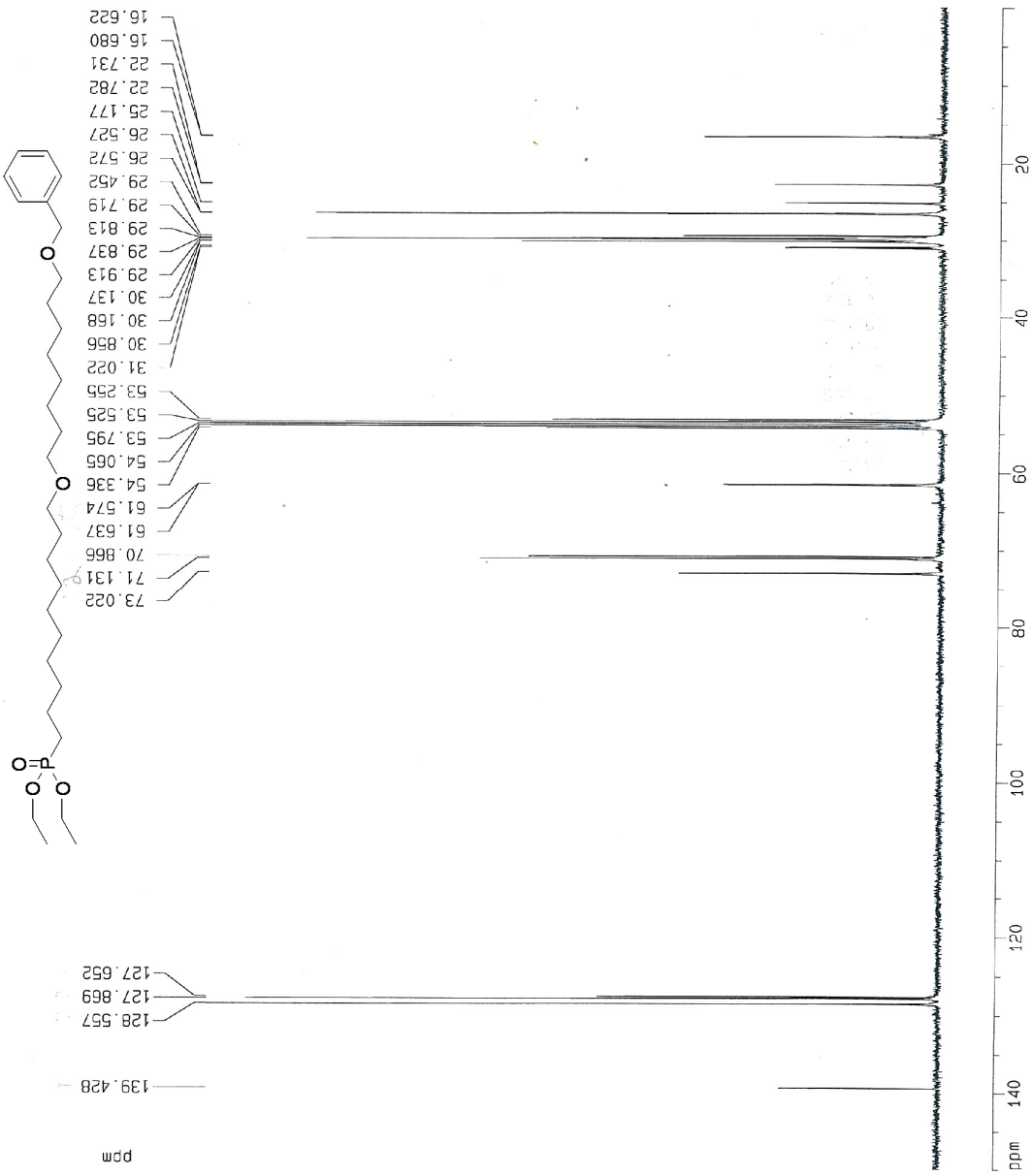

Appendix B

B.1 Preliminary Experiments on the Attachment of Biomolecules to ZnO

The ability to modify zinc oxide has been demonstrated and characterized, and while complete studies have not been conducted, some preliminary data has been obtained on using phosphonic acids to bind bioactive molecules to the surface of ZnO. 10-mercaptophosphonic acid (MPA) was bound to the ZnO surface and this used to attach a crosslinker that can then bind fluorescent antibodies to the ZnO surface (Figure B.1).

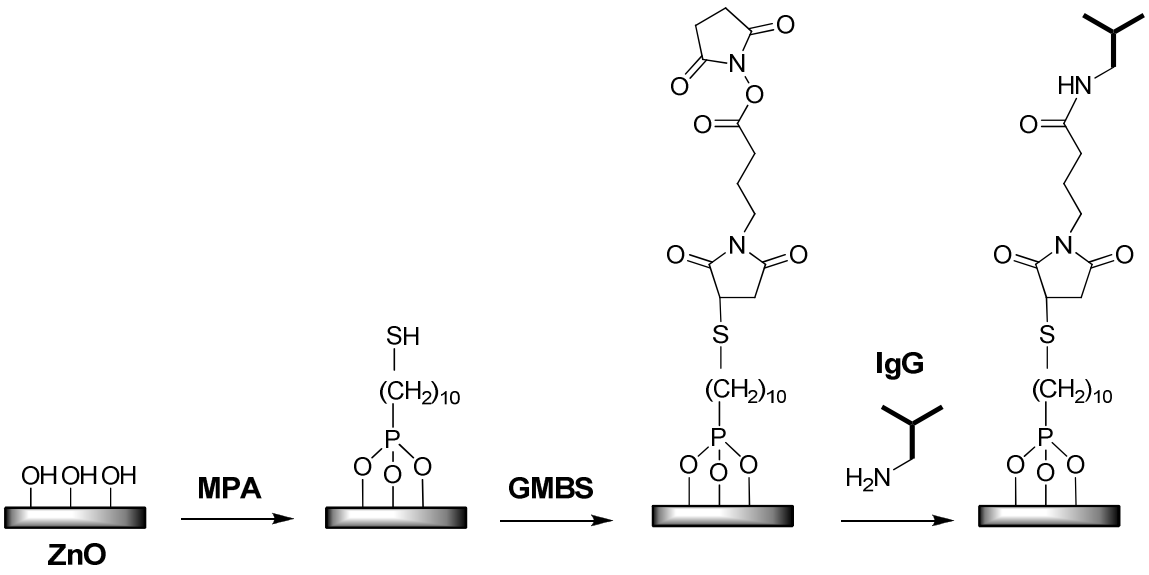

Figure B.1 Steps for the immobilization of antibodies (IgG, for example) onto a ZnO surface using mercaptophosphonic acid and a crosslinker N-(γ-Maleimidobutyryloxy)succinimide (GMBS).

Fluorescence microscopy shows that that the antibody attaches only when the phosphonic acid is present (Figure B.2), and AFM shows clearly a change in surface morphology upon addition of the MPA, the crosslinker, and the antibodies (Figure B.2). The fluorescence microscopy image shows the edge of a spot where the phosphonic acid was delivered to the surface *via* a very small drop of solution. After the additional protocol as outlined above, fluorescence can be seen from this spot, but not from the surrounding area, indicating that the antibody bound (after washings in PBS buffer and water) only where the surface was treated with MPA.

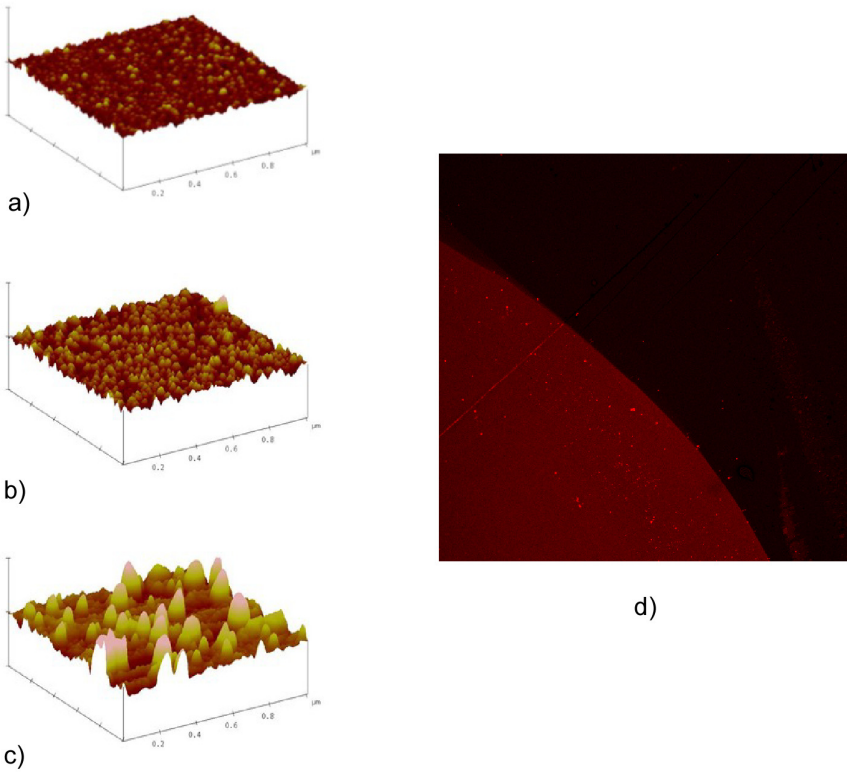

Figure B.2 AFM topography images (z-axis is 65 nm) of the various steps shown in Scheme 2. a) Bare ZnO surface. b) ZnO surface modified with mercaptophosphonic acid and the GMBS crosslinker. c) A ZnO surface modified with mercaptophosphonic acid, the GMBS crosslinker, and the antibodies. d) Fluorescence microscopy image of IgG antibody attached to a ZnO surface (image is 1 mm^2). (Data collected and figures prepared by C. Corso)

These initial results demonstrate that antibodies can be successfully attached to the surface of ZnO by using MPA and the appropriate crosslinker. Further studies need to be conducted to optimize the conditions of attachment and to test the actual sensing ability of devices incorporating phosphonic acids.

B.2 Preliminary Results on the Crosslinking of Molecules to the ITO Surface

In terms of ITO modification, while detailed studies have been completed on the ability to tune the work function and surface energy of the surface in a controlled fashion, little has been completed on studies related to covalently attaching subsequent organics to the surface. While modifying the surface energy such that subsequent small molecule and polymer layers form a better interface with ITO is a promising approach, covalently attaching the organics to the surface may lead to even better interfacial properties and stability. Molecules with which these studies can be conducted, such as phosphonic acids functionalized with benzophenone and cinnamate crosslinking units, as well as phosphonic acids which are functionalized with monomer units or polymer initiators, have all been synthesized. Additionally, initial studies have been conducted and indicate an ability to bind organics to the ITO surfaces by means of phosphonic acids.

As a first attempt to crosslink materials to surfaces, a cinnamate-terminated phosphonic acid was used to modify ITO surfaces for subsequent 2+2 cycloaddition with cinnamates in solution. The 2+2 cycloaddition of cinnamates often achieved by irradiation with ultraviolet light is well-known in the literature.[1] An ITO substrate was

modified with a phosphonic acid containing a terminal cinnamate group. A fluorinated cinnamate small molecule was then dropcast on the surface and the substrates irradiated with UV light for varying lengths of time (Figure B.3).

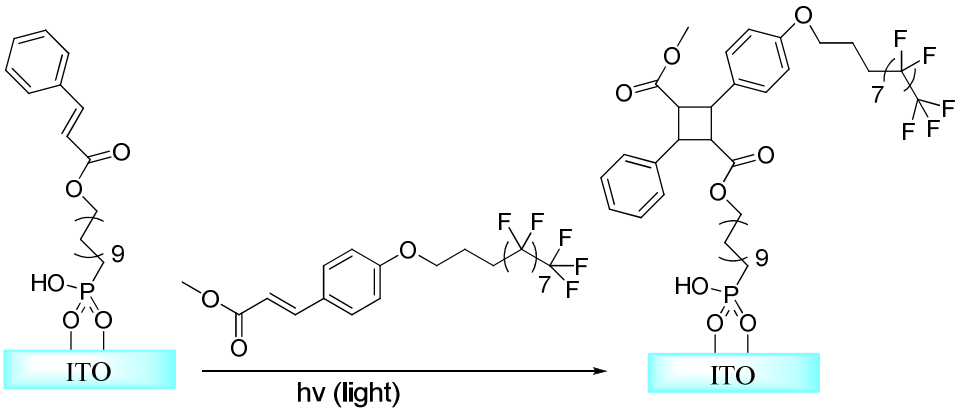

Figure B.3 Schematic showing the cycloaddition of a small molecule cinnamate to an ITO surface modified with a cinnamate functionalized phosphonic acid.

The composition of the samples surface was analyzed by XPS. The results suggest that, as the irradiation time increases, the amount of fluorinated molecule crosslinked to the surface also increases (Figure B.4). This is evidenced by an increase of the F(1s) peak (~ 689 eV) with increasing irradiation time.

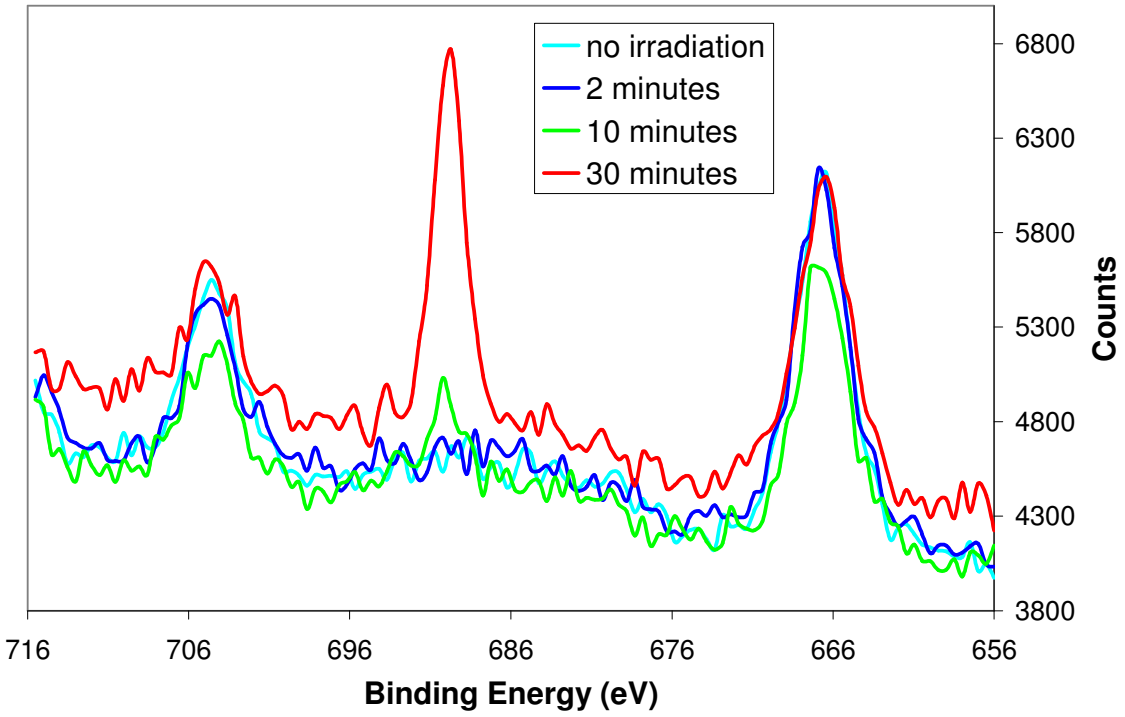

Figure B.4 XPS spectra of modified ITO surfaces crosslinked with a fluorinated cinnamate derivative for various irradiation times. The peak ~ 689 eV corresponds to the F(1s) electrons in the sample.

The atomic composition of the surface before and after the crosslinking step (assuming that all surface bound cinnamates undergo cycloaddition with the fluorinated counterparts) was calculated and compared with the experimental results (Table B.1). Here, again, it can be seen that the surface becomes enriched in fluorine with irradiation. The experimental results, however, do not approach the condition where each surface cinnamate is crosslinked to a fluorinated cinnamate from solution, for the irradiation condition utilized.

Table B.1 Theoretical and experimental atomic compositions (for F, C, and P) on the various crosslinked cinnamate ITO substrates. The % detected compositions take into account only the elements involved with the monolayer or the fluorinated cinnamate. Oxygen is not included because it is also present in the substrate. Hydrogen cannot be detected with XPS.

Sample	% detected composition		
	Fluorine	**Carbon**	**Phosphorus**
Monolayer (theoretical)	0	95	5
Post-functionalization (theoretical)	29	69.5	1.5
bare ITO	0	100	0
monolayer on ITO	0	94	6
monolayer, small molecule, no irradiation	0	92	8
monolayer, small molecule, irradiation (2 min)	0	96	4
monolayer, small molecule, irradiation (10 min)	7	87	6
monolayer, small molecule, irradiation (30 min)	10.5	87	2.5

These initial results using a cinnamate functionality to photocrosslink other cinnamates to the surface are promising, however the experiments need to be repeated and verified. Additionally, experiments need to be conducted using a benzophenone-terminated phosphonic acid, which has the ability to crosslink any molecules that have C-H bonds to the surface.

B.3 References

1. Sung, S. J.; Cho, K. Y.; Hah, H.; Lee, J.; Shim, H. K.; Park, J. K., Two different reaction mechanisms of cinnamate side groups attached to the various polymer backbones. *Polymer* **2006,** 47, (7), 2314-2321.